ISSN 1377-0950

MARID 2013

MARINE & RIVER MARID 4 DUNE DYNAMICS

Fourth International Conference on

Marine and River Dune Dynamics

Bruges, Belgium
15 to 17 April 2013

Editors : V. Van Lancker and T. Garlan

VLIZ special publication number 65

MARID IV

Marine and River Dune Dynamics

Bruges, Belgium
15 - 17 April, 2013

Organising Committee

Prof. Dr. Vera Van Lancker (Royal Belgian Institute of Natural Sciences / Ghent University)
Dr. Jan Seys (Flemish Marine Institute, VLIZ)
Dr. Marc Roche (Federal Public Service Economy, Self-employed, SMEs and Energy)
Dr. Yves Plancke (Flanders Hydraulics)
Dr. Tomas Van Oyen (Ghent University)
Sonia Papili (Belgian Navy)
Ir. Guido Dumon (Agency for Maritime & Coastal Services, Coastal Division, Flanders Hydrography)
Dr. Matthias Baeye (Royal Belgian Institute of Natural Sciences)
Dr. Thierry Garlan (French Naval Hydrographic and Oceanographic Service, SHOM)

Scientific committee

Chair: Prof. Dr. Vera Van Lancker (Royal Belgian Institute of Natural Sciences / Ghent University)
Co-chair: Dr. Thierry Garlan (French Naval Hydrographic and Oceanographic Service, SHOM)
Dr. Sophie Le Bot (University of Rouen)
Prof. Dr. Alain Trentesaux (University of Lille)
Prof. Dr. Suzanne Hulscher (University of Twente)
Prof. Dr. Dan Parsons (University of Hull)
Prof. Dr. Jim Best (University of Illinois)
Dr. Katrien Van Landeghem (University of Bangor)
Dr. Marc Roche (Federal Public Service Economy, Self-employed, SMEs and Energy)
Dr. Yves Plancke (Flanders Hydraulics)
Dr. Tomas Van Oyen (Ghent University)

This publication should be cited as follows:
Van Lancker, V. and Garlan, T. (Eds), 2013. MARID 2013. Fourth International Conference on Marine and River Dune Dynamics. Bruges, Belgium, 15-17 April 2013. Royal Belgian Institute of Natural Sciences and SHOM. VLIZ Special Publication 65 – Flanders Marine Institute (VLIZ). Oostende, Belgium. 338p. ISSN 1377-0950. ISBN 978-2-11-128352-7

ISSN 1377-0950
ISBN 978-2-11-128352-7

Organized and sponsored by:

Royal Belgian Institute of Natural Sciences
Management Unit of the North Sea Mathematical Models
Gulledelle 100, 1200 Brussels, Belgium - http://www.mumm.ac.be

French Naval Hydrographic and Oceanographic Service
SHOM – Oceanographic Centre - 13, rue du Chatellier
CS 92803, 29228 Brest Cedex 2, France - http://www.shom.fr

This conference is also supported by:

Flanders Marine Institute (VLIZ)
Federal Public Service Economy Self-employed, SMEs & Energy
Flanders Hydraulics Research
Ghent University (Dept. of Civil Engineering, Coastal Engineering)
Belgian Navy (Research group)
Agency for Maritime and Coastal Services (Coastal Division, Flanders Hydrography)

Golden Sponsorship

Belgian Science Policy Office (BELSPO)
Avenue Louise 231 Louizalaan, 1050 Brussels, Belgium - http://www.belspo.be

Silver Sponsorship

Flemish Authorities, Department Mobility and Public Works
Maritime Access
Tavernierkaai 3, 2000 Antwerpen, Belgium – http:// www.maritiemetoegang.be

Flemish Authorities, Agency for Maritime and Coastal Services
Coastal Division, Flanders Hydrography
Vrijhavenstraat 3, 8400 Oostende, Belgium –
http://www.afdelingkust.be and http://www.vlaamsehydrografie.be

Picture cover:
© Service Continental Shelf - FPS Economy, Belgium. NW flank of the Oosthinder sandbank showing an alignment of very large "barchanoid" dunes that stretch into the adjacent channel. The troughs of these large majestic dunes host a high biodiversity, discovered by our colleague Jean-Sébastien Houziaux, marine biologist (09/05/1970 - † 15/06/2012).

Preface & Welcome

Under the auspices of the North Sea Hydrographic Commission, a first workshop on marine sandwave dynamics was organised by SHOM and the University of Lille 1 (France) in 2000. This successful event was followed up in April 2004 (University of Twente, the Netherlands) and in April 2008 (University of Leeds, United Kingdom). These MARID conferences provided state-of-the-art overviews and outlined progress in our knowledge on marine sandwaves and river dunes in a format that stimulated cross-disciplinary knowledge exchange and cooperation. Earth scientists, oceanographers, engineers, hydrographers and biologists from across the world shared results derived from field observations, modelling studies and laboratory experiments.

The present, fourth conference, *Marine and River Dune Dynamics IV*, held in the City of Bruges in Belgium, April 15-17 2013, is piloted by the Royal Belgian Institute of Natural Sciences (Management Unit of the North Sea Mathematical Models) and the French Naval Hydrographic and Oceanographic Service (SHOM).
The central theme of this fourth edition is **Integrated Data-Modelling Approaches and Societal Relevance**. Discussions are encouraged to stimulate new research initiatives that will result in better integration of field data on marine and river bedforms, numerical/analytical model outputs and laboratory experiments. A plea is held for thorough and systematic data–model comparisons to test the capabilities and sensitivities of numerical models and, thus improve model accuracies and performances for better applications and assessments needed in environmental management. As such, we want to highlight the importance of interaction with end-users. Establishing and maintaining the societal relevance of research on bedform dynamics helps to maximize the impact of our work and ensures its long-term funding**.** We face new challenges in river and seabed management as human utilization is increasing and good environmental status needs safeguarding. For better practice in observations, modelling and experiments, often combined in integrated approaches, there is a growing need for new technologies, strategies and standardized methodology. This is a challenge for all disciplines.

MARID IV is open to all professionals and stakeholders dealing with bedform dynamics. It presents cutting-edge science and provides real-life examples from many areas and perspectives. Ample opportunity for networking is provided to what we know is a close-knit, global community of scientists, practitioners, industry representatives, policy advisors and managers.

In keeping with the previous MARID conferences, we maintain the concept of a small, focused event with only plenary sessions to stimulate discussion and cross-fertilization among disciplines and to learn from each other. New areas for future investigation and collaboration will undoubtedly emerge.

Enjoy the conference!

Vera Van Lancker & Thierry Garlan

Table of Contents

Gaps in understanding of sedimentary bedforms in the ancient, the present, the extraterrestrial and the kitchen

M.G. Kleinhans [(1)]

1. Faculty of Geosciences, Universiteit Utrecht, Utrecht, the Netherlands, m.g.kleinhans@uu.nl http://www.geo.uu.nl/fg/mkleinhans

Abstract

Much is known about bedforms, but a number of critical gaps in understanding remain. These gaps become clear when present understanding is extrapolated to extreme materials, conditions or environments. Advanced physics-based modelling demonstrates that dunes and upper-stage plane bed are predictable from the laws of physics, but may be sensitive to constitutive relations for flow and particle friction and sediment transport. Furthermore the question whether current ripples and dunes are distinct forms or the same forms with different sizes remains unanswered. Empirical work and experiments shows that a zoo of phenomena and bedforms emerge in cohesive sediments or sand-gravel mixtures, in hyperconcentrated flows and turbidity currents, showing that mixtures of particle sizes with different weight or other properties require basic exploration. Finally, the angle of repose is the most basic characteristic of sediment relevant for inter-particle friction and the steep lee side of bedforms, but prediction from physics remains poorly understood as demonstrated by measurements in lower gravity. The above phenomena arise because of three general mechanisms that can generally be called 'friction' and are incompletely understood: 1) the laminar to turbulent flow transition, 2) friction between particles and 3) cohesive forces.

1. INTRODUCTION

Bedforms and bed states such as Upper Stage Plane Bed or Upper Flow Regime Plane Bed have always been ubiquitous in many environments on Earth but our understanding of their formation, dynamics and sedimentary products is patchy. Classically bedforms and plane bed have been described for pure sand with low concentrations under unidirectional currents, tides and waves. Other species of bedforms emerge in cohesive sediments or poorly sorted sediment and in starkly different environments such as hyperconcentrated surface flows and turbidity currents. Finally, bedforms were discovered on Mars where a most fundamental condition differs from that on Earth: gravitational acceleration is only 3.74 m/s^2, yet we have no clue how this affects bedforms.

The objective of this paper is to uncover critical gaps in our mechanistic understanding of bedforms. The method is to explore the extreme limits of applicability of current concepts for material properties, conditions and environments. Building on the value of empiricism and physics, three complementary styles of logical reasoning: deduction, induction and abduction are used:

1) Deduction: laws of physics and numerical physically-based models are applied to initial+boundary conditions to predict bedforms.
2) Induction: initial+boundary conditions are measured or experimentally controlled to map the resulting bedforms to create 'laws'.
3) Abduction: the end result is observed and 'laws' are considered known, but the formative conditions are inferred.

2. PHYSICS-BASED MODELLING

2.1. Modelling ripples, dunes and plane bed

A decade ago the physics of full development of bedforms (as opposed to incipient bedforms predicted in linear stability analyses) were deemed so complicated that some doubted a model would ever be possible. Recently Nabi (2011) modelled three-dimensional flow and particle motion in great physical detail to show that ripples, dunes and upper stage plane bed emerge autonomously. Furthermore it produces hysteretic dune development in discharge waves, which can be used to develop new constitutive relations for dune dimensions and drag to use in large-scale morphological engineering models.

The physical nature of the model suggests that these exciting results are universally valid, but the sediment transport description implemented in the model is necessarily semi-empirical. Indeed, alternative constitutive sediment transport relations did not form dunes. This raises the question what the effect would be of alternative physical mechanisms and constitutive relations. Vice versa, alternative choices can provide clues about the best forms that constitutive relations for transport could have, independent of empirical measurement.

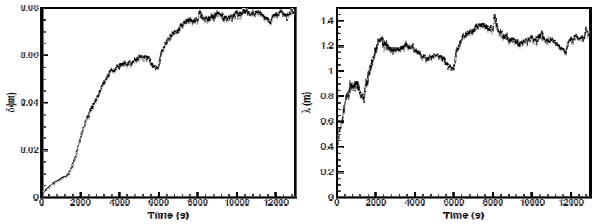

Figure 1. Bedform height (left) and length (right) development in the Nabi (2011) model under constant conditions starting from flat bed.

A long standing dispute is whether dunes and ripples are distinct features or simply different in scale. In bedform stability diagrams ripples occur in hydraulically smooth bed conditions, i.e. when laminar sublayer thickness exceeds particle size. In such conditions local turbulence production over an irregularity or bedform crest locally enhances shear stress. This causes formation of a scour hole which maintains local turbulence strong enough to suppress the laminar sublayer. If this is true then dunes replace ripples only due to an increase of shear stress or grain size and cannot occur in superposition unless in the transition zone. On the other hand, these scour holes are also observed without ripples in near-critical flow, where they add unrealistic effects to scale models for rivers and tidal systems. This suggests that scour holes and rhythmic bedforms are independent forms that are superimposed in the case of ripples, which otherwise are the same phenomenon as dunes.

A model such as Nabi's (2011) can be used to remove or add model components representing physical effects and processes, and can be used to model scenarios. Modelling started from plane bed for a flume-sized domain shows that at small bedforms develop that Nabi calls ripples, which then merge to grow into dunes. Indeed dune height growth temporarily stalls during the transition (Fig. 1). However, the most systematic set of controlled experiments producing ripples (Baas 1994) show that equilibrium ripples have well-defined dimensions independent of flow velocity, water depth and particle sizes (except close to the boundaries of their stability field), namely 0.02 m high and 0.2 m with a spread of a factor of two. Current work is aimed at understanding the relation between scour holes and ripples and the consequence for the ripple-dune transition.

2.2. Sorting of sand and gravel in dunes

In seemingly simple unidirectional flow with sandy gravel several sorting patterns occur, such as fining upward in dunes and transverse sorting in river bends. The sorting has large effects on equilibrium morphology and time scales of adaptation (Blom et al. 2008), which is highly relevant for managed rivers such as the Rhine. Furthermore it interferes with sorting patterns at the scale of bars and bends. But grain-scale sorting on reach-scale river morphology pose a rather large challenge to numerical modelling.

Blom et al. (2008) present a sophisticated model that conserves mass of all grain size fractions, models vertical sediment fluxes, and accounts for stochastic temporal variability of dune trough depth. This model constitutes an important improvement over the classic active layer depth where the layer thickness must be calibrated and strongly determines time scales of morphological and or sorting adaptation. The model also points towards the importance of initial sorting conditions and history effects in sorting, which adds a complication to hysteretic bedform dynamics.

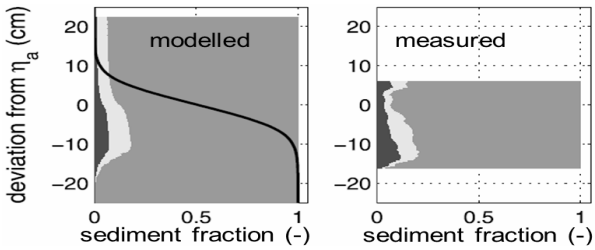

Figure 2. Vertical sorting by dunes (Blom et al. 2008).

One important question is what the effect is of constitutive relations for sediment transport. Several mechanisms must be included semi-empirically. Sediment pickup and deposition must be corrected for hiding effects occurring with particles of different sizes. Some processes are too poorly understood to be included. Due to hiding, armouring occurs in a mobile layer of a few grains thickness, whereas in partly mobile sediments the

smallest particles contributing to morphological change may be winnowed out of an otherwise nearly static bed by turbulence penetrating the bed, or deposited and percolated into the deeper bed.
A second major question is to what extent particle-scale phenomena are relevant for reach-scale river morphology. Yet the thin layers used in the discretised numerical model require very small time steps unsuitable for large-scale morphodynamic modelling. Yet dunes modify near-bed flow and thus interfere with transport and sorting processes on transverse bed slopes on bars and in bends. These phenomena call for further study by combination of detailed sorting models, engineering models and dedicated flume experiments to unravel the dynamic interaction between dunes and bars and the transverse slope effect on sediment transport and sorting.

3. EMPIRICAL EXTREMES

3.1. Angle of repose dependence on '*g*'

Noncohesive granular materials are found in many contexts, from kitchen to industry and, notably, the lee side of ripples, dunes and other steep bedforms. A basic property is the angle of repose a: the maximum slope angle at which the material is at rest. Above this slope angle, the material starts to flow. The angle is related to the friction angle of sediment that figures in semi-empirical relations for incipient sediment motion and transport.
It is generally believed that this angle is independent of gravitational acceleration g as on other terrestrial planets, moons and asteroids in the Solar system. This belief follows from the Coulomb law and the first law of Amontons. It follows that the driving gravitational force along the slope of a granular flow, $F_z = mg_{eff} \sin a$, is balanced by friction, which depends on the force normal to the slope, $F_f = mg_{eff} \cos a$. As both scale with the weight of the flow, the dynamic angle of repose for a granular flow is independent of gravity. Although some observations were done for granular materials under hypergravity, direct measurements of the angle of repose are rare.
In 33 parabolic flights in a well-controlled research aircraft Kleinhans et al. (2011) recorded avalanching granular materials in rotating drums at effective gravitational accelerations of 0.1 and 0.38 times the terrestrial value and at 1.0g as a control experiment. The granular materials varied in particle size and rounding and had Utrecht air or tap water as interstitial fluid. Materials with angular grains had time-averaged angles of about 40° and with rounded grains about 25° for all effective gravitational accelerations, except the finest glass beads in air, which was explained by static electricity. For all materials, the *static* angle of repose *in*creases about 5° with reduced gravity, whereas the *dynamic* angle *de*creases with about 10°. Surprisingly, both depend on gravity and avalanche size increases with reduced gravity.

Figure 3. Typical angles of repose under reduced g.

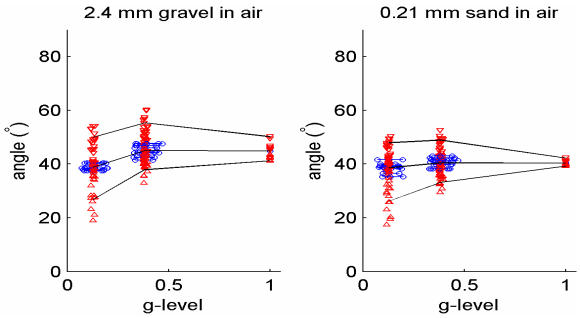

Qualitative explanations are that friction is lower in more dilated grain flows in reduced gravity so that the dynamic angle of repose is smaller. The static angle of repose, on the other hand, is related to 'cohesive' forces including Vanderwaals and electrostatic forces, which continue to act in vanishing gravity and increase the static angle.
We lack the mechanistic understanding to predict angle of repose and friction angle depending on material properties (and gravity). Hence this causes empirical uncertainty in transport predictors. It also raises questions about what happens in bedforms with low density sediments such as shell hash and mud clasts. Furthermore it is the question which angle is likely to be preserved at the planetary surface and in the rock record. Ubiquitous disturbances render the lower dynamic angle of repose dominant in nature. Lower slip face angles reduce flow separation and turbulence generated by flow over bedforms (Nabi 2011).

3.2. Bedforms in sand-mud mixtures

Mud occurs in abundance in fluvial and coastal systems since the emergence of plant life on Earth ~400 million years ago. Although mud consists of much finer particles than sand or of low-density flocs with much lower settling velocity, mud and sand often mix. Mud adds a plethora of effects to sediment, including cohesion and reduced pore flow due to blocking. Furthermore mud modifies near-bed turbulence. In novel experiments Baas et

al. (2011) found a bewildering variety of bedforms and layer patterns in sand-mud mixtures relevant for tidal environments and turbidity currents.
Baas et al. found that bedforms generated in turbulent flow and in turbulence-modulated, cohesive flows differ greatly in their size, texture, sedimentary structure and migration rate as a function of the duration of the formative flow and the texture of the initial flat bed. In particular, the mud, silt and sand fractions mix, segregate or layer rhythmically depending on Reynolds number and near-bed mud concentration. These findings are relevant for mud-silt-sand stratification formed in tidal environments, where critical shear stress for motion will be affected, and for rapidly decelerating turbidity currents in deep water.

4. BEDFORMS CARVED IN ROCK

4.1. Hyperconcentrated supercritical flow

The classical Bouma sequence of layering in rocks has been used as a conceptual model to infer the formative conditions of turbidity currents. But new systematic experimentation in supercritical hyperconcentrated flow demonstrated that antidunes, breaking antidunes, chutes-and pools and, notably, large, upslope migrating cyclic steps are transitional into each other with increasing Froude numbers (Cartigny et al. in review). In particular such large cyclic steps were hitherto unrecognised bedforms, that now appear to have recognisable stratification in outcrops of turbidity currents. Point characterisation of the flow with migrating bedforms inevitably covers both bedform troughs and crests, and experimentally it was found that a high percentile of the Froude number distribution over time discriminated better than the median between the bedform patterns. Temporally stable bedform types (in dynamic equilibrium) occupy distinct fields in a two-dimensional phase diagram with sediment mobility and particle size. However, the fields are modified by sediment concentration and fall-out rate.
Cartigny et al. find that various patterns of stratification resembling hummocky cross-stratification can be caused by multiple completely different bedforms and conditions. Fortunately, detailed differences exist so that otherwise vague deposits hitherto interpreted as the result of one process can now be ascribed to distinct locations and phases in a turbidity current system and provide detailed information on the formative conditions. This work illustrates that the geologic record may contain a zoo of bedforms that are hitherto unrecognised and poorly understood.

5. CONCLUSIONS

The science of bedforms is ultimately founded on classical physics, but three related groups of mechanisms are poorly understood and yet cause a plethora of phenomena highly relevant to the field:

1. laminar-turbulent flow transitions
2. friction between static and mobile particles, particularly of different sizes
3. cohesion: a bulk term for attractive forces between particles of clay-size and larger.

The examples further illustrate that complementary approaches in the disciplines studying bedforms reveals where significant progress can be made.

6. ACKNOWLEDGMENT

I am grateful to Astrid Blom, Mohamed Nabi, Jacco Baas and George Postma for discussion. Presented views are entirely my responsibility.

7. REFERENCES

Baas, J.H. 1994. A flume study on the development and equilibrium morphology of small-scale bedforms in very fine sand. Sedimentology, 41, 185–209.

Baas, J.H., Best, J.L. & Peakall, J. 2011. Depositional processes, bedform development and hybrid bed formation in rapidly decelerated cohesive (mud–sand) sediment flows. Sedimentology 58: 1953-1987

Blom, A., Ribberink, J.S. & Parker, G. 2008. Vertical sorting and the morphodynamics of bed form-dominated rivers: A sorting evolution model. J. Geophys. Res., 113: F01019

Cartigny, M.J.B., Ventra, D., Postma G. and Van Den Berg, J.H. submitted. Morphodynamics and sedimentary structures of bedforms under supercritical-flow conditions: new insights from flume experiments. Sedimentology, also open access PhD thesis Utrecht University 2012.

Kleinhans, M.G., Markies, H. de Vet, S.J. in ’t Veld, A.C. & Postema, F.N. 2011. Static and dynamic angles of repose in loose granular materials under reduced gravity. J. Geophys. Res. 116: E11004

Nabi, M. 2012. Computational modelling of small-scale river morphodynamics. Open access PhD thesis Delft University of Technology, 224 p.

Acoustic developments for the measurement of sediment processes over bedforms

Peter D. Thorne [(1)]

1. National Oceanography Centre, Liverpool, UK - pdt@noc.ac.uk

Abstract

The processes of near bed sediment dynamics involves feedback mechanisms, with the hydrodynamics, bedforms and sediment transport each mutually interacting and modifying one another. To understand these interactions requires co-located, simultaneous, high temporal-spatial resolution measurements of the three components of this interacting sediment triad. To study the triad, acoustics has been increasingly utilised over the past two decades. The development and application of acoustic systems capable of measuring near bed hydrodynamics, suspended sediments, bedload and bedforms is now contributing significantly to the measurement of sediment transport processes. Here we look at the application of these acoustic techniques to the study of sediment transport in large scale wave flume facilities and present results on sediment dynamics over sandy rippled beds under waves.

1. INTRODUCTION

To predict sediment transport requires a detailed understanding of the fundamental physical processes that lead to the movement of sediments. The processes can be thought of as dynamic interactions with feedback between: (i) the seabed morphology; (ii) the sediment field; and (iii) the hydrodynamics. This process has been coined the 'Sediment triad'.

The vision two to three decades ago was that acoustics may provide simultaneous measurements of all three components of the sediment triad. Acoustics was considered to have the potential to measure non-intrusively, with high temporal-spatial resolution, co-located profiles of suspended sediment particle size, concentration, the three orthogonal components of flow and bedforms, at intra-wave, intra-ripple and turbulent scales.

Here we look at the application of acoustics to sediment transport processes (Huther et al 2011) and illustrate its use through a study on sediment diffusivity (Thorne et al 2009)

2. ACOUSTIC INSTRUMENTS

2.1 Acoustic backscatter systems, ABS

As illustrated in figure 1 Multi-frequency ABS are used to measure near bed vertical profiles of suspended particle size and concentration, usually over the bottom 1-2 m above the bed with centimetric/millimetric spatial resolution and sub-second temporal resolution.

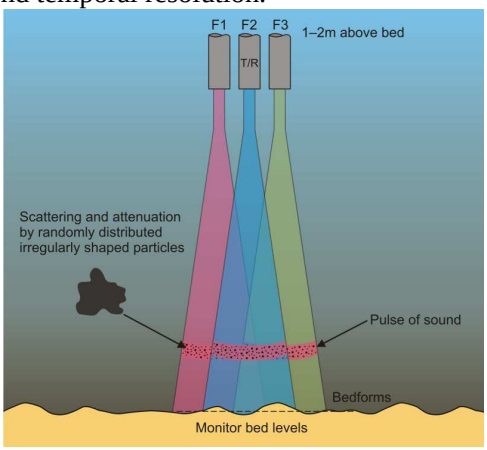

Figure1 Schematic of a Multi-frequency ABS for measuring vertical profiles of suspended particle size and concentration.

Using a combination of theoretical inversions (Thorne et al 2011), formulations for the scattering properties of natural irregularly shaped non-cohesive sediments (Moate and Thorne 2012) and exploiting the differential scattering characteristics with size and frequency, quantitative measurements of suspended sediment profiles can be obtained (O'Hara Murray et al 2012). Also because the echo from the bed is included in the acoustic backscattered signal the suspended sediment profiles can be referenced to the bed location.

To illustrate the type of measurements obtained from an ABS, figure 2 shows measurements of suspended sediments under waves over a vortex rippled sandy bed. The figure shows a high concentration even on the leeside of the ripple associated with the formation of a vortex, entraining and trapping sediments which was ejected over the ripple crest at flow reversal and up into the water column.

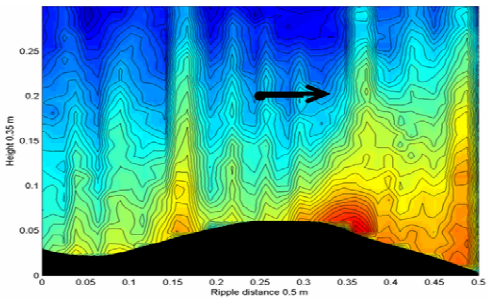

Figure 2. ABS image of suspended sediment entrainment over a vortex sand ripple under waves, with the arrow showing the instantaneous direction of flow.

2.2 Acoustic ripple profiles, ARP

As indicated above, bedforms impact on sediment transport processes and therefore it is essential to measure the features on the bed. Imaging from high frequency acoustic sector scanners has been around for a number of years (Hay and Wilson 1994). More recently two and three dimensional ripple profilers, ARP, which provide transects of the bed and actually measure the detailed bed topography have become available in recent years (Traykovski 2007).

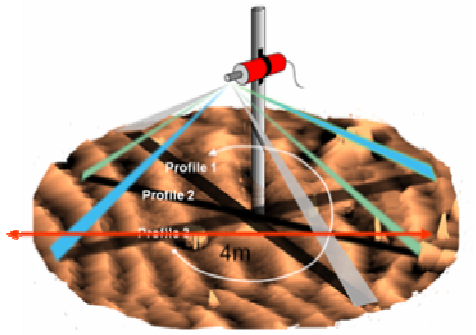

Figure 3. Illustration of a 3D-ARP covering a 4 m transect.

Figure 3 illustrates the mode of operation of a 3D-ARP. A narrow sound beam bisects a line along the bed and generates a two dimension transect of the bed providing a height profile, h(x,z). The system rotates through an angle and measures another transect. The system rotates through 180^o and builds up the topography shown in figure 3. From such measurements ripple height, wavelength, orientation and migration rates can be obtained.

2.3 Acoustic Doppler velocity profilers, ADVP

Measurement of the hydrodynamics is central to any sediment transport study. For near bed studies the acoustic Doppler velocimeter, ADV, is often the instrument of choice. This provides the three orthogonal components of flow at one height above the bed. In more recent years, profiling systems, ADVP, based on the same coherent signal processing of the backscattered signal have been developed (Hurther and Lemmin 2008. Hay et al 2012). Figure 4 illustrates the arrangement.

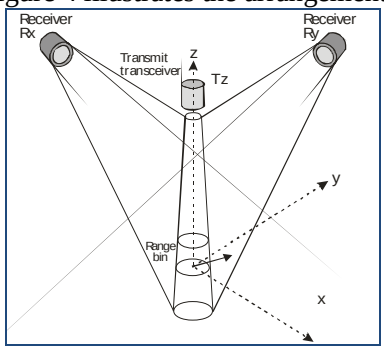

Figure 4 Schematic of an acoustic Doppler velocity profiler, ADVP

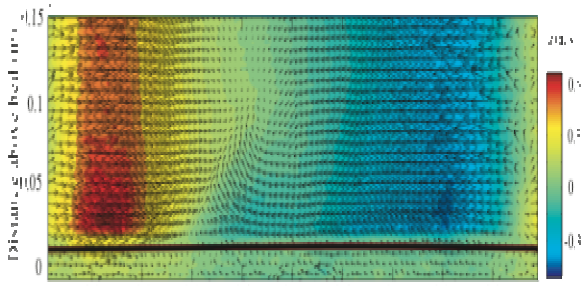

Figure 5. Vector v(u,w,z,t) flow structure during a 6.5 s wave period over a rippled bed underwaves .

Transducer Tz transmits a short pulse of sound and transducers Tz, Rx and Ry, receive the backscattered sound from sediment in suspension. Using coherent processing on the backscattered signal, high temporal-spatial profiles of the three orthogonal components of velocity can be

calculated. Figure 5 illustrates the type of measurements that can be collect. An ADVP was mounted above a rippled bed and profiles of the horizontal, u, and vertical, w, flow were collected. The vectors and colours show the detailed flow over a wave period at one location above a rippled bed.

3. ACOUSTIC PROCESS STUDY

3.1 Sediment diffusivity

Predictions for the form of the suspended sediment concentration profile are varied, differing according to the flow regime, the seabed sediment type and the bedforms. Most of the formulations to date have been underpinned by the classical concept of gradient diffusion (eg van der Werf et al 2006) In the simplest case the time averaged vertical turbulent diffusive flux of sediment, q_v, is considered to be balanced by the settling of the suspended sediment under gravity, such that:

$$q_v = w_s C \quad \text{where} \quad q_v = -\varepsilon_s \frac{\partial C}{\partial z} \tag{1}$$

Here C is the time-averaged sediment concentration at height z above the bed, w_s is the sediment settling velocity, and ε_s is the sediment diffusivity.

Despite the wide use of gradient diffusion, several studies (eg O'Hara Murray et al 2011) have indicated that this is not always the dominant process generating the suspended sediment concentration profile, particularly for sediment entrainment by waves over steeply rippled beds with $\eta_r/\lambda_r \geq 0.12$, where η_r is the ripple height and λ_r is the ripple wavelength. The mixing close to the bed is then dominated by a coherent process involving boundary layer separation on the lee-side of the ripple crest during each wave half-cycle near maximum flow velocity. The resulting lee-wake vortex remains attached to the bed entraining sediment into the flow as it grows in size and strength. At flow reversal the sediment-laden vortex is ejected into the water column, carrying sediment to several ripple heights above the bed. This process is coherent and repeatable and thus fundamentally different from that associated with gradient diffusion.

3.2 Sediment diffusivity models

Three diffusivity models are investigated. i) Nielsen's (1992) wave-averaged sediment diffusivity for rough and rippled bed is given by

$$\varepsilon_s = 0.016 k_s U_o \tag{2}$$

where U_o is the near-bed velocity amplitude and $k_s=25\eta_r(\eta_r/\lambda_r)$ is the equivalent bed roughness. ii) The formulation of Van Rijn (1993) is expressed as

$$\varepsilon_{s1} = \alpha_b k_s U_o \qquad z \leq \zeta_s \tag{3a}$$

$$\varepsilon_{s2} = \alpha_m \frac{Hh}{T} \qquad z \geq 0.5h \tag{3b}$$

$$\varepsilon_{s3} = \varepsilon_{s1} + (\varepsilon_{s2} - \varepsilon_{s1})\left[\frac{z-\zeta_s}{0.5h-\zeta_s}\right] \qquad \zeta_s < z < 0.5h \tag{3c}$$

Here ε_{s1} and ε_{s2} are, respectively, constant values for the sediment diffusivity near the bed and in the upper half of the water column, with the latter value being the larger; ζ_s is the thickness of the near-bed mixing layer and h is the water depth. In this present study the expression $\zeta_s = k_s$ $(=25\eta_r(\eta_r/\lambda_r))$ has been adopted for ease of comparison with Nielsen's formulation. Coefficient $\alpha_b = 0.004D_*$, where D_* is the dimensionless grain size , H is the wave height, T is the wave period and the coefficient $\alpha_m=0.035$. iii) The form often used for the sediment diffusivity is a simple linear increase in ε_s with height above the bed. This is commonly expressed as

$$\varepsilon_s = \beta\kappa\bar{u}_* z \tag{4}$$

where $\kappa=0.4$ is Von Karman's constant. Here the mean magnitude of the friction velocity, $\bar{u}_*$, over the wave cycle is used to be representative of the turbulent mixing during the wave cycle as a whole.

$$\bar{u}_* = 0.763(f_w/2)^{0.5} U_o \ , \ f_w = 0.237\left(\frac{k_s}{A_o}\right)^{0.52} \tag{5}$$

where f_w is the friction factor formulated by Soulsby (1997).

3.3 Acoustic and auxiliary measurements

The study was conducted in the Deltaflume of the Netherlands. The large size of this flume, 240 m in length, 5 m in width and 7 m deep, allow hydrodynamic and sediment transport to be studied at full scale. The experiments were conducted beneath weakly-asymmetrical, regular, surface

waves with heights, H, and periods, T, in the respective ranges H=0.6-1.1 m and T=4–6 s over medium sand and H=0.5-1.1 m and T=4–5 s over fine sand. The medium sand had d_{50}=330 μm and the fine sand had d_{50}=160 μm; both the sands were reasonably well sorted.

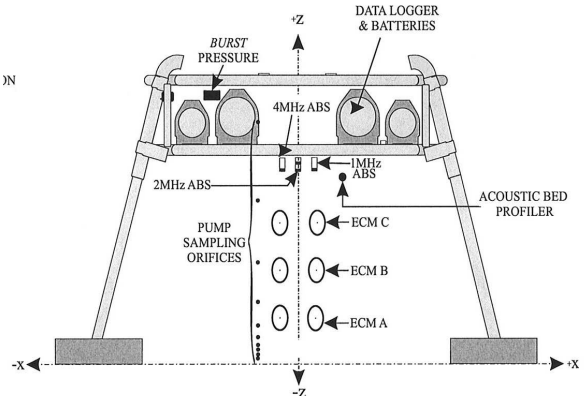

Figure 6 Schematic of the instrumented tripod used for the measurements. Shown is the triple frequency acoustic backscatter system, ABS, the acoustic ripple profiler, ARP, the pumped sampling heights and the electromagnetic current meters, ECMs.

Figure 6 shows the instrumented tripod platform used to collect the measurements. The main acoustic instruments relevant to the study were an ABS and a 2D-ARP. Auxiliary measurements using pumped sampling and electromagnetic current meters, ECMs, were collected.

High-resolution vertical profiles of the suspended sediments were measured using a triple-frequency ABS. The ABS provided 128 backscatter profiles each second, at each of the three frequencies, 1 MHz, 2 MHz and 4 MHz. Each profile consisted of 128 range bins, with a spatial resolution of 0.01 m, thereby covering a range of 1.28 m. Physical samples of the suspension were obtained by pumping through nozzles located at ten heights above the bed between 0.053 and 1.55 m. The samples were used to calibrate and assess the veracity of the acoustic backscatter measurements and provide profiles of w_s. To establish whether ripples were present on the bed, and to monitor their evolution and migration, a 2D-ARP, was used. The ARP operated at 2.0 MHz, and provided sub-centimetric measurements of the bed location over a 3m transect along the direction of wave propagation. Three ECMs located at 0.3, 0.6 and 0.91 m above the bed provided measurements of the along-flume and vertical components of the flow velocity at 8 Hz.

The measured ABS concentration profiles and w_s determined from the d_{50s} particle size profile from the pumped sample data, were used to calculate the sediment diffusivities ε_s with

$$\varepsilon_s = \frac{-w_s C}{dC/dz} \tag{6}$$

w_s is given by Soulsby (1997) as:

$$w_s = \frac{\nu}{d_{50s}}[(10.36^2 + 1.049D_*^3)^{0.5} - 10.36] \tag{7}$$

To compare results from all the different experiments the resulting sediment diffusivity profiles were normalised by plotting the parameters z/k_s and $\varepsilon_s/U_o k_s$.

3.4 Analysis and interpretation

Medium sand case. Using equation (6)and (7), ε_s was calculated from the ABS concentration profiles and the pumped sample particle size profiles. The results for the 39 sediment diffusivity profiles, from the 13 experiments were normalization and averaged to obtain the profile shown by the large solid circles with error bars in figure 7a. The data show approximately constant normalised sediment diffusivity in the region below $z/k_s \approx 1.3$. At heights greater than $z/k_s \approx 1.3$, $\varepsilon_s/U_o k_s$ increases linearly.

Using equation (2), Nielsen's empirical prediction for the constant normalized sediment diffusivity was calculated. This is shown by the dotted line in figure 7a and has a value of 0.016. This prediction is somewhat less than the presently measured value of 0.029. Considering the Van Rijn formulation for the constant sediment diffusivity layer, the value predicted by equations (3a) is 0.028, which is close to the measured value obtained here. Using equation (3a-3c) the predicted linear portion of the normalized sediment diffusivity does not result in a single curve for the present normalization. Therefore, rather than showing the calculations for each case, the bounds from the calculations are given by the two dashed lines. Given the limited data upon which equations (3a-3c) were based, the predictions are considered to be in reasonable agreement with the present data.

To complete the comparison of predictions with observations, equation (4) has been evaluated

using equation (5), and the result has then been normalised to yield

$$\frac{\varepsilon_s}{k_s U_o} = 0.763\kappa\beta\sqrt{\frac{f_w}{2}}\frac{z}{k_s} \qquad (8)$$

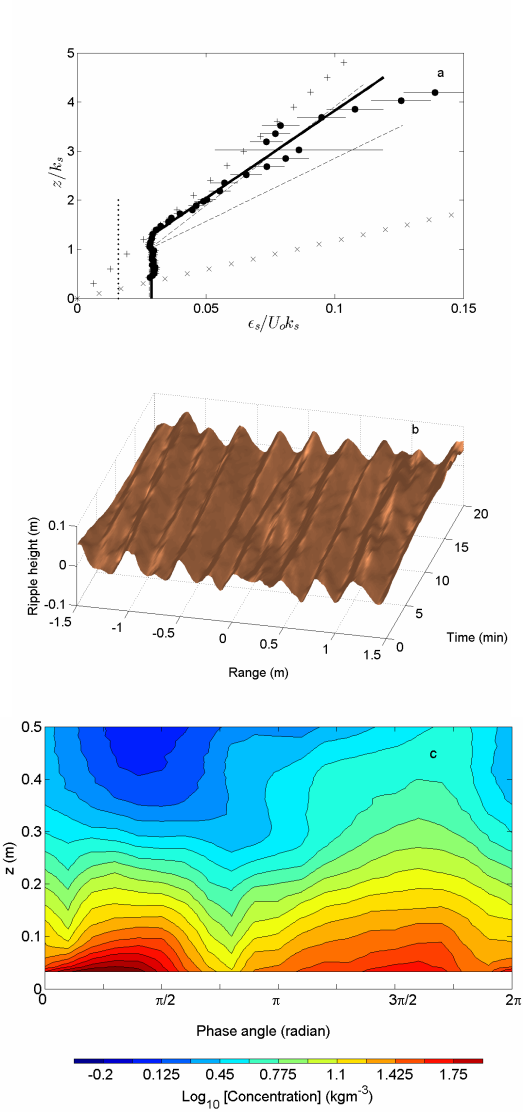

Figure 7. Comparison of the mean measured normalised sediment diffusivity (●) over the medium sand bed, with the calculations from equations (2) (····), (3) (----), (8) (x,+, see text) and (9) (▬). b) A transect of the bed over time for an experimental run with H=0.81 m and T= 5s and c) variation in concentration with the phase of the wave and height above the bed for the medium sand.

If equation (8) is evaluated using a mean value for f_w, from all the medium sand experiments, calculated using $k_s=25\eta_r(\eta_r/\lambda_r)$ in equation (5) and with $\beta=1$, the predictions for the sediment diffusivity ('×') substantially overestimate the observed values in the linear region. However, if f_w is calculated using a flat bed approximation $k_s=2.5d_{50}$ based on the grain size, then equation (8), again with $\beta=1$, yields the line in figure 7a represented by the '+' symbols. Evidently this latter outcome compares favourably with the data in the linear region

Finally, in order to capture the behaviour of the diffusivity in this case involving the medium sand, simple expressions have been fitted to the present data set to yield empirical expressions for the variation of sediment diffusivity with height above the bed. These expressions are as follows:

$$\varepsilon_s = \xi_1 U_o k_s \qquad z \leq 1.3k_s \qquad (9a)$$

$$\varepsilon_s = \xi_2 U_o z - \xi_3 U_o k_s \qquad z \geq 1.3k_s \qquad (9b)$$

where $\xi_1=0.029$, $\xi_2=0.028$, $\xi_3=0.007$ and the expression is given by the solid line in figure 7a. Further studies are required to assess the general applicability of equation (9)

To investigate the processes underlying the form of the sediment diffusivity profile, both the bedforms and the variation of suspended sediment concentration with the phase of the wave and height above the bed were examined. To illustrate the type of bedforms present on the medium sand, a typical measurement from the ARP is shown in figure 7b. The plot shows the development of a transect, over a 17 min period, for the case of T=5 s and H=0.81 m. The ripples were well developed with dimensions of $\lambda_r=0.34$ m, $\eta_r=0.047$ m, and slope of $\eta_r/\lambda_r=0.14$. This was typical for the medium sand, with $\langle\eta_r\rangle=0.05\pm0.01$ m, $\langle\lambda_r\rangle=0.36\pm0.07$ m, $\langle\eta_r/\lambda_r\rangle=0.14\pm0.01$ and $\langle k_s\rangle=0.17\pm0.03$ m, where $\langle\ \rangle$ represents an average over all experiments. The value for k_s is quite large indicating that the bed is having a major impact on the near-bed flow. To assess the mechanisms of sediment entrainment directly over the medium sand, intra-wave processes were investigated. The results are shown in figure 7c; here the intra-wave height variation of the ripple-averaged suspended sediment concentration, has been constructed over the 17 min recording period. It can be seen clearly that there are two main entrainment events and that these occur close to flow reversal ($\pi/2$, $3\pi/2$). Further analysis of this

data (Davies and Thorne 2005, Thorne et al 2009) supported the concept that the observations shown in figure 7c can be interpreted as arising from flow separation on the lee slope of the ripple, with the consequent generation of growing lee slope vortices. The processes are not random, but are repeatable and coherent. Importantly, the layer in which these effects occur may be seen to correspond to several ripple heights in thickness.

The intra-wave observations in figure 7c may be related to the sediment diffusivity profile in figure 7a in the following way. Due to the formation of vortices on the ripple lee slopes, suspended sediments were contained within a relatively fixed mixing region, of height comparable with the ripple height η_r, for most of the wave cycle. Near flow reversal the vortices were lifted up into the water column, retaining their structure to a height of the order of k_s. It is the associated coherence of sediment entrainment and structure that leads to the constant value for the sediment diffusivity within about $z/k_s \leq 1.3$ ($3\eta_r$-$4\eta_r$ for the medium sand). At heights greater than $z/k_s \approx 1.3$, the coherent structure of the vortices breaks down, with mixing of momentum increasingly becoming dominated by random turbulent processes (Ranasoma and Sleath, 1992). Here, therefore, gradient diffusion dominates and mixing increases due to an increase in the mixing length scale with height above the bed, leading to the linear increase in sediment diffusivity above the vortex layer.

Fine sand Using equation (6) and (7), ε_s was calculated for the fine sand bed, using the ABS concentration profiles together with the pumped sample particle size profiles. The normalised averaged results for the 21 sediment diffusivity profiles, from the 7 experiments are shown in figure 8a. The results show no indication of a constant diffusivity near-bed layer, but instead exhibit a sediment diffusivity that increases linearly with height above the bed. This shows no indication of a near-bed constant sediment diffusivity, associated in the medium sand measurements with vortex formation and entrainment of sediments. Instead, the results show, in the near-bed region, that the normalised sediment diffusivity increases linearly with height above the bed. Because there is no obvious constant near-bed sediment diffusivity, no useful comparison can be made with the formulations of Nielsen (Eq. (2)) or Van Rijn (Eq. (3a)). However, it is possible to compare Van Rijn's linearly increasing sediment diffusivity region with the present data. If, in equation (3c), ζ_s and ε_{s1} are set to zero, then using linear wave theory in the determination of ε_{s2} we have

$$\frac{\varepsilon_s}{k_s U_o} = \frac{2\alpha_m}{\pi} \sinh(kh) \frac{z}{k_s} \qquad (10)$$

where k is the wave number of the surface waves. Using this expression and taking the mean value of k for all the fine sand experiments, the dashed line in figure 8a is obtained. The resulting, predicted, normalised sediment diffusivity is comparable with the observed values, though it somewhat overestimates them. Reducing α_m from 0.035 to 0.022 brings Van Rijn's expression into line with the observations. Given the limited data set upon which equation (3b-3c) is based, this adjustment does not seem unreasonable. Secondly, equation (4) expressed in the form of equation (8) was compared with the data. It is interesting to note that, if equation (8) is evaluated using $k_s = 25\eta_r(\eta_r/\lambda_r)$ in equation (5), with $\beta=1$, as shown by the '×' symbols in figure 8a the predictions again significantly overestimate the observed values. However, if the flat bed approximation $k_s = 2.5d_{50}$ is used, the line in figure 8a represented by the '+' symbol is obtained, which can be seen to compare favourably with the data, with only a minor overestimation occurring. Given both these fine sand results and also those for the medium sand, it does appear to be the case that the use of $k_s = 25\eta_r(\eta_r/\lambda_r)$, for a rippled bed, overestimates the roughness length substantially if equation (4) is used to calculate ε_s.

Finally if, as in the medium sand case, an empirical fit is made to the data, forcing $\varepsilon_s = 0$ at $z=0$, then the following expression results:

$$\varepsilon_s = \chi_1 U_o z \qquad (11)$$

where $\chi_1 = 0.017$. This is comparable, though a somewhat smaller gradient than that for the linearly increasing region of the sediment diffusivity in the medium sand case.

To explain the form of the sediment diffusivity over the fine sand and its difference from the medium sand, we have again looked at the bedforms. Figure 8b shows a typical example of the ripple formation for waves with T=5 s and H=0.79 m; these inputs are very comparable with

the case shown in figure 7b for the medium sand. However, for the fine sand the ripples can be seen to be less well developed and less coherent in form, with, in the case shown, η_r=0.019 m, λ_r=0.27 m and η_r/λ_r=0.07.

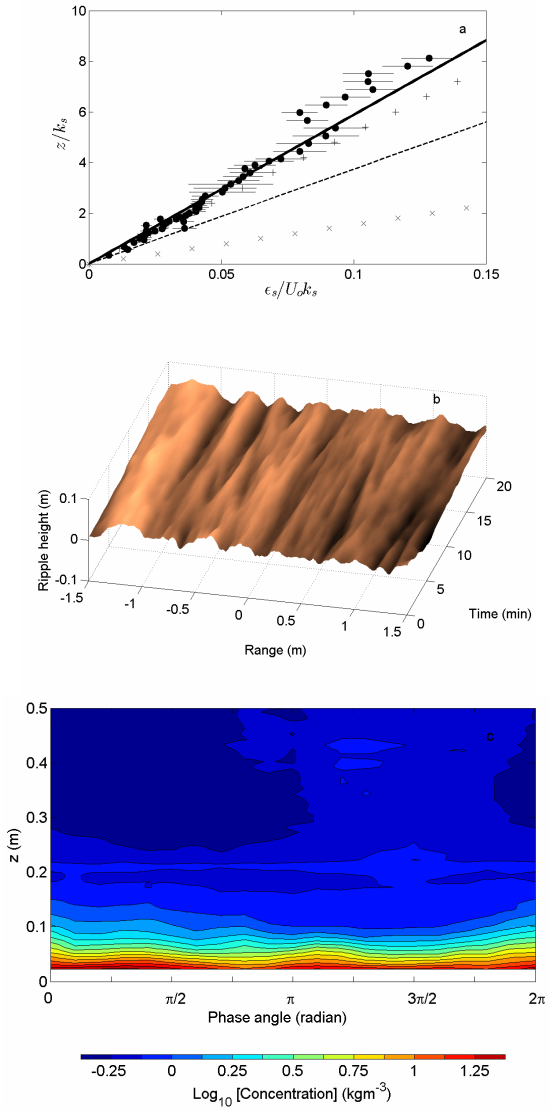

Figure 8 a) Comparison of the mean measured normalised sediment diffusivity (●) over the fine bed, with the predictions from equations (10) (– –), (8) (x,+ see text) and (11) (▬). b) A transect of the bed over time for an experimental run with H=0.79 m T=5s and c) variation in concentration with the phase of the wave and height above the fine bed.

These dimensions were typical of all the experiments, with $\langle\eta_r\rangle$=0.027±0.02 m, $\langle\lambda_r\rangle$=0.37±0.25 m, $\langle\eta_r/\lambda_r\rangle$= 0.07±0.01 and $\langle k_s\rangle$=0.05±0.03 m. For this range of slopes little significant flow separation or vortex formation is expected to occur (e.g. Sleath 1984).

Therefore, although the ripples enhanced the bed roughness somewhat, they acted on the flow dynamically like a plane bed. The equivalent roughness of the bed, if based upon $k_s=25\eta_r(\eta_r/\lambda_r)$, was just over a quarter that of that in the medium sand case, indicating that the impact of the bed on the flow is restricted to a region much closer to the bed than for the medium sand.

To assess the impact of ripples of low slope on sediment entrainment, the variation of the suspended sediment with the phase of the wave and the height above the bed for the fine sand was examined. An example of the results is shown in figure 8c for H=0.82 m and T=5s. The structure of the intra-wave suspended sediments is seen to be quite different from that shown in figure 7c; there are no significant suspension events near flow reversal lifting sediment well up into the water column. High concentrations are confined to a relatively thin layer within a few centimetres of the bed and the variation in the suspended load seems to be only weakly dependent on the phase of the wave, with only marginal increases in suspended concentration levels at maximum flow speed. The results in figure 8c indicate that the bed is behaving dynamically more like a plane bed, rather than a bed that is inducing vortex formation and entrainment. Therefore, the lack of a constant sediment diffusivity region in the fine sand case is not surprising, since the conditions for vortex entrainment were not present and it is the formation of vortices which are considered to be the underlying process leading to the constant sediment diffusivity region. For the fine sand case it is considered that the dynamics are comparable with the classical flat bed situation and that turbulent processes dominate the near-bed sediment entrainment. In this case the turbulent eddies are considered to grow with height above the bed (Davies and Villaret, 1997), leading to the linear increase in sediment diffusivity measured in this study over the bottom quarter of the water column.

4. CONCLUSIONS

Acoustics is now being used to measure, bedforms, suspended sediment, bedload, and hydrodynamics. The aim of the present paper was to describe and illustrate the use of acoustics in boundary layer sediment transport process studies. An example of the application of acoustic measurements has been

presented on sediment diffusivity profiles and comparisons made with three standard models and suggested new formulations have been presents. The work has shown how acoustics can be used to provide insight into understanding fundamental mechanisms of sediment processes

5. ACKNOWLEDGMENT

The work was supported by the EU contract MAS3-CT97-0106 and by the NERC, UK. The author is grateful to Professor Alan G Davies and Dr Paul S Bell for contributions to this work. Further details on this application of acoustics to sediment diffusivity studies can be found in Thorne, Davies and Bell (2009).

6. REFERENCES

Davies A.G. and C. Villaret, 1997. Oscillatory flow over rippled beds: Boundary layer structure and wave-induced Eulerian drift. Chapter 6 in Gravity Waves in Water of Finite Depth, ed. J.N. Hunt, Advances in Fluid Mechanics, Computational Mechanics Publications, 215-254.

Davies A.G. and Thorne P.D. 2005. Modelling and measurement of sediment transport by waves in the vortex ripple regime. Journal of Geophysical Research. Vol 110, C05017, doi:1029/2004JC002468, 2005. pp25.

Hay, A.E., Wilson, D., 1994. Rotary sidescan images of nearshore bedform evolution during a storm. Marine Geo. 119, 57-65.

Hay A.E., Zedel L., Cheel R. and Dillon J., 2012. On the vertical and temporal structure of flow and stress within the turbulent oscillatory boundary layer above evolving beds. Continental Shelf Research, 46, 31-49.

Hurther, D. and Lemmin U. (2008). Improved turbulence profiling with field adapted acoustic Doppler velocimeters using a bi-frequency Doppler noise suppression method. *J. Atmos. Oceanic Technol*., 25 (2), 452-463.

Hurther, D, Thorne, PD and Bricault M, Lemmin U and Baroud JM. 2011. A multi-frequency acoustic concentration and velocity profiler (ACVP) for boundary layer measurements of fine-scale flow and sediment transport processes. Coastal Engineering. 58, 294-605 doi: 10.1016/j.coastaleng.2011.01.006.

Moate BD and Thorne PD. 2012. Interpreting acoustic backscatter from suspended sediments of different and mixed mineralogical composition. Continental Shelf Research, 46, 67-82.

Nielsen P. 1992. Coastal Bottom Boundary Layers and Sediment Transport. Advanced series on ocean engineering, volume 4. World Scientific, Singapore, 324 pp.

O'Hara Murray, R.B., Thorne, PD and Hodgson DM. 2011. Intrawave observations of sediment entrainment processes above sand ripples under irregular waves, J. Geophys. Res., 116, C01001, doi:10.1029/2010JC006216.

O' Hara Murray, Hodgson D.M and Thorne P.D. 2012. Wave groups and the character of sediment resuspension over an evolving sandy bedforms. Continental Shelf Research, 46, 16-30.

Ranasoma, K.I.M., and . Sleath J.F.A. 1992. Velocity measurements close to rippled beds, in Proceedings of the 23rd International Conference on Coastal Engineering, pp. 2383-2396, American Society of Civil Engineers, Venice, Italy.

Sleath J.F.A. 1982. The suspension of sand by waves. J. of Hydraulic Research, 20, 5, 439-452.

Soulsby R.L. 1997 Dynamics of marine sands. Thomas Telford publication, UK. 249 pp.

Thorne, P.D., Davies, A.G. and Bell P.S. 2009. Observations and analysis of sediment diffusivity profiles over sandy rippled beds under waves, J. Geophys. Res., 114, C02023, doi:10.1029/2008JC004944.

Thorne P.D., Hurther D. and Moate B.D. 2011. Acoustic inversions for measuring boundary layer suspended sediment processes. J Acoust Soc Amer 130(3) 1188-1200.

Traykovski, P. (2007). Observation of wave orbital scale ripples and a nonequilibrium time-dependent model. J. Geophys. Res. 112, C06026, doi:10.1029/2006JC003811

van der Werf J.J. Ribberink, J.S, O'Donoghue T and Doucette J.S. 2006. Modelling and measurement of sand transport processes over full-scale ripples in oscillatory flow. Coastal Engineering, 53, 657-673

Van Rijn L.C., 1993 Principles of sediment transport in rivers, estuaries and coastal seas. Aqua publications, the Netherlands. 633 pp.

Modeling offshore sandwaves

Suzanne JMH Hulscher [(1)]

1. University of Twente, Faculty of Engineering Technology - Civil Engineering. Department of Water Engineering & Management, Enschede, The Netherlands

ABSTRACT

The offshore seabed shows various types of seabed patterns. This keynote will focus on one of these, being sandwaves. These features have elongated crests, about 500 ma apart, and show a wavy patters perpendicular. The sandwaves have heights up to 25% of the water column, so typically amplitudes of 5-10 meters. Sand waves are abundant: they cover the major part of the southern North Sea. They are also dynamic as the features migrate up to 20m/year. Apart from being scientifically relevant (what forms these features?) they are also practically relevant: when planning pipeline trajectories and offshore windparcs and shipping lanes one has to deal with the sandwave dynamics. In this presentation the focus will be on the modeling part of the sand waves. So what mechanism forms them and what approaches are available to describe the generation and evolution of sand waves. Typical approaches are idealized modeling (stability analysis) and modeling using complex models as Delft3D. I will discuss them and show the possibilities and limitations of both. Special attention will be given on the link between sandwaves and biologic activity.

Large-eddy simulations in dune-dynamics research

Ugo Piomelli [(1)] and Mohammad Omidyeganeh [(1)]

1. Department of Mechanical and Materials Engineering, Queen's University, Kingston (ON), Canada - ugo@me.queensu.ca, omidyeganeh@me.queensu.ca

Abstract

We discuss the recent use of large-eddy simulations (LES) for the analysis of the flow over dunes. In large-eddy simulations the governing equations of fluid motion are solved on a grid sufficiently fine to resolve the largest eddies, while the effect of the smallest ones is modelled. Examples are shown to demonstrate how this technique can be used to complement experiments, by exploiting its ability to calculate full-field information, and to highlight the temporal development of the flow. The main challenges slowing a more widespread application of this method are discussed.

1. INTRODUCTION

The study of environmental and geophysical flows presents considerable challenges. Geometrical complexities, stratification, two-phase flows are often present. Field experiments are extremely difficult, due to the often adverse conditions, and to the difficulty in obtaining accurate full-field measurements, especially near solid boundaries, and to the lack of control over the boundary conditions. Laboratory-scale studies can overcome some of these issues, but are still limited: in addition to the fact that a reduced Reynolds number must be used, present experimental techniques force the researcher to compromise between conflicting requirements: the needs for time-resolved measurements, for all components of the velocity, and for full-field information are difficult to reconcile. Furthermore, simultaneous measurements of velocity and scalars cannot always be obtained, and some quantities (vorticity, pressure, for instance) are difficult to measure.

Numerical models have recently been applied with increased frequency, due to the decreasing cost of computational power. Early simulations solved the Reynolds-Averaged Navier-Stokes (RANS) equations (Mendoza & Shen, 1990; Yoon and Patel, 1996). In RANS solutions the contribution of all the turbulent motions (eddies) is parameterized; in complex flows out of fluid-dynamical equilibrium these models may be inaccurate; moreover, they cannot account for the unsteady nature of turbulence. In many cases large coherent motions ("macroturbulence", Best 2005) are responsible for much of the momentum, energy and scalar transport. In this conditions, more advanced models are required to give accurate predictions of the flow, and help understand the turbulence physics underlying the transport processes.

One of these methods is the large-eddy simulation (LES). In LES the contribution of the large, energy-carrying structures to momentum and energy transfer is computed exactly, and only the effect of the smallest scales of turbulence is modelled. Since the small scales tend to be more homogeneous and universal, and less affected by the boundary conditions than the large ones, there is hope that their models can be simpler, and require fewer adjustments when applied to different flows, than similar models for the RANS equations.

LES provide a three-dimensional, time dependent solution of the Navier-Stokes equations. Among the objectives of LES are to provide data for low-

er-level turbulence models at moderate to high Reynolds numbers, and to study complex physics in realistic configurations.

While LES has a long history in the environmental sciences (in particular, meteorology), and in mechanical and aerospace engineering, its use for the study of dune dynamics is more recent. The first LES of this type was carried out by Yue and coworkers (Yue *et al.*, 2005). They modelled the flow over two-dimensional dunes for two depths. The results showed that the interaction of the free surface and the flow structures is significantly affected by the flow depth. The same authors (Yue *et al.*, 2006) subsequently performed LES in nearly the same configuration, and visualized periodically flapping spanwise rollers in the recirculation zone.

Stoesser *et al.* (2008) showed rollers at the crest that expanded to the size of the dune height as they were convected towards the reattachment point, and conjectured that the boils on the surface were originally hairpin eddies generated in the reattachment region as a result of secondary instabilities of rollers that are elongated in the streamwise direction and tilted upward. However, the instantaneous visualizations of velocity fluctuations do not show a strong upwelling at the surface, but rather a structure more similar to the smaller, weaker boils that occur at the surface of open-channel flows over flat surfaces**.**

Grigoriadis *et al.* (2009) studied two cases with Reynolds numbers (based on average flow depth and mean bulk velocity) equal to 17,500 and 93,500. They examined the turbulent eddies in more detail than previous investigators. Their results, however, differ somewhat from previous experimental and numerical observations: in their simulations the horseshoe structures do not reach the surface. They, however, observed kolk vortices generated by the interaction between streamwise vortices that reach the dune crest from upstream and rollers generated at the crest. Kolk vortices were found to last for long times, and were the most significant structure observed at the surface in their simulations.

Recently, we have applied LES to the study of two and three-dimensional dunes, at laboratory scale (Omidyeganeh & Piomelli, 2011, 2013). Our studies have focused on the relation between the largest coherent eddies, which may be generated in the separated or by the three-dimensionality of the bedform, to the mean and instantaneous flow. The type of understanding that can be obtained through a quantitative and qualitative analysis of the data obtained from such simulations will be discussed in Section 3.

In the following, first, a typical LES model will be described. Then, some representative results will be shown to illustrate the potential of this method. Finally, the potential and shortcomings of LES, *vis-à-vis* its application to dune dynamics, will be discussed.

2. METHODOLOGY

2.1 Governing equations

Large-eddy simulations (LES) are based on the assumption that small-scale turbulent eddies are more isotropic than the large ones, and are responsible mostly for energy dissipation in the mean. Modelling the small scales, while resolving the larger eddies, may be very beneficial: first, since most of the momentum transport is due to the large eddies, model inaccuracies are less critical; secondly, the modelling of the unresolved scales is easier, since they tend to be more homogeneous and isotropic than the large ones, which depend on the boundary conditions.

Thus, LES is based on the use of a filtering operation: a filtered (or resolved, or large-scale) variable, denoted by an overbar, is defined as

$$\overline{f}(\mathbf{x}) = \int_D f(\mathbf{x}')G(\mathbf{x},\mathbf{x}')d\mathbf{x}' \qquad (1)$$

where D is the entire domain and G is the *filter* function (Leonard 1974).

The filter function determines the size and structure of the small scales. The size of the smallest eddies that are resolved in LES is related to the length-scale of the smoothing operator, the "filter width", $\overline{\Delta}$. The grid size, h, should be sufficiently fine to allow eddies of size $\overline{\Delta}$ to be represented accurately.

If the operation (1) is applied to the governing equations, one obtains the filtered equations of motion, which are solved in large-eddy simulations. For an incompressible flow of a Newtonian fluid, they take the following form:

$$\frac{\partial \overline{u}_i}{\partial x_i} = 0 \qquad (2)$$

$$\frac{\partial \overline{u}_i}{\partial t} + \frac{\partial}{\partial x_j}(\overline{u}_i\overline{u}_j) = -\frac{1}{\rho}\frac{\partial p}{\partial x_i} - \frac{\partial \tau_{ij}}{\partial x_j} + \nu\nabla^2\overline{u}_i \qquad (3)$$

$$\frac{\partial \overline{c}}{\partial t}+\frac{\partial}{\partial x_j}(\overline{c}\overline{u}_j)=-\frac{\partial Q_j}{\partial x_j}+\kappa\nabla^2\overline{c} \qquad (4)$$

where c is an arbitrary transported scalar, ρ is the fluid density, p its pressure, ν and κ are, respectively, the kinematic viscosity and the molecular diffusivity of c, and τ_{ij} and Q_j are the subgrid-scale (SGS) stresses and scalar flux, defined as

$$\tau_{ij}=\overline{u_i u_j}-\overline{u}_i\overline{u}_j; \qquad Q_j=\overline{u_j c}-\overline{u}_j\overline{c} \qquad (5)$$

These terms must be parameterized; eddy-viscosity and diffusivity models are generally considered adequate (Piomelli 1999, Meneveau & Katz 2000).

2.2 Numerical approach

Most of the applications of LES to dune dynamics employ structured, finite difference or finite-volume codes, either using body-fitted or Cartesian grids. Our numerical method, in particular, is a curvilinear finite-volume code. Both convective and diffusive fluxes are approximated by second-order central differences. A second-order-accurate semi-implicit fractional-step procedure (Kim & Moin 1985) is used for the temporal discretization. The Crank-Nicolson scheme is used for the wall-normal diffusive terms, and the Adams-Bashforth scheme for all the other terms. The pressure is obtained from the solution of a Poisson equation, which will be discussed later. The code is parallelized using the Message-Passing Interface and the domain-decomposition technique, and has been extensively tested for turbulent flows (Silva Lopes & Palma 2002; Silva Lopes et al. 2006; Radhakrishnan et al. 2006, 2008; Omidyeganeh & Piomelli 2011).

2.3 Turbulence models

Most subgrid scale models in use presently are eddy-viscosity models of the form

$$\tau_{ij}-\delta_{ij}\tau_{kk}/3=-2\nu_T\overline{S}_{ij}=-2C\overline{\Delta}^2|\overline{S}|\overline{S}_{ij}. \qquad (6)$$

Here

$$\overline{S}_{ij}=\left(\partial\overline{u}_i/\partial x_j+\partial\overline{u}_j/\partial x_i\right)/2 \qquad (7)$$

is the resolved strain-rate tensor, |S| is its magnitude, ν_T is the eddy viscosity, and C is a coefficient that, in the present simulations, is calculated using the Lagrangian-dynamic eddy-viscosity model (Meneveau *et al.*, 1996). This technique allows the eddy viscosity to respond to the local state of the flow, and adapt to fluid-dynamical non-equilibrium better than fixed-constant models.

3. CASE STUDIES

In this Section we show two examples of recent results obtained by our group, to demonstrate how numerical simulations can complement experimental studies, both at the field and at the laboratory scale to answer outstanding questions in dune dynamics.

3.1 The origin of boils

One feature of the flow over dunes that has attracted significant attention is the variety of very large (with size comparable to the river depth) coherent structures that are observed. Several researchers have discussed these structures, and their role in the transport of mass and momentum. Best (2005) observed boils (upwelling motions at the water surface, that usually occur when a horizontally oriented vortex attaches to the surface) in a high Reynolds-number flow over dunes in the laboratory and in the Jamuna River, Bangladesh, and proposed a schematic model for the interaction of coherent structures with the flow surface that results in boils. Discussion on the generation of large vortex loops that cause the strong upwelling at the surface is still inconclusive. Müller and Gyr (1986) proposed a mixing-layer analogy in which separated spanwise vortices at the crest undergo three-dimensional instabilities, which eventually cause hairpin-like vortices associated with low-speed fluid that rises up to the surface and generates boils. Nezu & Nakagawa (1993) identified vortices in the separated-flow region that move towards the reattachment point; they conjecture that kolk-boil vortices are formed due to oscillations of the reattachment line.

To determine which of the above conjectures is the correct one, we performed numerical simulations of the flow over a two-dimensional dune, at laboratory scale (Omidyeganeh & Piomelli 2011). The simulation used 416×128×384 grid points to discretize a domain of dimensions $20h\times4h\times16h$ (where h is the dune height) at Re=18,900. The results of the model were validated by comparison against experimental data (Balachandar *et al.*

$|\overline{S}|$

2003).

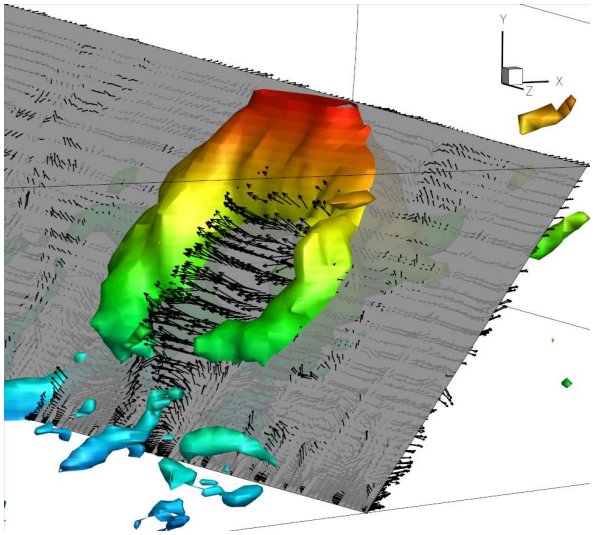

Figure 1. Visualization of the flow near a large horseshoe structure (visualized through isosurfaces of p' coloured by the vertical coordinate) when it touches the surface. The vectors show the upwash between the vortex legs that results in the appearance of a boil on the surface.

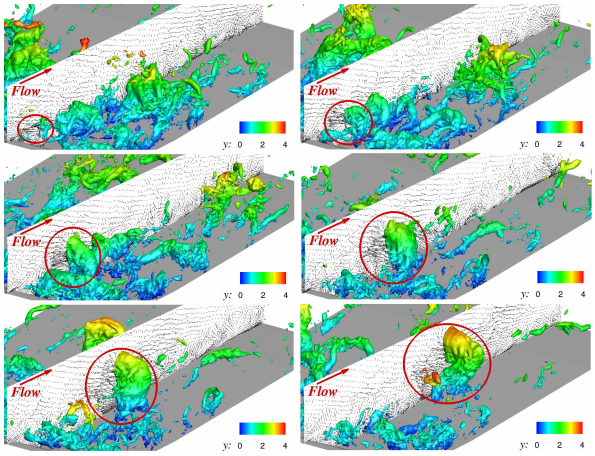

Figure 2. Evolution of a large horseshoe structure, visualized through isosurfaces of p' coloured by the vertical coordinate; the time interval between snapshots is $3h/U_b$; vectors of velocity fluctuations are shown on a vertical plane at z = 10.7h for every 5 grid points.

The availability of three-dimensional velocity fields makes it possible to use advanced flow-visualization techniques. Moreover, since several snapshots of the flow, closely spaced in time, are available, one can observe a feature of interest, and then march forward in time to study its development, but also backwards to investigate its origins. Taking advantage of these features of the numerical model, and coupling the (qualitative) flow visualization with a quantitative analysis, allows us to obtain in-depth understanding that would be difficult to achieve using experimental techniques, especially at field scale.

Figure 1, for instance, shows the flow field associated with a horseshoe vortex that reaches the water surface. The vortex is visualized through isosurfaces of the pressure fluctuations, negative values of which highlight the core of large scale vortices. We observe, first, that the scale of the vortex is comparable to the depth, consistent with many experimental observations. Second, that the vortex induces a very strong upwash between its legs, which causes with the vertical velocity, high pressure and diverging streamlines associated with a boil.

The temporal development of a horseshoe vortex of this type is illustrated in Figure 2, which shows how a spanwise vortex generated at the separation point undergoes a 3D instability, and moves towards the surface while, at the same time, becoming more and more 3D and assuming its characteristic horseshoe shape.

A more quantitative illustration of this development is given in Figure 3, in which we show the probability of the occurrence of the vortices that cause the boils. A very clear high-probability region extends from the separation point at the dune top, towards the free surface over the stoss side. Spectra measured along this path show a distinct peak that corresponds to the shedding frequency; this signature can be observed even at the surface, in regions where boils prevalently occur. The reattachment region, or the boundary layer on the stoss side, by contrast, do not show this signature.

3.2 Dune three-dimensionality

A similar approach was taken by Omidyeganeh & Piomelli (2013) to study the effect of crest three-dimensionality on the flow field. A sinusoidal deformation was imposed on the crestline, and cases with varying amplitude and wavelength were studied. One case in which the lobes and saddles were staggered was also considered.

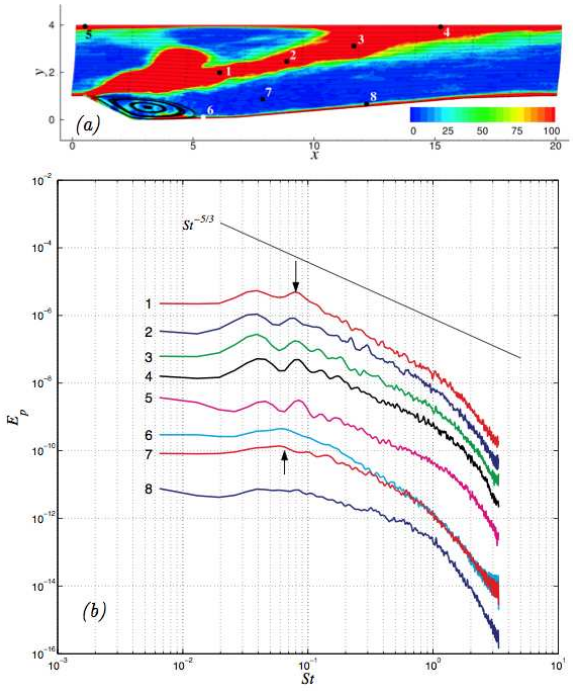

Figure 2. *(a)* Contours of the number of occurrence of the event $p' < -5p_{rms}$; *(b)* pressure spectra at the points marked in *(a)*; each curve is shifted downward by a factor of 10 for clarity.

Allen (1968) studied near bed streamlines of a series of sinusoidal crestline dunes and obtained some insight of the developed secondary flow across the channel. The induced streamwise vortices with a size of the flow depth are measured by Maddux and co-workers (Maddux *et al.* 2003a, 2003b) for a staggered crestline configuration. The characteristics of these vortices have been related to the characteristics of the sinusoidal crestline by Venditti (2007) for aligned crestline configurations. Our simulations provide features of the secondary flows, their impact on the bed shear stress distribution, characteristics of the separation and reattachment regions, and sensitivity of turbulence statistics to the geometrical parameters of the crestlines.

Figure 4 shows contours of the streamwise component of the wall stress, for three selected cases. The dashed white lines highlight the $\tau_{w,x} = 0$ contour. First, we note that longitudinal regions of low wall stress can be observed in all cases. In the first case (Figures 4*(a)*) they are aligned with the lobe, and are due to pairs of streamwise vortices, which advect low-speed fluid close to the bed towards the lobe and high-speed fluid from the outer flow towards the wall, thereby decreasing τ_w at the lobe and increasing it at the saddle. These vortices can be observed in Figure 5*(a)*. In Case 9 (Figure 4*(b)*), in which the wavelength of the crest is short, streaks are due to a streamline convergence caused by the bottom topography, whereas in Case 10 (long wavelength and staggered dunes), two pair of vortices are present, one generated at the lobe, the other at the lobe of the upstream dune.

Case 9 has the lowest crestline wavelength, and different mean-flow characteristics. The typical secondary flow with large streamwise vortices between the lobe and the saddle, observed in the other cases, is not observed here (Figure 5*(b)*). In the channel interior, the spanwise velocity is negligible compared to the vertical one, and the flow characteristics are similar to the 2D dunes (Omidyeganeh & Piomelli 2011), as fluid moves downward in the first half of the channel and upward in the second half. Nezu & Nakagawa (1993) pointed out that large secondary currents occur when the wavelength of the bed deformations in the spanwise direction is more than twice the flow depth; in Case 9 the wavelength is equal to the maximum flow depth ($\lambda = 4h$), and large-scale streamwise vortices are not observed. Although the streamwise vorticity in the interior of the channel is small, due to the waviness of the bed in the spanwise direction, the spanwise pressure gradient becomes significant, driving high-momentum fluid toward the lobe, causing high-pressure zone at the lobe and low wall-shear stress stripes along the saddle plane in Figure 4*(b)*.

In Case 10, because of the staggered lobes and saddles, the flow develops quite differently (Figures 4*(c)* and 5*(c)*). First, as was also observed experimentally (Figure 6 in Maddux et al. (2003a)), the flow is faster over the node plane. After the reattachment on the stoss side (e.g., in the vertical planes in Figure 5*(c)*), two strong vorticity contours with opposite signs are observed near the lobe. These vortices decay as they travel over the saddle plane of the following dune, but can still be observed in the vertical plane in Figure 5*(c)*, and in the wall-stress contours in Figure 4*(c)*.

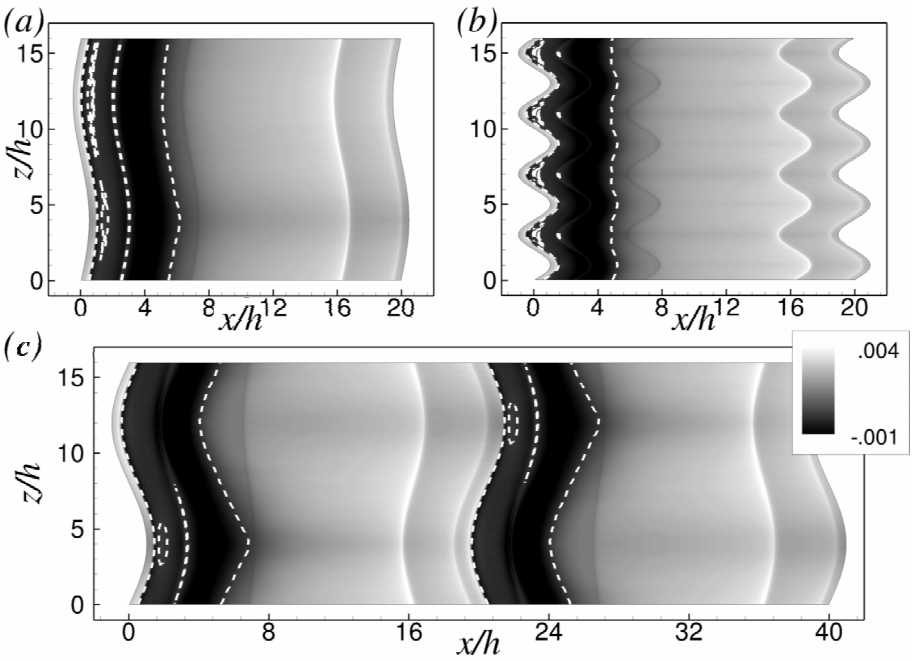

Figure 4. Contours of the streamwise component of the wall stress, $\tau_{w,x}/\rho U_b^2$. The dashed white lines highlight the $\tau_{w,x} = 0$ contour. (a) Case 1 (long crest wavelength) *(b)* Case 9 (short crest wavelength); *(c)* Case 10 (long crest wavelength, staggered dunes).

4. CHALLENGES AND ACHIEVEMENTS

Numerical simulations will not replace experiments, either at the laboratory scale, or at the field scale, in the near future. They can, however, complement them, and help researchers gain a stronger foothold on the very complex and challenging problem of turbulence in environmental flows.

Numerical models present several useful characteristics: they allow very careful definition of the boundary conditions; they yield three-dimensional and time-dependent fields, from which quantities that are hard to measure may be extracted (pressure, vorticity, higher-order moments); they allow the researcher to "travel back in time", by isolating a flow feature of interest, and examining the flow at previous times to determine its origin; finally, in wall-resolved calculations, the flow field extends all the way to the wall. In the previous Section, through two examples of recent calculations, we have tried to show how these potential advantages can be beneficial, and allow to answer conclusively questions that had been raised by experimentalists, but could not be answered completely based on the data available in field or laboratory studies. Additional features that can be easily added to the model are more complex geometries (either through body-fitted grids or using Immersed-Boundary Methods (Mittal & Iaccarino, 2005), the transport of pollutants or nutrients, or roughness (which, again, can be included through immersed-boundary methods).

Several challenges still limit the application of numerical models. First is the computational cost. Wall-resolved LES of the type described here are expensive, since the equations of motion need to be integrated for long times to accumulate the sample required for convergence of the statistics. In the present case, this resulted in approximately 6,000 CPU hours, or four weeks of continuous running on 64 processors. Increasing the Reynolds number to field scale is, at the present time, unfeasible, as the number of points required to resolve the flow scales like $Re^{13/7}$ (Choi & Moin 2012). The use of wall-models may allow such extension, but the additional modelling required may make the prediction of flow features that are driven by near-wall dynamics (some of the secondary flows described above, for instance) inaccurate.

Another important addition to the model is the inclusion of the motion of sand, which could help predict dune motion, or scouring. Models that include the motion of solid particles are in widespread use in engineering. Methods in which the motion of the particles (and their effect on the flow field) is simulated using a Lagrangian viewpoint are very successful for heavy particles with low concentration (solid particles in gases, for instance). In the case of flow over dunes, the density ratio between sand and water is not large, and the concentration of particles may be very large near the bottom; Eulerian approaches in which the suspended sediment is modelled as a transported scalar may be more successful. A model for the particle lift up from the wall that is accurate locally and instantaneously (and not only capable of predicting average quantities) is crucial to the development of this type of technique.

In summary, the application of LES to dune flows is quite new, but has already shown potential. A wise use of numerical simulations will, at this time, focus on fairly simple geometries, to maximize the accuracy of the model, and try to address questions that cannot be resolved adequately by present experimental techniques. As computational power continues to increase, however, there is reason to believe that predictive calculations in realistic geometries may become more and more common.

5. ACKNOWLEDGMENT

This research was supported by the Natural Sciences and Engineering Research Council (NSERC) under the Discovery Grant program. The authors thank the High Performance Computing Virtual Laboratory (HPCVL), Queen's University site, for the computational support. MO acknowledges the partial support of NSERC under the Alexander Graham Bell Canada NSERC Scholarship Program. UP also acknowledges the support of the Canada Research Chairs Program.

6. REFERENCES

Allen, J. R. L. (1968). *Current ripples: their relation to patterns of water and sediment motion*. North-Holland Pub. Co.

Best, J. (2005). The fluid dynamics of river dunes: A review and some future research directions. *J. Geophys. Res.*, 119(F04S02):1–21.

Choi, H. and Moin, P. (2012). Grid-point requirements for large eddy simulation: Chapman's estimates revisited. *Phys. Fluids*, 011702.

Grigoriadis, D. G. E., Balaras, E., and Dimas, A. A. (2009). Large-eddy simulations of unidirectional water flow over dunes. *J. Geophys. Res.*, 114.

Kadota, A. and Nezu, I. (1999). Three-dimensional structure of space-time correlation on coherent vortices generated behind dune crests. *J. Hydr. Res.*, 37(1):59–80.

Kim, J. and Moin, P. (1985). Application of a fractional step method to incompressible Navier-Stokes equations. *J. Comput. Phys.*, 59:308–323.

Leonard, A. (1974). Energy cascade in large-eddy simulations of turbulent fluid flows. *Adv. Geophys.*, 18A:237–248.

Maddux, T. B., McLean, S. R., and Nelson, J. M. (2003a). Turbulent flow over three-dimensional dunes: 2. Fluid and bed stresses. *J. Geophys. Res.*, 108-F1(6010):11–1—17.

Maddux, T. B., Nelson, J. M., and McLean, S. R. (2003b). Turbulent flow over three-dimensional dunes: 1. Free surface and flow response. *J. Geophys. Res.*, 108-F1(6009):10–1—20.

Mendoza, C. and Shen, H. W. (1990). Investigation of turbulent flow over dunes. *J. Hydr. Engng*, 116:459–477.

Meneveau, C., Lund, T. S., and Cabot, W. H. (1996). A Lagrangian dynamic subgrid-scale model of turbulence. *J. Fluid Mech.*, 319:353–385.

Meneveau, C. and Katz, J. (2000). Scale-invariance and turbulence models for large-eddy simulations. *Annu. Rev. Fluid Mech.*, 32:1–32.

Mittal, R. and Iaccarino, G. (2005). Immersed boundary methods. *Annu. Rev. Fluid Mech.*, 37(1):239–261.

Müller, A. and Gyr, A. (1986). On the vortex formation in the mixing layer behind dunes. *J. Hydr. Res.*, 24:359–375.

Nezu, I. and Nakagawa, H. (1993). *Turbulence in Open-Channel Flows*. Balkema.

Omidyeganeh, M. and Piomelli, U. (2011). Large-eddy simulation of two-dimensional dunes in a steady, unidirectional flow. *J. Turbul.*, 12(N42):1–31.

Omidyeganeh, M. and Piomelli, U. (2013). Large-eddy simulation of three-dimensional dunes in a steady, unidirectional flow. Part 1: Turbulence statistics. *J. Fluid Mech.*

Piomelli, U. (1999). Large-eddy simulation: achievements and challenges. *Prog. Aerosp. Sci.*, 35:335–362.

Radhakrishnan, S., Piomelli, U., Keating, A., and Silva Lopes, A. (2006). Reynolds-averaged and large-eddy simulations of turbulent non-equilibrium flows. *J. Turbul.*, 7(63):1–30.

Silva Lopes, A. and Palma, J. M. L. M. (2002). Simulations of isotropic turbulence using a non-orthogonal grid system. *J. Comput. Phys.*, 175(2):713–738.

Silva Lopes, A., Piomelli, U., and Palma, J. M. L. M. (2006). Large-eddy simulation of the flow in an S-duct. *J. Turbul.*, 7(11):1–24.

Stoesser, T., Braun, C., Garcìa-Villalba, M., and Rodi, W. (2008). Turbulence structures in flow over two-dimensional dunes. *J. Hydr. Engng*, 134(1):42–55.

Venditti, J. G. (2007). Turbulent flow and drag over fixed two- and three-dimensional dunes. *J. Geophys. Res.*, 112(F04008):1–21.

Yoon, J. Y. and Patel, V. C. (1996). Numerical model of turbulent flow over sand dune. *J. Hydr. Engng*, 122:10—18.

Yue, W., Lin, C., and Patel, V. (2005). Large eddy simulation of turbulent open-channel flow with free surface simulated by level set method. *Phys. Fluids*, 17:025108.

Yue, W., Lin, C.-L., and Patel, V. C. (2006). Large-eddy simulation of turbulent flow over a fixed two-dimensional dune. *J. Hydr. Engng*, 132(7):643–651.

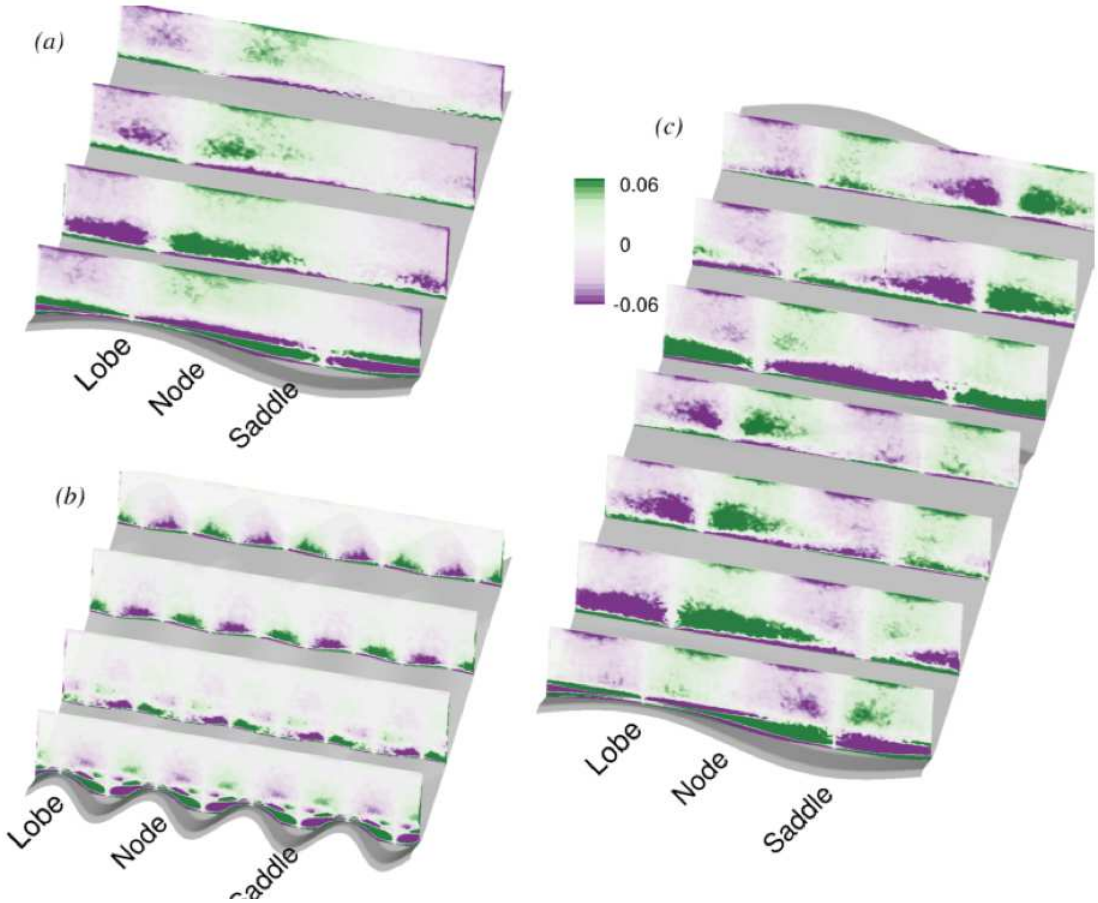

Figure 5. Contours of mean streamwise vorticity, $\Omega_x h/U_b$. (a) Case 1, long wavelength; (b) Case 9, short wavelength; (c) Case 10, long wavelength, staggered crests.

Physical and Biological Cohesion Within Mixed Sand-Mud Beds: Implications for Erosion and Bedform Development

Jaco H. Baas [(1)] and Jonathan Malarkey [(1)]

1. School of Ocean Sciences - Bangor University, Menai Bridge, Isle of Anglesey, LL59 5AB, Wales, UK- E-mail: j.baas@bangor.ac.uk

ABSTRACT

Flow and sediment transport predictions from sedimentary structures found in modern environments and within the geological record are impeded by an almost complete lack of process-based knowledge of the behaviour of natural sediments that consist of mixtures of cohesionless sand and biologically-active cohesive mud. Indeed, existing predictive models are largely based on non-organic cohesionless sands, despite the fact that mud, in pure form or mixed with sand, is the most common sediment on Earth, and is also the most biologically active interface across a range of Earth-surface environments, including rivers and shallow seas.

The multidisciplinary COHBED project uses state-of-the-art laboratory and field technologies to measure the erosional properties of mixed cohesive sediment beds and the formation and stability of sedimentary bedforms on these beds, integrating the key physical and biological processes that govern bed evolution.

The erosive behaviour of cohesive mixed sand-mud beds and bedform development on these beds was quantified as a function of physical control on bed cohesion versus biological control on bed cohesion. The Shear Flume at Bangor University was used to measure the critical shear stress for bed erosion for different mixtures of fine sand, kaolin clay and xanthan gum. Kaolin clay is a proxy for physical cohesion within the mixed bed. Xanthan gum is a polysaccharide of bacterial origin used commonly in experimental biostabilisation research, and thus provided control over biologically-induced cohesion in the experiments. The experiments involved the determination of suspended sediment concentration over a premixed and pre-consolidated sediment bed at progressively higher bed shear stress until an abrupt increase in concentration signified the critical shear stress for bed erosion.

Preliminary results show that the critical shear stress for bed erosion increases as the volume fraction of kaolin clay and xanthan gum in the sand bed is increased, but this effect is more pronounced for xanthan gum than for kaolin clay at similar volume fractions. This suggests that biological cohesion is more important than physical cohesion, and sedimentological process models should refocus on biostabilisation processes. However, this ignores any differences in the rate of production of biostabilisers versus the availability of cohesive clay in natural environments. Examples of sedimentary environments where biological cohesion might be more important than physical cohesion will be discussed and compared with environments where physical cohesion might outcompete biological cohesion.

The first results of experiments on bedform development in cohesive mixed sand will also be presented. These experiments show that winnowing of fine-grained cohesive sediment, including biological stabilisers, is an important process affecting the development rate, size and shape of the cohesive bedforms. Recommendations will be made if and how existing bedform predictors need to be modified to allow for cohesive bed behaviour by physical and biological processes.

Conceptual model of object burial in turbid waters on a sandy seabed

Matthias Baeye [(1)], Michael Fettweis [(1)], Frederic Francken[(1)], Dries Van den Eynde [(1)], Vera Van Lancker [(1)]

1. Royal Belgian Institute of Natural Sciences - Management Unit of the North Sea Mathematical Models (MUMM)- Gulledelle 100, B-1200 Brussels, Belgium
E-mail: m.baeye@mumm.ac.be

ABSTRACT

Highly turbid waters are characterized by high-concentrated suspensions of fine-grained sediments near the seabed. The dynamics of these fluffy mud layers on a sandy seabed have been studied in the turbid Belgian nearshore area using a test mine in combination with an instrumented, benthic tripod lander (Baeye et al. 2012). The latter measured currents and suspended particulate matter (SPM) concentration using optical (OBS) and acoustic devices (ADP, ADV). Besides time series of current velocities and acoustic amplitude, the ADV (5MHz) and ADP (3MHz) were configured to also measure and store the distance between the sensor and the seabed, i.e. seabed evolution (altimetry). Further, the optical sensors, integrated in the mine, also measured seabed evolution, or in this case burial-and-exposure cycles, as a function of hydrodynamic and meteorological conditions. Typically, near-bed hydrodynamics and SPM dynamics are dominated by tidal forcing. Maximal ebb and flood currents induce alternately scour at the mine's ends, and increased SPM concentrations. Further, short-term burial-and-exposure events (few hours) throughout the tidal cycle were also revealed: during slack water (reduced current speeds) the SPM settles massively and the mine is buried; after slack tide (increasing currents) re-suspension of this high-concentrated fluffy mud layer occurs, and the mine is again 'visible' with a scour pit at one end. The temporal pattern of this burial mechanism (ephemeral muddy bedform) mimics the cyclicity of the lutocline as recorded by ADV and ADP altimetry. A significant modification of the tidal forcing results from alongshore advection due to wind-induced flows and wave-induced re-suspension; these modifications can cause the fluffy mud layer to persist through some tidal cycles. In these conditions, the risk of long burial events is highest for mines, and objects in general, present in the nearshore area.

REFERENCES

Baeye M, Fettweis M, Legrand S, Dupont Y, Van Lancker V. 2012. Mine burial in the seabed of high-turbidity area - Findings of a first experiment. Continental Shelf Research 43, 107–119. doi:10.1016/j.csr.2012.05.009

Bedform morphology across the fluvio-tidal transition, Columbia River, USA.

Jim Best[(1)], Phil Ashworth[(2)], Andrew Nicholas[(3)], Dan Parsons[(4)], Eric Prokocki[(1)], Greg Sambrook Smith[(5)], Chris Simpson[(6)] and Steve Sandbach[(3)]

1. Departments of Geology, Geography and Geographic Information Science, Mechanical Science and Engineering and Ven Te Chow Hydrosystems Laboratory, University of Illinois at Urbana-Champaign, 1301 W. Green St., Urbana, IL, 61801, USA.
E-mail: jimbest@illinois.edu
2. Division of Geography and Geology, School of Environment and Technology, University of Brighton, UK
3. Department of Geography, University of Exeter, UK
4. Department of Geography, Environment and Earth Sciences, University of Hull, UK
5. School of Geography, Earth and Environmental Sciences, University of Birmingham, UK
6. Fulcrum Graphic Communications Inc., TH2-168, North Vancouver, Canada

ABSTRACT

Bedload transport within the fluvio-tidal zone is governed by the interaction between unidirectional currents with tidal flows of varying magnitude, with the additional superimposition of waves, and which all display an appreciable spatio-temporal variation across a range of scales. These changes in the hydrodynamics should control the differing characteristics of bedforms within this region, and thus ultimately determine the subsurface preserved sedimentary facies. This paper will detail the morphology of bedforms in the fluvio-tidal transition in the Columbia River, USA, through analysis of high-resolution multibeam echo sounder data collected in 2009 by NOAA (US National Oceanic and Atmospheric Administration) and extending from near the mouth of the river to *c.* 82 km upstream. These data have been used to quantify the different types of bedforms in the main channels (c. 500-1000m wide and 10-20m deep) and on barforms in the Columbia River and their geometric characteristics, including planform geometry, dune orientation, bedform asymmetry index and leeside angle. The data show a marked increase in the planform two-dimensionality of bedforms near the river mouth, where the dunes are also both more symmetric and smaller in amplitude than those further upstream, likely reflecting the modulation of bedforms by waves and tidal flows in this region. The data also shows dune orientation to depend on both the distance from the river mouth and lateral position in the channel and superimposed on the larger (c. 500-1500 long and 200-500 m wide) sand bars. Dunes within the fluvially-dominated reach are typically asymmetric in profile and displayed less superimposition of smaller forms than in the fluvio-tidal transition zone at the time of these surveys. Additionally, there are regions of channel bed in the fluvially-dominated reach where the mobile sand appears to be moving over a more resistant substrate that influences the geometry of the bedforms, with smaller barchanoid dunes being present. This paper will illustrate the nature of bedforms across this transition, examine their scaling with mean flow depth, and discuss the implications of these results for sedimentary facies in the tidally-influenced fluvial zone.

The dynamics of bedform amalgamation: new insights from a very thin flume

Jim Best [(1)], Gianluca Blois [(1)], Julio Barros [(1)] and Kenneth Christensen [(1)]

1. University of Illinois, Urbana-Champaign, Illinois, USA
jimbest@illinois.edu; blois@illinois.edu; jmbarros@illinois.edu; ktc@illinois.edu

Abstract
Bedform superimposition and amalgamation are ubiquitous in many sedimentary environments and yet we possess a sparse knowledge of the fluid dynamics of such bedform interactions and both their sediment transport and morphological consequences. In this paper, we report on results concerning the morphology and flow fields of amalgamating *mobile* bedforms using a unique, narrow (5 mm wide) flume, which allows the behavior of strictly two-dimensional bedforms to be observed and quantified. Measurement of the morphology and flow fields associated with bedform amalgamation reveals the importance of interactions between the separation zones of the upstream and downstream bedforms, with flow sheltering, shear layer interactions, bedform stalling and leeside erosion being central to the amalgamation process. These fluid dynamic patterns reveal a distinct sequence of stages during bedform superimposition and amalgamation, which leave a characteristic record in the preserved sedimentary cross-strata.

1. BACKGROUND

Bedform superimposition and amalgamation are ubiquitous in all river and marine environments and lay behind the processes of bedform growth and diminution, and are also central to the preservation of the deposits of bedforms in the subsurface. Recent years have witnessed increased study of the interactions between bedforms, yet we still possess a rudimentary knowledge of the fluid dynamic interactions between bedforms under mobile bed conditions (Best, 2005). Research has shown how the dynamics of such bedform interactions may be critical across the transition from ripples to dunes (Bennett and Best, 1996; Robert and Uhlman, 2001; Schindler and Robert, 2004, 2005), Additionally, experimental work has indicated that the interactions of two bedforms may produce non-linear effects in the production of turbulence in the bedform leeside, with the interactions between the shear layers produced from adjacent leeside separation zones being critical (Fernandez et al., 2006; Palmer et al., 2011). Recent research documenting the interactions between barchan dunes (Schwämmle and Herrmann, 2003; Endo et al., 2004; Hersen and Douady, 2005; Duran et al., 2005, 2007; Hugenholtz and Barchyn, 2012) has also shown the complex behaviour of such interactions, and that these dynamics may produce a range of kinematic characteristics in dune evolution and migration (Schwämmle and Herrmann, 2003; Endo et al., 2004). Additionally, recent work documenting the cross-stratification produced by bedforms (Reesink and Bridge, 2007, 2009) has pointed to the importance of bedform superimposition and amalgamation in controlling the geometry and internal structure of bedding produced by a range of different size bedforms, from ripples to larger bar forms in rivers.

Such experimental studies are often made more complex due to the 3D nature of mobile bedforms, which makes quantification of their flow fields difficult, if not impossible, especially in the leeside region when superimposition and amalgamation are occurring and are strongly 3D processes.

2. METHODOLOGY

In order to examine the interactions between bedforms, we constructed a 5 mm wide flume (Fig. 1) that is designed to remove any three-dimensionality in the bedform planform, and thus allow interactions between 2D bedforms to be investigated and quantified. The working section of the flume is 3.0 m long, 0.25 m high and 0.005 m wide. A distribution plenum, fabricated of clear acrylic, guides fluid into the working section, whilst a return plenum collects the flow at the downstream end of the working section. An acrylic roof is fitted to the top of the flume to provide support and maintain the width of the channel throughout its length. An integral sediment trap funnels any sediment down into the return piping where it is recirculated back to the inlet section. The water and sediment circulation is driven by a magnetic drive, glass fiber reinforced polypropylene, centrifugal pump. An inline electromagnetic flow meter in the return line provides a real-time display of discharge, with values being adjustable from *c.* 3 to 48 L min^{-1}(*c.* 50-800 cm^3s^{-1}). An acrylic stop-gate is inserted at the end of the flume to provide a control on the thickness of the sediment bed and help set the flow depth. The required flow depth and velocity are thus controlled by selecting the appropriate volume of water within the flume and the pumped discharge. The entire flume is mounted on a steel framework that provides both support and allows the flume slope to be adjusted via a jack at the inlet end of the flume. Adjustment of the slope thus allows a constant flow depth to be imposed along the entire test section.

The sediment used in these experiments consisted of 212-325 μm soda lime glass beads (density 2.47 g cm^{-3}) that formed a bed *c.* 5 cm thick along the entire length of the flume. A small quantity of 150 μm mean diameter silica carbide (density 3.2 g cm^{-3}) sand was added to the mixture during the experiments to aid visualization of the cross-stratification produced by the migrating bedforms. A flow depth of *c.* 0.13 m was employed in these experiments with a discharge of 23.6 L min^{-1} yielding a mean velocity in the test section of *c.* 0.59 ms^{-1}. Measurements of the bedform profiles were taken using cameras mounted at the side of the flume. A Nikon D90 DSLR was used with a remote control timer to take images every 5 s, whilst the PIV camera (see below) was also used to provide a record of the changing bed elevation through time. These images were used to examine the geometrical characteristics of the bedforms, including their height, wavelength and shape, and migration celerity and characteristics. A grey-level thresholding scheme was found to well capture the profiles of the bedforms as they evolved through time (Fig. 2).

In addition to this morphological study, particle image velocimetry (PIV) was used to quantify the flow fields during bedform growth, superimposition and amalgamation. PIV permits study of the mutual interactions between the flow field and mobile bed in all phases of bedform development. A dual-cavity Nd:YAG laser (15 Hz and 35 mJ per pulse) was used to project a 0.5 mm thick light sheet, through a series of mirrors, into the working section of the flume. This allowed illumination of an area *c.* 200 mm × 200 mm. Neutrally-buoyant 10 μm diameter fluorescent particles (emission approx. 670 nm – LeFranc & Bourgeois Flashe Light Orange) were introduced into the flow and the light scattered by these particles was collected by a 12-bit, frame-straddle CCD camera (11 Mpixel) coupled with a 60 mm focal-length lens and high-pass filter (cutoff at 650 nm). This set-up allowed us to selectively collect the light from the tracer particles and filter out the light from the suspended sediment that was significant in the lee side of the bedforms. Sequences of images were collected at a rate of 2 Hz. Pre-processing of these images involved the development of dynamic masking procedures based upon detection of the position of the bedform. Interrogation of these images was performed using recursive cross-correlation techniques and adaptive interrogation windows to maximize the spatial resolution of the associated instantaneous velocity fields. Post-processing of the data set involved detection of the flow fields associated with specific stages of bedform evolution that allowed production of maps of downstream and vertical velocities, turbulence intensities and vorticity.

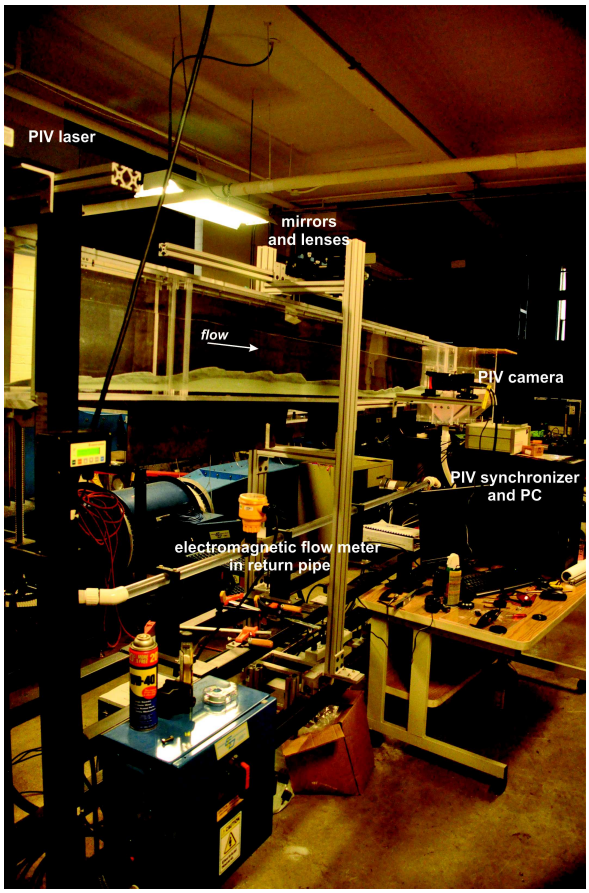

Figure 1. The 5 mm wide flume with the PIV laser and camera installed. Flow is away from the observer.

3. RESULTS

In this paper, we will detail the interactions between ripples migrating within the flume, and document the changing flow fields during superimposition and amalgamation of mobile bedforms. We will use these observations to propose a model for flow as bedforms become superimposed and amalgamate, and to detail the internal stratification such processes produce.

The superimposition of ripples in the flume involves five principal stages: 1) initial migration of a smaller, larger celerity, upstream ripple that initially has little or no fluid dynamic influence on the downstream bedform (Fig 2A); 2) As the smaller ripple migrates up the stoss side of the downstream form, the leeside flow separation zone of the upstream form begins to exert a sheltering effect on the downstream bedform (Figure 2B). This results in both less sediment being transported to the downstream bedform, as it is trapped by the upstream ripple, and also lower flow velocities over the crest of the downstream bedform. Both of these factors serve to decrease the celerity of the downstream bedform; 3) As the upstream bedform continues to migrate and catch the downstream bedform, its flow separation zone, and erosion at its reattachment region, begins to erode the crest of the downstream bedform (Fig. 2C). This produces an erosion surface over which the upstream bedform migrates, and lowers the height of the downstream bedform; 4) Bedform migration continues upon the now essentially static and stalled downstream bedform (Fig. 2D) and leads to eventual amalgamation of the two bedforms (Figure 2E). This resultant bedform now possesses a larger and renewed flow separation zone, and this amalgamated bedform then begins to migrate downstream (Fig. 2E). This amalgamation process thus produces a distinct reactivation surface between the lower and upper cross-stratification produced by these two bedforms, with this surface being the product of bedform amalgamation and not any change in mean flow conditions; 5) The process may then begin again with the stoss side migration of another smaller upstream ripple (Fig. 2F).

Results from the PIV show the changing patterns of flow around bedforms during their migration, with the high resolution data showing the details of flow near the bed as well as in the bedform leeside. A sequence of four images (Fig.3) shows flow around a migrating bedform that is in the initial stages of superimposition. Initial migration of the bedform (Figs 3A,B) shows no influence of an upstream bedform, with a region of maximum streamwise velocity over the crest, a marked region of flow separation in the leeside with recirculating flow, a strong shear layer surrounding this region and reattachment on the toe of the bedform. The presence of an advancing superimposed bedform is shown by the appearance of a lower velocity region upstream (Fig. 3C), a result of an upstream bedform wake, that begins to both decrease velocities at the crest and also decrease the size of the flow separation zone. Continued migration of this bedform, whose morphology is not seen in this sequence, begins to allow erosion of the crest of the downstream bedform (Fig. 3D) and shows an advancing lower-

velocity wake region on the stoss side of the bedform.

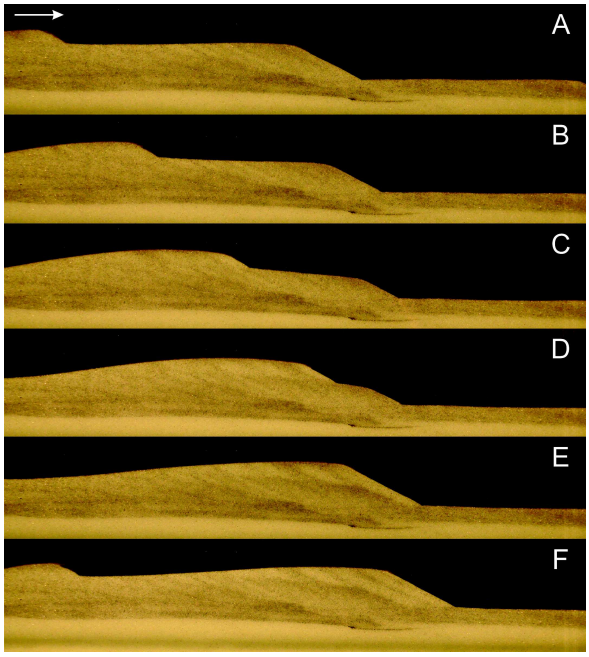

Figure 2. Images of ripples imaged through the flume sidewalls. These six images are each 20 s apart (total sequence = 100 s) and show the superimposition and eventual amalgamation of a smaller ripple with an initially larger downstream bedform. The ripple height is *c.* 1.5 cm. Flow left to right.

Plots of the flow field during another instance of bedform superimposition show a similar sequence of events, in maps of changing streamwise velocity (Fig. 4) and spanwise vorticity (Fig. 5). Initial migration of the bedform shows a larger leeside flow separation zone (Figs 4A,B) and associated spanwise vorticity along the shear layer (Figs 5A,B). The separation zone becomes smaller (Figs 4C,D,E) as an upstream bedform approaches, with the shear layer also becoming less extensive (Figs 5D,E). Impingement of the shear layer from the upstream bedform onto the stoss side of the downstream ripple (Figs 4D,E,F and 5D,E,F) results in erosion of this surface and a decrease in the bedform height.

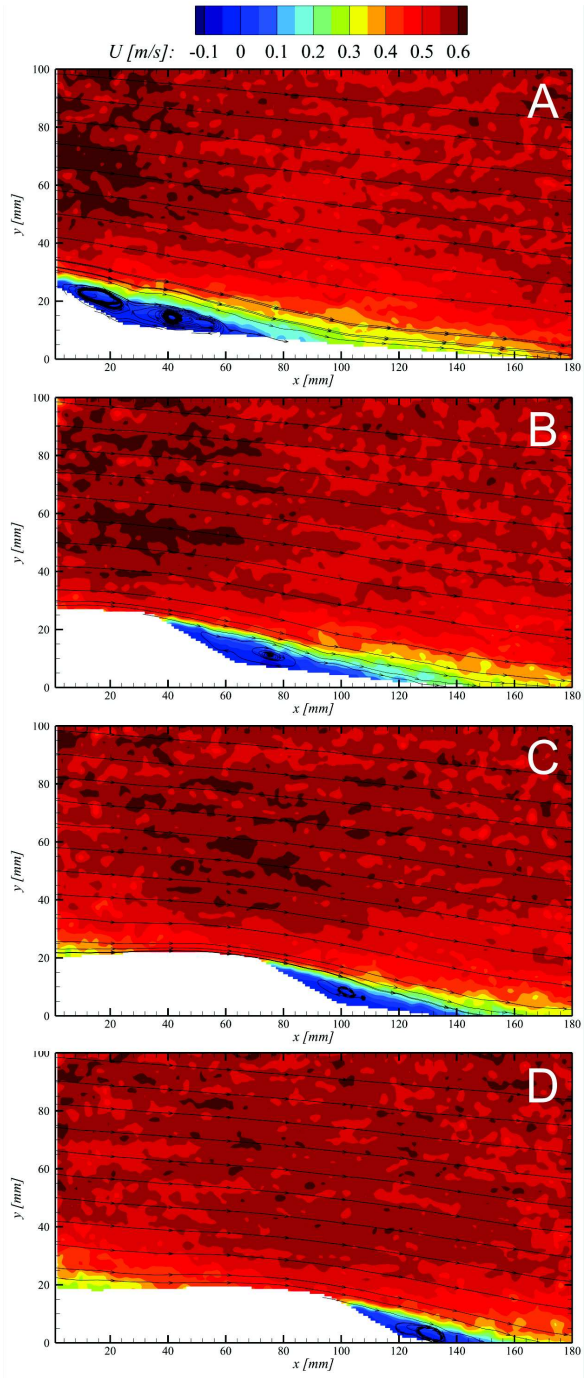

Figure 3. Instantaneous PIV flow field maps showing streamwise flow velocity (in ms^{-1}) and streamlines over a migrating bedform (A,B) that begins to show the influence of an upstream superimposed bedform (C,D). Flow fields are 15 s apart and the ripple height is *c.* 2 cm. Flow left to right.

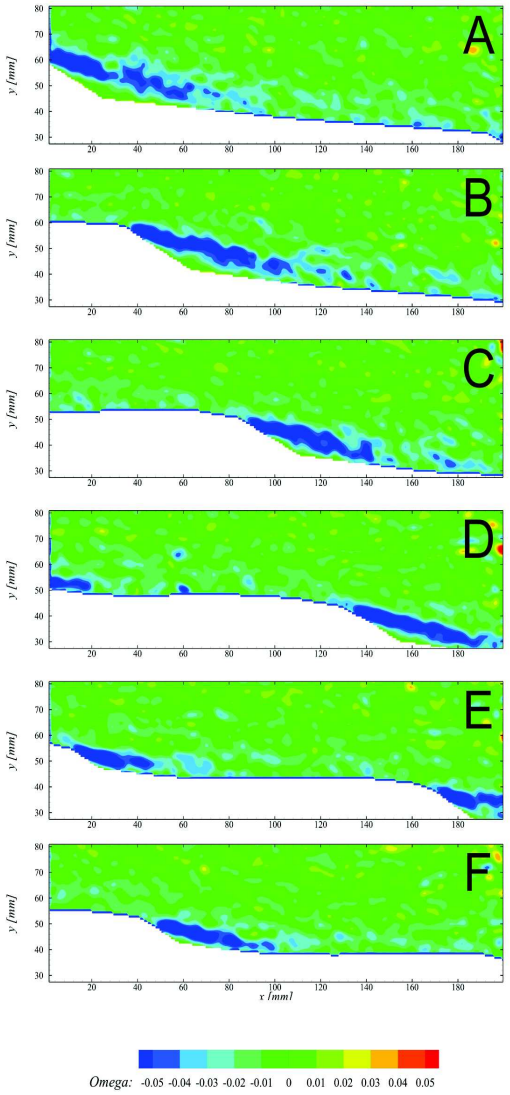

Figure 4. Instantaneous PIV flow field maps showing streamwise flow velocity (in ms^{-1}) over a migrating bedform (A,B,C) that has a superimposed bedform migrating over its stoss side (D,E,F). Note the change in the size of the separation zone associated with the downstream bedform as the upstream ripple approaches (C,D,E), and that the impingement of the shear layer from the upstream bedform upon the bed causes erosion and lowering of the stoss side of the downstream bedform (D,E,F). Flow fields are 20 s apart and the ripple height is *c.* 1.5 cm. Flow left to right.

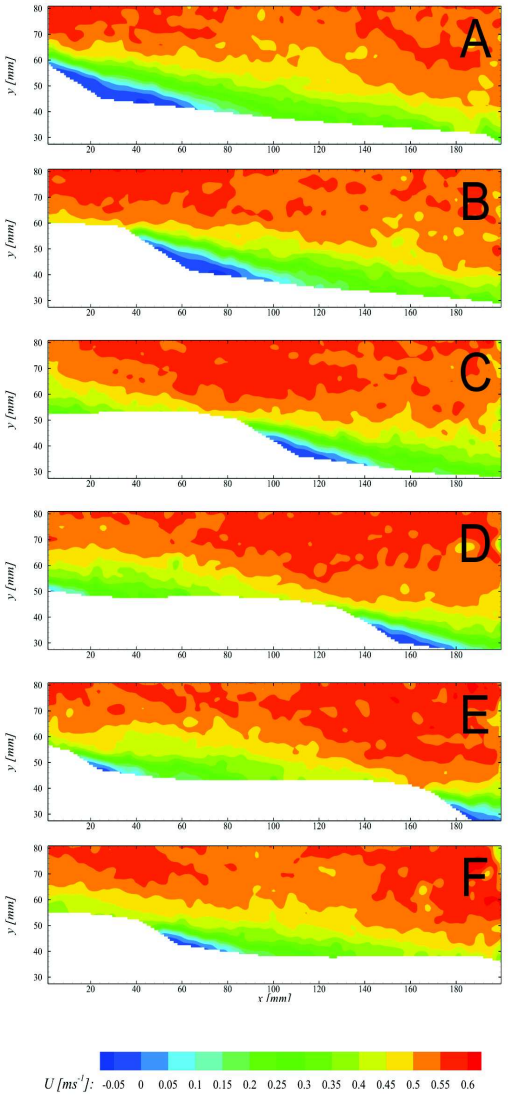

Figure 5. PIV flow field maps showing instantaneous spanwise vorticity over a migrating bedform (A,B) that has a superimposed bedform migrating over its stoss side (D,E,F) for the same realizations as shown in Figure 4. Flow fields are 20 s apart and the ripple height is *c.* 1.5 cm. Flow left to right.

4. REFERENCES

Bennett, S.J. and Best, J.L. (1996) Mean flow and turbulence structure over fixed ripples and the ripple-dune transition, in *Coherent Flow Structures in Open Channels*, edited by P. J. Ashworth et al., pp. 281– 304, John Wiley, Hoboken, N. J.

Best, J. 2005. The fluid dynamics of river dunes: A review and some future research directions. *Journal of Geophysical Research F: Earth Surface*, 110, F04S02.

Durán, O., Schwämmle, V. and Herrmann, H.J. (2005) Breeding and solitary wave behavior of dunes, *Phys. Rev. E*, 72, 021308, doi:10.1103/PhysRev E.72.021308.

Durán, O., Schwämmle, V., Lind, P.G. and Herrmann H.J. (2011) Size distribution and structure of barchan dune fields, *Nonlinear Processes Geophys.*, 18, 455–467, doi:10.5194/npg-18-455-2011.

Endo, N., Taniguchi, K. and Katsuki, A. (2004) Observation of the whole process of interaction between barchans by flume experiments, *Geophys. Res. Lett.*, 31, L12503, doi:10.1029/2004GL020168.

Fernandez, R., Best, J. and Lopez, F. (2006) Mean flow, turbulence structure and bedform superimposition across the ripple-dune transition, *Water Res. Research*, 42, W05406, doi:10.1029/2005WR 004330.

Hersen, P. and Douady, S. (2005) Collision of barchan dunes as a mechanism of size regulation, *Geophys. Res. Lett.*, 32, L21403, doi:10.1029/2005GL024179.

Hugenholtz, C.H. and Barchyn, T.E. (2012) Real barchan dune collisions and ejections, *Geophys. Res. Lett.*, 39, L02306, doi:10.1029/2011GL050299.

Palmer, J. A., Meja-Alvarez, R., Best, J.L. and Christensen, K.T. (2012) Particle-image velocimetry measurements of flow over interacting barchans dunes, *Exp. Fluids*, 52, 809-829, doi:10.1007/s00348-011-1104-4.

Reesink, A.J.H. and Bridge J.S. (2007) Influence of superimposed bedforms and flow unsteadiness on formation of cross strata in dunes and unit bars, *Sed. Geology*, 202, 281-296.

Reesink, A.J.H. and Bridge J.S. (2009) Influence of bedform superimposition and flow unsteadiness on the formation of cross strata in dunes and unit bars — Part 2, further experiments, *Sed. Geology*, 222, 274-300, 10.1016/j.sedgeo.2009.09.014.

Robert, A., and Uhlman, W. (2001) An experimental study on the ripple dune transition, *Earth Surf. Processes Landforms*, 26, 615– 629.

Schindler, R.J. and Robert, A. (2004) Suspended sediment concentration and the ripple-dune transition, *Hydrol. Processes*, 18, 3215–3227.

Schindler, R.J. and Robert, A. (2005) Flow and turbulence structure across the ripple-dune transition: An experiment under mobile bed conditions, *Sedimentology*, 52, doi:10.1111/j.1365-3091.2005.00706x.

Schwämmle, V. and Herrmann, H. J. (2003) Solitary wave behaviour of sand dunes, *Nature*, 426, 619–620, doi:10.1038/426619a.

An experimental investigation of 3D subaqueous barchan dunes and their morphodynamic processes

G. Blois [(1)], J. M. Barros [(1)], K. T. Christensen [(1)] and J. L. Best [(1)]

1. University of Illinois, Urbana-Champaign, Illinois, USA blois@illinois.edu; jmbarros@illinois.edu; ktc@illinois.edu; jimbest@illinois.edu

Abstract

In order to experimentally investigate the flow dynamics around a 3D barchan dune, herein we adopt a new experimental approach that enables us to quantify flow around complex morphologies using a refractive index matching (RIM) flume. This technique allows the model barchan to be rendered invisible, thus permitting use of standard optical techniques for flow-field quantification. Here, we present full details of this unique new RIM facility and detail its use to investigate flow around a model barchan dune. These results are compared to past experimental and numerical models of barchan dune flow dynamics.

1. BACKGROUND

River, marine and submarine flows shape the Earth's surface through complex turbulence-sediment interactions that often result in 3D bedform topographies. Flow direction variability, turbulence levels, sediment size and sediment supply are among the most important factors that determine the shape of bedforms. For example, barchan dunes, common topographic features on the Earth's surface, are generated under both aeolian and aqueous flows in regions of strong unidirectional flow and restricted sediment supply. Barchan dunes are characterized by a crescentic planform shape, with the horns of the barchan pointing downflow. Many 3D subaqueous dunes possess such a crescentic shape, but with a less pronounced three-dimensionality than that of aeolian barchans. While aeolian barchans have been extensively investigated, little has been reported on the formation and evolution of subaqueous 3D barchan-like dunes that have been observed on the sea floor and in rivers. As recently observed (Franklin and Charru, 2011), subaqueous barchan dunes are characterized by a high stability that may be due to a moderate spanwise flux. However, at present such a spanwise characterization of flow is largely missing, due to the experimental challenges involved in collecting data in such configurations.

The objective of the present experimental study is to quantify the turbulent flow generated by fixed-bed barchan dunes, and, in particular, to investigate the spanwise flow characteristics produced by such bedform three-dimensionality.

2. METHODOLOGY

In order to minimize reflection from the solid-fluid interface and gain full optical access within the flow regions in which imaging is typically obstructed (i.e. in the leeside), a refractive-index matching (RIM) approach was used. A transparent barchan dune was constructed from an idealized contour map based upon previous empirical studies of dune morphology (Palmer *et al.*, 2012). The transparent model cast from the polymer Uoptic2 was immersed within a turbulent flow of aqueous sodium iodide at 64% by weight that has the same refractive index, and thus rendered invisible.

Experiments were conducted in a specially designed RIM facility (Figure 1). This RIM facility comprises

two main components: 1) a recirculating, fully temperature-controlled, fluid channel and 2) a dedicated storage/processing vessel, designed to provide mixing, deoxygenation and safe storage of the working fluid. Both of these components were designed to handle corrosive working fluids under a broad range of pressure conditions.

The tunnel test section, entirely constructed with clear acrylic (19.10 mm thickness), is 2.50 m long with a constant cross-section of 0.1125×0.1125 m^2. The slope of the test section is adjustable from 0 to +2% and the slope can be monitored using a liquid capacitive, gravity-based inclinometer.

Flow conditioning was provided by a contraction section (area ratio = 4.375:1) and a series of perforated plates and screens. The flow quality downstream of this flow-conditioning arrangement was ascertained via 2D PIV measurements 0.6 m downstream of the test-section entrance. Finally, the contraction section cover was equipped with a cupola that assisted in trapping bubbles generated and advected by the flow.

The pump system was designed to generate high flow discharges, handle corrosive liquids (e.g. NaI, ZnI_2 solutions) and recirculate sediment up to 2 mm in diameter. The flume was equipped with two identical, close–coupled, fiberglass-reinforced centrifugal pumps that deliver a combined discharge in the range 1–0.016 m^{3}s^{-1} when utilizing an aqueous solution of NaI as the working fluid and operating at 0% slope. The volumetric flow rate through the tunnel is monitored by an electromagnetic flow meter mounted in the return line of the system piping.

To maintain a constant RI of the working fluid, the temperature of the system must be carefully maintained. The temperature control system was designed by coupling an in-line heat exchanger and an electronically-controlled modulating valve. A tube and shell heat exchanger was installed in the supply pipe. The working fluid is conveyed through a set of 36 titanium tubes (0.019 m diameter) held inside a PVC shell while the cooling fluid (at 15 ^{o}C) is circulated through the shell. The modulating valve regulates the flow rate of the cooling fluid, while a set-point controller monitors the temperature of the working fluid through input from a thermocouple probe installed in the upstream duct. If the temperature is higher than the set-point value, the modulating valve is opened by a 4-20 mA positioner and integral actuator. The temperature control process is fully automated and is able to maintain the temperature constant to within 0.1 ^{o}C, which translates to a 0.001% change in the fluid RI.

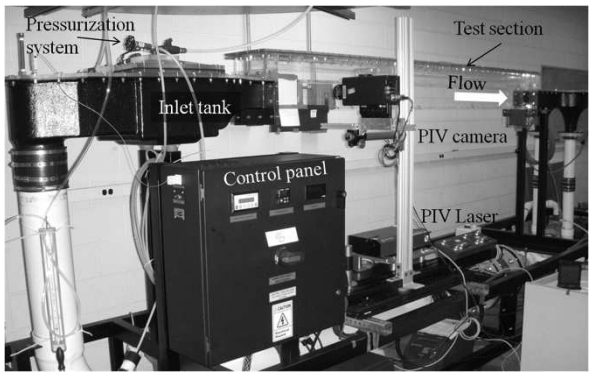

Figure 1. Photo of the model RIM flow facility showing the PIV system setup.

The entire facility was designed to be airtight, handle low values of negative pressure and operate with low values of positive pressure. The pressure is regulated through a manifold installed in the cupola (see Fig. 1). The manifold is connected to: 1) a vacuum pump for ambient air removal; 2) a nitrogen tank that is used to maintain an inert gas-saturated environment within the tunnel; and 3) a manual relief valve for pressure regulation. Additionally, the cupola is equipped with a safety pressure relief valve that ensures the system cannot be dangerously over-pressurized (pressure safety value was 5 psi). This capability allows us to generate free-surface flows by filling the test section only partially with the working fluid and introducing nitrogen gas (N_2) into the overlying space under a slight positive pressure. The use of N_2 avoids the risk of discoloration of the salt solution (that occurs by I_3^- ions formed by simultaneous exposure to oxygen and visible light) during operation of the facility. The ability to produce free-surface flow and adjust the slope allowed us to perform a wide range of Froude-number-dependent flow experiments and ensures attainment of equilibrium, equal-depth, flows within the flume for open-channel applications. We used this capability to investigate both subcritical and supercritical flow conditions, with the flow depth being controlled by an adjustable overshot weir at the downstream end of the test section.

A dedicated processing vessel allowed mixing of the solution while also preserving it from discoloration. To achieve this goal, a deoxygenation procedure was required. The processing vessel is connected to the vacuum pump through a fluid trap and to a high-pressure nitrogen tank. The pressure is monitored

through a compound pressure gauge. The tank is connected to the tunnel via a piping system and the solution is transferred using a magnetically driven pump. The RI of the working fluid was varied in two ways: 1) gross variations achieved by altering the salt concentration of the solution; and 2) fine tuning by carefully adjusting the temperature of the working fluid.

Measurements of flow around the clear complex topography models were carried out using a 2D PIV system. A 4 MP frame-straddle CCD camera (2048 · 2048 pixels) coupled with a 105 mm focal-length lens was used to image the flow, while a dual-cavity Nd:YAG laser (15 Hz and 120 mJ per pulse) provided coherent (λ = 532 nm) illumination. Optics were used to form a light sheet (in the streamwise–wall-normal plane) that was wide enough to illuminate the entire flow around the rectangular prism and to obtain a constant lightsheet thickness (~ 1.5 mm). The light was conveyed from the bottom of the channel using a system of optics mounted on a transition stage, which facilitated positioning of the light sheet at different spanwise locations. Measurements were performed with different magnifications in order to image the entire flow around the topography, as well as resolve the flow within the trough of the topography. Silver-coated hollow glass spheres (mean diameter, ϕ = 14 μm) with a density of 1.7 g cm^{-3} were added to the flow to serve as PIV tracer particles (the specific gravity of the RI-matched fluid is ~1.8).

Topographic models were constructed by casting a special clear polymer (Uoptic2) which has the same RI as the NaI solution. Negative molds based upon the digital model were built by rapid prototyping. Figure 2A shows the negative obtained using the digital model previously utilized by Palmer *et al.* (2012). The final bedform model was then cast using a proper mix of the polymer in its liquid form with a catalyst into these negatives. The resulting transparent bedform (Fig. 2B) was then introduced to the flow test section and rigidly mounted to the floor to ensure it remained static in the presence of the high *Re* flows under study.

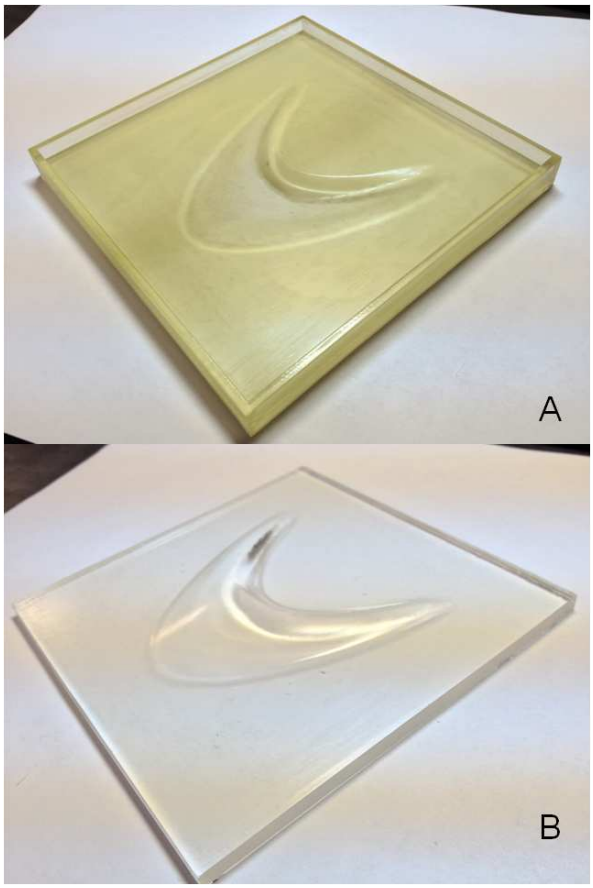

Figure 2. Photos of: A) barchan model mold; B) transparent barchan model used in experiments.

The model consisted of a 5 mm thick square tile (11.25 mm side) on top of which the topography was built. The larger dune fabricated was 0.08 m long and 0.07 m wide. The tile was mounted on the wall of the test section. The distance between the inlet section of the channel and the model leading edge was 0.61 m.

PIV measurements of the turbulent flow field were made in the streamwise–wall-normal plane along the centerline of the topography and in the streamwise-spanwise planes at three different elevations. Two different barchan configurations were investigated: i) isolated, and ii) two co-axially aligned identical dunes.

Four different volumetric flow rates were considered (Q = 3.1, 4.0, 4.9, 7.2·10^{-3} m^{3}s^{-1}) and the mean velocity of the incoming flow, U_0, was estimated as $U_o = Q/(h_w \cdot B)$ where h_w is the flow depth and B is the width of the test section. These conditions yielded *Re* ($Re = U_o h_w/\nu$, where ν is the kinematic viscosity of the working fluid) in the range 2.5 – 6.5 (10^4).

3. RESULTS

The efficacy of our RIM technique was assessed through immersion of a barchan model within the NaI solution. Figure 3A shows the effect of immersion of the transparent barchan bedform in water; the distortion of the image is due to the RI mismatch between the liquid and the solid phase. In Figure 3B, the same barchan model is immersed in the NaI solution. The image shows how an accurate index match renders the solid phase optically invisible.

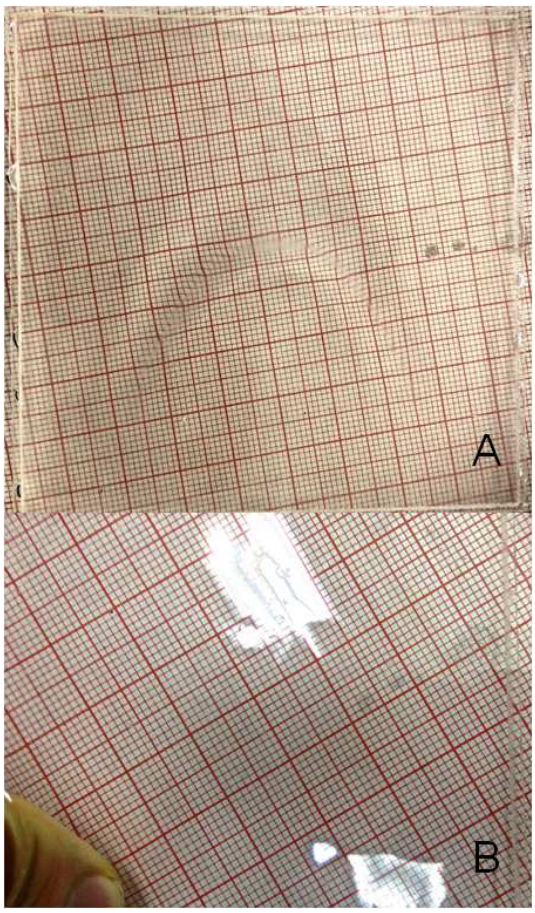

Figure 3. Photos of transparent barchan model immersed in A) water and B) aqueous solution of NaI.

This paper will present the first results of using this innovative new RIM method to examine flow around a 3D barchan dune, as well as modifications to the flow field produced by the presence of an upstream barchan dune.

4. REFERENCES

Blois, G., Christensen, K.T., Best, J.L., Elliott, G., Austin, J., Garcia, M., Bragg, M., Dutton, C. and Fouke, B. 2012 A Versatile Refractive-Index-Matched Flow Facility for Studies of Complex Flow Systems Across Scientific Disciplines, *50th American Institute of Aeronautics and Astronautics (AIAA) Aerospace Sciences Meeting, Nashville, TN, AIAA* Paper 2012-0736 (INVITED), January 2012.

Bons, J.P., Taylor, R.P., McClain, S.T. and Rivir, R.B. 2001 The many faces of turbine surface roughness, *J. Turbomach.* 123, 739.

Franklin, E.M. and Charru, F. 2011 Subaqueous barchan dunes in turbulent shear flow. Part 1. Dune motion, *Journal Fluid Mechanics*, 675, 199-222, DOI: http://dx.doi.org/10.1017/S0022112011000139.

Palmer, J.A., Mejia-Alvarez, R., Rivera, E.M., Best, J.L. and Christensen, K.T. 2012 Particle-image velocimetry measurements of flow over isolated and interacting barchan dunes, *Experiments in Fluids*, 52, 809-829.

On the influence of bed permeability on flow in the leeside of coarse-grained bedforms

G. Blois [(1)], J. L. Best [(1)], G. H. Sambrook Smith [(2)], R. J. Hardy [(3)]

1 University of Illinois, Urbana-Champaign, Illinois, USA - blois@illiois.edu; jimbest@illinois.edu
2 University of Birmingham, Birmingham, UK - g.smith.4@bham.ac.uk
3 Durham University, Durham, UK - r.j.hardy@durham.ac.uk

Abstract
This paper details the dynamics of coherent flow structures generated in shallow flows *around* impermeable and permeable 2-dimensional bedforms overlaying a highly-permeable idealised bed. Particle imaging velocimetry (PIV) measurements were conducted in order to characterise flow both over and underneath idealised 2-dimensional dunes overlaying a packed bed of uniform size spheres. Experiments were conducted in free surface flow conditions (Froude number = 0.1; Reynolds number = 25,000) for one bedform height: flow depth ratio (0.31). The flow above the dune was measured using a standard PIV technique while a novel endoscopic PIV (EPIV) system allowed collection of flow data within the pore spaces beneath the dune. These results show that the permeability of the bed has a critical impact on flow around the bedform, inducing a significant interaction between the freeflow and subsurface flow. The interaction between the free-flow and hyporheic flow is significant; in the leeside, recirculation in the separation zone is replaced by a mechanism of asymmetric alternate vortex shedding. The paper will discuss the implications of these results for the morphodynamics of coarse-sediment bedforms.

1. BACKGROUND

In many natural shallow channel flows, the deposition of sediment creates a complex bedform geometry that provides both resistance to flow and can dominate the flow structure. This is witnessed by the presence of a multitude of bedforms in nearly all river channels, and by the presence of bedforms of different size, shape and internal structure, dependent on the grain size distribution of the bed sediment and the flow characteristics. Even though in most natural channels the bed can be regarded as permeable, many previous experimental, numerical and theoretical studies have treated such surfaces as essentially impermeable. However, the deposition of cohesionless sediments generates porous layers in which the permeability may be relatively high (especially in gravel-sized sediments) and, more importantly for shallow flows, where the subsurface flow may comprise a significant portion (up to 30-40%) of the total flow discharge. Recent large-eddy simulations (LES; Stoesser and Rodi, 2007) have shown that interactions between the freestream and subsurface flow of a highly permeable bed can dramatically alter the mechanisms of momentum exchange across the interface, and that this has direct implications for the stability of grains at the bed interface. These surface-subsurface flow interactions are expected to be even greater in the presence of bed topography that will generate pressure gradients at, and within, the bed surface. However, most models of bedform dynamics assume that the bed, and bedforms, are impermeable or characterized by laminar flows within the pore space (Cardenas and Wilson, 2007), and neglect the existence of any transitional layer in the upper sediment bed. The current lack of understanding of this transitional zone may be one of the reasons why the morphodynamics of coarse-grained bedforms are rather poorly understood.

Here, we investigate the role played by bed permeability on flow around an idealised bedform, in order to gain new insight on the formation and evolution of bedforms in cohesionless sediment. This paper details the dynamics of coherent flow structures generated around a model of a 2D impermeable bedform overlaying a permeable bed of cubically-packed uniform spheres (D = 0.04 m diameter). This simplified case of an isolated bedform concentrates on the structure and dynamics of the wake produced by such topography in the presence of bed permeability.

2. METHODOLOGY

Laboratory experiments were conducted in a recirculating hydraulic flume (Figure 1) that was 4.8 m long and had a cross-sectional width, W, = 0.35 m and height, H, = 0.60 m, in order to maximize the thickness (h_{bed}) of the permeable domain and the range of water depths (h_w) that could be investigated. Additional details on the flume characteristics, including flow conditioning and instrumentation can be found in Blois et al. (2011). For the present study, both h_{bed} and h_w were kept constant (h_{bed} = 0.24 m, h_w = 0.18 m), thus yielding a flow depth: bed thickness ratio, h_w/h_{bed}, of 0.75. The sediment bed, which covered the entire length and width of the flume test section, was built using a simplified geometry comprising six layers of uniform spheres (D = 0.04 m diameter) that were rigidly fixed in a cubic arrangement. A 2D bedform with a triangular cross-section (length, L_d = 0.41 m and height h_d= 0.056 m, with a leeside angle, α_{lee}, = 27°) was used. The grain roughness and bedform submergence were $h_w/(D/2) = 9$ and $h_w/h_d \approx 3.2$ respectively, this simulating a simplified dune in such coarse-grained sediment. The total flow discharge, Q_t, = Q_{bed} + Q_{stream} (see definitions below) was measured using a magnetic flow meter in the return pipe to the pump. An ultrasonic Doppler velocimetry profiler (UDVP) was used to measure the mean velocity of the freestream flow, U_0, for a number of flow conditions. The mean flow discharge over the bed, Q_{stream}, was estimated as $Q_{stream}=U_0 \cdot h_w \cdot W$. The flow uniformity over the permeable bed was characterised (without the bedform) by collecting UDVP data for different flow conditions and at different locations. Flow uniformity was achieved at a distance approximately 2 m downstream from the inlet section. Due to constraints in the experimental set-up, the measurement location was kept unchanged while the location of the bedform was varied to maximise the number of flow regions investigated. The bedform was placed in the flume at variable distances from the inlet section in the range 2.2 – 3.6 m, and in which the oncoming flow was uniform.

U_0 was also used to compute the freestream flow Reynolds number, $Re_s = U_0 \cdot h_w/\nu$ (where ν is the kinematic viscosity = $1.004 \cdot 10^{-6}$ m$^2 \cdot$s^{-1}) and Froude number $Fr_s = U_0 \cdot (g \cdot h_w)^{-0.5}$ (where g is acceleration due to gravity = 9.81 m$\cdot$s^{-2}). For the data reported herein, these dimensionless numbers are $2.1 \cdot 10^4$ and 0.18 respectively.

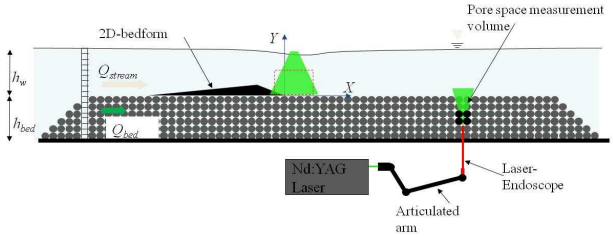

Figure 1. Schematic diagram of the experimental set-up.

The flume was instrumented with two different PIV systems: i) a standard PIV for above-bed measurements, and ii) an endoscopic PIV system (EPIV) for subsurface measurements (Fig. 1) as described in Blois et al. (2011). A photograph of the experimental set-up showing the solid dune placed on the permeable bed and both PIV systems is shown in Fig. 2. Above the bed, the flow was illuminated by a 50 mJ Nd:YAG laser (Litron Lasers) and was imaged by a 4 Mp camera (Redlake MotionPro Y5). Image capture was kept constant at 10Hz, thus obtaining time-resolved flow fields while allowing sufficient images (n = 2000, time series was tested for stationarity) to be collected to obtain robust statistics. The laser light was introduced from the top (see Fig. 1) as the water surface was relatively flat and the laser light could be provided in this configuration without any major refraction. For the subsurface flow, a two-borescope configuration was employed (Blois et al., 2011), with the seeding particles and image interrogation/ validation schemes being the same as those used for EPIV (see details in Blois et al. 2011).

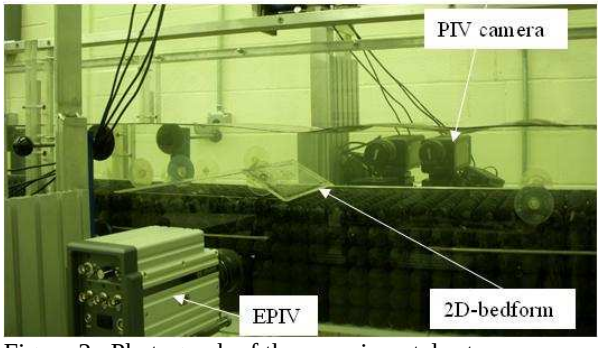

Figure 2. Photograph of the experimental set-up.

3. RESULTS

Figure 3 shows the time-averaged flow in the leeside of the impermeable bedform overlaying a highly-permeable bed. Our PIV data reveal that the wake generated in such a bed configuration is dramatically different when compared to classical cases of 2D impermeable bedforms on an impermeable bed (see review in Best, 2005). Specifically, our data show that: a) the flow separating at the crest does not reattach at the bed due to its interaction with flow in the near-bed region, which is characterized by continuous upwelling; b) this flow upwelling is so intense that it produces flow separation from the individual spheres, as suggested by the streamlines reported in Fig. 3; c) as a result of b), the flow separation zone, a major feature associated with flow transverse bedforms on beds that are impermeable, is absent and replaced by two large-scale counter-rotating vortices of comparable size; and d) the magnitude of vorticity is high both at the crest *and* at the toe of the bedform, thus highlighting the presence of two counteracting shear layers with opposite vorticity.

Figures 4 and 5 illustrate the mean flow *around* the bedform, meaning that flow both above *and* below the bedform was quantified. Pore space flow was collected using EPIV at 15 different X locations, at the same depth within the bed ($Y = -2D$). By examining Figs 4 (v component) and 5 (u component), we identified four different subsurface flow regions, herein termed A, B, C and D. This classification was based upon qualitative criteria that considered flow structure, velocity magnitude and the principal flow direction in the pore space. Region A is characterized by downward-moving flow that is generated by the high-pressure region upstream of the bedform. In region B, the flow can be mainly considered horizontal and flowing parallel to the bed surface. In region C, however, the pore flow has a strong upward-component, which is consistent with flow towards the low-pressure region above the bed associated with the bedform wake, which induces significant suction of the subsurface flow. Finally, region D has an upward-moving component but, contrary to regions A-C, the horizontal component is significantly negative. The relative extent of these regions highlights changes in the large-scale flow paths that are due to the specific bedform used. In all the pore space locations considered herein, the pore flow has high velocities and turbulence intensities ($Re_p > 300$, with $Re_p = U_p \cdot D/\nu$, where U_p is the mean pore space velocity magnitude). This onset of turbulence within the subsurface contrasts with recent numerical models that are based upon the assumption of a laminar subsurface flow (Cardenas & Wilson, 2007). In our present results, the mutual interaction between the turbulent wake and subsurface flow appears significant in the mechanisms governing these phenomena. Additional evidence to suggest that previous numerical methods may provide incorrect results can be found in the location of the low-pressure peak. Numerical models predict that the peak of low-pressure occurs very close to the crest (Cardenas & Wilson, 2007). The location of the peak in low pressure, qualitatively inferred from our velocity data by considering the direction and magnitude of the flow, is shown in Fig. 4. The data suggest that this low-pressure peak may be shifted downstream and that the distance between this peak and the bedform crest scales with the bed permeability. The existence of strong upstream-moving flow (region D) at a relatively long distance from the bedform supports this hypothesis. The effects observed at the bedform may also be influenced by grain roughness as well as bedform permeability, and thus additional experiments are needed in which these features of the bedform are isolated.

Figure 4 shows a very strong jet concentrated at the toe of the impermeable bedform and directed at 45 degrees up into the flow, while the flow upwelling progressively decreases in its magnitude downstream. These observations are supported by the patterns of subsurface flow, which show that the magnitude and distribution of upward-moving flow in the subsurface (region C) is proportional to the v component of the freestream flow at the same vertical location.

Figure 5 illustrates that the wake is characterized by a low-momentum region that is consistent with deceleration of flow in the subsurface.

The mean flow structure described above is the result of complex dynamic mechanisms taking place in the wake and involving the interaction between two shear layers of opposite vorticity. Figure 6 shows an example of the instantaneous flow fields in the wake of the bedform. Similar to

past descriptions of flow over backward-facing negative steps and bedforms, the shear layer originating at the crest generates clockwise-rotating vortices that tend to dominate the wake. However, in the case reported herein, the wake is dominated by a quasi-vertical jet that originates at the toe of the bedform (Fig. 6) and impinges against the clockwise vortices generated above near the bedform crest (see label A in Fig. 6). The jet dynamics are complex, involving pulsations and flapping dominating the motion in region A. In turn, the jet originating at the bed generates anticlockwise rotating vortices at the bedform toe (see B in Fig. 6) that subsequently interact with the vortices shed from the crest. The flow dynamics observed herein can thus be described as *asymmetrical vortex shedding*, since the vortex at the bedform toe (B) remains confined to the lee side, and only vortices generated at the crest (A) are shed downstream. Further downstream, the wake is dominated by larger-scale clockwise rotating vortices (C) that originate through the interaction between vortex A and the jet.

4. CONCLUSIONS

The present results show that the permeability of the bed has a marked impact on flow around the bedform, inducing a significant interaction between the freeflow and subsurface flow. As expected, the high pressure region generated on the stoss side of the bedform acts to force flow through the bed, whilst the low pressure region in the leeside induces an upwelling of fluid from the bed *into* the free flow. This upwelling flow in the leeside dramatically changes the dynamics of flow in the wake of the bedform. Bed permeability is thus shown to control the dynamics of coherent flow structures generated in the leeside and near-wake region of these porous, coarse-grained, bedforms.

The main findings of this paper are:

1) Flow upwelling in the bedform leeside appears in the form of pulsating jets, which are particularly intense at the toe of the bedform leeside and gradually decrease in their effect downstream.

2) Flow in the separation zone is dominated by a mechanism of asymmetric, *alternate*, vortex shedding that appears to trigger pulsing jet motions from the bed.

3) Three discrete flow regions can be identified *within* the bed: i) upstream of the bedform (region A): downward-moving flow is deflected downstream with significant horizontal flow accelerations; ii) beneath the bedform (region B): flow is predominantly horizontal and characterized by the interaction of multiple interacting jets, which results in a complex flow pattern; and iii) downstream of the bedform (regions C and D): pore space flow, although displaying a strong upward component, is predominantly directed diagonally, before converging at $x/D \sim 7$ and moving vertically upwards.

Based on these observations, it is suggested that the movement of fluid from the permeable bed *into* the freeflow may have a significant impact upon the recirculation zone in the wake of the bedform that has hitherto not been quantified, and will have considerable implications for the geometry and characteristics of bedforms generated in such coarse-grained, permeable, sediments.

5. REFERENCES

Best, J. 2005 Kinematics, topology and significance of dune-related macroturbulence: some observations from the laboratory and field. In: *Fluvial Sedimentology VII* (Eds. Blum, M.D., Marriott, S.B. & LeClair, S.), 41-60, Spec. Publ. Int. Assoc. Sediment., 35, Blackwells .

Blois, G., Sambrook Smith, G. H., Best, J. L. , Hardy, R.J. and Lead, J.R. (2011) Quantifying the dynamics of flow within a permeable bed using time-resolved endoscopic particle imaging velocimetry (EPIV). *Exp. in Fluids*, (in press) doi:10.1007/s00348-011-1198-8.

Cardenas, M.B. and Wilson J.L. (2007) Dunes, turbulent eddies, and interfacial exchange with permeable sediments. *Water Res. Research*, vol. 43, W08412, doi:10.1029/2006WR005787.

Stoesser, T. and Rodi W. (2007) Large eddy simulation of open-channel flow over spheres. *High Perform. Comput. Sci. Eng.*, vol. 4:321–330. doi:10.1007/978-3-540-36183-1_23.

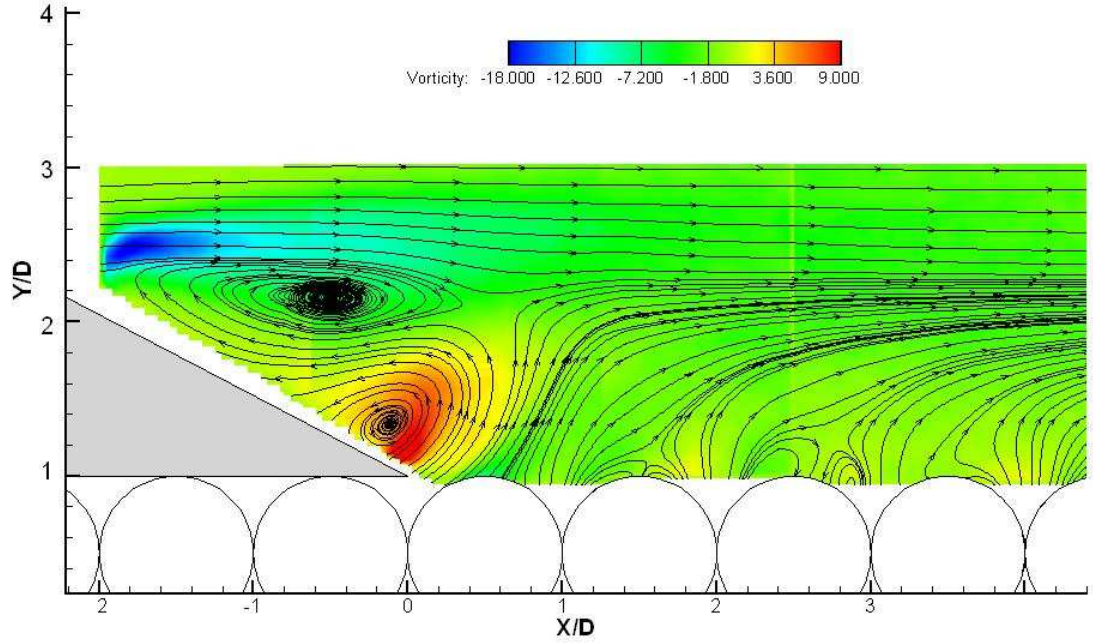

Figure 3. Mean flow in the leeside of an impermeable bedform showing the distribution of vorticity. Flow left to right. Streamlines are also shown to highlight the structure of the flow.

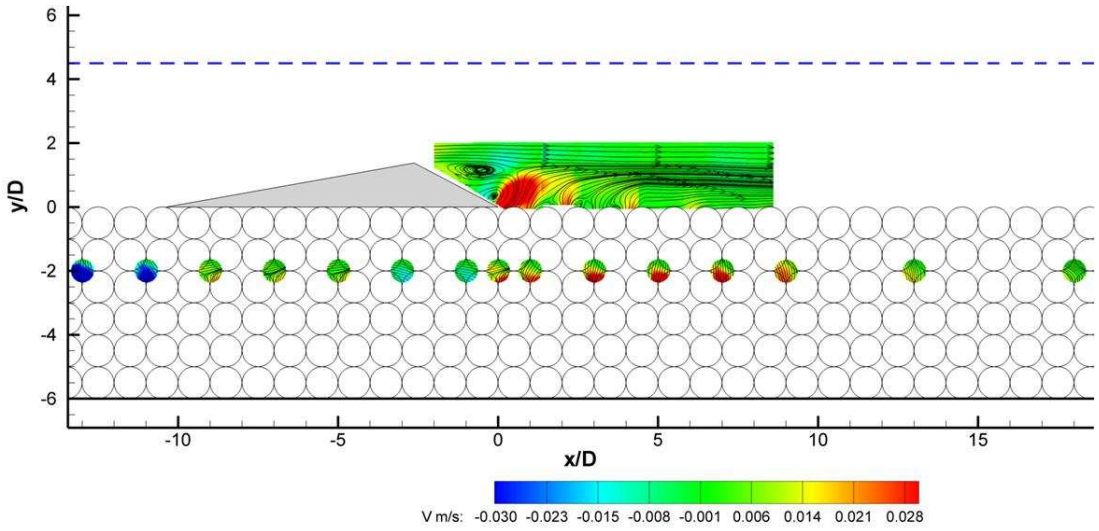

Figure 4. Distribution of *v* component around the bedform. The arrows on the figure represent the mean direction of the flow at the different pore space locations. The red dot represents the location of the low-pressure peak at the near bed.

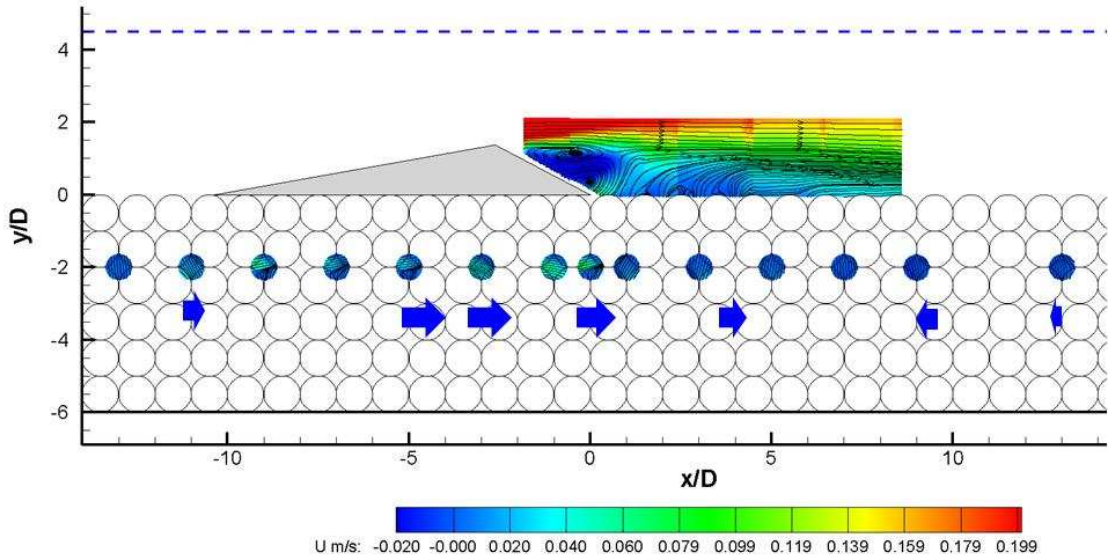

Figure 5. Distribution of *u* component around the bedform. The arrows on the figure represent the mean magnitude of *u* at the different pore space locations.

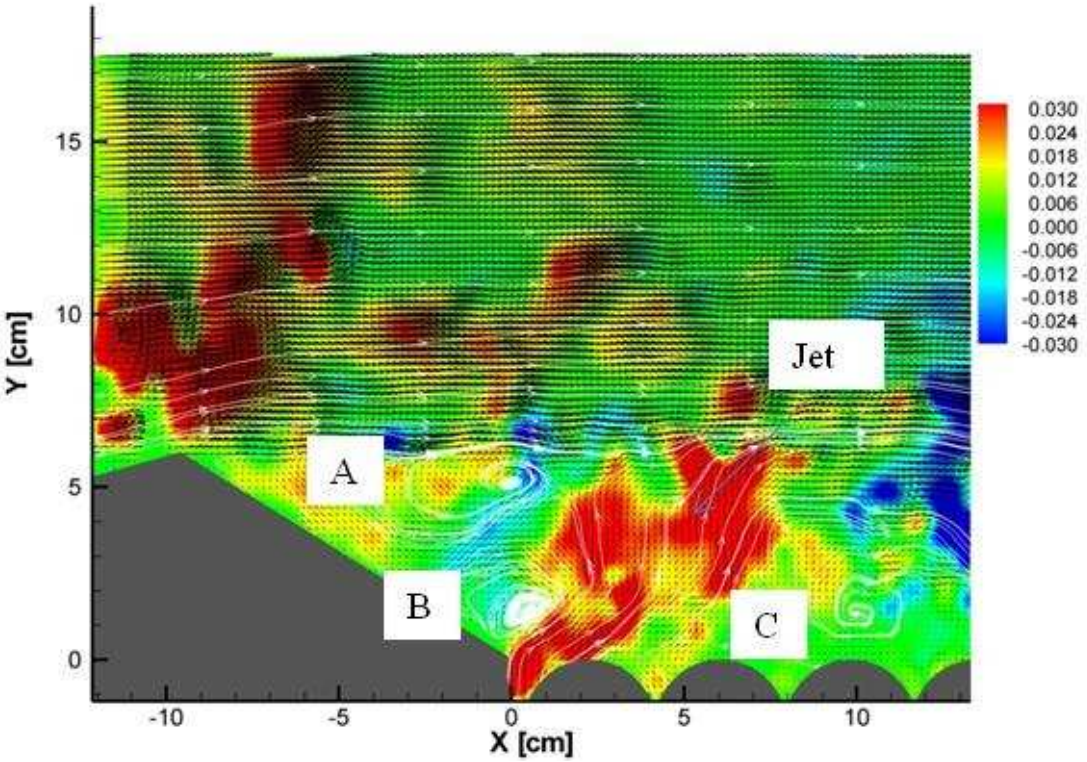

Figure 6: Example of instantaneous flow field in the bedform leeside, showing the *asymmetrical vortex shedding* mechanism. The colormap refers to the *v* component (ms^{-1}).

How the Belgian wind farm business made us discover the challenging environment of marine sand dunes

Annelies Bolle [(1)], Mieke Mathys [(1)], Piet Haerens [(1)]

1. International Marine and Dredging Consultants (IMDC nv), Coveliersstraat 15, 2600 Berchem, Antwerp, Belgium
E-mail: annelies.bolle@imdc.be.

Abstract
During the last decade, it has become clear that sand dunes are important features in the Belgian wind farm concession area. Because they influence not only the design seabed levels, but also the hydrodynamic forcings and installation methods for both cable and foundations, the study of the seabed morhodynamics is essential for all wind farm projects.
This paper starts with an overview of the geographic and morphological setting of the Belgian wind farm concession areas and presents an overview of the key features of the bedforms in the different concessions.
Next the importance and impact of the sand dunes during the design and development of these wind farms is illustrated by exploring the different types of studies and investigations which have been performed in relation to seabed & morphology, the hydrodynamic loadings, the installation methods and the environmental impact assessments.

1. INTRODUCTION

Thanks to C-Power, the pioneers of the Belgian offshore wind energy sector, IMDC has had the opportunity to start to work on and to study the Belgian Part of the North Sea (BPNS) since 2003. During the following 10 years we did not only got to know the sand dunes on the Thornton Bank, but also the bed forms in the concession areas of Norther, Rentel, Northwind, SeaStar, Belwind, and Mermaid.
For the permits of these wind farms , the design of the wind turbine foundations and the cable laying not only the effect of the moving sand dunes on the structures is investigated, but also the influence of the constructions works and these artificial features should be scrutinized.

2. THE WIND FARMS

1.1. Geographical setting

In the KB (Koninklijk Besluit) of 17 May 2004 (and adapted by the KB of 3 February 2011) a preferential zone for the development of offshore wind farms has been indicated by law. This Belgian wind farm area is situated along the Northeastern boundary of the BPNS encloses the 7 concession areas. From shore towards the sea the concession areas are: Norther, C-Power, Rentel, Northwind, SeaStar, Belwind and Mermaid (see figure 1, end of paper).
The location of the concession zones ranges between 21 km (for the Norther wind farm) and 50 km (for Mermaid) offshore. Also water depth greatly varies: 12 m on top of the Thornton Bank, till 50 m far offshore (see table 1, end of paper).
The total installed capacity offshore wind energy in Belgium end 2012 was about 380 MW spread over 91 turbines, across two wind farms (C-Power and Belwind). This represents 7.6% of the total installed (offshore) capacity in Europe (EWEA, 2013).

1.2. Morphological setting

The bottom topography of the BPNS consists of a complex of sandbanks and swales, where the channels reach maximum depths of 30 to 40 m below LAT. The sandbanks are traditionally divided into four groups: the Coastal Banks, the

Flemish Banks, the Hinder Banks and the Zeeland Ridges. The Zeeland Ridges are roughly SW-NO oriented. From north to south they consist of the Lodewijkbank, the Thornton Bank, the Gootebank and the Akkaertbank. These banks are part from a group which is also situated on Dutch territory.
A fundamental process for the existence of the sandbanks is the presence of ebb and flood channels on both sides of the bank. This causes the circular sand movement over and around the bank which maintains the stability of the bank. Normally there exists an asymmetry in current velocity on both sides of the banks. This is because the sandbanks are positioned with a small angle relative to the tide, which makes that one side of the bank is more exposed to the flood current, while the other side is more exposed to the ebb current (Dyer en Huntley, 1999). The strongest current erodes most often one side of the bank and maintains in this way the steepest flank. The Zeeland Ridges have a steep eastern flank and the maximal current velocity is directed in the flood direction (NE) (Lanckneus et al., 2001). This points towards a circular sand movement around the Zeeland Ridges anti-clockwise, in contrast to the rest of the BPNS.
The occurrence and morphology of the sandbanks as a whole has generally not drastically changed over the last 200 years, despite of the very dynamic environment. Movements are only located within the area of sandbanks themselves and especially towards their summits. Generally sandbanks witness a major stability and this at least since 1800 (Le Bot et al., 2005; Van Lancker et al. 2009).
Throughout the area, the surface is covered with Holocene sea sand. This sand has a medium grain size between 250 and 500 μm and is generally coarser on the banks than in the swales. The sand on the banks can reach a total thickness of 20 m. In the swales possibly gravel and mud can be present.

1.3. Bedforms

An important phenomenon on top of the sandbanks and in the gullies in between are the sand dunes. Sand dunes are significantly smaller than sandbanks (a couple of meters high), but are more dynamic and, as the tidal banks, prominent in the Belgian part of the North Sea (BPNS). Usually they are perpendicular to the direction of the net present flow. Like the tidal banks they incurred due to an unstable seabed area subject to tidal currents. In general the highest sand dunes occur on the northern end of the Flemish Banks (up to 8 m) and in the northern part of the Hinder Banks (up to 11 m) (Deleu, 2001).
Dunes can strongly migrate (e.g. more than 50 m in 1.5 year for the dunes on the Westhinder bank) (Deleu et al., 2004), although sometimes with an oscillating movement. Sand dunes are oriented perpendicular to the main current direction, on both sides of the bank they are often oriented towards the crest of the bank.
The dunes are usually covered with smaller dunes and (mega)ripples, which dimensions change at a short time scale (tidal cycle). The size of ripples is controlled by water depth and grain size (O'Conner, 1992). Ashley (1990) has classified the bed forms according to amplitude and wave length into ripples, small, medium, large and very large dunes (see table 2).

Table 2: Classification of bed forms according to Ashley (1990)

Bed form	**Amplitude [m]**	**Wave length [m]**
Ripples	< 0,075	< 0,6
Small dunes	0,075 - 0,4	0,6 - 5
Medium dunes	0,4 - 0,75	5-10
Large dunes	0,75 – 5	10 – 100
Very large dunes	> 5	> 100

In the Belgian wind farm area, a variation of bed forms has been observed (see table 3, end of paper). On top of the sandbanks quite often large to very large sand dunes are present with heights from 2 to 7 m and wave lengths of 150 – 500 m (Haerens et al. 2008). Superposed on these sand dunes smaller bed forms, such as ripples, can be present. Quite often, in the gullies in between the sandbanks, bed forms are less important (e.g. Norther), although for example in the Rentel area also there large dunes are present.

3. DESIGN OF WIND TURBINE FOUNDATIONS

During the design, bed forms have an influence on the selection of the foundation type, the foundation level, and the scour protection type. Three

foundation types are currently present in the BPNS: monopile, jacket and gravity based foundations (GBF) (see figure 2 and 3). To be able to make a smart choice for one of these foundation types, amongst others long term predictions of the dune mobility and possible seabed levels are required.

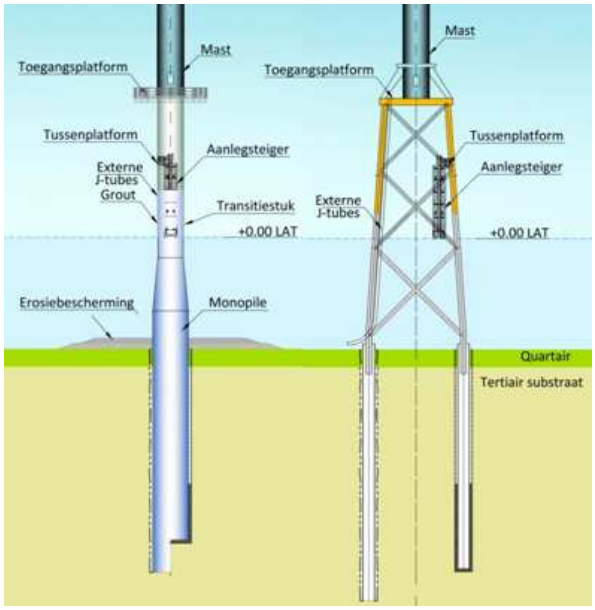

Figure 2: Monopile (left) and jacket foundation (right) (source: Technum-IMDC)

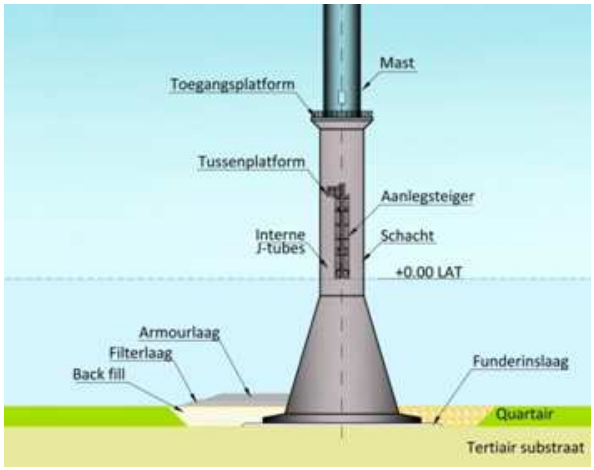

Figure 3: Gravity Based Foundation (GBF) (source: Technum-IMDC)

Depending on the foundation type, changing seabed levels around the foundation can easier be dealt with (e.g. jacket foundations) or should be prevented by the placement of an adequate scour protection (e.g. GBFs and most monopole foundations). Whereas for GBFs a constant seabed level is a firm condition for the design and construction, an interaction exists between the variation of the seabed level during the lifetime of the foundation and the design of the steel structures: varying levels might change the eigen frequencies and influence the fatigue behaviour of the structure.

Also for the scour protection different options can be considered: the so called “static” or “dynamic” scour protections. Whereas the first type cannot deal with dropping seabed levels, the second type is designed to remain functional. In the BPNS currently the static scour protection has been chosen for the GBFs (C-Power) and monopiles (Belwind). For the jackets structures of C-Power, it has been chosen to leave the seabed unprotected, and thus to allow the scour of the seabed due to the presence of the structures.

Not only for the selection of the foundation type, but also for the actual design of the foundation, sand dunes and their mobility remain important. The passing of a sand dune introduces changes in the hydrodynamic loadings on the foundation, not only in terms of water depth, but also the wave characteristics might change. Steep slopes in shallow areas introduce different types of wave breaking, each having their own influence on the loading (e.g. IMDC 2009a & 2012a).

Construction and installation methods are influenced as well by the presence of sand dunes. Gravity based foundations for example require a perfect horizontal foundation surface and thus quite some seabed preparation. For the GBFs a foundation pit has been dredged, and a horizontal gravel bed has been installed to provide a solid base for the foundations (Bolle et al., 2010 & 2012). Also for the jacket foundations some seabed preparation was necessary: the seabed had to be (locally) flattened (or dredged) in order to be able to position the installation frame for the pin piles of the jacket foundation (Bolle et al., 2012).

During the lifetime of the project cables can become exposed as a consequence of mobile sand dunes. Therefore enough coverage of the cables will be aimed for during installation. But on the other side, cable installation (e.g. by means of a plough) is hindered if dune slopes are too steep, which might result in insufficient burial and a higher risk of cable exposure later on.

But let's not forget the other way around as well, namely the influence these rigid structures might have on the dynamic, sandy surroundings. The environmental impact assessment (EIA) procedures force us to investigate, describe and predict these changing environments and the possible impacts in the best possible way for both the short and the long term (e.g. IMDC, 2012b & c). Typically the expected effects during construction of the foundations, during operation of the farm and in case of dismantling are described. Regarding morphology, a slightly bigger effect is expected during construction of the GBFs, compared to the installation of monopiles or jackets due to the more important seabed preparations (IMDC, 2012d).

4. STUDY OF DESIGN PARAMETERS AND FUTURE CHALLENGES

For all these studies numerous tools and models are applied and further developed: historic data and brand new high-resolution measurements are analysed and numerical models are put in place to predict waves, currents and the morphodynamics of the seabed.

The type and detail of the studies depend not only from the amount and quality of the data available, but also from the aim of the study. Whereas during feasibility and preliminary design studies, a more general approach will be followed (because a choice for a foundation type still has to be made, or because only limited data are available at that stage), for the detailed design one should be much more precise in order to limit the variation of all parameters to be taken into account in the design.

An overview of the current practice and some of the evolutions over the past 10 years follows below.

1.4. Seabed & morphology

A basic bathymetry will provide a first idea of the expected water depths. However, since the seabed level is an important design parameter, foundation designers do not only want to know the present seabed level, but also the level throughout the lifetime of the foundation and the variations which can occur.

Although ideally several detailed bathymetries (e.g. full coverage multibeam surveys) are needed to assess the seabed stability, quite often and almost certainly for the first orienting studies, one has to deal with less dense datasets (e.g. single beam surveys with a large spacing).

To give the designers the data they need, typically the following studies are performed. When only one dataset is available, the studies are limited to the observations which can be made: the presence of sand dunes and bed forms, the amplitudes and wave lengths and the orientation of their slopes, which give already a first indication of the seabed mobility (see table 3 for estimates for the different concession areas). In this case, literature remains a very important source to compare with earlier studies.

If more detailed datasets are available, difference maps can reveal an erosion or sedimentation trend, and the migration rate of the bed forms over the years can be determined. The combination of all this information allows to predict the minimum and maximum seabed levels which can be expected during the lifetime of the foundation due to the autonomous evolution (Haerens et al. 2008).

Of course it is still a bit more complex than this: migration rates are often roughly estimated without any link to the hydrodynamics. Last decade some successful attempts were reported to model these sand dune migration with numeric models (e.g. Hulscher & Van Den Brink, 2001; Roos & Hulscher, 2003; van den Berg & van Damme, 2004; Borsje, 2011) and to model several of this processes or impacts separately (e.g. Knaapen & Hulscher, 2002). But still a lot of the interactions between sand dunes and different foundation types are not very clear yet. How do sand dunes influence the scour holes and depths around jacket foundations without scour protection? How do sand dunes influence the scour protection around monopiles and GBFs? And what's the effect of seabed preparation or dredging, which lowers the seabed around the foundation below the surrounding levels? Studies are still ongoing and hopefully field data from existing wind farms can give us more insight in the future.

1.5. Hydrodynamic loading

The hydrodynamic forcing on a foundation is a combination of the water levels, the currents and

the waves. Not only the regular conditions, but especially the extreme conditions will influence the design. Typical values with a return period of 50 or 100 years are taken as design values.
In the Belgian part of the North Sea, the "Meetnet Vlaamse Banken" (2012) has collected over the years a valuable data set which allows us to determine these extreme values. However, when the first wind farm was designed, no site specific data were available yet, so measurements had to be performed on the Thornton Bank. A wave rider buoy has been installed and through tide measurements have been performed to capture the current distributions on top and around the sandbanks (Technum, IMDC & Elsam, 2006). Another option is to perform numerical modeling both for the currents and the waves. But also then, these new datasets are very useful, to validate the models.
If we focus a bit more on the waves, there has been an evolution in the type of models which are applied. The spectral models (e.g. SWAN) are typically used to determine the wave climate on a large scale and are already a long time part of the current practice. Extreme values can be calculated, and maximum wave heights and locations with wave breaking are typically determined according to rules of thumb.
For some locations however, for example the sandbanks and locations with sand dunes, non-linear interactions become important and spectral models cannot give an answer anymore. A combination with Boussinesq type models (e.g. MIKE21BW) can offer a solution, since all processes and non-linear interactions are included so the effects of the seabed can be better predicted. Indeed, some sandbanks and sand dunes can influence (also increase!) the local wave heights, or can introduce wave breaking (IMDC, 2009b and 2012a).
Even one step further, we can determine the loading of one single wave on a foundation with CFD models (Christensen et al., 2011). These models allow also taking into account a specific bathymetry and can provide the designer with time series of the pressure distribution on the foundation and the conditions for wave breaking (DHI, 2009a & b). This type of modeling is certainly useful for all foundations with a particular shape (e.g. GBFs).

1.6. Installation techniques

Also installation techniques depend on the water depth and the seabed morphology. Although for the installation itself, mainly information about the actual state is needed, which can be provided with a multi-beam survey, for some aspects also the bed evolution has to be considered.
The water depth is the main factor which influences the choice of the vessels. Also to place a frame on the seabed and to install the pin piles for C-Power's jacket foundations, a minimum water depth was required, which implied (limited) local dredging on top of the sandbank, in the shallowest locations.
For the cable however, both bed forms and bottom type impact the installation. Whereas the bottom type determines the installation technique (plough, jetting, ...), the seabed erosion and the migrating bed forms will influence the burial depth. This depth has to be chosen sufficiently large to prevent cable exposure during the wind farm's lifetime, but putting the cable too deep will make installation too expensive (if even possible). Also the steep slopes on some dunes might cause problems during cable installation. So typically a profound analysis of the cable trajectory is advisable before starting any works.

1.7. Environmental impact assessment

Last but not least, the seabed is one of the topics that has to be addressed in the EIAs which are performed to obtain the concession.
Although this study has to be made in a very preliminary stage of the project, and often the choice between different foundation options and lay-outs is still to be made, all possible impacts from the structures and the works have to be identified (IMDC, 2012d). For these studies typically all the available information from literature or previous projects is collected. In some cases, numerical modelling is performed though, to estimate for example the local sediment transport (IMDC, 2012b), or the sediment plumes during the dredging operations more accurately (IMDC, 2012c).
For the first wind farms, information was fairly limited, but every year more and more information becomes available from the wind farms in operation. Long term monitoring and analysis of these data will certainly improve the insight in the

system (e.g. Degraer, & Brabant, 2009; Degraer et al., 2011, 2012).

5. CONCLUSIONS

Sand dunes are important features in the Belgian wind farm concession area, as has been illustrated in this paper. Not only they are evidence for the dynamic environment of the sandbanks, they can certainly not be neglected during the design and installation of the wind turbine foundations and electrical cables.

Since 2003, studies have been performed to qualify and quantify their temporal evolution, to determine their impact on the design bottom levels for the foundations and their impact on the hydrodynamic forcing and installation methods. Over the past years not only the amount of available information has drastically increased, but also the quality of the data has been improved as a result of the important investments the wind farm industry has done into research. In the framework of this search towards better defined boundary conditions and design values, consultants have been pushed towards more performant numerical models.

Also scientists have been focusing on this research, trying to understand the physics behind all these processes and to capturing these processes in often complicated and time consuming models. Monitoring on the other hand remains essential to improve the understanding of the processes, and to validate the developed models.

One of the major challenges for the future will be to build a bridge between scientists and engineers, to be able to use this knowledge for new projects, within the often short time frames available for these studies.

6. REFERENCES

Ashley, G.M. (1990). Classification of large-scale subaqueous bedforms: a new look at an old problem. Journal of Sedimentary Petrology, 60(1): 160-172.

Bolle A., Mercelis P., Goossens W. and Haerens P. (2010). „Scour monitoring and scour protection solution for offshore gravity based foundations‟ . Proceedings of ICSE5, San Francisco, 7-10 November 2010. Geotechnical Special Publication No. 120, ASCE (ISBN 978-0-7844-1147-6)

Bolle A., De Winter J., Goossens W., Haerens P. and Dewaele G., (2012). Scour monitoring around offshore jackets and gravity based foundations, Proceedings of the ICSE6, 27-31 August 2012, Paris, France, pp. 127-134.

Borsje, B., Roos, P., Kranenburg, W. and Hulscher, S., 2011. Modeling sandwave formation in a numerical shallow water model. River, Coastal and Estuarine Morphodynamics conference, RCEM, 2011.

Christensen, E.D., Lohmann, I.P., Hansen, H.F., Haerens, P., Demuynck, A., Mercelis, P., 2011. Irregular wave loads on a gravity based foundation in shallow water. In press, Proceedings of the 30th International Conference on Ocean, Offshore and Arctic Engineering (OMAE 2011) in Rotterdam.

Degraer, S. & Brabant, R. (Eds.) (2009). Offshore wind farms in the Belgian part of the North Sea: State of the art after two years of environmental monitoring. Royal Belgian Institute for Natural Sciences, Management Unit of the North Sea Mathematical Models. Marine ecosystem management unit. 287 + annexes.

Degraer, S., Brabant, R. & Rumes, B., (Eds.) (2011). Offshore wind farms in the Belgian part of the North Sea: Selected findings from the baseline and targeted monitoring. Royal Belgian Institute of Natural Sciences, Management Unit of the North Sea Mathematical Models. Marine ecosystem management unit. 157 + annex.

Degraer, S., Brabant, R. & Rumes, B., (Eds.) (2012). Offshore wind farms in the Belgian part of the North Sea: Heading for an understanding of environmental impacts. Royal Belgian Institute of Natural Sciences, Management Unit of the North Sea Mathematical Models, Marine ecosystem management unit.

Deleu, S. (2001). Zeebodemmobiliteitsstudie van de Hinderbanken regio. Scriptie voorgelegd voor het verkrijgen van het Diploma van licentiaat in de Geologie. Universiteit Gent.

Deleu S., Van Lancker V., Van den Eynde D., Moerkerke G. (2004). Morphodynamic evolution of the kink of an offshore tidal sandbank: the Westhinder Bank (Southern North Sea). Continental Shelf Research, 24, 1587–1610.

DHI (2009a). 2D Analyses of Shoaling Wave Loads, Screening of Scenarios, Report prepared for C-Power.

DHI (2009b) Breaking Wave Loads on GBS Foundation . Report prepared for C-Power.

Dyer, K.R. and Huntley, D.A. (1999). The origin, classification and modelling of sandbanks. Continental Shelf Research, 19, 1285-1330.

European Wind Energy Association (EWEA), 2013. The European offshore wind industry - key trends and statistics 2012. Available from: http://www.ode.be/images/nieuws0103/european_offshore_statistics_2012_embargo.pdf

Haerens, P., Trouw, K, Rits, S., Martens, F., Sas, M., Smits, J., Houthuys, R., Kirkegard, J., Sanchez, M., Doorme, S., Ponnet, L. and De Vos, L. (2008). C-Power – Offshore wind turbine farm – Bank Morphology and scour protection. CEDA Dredging Days 2008.

Hulscher, S.J.M.H., Van Den Brink, G.M. (2001). Comparison between predicted and observed sand dunes and sandbanks in the North Sea. Journal of Geophysical Research 106 (C5).

IMDC (2009a). Windfarm Thornton Bank phase 2: design basis for sub area B. 2-ENG-BOD-TN-003-C.

IMDC (2009b), "Wind Farm Thornton Bank Phase2 – MIKE21 Wave analyses", Report prepared for C-Power, I/NO/14125/09.058/PEM.

IMDC (2012a). Norther offshore wind farm, Design Basis Part A - Site conditions: Part A.2 - Hydrodynamic conditions - Annex A - Wave modelling. I/RA/14159/11.187/PEM.

IMDC (2012b). Environmental Impact Report windmill farm Rentel. Numeric modelling of sediment transport. I/RA/11397/12.072/LWA.

IMDC (2012c). Environmental Impact Report windmill farm Rentel. Numeric modelling of dredging plume dispersion. I/RA/11397/12.114/VBA.

IMDC, (2012d). Milieueffectenrapport windturbinepark Rentel. Report prepared for Rentel NV, I/RA/11397/11.188/RDS

Knaapen, M.A.F., Hulscher, S.J.M.H. (2002). Regeneration of sand dunes after dredging. Coastal Engineering 46 (4), 277– 289.

Lanckneus, J., Van Lancker, V., Moerkerke, G., Van den Eynde, D., Fettweis, M., De Batist, M. & Jacobs, P. (2001) – "Investigation of the natural sandtransport on the Belgian Continental Shelf (BUDGET)", Final Report. Federal Office for Scientific, Technical and Cultural Affairs (OSTC), 104 +87 Annex.

Le Bot, S., Van Lancker, V., Deleu, S., De Batist, M., Henriet, J.P. & Haegeman, W., (2005). Geological characteristics and geotechnical properties of Eocene and Quaternary deposits on the Belgian continental shelf: synthesis in the context of offshore wind farming. Netherlands Journal of Geosciences — Geologie en Mijnbouw, 84 – 2, 147 – 160.

Meetnet Vlaamse Banken (2012). Vlaamse Hydrografische gegevens, Hydro Meteo Atlas, available from http://www.vlaamsehydrografie.be/hm_atlas_cd/www/index.htm.

O'Conner, B.A. 1992. Prediction of seabed sand dunes. In: Partridge, P.W., Editor, *Computer Modelling of Seas and Coastal Regions*. Computational Mechanics, Elsevier, Amsterdam. 312-338.

Roos, P. C., and S. J. M. H. Hulscher (2003), Large-scale seabed dynamics in offshore morphology: Modeling human intervention, Rev. Geophys., 41(2), 1010, doi:10.1029/2002RG000120.

Technum, IMDC & Elsam (2006), Wave and current measurements on the Thornton Bank. report 1/ENG/BOD/TSP/009.

van den Berg, J., and R. M. J. van Damme (2004), A simplified sand dune model, paper presented at MARID 2004, Univ. of Twente, Enschede, Netherlands.

Van Lancker, V.R.M., Du Four, I., Degraer, S., Fettweis, M., Francken, F., Van den Eynde, D., Monbaliu, J., Toorman, E., Verwaest, T., Janssens, J., Vincx, M., Houziaux, J.-S. (2009). Changes in the marine environment: the Belgian part of the North Sea revisited, in: (2009). 41st International Liège Colloquium on Ocean Dynamics: Science-Based Management of the Coastal Waters, 4-8 May 2009.

Wiertsema & Partners, 2008. "Long term stability analysis Bligh Bank"

Table 1: Basic characteristics of the 7 wind farm concession areas.

Wind farm	Distance from shore [km]	Water depth [m]	Location	Surface [km²]	Number of turbines	Total capacity [MW]
1. Norther	21	14-30	Rabs bank and Gootebank	44	47-100	420
2. C-Power	27	12-27	Thorntonbank	18	54	300
3. Rentel	31	22-28	Zuidwest-Schaar	27	47-78	289-468
4. Northwind	37	16-29	Lodewijkbank (Bank zonder naam)	14.5	72	216
5. SeaStar	41	20-25		18	41	246
6. Belwind	42	15-37	Bligh Bank	35	55	330 (2x165)
7. Mermaid	50	25-50		28	75	450

Table 3: Morphologic characteristics of the 7 wind farm concession areas.

Wind farm	Water depth [m]	Location	Height sand dunes [m]	Spacing sand dunes [m]	Classification (Ashley, 1990)	migration rate [m/year]
1. Norther	14-30	Rabs bank	3.4-5.7	200-340	Large and very large dunes	2.4-7
		Gootebank	1.5-3.9	170-320		1-7
		gully between Rabs & Thornthonbank	<0.5	10-20	Small to medium dunes	stable
2. C-Power	12-27	Thorntonbank	2-7	100-500	Large to very large dunes	1-3
3. Rentel	22-28	Zuidwest-Schaar	2-7	200-500	Large to very large dunes	
4. Northwind	16-29	Lodewijkbank (Bank zonder naam)	3.7-7.5	170-350	Large to very large dunes	2.5-3.3
5. SeaStar	20-25		2-4	?	Large dunes	?
6. Belwind	15-37	Bligh Bank	3-4 °	150- 225	Large dunes	1 -2.5
7. Mermaid	25-50		2-4	?	Large dunes	?

° Wiertsema & Partners (2008)

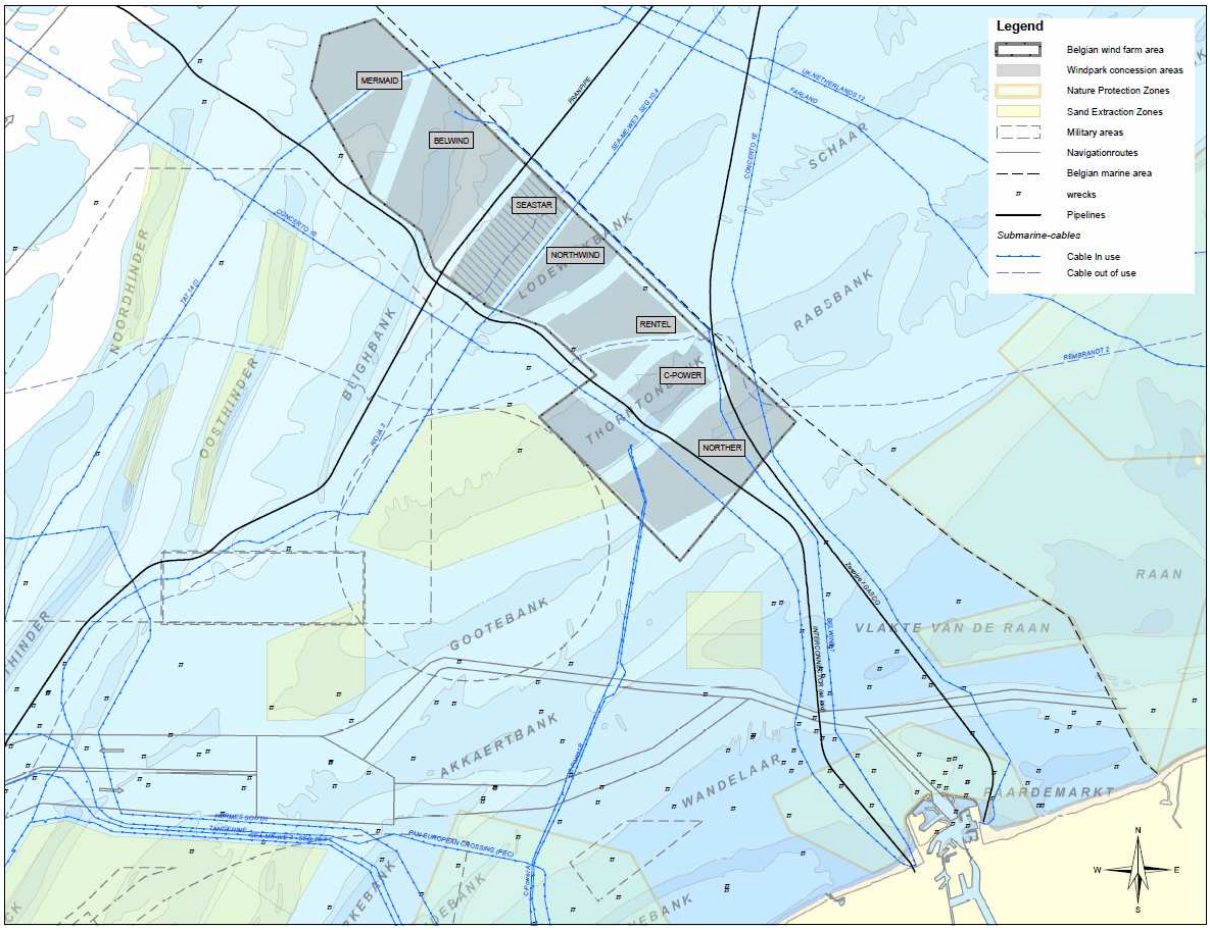

Figure 2. Concession zones in the Belgian wind farm area.

Biogeomorphological self-organization in sandy shelf seas

B.W. Borsje [1,2], S.J.M.H. Hulscher [1], P.M.J. Herman [3], S. Degraer [4]

1. University of Twente Enschede, The Netherlands. - b.w.borsje@utwente.nl
2. Deltares, Delft, The Netherlands
3. Netherlands Institute of Sea Research (NIOZ-Yerseke) The Netherlands
4. Royal Belgian Institute of Natural Sciences, Brussel, Belgium

Abstract

Benthic organisms live in the top centimeters of the seabed and change the structure of the seabed in ways not done by physical processes alone, either by reworking the sediment (e.g. bioturbators) or by providing structures (e.g. tube-building worms) and thereby create, modify and maintain habitats. Due to the interaction between the tidal current and the sandy seabed tidal sand waves are formed, which change in form continuously and thereby controlling the spatial and temporal distribution of benthic organisms. This paper investigates the mutual interactions between small-scale benthic organisms and the large-scale underwater landscape of coastal seas, by combining field observations, flume experiments and model studies.

1. INTRODUCTION

There is growing recognition of the importance of feedbacks between organisms and physical forces in landscape formation; a field labeled biogeomorphology. Biogeomorphological processes typically involve so-called ecosystem engineering species, which are organisms that modify the abiotic environment via their activity or physical structures and thereby create, modify and maintain habitats. Biogeomorphological processes are known to shape a broad range of landscapes. However, in the underwater landscape these interactions have received little attention, despite the high abundance of ecosystem engineering species in the bed of coastal seas.

This paper aims at understanding the interaction between ecosystem engineering species, hydrodynamics and sediment dynamics in the formation of the underwater landscape. In order to understand this interaction, we followed a model approach. Additionally, field observations and flume experiments are executed to obtain input parameters and validation data for the model studies.

Figure 1. The ecosystem engineering species *Lanice conchilega* occurs in dense patches and stabilizes the sediment. Patches of these tube-building worms are observed at both the intertidal and subtidal seabed. Location of photo: Zeebrugge (Belgium). Photo courtesy: Prof. Dr. Steven Degraer - Ghent University.

2. MODELING SAND WAVE FORMATION

Large parts of the sandy seabed of shallow seas, such as the North Sea, are covered with rhythmic bed patterns. These bed patterns are the result of the complex interaction among hydrodynamics, sediment transport and morphology. The most dynamic large scale bed patterns are tidal sand waves, which regenerate in several years time (e.g. after dredging), may grow up to 25% of the water depth, have wavelengths (distance between two successive crests) in the order of hundreds of meters and migrate at a speed up to tens of meters per year.

Given their dynamic behavior, sand waves may pose a hazard to offshore activities, by reducing the water depth of navigation channels, exposing pipelines and telecommunication cables and scouring offshore platforms or wind turbines. Consequently, insight in the processes controlling the variation in tidal sand wave characteristics is essential for cost-effective management practices.

Up to now, the processes controlling the dynamics of sand waves are only partly understood and the formation of sand waves has only been studied in idealized models, in which geometry, boundary conditions and turbulence models are strongly schematized. Alternatively, in this paper we present simulations of sand wave formation with a numerical shallow water model (Delft3D), in which process formulations are more sophisticated. We demonstrate that reproducing the basic sand wave formation mechanisms is possible, but requires careful treatment of vertical resolution and boundary conditions.

By using an advanced spatially and temporally variable turbulence model and modeling sediment transport both as bedload and suspended load transport, we were able to find critical conditions for sand wave formation. The simulations showed that sand waves were only formed when bedload transport was the dominant transport mode. As soon as suspended load transport became the dominant transport regime, sand waves were absent; a relation we also found in field observations.

In a pilot study, we succeeded in generating a sand wave field, starting with randomized bed perturbations in three dimensions (Figure 2). Due to the limited calculation time, the height of sand waves is limited. However, in 2D the sand waves were growing and showed realistic values after sufficient calculation time. So far, no one was able to model the physical generation of sand wave fields, which has been formulated as an open question already for 15 years (Hulscher, 1996). Thanks to the numerical sand wave model, the way is open to incorporate the heterogeneous distribution of ecosystem engineering species in space and time, thus allowing us to model the patchily distributed species for which we have empirical field data.

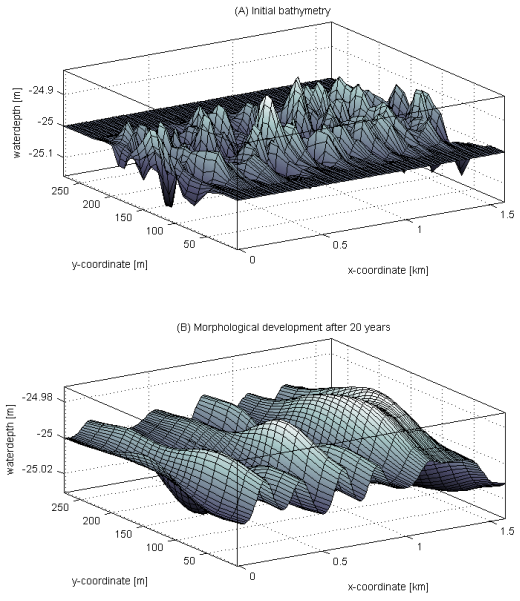

Figure 2. Self-organization in a tidal sand wave field. Starting from a bed with random perturbations (top) a regular sand wave field is generated (under) in a time span of 20 years. Flow velocity amplitude = 0.65 m s^{-1}, mean water depth = 25 m and grain size = 0.35 mm.

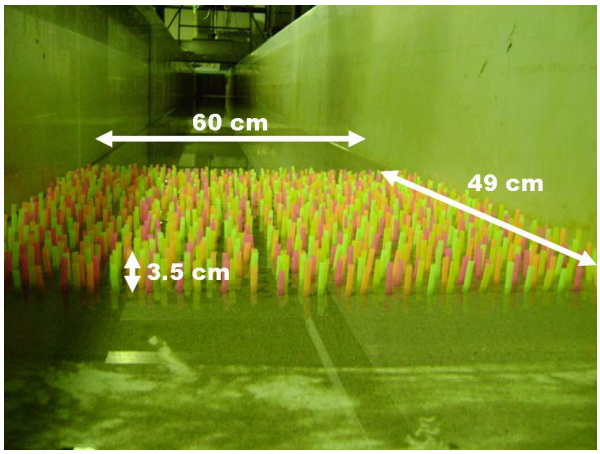

Figure 3. Lay-out of the flume experiment, in which a patch of 3.5 long straws was placed. The flume is located at NIOZ-Yerseke, The Netherlands.

3. PARAMETERIZATION OF ECOSYSTEM ENGINEERING SPECIES ACTIVITY

In order to include ecosystem engineering species in an idealized geomorphological model, we linked their activity to physical properties of the seabed. We focused on three ecosystem engineering species on the basis of (i) their abundance in sandy coastal seas, (ii) their strong modification of the environment, and (iii) their contrasting type of feeding and burrowing, and thereby contrasting influence on the sediment dynamics and hydrodynamics. The species selected are the tube-building worm *Lanice conchilega*, which reduces the near-bottom flow and consequently lowers the ripple height, the clam *Tellina fabula* which destabilizes the sediment and thereby decreases the critical bed shear stress for erosion and the sea urchin *Echinocardium cordatum* which redistributes the sediment, resulting in a coarser surface layer and a finer subsurface layer.

To model the influence of *Lanice conchilega* on the near bottom flow, we represent the tube-building worm by thin piles on the bottom of the seabed. This model is able to calculate the turbulent flow over and through vegetation (thin piles) in water of limited depth. The model explicitly accounts for the influence of cylindrical structures on drag and turbulence. The model is included in Delft3D-FLOW model. We validated this module in a flume experiment in which we measured the flow adaptation both within and outside a patch of worm mimicks with varying tube densities (Figure 4). In the test section of the flume (2 m long, 0.6 m wide) we placed 7 cm long rigid drinking straws (0.5 cm diameter) from which 3.5 cm length protruded into the water column. The patch size of the straws was 0.6 m in width and 0.49 m in length. In order to construct an even but non-regular distribution, a grid was placed with a mesh size of 3.5 x 3.5 cm on the bed of the flume. Within every mesh of the grid 4 straws with a different color were placed randomly. This resulted in an even distribution at a scale > 3.5 cm, but with random inter-individual distances at the smaller scale. By removing one color from the patch the tube density of the patch was reduced, but still evenly and non-regularly distributed over the area.

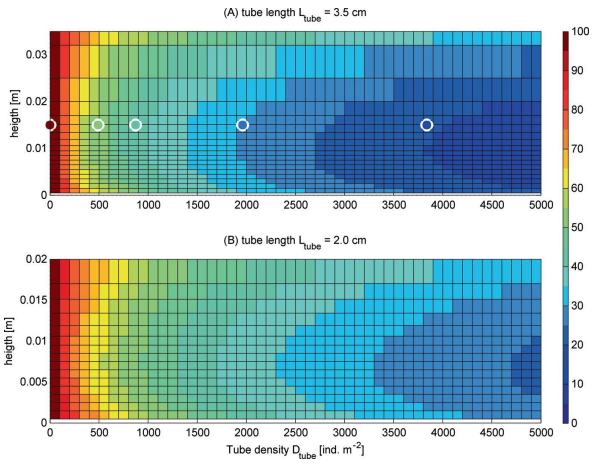

Figure 4. Relative flow velocity [%] at the end of a patch with a tube length of 3.5 cm (A) and 2.0 cm (B). Results are given at different heights [m] above the sediment bed (Y-axis) and for increasing tube densities [ind. m^{-2}] (X-axis). Filled circles are flume measurements and colored area is model outcome. In both cases, flow velocity is expressed as percentage of a reference velocity over bare sediment, using a color scale from 0% (i.e., flow = 0 m s^{-1}) to 100% (i.e., no flow deceleration) for visualization.

4. IMPACT OF ECOSYSTEM ENGINEERING SPECIES ON SAND WAVE CHARACTERISTICS

Based on field observations for the Dutch part of the North Sea, we determined the contours of high densities of the three selected ecosystem engineering species. Model simulations showed that their activity can be sufficient to change the model behavior from presence to absence of sand waves and thereby significantly improving the model prediction on sand wave occurrence. Moreover, seasonal variation in both the migration rate and wavelength of sand waves is observed in the Marsdiep tidal inlet (The Netherlands). With help of our idealized biogeomorphological sand wave model, we demonstrated that variations in both physical (flow velocity and water temperature) and biological processes (density of tube-building worms) are capable of inducing the observed seasonal variation.

Next, we modeled the impact of tube-building worm patches on a flat seabed. On the small-scale (within the patch) mounds were formed within one year. These mounds affected the hydrodynamics and sediment dynamics on the landscape scale.

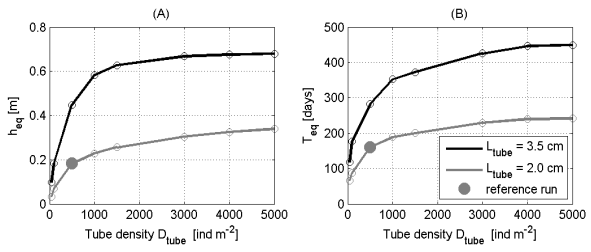

Figure 5. Equilibrium mound height h_{eq} (A) and equilibrium time T_{eq} (B) for increasing tube densities D_{tube} and for a tube length L_{tube} = 3.5 cm (black line) and L_{tube} = 2.0 cm (gray line).

Finally, we studied the self-organization in the underwater landscape in a two-way coupled biogeomorphological model. Within this model, the initial seabed consisted of small-amplitude randomized perturbations and the seasonal and patchy distribution of tube-building worms was prescribed by a simple tube-building worm growth model. In order to prescribe the spatial and temporal variation in tube-building worm density we make five assumptions: (1) there are three recruitment periods for the tube-building worms (spring, summer and autumn), following field observations during a sampling campaign along the Belgian coastline. (2) 10% of the area is covered by tube-building worms after seeding, following field observations at the Belgian coastline.(3) Once a patch is formed, all recruitment occurs within the patch, since field observations in the German Wadden Sea show that all juvenile tubes were directly attached to the tubes of the adult worms. (4) Recruitment factors are higher at locations where the suspended sediment concentrations are higher since tube-building worms are filter-feeders. (5) All tube-building worm patches disappear during winter, since tube-building worms are sensitive to low water temperatures.

At locations near the critical conditions of sand wave formation, mounds constructed by tube-building worms were able to suppress the formation of sand waves. However, at locations in the bedload regime, the landscape consisted of mounds on the flanks of tidal sand waves.

Given the similarities in model results for tube-building worms, we recommend to use both modeling approaches in a complementary way in future biogeomorphological research: idealized models for the long-term qualitative behavior and numerical shallow water models for short-term detailed predictions.

5. ACKNOWLEDGMENT

This work is part of the PhD research of the first author, which is supported by the Dutch Technology Foundation STW, applied science division of NWO and the Technology Program of the Dutch Ministry of Economic Affairs. Deltares funded part of the research and made its Delft3D software available. Finally, we acknowledge Lowie Hazen, Bert Sinke, Achmad Adhitya and Jelmer Schellingerhout for assisting in the flume experiments and analysis.

6. REFERENCES

Borsje, B.W., 2012. Biogeomorphology of coastal seas. University of Twente, PhD thesis, 168 pp.

Degraer, S., Moerkerke, G., Rabaut, M., Van Hoey, G., Du Four, I., Vincx, M., Henriet, J.P. and Van Lancker, V. 2008. Very high resolution side-scan sonar mapping of biogenic reefs of the tube-worm Lanice conchilega. Remote Sensing of Environment 112, 3323-3328.

Hulscher, S.J.M.H. 1996. Tidal-induced large-scale regular bed form patterns in a three-dimensional shallow water model. Journal of Geophysical Research C9, 101, 20727-20744.

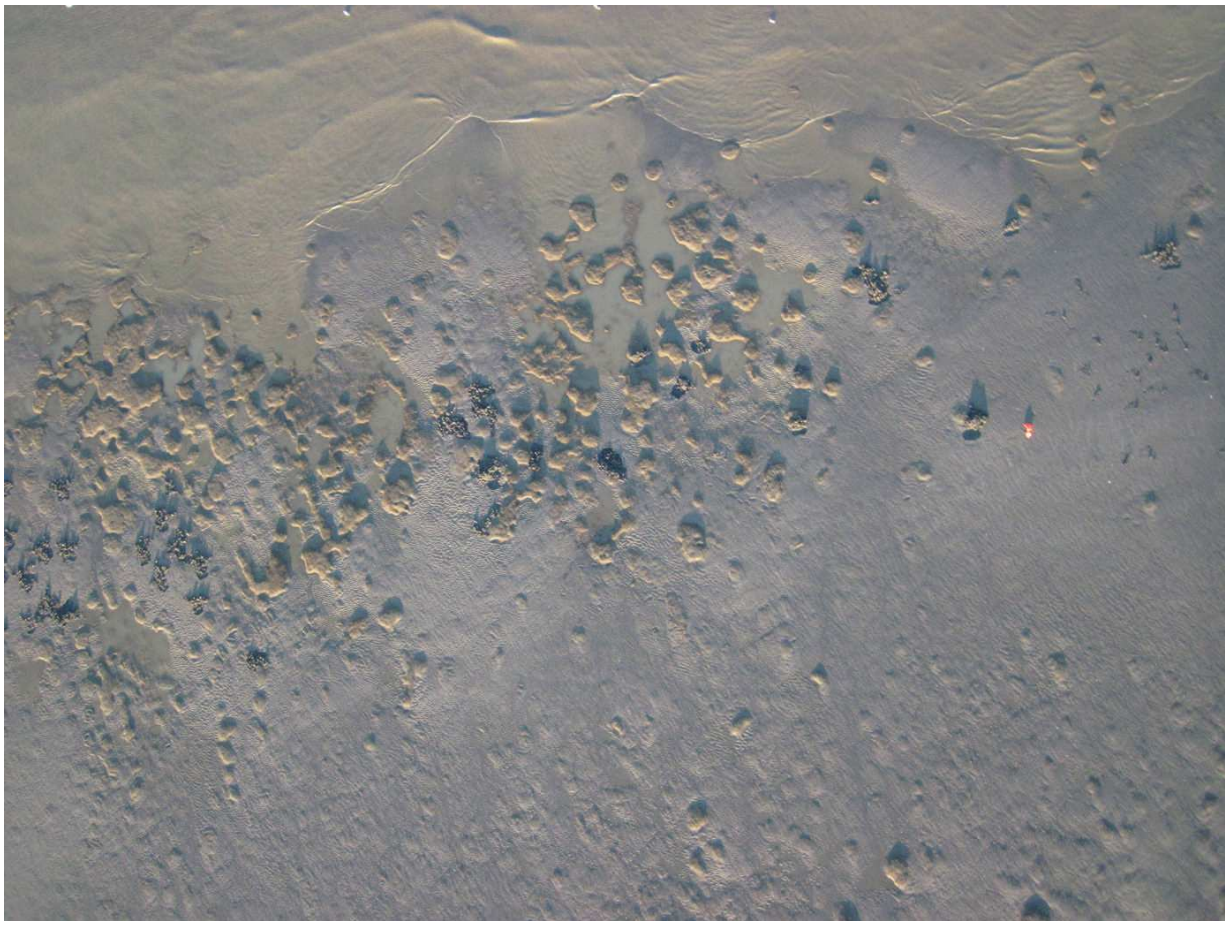

Figure 6: Kite Aerial Photography (KAP). Aerial picture of intertidal area with Lanice conchilega reefs. Total area is around 100 x 100 m. Picture taken with camera Canon D10 attached to a kite type Flow Form 4. Intertidal area of Boulogne-sur-mer during spring low tide: 14 October 2011. Picture under copyright. Picture courtesy: Dr. Klaas Pauly and Dr. Marijn Rabaut - Ghent University.

A GIS-based hydrographic resurvey strategy of the Belgian Continental Shelf

N. Bos [(1)], G. Dumon [(1)], J. Verstraeten [(1)], F. Claeys [(2)], F. Waûters [(3)], G. Eggermont [(3)]

1. Agency for Maritime and Coastal Services, Oostende, Belgium – kust@vlaanderen.be
2. Eurosense Planning and Engineering NV, Wemmel, Belgium - info@eurosense.com
3. Esri BeLux, Wemmel, Belgium - geraldine.eggermont@esribelux.com

Abstract

Using a GIS-based approach, bathymetric surveys and maritime traffic records were combined to determine resurvey priorities within the Belgian Continental Shelf (BCS). Four reference layers were produced: (1) water depth; (2) maximum absolute change in water depth; (3) ship traffic intensity; (4) maximum ship draught. The reference layers were reclassified and merged into a weighted overlay analysis. Two combinations of layers and weight factors were used and resulted in priority maps differing greatly from each other.

The reliability of the analysis depends on the way weight factors are assigned, and on the availability and accuracy of the data. These are limited for bathymetric surveys.

This empirical GIS-based methodology can be applied as a whole to a zone showing various morphodynamic patterns. It can also be automated: additional datasets can be included in the analysis, and different scenarios and assumptions can be easily tested.

1. INTRODUCTION

This study aims at defining a resurvey policy for the Belgian Continental Shelf (BCS). This policy should divide the BCS into zones classified according to their resurvey priority.

2. METHOD

2.1 Study area

The BCS has an area of about 3470 km^2. Dredging zones (56 km²) were excluded from the study because they are surveyed and dredged on a regular basis. Coastal zones (118 km²) were not considered neither: a 1.5-km wide buffer zone along the Belgian coast was defined (Figure 1).

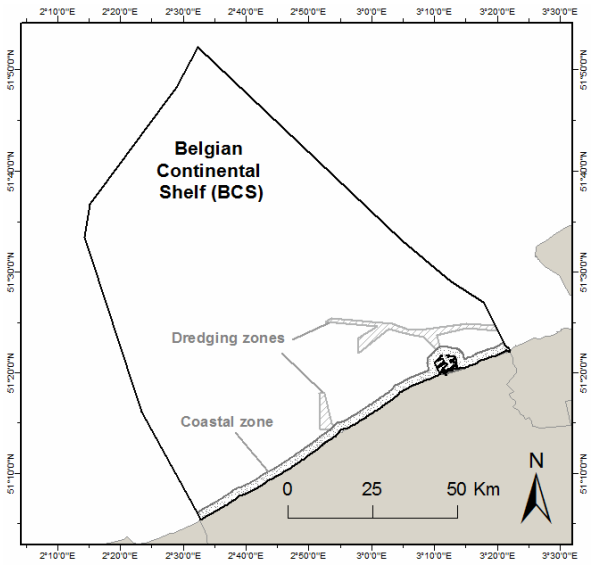

Figure 1. Study zone (Belgian Continental Shelf).

2.2 Data

2.2.1 Bathymetric data

A series of 38 bathymetric surveys conducted between 1997 and 2011 was provided by the Flemish Hydrographic Service (Vlaamse Hydrografie) for this study. Most of the surveys (32) were carried out using single beam echo sounders (SBES), with a track spacing of 100 or 200 m. The rest of the surveys were carried out using SBES with a narrower track spacing (4 surveys) or using multibeam echo sounders -

MBES (2 surveys). All surveys were provided as tabular files.

2.2.2 Maritime traffic data

Ship traffic intensity and draught are measured by Automatic Identification System (AIS) signals. AIS is an automatic tracking system used on ships for identification and location. AIS signals for the period October 2010 - September 2011 were provided by Agentschap voor Maritieme Dienstverlening en Kust, the agency for maritime services, coastal mobility and public works of the Flemish Government (Maritime Rescue and Coordination Centre or MRCC) as tabular files. This represents about 3,843,000 records within the extent of the BCS.

The source records were filtered by the MRCC so that the minimum distance between two signals from the same vessel is 1 km. But there is at least one signal per hour, which means that records for an anchored vessel are less than 1 km apart.

In order to avoid counting anchored vessels as separate vessels, an extra filtering has been applied to the data. Using a grid of 1 km-wide cells, records were filtered to keep only one signal from each ship per day and per cell. When those signals from the same ship had different draught values, the signal with the largest draught value was selected. This filtering process might delete signals from a ship doing a round trip via the exact same route in the BCS the same day.

2.3 Coordinate systems

2.3.1 Horizontal coordinate system

The horizontal coordinate system of all data and maps used in this study is WGS 1984 UTM Zone 31N.

2.3.2 Vertical coordinate system

The vertical coordinate system of data used in this study is LAT (Lowest Astronomical Tide).

2.4 Method

The methodology developed here is based mainly on the validation of the resurvey policy of the Netherlands Hydrographic Office (Van Dijk et al., 2011), which is the most advanced study on resurvey strategy available among countries of the North Sea Hydrographic Commission (NSHC).

All data processing was executed using ArcGIS Desktop 10.0, the Esri GIS software.

2.4.1 Bathymetric data

Bathymetric point datasets were converted to DEMs (Digital Elevation Models) using the IDW (Inverse Distance Weighted) interpolation method, with a cell size of 25 m, search radius of 100 m, neighbours comprised between 4 and 15. These parameters were chosen based on the assumptions made by Van Dijk et al. (2011) and on the specificities of the datasets (e.g. track spacing).

A surface of minimum water depth was produced. The maximum absolute change in water depth was also computed. This maximum depth change value allows detecting zones with seafloor dynamics. Due to the lack of available bathymetric data, annual variation rates (m/year) were not calculated. For the same reason, the vertical node approach used by Van Dijk et al (2011) could not be implemented: it requires time series of at least 3 depth values to be reliable.

2.4.2 Maritime traffic data

AIS records were filtered as described in paragraph 2.2.2. Raster grid maps with a resolution of 1 km² were produced for ship traffic intensity (ships/km².year) and maximum draught (m).

2.4.3 Weighted overlay analysis

All four grids (minimum water depth, maximum absolute depth change, traffic intensity and maximum draught) were combined in a weighted overlay analysis. Values were reclassified into five classes prior to overlay in order to avoid a very large number of resulting categories. In a weighted overlay analysis, each parameter is assigned a weight factor, so that it is possible to fine-tune its importance (see equation 1):

$$RP = a*WD + b*DC + c*TI + d*MD \quad (1)$$

where RP = resurvey priority; WD = minimum water depth category; DC = water depth change category; TI = traffic intensity category; MD = maximum draught category; a, b, c and d = weight factors. The sum of all weight factors should be equal to 1. Parameters with a major influence, or with a higher accuracy, should have a greater

weight factor than parameters with a minor influence.

2.5 Results

2.5.1 Bathymetric data

The maximum absolute variation of water depth was calculated for zones with at least two available surveys. Depending on the zone, this variation is observed over a period ranging from 1 to 11 years. Mapping these changes gives a first insight into dynamic and stable zones. Zones covered with less than two bathymetric surveys represent more than half the BCS (Figure 2). The variation of water depth in these zones could not be calculated and has been fixed to a constant value (0.194 m, i.e. mean water depth change for zones with at least two surveys available).

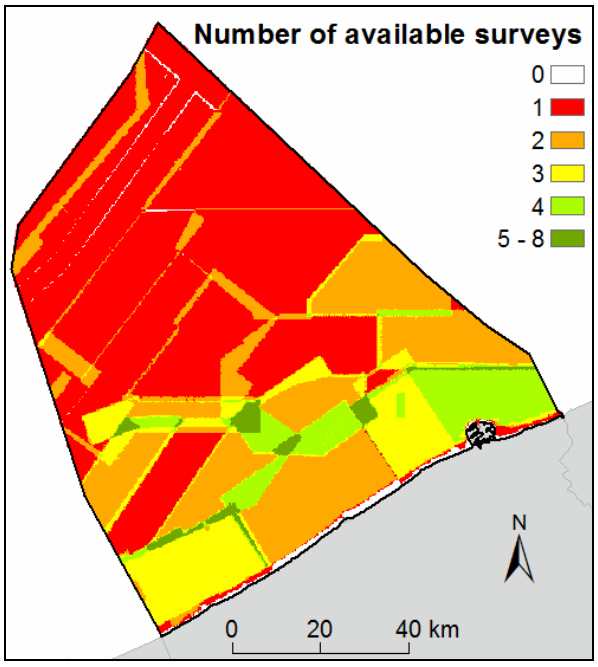

Figure 2. Availability of bathymetric surveys.

2.5.2 Maritime traffic data

AIS signal density and maximum draught were mapped after filtering of the anchored or dredging ships. Ship traffic intensity varies from 0 to 31,953 ships/km².year. Maximum draught is comprised between 1.2 and 25 m.

2.5.3 Weighted overlay analysis

Values from each dataset were reclassified into 5 categories, as detailed in Table 1.

Table 1. Initial and reclassified values and weight factors for water depth, water depth change, ship traffic intensity and maximum draught.

Layer	Initial range of values	Reclas-sified value	Weight	
			1	2
Water depth (m)	< -20	1	0.50	0.50
	-15 - -20	2		
	-8 - -15	3		
	-3 - -8	4		
	> -3	5		
Maximum water depth change (m)	< 0.1	1	0	0.20
	0.1 - 0.3	2		
	0.3 - 0.5	3		
	0.5 - 1	4		
	> 1	5		
Ship traffic intensity (ships/km².year)	< 10	1	0	0.10
	10-100	2		
	100 - 500	3		
	500 - 1000	4		
	> 1000	5		
Maximum draught (m)	< 3	1	0.50	0.20
	3 - 8	2		
	8 - 15	3		
	15 - 20	4		
	20 - 25	5		

The greater the reclassified value and weight, the greater the resurvey priority should be.

The values used to reclassify water depth and maximum draught correspond to the maximum ship draught allowed in the following ports: Nieuwpoort (up to 3 m); Oostende (up to 8 m); Zeebrugge (up to 15 m); Antwerp (up to 20 m); Rotterdam (above 20 m).

Maps of the reclassified parameter values are shown in Figure 3 through Figure 6.

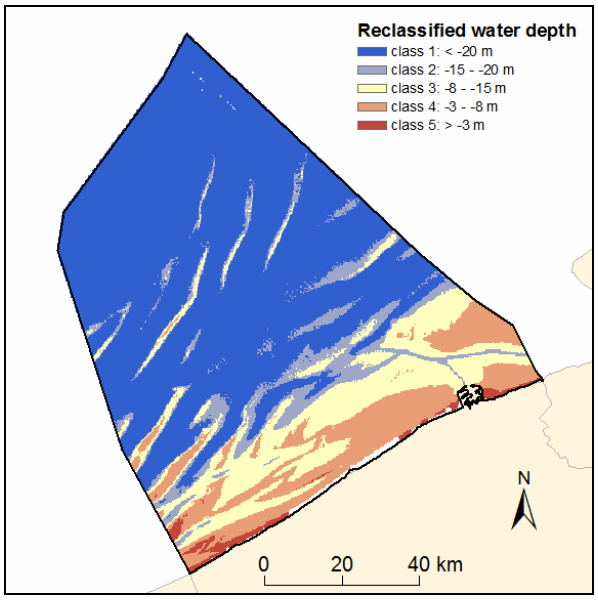

Figure 3. Reclassified water depth values.

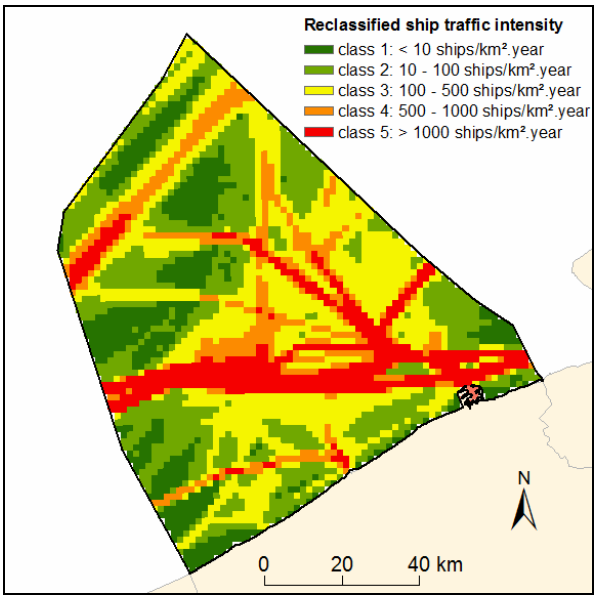

Figure 5. Reclassified ship traffic intensity values.

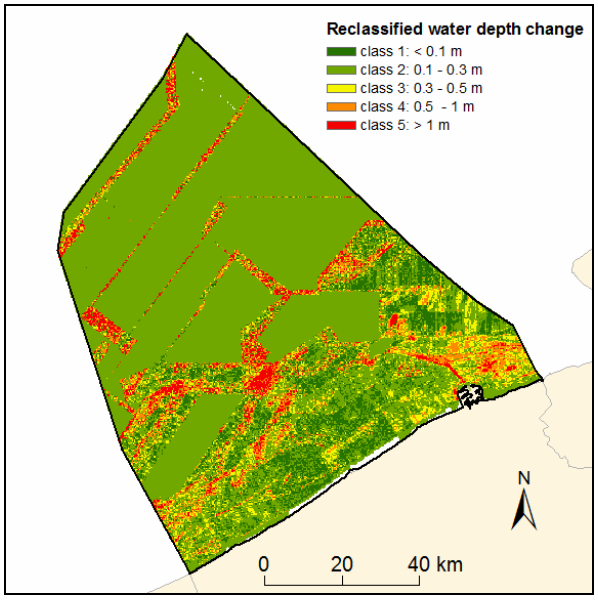

Figure 4. Reclassified water depth change values.

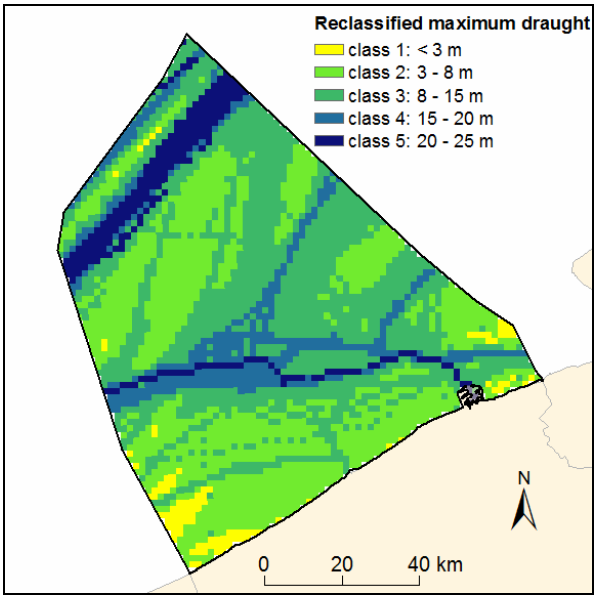

Figure 6. Reclassified maximum draught values.

The weighted overlay analysis was performed using two different combinations of parameters and weight factors: (1) only water depth and maximum draught are considered and have the same influence (50% each); (2) all four parameters are considered and have various weights (see Table 1).
The result of the weighted overlay analyses is shown in Figure 7 and Figure 8.

Priority zones were then drawn manually to fit the limits of the BCS, the dredging and coastal zones, and as much as possible, the overlay layers (Figure 9 and Figure 10). These priority maps show noticeable differences, emphasizing the importance of the choice of parameters to be included in the analysis and of the weight factors assigned to these parameters. Only four categories could be distinguished for both cases.

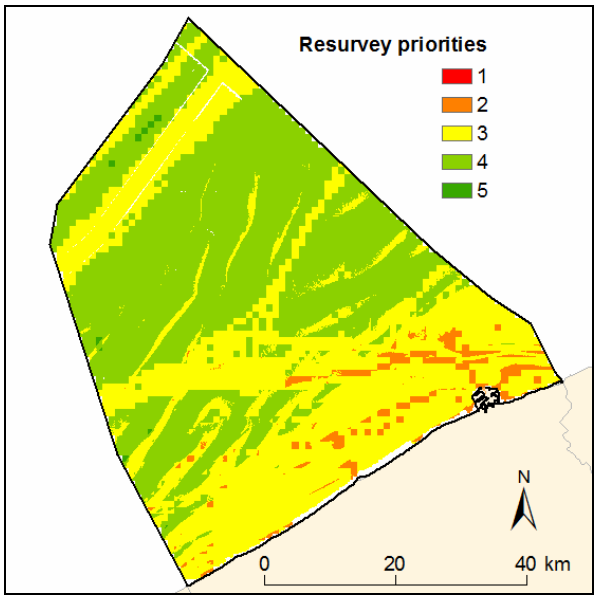

Figure 7. Result of the weighted overlay analysis based on two equally weighted parameters. Category 1 should have the highest resurvey frequency and category 5 should have the lowest frequency.

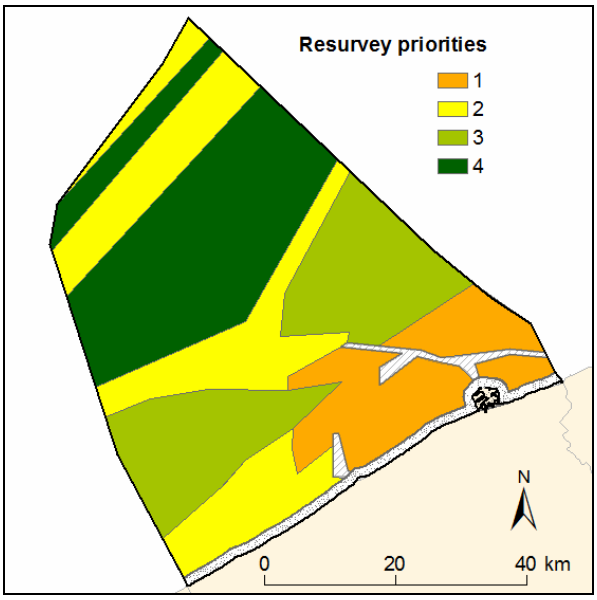

Figure 9. Proposed resurvey priorities based on the 2-parameters weighted overlay analysis. Category 1 has the highest resurvey priority and category 4 has the lowest priority.

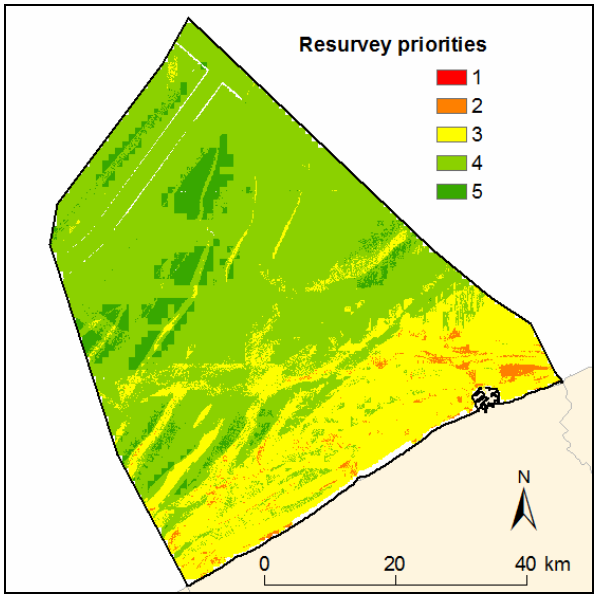

Figure 8. Result of the weighted overlay analysis based on four parameters. Category 1 should have the highest resurvey frequency and category 5 should have the lowest frequency.

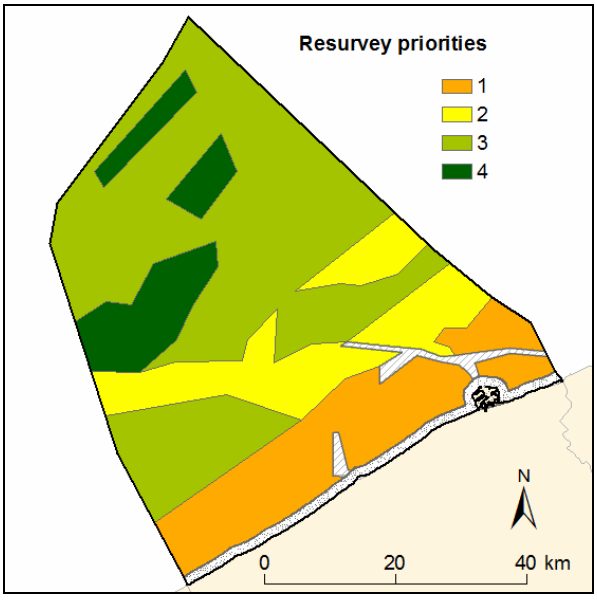

Figure 10. Proposed resurvey priorities based on the 4-parameters weighted overlay analysis. Category 1 has the highest resurvey priority and category 4 has the lowest priority.

The relative area of priority zones is given in Table 2.

Table 2. Relative area of the resurvey priority zones and other activity zones in the BCS.

Zone	Area – Case 1	Area – Case 2
	Percentage of the BCS	Percentage of the BCS
Priority 1	15	18.5
Priority 2	27	16
Priority 3	23.5	50.5
Priority 4	29.5	10
Dredging zones	1.5	1.5
Coastal area	3.5	3.5

3. CONCLUSIONS

A resurvey priority scheme was defined based on bathymetric data and maritime traffic data (AIS). The data was processed using the ArcGIS software and four reference layers were obtained (water depth, maximum absolute change in water depth, traffic intensity and maximum draught values). These reference layers were combined in a weighted overlay analysis to produce maps of the BCS split into zones indicating resurvey priority.

The weighted overlay analysis was chosen because it allows modifying the influence of each parameter on the final result. In the future, the following improvements could be brought in order to get a more reliable picture of the resurvey priorities:

- Analyse a larger number of bathymetric datasets. Less than two datasets were available for about half the BCS, making it impossible to detect bathymetric variations in these zones.
- Use MBES datasets instead of SBEs datasets. The accuracy of MB echo soundings is much greater than SB echo soundings.
- Validate the draught values of AIS signal records. These values are entered manually by the vessel staff and are prone to errors. It was not possible in this study to validate the draught values.
- Fine-tune the reclassification of values and choice of weight factors assigned to each parameter in the weighted overlay analysis, to better reflect the influence of each factor on resurvey priority. This implies a sound understanding of bathymetry, sand dynamics and maritime navigation.

4. ACKNOWLEDGMENT

The following persons have contributed to this study:

- Nadia Bos, Johan Verstraeten, Stijn Van Bossuyt and Guido Dumon from Maritieme Dienstverlening en Kust provided data and literature, and supervised the project throughout its whole course.
- Marc Roche and Koen Degrendele from the Continental Shelf Service of the FPS Economy, SMEs, self-employed have provided a lot of valuable advice, data and literature about sand dynamics and bathymetry in the BCS in general and in Flemish banks in particular.
- Gerrie Eikenhout and Lieven Dejonckheere from MRCC have provided AIS signal data and answered my many questions regarding the format and specificities of the data.
- Leendert Dorst from the Hydrographic Service of the Royal Netherlands Navy invited me to attend the minisymposium ‘Resurvey planning in the North Sea’ he organised in August 2011. This symposium provided me with a broad insight on bathymetric survey policies and practices and allowed me to meet helpful persons.
- Sandrine Le Jeune, student in Hydrography at ENSIETA and Serge Lannuzel from SHOM, provided information about the resurvey policy of France. Sandrine also sent the questionnaires she developed in the framework of her traineeship.

5. REFERENCES

Van Dijk, T.A.G.P., Van der Tak, C., De Boer, W.P., Kleuskens, M.H.P., Doornenbal, P.J., Noorlandt, R.P. and Marges, V.C. 2011. The scientific validation of the hydrographic survey policy of the Netherlands Hydrographic Office, Royal Netherlands Navy. Deltares report 1201907-000-BGS-0008, 165 pp.

Sand waves morphology and small-scale migration at a macrotidal tropical estuary (São Marcos bay, Brazil).

Felipe Murai Chagas [(1)], Leonardo Samaritano [(1)], José Carlos de Melo Bernardino [(1)], Eduardo Siegle [(2)], Moyses Gonsález Tessler [(2)] and Sandra Uemura [(1)]

1. FCTH, Fundação Centro Tecnológico de Hidráulica da Escola Politécnica da Universidade de São Paulo, Avenida Pedroso de Morais, 1619 - cj 507/508, 05419-001. São Paulo, São Paulo, Brasil. E-mail: felipe.chagas@fcth.br
2. IOUSP, Instituto Oceanográfico da Universidade de São Paulo, Dep. de Oceanografia Física, Química e Geológica. Pça do Oceanográfico, 191, Cid. Universitária. 05508-900. São Paulo, Brasil

ABSTRACT

Bottom features generated by strong currents at coastal estuarine regions are frequently referred to as sand waves. Shape, orientation, morphology and migration provide significant information about sediment dynamics and direction of bottom transport. Defining migration of dunes, Bartholomä (2008) indicates that most of the studies working with transect lines use hand-picked longitudinal profiles. Small-scale flow structure, local hydrodynamic regimes and residual sediment transport can be described by bottom morphology sequences and migration analysis (Barnard, 2012).

São Marcos Bay, northern of Brazil is characterized by strong currents (above 2.6m.s^{-1}) generated by a semidiurnal macrotidal regime, where the high levels reach up to 7m at spring equinox tides. Intense port activities contribute to the system complexity, thus socio-economic importance of understanding local sediment dynamics is of prime importance.

Sand waves migration at São Marcos Bay were studied through 6 multibeam bathymetric surveys, performed from May-2011 to Fev-2012 over the same area. Odom Hydrographyc ES3 Multibeam Bathymeter coupled to Hemisphere DGPS has been applied, at 200 kHz frequency, precision of 0.1% of local depth. Elevation data were interpolated, providing 6 digital depth models. Three hand-picked transects transversal to the crests were assumed for migration rates calculation and orientation analysis.

The sequence of high-resolution multibeam bathymetry surveys allowed us to assess the migration of sand waves at São Marcos Bay. These bedforms were found along the whole surveyed area, concentrated on Boqueirão Channel mainly due to the strong fluxes generated by the confluence of Medo and Irmãs Islands. The height and wavelength of sand waves ranged approximately from 0.5m to 5.8m and from 20m to 250m, respectively. The crests analyzed where located at depths ranging from 6.2m to 35.3m.

Unidirectional crest variation was stronger at shallower depths, where sand waves move along the longitudinal axis of the Boqueirão Channel. Wavelengths were smaller (30-150m) at deeper depths and wider at intermediate and shallower depths (100-250m).

From shallower to deeper areas the movement of sand waves was mainly bidirectional. At depths from 11m to 22m, crest horizontal position varied up to 180m between the surveys. Deeper sand waves moved less than 50 m during the surveyed period. Intense southwesterly bedload transport is observed at the northern region of Boqueirão Channel, a shallow area with strong currents, where crest

migration reached 50m.month^{-1} from Jul-2011 to Sep- 2011.

In the central part of the studied area, where intermediate depths occur, a standard transport direction has been observed. From May-2011 to Sep-2011northwesterly movement has dominated in 2 main crests, while from Sep-2011 to Nov-2011 a strong southward change of position has occurred.

Hand-picked transects analysis indicate that São Marcos Bay's main bedforms are dynamic and move along the longitudinal axis of the leading channels, influenced by the strong fluxes of currents and exhibiting intense growth and decay along small scale periods, typically under one month.

REFERENCES

Bartholomä A., Schrottke K., Winter C., 2008. Sand wave dynamics: Surfing between assumptions and facts. In: Parsons, D., T. Garlan and J. Best (eds) Marine and River Dune Dynamics, p. 17-24.

Barnard P.L., Hanes D.M., Erikson L.H.; Rubin D.M., Dartnell P., Kvitek R.G. 2012. Analyzing bedforms mapped using multibeam sonar to determine regional bedload sediment transport patterns in the San Francisco Bay coastal system. In: Li M., Sherwood C., Hill P. Special Publication Book on Self Sedimentology, 33 pp. An. de l'Inst. Océanog. 59:117-126.

.

Sand transport over a barchan dune

F. Charru [(1)], V. Laval [(1)]

1. IMFT, Toulouse, France - corresponding author: francois.charru@imft.fr

Abstract

The present work investigates an important and yet unsolved issue: the relationship between the sand flux and the fluid shear stress over a spatially varying bed of particles. It is now recognized that over such a bed, the particle flux is not in equilibrium with the shear stress: there is some lag related to the particle inertia or particle settling. A confident modelling of this relaxation phenomena and the corresponding length scales, is still lacking (Charru, Andreotti and Claudin 2013). This question is investigated here from experiments on barchan dunes in a closed-conduit water flow. From visualizations with a high-speed camera and a tracking algorithm, the particle motion over the whole dune surface is determined: particle trajectories, local velocity and surface density of the moving particles, and local particle flux. The relationship between the local particle flux and local shear stress (estimated from previous analyses) is investigated. Surprisingly, the particle flux appears to be out-of-equilibrium over the whole dune surface, with saturation length much larger than expected.

1. INTRODUCTION

When a fluid flows over an erodible bed (e. g. in a channel, river, or marine current), particles forming the bed are eroded and transported downstream. As a consequence, an intially flat bed generally does not remain flat: bedforms such as ripples and dunes are observed to grow and propagate.

Although these phenomena are known for a long time, and have been widely studied both in the natural environment and laboratory flumes, their understanding is far from complete. From the experimental point of view, wavelength measurements exhibit large scatter, over one order of magnitude (Yalin 1985). From the theoretical point of view, the modelling of the bed shear stress τ_b exerted by the fluid flow on the bed is dependent on uncertain knowledge about the turbulence over an undulated wall (Abrams and Hanratty 1985). Moreover, the sediment transport over a variable bed is not well-known, and the use of the classical laws $q_{sat}(\tau_b)$ for the particle flux, which assume q_{sat} to be in equilibrium with τ_b, is now recognized to lead to wrong predictions, i.e. ripple lengths much to small (Charru, Andreotti and Claudin 2013).

Crucial improvements for the sand transport law have been proposed during the last decade, based on the idea that as the shear stress varies, the particle flux does not adapt immediately, but after a certain relaxation time of length. The simplest transport law accounting for this relaxation is the first-order equation (Sauermann, Kroy and Herrmann 2001; Andreotti, Claudin and Douady 2002):

$$L_{sat}\,\partial_x q = q_{sat}(\tau_b) - q. \qquad (1)$$

This law states that when the actual flux q differs from the saturated -- or equilibrium -- flux $q_{sat}(\tau_b)$, it relaxes exponentially towards $q_{sat}(\tau_b)$ over the relaxation length L_{sat} (figure 1). This equation holds for quasistatic situations where time variations of the bed are slow, i.e. when the bedform velocity is much smaller that the particle velocity, which is generally the case. For situations where such a condition would not be met, the term $T_{sat}\partial_t q$ should be added to the l.h.s. of Eq. (1), where T_{sat} is a relaxation time.

Eq. (1) has been first introduced from phenomenological considerations. A different introduction of this equation was proposed by Charru and Hinch (2006) and Charru (2006), based on the modelling of the erosion and deposition rates (Figure 2). The expression of the saturation length is discussed below.

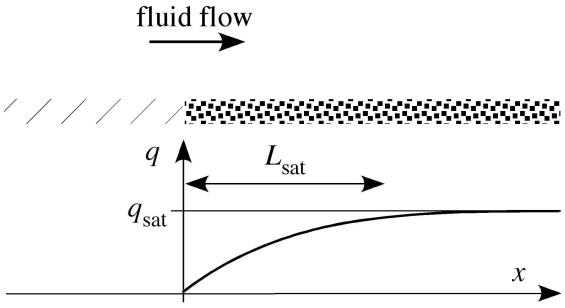

Figure 1. Fluid flow coming over an erodible bed (for $x > 0$) and corresponding particle flux increasing from zero to q_{sat} over the length L_{sat}..

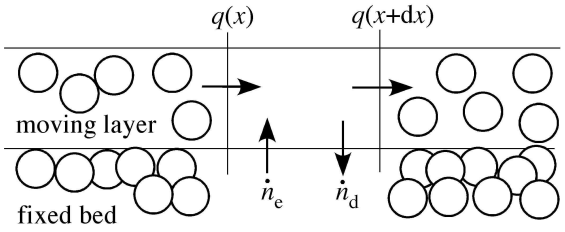

Figure 2. Sketch of the mass conservation balance between the flux divergence $\partial_x q$, and the erosion and deposition rates n_e and n_d, from which Eq. (1) may be derived.

When Eq. (1) is used in bed stability calculations (instead of the usual equilibrium law $q = q_{sat}(\tau_b)$ which corresponds to $L_{sat} = 0$), ripple length predictions are much improved (Charru 2006). Indeed, bed instability is rooted in the fact that the phase of the bed shear stress leads that of the bed deformation, due to fluid inertia. Within the equilbrium assumption, the phase of the particle flux is the same as that of the bed shear stress, so that particles are dragged from troughs to crests (figure 3a). Accounting from the stabilizing (diffusive) effect of gravity on inclined slopes, a cut-off wavenumber arises, which defines the most amplified wavelength which can be compared to ripple length measurements. Within the new non-equilibrium model (figure 3b), the particle flux lags, which corresponds to a stabilizing effect : a relaxation length L_{sat} larger than the fluid inertia length L_τ carries the maximum particle flux downstream of the crest of the disturbance, so that the bed deformation vanishes and the flat bed is stable.

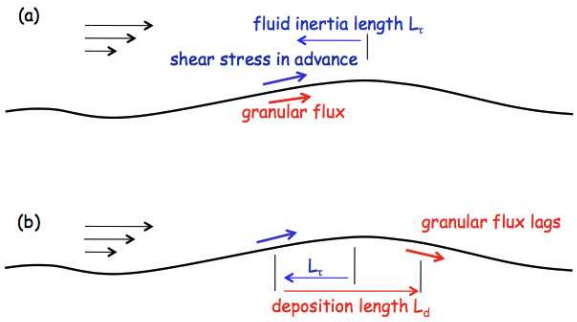

Figure 3. (a) Within the equilibrium assumption $q = q_{sat}(\tau_b)$, the shear stress and particle flux disturbances are in phase and the flat bed is unstable. (b) Accounting for relaxation effects stabilizes the bed (apart from gravity effects).

Predictions of the most amplified wavelength imply that some expression is given for L_{sat}. Two heuristic models have been proposed. When particle inertia dominates, L_{sat} scales with the acceleration length $(\rho_p/\rho)\, d$, where ρ_p and ρ are the particle and fluid density and d is the particle diameter (Andreotti, Claudin and Pouliquen 2010). When settling effects dominate, L_{sat} scales with the deposition length $(u_*/V_{fall})\, d$, where u_* is the friction velocity (which is a scale for the particle velocity) and V_{fall} is the settling velocity of the particles (Charru 2006). The first situation is more likely relevant for aeolian transport (where the ratio ρ_p/ρ is large), whereas the second is expected to hold for aqueous transport where ρ_p/ρ is about two. Thorough measurements in water and oil, of the erosion and deposition processes at the particle scale, have allowed some determination of L_{sat}, for both laminar flow (Charru, Mouilleron and Eiff 2004) and turbulent flow (Lajeunesse, Malverti and Charru 2010). However, direct measurements of L_{sat} in non equilibrium conditions have never been performed. The aim of this paper is to present such measurements.

2. BARCHAN DUNES

A nice situation of non-equilibrium particle flux is provided by barchan dunes. Such dunes form when sand is transported by a fluid flow (gas or liquid) over a non-erodible bed. These dunes exhibit a remarkable crescentic shape with horns pointing downstream (figure 4). They are commonly observed in deserts, with height of a few meters and velocity of a few tens of meters per year. In his famous book, Bagnold (1941) first pointed out their significance for understanding the physics of blown sand. Their outstanding shape and stability properties have triggered a number of studies, aiming at understanding the conditions for their formation, their migration velocity and time evolution, and also the striking existence of a minimum length, of about ten meters in air, below which no dune is observed. A model accounting for their main properties was derived by Kroy, Sauermann and Hermann (2002) and Andreotti, Claudin and Douady (2002), from calculations of the shear stress at the dune surface by Hunt, Leibovich and Richards (1988) and Eq. (1) for the sand flux accounting for the retarding effect of grain inertia (Sauermann, Kroy and Hermann 2001).

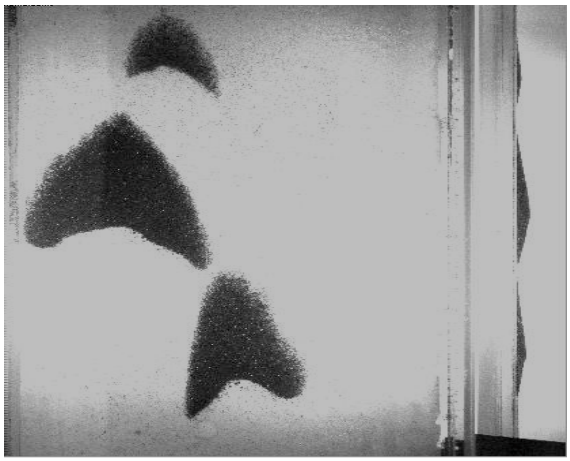

Figure 4. Three barchan dunes under a water flow, seen from above. Top of the photo: side view from an inclined mirror. The width of the largest dune is 4 cm (photograph from V. Laval, IMFT).

Similar barchan dunes have also been observed under water flows when, again, the sediment supply is limited. The size of these aquaeous dunes is however much shorter than in air, of a few centimeters, say. Such dunes formed in an open channel flow are reported by Mantz (1978), with typical width of about three centimeters; in this paper the resemblance with the aeolian dunes observed by Bagnold was noted. This resemblance was investigated further by Hersen (2005) from experiments in which the dunes were formed on a tray oscillating asymmetrically in a water tank. Barchan dunes also form in circular pipes where they may cause damages to industrial installations (Al-lababidi *et al.* 2008). An extensive study of barchan dunes in water has been performed by Franklin and Charru (2011), discussing their geometry, velocity, and long time evolution. The existence of a smallest dune size of about one centimeter was evidenced, supporting the idea that the relaxation length scsale on the deposition length $(u_*/V_{fall})d$ rather than the acceleration length $(\rho_p/\rho)d$. Again, no direct measurement of L_{sat} was provided.

3. EXPERIMENTAL RESULTS

1.1. Experimental arrangement

The experimental arrangement mainly consists of a horizontal plexiglass channel, six meters long, with rectangular cross-section of height $2\delta = 60$ mm and width $b = 120$. Water flows from a head-tank with free surface 2.5 meters above the channel, and enters the channel through a divergent-convergent device with a honeycomb section in order to suppress large eddies and homogeneize the small-scale turbulence. At the open end of the channel, particles are separated by sedimentation in a large tank, and a pump drives the water up to the head-tank. The volumetric flow rate is measured with an electromagnetic flow-meter. For more details see Franklin and Charru (2011).

The particles (glass beads, with diameter $d = 1.1$, 0.2 or 0.5 mm) were deposited in the channel, previously filled with water, with the help of a syringe through a small hole in the upper wall located at 4.15 m form the entrance. The sand settles in the water at rest and forms a conical heap. Then the flow is started up, and the heap deforms. A slip face develops on the lee-side where particles avalanche, and horns grow on both sides. The equilibrium shape of the dune is quickly

reached, as it has travelled over a distance of the order of its own size. Varying the shape of the initial heap does not change the final dune shape. When the heap is large, it may split and form several interacting barchan dunes, as shown in Figure 4.

The evolution of the shape of the dune was recorded with a video camera placed above the channel and mounted on a travelling system. The resolution of the camera was 2048x2048 pixels, with field of view at the bottom wall of about 140x140 mm^2. The side view of the dune was recorded on the same images thanks to a mirror inclined at 45°.

1.2. Particle motion

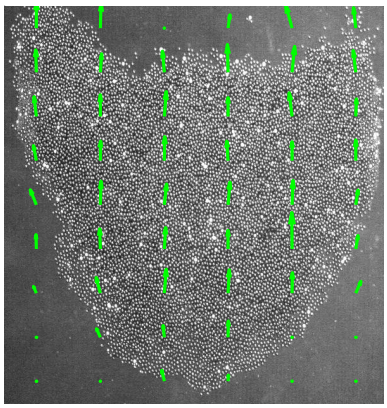

Figure 5. A barchan dune seen from above, and the particle velocity field averaged over a rectangular mesh (green arrows).

The motion of a few dyed particles (5%) was recorded, allowing the determination of the surface density of the moving particles (number of moving particles per unit horizontal area) and their velocity. Figure 5 displays a typical particle velocity field over a moving barchan dune, where the measured velocity of individual particles has been averaged over a rectangular area with size of 1/10 and 1/6 of the length and width of the dune, respectively. The velocity increases from the upstream foot of the dune towards the crest, and is larger in the central part of the dune than at the horns, as expected.

From the velocity $u(x, y)$ and moving particle density $n(x, y)$, the field of the particle flux, $q(x, y) = n(x, y)\, u(x, y)$, can be obtained. An example of the resulting profiles is shown in figure 6, along three slices : (i) the central part of the dune, (ii) the side parts, and (iii) the horns. It can be seen that, firstly, the flux increases from the dune foot towards the crest (located at x = 40 mm), as expected. Secondly, the flux is the largest in the central part, and minimum over the horns. Thirdly, the flux increases everywhere, with no indication of saturation in the vicinity of the crest.

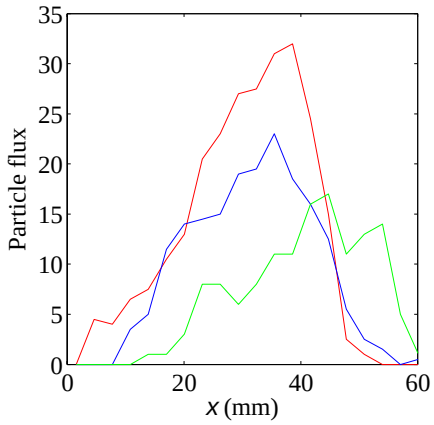

Figure 6. Sand flux along the dune (cm^{-1}), with x=0 at the dune foot. Red: central part ; blue : side part ; green: horns.

4. RELAXATION LENGTH

The above measurements may be put together by (i) shifting the x-origin of each slice, initially at $x_d(y)$, up to the foot of the slice, and (ii) normalizing the flux in each slice by a saturated flux $q_{sat}(y)$ obtained by fitting the data points with Eq. (1). The result is shown in figure 7. It can be seen that the data points nicely fall close to the exponential relaxation curve corresponding to Eq. (1) (except very near the foot), with

$$L_{sat} = 300\ (u_*/V_{fall})\ d$$

where u_* is the friction velocity on the bottom wall of the channel. This length appears to be one of magnitude larger than those obtained from measurements of the equilibrium erosion and

deposition rates. Further investigation is needed here to clarify this point.

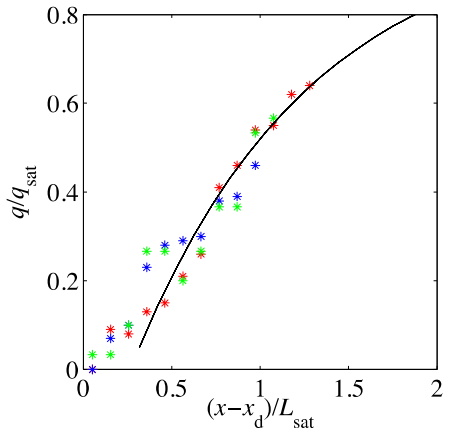

Figure 7. Normalized sand flux along the dune (see text for the normalizations). Red: central part ; blue : side part ; green: horns. Solid line: Eq. (1) with L_d = 300 (u_*/V_{fall}) d.

5. CONCLUSIONS

Understanding relaxation effects of the particle flux over a variable erodible bottom is a key point for confident prediction of the sediment transport over a variable bottom. In particular, such an understanding is necessary for predictions of the ripple length under water. We have shown here that field measurements of the particle flux $q(x, y)$ over barchan dunes allows the determination of the relaxation length. Our results show that the particle flux increases from the dune foot up to the crest, where it is not yet saturated. Fitting these measurements with the non-equilibrium model corresponding to Eq. (1) provides a relaxation length much larger than expected from previous analyses. Further analyses are in progress, which include the variations of the shear stress over the dune.

6. REFERENCES

Abrams, J. ans Hanratty, T. J. 1985. Relaxation effects observed for turbulent flow over a wavy surface. J. Fluid Mech. 151: 443-455.

Al-lababidi S., Yan W., Yeung H., Sugarman P. and Fairhurst C. P. 2008. Sand transport characteristics in water and two-phase air/water flows in pipelines. 6th North American Conference on Multiphase Technology. 159-174.

Andreotti, B., Claudin, P. and Douady, S. 2002. Selection of dune shapes and velocities. Part 2: A two-dimensional modelling. Eur. Phys. J. B 28: 341-352.

Andreotti, B., Claudin, P. and Pouliquen, O. 2010. Measurements of the aeolian sand transport saturation length. Geomorphology 123: 343--348.

Bagnold, R. A. 1941 The physics of blown sand and desert dunes. Methuen, London.

Charru, F. 2006. Selection of the ripple length on a granular bed sheared by a liquid flow. Phys. Fluids 18: 121508.

Charru, F. and Franklin, E. 2012. Subaqueous barchan dunes in turbulent shear flow. Part 2. Fluid flow. J. Fluid Mech. 694: 131-154.

Charru, F. and Hinch, E.J. 2006. Ripple formation on a particle bed sheared by a viscous liquid. Part 1. Steady flow. J. Fluid Mech. 550: 111-121.

Charru, F., Andreotti, B. and Claudin, P. 2013. Sand ripples and dunes. Annu. Rev. Fluid Mech. 45: 469-493.

Claudin, P., Charru, F. and Andreotti, B. 2011. Transport relaxation time and length scales in turbulent suspensions. J. Fluid Mech. 671: 491-506.

Franklin, E. and Charru, F. 2011. Subaqueous barchan dunes in turbulent shear flow. Part 1. Dune motion. J. Fluid Mech. 675: 199-222.

Hersen P. 2005. Flow effects on the morphology and dynamics of aeolian and subaqueous barchan dunes. J. Geophys. Res. 110: F04S07.

Hunt, J. C. R., Leibovich, S. and Richards, K. J. 1988. Turbulent shear flows over low hills. Q. J. R. Meteorol. Soc. 114: 1435-1470.

Kroy, K., Sauermann, G. and Herrmann, H. J. 2002. Minimal model for aeolian sand dunes. Phys. Rev. E 66: 031302.

Lajeunesse, E., Malverti, L. and Charru, F. 2010. Bedload transport in turbulent flow at the grain scale: experiments and modeling. J. Geophys. Res. 115: F04001.

Mantz P. A. 1978. Bedforms produced by fine, cohesionless, granular and flakey sediments under subcritical water flows. Sedimentology 25: 83--103.

Richards, K. J. 1980. The formation of ripples and dunes on an erodible bed. J. Fluid Mech. 99: 597-618.

Sauermann, G., Kroy, K. and Herrmann, H. J. 2001. Continuum saltation model for sand dunes. Phys. Rev. E 64: 031305.

Yalin, M. S., 1985. On the determination of ripple geometry. J. Hydraul. Eng. 111: 1148-1155.

On the role of fine-sand dune dynamics in controlling water depth changes in Rio Parapeti, Serrania Borebigua (Southern sub-Andean zone of Bolivia)

N. Deville [(1)], D. Petrovic [(1)] & M.A. Verbanck [(1)]

1. Department of Water Pollution Control, Université Libre de Bruxelles (ULB), Boulevard du Triomphe, CP208, B-1050 Brussels, Belgium. E-mail : ndeville@ulb.ac.be

Abstract

The role of the fine-dune sand dynamics in controlling the natural regeneration of the upper layer of a riverbed used for filtration is studied at the Choreti test reach of Rio Parapeti, in the Southern sub-Andean zone of Bolivia. Local production of drinking water relies on Riverbed Filtration, the delivery of which depends on the river water depth and the riverbed permeability. There is a strong, natural, declamation process of the upper layer maintained by dune bed-forms migrating downstream. It is thus essential to understand and represent local water depth changes as a function of the incoming discharge. We show the vortex-drag model can be used to correctly calculate the stream velocity in natural environment. Then we study the sand dunes characteristic (wavelength and celerity) in the Rio Parapeti. Because of the shallow-flow configuration the dominant dune length can be easily extracted from satellite images taken at various dates. We also show that it is more than likely that dune movement can be followed by the simple deployment of a pressure probe into the water under stable discharge condition, even if further data and investigation are necessary to confirm this.

1. INTRODUCTION

The role of the fine-dune sand dynamics in controlling the natural regeneration of the upper layer of a riverbed used for filtration is studied at the Choreti test reach (20°1'0" N 63°31'60" E) of Rio Parapeti, in the Southern sub-Andean zone of Bolivia. The site is located at 800m elevation, mid-slope from the Central Cordillera towards the Chaco plain (Baby et al. 2009). The subtropical climate is characterised by two distinct seasons. During the summer is a heavy rainy season from November to April (Ministerio de saneamiento basico 2005) accompanied by melting ice from the Andean mountains, while winter is dry. From this results a high variation in the discharge value of the Rio Parapeti (Table 1).

	Min	Max	Average
Discharge Q (m^3/s)	5.2	940	90

Table : Daily data of Rio Parapeti discharge 1975-1984 at the San Antonio site, 550 m elevation, at the bottom of sub-Andean foothills (Guyot et al. 1994)

The subandean ground is composed by the late Cenozoic sedimentary strata of sandstone, in this case the Yecua and Tariquia formations of late Miocene (Hulka et al. 2006, Hulka & Heubeck 2010). This explains the particularly small granulometry found for streambed particles in Choreti, with a median grain size of 250④m of non-cohesive, very homogeneous, silica sand. Size-distribution analysis indicates that sand particles sizing between 210µm and 290µm constitute more than 55% of the active layer of local riverbed deposits. For this reason rio Parapeti in Choreti forms a remarkable field investigation site to study alluvial adaptations and consequences for bedform roughness. The combination of small granulometry and high discharge during the rainy season explains the highly dynamic riverbed present at the Choreti site. Even if the river is around 90 m wide, it is a shallow river with a mean depth of only 1 m even if in extreme events, it can goes up to 4-5m (Camacho 2004).

Local production of drinking water relies on Riverbed Filtration (RBeF). The system, which derives from the well-known riverbank filtration used in Europe since last century (Stuyfzand *et al.* 2006), consists in extracting water from a lateral well directly connected to an infiltration gallery installed perpendicularly under the riverbed. The filtering layers at that location of the riverbed are formed by top-down increasing sand and gravel beds laid there for the purpose (Camacho 2004).

The production of such a system is mainly dependent of the river water depth (D) and the riverbed permeability. But the system eventually starts to clog with infiltration of small particles into lower layers and biological development (Schalchli 1992, Stoquart 2009, Craddock 2012). This causes the productivity to decrease in time and water quality is mainly dependent on the upper sand-bed layer. Indeed, there is a strong, natural, declamation process of the upper filtration layer maintained by dune bed-forms migrating downstream. This renewal avoids the upper layer to clog and preserve its capability to clean infiltrating water. It is thus important to understand and represent local water depth changes as a function of the incoming discharge. Water depth is controlled by alluvial hydraulic roughness and by sand-bed adaptive morphology (Simons & Richardson 1961). Our observations take place during the rainy season thus high stream power conditions were present all the time. In a fine non-cohesive sand particles system like this one, the riverbed is highly dynamic and adapts itself quickly to the stream velocity (U) changes. Basically, the system can be separated, as a function of ambient specific stream power (W/m²), into two different regimes which are lower alluvial regime, associated to fully developed dunes (FDD) and upper alluvial regime with In-phase waves (IPW) (Simons & Richardson 1961). IPW presence is easily identifiable on the spot (see Fig.3) because of the characteristic undular water surface deformations.

1.1 The control factor m and stream velocity determination

FDD flow is characterised by a phase opposition between water surface and sand wave profiles. The water flow is accelerated due to the topographic forcing on the back of the dune (Fig. 1) until the crest where it loses contact at the separation edge. At this moment an eddy is formed which creates a strong velocity gradient between the recirculation zone and the overlying free stream. Kelvin-Helmholtz instabilities therefore develop at the shear layer (Muller and Gyr 1982, 1986). These instabilities reach the back of the next dune, generating a secondary perturbation in the form of a vortex, or kolk-boil, that in a sufficiently shallow stream can be observed at the water surface (Best 2005, Barua & Rahman 1998).

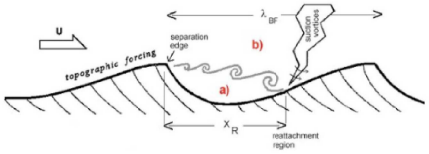

Figure : Attached/detached flow model. The movable-bed resistance problem can be seen as a combinaison of (a) topographically-forced attached flow, and (b) instabilities in the separated shear layer which originates at the bedform crest

Levi (1983) introduced the universal Strouhal law (Eq. 1.1) to describe the frequency of vortex shedding as Strouhal did for aeolian tones.

$$f_{detached} = \frac{1}{2\pi}\frac{U}{xr} \qquad (1.1)$$

where $f_{detached}$ = frequency of perturbation (s^{-1}), U = stream velocity (m/s) and x_r = characteristic length (m). Later, Verbanck (2008) introduces the « control factor m » from Kiya's theoretical development into the universal Strouhal law to take into account the different harmonic modes. m value of one corresponds to the fundamental mode described initially by Levi (with IPW) and m value of two corresponds to the second harmonic with the presence of FDD (Verbanck 2008, Huybrechts *et al* 2011). This gives us the equation:

$$f_{detached} = \frac{1}{T_{kolk-boil}} = \frac{mU}{2\pi D} \qquad (1.2)$$

where $T_{kolk\text{-}boil}$ = kolk-boil period (s), D = water depth (m) and m = control factor.

Verbanck pursuits the development by formulating the vortex-drag equation which is a combination of both the detached effect (universal Strouhal law) and the attached effect. The local topography of the dune forces the flow to accelerate . This creates a gravity wave which tries to plan the water surface. The propagation of this wave (neglecting surface tension) is described by Airy's law.

$$c = \sqrt{\frac{g\,\lambda_{bf}}{2\pi}\tanh\frac{2\pi D}{\lambda_{bf}}} \qquad (1.3)$$

where c = gravity wave celerity (m/s), g = gravitational constant (m/s^2) and λ_{bf} = dune wavelength (m).

The two phenomenons participate in the dissipation of energy. The attached phenomenon is the most efficient way to evacuate the excess water and thus tends to reduce the energy loss of the stream, while the detached phenomenon consumes energy for maintaining the vortex turbulences. Verbanck assumes then these two effects can be reunited into a single formulation of the energy gradient:

$$S = \beta\left(\frac{\frac{mU}{2\pi D}}{\sqrt{\frac{g\,\lambda_{bf}}{2\pi}\tanh\frac{2\pi D}{\lambda_{bf}}}}\right)^{\alpha} \qquad (1.4)$$

where S = surface water slope and α, β = coefficients. An empirical analysis was conducted to give value to the coefficients, which leads us to the vortex-drag equation used in this work.

$$U = \frac{2\pi}{m}\sqrt{\frac{g\,\lambda_{bf}}{2\pi}\tanh\frac{2\pi D}{\lambda_{bf}}}\,S^{0.3} \qquad (1.5)$$

1.2 Field measurements

Field measurements were performed for several years on the spot in Choreti (2009-2012) during the rainy season. Measures of water depth were recorded daily by both limnimeter and pressure probe OTD Diver Schlumberger (Fig. 2).

Water velocity was recorded by General Oceanics 2030 currentmeter with standard 2030-R mechanical rotor. We arbitrarily took the measure in the middle of the stream with two measures at respectively 20 and 80 % of the water depth in appreciation of the vertical logarithmic velocity profile.
The alluvial regime is easily recognizable in this river. Upper alluvial regime is represented by IPW (Fig. 3) and lower alluvial regime by FDD. As we explained earlier, kolk-boils are visible when there are FDD and thus we could measure the time between each of them determining $T_{kolk\text{-}boils}$.

Figure : Installation of the limnimeter in the Rio Parapeti. The pressure probe is inserted into the pole.

Figure : IPW formation at Choreti test reach, Bolivia (Photo credit: F.Craddock).

Because of high particles concentrations and thus water opacity, dunes lengths were not directly visually discernable on the spot. But we show that satellite images can be used to determine their length

relatively precisely. Thanks to the shallow-stream, dunes migration were visible with only the installation of a pressure sensor into a protecting pole (Fig. 2). The study of the water surface slope has been done between two bridges separated by a curvilinear distance 1.8km from each other. The determination of the reference piezometric level at the two points has been done by a theoretical development due to a lack a precision of our GPS.

2. RESULTS

2.1 On the determination of stream flow velocity by the vortex-drag model

The vortex-drag equation needs four terms to be applied. The control factor "m", dunes length, water depth and water slope.

2.1.1 The control factor m

There are different ways to determine the value of the control factor m. It can be based on water surface slope or kolk-boil frequency.
First of all, we try to confirm the link between the kolk-boil period and the expected value of control factor m = 2. The determination of kolk-boil period has been done by visual observation on the spot. Equation (1.2) is used to calculate the m value associated with these kolk-boils (Table 2).

	5/4/10	17/03/11	18/03/11
Observed period (s)	4.0	2.6	4.0
m with $T_{detached}$	1.92	2.35	2.27
Q (m^3/s)	49	116	122

Tableau : Field observations of the time elapsed between two consecutive kolk-boils appearing at the water surface. The second line is the m value calculated with Equ. 1.2. The discharge, obtained using the local Choreti hydrometric rating curve (Stoquart 2009), is represented at the third line.

As we can see, the m value is close to the expected value of m=2 for the three observations**.** This means that we can allow us to attribute a "visual" value for the parameter m = 2 when we observed FDD. And when we observed IPW, the control factor value is m=1 (Huybrechts *et al.* 2011a). We can also see that m value of 2 can be found for contrasted values of discharge.

2.1.2 Water surface slope

First of all we determine the absolute level difference between our two (upstream-downstream) measurement points. As explained before, m equals 2 when kolk-boils are present. Therefore, we base this study on the 18/3/2011 where kolk-boils were visible and calculate the water surface slope with the equation (1.5). This gives us a standard slope value that we used to determine comparatively the water surface slope for all the other days. The surface water slope on the 18/3/2011 was S = 0.00022.
We also used these values of S to determine the daily control factor m that we compare with the values obtained with the flow resistance prediction rule proposed by Huybrechts et al. 2011b (Fig. 4). We can see we have an acceptable agreement between the two estimation methods.

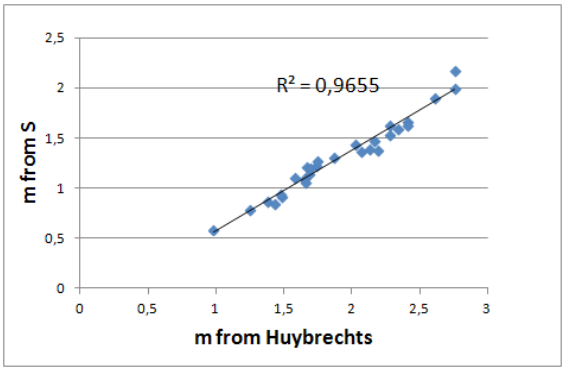

Figure : Comparison of the control factor m calculated with the method of Huybrechts (abscissa) and calculated with the measured surface water slope (equation (1.5)) (ordinate).

Huybrechts' method gives slightly higher values of m than the ones extracted from the local experimental water slope. However, it seems that it is Huybrechts who over-estimates the control factor m value because the stream power calculated with his values are too

big to describe what has been observed (Pw_{mean} = 11.5 W/m^2). Indeed, it would mean that upper alluvial regime has been there every single day which, from field observations, is known not to be true. Therefore, we will work with our measured values.

2.1.3 Dune wavelengths

Due to local constraints no detailed bathymetry survey was possible. The information about dominant dunes length (λ_{bf}) was thus extracted from available satellite images. Three satellite images were used to have a mean value of dunes length (See example at Fig. 5). The value we kept in this work is λ_{bf}=6.7m.

Figure : September 2007, we count 11 sand waves on 76 m, thus λ_{bf} = 6.9m. Source: Google earth©.

This result is in good agreement with the proposition of Julien and Klaassen (1995) who predict $\lambda_{bf} \approx 6.5D$. Indeed, the flow depth measured in the Rio Parapeti at the Choreti site is around 1.0 m deep which corresponds then to $\boldsymbol{\lambda_{bf}}$=6.5m. The equation of Liang (2003) also gives us the same magnitude of sand waves length.

	Satellite image (m)	Liang 2003 (m)	Julien & Klaassen 1995 (m)
14/4/09	6.7 ±0.5	1.40	3.84
26/3/11	6.7 ±0.5	2.95	4.81
1/04/11	6.7 ±0.5	4.95	7.99

Table : Dune wavelength estimates

2.1.4 The vortex-drag model

Finally, we use the vortex-drag equation to determine the water velocity, taking into account the measured water depth, measured water surface slope, visual control factor "m" (thus m=1 when IPW or 2 when FDD) and the dunes length (satellite images). We plot it with the velocity obtained with the currentmeter (Fig. 6). The calculated velocity correctly follows the variation of the stream velocity. This encourages us to pursue our further work relying on this equation.
This means also that when there are FDD, we can use the same equation to approximate the water slope of a river by measuring the stream velocity, the dunes length and the water depth only in one point. One way to get better results would be to improve the determination of the control factor m (not only m=1 or 2) to be closer to the measured velocity as well as the measured water surface slope.

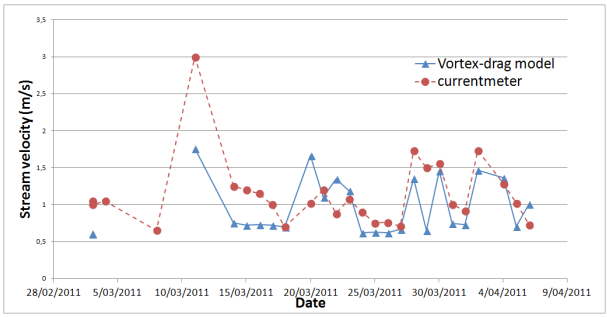

Figure : Comparison of the stream velocity determined by the vortex-drag model with the experimental data at the Choreti test reach in 2011.

2.2 On the determination of sand dunes celerity

As is well explained in the literature, the passage of a FDD in a shallow stream is associated with a phase opposition of the water surface (Simons & Richardson 1961). Where the dune crest exactly stands, the observed water level will be lower due to the topographical forcing effect mentioned before. Therefore, we argue that the dunes movement can be followed by the simple deployment of a (fixed-altitude) pressure probe into water during stable-discharge conditions (no rainfall nor tributary discharge). As an example, the 1-minute water level record in the Choreti test reach on April 1st, 2011 is represented in Fig. 7. We can see that the dune took about 4.5 hours to pass the sensor. As perceived by the Eulerian pressure sensing, the rapid raising of the water level at 15:10 (but also from 11:20 to 11:40) corresponds to the moment when the dune crest suddenly disappears underneath the probe. That is why all our water level records, here exemplified by Fig. 7, provide a transposed (top to bottom) representation which is exactly the reverse of the expected dune longitudinal shape. Besides, as shown

by a FFT analysis, the available records indirectly suggest that ripples (or mini-dunes) are actually migrating on the back of the big dunes. Their wavelength is about 20 times shorter than the reference 6.7m scale characteristic of the large-sized dunes evoked so far (those which are sufficiently large to be discernable by satellite imagery). Indeed, as shown in Fig. 7, we can count 21 ripples passing under the probe on the back of one big dune.

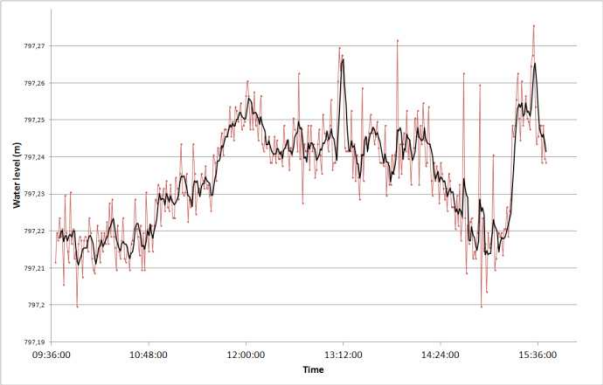

Figure : 1-min record of the water level evolution obtained with the (fixed-altitude) immersed pressure probe. Choreti test reach, 1 April 2011. The black line is the moving average with a period of 6 minutes.

To confirm these observations for the large dunes, we will compare the dune celerity determined with the pressure probe with the celerity determined by different authors.

Several authors have proposed a method (Pushkarev 1936, Kondratiev 1962, Simons et al. 1965, Thomas 1967, Kondap & Garde 1973, Orgis 1974, Fedele 1995) to predict the dune celerity. Strasser (2008) made a comparative study on those equations and showed that the correlations of Kondap & Garde, Pushkarev, Orgis and Fedele give good agreement on both laboratory (Guy et al. 1966) and river data (Rhine, Waal and Dommel). However, Pushkarev, Orgis and Fedele primarily consider coarser (gravel) grain-sizes and thus do not provide satisfactory predictions for fine-size (sand) granulometry (Fig. 8 and Table 4) (data from Guy *et al.* 1966, Termes 1986 and Driegen 1986). Therefore, despite the fact that granulometry is not explicitly represented in the relation, we will use the one of Kondap and Garde to evaluate the dune celerity in the Choreti site (Equ.2.2).

$$\frac{c_w}{\sqrt{gD}} = 0.021\, Fr^4 \qquad (2.2)$$

where c_w = sand wave celerity (m/s) and Fr = Froude number.

	Fedele	Orgis	Kondra-tiev	Simons	Kondap
	0.14	0.39	0.27	0.52	0.49
AGD	12.3	60.9	48.0	67.4	1.75

Table : R-square and AGD value for the different equations with the experimental data (Guy et al. 1966, Driegen 1986 and Termes 1986). The Average Geometric Deviation proposed by Zanke (AGD) (Huybrechts et al. 2011b) describes the discrepancy between the predicted and measured data. (AGD = 1 corresponds to a perfect match).

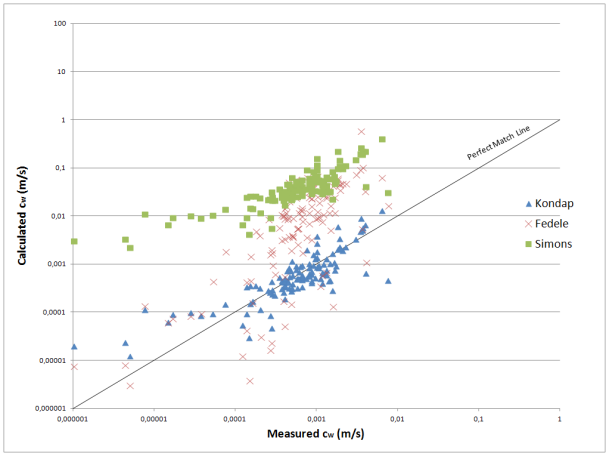

Figure : Comparison of the calculated sand dunes celerity by different authors (Kondap, Fedele and Simons) and the experimental data (Guy et al. 1966, Driegen 1986 and Termes 1986).

The sand wave celerity at the Choreti site is simply obtained by dividing the dune length extracted from satellite images (Table 3), by the time necessary for the dune to pass under the (water-column measuring) Schlumberger sensor. The results are given in Table 5.

Date	Choreti test reach (m/h)	Kondap & Garde (m/h)
14/4/09	1.01	0.45
26/3/11	4.48	1.27
1/04/11	1.34	1.26

Table : Comparison of the measured dunes celerity with the celerity calculated by the equation of Kondap & Garde.

As we can see, there is an acceptable relationship between sand wave celerities. This tends to confirm our hypothesis that records such as the one in Fig. 7 (we have many of them) indeed correspond to the indirect visualisation of the sand wave (the dune) migrating under the pressure probe. Further investigations and more data are needed to confirm this hypothesis in the future.

3. CONCLUSION

We study the applicability of the vortex-drag equation on the Choreti test reach of Rio Parapeti, Camiri (Bolivia). In the shallow-water condition prevailing here, Fully Developed Dunes are associated with marked kolk-boils periodicity appearing at the water surface. We show that field observation of kolk-boil periods leads us to the expected value of the control factor (m equal 2). Then we make use of the vortex-drag equation to study the stream velocity change taking into account bedforms configuration (m, wavelength λ_{bf}), water depth and water surface slope (S). The results show a satisfactory description of the stream velocity changes. This means that, reversely, the same equation could be used to correctly assess the water surface slope over fluvial dune fields by simply measuring the stream velocity, water depth and dunes length. A universal method to predict the value of control factor m as a function of local stream circumstances (and increasing stream power) would thus be most welcome.

We also show that the sand wave celerity can be followed by the simple deployment of a (fixed-altitude) pressure probe within the right conditions. Indeed, we obtain the dune celerity with the determination of the time needed for the dune to pass the probe and the sand wavelength determined by satellite images (confirmed by the equation of Julien & Klaassen, 1995, and Liang, 2003). The comparison of this celerity with the one obtained by the equation of Kondap and Garde (1973) shows that it is reasonable to argue that it is actually a sand wave passing under the probe. This is also indicated by the recurrence of this observation in our database. Further investigation and data collection are needed to continue the study of the Riverbed filtration at the Choreti test reach.

4. NOTATION

c	Gravity wave celerity (m/s)
D	Water depth (m)
d_{50}	median grain size (m)
$f_{detached}$	vortex shedding frequency (s^{-1})
Fr	Froude number (-)
g	Gravitational constant (m/s^2)
λ_{bf}	Dune length (m)
m	Control factor m (-)
Pw	Specific stream power (W/m^2)
Q	Discharge (m^3/s)
S	Water surface slope (-)
$T_{kolk-boil}$	Kolk-boil period (s)
U	Stream velocity (m/s)
c_w	Sand wave celerity (m/s)
x_r	Length of separation zone (m)

	D (m)	U (m/s)	Q (m^3/s)	S
Average	0.88	0.82	90	0.00023

	λ_{bf} (m)	H_{bf} (m)	c_w (m/s)	d_{50} (m)
Average	6.72	0.25	1-4 m/h	250 10^{-6}

Table : Average hydraulic characteristics of rio Parapeti at the Choreti test reach. H_{bf} value has been estimated with the equation of Flemming (2000) and Julien & Klaassen (1995).

5. ACKNOWLEDGMENTS

This study contributes to the project (WBI-Bolivie 2010-Projet 8) entitled 'Analysis & optimization of the RiverBed Filtration extraction system used to pre-treat the drinking waters feeding the city of Camiri in Santa Cruz Province, Bolivia, funded by the Wallonie-Bruxelles-International agency (www.wbi.be). The efficient technical help provided by the Coopagal staff in Camiri was greatly appreciated. In addition to this, the first author benefitted in 2011 of a travel grant to Bolivia financed by the Universities Cooperation Development Fund (www.cud.be) in Brussels.

6. REFERENCES

Camacho Garnica, A. 2004. Estudio de galerías filtrantes en lechos aluviales de Bolivia. Master thesis, Universitad del Valle, Cali, Columbia.

Barua, D.K., Rahman, K.H. 1998. Some aspects of turbulence flow structure in large alluvial rivers. J. Hydraulic Res. 36(2): 235–252.

Best, J. 2005. Kinematics, topology and significance of dune-related macroturbulence: some observations from the laboratory and field. Spec. Publs int. Ass. Sediment, 35 : 41–60.

Craddock, F. 2012. Modélisation de la productivité d'un système de filtration sur lit de rivière pour la production d'eau potable. Master Thesis, ULB.

Driegen, J. 1986. Flume experiments on dunes under steady flow conditions (uniform sand, d_{50} = 0.77mm). Description of bed forms. TOW Report R 657 – XXVII / M1314 part XV, WL / Delft Hydraulics, Delft, the Netherlands.

Flemming, B.W. 2000. The role of grain size, water depth and flow velocity as scaling factors controlling the size of subaqueous dunes. In: Trensetaux A, Garlan T (eds) Proc Worksh Marine Sandwave Dynamics : 55-60. 23-24 March 2000, University of Lille, France

Guy, H., Simons, D.B., Richardson, E.V. 1966. Sediment transport in alluvial channels: Summary of alluvial channel data from flume experiments, 1956-61. Geological survey professional paper 462-1.

Harbor, D.J. 1998. Dynamics of bedforms in the lower Mississippi River. Journal of Sedimentary Research, Vol. 68, N°5: 750-762.

Hulka, C. Heubeck, C. 2010. Composition and Provenance History of Late Cenozoic Sediments in Southeastern Bolivia: Implications for Chaco Foreland Basin Evolution and Andean Uplift. Journal of Sedimentary Research (SEPM), 80 (3): 288-299.

Hulka, C., Gräfe, K.-U., Sames, B., Uba, C.E. and Heubeck, C. 2006. Depositional setting of the middle to late Miocene Yecua formation of the Chaco Foreland Basin, southern Bolivia. Journal of South American Earth Sciences, 21(1-2): 1-16.

Huybrechts N, Luong G.V., Zhang Y.F. & Verbanck M.A. 2011a. Observations of canonical flow resistance in fast-flowing sand-bed rivers. Journal of Hydraulic Research, 49(5): 611-616.

Huybrechts, N., Luong, G., Zhang, Y., Villaret, C., and Verbanck, M.A. Sept. 2011b. Dynamic Routing of flow resistance and alluvial bed-form changes from the lower to the upper regime. Journal of Hydraulic Engineering, 137(9): 932-94.

Julien, P.Y. and Klaassen, G.J. Sept. 1995. Sand-dune geometry of Large Rivers during floods, Journal of Hydraulic engineering: 657-663.

Levi, E. 1983. A Universal Strouhal Law. J. Eng. Mech.109: 718–727.

Liang, Z.Y. and al. 2003. Anti-dunes in Hyper-concentrated flows. Journal of Sediment Research, 4: 14-18 (in Chinese).

Müller, A. and Gyr, A. 1982. Visualization of the Mixing Layer Behind Dunes. In: Sumer, B.M. and Müller, A. (eds.), Mechanics of Sediment Transport: 41-45. A. A. Balkema, Brookfield, Vt.

Müller, A. and Gyr, A. 1986. On the Vortex Formation in the Mixing Layer Behind Dunes. Journal of Hydraulic Res. 24(5): 359–375.

Schalchli U. 1992. The clogging of coarse gravel river beds by fine sediment. Hydrobiologia, No. 235/236: 189-197.

Simons, D.B., and Richardson, E.V. 1961. Forms of bed roughness in alluvial channels. ASCE, Proc. Journal of hydraulic Division 87 (HY8) : 87-105.

Stoquart, C. 2009. Contribution à la caractérisation du système de production potable, par la technique de River Bed Filtration, du district de Choreti, Camiri (Bolivie). Master Thesis, ULB.

Strasser, M.A. 2008. Dunas fluviais no rio Solimões – Amazonas : dinâmica e transporte de sedimentos. Tese, Universidade Federal do Rio de Janeiro, Coppe.

Stuyfzand, P.J., Juhàsz-Holterman, M.H.A., and de Lange, W. 2006. Riverbank Filtration in the Netherlands : Well fields, clogging and geochemical reactions. Springer Netherlands. NATO Science Series, Vol. 60: 119-153.

Termes, A.P., 1986. Dimensies van beddinvormen onder permanente stromingsomstandigheden bij hoog sedimenttransport. Waterloopkundig laboratorium, Delft hydraulics laboratory.

Verbanck, M.A. 2008. How fast can a river flow over alluvium? Journal of hydraulic research, Vol 46 Extra Issue: 61-71.

Vice Ministerio de Saneamiento Básico. 2005. Investigación sobre galerías filtrantes en Camiri. Technical report, inisterio de Servicios y Obras Públicas, Cochabamba, Bolivia.

Developments in North Sea wide resurveying and charting of dynamic sand wave areas

L. Dorst [(1)], T. Dehling [(2)], C. Howlett [(3)]

1. Hydrographic Service, Royal Netherlands Navy (NLHS), The Hague, The Netherlands - ll.dorst@mindef.nl
2. Bundesamt für Seeschifffahrt und Hydrographie (BSH), Hamburg, Germany - thomas.dehling@bsh.de
3. United Kingdom Hydrographic Office (UKHO), Taunton, United Kingdom - chris.howlett@ukho.gov.uk

Abstract

We discuss two cases of international cooperation between hydrographic offices. The first case is the unified approach to populate the CATZOC indicator for bathymetric quality in nautical charts, in the presence of sand wave fields. The second case is the North Sea wide formulation of resurvey policies. The two cases can only be successful if it is understood and agreed how the sea floor develops. For both of the cases, it is very relevant to distinguish between the growth of a pattern, and its migration. Therefore, hydrographic offices need accurate morphodynamic models, an appropriate set of methods for the analysis of time series of bathymetric data, and versatile remote sensing techniques.

The two cases are discussed using the example of a sand wave field near the Port of Rotterdam, in the Southern North Sea. The development of the field is potentially influenced by the maintenance of dredged channels and an emergency turning zone; extensive sand pits; and two infrastructural projects in the coastal vicinity: Maasvlakte 2 and the Zandmotor.

1. INTRODUCTION

Hydrographic offices around the North Sea are faced with the challenge to resurvey and rechart areas with rhythmic patterns on the sea floor. Especially tidal sand wave fields, with wavelenghts of several hundreds of metres and heights of up to several meters, are found at many locations. It is mostly unknown whether the observed patterns are dynamic, although time series of modern high resolution surveys have become available for more and more areas [Van Dijk et al., 2012a].

The most common change of a sand wave pattern is a migration, due to e.g. asymmetries in the tidal currents [Németh et al., 2002]. In such a situation, the charted depth values remain constant, according to the nautical charting principle of shoal biasing [Smith et al., 2002]: the shallowest values are selected for visualisation in the chart, implying that these values represent the shallowest values that are likely to appear in the surrounding area. Consequently, the mariner will not notice the migratory character of the sea floor, and has to trust the prudent monitoring of pattern development by the hydrographic office.

This practice is acceptable as long as the hydrographic office is able to maintain a safe resurvey frequency for the area, and as long as there are no large-scale human interventions in the greater region of the sand wave field, with the potential to disturb the morphodynamic processes that have created the migratory sand wave field. National hydrographic survey budgets are under pressure though, which translates into a reduction in bathymetric survey capacity [Ward, 2012].

Yet the mariner expects accurate and recent information. Users of digital products, a group that grows fast now that this is mandatory for certain types of ships, are often not even aware that the source data could be less accurate due to survey age. Ship owners are aiming for a maximum

quantity of cargo, allowing for a minimum under keel clearance, also along coasts with heavy maritime traffic, sensitive ecosystems and a flourishing tourism industry. The Southern North Sea is a perfect example of such a combination of risks.

The hydrographic offices that constitute the North Sea Hydrographic Commission (NSHC) have reacted to these developments by intensifying their cooperation. This takes place on different levels. We present some developments on three levels: global, European, and North Sea wide.

2. AN EXAMPLE: THE PORT OF ROTTERDAM APPROACH

An example of an area with a challenging mix of human activities and critical depth values is the approach area to the Port of Rotterdam. The larger ships can only enter during high tide, which puts serious constraints on the quality of the survey and the chart, both in terms of measurement accuracy and in terms of update frequency. The sea floor is characterised by a dredged channel through an extensive field of rhythmic patterns with different wavelengths [Knaapen et al., 2001].

An example of a survey of the area and the large-scale chart is given in Figure 1, and the contents of the bathymetric database in Figure 2. Obviously, the sand pits are not relevant for navigation at sea. Hence they did not generate new editions of nautical charts or Notices to Mariners.

The patterns in the deeper, Western part of the area are found to be hardly dynamic [Van Dijk et al., 2012b; Dorst et al., 2011], while the pattern in the shallower Eastern part shows a clear migration [Van Dijk et al., 2012b; Dorst et al., 2008]. The heights of the sandwaves are generally found to be constant [Van Dijk et al., 2008; Knaapen, 2005], which implies that the shallowest likely depth values in the area do not change [Dorst et al., 2012a][1].

In the area of the example, several human interventions are in progress. The coastline changes, due to the Maasvlakte 2 extension to the Port of Rotterdam and the Zandmotor megascale beach nourishment project, are of such a scale that the tidal currents change[Dorst et al., 2012b]. The sandy sediment that the two projects use is taken out of sand pits (Figure 1) that are sufficiently extensive to affect the hydrodynamic conditions, potentially inducing a corresponding change in morphodynamic conditions [Roos et al., 2008].

3. GLOBAL DEVELOPMENTS

Within the International Hydrographic Organization (IHO), there is consensus that the visualisation of the quality of bathymetric data in Electronic Navigational Charts (ENCs) needs to be improved [Dorst & Howlett, 2012]. For future ENCs, the S-101 data model containing a hierarchical series of new quality indicators is under development. For current ENCs, produced in the S-57 data model, the "Zone Of Confidence" indicator will be populated in a more consistent manner by the national hydrographic offices.

An important consistency aspect is the assignment of a category for the Zone Of Confidence (CATZOC) in case of a mobile seafloor. Six categories can be distinguished, five of those ranging from A1 (best quality) to D (worst quality), and the sixth being U (unassessed) [Johnson, 2004]. Currently, a proposal to degrade CATZOC to category C in this case of seafloor mobility is under discussion, even in case of a recent, accurate survey without gaps. This category is described with the words "depth anomalies may be expected".

For a migrating sand wave field, different arguments about the appropriate CATZOC value can be made. On one hand, one may argue that depth anomalies cannot be expected, as the charted depth values remain constant. Such an argument ignores the changes in surveyed depth values, which it justifies by pointing out that CATZOC applies to the charted product, not to the observed data set. Advocates of this argument even fear that degradation of such a "safe" sand wave area to a CATZOC of C could tempt mariners to enter other CATZOC C areas with insufficient care.

On the other hand, one may argue that the mariner should be informed about the mobile character of the sea floor, especially if human activities may change the hydrodynamics that drive the sea floor dynamics. Hydrographic offices may not have the resources to resurvey the area with a sufficiently

[1] In the terminology of Dorst et al. [2012a], the overall shoaling rate of the area is zero, while the maximum shoaling rate at a location within the area is larger than zero.

high frequency to detect changes in the behaviour of the pattern in time, or may otherwise not be willing to accept the risk of assigning the area with a CATZOC value of A or B. This argument would satisfy the desire to indicate the potential danger of mobile areas, rather than give a potentially false indication of a highly accurate depiction of the seafloor.
Given the challenges that the example provides, we are inclined to, at least, allow hydrographic offices to artificially degrade CATZOC to a category C for areas with dynamic patterns. Perhaps the ideal of an internationally fully consistent assignment procedure is not feasible for CATZOC, and the specifics of each sea area, as known at the national hydrographic office, have to be taken account.

4. EUROPEAN DEVELOPMENTS

On the European scale, the INSPIRE directive contributes to a European Marine Spatial Data Infrastructure (SDI) by setting requirements to publish bathymetric data in a unified and automatic way. The European EMODNet project will take this one step further by creating a single portal[2] from which marine datasets, like bathymetry, can be viewed and downloaded [Longhorn, 2012]. These facilities will create new opportunities for morphodynamic research, provided that researchers have powerful tools for the analysis of large volumes of spatial data.

5. NORTH SEA DEVELOPMENTS

The North Sea Hydrographic Commission (NSHC) established a Resurvey Working Group, which has been active since 2007. National hydrographic offices share their resurvey plans, with the aim to unify survey efforts at their maritime boundary areas and for international shipping routes. These routes cross several international maritime boundaries, which makes access to all major ports dependent on the survey and charting efforts of neighbouring countries[3]. It is a potential waste of resources to survey more frequently than your neighbour, and a potential risk to survey less frequently.
At present, Belgium, Germany, the Netherlands and the United Kingdom have agreed to publish their resurvey prioritization together, in a single online map, for at least a part of their North Sea area. The current status of this plan is shown in Figure 3.

6. APPLICATION OF THE DEVELOPMENTS TO THE EXAMPLE

The dredged channel to the Port of Rotterdam currently has a CATZOC value of A1, and the sand wave field a CATZOC value of A2. Category A indicates that "significant seafloor features [were] detected and [their] depths measured". Subcategory A1 and A2 differ only in their requirements for survey accuracy [Johnson, 2004]. The Netherlands Hydrographic Service is confident that these requirements are met, as frequent resurveys are done by Rijkswaterstaat (the dredged channel, several times a year to once a month) and the Hydrographic Service (the sand wave field, once every other year).

Deep draught ships are led into the channel by pilots, taking advantage of the maintained depths in the channel. This guarantees that ships with a critical depth will not access the sand wave field. Although considerations like shipping intensity and draught are not included in the assignment process of an indicator in a nautical chart, they do play a role in the determination of a safe resurvey frequency, especially when such information is available through AIS data [Ward & Gallagher, 2011; Van Dijk et al., 2011].

The assignment of a CATZOC value of C to the mobile sand wave field would require an assessment of a line where the migration becomes significant. This could for instance be done by a comparison of the CATZOC position accuracy requirements to the expected migration between

[2] A comprehensive bathymetric data set at a coarse resolution is directly available at the portal www.emodnet-hydrography.eu, for high resolution sub-datasets it refers to the relevant authorities.

[3] Until 2012, the four countries around the English Channel had a shared policy on transboundary surveys around the selected track for deep draught ships. The so-called Dover Straight Survey Policy was revised, in order to better reflect the national responsibilities of each country to survey its own waters.

consecutive surveys. This immediately leads us to a requirement to accurately predict migration rates. As it currently is not feasible to make reliable predictions for large parts of the sand wave fields in the North Sea, we either need to set CATZOC to a value of C for all these sand wave fields, or accept that sand wave migration is excluded from the assignment process of a CATZOC value. We reject the option to only assign a CATZOC value of C to areas, like our example, where the migration is known and deemed significant, as this option would indicate the areas of known migration as less safe to the mariner than areas of unknown migration.

The area of the example does not only facilitate intercontinental shipping through the English Channel. There is an inshore traffic zone towards Belgian and French ports, the Maas Northwest Traffic Separation Scheme (TSS) towards English and Scottish ports, and the Maas North TSS towards German and Danish ports[4].

In the virtual case that the Netherlands were to decide to reduce resurveying efforts, there would come a moment that it is no longer defendable to classify the area with a CATZOC value of A. It would be in the interest of the national economies around the North Sea to prevent such a reduction in accessibility of their ports. But, in the absence of accurate predictions on the development of the sand wave field in the presence of the sand pits, the moment that the CATZOC value has to be degraded cannot be determined with any certainty, and such a decision cannot be discussed between the North Sea countries with factual evidence.

7. CONCLUSIONS

We discussed two cases of international cooperation between hydrographic offices: the unified approach to populate the CATZOC quality indicator for sand wave fields and the North Sea wide formulation of resurvey policies. The two cases can only be successful if it is understood and agreed how the sea floor develops. For both of the cases, it is very relevant to distinguish between the growth of a pattern, and its migration.

Within the North Sea, all national hydrographic offices have an interest in the decisions that the other hydrographic offices make. Poor decisions may jeopardize the coasts around the North Sea, or limit the accessibility of the ports of each country.

Scientific progress will enhance the insights of the hydrographic community into marine sand wave behaviour, opening up opportunities to improve survey efficiency and correct use of quality indicators in nautical charts. Hydrographic offices need accurate morphodynamic models, an appropriate set of methods for the analysis of time series of bathymetric data, and versatile remote sensing techniques.

Meanwhile, European policy decisions allow scientific institutions easier access to the bathymetric data that hydrographic offices possess. This could facilitate further progress in scientific knowledge on sand wave dynamics, satisfying the need for accurate hydrodynamic models.

[4] The TSS structure in the Netherlands EEZ will change per 1 August 2013.

8. ACKNOWLEDGMENTS

We would like to thank the crew of HNLMS Snellius, Daniëlle van Kuijk, Marcel Lans and Riejet Willemsen of NLHS, as well as Bernd Vahrenkamp of BSH for providing us with the figures. We also would like to thank Pieter Roos of the University of Twente, Jan Schaap of NLHS, and Janneke Bos, Niels Kinneging and Jos Kokke of Rijkswaterstaat for providing us with comments on an earlier version of this paper.

9. REFERENCES

Dorst, L.L., Roos, P.C., Van der Meer, F.M. & Hulscher, S.J.M.H. 2008. Sand wave migration in an anchorage area in the Southern North Sea. In D. Parsons, T. Garlan & J. Best (eds.), Proc. MARID2008, Leeds (UK), 1-3 April 2008. Leeds: University of Leeds.

Dorst, L.L., Roos, P.C. & Hulscher, S.J.M.H. 2011. Spatial differences in sand wave dynamics between the Amsterdam and the Rotterdam region in the Southern North Sea. Continental Shelf Research 31: 1096-1105.

Dorst, L. & Howlett, C. 2012. Safe navigation with uncertain hydrographic data – the representation of data quality in the IHO S-101 data model. Hydro International 16(4): 18-21.

Dorst, L., Roos, P. & Hulscher, S. 2012a. Improving a bathymetric resurvey policy with observed sea floor dynamics. Journal of Applied Geodesy, published online.

Dorst, L, Oude Elferink, A. & Ligteringen, T. 2012b. Recent changes in the Dutch baseline: the inseparable connection of human activities and natural processes. In Proc. ABLOS2012, Monaco, 3-5 October 2012. Monaco: International Hydrographic Organization.

Johnson, P. 2004. ZOCMAN cometh, or the application of Zones of Confidence in the Australian Hydrographic Service. International Hydrographic Review, New Series 5(3): 6-16.

Knaapen, M., Hulscher, S., De Vriend, H. & Stolk, A. 2001. A new type of sea bed waves. Geophysical Research Letters 28(7): 1323-1326.

Knaapen, M.A.F. 2005. Sandwave migration predictor based on shape information. Journal of Geophysical Research 110(F04S11).

Longhorn, R., 2012. Assessing the impact of INSPIRE on related EU marine directives. In Taking care of the sea; Proc. Hydro12, Rotterdam (NL), 12-15 November 2012. Hydrographic Society Benelux.

Németh, A., Hulscher, S. & De Vriend, H. 2002. Modelling sand wave migration in shallow shelf seas. Continental Shelf Research 22: 2795-2806.

Roos, P., Hulscher, S. & De Vriend, H. 2008. Modelling the morphodynamic impact of offshore sandpit geometries. Coastal Engineering 55: 704-715.

Van Dijk, T., Lindenbergh, R. & Egberts, P. 2008. Separating bathymetric data representing multiscale rhythmic bed forms: a geostatistical and spectral method compared. Journal of Geophysical Research 113(F04017).

Van Dijk, T.A.G.P., Van der Tak, C., De Boer, W.P., Kleuskens, M.H.P., Doornenbal, P.J., Noorlandt, R.P. & Marges, V.C. 2011. The scientific validation of the hydrographic survey policy of the Netherlands Hydrographic Office, Royal Netherlands Navy. Utrecht (NL): Deltares.

Van Dijk, T., Van Heteren, S., Kleuskens, M., Vonhögen-Peters, L., Doornenbal, P., Van der Spek, A., Hoogendoorn, B., Dorst, L. & Rodriguez Aguilera D. 2012a. Quantified sea-bed dynamics of the Netherlands Continental Shelf and the Wadden Sea: a morphological and sedimentological approach. In Taking care of the sea; Proc. Hydro12 Rotterdam (NL), 12-15 November 2012. Hydrographic Society Benelux.

Van Dijk, T.A.G.P., Van der Mark, C.F., Doornenbal, P.J., Menninga, P.J., Keppel, J.F., Rodriguez Aguilera, D., Hopman, V. & Erkens, G. 2012b. Onderzoek meetstrategie en bodemdynamiek. Utrecht (NL): Deltares.

Ward, K. & Gallagher, B. 2011. Utilizing Vessel Traffic and Historical Bathymetric Data to Prioritize Hydrographic Surveys. In Proc. USHydro2011, Tampa Bay (USA), 25-28 April 2011. The Hydrographic Society of America.

Ward, R., 2012. IHO committed to serve the mariner. Hydro International 16(8): 10-13.

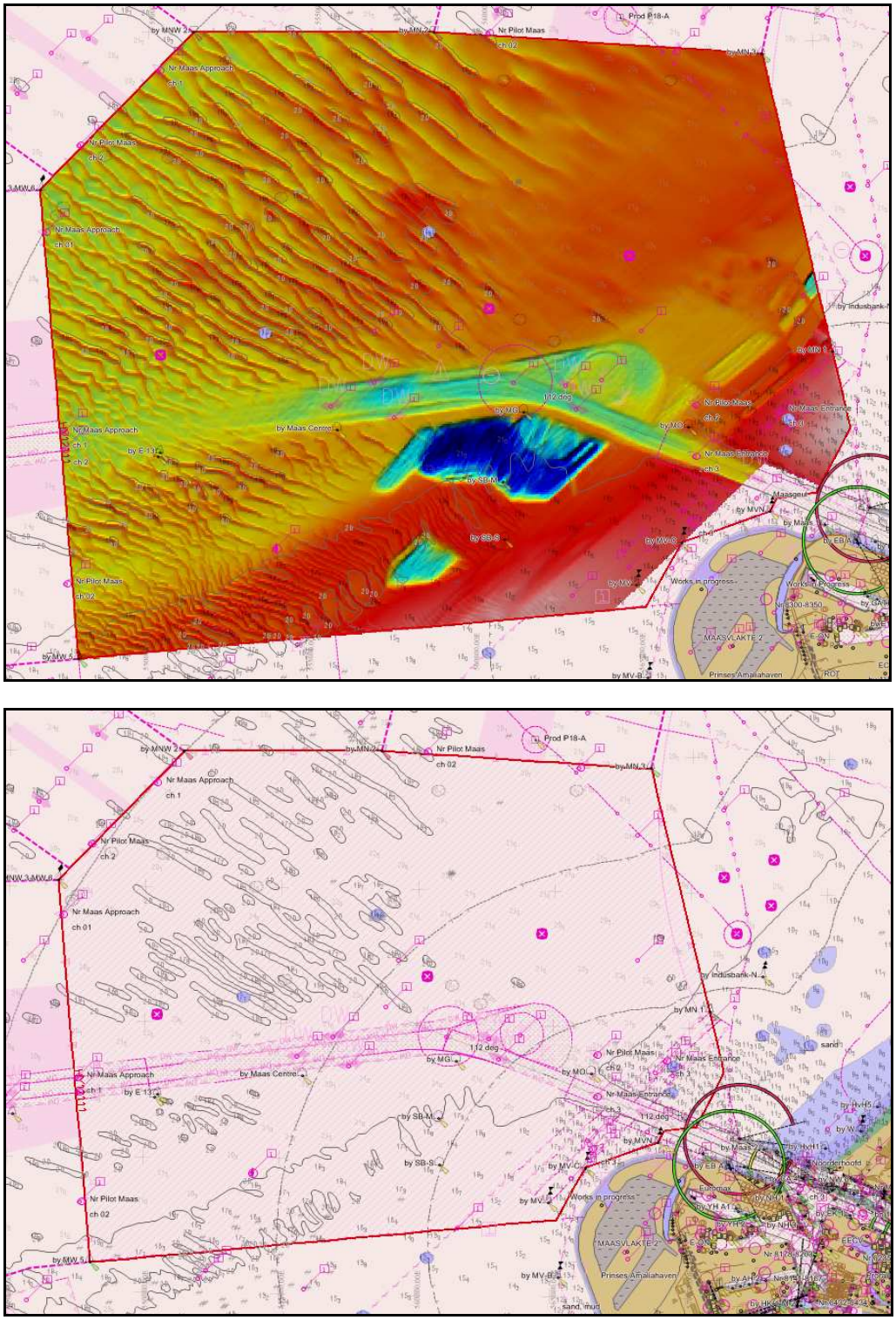

Figure 1. Bathymetric survey of the approach area to the Port of Rotterdam, HNLMS Snellius, May-July 2012 (top): notice the presence of the dredged channels, the emergency turning zone, and the sand pits for infrastructural projects like the Maasvlakte 2 (lower right) and the Zandmotor (not visible) [Dorst et al., 2012b]. Bathymetry of the approach area to the Port of Rotterdam in Electronic Navigational Chart NL400122 (bottom): notice the absence of the rather recent sand pits. A new edition is expected in the Summer of 2013. (figure courtesy of crew HNLMS Snellius)

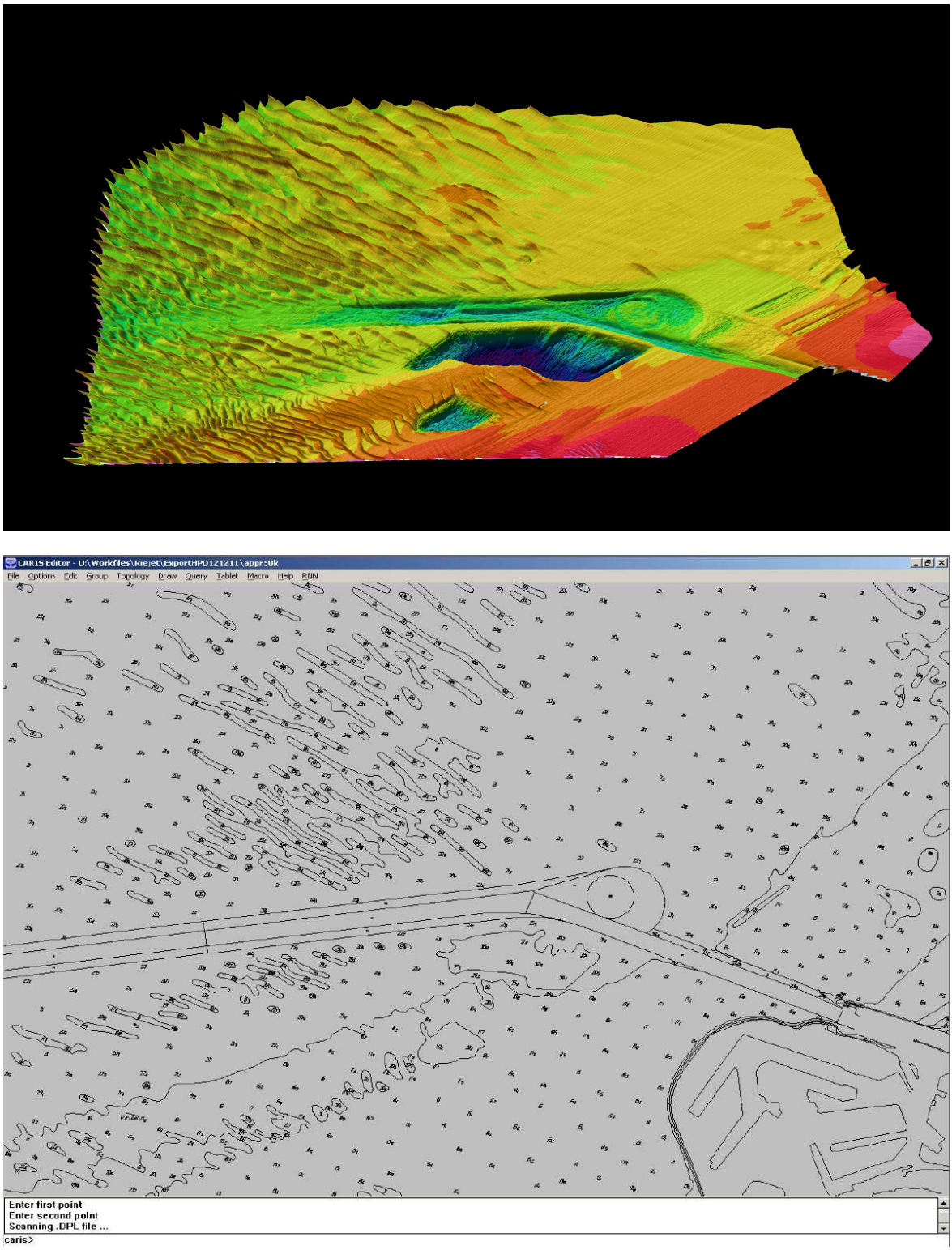

Figure 2. Bathymetry of the approach area to the Port of Rotterdam in the database of the Netherlands Hydrographic Service: digital terrain model (top) and isolines (bottom). Notice the presence of the sand pits. The isolines will be published in new chart editions expected in the Summer of 2013. (figure courtesy of Data processing department, Netherlands Hydrographic Service)

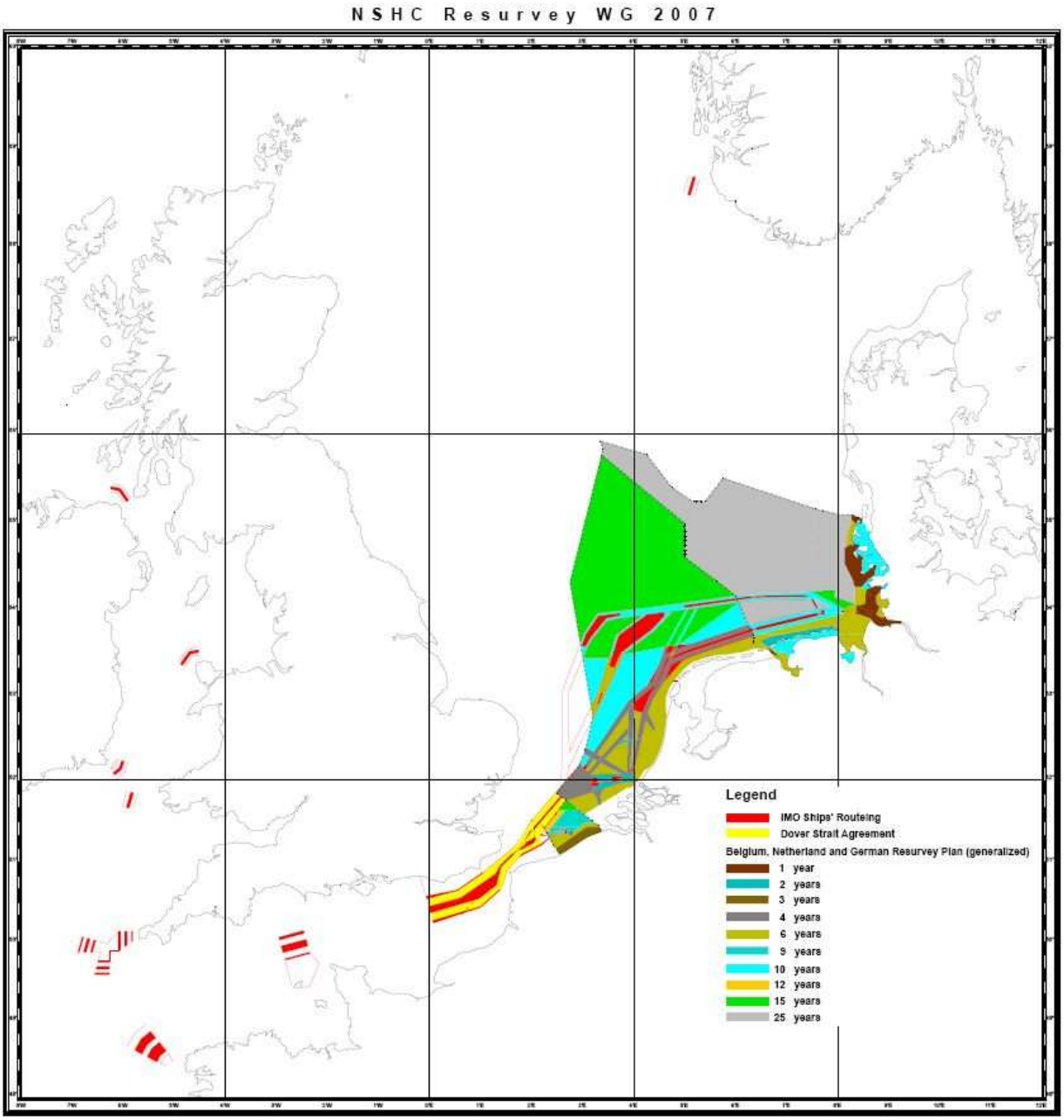

Figure 3. Resurvey prioritization map of the NSHC Resurvey Working Group. (figure courtesy of BSH)

Modelling sediment pick-up and deposition in a dune model

Olav J.M. van Duin [(1)], J.S. Ribberink [(1)], C.M. Dohmen-Janssen [(1)], S.J.M.H. Hulscher [(1)]

1. University of Twente, Enschede, The Netherlands – o.j.m.vanduin@utwente.nl

Abstract
Often river bed form modelling is done with an equilibrium bed load transport formula like that of Meyer-Peter & Müller (1948). However, a physically more correct way would be to model it with separate models for the sediment pick-up and deposition processes as described by Nakagawa & Tsujimoto (1980). Besides the physics of the sediment transport itself, using such a method allows for the modelling of higher-order processes as well like spatial lag in bed load transport.
As shown by Shimizu et al. (2009) applying the aforementioned pick-up and deposition model in a dune evolution model, makes is possible to model dunes well. Specifically it made it possible to determine a transition to upper stage plane beds, as well as capturing hysteresis well.
In this paper we will explore the effect of using different kinds of bed load models in a relatively simple dune evolution model. The Nakagawa & Tsujimoto (1980) bed load model, will be implemented in the dune evolution model of Paarlberg et al. (2009). Results of this model version will be compared with the original version (using the Meyer-Peter & Müller formula) and a later version that directly models spatial lag with a relaxation equation.

1. INTRODUCTION

Hydraulic roughness values play an important role in correctly determining water levels (Casas et al., 2006; Vidal et al., 2007; Morvan et al., 2008), which is critical for flood management purposes.
River dunes increase the hydraulic roughness significantly, because their shape causes form drag. Water level forecasts during a high river water discharge therefore depend on accurate predictions of the evolution of river dune dimensions.
In the past, many approaches have been used to model dune dimensions, varying from equilibrium dune height predictors (e.g. Yalin, 1964; Allen, 1978; Van Rijn, 1984) to different forms of stability analyses (e.g. Kennedy, 1963; Engelund, 1970; Fredsøe, 1974; Yamaguchi & Izumi, 2002). Recently, models have been developed that calculate the turbulent flow field over bedforms, in some cases in combination with morphological computations (e.g. Nelson et al., 2005; Tjerry & Fredsøe, 2005; Shimizu et al., 2009; Nabi et al., 2010). These models are valuable to study detailed hydrodynamic processes, but are computationally intensive.

To be able to efficiently predict dune dimensions over the time-scale of a flood wave Paarlberg et al. (2009) developed a model in which the flow and sediment transport at the flow separation zone is parameterized instead of using complex hydrodynamic equations. This model is able to predict the evolution of dunes from small initial disturbances up to equilibrium dimensions with limited computational time. In addition, this model has been coupled with an existing hydraulic model to form a 'dynamic roughness model' (Paarlberg et al., 2010). Results are promising, as the coupled model clearly shows the expected hysteresis effects in dune roughness and water levels and different behaviour of sharp-peaked versus broad-peaked flood waves (Paarlberg et al., 2010).
Paarlberg et al. (2009) assume that equilibrium between shear stress and transport is present, so the formula devised by Meyer-Peter and Müller (1948) is used. As Nakagawa & Tsujimoto (1980) argue, a lag distance between flow properties (and thereby bed shear stress) and sediment transport is the principal cause of bed instability and thereby regime transitions. They further identify two sources of this lag distance. The first is the spatial distribution of bed shear stress, which is handled in the Paarlberg et al. (2009) model by applying the transport formula to the local bed shear stress. The second is the probability distribution of sediment particle step length, which is the distance travelled from dislodgement to rest according to Einstein (1950). This effect is not taken into account in the bed load formulation of the original model.

To be able to model the latter effect with bed load transport, the Paarlberg et al. (2009) model is first extended with a linear relaxation equation applied on the Meyer-Peter and Müller (1948) transport, and secondly with the pick-up and deposition model of Nakagawa & Tsujimoto (1980). This bed load formula is also used in the model of Shimizu et al. (2009), with good results. The pick-up is determined from local bed shear stress. The sediment is deposited from the pick-up point with a distribution function, which uses a mean step length, exponentially decreasing with distance. By handling the transport like this a lag distance between shear stress and sediment transport is introduced.
The effects on bed morphologies and development characteristics of using the non-equilibrium transport relations versus the previous equilibrium transport relation will be explored. Different values of step length are used to see how it influences the results. It is expected that the dune shape will differ significantly between versions of the model due to the introduction of spatial lag with the two new model versions. This should improve the predictions of the model for future applications, as this lag is one of the causes of bed instabilities, and thereby controls transitions between bed form regimes.

2. MODEL SET-UP

1.1 General set-up

The basis of the present model is the dune evolution model developed by Paarlberg et al. (2009). Paarlberg et al. (2009) extended the process-based morphodynamic sand wave model of Németh et al. (2006) , which is based on the numerical model of Hulscher (1996), with a parameterization of flow separation, to enable simulation of finite amplitude river dune evolution.

Figure 1. Schematization of a dune (flow left to right)

Flow separation is forced in the model when the leeside slope exceeds 10°. The form of the flow separation zone (see Figure 1) behind the dune and the effect it has on flow, bed shear stress distribution and the sediment transport is included in a parameterized way using experimental data of turbulent flow over two-dimensional subaqueous bedforms (Paarlberg et al. 2007). In the flow separation zone the bed shear stress is assumed to be zero and all the sand transport that reaches the crest of the dune is avalanched under the angle of repose on the leeside of the dune (Paarlberg et al., 2009). This enables the model to predict river dunes with their characteristic shape and realistic dimensions without resolving the complex recirculating flow in the flow separation zone and remaining computationally cheap.
The model consists of a flow module, a sediment transport module and a bed evolution module which operate in a decoupled way. The model simulates a single dune which is assumed to be in an infinite train of identical dunes. Therefore periodic boundary conditions are used. The domain length and thereby dune length is forced by either using the simple relation Van Rijn (1984) found or using a numerical stability analysis as the original model by Paarlberg et al. (2009) does. In the first case the dune length is seven times the water depth, a reasonable approximation of the values Julien & Klaassen (1995) find, namely 7.3 and 2π times the water depth. In the latter case the length of the fastest growing disturbance is determined during simulation. Only the first approach will be used in this paper.

1.2 Flow model

In general the flow is forced by the difference in water level across the domain. Though the water depth at the start and end of domain are the same due to the periodic boundary conditions, the water level differs because the domain is sloped. The average bed level is taken as zero but has a slope (this average bed slope is an input parameter for the model). By solving the flow equations with a certain average water depth a discharge is found. The average water depth is adjusted until this discharge matches the discharge given as input.

1.2.1 Governing equations

The flow in the model of Paarlberg et al. (2009) is described by the two-dimensional shallow water equations in a vertical plane (2-DV), assuming hydrostatic pressure conditions. For small Froude numbers the momentum equation in vertical direction reduces to the hydrostatic pressure

condition, and that the time variations in the horizontal momentum equation can be dropped. The governing model equations that result are shown in equations (1) and (2).

$$u\frac{\partial u}{\partial x}+w\frac{\partial u}{\partial z}=-g\frac{\partial \zeta}{\partial x}+A_v\frac{\partial^2 u}{\partial z^2}+gi \tag{1}$$

$$\frac{\partial u}{\partial x}+\frac{\partial w}{\partial z}=0 \tag{2}$$

The velocities in the x and z directions are u and w, respectively. The water surface elevation is denoted by ζ, i is the average channel slope, and g and A_v denote the acceleration due to gravity and the vertical eddy viscosity respectively.

1.2.2 Boundary conditions

The boundary conditions are defined at the water surface (z=h) and at the bed ($z=z_b$). The boundary conditions at the water surface are (3) no flow through the surface and (4) no shear stress at the surface. The kinematic boundary condition at the bed is (5) that there is no flow through the bed.

$$\left.\frac{\partial u}{\partial z}\right|_{z=h}=0 \tag{3}$$

$$\left.u\frac{\partial \zeta}{\partial x}\right|_{z=h}=w \tag{4}$$

$$\left.u\frac{\partial z_b}{\partial x}\right|_{z=z_b}=w \tag{5}$$

As basic turbulence closure, a time- and depth-independent eddy viscosity is assumed, leading to a parabolic velocity profile. In order to represent the bed shear stress correctly for a constant eddy viscosity, a partial slip condition at the bed (6) is necessary.

$$\tau_b=\left.A_v\frac{\partial u}{\partial z}\right|_{z=z_b}=Su_b \tag{6}$$

In this equation τ_b (m^2/s^2) is the volumetric bed shear stress and the resistance parameter S (m/s) controls the resistance at the bed. For more details about the model equations and numerical solution procedure, reference is made to Paarlberg et al. (2009), Van den Berg and Van Damme (2005), and Van den Berg (2007).

1.3 Bed load transport model

For this work we compare three versions of the bed load model : the original, a later version with spatial lag via a relaxation equation, and a new version with the Nakagawa & Tsujimoto (1980) pick-up and deposition model. These three versions are explained in the next paragraphs.

1.3.1 Equilibrium transport model

In the original dune evolution model equilibrium bed load transport is taken into account. This is calculated by applying the formula of Meyer-Peter and Müller (1948) including gravitational bed slope effects. Below this formula is given in dimensional form (as volumetric bed load transport per unit width, m^2/s):

$$q_{b;e}=\begin{cases}\beta\left(\tau_b(x)-\tau_c(x)\right)^n\left(1+\eta\dfrac{\partial z_b}{\partial x}\right)^{-1} & \text{if} \quad \tau>\tau_c \\ 0 & \text{if} \quad \tau\le\tau_c\end{cases} \tag{7}$$

where $\tau_c(x)$ is the local critical (volumetric) bed shear stress (m^2/s^2), n=3/2 and $\eta=\tan(\varphi)^{-1}$ with the angle of repose φ=30°. The proportionality constant β (s^2/m) describes how efficiently the sand particles are transported by the bed shear stress (Van Rijn, 1993) and its value can be estimated with

$$\beta=\frac{m}{\Delta g} \tag{8}$$

where $\Delta=\rho_s/\rho-1=1.65$ (ρ_s/ρ is the specific grain density), and m is an empirical coefficient which is set to 4 by Paarlberg et al. (2009) based on analysis done by Wong and Parker (2006). The local, critical bed shear stress $\tau_c(x)$, corrected for bed slope effects, is given by the following equation:

$$\tau_c(x)=\tau_{c0}\frac{1+\dfrac{\partial z_b}{\partial x}}{\sqrt{1+\left(\dfrac{\partial z_b}{\partial x}\right)^2}} \tag{9}$$

with τ_{c0} the critical bed shear stress for flat bed, defined by equation (10). In this equation θ_{c0} is the critical Shields parameter and D_{50} is the median grain size.

$$\tau_{c0} = \theta_{c0} g \Delta D_{50} \tag{10}$$

1.3.2 Linear relaxation of transport

Here the model differs from the model presented by Paarlberg et al. (2009). Instead of calculating the equilibrium transport (see previous paragraph) and taking that as the actual transport, the following relation is applied:

$$\frac{dq_b}{dx} = \frac{q_{b;e} - q_b}{\Lambda} \tag{11}$$

where q_b is the actual sediment transport and Λ is the mean step length. This is determined by:

$$\Lambda = \alpha D_{50} \tag{12}$$

where α is the non-dimensional step length (as used by Nakagawa & Tsujimoto, 1980). It should be noted that equation 11 needs a boundary condition (at x=0) whereas only a periodic boundary condition is defined. Therefore a value is guessed for x=0 and the rest of the values are determined using equation 11 and a backwards Euler scheme. The value at the end of the domain should be the same as the value at x=0, if this is not the case a new guess is made. This process is repeated until a satisfactory result is found (i.e. when the periodic boundary condition is met).

1.3.3 Pick-up and deposition model

The pick-up and deposition model of Nakagawa & Tsujimoto (1980) uses the following formulae to determine bed load transport. Pick-up of sediment (probability of a particle being picked up in s^{-1}) is determined by

$$p_s(x) = F_0 \sqrt{\frac{\Delta g}{D_{50}}} \tau_*(x) \left(1 - \frac{\tau_{*_c}}{\tau_*(x)}\right)^3 \tag{13}$$

where F_0=0.03. Deposition at a location is determined by summing the sediment that arrives at that location. So, to determine the deposition at a certain location *x* the distribution of picked up sediment from upstream locations is needed. The determination of deposition is done by applying the following formula:

$$p_d(x) = \int_0^\infty p_s(x-s) f(s) ds \tag{14}$$

where the distribution *f(s)* determines the fraction of sediment that is deposited a distance s away from the pick-up point *(x-s)*. The distribution function is defined as follows:

$$f(s) = \frac{1}{\Lambda} \exp\left(\frac{-s}{\Lambda}\right) \tag{15}$$

where λ is the step length. By using this function, all the sediment that has been picked up at certain location is deposited between that location and 5 times the step length in downstream direction. Finally the transport gradient is determined as follows:

$$\frac{dq_b(x)}{dx} = D_{50}\left[p_s(x) - p_d(x)\right] \tag{16}$$

1.4 Step length

Francis (1973), Fernandez Luque & Van Beek (1976) and Sekine & Kikkawa (1984) have done experiments to determine the dependence of particle velocity on various parameters under flat bed conditions. The latter authors have used this data to verify a numerical model of saltation of particles (Sekine & Kikkawa, 1992). All computed values are no more than two times larger or smaller than the observed values.

Their model further shows that the mean step length can vary between near zero and about 350 times the particle diameter, mostly dependent on friction velocity (positively) and settling velocity (negatively). The data shows a range of approximately 40 to 240 times the particle diameter. For this paper the step length will therefore be varied between 25 and 300 times the particle diameter, to get an idea of how sensitivite the results are to this parameter.

1.5 Bed evolution

The bed evolution is modelled using the Exner equation given by (17), where the sediment transport rate is calculated with one of the three options and ε_p=0.4 is the bed porosity.

$$\left(1-\varepsilon_p\right)\frac{\partial z_b}{\partial t}=-\frac{\partial q_b}{\partial x} \qquad (17)$$

It should be noted that in the case of flow separation this equation is only applied outside the flow separation zone. In the separation zone the bed transport at the crest of the dune is deposited on the leeside of the slope under the angle of repose (i.e. avalanched). So, an integral form of equation is used for the lee slope of the dune.

3. RESULTS

The reference case used for this study is an experiment done by Venditti et al. (2005). The relevant parameters can be found in the table below.

h_i [m]	0.152
i [10^{-4}]	12
q [m^2/s]	0.077
D_{50} [mm]	0.5
l_e [m]	1.3172
Δ_e [m]	0.048
h_e [m]	0.17
$\theta_{c;0}$ [-]	0.050

Table 1. Used parameters

New parameters in this table are h_i (initial water depth), q (discharge per unit width), l_e (equilibrium dune length), Δ_e (equilibrium dune height) and h_e (equilibrium water depth).

1.6 Results with the original bed load model

Using the original bed load model, Meyer-Peter and Müller (1948), an equilibrium dune height of 0.064m, dune length of 1.33m and water depth of 0.19m are found. The dune length is predicted well (the experimental result was 1.32m), but the dune height is overestimated by about 25%. The resulting water depth is reasonably close to the experimental result of 0.17m. In figure 2 the evolution of the dune shape is shown.

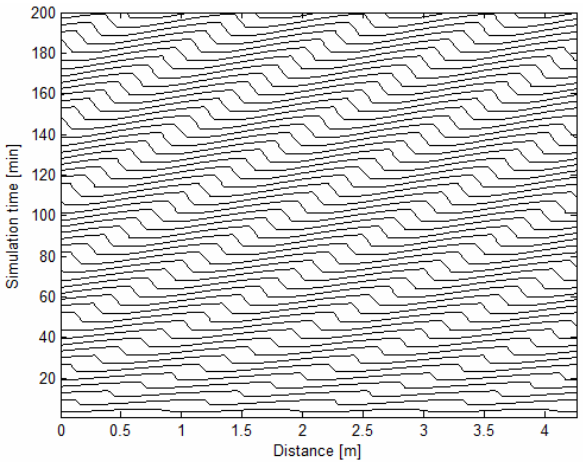

Figure 2. Dunes of the original model (flow left to right)

It should be noted that this figure is obtained by plotting the resulting single dune as a train of four identical dunes to make the results more clear.

1.7 Results with linear relaxation

Using the original bed load model, but with an additional forcing of spatial lag with a relaxation equation the following is found.

α [-]	Δ_e [m]	l_e [m]	h_e [m]
[original]	0.064	1.33	0.19
25	0.029	1.11	0.16
50	0.023	1.10	0.16
75	0.000	1.07	0.15
100	0.000	1.07	0.15

Table 2. Linear relaxation results.

As can be seen applying spatial lag in this way leads to a very strong suppression of the dune height and length. The first is because the spatial lag decreases the total transport and the lee side angle, and no more flow separation occurs. This severely limits the dune growth, leading to these very small dunes. The less steep dunes of limited height are shown in figure 3, presenting the bed morphology with a non-dimensional step length of 25.

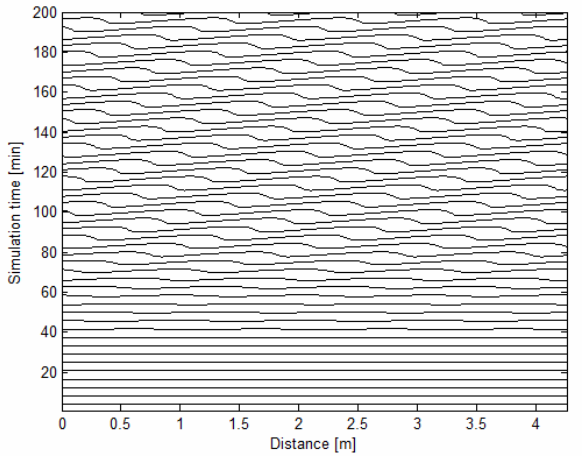

Figure 3. Dunes of the model with linear relaxation, α=25 (flow left to right)

With a stronger lag (non-dimensional step length of 75 and greater) this 'smearing' effect is so strong that no more dune growth occurs at all. This is similar to what would occur when going towards an upper stage plane bed, where the bed washes out. Because the dune height is small, there is less hydraulic roughness so the water depth is limited as well. The dune length directly follows from this, so that remains small as well.

As presented at RCEM 2011, the authors found that this same analysis but then with the dune length selected by a stability analysis (see Paarlberg et al., 2009) led to different results. The dune height was still supressed, but not so strong as presented here (Van Duin et al, 2011). For higher values of the non-dimensional step length dunes kept appearing as opposed to now. Interestingly the dune *length* was not supressed at all, and greatly increased for larger values of the step length. During the selection for dune length, the transport with linear relaxation was used to determine which dune length lead to the strongest growth, and that method selected progressively longer dunes up until values of 200 for the non-dimensional step length before decreasing again. This interplay between the selected dune length and the introduced spatial lag is not fully understood (Van Duin et al, 2011), but should be taken into account in further model development.

1.8 Results with pick-up and deposition

Using the pick-up and deposition model of Nakagawa & Tsujimoto (1980) as the bed load model, the following is found.

α [-]	Δ_e [m]	l_e [m]	h_e [m]
25	0.067	1.33	0.19
50	0.066	1.33	0.19
75	0.064	1.32	0.19
100	0.067	1.33	0.19
150	0.069	1.34	0.19
200	0.070	1.35	0.19
250	0.076	1.39	0.20
300	0.079	1.41	0.20

Table 3. Pick-up and deposition results.

Against expectation, the water depth and thereby dune length are very similar to the experimental and original model results. The dune height is still too high compared to the experimental results, but very near the original model. This at least shows that the new bed load formula still performs reasonably well.

With the linear relaxation method dune height was suppressed strongly, and now it is not. This is because with linear relaxation the transport was greatly reduced, while now it is still about as high as with the original model. Flow separation still occurs, and so all in all the dune is able to grow like it did with the original model. Even larger values for the non-dimensional step length don't lead to decreasing dune growth as it did with linear relaxation but actually *increasing* dune growth. With increasing step length in this model version, sediment is spread over a larger distance, so more sediment actually reaches the crest. Because flow separation still occurs, all the sediment that reaches the crest is avalanched there instead of being spread out over the lee side and trough as happened with linear relaxation.

The final resulting dune shape with a non-dimensional step length of 25 can be seen in figure 4.

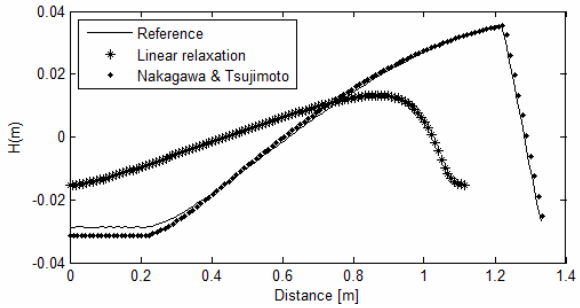

Figure 4. Dune shapes of the three versions, with α=25 for linear relaxation and pick-up and deposition (flow left to right)

It is clear that it is very similar to the result with the original model version but strongly differs from the linear relaxation result. While by itself it is promising that the model still performs well, it was expected that the dune shape would differ significantly from the original version. Had this been the case, it would signal that the model should be able to handle transitions to other regimes better because it allows for more different dune morphologies. Now, it is not known whether this is improved so further research is needed. It is likely that a non-constant step length will lead to more different results and a better prediction of transitions, as the model of Shimizu et al. (2009) has shown.

4. CONCLUSIONS

This paper has shown how a computationally cheap dune evolution model depends on the bed load transport formulation used. With the equilibrium transport formula of Meyer-Peter and Müller (1948) the results are reasonable, though the dune height is overestimated. Applying a linear relaxation equation introduces a spatial lag equal to the step length, and leads to a strong suppression of dune height and length. This is so strong that for a higher step length no more dunes form.
Using the Nakagawa & Tsujimoto (1980) pick-up and deposition model the results are very similar to the original version. By itself it is promising that the model still performs well, it was expected that the dune shape would differ significantly. It is likely that using a non-constant step length will lead to different and better results with regards to regime transitions.

5. FUTURE WORK

The model will be further refined by improving the relation between bed shear stress and the step length of transported material. For this the conceptual model of Shimizu et al. (2009), a step length model for flat bed (Sekine & Kikkawa, 1992) and a formulation that depends on the transport parameter by van Rijn (1984) will be tested. Also, experiments have been undertaken by the authors regarding step length. With this knowledge and the different step length models the model will be improved further.

6. ACKNOWLEDGMENT

This study is carried out as part of the project 'BedFormFlood', supported by the Technology Foundation STW, the applied science division of NWO and the technology programme of the Ministry of Economic Affairs.

7. REFERENCES

Allen, J.R.L. (1978). Computational methods for dune time-lag: Calculations using Stein's rule for dune height. Sedimentary Geology, 20(3), pp. 165-216.

Casas, A., G. Benito, V.R. Thorndycraft, M. Rico (2006). The topographic data source of digital terrain models as a key element in the accuracy of hydraulic flood modelling. Earth Surface Processes and Land Forms, 31, pp. 444-456.

Einstein, H.A. (1950). The bed load function for sediment transportation in open channel flows. Technical bulletin, No. 1026, U.S. Department of Agriculture, Soil Conservation Service.

Engelund, F. (1970). Instability of erodible beds. Journal of Fluid Mechanics, 42, pp. 225-244.

Fernandez Luque, R. and R. Van Beek (1976). Erosion and transport of bed sediment. Journal of hydraulic research, 14 (2), pp. 127-144.

Francis, J.R.D. (1973). Experiment on the motion of solitary grains along the bed of a water stream. Proceedings of the Royal Society of London, A332, pp. 443-471.

Fredsøe, J. 1974. On the development of dunes in erodible channels. Journal of Fluid Mechanics, 64, pp. 1-16.

Hulscher, S.J.M.H. (1996). Tidal-induced large-scale regular bedform patterns in a three-dimensional shallow water model. Journal of Geophysical Research, 101, pp. 20,727–20,744.

Julien, P.Y. and G.J. Klaassen, 1995. Sand-dune geometry of large rivers during floods. J. Hydr. Eng, Vol. 121, No. 9, pp. 657-663.

Kennedy, J.F. (1963). The mechanics of dunes and antidunes in erodible-bed channels. Journal of Fluid Mechanics, 16, pp. 521-544.

Meyer-Peter, E. and R. Müller (1948). Formulas for bed-load transport. Proceedings of the 2nd IAHR congress, Vol. 2, pp. 39–64.

Morvan, H., D. Knight, N. Wright, X. Tang, A. Crossley (2008). The concept of roughness in fluvial hydraulics and its formulation in 1D, 2D and 3D numerical simulation models. Journal of Hydraulic Research, 46(2), pp. 191-208.

Nabi, M., H.J. De Vriend, E. Mosselman, C.J. Sloff, Y. Shimizu (2010) – Simulation of subaqueous dunes using detailed hydrodynamics. River, Coastal and Estuarine Morphodynamics: RCEM 2009.

Nakagawa, H. & T. Tsujimoto (1980). Sand bed instability due to bed load motion. Journal of the Hydraulics Division, 106(12), pp. 2029-2051.

Nelson, J.M., A.R. Burman, Y. Shimizu, S.R. McLean, R.L. Shreve, M. Schmeeckle (2005). Computing flow and sediment transport over bedforms. River, Coastal and Estuarine Morphodynamics: RCEM 2005, 2, pp. 861–872.

Németh, A.A., S.J.M.H. Hulscher, R.M.J. Van Damme (2006). Simulating offshore sand waves. Coastal Engineering, 53, pp. 265–275.

Paarlberg, A.J., C.M. Dohmen-Janssen, S.J.M.H. Hulscher, P. Termes (2007). A parameterization of flow separation over subaqueous dunes. Water Resource Research, 43.

Paarlberg, A.J., C.M. Dohmen-Janssen, S.J.M.H. Hulscher, and A.P.P. Termes (2009). Modelling river dune evolution using a parameterization of flow separation. Journal of Geophysical Research. Pt. F: Earth surface, 114.

Paarlberg, A.J., C.M. Dohmen-Janssen, S.J.M.H. Hulscher, P. Termes, R. Schielen (2010). Modelling the effect of time-dependent River dune evolution on bed roughness and stage. Earth Surfaces Processes and Landforms, 35, pp. 1854-1866.

Sekine, M., and H. Kikkawa (1984). Transportation mechanism of bed-load inan open channel. Proceedings of the Japanese Society of Civil Engineering., 351, pp. 69-75 (in Japanese).

Sekine, M., and H. Kikkawa (1992). Mechanics of Saltating Grains II. Journal of Hydraulic Engineering, ASCE, 118 (4), pp. 536-558.

Shimizu, Y., S. Giri, I. Yamaguchi, J. Nelson (2009). Numerical simulation of dune-flat bed transition and stage-discharge relationship with hysteresis effect. Water Resources Research, 45.

Tjerry, S. & J. Fredsøe (2005). Calculation of dune morphology. Journal of Geophysical Research - Earth Surface, 110.

Van den Berg, J. (2007). Non-linear sand wave evolution. PhD thesis, University of Twente, the Netherlands.

Van den Berg, J. & R. Van Damme (2005). Sand wave simulation on large domains. River, Coastal and Estuarine Morphodynamics: RCEM 2005, 2, pp. 991–997.

Van Duin, O.J.M., J.S. Ribberink, C.M. Dohmen-Janssen and S.J.M.H. Hulscher. (2011). Modelling non-equilibrium bed load in a parameterized dune evolution model. In Shao, X., Z. Wang and G. Wang (Ed.), Proceedings of the 7th IAHR Symposium on River, Coastal and Estuarine Morphodynamics. Beijing, China: Tsinghua University Press.

Van Rijn, L.C. (1984). Sediment transport part III: Bedforms and alluvial roughness. Journal of Hydraulic Engineering, ASCE, 110(12), pp. 1733-1754.

Van Rijn L.C. (1993). Principles of Sediment Transport in Rivers, Estuaries and Coastal Seas. AQUA: Amsterdam.

Vidal, J.-P., S. Moisan, J.-B. Faure, D. Dartus (2007). River model calibration, from guidelines to operational support tools. Environmental Modelling & Software, 22, pp. 1628–1640.

Wong, M. & G. Parker (2006). Reanalysis and correction of bed-load relation of Meyer-Peter and Müller using their own database. Journal of Hydraulic Engineering, 132 (11), pp. 1159–1168.

Yalin, M.S. (1964). Geometrical properties of sand waves. Journal of the Hydraulic Division, ASCE, 90(5).

Yamaguchi, S. & N. Izumi (2002). Weakly nonlinear stability analysis of dune formation. Proceedings of River Flow 2002, pp. 843-850.

Numerical simulation of turbulent sediment transport

O. Durán [(1)], B. Andreotti [(2)], P. Claudin [(2)]

1. Laboratoire de Physique et Mécanique des Milieux Hétérogènes (PMMH), UMR 7636 CNRS ESPCI - Univ. Paris Diderot - Univ. P.M. Curie, 10 Rue Vauquelin, 75005 Paris, France – philippe.claudin@espci.fr
2. Department of Geological Sciences, Univ. North Carolina, 104 South Rd. Mitchell Hall, Campus Box 3315, Chapel Hill, North Carolina 27515, USA

Abstract

Sediment transport is studied by means of two phase numerical simulations based on a discrete element method for particles coupled to a continuum Reynolds averaged description of hydrodynamics.. We analyse the mechanisms at the grain scale in the case of bed load, in order to give support to empirical transport laws. The vertical velocities of the grains are small and sediment transport occurs in a thin layer at the surface of the static bed. Steady, or `saturated' transport is reached when the fluid borne shear stress at the interface between the mobile grains and the static grains is reduced to its threshold value. The number of grains transported per unit surface is therefore limited by the flux of horizontal momentum towards the surface. However, the fluid velocity in the transport layer remains almost undisturbed so that the mean grain velocity scales with the fluid shear velocity u_*, eventually leading to a sediment flux scaling with the third power of u_*. The influence of the grain to fluid density ratio is systematically studied to reveal the transition between sub-aqueous bedload and aeolian saltation, for which the transport law has a different scaling with u_*. Based on the mechanisms identified in the steady case, we discuss the transient of saturation of sediment transport and in particular the saturation time and length. Finally, we investigate the exchange of particles between the mobile and static phases and we determine the exchange time of particles.

1. INTRODUCTION

Despite a wide literature, some fundamental aspects of sediment transport in turbulent flows are still only partly understood. In particular, derivations of transport laws, relating the sediment flux to the flow velocity, have a strong empirical or semi-empirical basis (see e.g. among many others Meyer-Peter and Muller (1948), Ribberink (1998), Camemen and Larson (2005), Greeley et al. (1996), Iversen and Rasmussen (1999), Kok and Renno (2009) and references therein), thus lacking more physics-related inputs. Also, the dynamical mechanisms limiting sediment transport, in particular the role of the bed disorder (Charru, 2006) and turbulent fluctuations (Marchioli et al., 2006; Baas, 2008; Le Louvetel-Poilly et al., 2009), remain matter of discussion.

Here we investigate the properties of steady homogeneous sediment transport using a novel numerical description of particle-laden flows, using two-phase numerical simulations based on a discrete element method for particles coupled to a continuum Reynolds averaged description of hydrodynamics. In particular, we examine the transition from bed-load to saltation by studying the influence of the grain to fluid density ratio ρ_p/ρ_f. A similar approach has recently been used to study the onset of aeolian saltation (Carneiro et al., 2011). The present paper summarizes the MARID presentation. More details on this work, as well as a more developed bibliography on the subject, can be found in Durán et al. (2012).

2. THE MODEL

The idea is to use a continuum description of hydrodynamics, averaged at a scale larger than the grain size. This means that the feedback of the particles on the flow is treated in the mean field manner. This method allows us to perform very long numerical simulations (typically $1000\sqrt{d/g}$), using a (quasi) 2D large spatial domain (typically 15000 spherical grains in a xyz box of respective dimensions $1000d \times 1d \times 1000d$), while keeping the complexity of the granular phase. Periodic boundary conditions are used in the x (flow) direction. We will now detail the different ingredients of the model - see table 1 for notations.

General:	length l	d
	acceleration	g
	time t	$\sqrt{d/g}$
	velocity v	$\sqrt{gd}$
Particles:	angular velocity ω	$\sqrt{g/d}$
	mass m	$\frac{\pi}{6}\rho_p d^3$
	moment of inertia I	md^2
	force f	mg
	contact stiffness k	mg/d
	damping constant γ	$m\sqrt{g/d}$
Fluid:	shear stress τ	$(\rho_p-\rho_f)gd$

Table 1: Units used in the model, expressed in terms of the grain density (ρ_p), the fluid density (ρ_f), the gravity (g) and the mean grain diameter (d).

2.1 Forces on particles

The grains have a spherical shape and are described by their position vector $\vec{r}$, velocity $\vec{u}$ and angular velocity $\vec{\omega}$. A given grain labelled p inside a fluid obeys the equations of motion,

$$\begin{aligned} m\frac{d\vec{u}^p}{dt} &= m\vec{g}+\sum_q \vec{f}^{p,q}+\vec{f}^p_{fluid} \\ I\frac{d\vec{\omega}^p}{dt} &= \frac{d}{2}\sum_q \vec{n}^{p,q}\times\vec{f}^{p,q} \end{aligned} \quad (1)$$

where $\vec{g}$ is the gravity acceleration, $I=md^2/10$ is the moment of inertia of a sphere, $\vec{f}^{p,q}$ is the contact force with grain q, $\vec{n}^{p,q}$ is the contact direction, and $\vec{f}^p_{fluid}$ encodes forces of hydrodynamical origin.

We model the contact forces following a standard approach for the modeling of contact forces in MD codes (see e.g. DEM book (2011) and references therein), where normal and tangential components are described by spring dash-pot elements. A microscopic friction coefficient is also introduced. For simplicity we assume that the net hydrodynamical force ($\vec{f}^p_{fluid}$) acting on a grain p due to the presence of the fluid is dominated by the drag and Archimedes forces, $\vec{f}^p_{drag}$ and $\vec{f}^p_{Arch}$, respectively. The lift force, lubrication forces and the corrections to the drag force (Basset, added-mass, Magnus, etc.) are neglected.

Drag force — We hypothesize here that the drag force exerted by a homogeneous fluid on a moving grain only depends on the difference between the grain velocity $\vec{u}^p(x,z)$ and the fluid velocity $\vec{u}(z)$ at grain's height z. Introducing the particle Reynolds number R_u based on this fluid-particle velocity difference $R_u=|\vec{u}-\vec{u}^p|d/\nu$, the drag force can be written under the form

$$\vec{f}^p_{drag}=\frac{\pi}{8}\rho_f d^2 C_d(R_u)|\vec{u}-\vec{u}^p|(\vec{u}-\vec{u}^p) \quad (2)$$

where $C_d(R_u)$ is the drag coefficient. We use the following convenient phenomenological approximation (Ferguson and Church, 2004): $C_d(R_u)=[\sqrt{C_d^\infty}+\sqrt{R_u^c/R_u}]^2$, where $C_d^\infty\approx 0.5$, is the drag coefficient of the grain in the turbulent limit ($R_u\to\infty$), and $R_u^c\approx 24$ is the transitional particle Reynolds number above which the drag coefficient becomes almost constant.

Archimedes force — This force results from the stress which would have been exerted on the grain, if the grain had been a fluid. Thus,

$$\vec{f}^p_{Arch}=\frac{\pi}{6}d^3 div\sigma^f \quad (3)$$

where $\pi d^3/6$ is the grain volume and $\sigma^f_{ij}=-p^f\delta_{ij}+\tau^f_{ij}$ is the undisturbed fluid stress tensor (written in terms of the pressure p^f and the shear stress tensor τ^f_{ij}). In first approximation, the stress is evaluated at the center of the grain.

2.2 Hydrodynamics and coupling

In the presence of particles occupying a volume fraction ϕ, the hydrodynamics is described by the two-phase flow Reynolds averaged Navier-Stokes equations:

$$\rho_f(1-\phi)D_t u_i=-\partial_i p^f+\rho_f(1-\phi)g_i+\partial_j\tau^f_{ij}-F_i \quad (4)$$

where $D_t u_i=\partial_t u_i+u_j\partial_j u_i$ denote the fluid inertia. τ^f_{ij} is the total shear stress tensor resulting both from viscous diffusion of momentum (viscous stress) and transport of momentum by turbulent fluctuations (Reynolds stress). $\vec{F}$ is the body force exerted by the grains on the fluid. In the steady and

homogeneous case investigated here, These RANS equations simplify into

$$\partial_z p^f = -\rho_f g \tag{5}$$

$$\partial_z \tau^f = F_x \tag{6}$$

where we note $\tau^f = \tau^f_{xz}$ the fluid shear stress, and later on $u = u_x$ for the fluid horizontal velocity.

The coupling term $\vec{F}$ can then be obtained by averaging the hydrodynamical force $\vec{f}^p_{fluid}$ acting on all the grains moving around altitude z, in a horizontal layer of area A and thickness dz:

$$\vec{F}(z) = \frac{1}{Adz}\left\langle \sum_{p\in\{z;z+dz\}} \vec{f}^p_{fluid} \right\rangle \tag{7}$$

We take for A the total horizontal extent of the domain (i.e. $1000d \times 1d$). The symbols $\langle . \rangle$ denote ensemble averaging. Here, we retain its x-component only, which simplifies into

$$F_x = \frac{\phi}{1-\phi}\left\langle \sum_{p\in\{z;z+dz\}} f^p_{drag,x} \right\rangle / \sum_{p\in\{z;z+dz\}} \frac{\pi}{6} d^3 \tag{8}$$

where the grain's volume fraction ϕ is defined as

$$\phi(z) = \frac{1}{Adz} \sum_{p\in\{z;z+dz\}} \frac{\pi}{6} d^3 \tag{9}$$

Eq 6 integrates as $\tau^f(z) = \rho_f u_*^2 - \tau^p(z)$, where we have introduced the shear velocity u_*, defined by the undisturbed (grain free) wall shear stress, and the grain borne shear stress τ^p, computed from the integration of (8) over sufficient vertical extension to count all moving grains.

In order to relate the fluid borne shear stress to the average fluid velocity field, we adopt a Prandtl-like turbulent closure. Introducing the turbulent mixing length ℓ, we write

$$\tau^f = \rho_f (\nu + \ell^2 |\partial_z u|)\partial_z u \tag{10}$$

ν is the viscosity (a constant independent of the volume fraction). As for the mixing length ℓ, we know it should vanish below some critical Reynolds number R_c and should be equal to the distance to the surface z, far above the transport layer. To avoid the need of a somewhat arbitrary definition of an interface between he static and mobile zones of the bed, we propose the differential equation

$$\nu \partial_z \ell = \kappa \left[1 - e^{\sqrt{\frac{1}{R_c}\left(\frac{u\ell}{\nu}\right)}} \right] \tag{11}$$

where $\kappa \approx 0.4$ is von Karman's constant. In the case of a turbulent flow over a smooth and flat surface (no grains), we recover the prediction computed with the phenomenological expression for the mixing length suggested by van Driest (Pope, 2000), which reproduces well classical experimental results. Comparison to measurements determines the dimensionless parameter $R_c \approx 7$.

Starting integration deep enough in the static bed to be in the asymptotic limit that can be analyticaly derived, we obtain the different hydrodynamical fields. They are displayed in Fig. 1, in the case of sub-aqueous transport ($\rho_p / \rho_f = 2$).

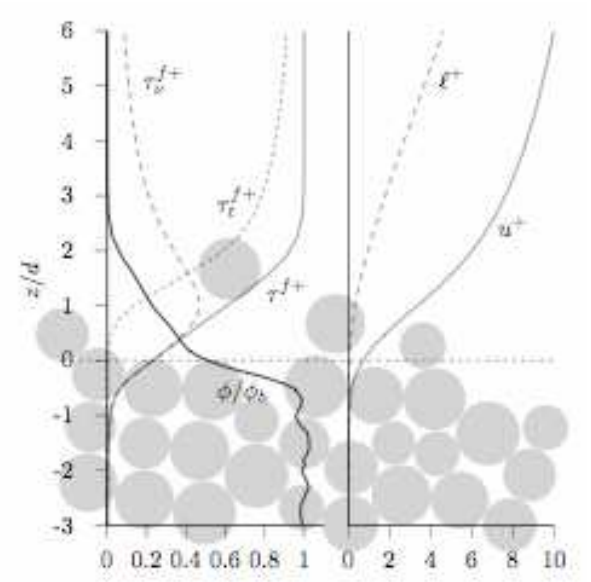

Figure 1. Vertical profiles of the rescaled volume fraction ϕ/ϕ_b, flow velocity $u^+ = u/u_*$, mixing length $\ell^+ = \ell/d$, fluid borne shear stress $\tau^{f+} = \tau^f/(\rho_f u_*^2)$, viscous shear stress $\tau^{f+}_\nu = \nu\partial_z u/u_*^2$ and turbulent shear stress $\tau^{f+}_t = (\ell\partial_z u)^2/u_*^2$ (by definition $\tau^{f+} = \tau^{f+}_\nu + \tau^{f+}_t$). The reference height $z = 0$ is set at the altitude such that $\phi = \phi_b/2$.

3. SEDIMENT FLUX

Steady and homogeneous sediment transport is quantified by the volumetric saturated flux q_{sat}, i.e. the volume of the particles (at the bed density) crossing a vertical surface of unit transverse size per unit time. It has the dimension of a squared length per unit time. In the simulations, we compute it as

$$q_{sat} = \frac{1}{A\phi_b}\frac{\pi}{6}d^3\sum_p u_p \qquad (12)$$

A key issue is the dependence of q_{sat} on the shear velocity or, equivalently, its dimensionless counterpart the Shields number Θ, defined by

$$\Theta = \frac{\rho_f u_*^2}{(\rho_p - \rho_f)gd} \qquad (13)$$

which encodes the strength of the flow.

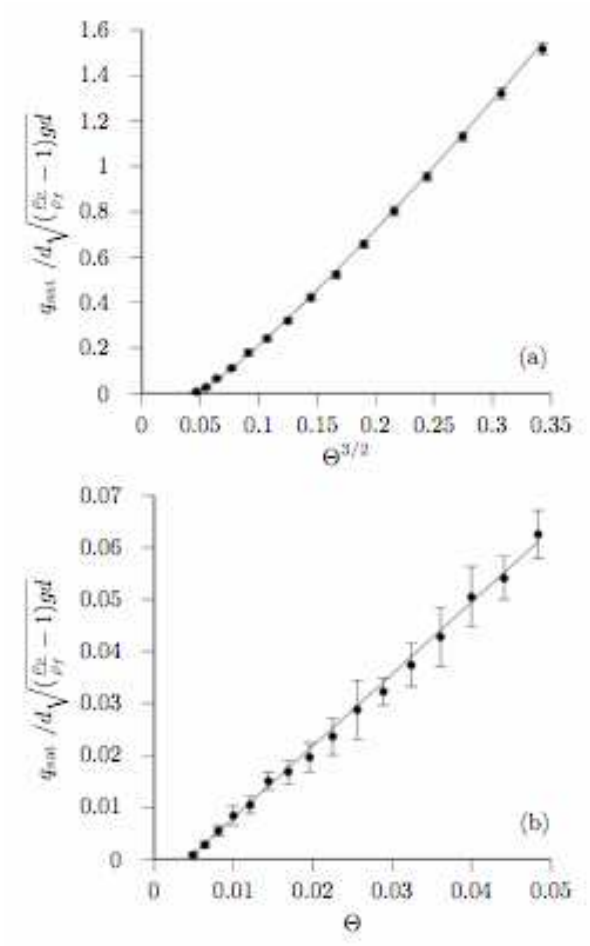

Figure 2. Rescaled saturated flux versus $\Theta^{3/2}$ for water (a) and Θ for air (b). Full lines are the predictions given in the text.

We show in Fig. 2 the saturated flux in both cases (water and air). In agreement with experimental observations (e.g., Meyer-Peter and Muller, 1948; Ribberink, 1998; Lajeunesse et al., 2010; Rasmussen et al., 1996; Creyssels et al., 1009), we find that q_{sat} scales asymptotically as Θ (or u_*^2) for saltation, while q_{sat} scales as $\Theta^{3/2}$ (or u_*^3) underwater. This figure also reveals the existence of a threshold shear velocity below which the flux vanishes. More precisely, we define the dynamical threshold Shield number Θ_d from the extrapolation of the saturated flux curve to 0, which gives in our case $\Theta_d \approx 0.12$ for water ($\rho_p/\rho_f = 2$) and $\Theta_d \approx 0.004$ for air ($\rho_p/\rho_f = 2000$), respectively. These values are consistent with experimental ones within a factor of 2.

4. MECANISMS AT WORK IN THE TRANSPORT LAYER

Bed load and saltation mainly differ by the vertical characteristics of the transport layer. At small density ratios the motion of grains is confined within a thin layer of few grain diameters. By contrast, for large density ratios, grains experience much higher trajectories: the transport layer is much wider and the flux density decreases exponentially with height with a characteristic size of the order of $50d$, roughly independent of the shear velocity. The transport layer thickness is effectively determined by the hop length for $\rho_p/\rho_f > 10$. Below this cross-over value, this thickness is given by the grain diameter d, as trajectories are almost horizontal. The transition from bed load to saltation therefore takes place when the vertical velocities of the particles are sufficiently large for these particles to escape the traps formed by the grains on the static bed.

Another difference between bed load and saltation is how the grain's feedback on the flow is distributed within the steady state transport layer. Fig. 3 presents the vertical profiles of the fluid shear stress, rescaled by the dynamical threshold τ_d (as defined by the saturated flux), for different shear velocities. For bed load (Fig. 3a), the different profiles of the fluid shear stress seems to

converge to the threshold value very close to the surface ($z=0$). In this transport layer, the fluid momentum decays over few grain sizes, in agreement with the vertical extension of the transport layer. By contrast, the fluid shear stress is below the threshold in the bed ($z<0$) but some (weak) transport still occurs there, which is sustained not by the fluid itself but by the momentum transferred to the surface by grain collisions.

This general picture is still valid for saltation (Fig. 3b), however now the dynamical threshold is reached much farther from the surface (at $z \approx 10d$) which implies that the kinetic energy of impacting grains is large enough as to sustain the transport below this height. Above it, the transport is driven by the fluid and most of its momentum is dissipated in a much larger layer (comprising tens of grain diameters) again in agreement with the size of the saltation layer. Notice that although this surface sublayer below $10d$ contains most of the grains, it still represents a small fraction of the overall transport layer.

An important consequence of this distinction in the vertical structure of the grain's feedback is that although for bed load transport is equilibrated when the fluid shear stress reaches its dynamical threshold below the transport layer, this condition is not enough for saltation to equilibrate. For saltation there is a sub-layer where transport is not directly driven by the fluid and thus its equilibration is not dictated by the threshold. There, the properties of grain's collisions become relevant and the equilibrium is described by the conservation of the number of saltating grains i.e. when the number of grains entering the flow exactly balance those grains trapped by the bed.

5. SCALING LAWS

The saturated flux can then be decomposed as the product of the number n of transported grains per unit area by the mean grain horizontal velocity $\overline{u}^p$: $q_{sat} = n\overline{u}^p \pi d^3/(6\phi_b)$. In the numerical simulations, we compute n and $\overline{u}^p$ as

$$n = \frac{\left(\sum_p u_p\right)^2}{A\sum_p u_p^2} \quad \text{and} \quad \overline{u}^p = \frac{\sum_p u_p^2}{\sum_p u_p} \qquad (14)$$

These quantities are plotted as functions of the Schields number in Fig. 4. A scaling law $n \propto \Theta - \Theta_d$ is well verified over two decades, independently of ρ_p/ρ_f. By contrast, the density ratio has a strong effect of $\overline{u}^p$. The mean grain velocity is independent of Θ for large ρ_p/ρ_f (aeolian case), whereas it varies linearly with the fluid shear velocity at low density ratio (sub-aqueous case). Interestingly, $\overline{u}^p$ remains finite at the threshold, at a value independent of ρ_p/ρ_f. These behaviours are in agreement with experimental findings in the case of bedload (Lajeunesse et al., 2010).

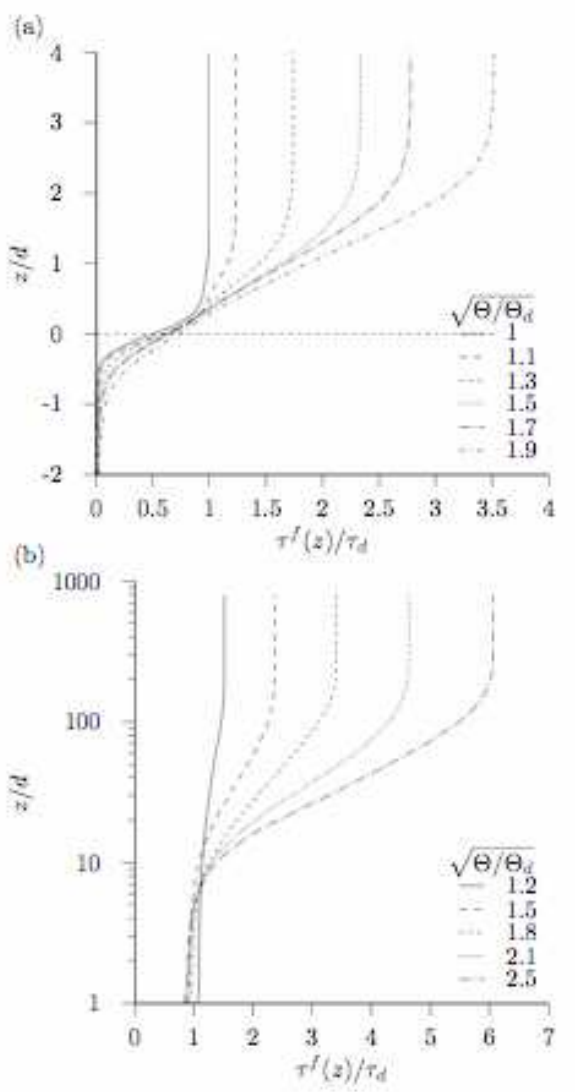

Figure 3. Vertical profiles of the fluid borne shear stress for different values of the shear velocity ratio (see legend), in water (a) and air (b).

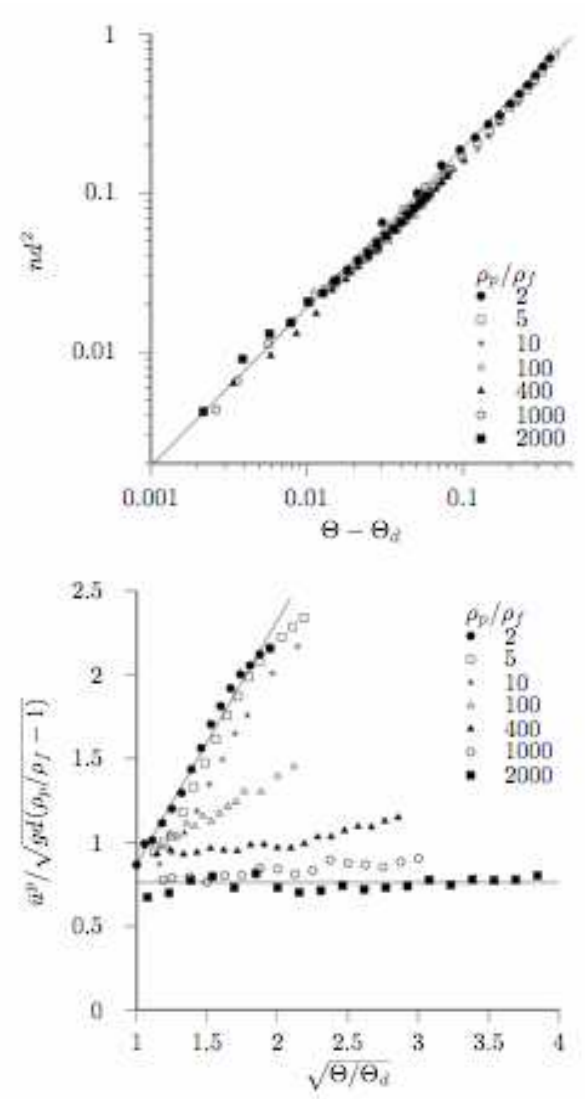

Figure 4. (a) Number of transported grains per unit area and (b) mean velocity of these grains as functions of the Shields number for different values of the density ratio (see legend).

We can derive these scaling laws from simple models. Following Bagnold's (1956) original ideas for the case of bedload, we write the grain born shear stress τ^p as proportional to the moving grain density n and to the drag force f_d acting on a moving grain. As these grains are in steady motion, f_d balances a resistive force due granular friction, collisions with the bed, etc. These different dissipative mechanisms can be modeled as an overall effective friction force characterized by a friction coefficient μ_d, leading to $f_d = \pi/6\mu_d(\rho_p - \rho_f)gd^3$. Saturation is reached when the fluid shear stress equals the transport threshold at the surface of the static bed, i.e. when $\tau^p = \rho_f u_*^2 - \tau_d$, with, by definition, $\tau_d = \Theta_d(\rho_p - \rho_f)gd = \rho_f u_d^2$. As consequence, the number of transported particles per unit area is solely determined by the excess shear stress: $n = (\rho_f u_*^2 - \tau_d)/f_d$. Assuming that the transported grains do not disturb the flow, the flow velocity around grains u must be proportional to the shear velocity, so that $u/u_d = \sqrt{\Theta/\Theta_d}$. One can then deduce: $\bar{u}^p = u_d(\sqrt{\Theta/\Theta_d} - \sqrt{\mu_d/\mu_s})$, where μ_s is a friction coefficient characterising the drag force necessary to set into motion a static grain. This predicts that the grain velocity does not vanish at the threshold, if friction is lowered during motion ($\mu_d < \mu_s$). The velocity at threshold can be interpreted as the velocity needed by a grain to be extracted from the bed and entrained by the flow.

We can proceed in a similar manner for the aeolian saltation regime, following ideas initially proposed by Owen (1964) and Ungar and Haff (1987). The momentum balance $\tau^p = \rho_f u_*^2 - \tau_d$ still holds, so that n has the same form as in the bed-load case, but with a different effective drag force f_d, not related to friction anymore but to grain velocities. For saltation, steady transport also implies that the number of grains expelled from the bed into the flow exactly balances those trapped by the bed, i.e. a replacement capacity equal to one. Due to the grain feedback on the flow, in contrast with bed load, grains in the transport layer feel a flow independent of the wind strength (see Fig. 3). Thus, new moving grains come only from high energy bed collisions. Since the number of ejected grains is a function of the impact energy (or equivalently, of the impact velocity), the mean grain velocity $\bar{u}^p$ must be constant, independent of the shear velocity, scaling with u_d. In fact, all particle surface velocities also scale with u_d, so that f_d is a constant too, leading again to $n \propto \Theta - \Theta_d$.

These scaling laws explain the different behaviours of $q_{sat}(\Theta)$ in the sub-aqueous bedload and aeolian saltation cases, as shown in Fig. 2.

6. CONCLUSIONS

The aim of this paper was to present a novel numerical approach for sediment transport based on a discrete element method for particles coupled to a continuum Reynolds averaged description of hydrodynamics. We have studied the effect of the grain to fluid density ratio and showed that we can reproduce both (sub-aqueous) bed load at ρ_p/ρ_f close to unity, where transport occurs in a thin layer at the surface of the static bed, and (aeolian) saltation at large ρ_p/ρ_f, where the transport layer is wider and more dilute. Scaling laws for the density of moving grains, and for the average velocity of these grains, as functions of the Schields number are found in agreement with experiments, and support simple mechanisms at work in steady and homogeneous transport.

Further work will be focused on transient situations, in order to study the time and length scales encoding the relaxation properties of out-of-equilibrium transport. Also, it would be interesting to investigate the case of bimodal or more polydisperse grains (Houssais and Lajeunesse, 2012)

7. ACKNOWLEDGMENT

We thank S. Luding for allowing us to use his MD code to simulate the granular system. This work has benefited from the financial support of the ANR, grant #ERCS07_18.

8. REFERENCES

Baas, A.C.W. 2008 Challenges in aeolian geomorphology: investigating aeolian streamers. Geomorphology 93, 3-16.

Bagnold, R.A. 1956 The flow of cohesionless grains in fluids. Phil. Trans. R. Soc. Lond. 249, 235-297.

Camemen, B. and Larson, M. 2005 A general formula for non-cohesive bed-load sediment transport. Esturarine Coastal 63, 249-260.

Carneiro, M.V., Pahtz, T., and Herrmann, H.J. 2011 Jump at the onset of saltation. Phys. Rev. Lett. 107, 098001.

Charru, F. 2006 Selection of the ripple length on a granular bed. Phys. Fluids 18, 121508.

Creyssels, M., Dupont, P., Ould el Moctar, A., Valance, A., Cantat, I., Jenkins, J.T., Pasini, J.M., Rasmussen, K.R. 2009 Saltating particles in a turbulent boundary layer: experiment and theory. J. Fluid Mech. 625, 47-74.

Discrete-element Modeling of Granular Materials. Edited by F. Radjai and F. Dubois, ISTE, Wiley, 2011.

Durán, O., Andreotti, B. and Claudin, P. 2012 Numerical simulation of turbulent sediment transport, from bed load to saltation. Phys. Fluids 24, 103306.

Ferguson, R.I. and Church, M. 2004 A simple universal equation for grain settling velocity, J. Sedim. Res. 74, 933-937.

Greeley, R., Blumberg, D.G. and Williams, S.H. 1996 Field measurement of the flux and speed of wind blown sand. Sedimentology 43, 41-52.

Houssais, M. and Lajeunesse, E. 2012 Bedload transport of a bimodal sediment bed. J. Geophys. Res. 117, F04015.

Iversen, J.D. and Rasmussen, K.R. 1999 The effect of wind speed and bed slope on sand transport. Sedimentology 46, 723-731.

Kok, J.F., Renno, N.O. 2009 A comprehensive numerical model of steady state saltation (COMSALT). J. Geophys. Res. 114, D17204.

Lajeunesse, E., Malverti, L. and Charru, F. 2010 Bedload transport in turbulent flow at the grain scale: experiments and modeling. J. Geophys. Res. 115, F04001.

Le Louvetel-Poilly, J., Bigillon, F., Doppler, D., Vinkovic, I., Champagne, J.-Y. 2009 Experimental investigation of ejections and sweeps involved in particle suspension. Water Resour. Res. 45, W02416.

Marchioli, C., Armenio, V., Salvetti, M.V. and Soldati, A. 2006 Mechanisms for deposition and resuspension of heavy particles in turbulent flow over wavy interfaces. Phys. Fluids 18, 025102.

Meyer-Peter, E. and Muller, R. 1948 Formulas for bed load transport. Proc., 2nd Meeting, IAHR, Stockholm, Sweden, 39-64.

Owen, P.R. 1964 Saltation of uniform grains in air. J. Fluid Mech. 20, 225-242.

Pope, S.B. 2000 Turbulent flows. Cambridge University Press.

Rasmussen, K.R., Iversen, J.D., Rautaheimo, P. 1996 Saltation and wind flow interaction in a variable slope wind tunnel. Geomorphology 17, 19-28.

Ribberink, J.S. 1998 Bed-load transport for steady flows and unsteady oscillatory flows. Coastal Eng. 34, 58-82.

Ungar, J.E. and Haff, P.K. 1987 Steady state saltation in air. Sedimentology 34, 289-299.

Short and long term evolution of deep giant submarine dunes in continental shelf environment: the example of the "Banc du Four" (Western Brittany, France)

Marcaurelio Franzetti [(1)], Pascal Le Roy [(1)], Thierry Garlan [(2)], Christophe Delacourt [(1)], Rémy Thibaud [(3)], Romain Cancouet [(1)], David Graindorge [(1)], Christophe Prunier [(1)] and Alexey Sukhovich [(1)]

1. Université Européenne de Bretagne Occidentale, UMR-6538 Domaines Océaniques, IUEM / CNRS Place Copernic, 29280 Plouzané, France - marcaurelio.franzetti@gmail.com
2. SHOM, DOPS/HOM/REC-CFuD/Sédimentologie 13, rue du Chatellier 29228 Brest, France
3. Ecole Navale, IRENav BCRM Brest, CC 600, 29240 Brest, France

Abstract

The deep sandwave dynamics is still in debate. Understanding the migration processes and the resulting evolution of their 3D internal architecture are scientifically challenging. To address these questions we realized two swath bathymetry surveys complemented with seismic reflection across the large sandwaves field named "Banc du Four". It is located offshore the Western Brittany and is composed of more 500 dunes. Some of the dunes' wavelengths and heights exceed 1000m and 30m respectively placing them among the largest dunes ever described. Equilibrium laws obtained from our morphological analysis are not completely in agreement with those described in previous studies of similar structures in shallow waters. Relatively high migration velocities on deep continental shelves (from 3 to 20m.yr-1) attest of their still present dynamical equilibrium. Internal-external morphological and kinematical analyses show the existence of two different dynamic regimes. Interpretation of the seismic reflection data allowed to reconstruct long-term evolution of the sandbank and the establishment of progressive connections between stepped submarine channels and tidal dynamics during the last sea-level rise.

1. INTRODUCTION

Seabed is often covered with rhythmic sandy bedforms, the marine dunes, which are particularly wide-spread on macro-tidal continental shelves. According to Ashley (1990) and Berné et al. (1993), dunes are classified by their size (wavelength): small (0.04-0.25m), medium (0.25-0.44m), large (0.44-2.8m) and giant (>2.8m). Those are elongated bedforms, with angular variations frequently reaching up to 20°, perpendicular to the main current (Hulscher and Van den Brink, 2001). The latter ones differ from sandbanks which are defined as flow-parallel bedforms or slightly oblique (<30°) to the peak of tidal flow direction (Le Bot, 2001) and are also characterized by much larger sizes (>1000m large).

Morphology dunes parameters (wavelength, height and depth) are commonly correlated in order to determine universal relationships. Flemming (1988) gives an evidence of the existence of a geometrical equilibrium relationship between λ and h ($h=0.0677\lambda^{0.8098}$) and defines an upper height limit ($h_{max}=0.16\lambda^{0.84}$). However, recent studies on giant-deep dunes tend to invalidate this limit (Barrie et al., 2009; Van Landeghem et al., 2009). As Allen (1968) observed an increase of h in accordance with D, Francken et al. (2004) calculated another upper height limit ($h_{max}=0.25P$). Other studies (Werner et al., 1974; Van Landeghem et al., 2009) have produced contradictory evidence and have demonstrated that this relationship does not apply in general cases (Flemming et al., 2000).

Sandbodies are formed in response to the interaction between sedimentary characteristics and local hydrodynamics regime (Allen, 1968). It is usually assumed that migration velocities of dunes decrease as their size increases (Ernstsen et

al., 2006). However, inverse correlations have been observed (Garlan, 2004). Marine dunes tend to migrate in the direction of the residual current by acquiring asymmetric shapes facing the same direction (Hulscher and Dohmen-Janssen, 2005). Knaapen (2005) uses the degree of asymmetry to estimate their direction and their migration rates.

However, some field observations show asymmetries opposed to residual currents (Besio et al., 2004) and migrating directions (Van Landeghem et al., 2012).

Internal geometries of sandbodies partially reflect their paleo-morphologies. Indeed, the recognition of internal dune structures allows a reconstitution of depositional environments and processes on an annual-decadal timescale (Morelissen et al., 2003).

Berné et al. (1993) describe three orders of boundaring surfaces: (1) first order surfaces which are sub-horizontal and correspond to the erosional overlapping of small sandwaves superimposed

(Berné, 1991) (2) second order surfaces which dip in direction of lee-side and correspond to an erosive process of wind-current and wave-storm (Le Bot and Trentesaux, 2004) (3) third order surfaces, which are more inclined than the latter ones, and result from the alternation of avalanche phases and "sandy rainfalls" (Berné, 1991). Allen (1980) suggests that the layout of internal units is led to the tidal asymmetry degree.

2. DATA AND METHODS

The north Iroise Sea connects the English Channel and the North Atlantic Ocean on the western Brittany's continental shelf. The hydrodynamics is strong with tidal current velocities reaching up to $4m.s^{-1}$ (Hinschberger, 1962) and storm waves regularly exceeding 4m (Dehouck, 2006). The study area consists in a wide Northward opened triangular bay, bounded to the East by coastal reefs and to the South and West by the Molene-Ushant Archipelago. The island belt is interrupted by two narrow and shallow channels, the Fromveur channel (50m b.s.l.) and the Four channel (10m b.s.l.). The "Banc du Four" is located 100m b.s.l. in the middle of the bay (Fig. 1). The sandbody has been the subject of little investigation (Hinschberger, 1962) up to now.

DTMs were obtained by two multibeam echosounders (MBES) bathymetric surveys (Fig. 2). The Evalhydro2009 campaign, carried out in February 2009 by SHOM from the board R/V "Pourquoi-Pas?", yielded a DTM of 5m resolution. And the AlbertGeo2010 campaign, carried out in August-September 2010 by IUEM from the board R/V "Albert Lucas" yielded four DTMs (A to D) of 2m resolution. Internal sandbodies structures were investigated by seismic reflection acquisition. SHOM conducted very High Resolution (VHR) seismic profiles with SIMRAD EM120 CHIRP on R/V "Beautemps-Beaupré" in November 2010 (Daurade2010). HR seismic profiles were carried out by IUEM on R/V "Côtes de la Manche" with sparker (250 Joules) mono and multi-channels during several surveys GeoBrest (2005, 2006, 2010 and 2012).

Morphology dunes parameters were obtained either manually or automatically on bathymetric DTMs. Wavelength λ, lee side length Ls and height h were found manually from at least three 2D cross-sectional profiles perpendicular to the waves' crests. Crest depth D and dip direction of a lee side α are defined automatically by zonal statistics. The asymmetry A is defined as $(\lambda - 2Ls)/\lambda$ according to Knaapen (2005).

Two different methodologies were used to measure dunes' migration between February 2009 (EvalHydro2009) and August-September 2010 (AlbertGeo2010) in zone D: (1) firstly, the crosscorrelation, which is a rasterial technique, calculates migration vectors from the search of similar shapes between two grids obtained for two different times t1 and t2 (Delacourt et al., 2004; Duffy and Hughes-Clarke, 2005; Buijsman and Ridderinkhof, 2008) and (2) then, the spatiotemporal graph approach is based on an entitiesrelations conceptual model and on geometrical measurements between geographical entities (crests of dunes) related by filiation or sptatiotemporal links (Del Mondo et al., 2010; Thibaud et al., 2012). The results of these two methods were then compared.

3. RESULTS

The "Banc du Four" is a series of more than 510 bedforms extending between 70 and 105m b.s.l. It is characterized by a sandbank flanked by two dune fields, which define a V shape (Fig.2). The sandbank covers an area of 4x2km2 ranging

between 35 to 90m b.s.l. It is nearly symmetrical, with a flattened crest aligned to the East-West direction. To the south, it is preceded by a giant asymmetric straight dune (λ=1050 m, h=32 m, width=2000 m) oriented towards the Southwest direction. In one hand, the northwestern dune field is characterized by dunes decreasing in size (between 0.02 to 30m high and 10 to 600m wavelength) while increasing in depth (50 to 105m b.s.l.) as one goes away from the sandbank. They are generally asymmetric with a flexing of the upper part of the crests and polarity directions that rotate clockwise (from Southwest to Northeast) as the distance to the Northwest increases. In the other hand the northeastern dune field is characterized by giant asymmetric dunes (between 0.02 to 20m high and 10 to 500m wavelength) and an increasing depth as one goes away from the sandbank. Their morphologies delineate two distinct zones: (1) in the western part, dunes are nearly straight and oriented towards the Southwest (2) in the eastern part, dunes are smaller, yet with a greater sinuousness (even barkanoid) and inversely oriented (towards the Northeast). The separation of the latter ones manifests itself by a well-marked shear zone.

The dunes' morphological parameters analysis of "Banc du Four" gives interesting results. The geometrical equilibrium relationship between λ and h ($h=0.0121\lambda^{1.1902}$, $r^2=0.75$) has a similar trend to that of Flemming (1988) but with a steeper positive slope. Furthermore, some measurements values exceed the upper limit of Flemming (1988).

One can also assess that the calculated relation between h and D is not accurate ($h=13156.103D^{-3.4595}$, $r^2=0.3$). Yet, the height of the dunes decreases as the crest depth increases, this trend being opposed to Allen's observations (1968). Moreover, for some dunes, the ratio of h and D exceeds the upper limit calculated by Francken et al. (2004).

Cross-correlation parameters used were 32 pixels for the search window and 8 pixels for the shape matrix. Only migration vectors associated to SNR above 0.99 and magnitude vector greater or equal to 5m were kept. The calculated dune migration rates vary between 3 and 20m.yr-1. At 75%, the migration directions correspond to morphological directions of dunes with an angular spacing lower than 30°. As for the morphological analysis, the dune migrations delineate the same two zones: (1) the western part characterized by lower velocities ($6m.yr^{-1}$ mean) and motion directions towards the Southwest (2) the eastern part characterized by higher velocities (12 m.yr-1 mean) and an opposite migration direction (towards the Northeast). Here again, one can identify a central shear separation with no preferential motion direction. Similar dune migration results were obtained with the spatiotemporal graphs method (deviations less than 10% for migration rates and 15% for migration directions).

The analysis of internal geometry of Zone D dunes was performed with seismic CHIRP and sparker profiles. The observed reflectors can be split in two groups characterized by different layouts. The first group is composed of oblique third order reflectors parallel to the dune lee-slope and prograding towards the latter. These foresets downlap a first order (subhorizontal) reflector which is the prolongation of the next dune's stossside. According to Reineck and Singh (1980), this

geometry is due to dune migration which proceeds by successive avalanches at the lee-side and prograding on the next dune's stoss-side. The reflectors of second group form small units made of first and third order reflectors crosscut by slightly oblique second order reflectors dipping in direction of lee-side (Ferret et al. 2010). These units are accumulated vertically whithin the dune.

Internal structures of sandbank were derived from seismic sparker profiles (Fig. 3). Six different units have been individualized and numerated in chronological order. The first unit (U1) is the deepest and smallest one, localized in the center of the sandbank and lies on the substratum. The second unit (U2) is bigger, aggrades and progrades partially on the previous unit toward the Northwest. The third unit (U3) rests on previous unit side and progrades toward the WNW. The fourth unit (U4) aggrades and progrades towards the WNW with the same area that the sandbank itself. The fifth unit (U5) aggrades in the WNW part of the sandbank. The last active unit (U6) covers the entire sandbank with an aggrading component in the northwestern part.

4. DISCUSSION

Morphology parameters relationship results of "Banc du Four" are different from other authors'

studies. Flemming (1988) described well the general trend of increasing height as wavelength increases, without determining a universal law for the geometrical equilibrium relationship and an upper height limit. This assessment is consistent with other observations (Barrie et al., 2009; Van Landeghem et al., 2009). Moreover, the inverse relationship between height and crest depth observed here is contrary to that of Allen (1968) and some height values measured exceed the upper limit established by Francken, et al. (2004). Here again, these observations are consistant to similar studies (Werner et al., 1974; Flemming et al., 2000; Van Landeghem et al., 2009). The non universality of morphology parameters relationship can be linked to the failure to take into account particular environments such as deeper waters and highlights that the complex physical mechanisms of dunes' forming are still poorly known.

The migration directions of dunes in Zone D are in agreement with their morphological directions (Hulscher and Dohmen-Janssen, 2005). The dunes' dynamic study clearly shows two opposing dynamic sets in shearing. This is in accordance with numerical models of tidal residual current near the bottom (Guillou, 2007): (1) western part is characterized by a clockwise current eddy (2) eastern part is characterized by a tidal coast current oriented toward the Northeast. This spatial segmentation is also found in the analysis of morphodynamical parameters relationships: (1) in western part, the velocity increases with size (in agreement with Garlan, 2004) and asymmetry (in agreement with Knaapen, 2005) and (2) in the eastern part, the velocity decreases with an increase of dune size (in agreement with Ernstsen et al., 2006) and asymmetry. To this is added the difference of internal geometries observed with seismic profiles: (1) in western part, dunes are mainly formed by accumulation of prograding avalanche foresets in forward direction and (2) in eastern part, internal dunes' geometry consists in an alternative superposition of smaller dunes with different degrees of asymmetry. Based upon the model of internal structures of Allen (1980), we can assume that there is an asymmetry difference of tidal currents which induces two different dunes' dynamics: (1) in the western part, the clockwise current eddy leads to an asymmetric hydrodynamics regime and (2) in the eastern part, the tidal coast current presents a less asymmetrical behavior.

The internal structuration of sandbank reflects major developments over time in relation with the last sea-level rise and the establishment of progressive connections between stepped submarine channels and tidal dynamics. The U1 unit marks the first formation stage of the "Banc du Four" with the establishment of a small sandy structures (most likely a small sandbank or a dune field) in shallow water. At this time, the sand structure was no deeper than 80m below the current sea level (b.c.s.l.) and the north Iroise Sea could look like a wide open bay toward Northwest. The U2 unit marks a strong change of the sedimentary dynamics which can be explained by the opening of one of the South channels when the sea level was above 50m b.c.s.l. This episode is followed by a gradual displacement of the sedimentation in Northwest direction (U3, U4 and U5) due to the submersion of the Molene-Ushant Archipelago. The recent stabilization of coastline may explain the low mobility of sedimentation (U6).

5. ACKNOWLEDGMENT

This worked was founded by the Direction Générale de l'Armement (DGA). The authors are very grateful to the crew of vessels "Albert Lucas" and "Côtes de la Manche". They also thank Guillaume Fromant who has vetted this paper..

6. REFERENCES

Allen, J.R.L., 1968. The nature and origin of bed-form hierarchies. Sedimentology 10: 161-182.

Allen, J.R.L., 1980. Sand waves: A model of origin and internal structure. Sedimentary Geology, 26(4): 281-328.

Ashley, G.M., 1990. Classification of large-scale subaqueous bedforms: a new look at an old problem. Journal of Sedimentary Petrology 60: 160-172.

Barrie, J.V., Conway, K.W., Picard, K., Greene, H.G., 2009. Large-scale sedimentary bedforms and sediment dynamics on a glaciated tectonic continental shelf: Examples from the Pacific margin of Canada. Continental Shelf Research 29: 796-806.

Berne, S., 1991. Architecture et dynamique des dunes tidales. PhD Thesis, University of Lille 1, Villeneuve-d'Ascq: 295.

Berne, S., Castaing, P., Le Drezen, E., Lericolais, G., 1993. Morphology, internal structure, and reversal of asymmetry of large subtidal dunes in the entrance to Gironde estuary (France). Journal of Sedimentary Petrology 63: 780-793.

Besio, G., Blondeaux, P., Brocchini, M., Vittori, G., 2004. On the modeling of sand wave migration. Journal of Geophysical Research 109.

Buijsman, M.C., Ridderinkhof, H. 2008. Long-term evolution of sand waves in the Marsdiep inlet. I: High-resolution observations. Continental Shelf Research 28: 1190-1201.

Dehouck, A., 2006. Observations et conditions d'apparition de croissants de plage sur les littoraux de la mer d'Iroise. Norois 20: 7-16.

Delacourt, C., Allemand, P., Casson, B., Vadon, H., 2004. Velocity field of the "La Clapière" landslide measured by the correlation of aerial and Quick-Bird satellite images. Geophysical Research Letters 31: 1-5.

Del Mondo, G., Stell, J.G., Claramunt, C., Thibaud, R., 2010. A graph model for spatio-temporal evolution. Journal of Universal Computer Science, 16: 1452-1477.

Duffy, G.P., Hughes-Clarke, J.E., 2005. Application of spatial cross correlation to detection of migration of submarine sand dunes. Journal of Geophysical Research 110: 10.

Ernstsen, V.B., Noormets, R., Winter, C., Hebbeln, D., Bartholomä, A., Flemming, B.W., Bartholdy, J., 2006. Quantification of dune dynamics during a tidal cycle in an inlet channel of the Danish Wadden Sea. Geo-Marine Letters 26: 151-163.

Ferret, Y., Le Bot, S., Tessier, B., Garlan, T., Lafite, R., 2010. Migration and internal architecture of marine dunes in the eastern English Channel over 14 and 56 years intervals: the influence of tides and decennial storms. Earth Surface Processes and Landforms 35: 1480-1493.

Flemming, B.W., 1988. Zur Klassifikation subaquatischer, strömungstransversaler Transportkörper. Bochumer Geologische und Geotechnische Arbeiten, 29: 93-97.

Flemming, B.W., 2000. The role of grain size, water depth and flow velocity as scaling factors controlling the size of subaqueous dunes. A.

Trentesaux, T. Garlan (Eds.), Marine Sediment wave Dynamics, Proceedings of and Internaltional Workshop held in Lille, France, 23-24 March 2000, University of Lille 1, Lille: 55-60.

Francken, F., Wartel, S., Parker, R., Taverniers, E., 2004. Factors influencing subaqueous dunes in the Scheldt Estuary. Geo-Marine Letters 24: 14-24.

Garlan, T., 2004. Apports de la modélisation dans l'étude de la sédimentation marine récente, HDR thesis, Université d'Angers: 158.

Guillou, N., 2007. Rôles de l'hétérogénéité des sédiments de fond et des interactions houle—courant sur l'hydrodynamique et la dynamique sédimentaire en zone subtidale - applications en Manche orientale et à la pointe de la Bretagne. PhD thesis, Université de Bretagne Occidentale: 469.

Hinschberger, F., 1962. Résultats de 14 stations hydrologiques dans l'Iroise et à ses abords. Comptes Rendus de l'Académie des sciences 255 : 2629-2631.

Hulscher, S.J.M.H. & Van den Brink, G.M., 2001. Comparison between predicted and observed sand waves and sand banks in the North Sea. Journal of Geophysical Research 106: 9327-9338.

Hulscher, S.J.M.H. & Dohmen-Janssen, C.M., 2005. Introduction to special section on marine sand wave and river dune dynamics. Journal of Geophysical Research 110: 6.

Knaapen, M.A.F., 2005. Measuring sand wave migration in the field. Comparison of different data sources and an error analysis. Journal of Geophysical Research, Earth Surface 110: 152-159.

Le Bot, S., 2001. Morphodynamique de dunes sous-marines sous influence des marées et des tempêtes. Processus hydro-sédimentaires et enregistrement. Exemple du Pas-de-Calais. PhD thesis, Université de Lille 1: 300.

LeBot, S., Trentesaux, A. 2004. Types of internal structure and external morphology of submarine dunes under the influence of tide- and wind-driven processes (Dover Strait, northern France). Marine Geology 211: 143-168.

Morelissen, R., Hulscher, S.J.M.H., Knaapen, M.A.F., Németh, A.A., Bijker, R., 2003. Mathematical modeling of sand wave migration and the interaction with pipelines. Coastal Engineering 48 : 197–209. Reineck, H.E. & Singh, I.B., 1980. Depositional Sedimentary Environments. New York: Springer-Verlag: 22-30.

Thibaud, R., Del Mondo, G., Garlan, T., Mascret, A., Carpentier, C., 2012. A spatio-temporal graph model for marine dune dynamics analysis and representation - accepted of Journal Transactions in GIS in august 2012.

Van Landeghem, K.J.J., Uehara, K., Wheeler, A.J., Mitchell, N.C., Scourse, J.D., 2009. Post-glacial sediment dynamics in the Irish Sea and sandwave morphology: data-model comparisons. Continental Shelf Research 29: 1723-1736.

Van Landeghem, K.J.J., Baas, J.H., Mitchell, N.C., Wilcockson, D., Wheeler, A.J., 2012. Reversed sandwave migration in the Irish Sea, NW Europe: A reappraisal of the validity of geometry-based

predictive modelling and assumptions. Marine Geology 295-298: 95-112.

Werner, F., Arntz, W.E., Tauchgruppe, K., 1974. Sedimentoloie und Okologie eines ruhenden Riesenrippelfeldes. Meyniana 26: 39-59.

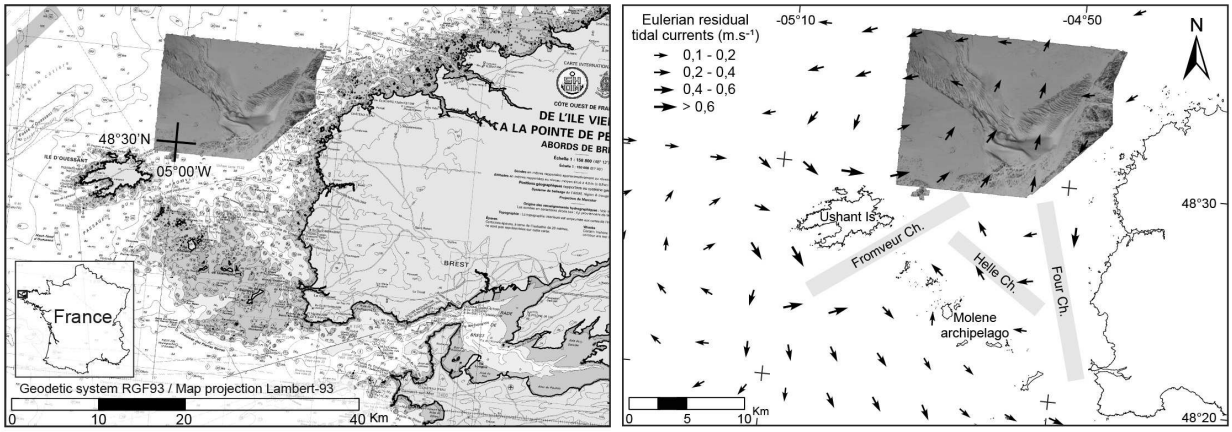

Figure 1. left) Map of the Iroise sea (situated between Brittany French coast and the Ushant-Molene Archipelago) showing the location of DTM EvalHydro2009. The study area covers 14x18 km2 with the water depth ranging up to 100 m. (right) Eulerian residual tidal currents according to PREVIMER for a tide range of 90.

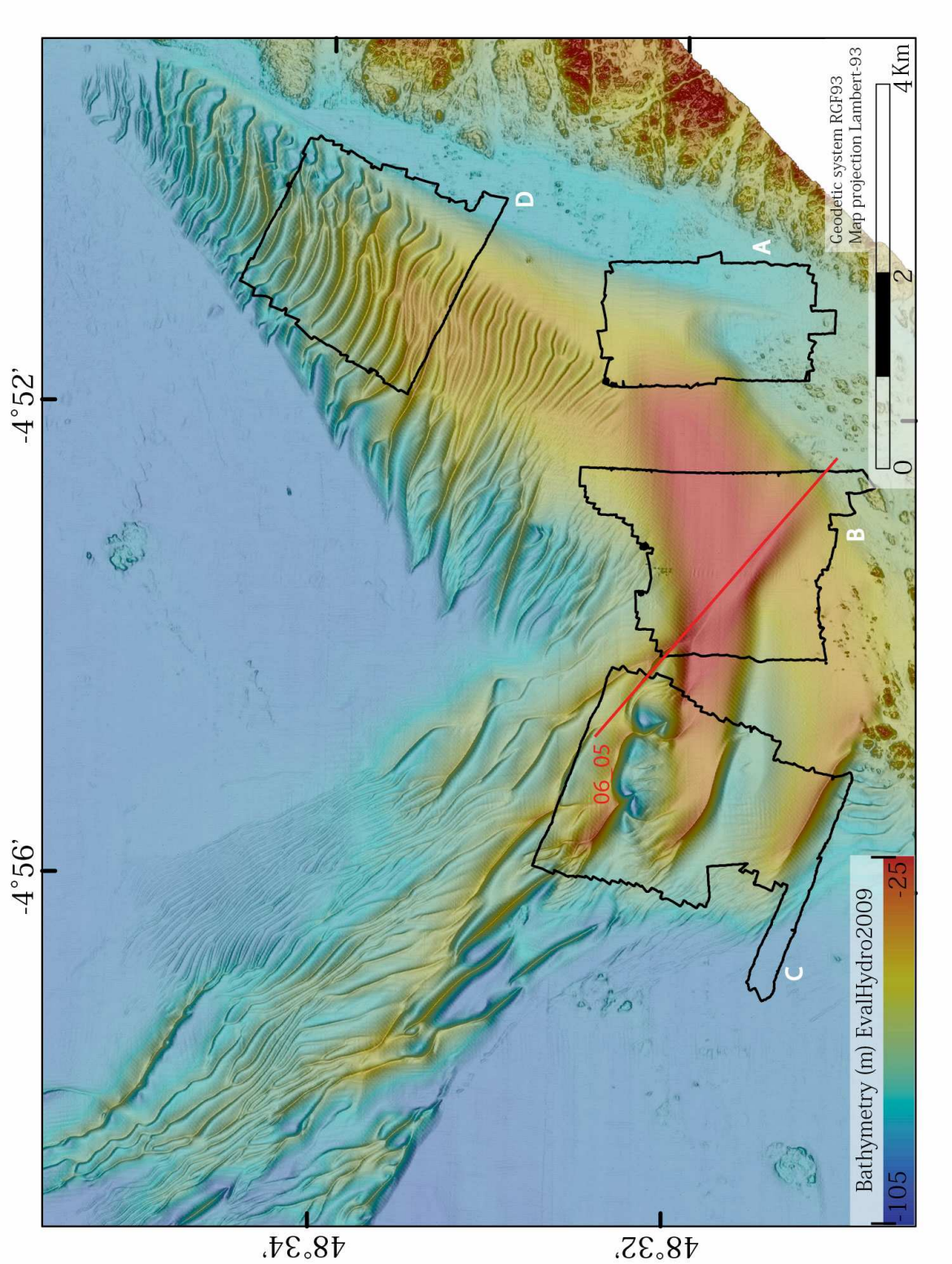

Figure 2. Bathymetry of "Banc du Four" on February 2009 defined with a 5 m resolution. Areas of AlbertGeo2010 swath surveys are outlined by black solid lines and labelled in white as A, B, C and D. Seismic sparker profile number 6 of GeoBrest2005 is located by a solid line.

Complex morphology and organisation of dunes in a giant dunes field

T. Garlan[(1)], A. Cartier[(1)], M. Franzetti[(2)], P. Le Roy[(2)], J. Duarte[(3)], J. Pombo[(3)], M. Peix[(4)], P. Guyomard[(1)], Y. Le Faou[(1)], I. Gabelotaud[(1)] and E. Marchès[(1)]

1. SHOM, HOM/REC-CFuD/Sedimentology, France - Thierry.garlan@shom.fr
2. Université Européenne de Bretagne Occidentale, IUEM, France - Pascal.leroy@univ-brest.fr
3. Instituto Hydrografico, Portugal - Joao.Duarte@hidrografico.pt
4. Université de Perpignan, CEFREM, France

Abstract

The most recent hydrographic surveys conducted by SHOM in the north and west of Brittany, at depths of 70 to 200m, delineated two very large dune fields, that until now, had been described only by a few old profiles. More than two thousands dunes were identified during surveys of 2011 and 2012. These one have been added to the GIS dedicated to banks and dunes of the French continental shelf. These surveys have highlighted the boundaries of these two dune fields, and the existence of fields of barchan, giant dunes and very large variations in the orientation of the dunes, characterizing the complexity of these environments. The dunes field of the Celtic Sea, cover a surface of 31 000 km^2. The main direction of the transit is to the south west, and most of the dunes are transverse and of some meters high. But when we look the morphology of dunes at the local scale, it appears morphologies that have been rarely described. After describing the Celtic dune fields, we establish a classification of dunes based on their shape, their dynamics and their environment in order to achieve a synthesis of the dunes of the Celtic Sea.

1. INTRODUCTION

During the bathymetric surveys achieved by the French Hydrographic Office (SHOM), submarine dunes were detected in the shallow water zone, at the end of the nineteenth century. We nevertheless had to wait until the late twentieth century, with the arrival of multibeam echo sounder and GPS, to have an accurate characterization of the morphology and location of these dunes. It has thus become possible over the past fifteen years to precisely quantify the speed of dunes and follow their morphological evolution over time. According sediments and hydrodynamics involved, these rates vary from a few meters to tens of meters per year. The study of the dunes is a young science, and knowledge of the movements of the dunes stay must await the results of surveys of different environments on recurring periods sufficiently significant. Synthesis of studies made by Wever (2004), gives the values of dunes displacements reported in the scientific literature. These studies are unfortunately limited to depths less than 40m and it must be necessary to take into account currents and regional characteristics of sediments. As Kocurek says during the precedent MARID « Boundary conditions makes each bedform field unique ». Studies on dunes of the French continental shelf were done at the beginning on some sandbanks environment and on some dune fields of estuaries or near the coast of Calais and Cherbourg (Berné et al 1989, 1993), Since 1988, SHOM has done hydrographic cruises devoted to the study of the dynamics of dunes of the North Sea and the English Channel. Since 2011, these surveys apply now to the Celtic Sea, and the region of dunes explored, will therefore from the border of Belgium to the continental slope of the Atlantic.

The objectives of our works are to answer to some questions about the time needed between hydrographic survey, the impact of these fields on benthic habitat mapping, on offshore renewable energy and on mine burial. In parallel we realised research on dunes (Le Bot, 2001; Ferret et al, 2010; Franzetti et al, 2013) and on numerical

modelling of dune dynamics (Idier, 2002; Idier et al, 2011). We develop a specific GIS on dunes which is the synthesis of knowledge from some decades of surveys (Garlan et al, 2008, Thibaud et al, 2012). This system is used to compare the knowledge of bedforms with charts, to modify the surveying strategy, to look at the historical movement of the dunes and to develop new cartographical products (Garlan, 2009). These works are done in the context of the second SHOM Dune projects (2013 to 2017) which concern research, GIS and products for the safety of navigation, sand mining, mine burial, wind farm, European marine strategy directive, marine protected areas, ...

2. DUNES SURVEYS

2.1. North Sea recurrent surveys

Recurrent hydrographical surveys in the French part of North Sea are done for the safety of navigation. Hydrographic Offices should ensure for sea transport a minimum depth of 26m. If the maximum height of a dune is 22 meters; areas with dunes and a maximum depth of 48m, thus present a potential risk. But we must take into account the impact of the water level, which is critical to the height of the dunes. In fact, the height of the dunes saturation is about 35% of the depth so, for a dune reaches a depth of 26m, it is a necessity that the bottom is of 40m. So, for safety of navigation, all areas containing dunes and whose depths are less than 48m are classified as risky; below 40m, they are classified as high risk. The surveys were done from 1988 to 2000 every 3 years on some specific zones. With a 3 weeks survey/year, a complete survey of the French part of the North Sea traffic separation channel was done from 2000 to 2012. We define a new protocol which consist of survey every 2 years a dozen of dunes all along the zone of navigation and study the movements of these dunes. These observations are sufficient to look at the normality of the dynamics of the dunes concerned by the safety of navigation and of the conformity of the reality with charts.

To define marine habitats, for mine hunting and to choose appropriated zones for marine cables or wind farm, the first need is to know if there is dune in the region and if so, do they move. If the delimitation of dunes and dune fields of North Sea are well known, it is not the case of the west of the English Channel and of the Celtic sea. For these regions the only documents which describe dunes are papers of Belderson et al (1971) and some works on small areas of the Celtic Sea for the research of petrol (SHOM and SNEAp, 1962), and research on Neogene stratigraphy (Reynaud et al., 1999).

2.2. West Channel and Celtic Sea Surveys

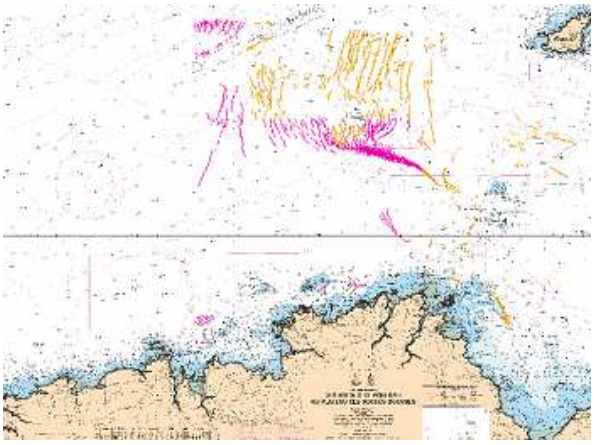

Figure 1. Fields of dunes of north Brittany defined by thirteen recent SHOM hydrographic cruises

From 2002 to 2007, thirteen hydrographic surveys were done in the north of Brittany in regions which had not been surveyed since more than fifty years. These MES surveys had been used to delineate the field of dunes and to characterize their properties.
In this area, tidal currents have a principal direction from WNW to ESE, with intensities of the bottom currents which go from 1 to 1.5 knots. The depth is from 70 to 120 m. 46% of the dunes are large ($10 < \lambda < 100$m, $0{,}75 < H < 5$m), 44% are very large dunes ($\lambda > 100$, $5\text{m} < H < 10$m), and 10% are dunes with heights between 10 and 22 meters.

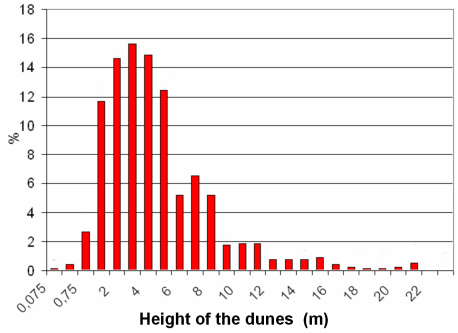

Figure 2. Height of dunes in the north Brittany in the area of 70 to 120 m depth

Studies on twenty parameters, measured on each of these dunes, allow regional comparisons using relationship between the height, the wavelength and sinuosity parameters. It remains to analyze the current meter measurements and sediment samplings which will continue to be performed during planned campaigns in 2013 and 2014.

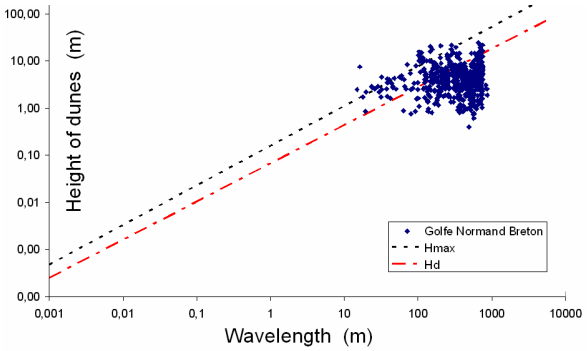

Figure 3. Comparison of Height/wavelength relation with Flemming's results

The characteristics of these dunes change with depth in this region. Height of dunes increases with bathymetry, and the higher dunes are on the edge of the central depression of the English Channel. It is why it is important to go deeper and look at the Celtic Sea with it's depths from 70 to 200m.

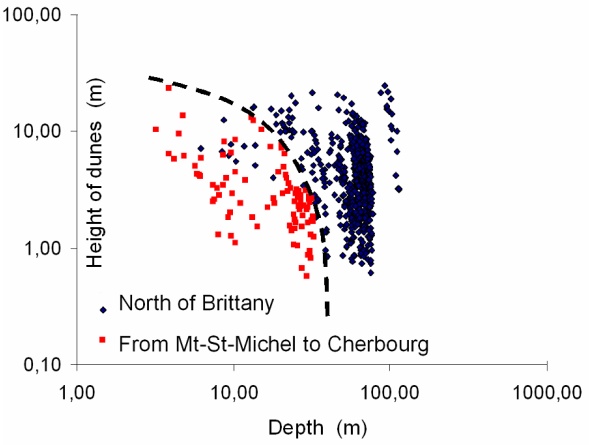

Figure 4. Evolution of the height of dunes with depth in the north of Brittany and between the English islands and Normandy

The study of directions of movements of the dunes shows three regions with a clear direction:

- in the north-east, to the English island
- in the south-east, to the Bay of Saint-Brieuc,
- in the south-west, to the extern part of the Channel.

The fourth part, located in the north-west shows displacement in very different directions and require additional surveys to clarify this system.

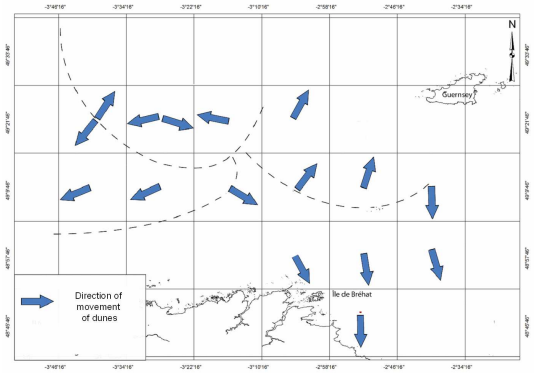

Figure 5. Variation of direction of movement of dunes in the north of Brittany.

3. SOME EXAMPLES OF DUNE FIELDS OF THE CELTIC SEA

The two sedimentological cruises of 2011 and 2012 with the Beautemps Beaupré and the Pourquoi Pas? were realized to define the limits of the dune fields, and to characterized the principal properties of the dunes and of their environment. The west limit of dunes, on the top of the continental slope, and the limit with the Bay of Biscay, where dunes are limited to coastal bays and estuaries, are not completely defined, but the French fields of dunes of Iroise Sea, Celtic Sea and west part of the English Channel are now globally delimited (Figure6).

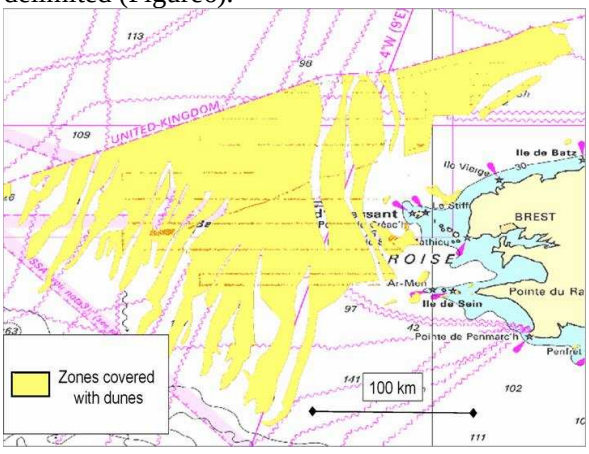

Figure 6. Location of the dunes of the Celtic Sea and the west part of the English Channel

Most of the analysis of the data from these surveys must be done and two new surveys are in preparation. Results on the Four Banks are presented by Franzetti et al (2013), for the rest of our observations, the following chapters show some of the first observations.

3.1. Ouessant sandbank and Ouessant Dunes field

The Ouessant sandbank (Figure 7) is the brother of the Four sandbank, they are at the two extremities of the Fromveur which is a channel with strong bottom currents up to 2.5m/s. In the north, a kind of corridor of dunes, go in the direction of the sandbank. Along this bank, the dunes turning around in an anticlockwise direction with speeds of the order of 20m/an (measured on two surveys spaced to 11 months)

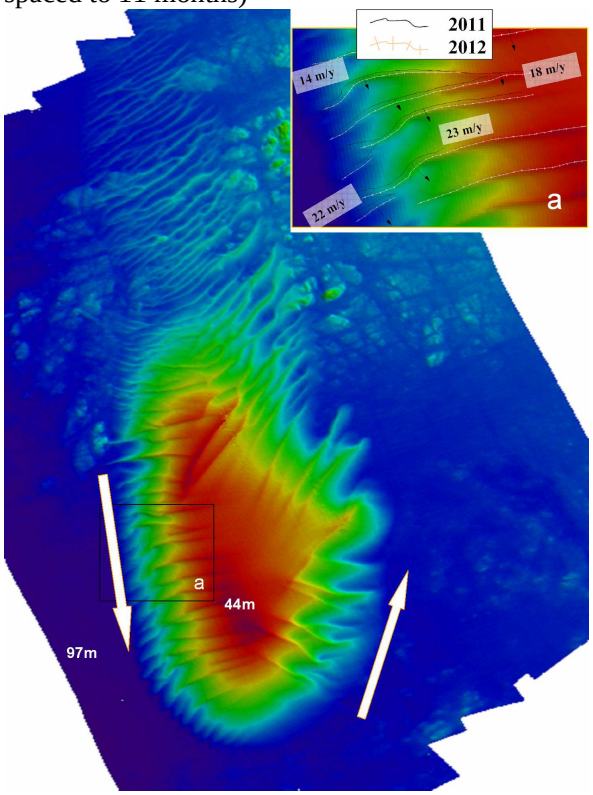

Figure 7. Bank of Ouessant and dunes with 20m/y dynamics

At some nautical miles in the South west of this sandbank, a large field of dunes presents the particularity to be the zone of life for a colony of dolphin. New observations must be done on this particular field.

3.2. Portsall Dunes

As an example of the poor knowledge of dunes of these regions, the Portsall field of dunes is at 50 kilometers to the French coast and it has been discovered during the PROTEVS-Dunes survey of October 2012. At a depth of 90 to 100 meters, more than 300 dunes associated to a low sandbank. 7.7 % of these dunes are higher than 10 meters and some of these higher dunes are barchans (figure 8).

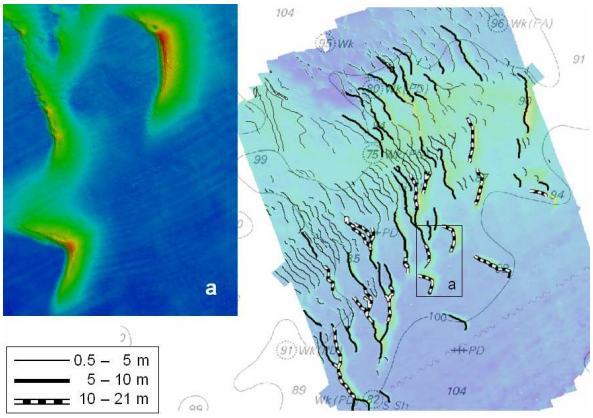

Figure 8. Portsall sandbank and it's very large dunes and barchans

In deserts, barchans are the dunes with the fastest speeds. Portsall sadbanks with barchans and longitudinal dunes, which is near the coast, is a particularly interesting environment to study the dynamics of dunes at depths of 100 meters.

3.3. Celtic Giant Dunes

The new surveys show that all the Celtic Sea shows dunes. These dunes are associated with great sandbanks which had been described since many years (Belderson et al 1962, Reynaud et al, 1999). Before MES, at these depth of 100 to 200 meters, the bathymetric systems didn't had a sufficient accuracy for the mapping of dunes. In 2011 a profile had showed a series of giant dunes with height from 25 to 29 meters. Eleven months after a survey in this area shows that these dunes did not seem to move, and that these symetrical structures are not numerous. These dunes are similar to those described by Van Landeghem (2009) and a study about morphology and regional currents is under process (Figure 9).

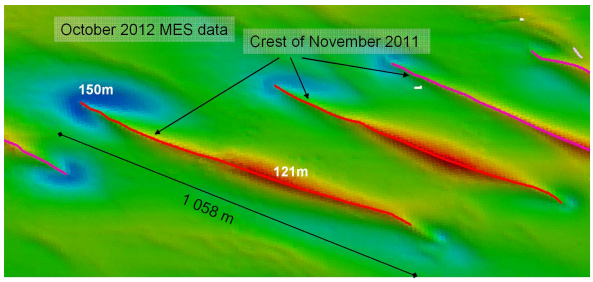

Figure 9. Comparison of 2011(lines) and 2012 (DEM) bathymetry of trochoidal dunes of the Celtic sea.

4. CONCLUSIONS

Dunes observed during surveys conducted in 2011 and 2012 shows different morphologies. The dynamics of these dunes appears possible even at depths of 200m. Many criteria shows that these movements exist locally, it is necessary to continue the measures to support these observations. Surveys on the dunes of the Celtic Sea and Western Channel will continue in 2013 and 2014, including new surveys of MES acoustic imagery and bathymetry, seismic profiles, measurements of currents, turbidity and recurrent photographs.

5. ACKNOWLEDGMENT

We are grateful to hydrographers of SHOM/GHA and SHOM/GOA which realized these surveys and to the crews of Hydrographic ships Borda, Lapérouse, Beautemps-Beaupré et Pourquoi Pas? We also would like to thank Sophie Le Bot, Claudia Guidat, Jeremy Ruest, Elodie Marchès, Morgan Peix, Sébastien Garnaud, … which spent time looking for the dunes.

6. REFERENCES

Belderson, R.H., Kenyon, N.H., Stride, A.H., Holocene sediments on the continental shelf west of the British Isles. The geology of the East Atlantic Continental Margin. Delany F.M. Ed, Institut of geological Sciences Report , 70/14, 157-170.

Berné, S., Allen, G., Auffret, J.P., Chamley, H., Durand, J., Weber, O, 1989. Essai de synthèse sur les dunes hydrauliques géantes tidales actuelles. *Bull. Soc. Geol. France, 6,* 1145-1160.

Berné, S., Castaing, P., Le Drezen, E., Lericolais, G., 1993. Morphology, internal structure, and reversal of asymmetry of large subtidal dunes in the entrance to Gironde estuary (France). Journal of Sedimentary Petrology 63: 780-793.

Ferret, Y., Le Bot, S., Tessier, B., Garlan, T., Lafite, R. 2010. Migration and internal architecture of marine dunes over 14 and 56 years intervals (Eastern English Channel). *Earth Surf. Process. Landforms* 35, 12 : 1480-1493

Idier, D. 2002. Dynamique des bancs et dunes de sable du plateau continental: observations in-situ et modélisation numérique. Mémoire de Doctorat, INP Toulouse.

Idier, D., Astruc, D., Garlan, T. 2011. Spatio-temporal variability of currents over a mobile dune field in the Dover Strait. Continental Shelf Research, 31, 19-20 : 1955 – 1966.

Franzetti, M., Delacourt, C., Garlan, T., Le Roy, P., Cancouët, R., Submitted, Giant sandwave morphologies and dynamics in a deep continental shelf environment: example of the Banc du Four (Western Brittany, France).

Garlan, T., 2004. Apports de la modélisation dans l'étude de la sédimentation marine récente. Mémoire d'Habilitation à Diriger la Recherche, Université des Sciences et Techniques de Lille, 155 p.

Garlan, T., 2007. Study on marine sandwave dynamics. International Hydrographic Review, 8 (1): 26-37

Garlan, T. Le Faou, Y. Guyomard, P., Gabelotaud, I. 2008. French marine sand dune project. In D. Parsons, T. Garlan & J. Best (eds.), Proc. MARID2008, Leeds (UK), 1-3 April 2008. Leeds: University of Leeds. pp. 133-140.

Garlan, T., 2009. GIS and Mapping of moving Marine Sand Dunes. Proceedings ICC2009, Santiago, Chili. http://icaci.org/documents/ICC_proceedings/ICC2009/

Le Bot, S., 2001. Morphodynamique de dunes sous-marines sous influence des marées et des tempêtes. Processus hydrosédimentaires et enregistrement. PhD Université de Lille, 273p.

Reynaud, J.-Y., Tessier, B., Proust, J-N., Dalrymple, R.W., Marsset, T., De Batist, M., Bourillet, J-F. & Lericolais, G., 1999. Eustatic and hydrodynamic controls on the architecture of a deep shelf sand bank (Celtic Sea). Sedimentology, 46, 703-721.

Thibaud, R., Del Mondo, G., Garlan, T., Mascret, A., Carpentier, C., 2012. A spatio-temporal graph model for marine dune dynamics analysis and representation - accepted of Journal Transactions in GIS in august 2012.

Van Landeghem, K.J.J. Uehara, K., Wheeler, A.J., Mitchell, N.C., Scourse, J.D. 2009. Post-glacial sediment dynamics in the Irish Sea and sediment wave morphology: Data–model comparisons. Continental Shelf Research 29: 1723–1736

Bed form dynamics in relation to headwater discharge and human influences in the tidal Elbe river, Germany

N. Gehres [(1)], A. Winterscheid [(1)], R.M. Frings [(2)], S. Vollmer [(1)]

1. Federal Institute of Hydrology, Koblenz, D - gehres@bafg.de
2. RWTH Aachen University, Aachen, D - frings@iww.rwth-aachen.de

Abstract

The major part of the navigation channel in the tidal Elbe river in Germany is covered with bed form structures. When increasing in height, these structures impair the safety of navigation and therefore have to be eliminated by dredging or water injection procedures. Hence it is important for river managers that the understanding of bed form dynamics is improved. Therefore we analyzed eleven echo-sounding datasets from March to August 2010 during different headwater discharge with the Rheno Bedform Tracking software. In our study area near St. Margarethen we detected over 10.000 individual bed form structures with an average height of 2m and an average length of 82m. Results of the bed form height and length do not show correlation with headwater discharge. But we identified a correlation between migration rate and headwater discharge. Using the example of one individual bed form structure we were able to monitor the re-development of this structure after it has been eliminated by water injection procedure. It could not be established whether sediment supply on relocation sites close to the navigation channel in the study area has an influence on growth rate of bed form structures in the navigation channel.

1. INTRODUCTION

The tidal Elbe river is the largest estuary at the German North Sea coast and it is an important waterway connecting the Port of Hamburg with the North Sea. To maintain the safety of navigational purpose and a certain navigational depth the system is frequently dredged since the last Elbe channel adjustment in 1999. The major part of the navigation channel in the tidal Elbe river is covered with bed form structures. When increasing in height these structures impair the safety of navigation, therefore the bed form crests have to be eliminated by dredging or water injection procedures. In 2010 about 36% of all water injection procedures in the tidal Elbe river were carried out between Elbe-km 680 and 690, where our study area is located. There are only a few studies on bed form dynamics having conducted a regional focus on the tidal Elbe river (Vollmers and Wolf, 1969; Nasner,1974; Dammschneider, 1983; Möhl, 1996 and Zorndt et al., 2011). Nasner (1974) for example analyzed echo-sounding data between Elbe-km 624.4 and 624.7 in an area of the Port of Hamburg with an average bed form height of 1.15m and bed form length of 21.5m. But to a large extend all these relevant reports except that from Zorndt et al. (2011) where done with former echo-sounding techniques. Study area of Zorndt et al. (2011) was a 3km long river section directly downstream of the Port of Hamburg. For the entire study period between 1995 and 2010 they determined an average bed form height and length of 1.8m and 49m. However, in the tidal Elbe is still a lack of studies with regional focus especially in more downstream regions. To improve sediment management strategies and to maintenance the navigational depth river managers need better answers to questions such as: (I) What is the geometry and the dynamic of the bed form structures, (II) What is the exact impact of headwater discharge on the rate of increase in bed form height. (III) Is there an impact of relocation sites on bed form dynamics?. To answer these questions river managers at least require an semi-automatic method to analyse geometry and migration of bed forms in an operational way. This case study is investigating the bed form dynamics in a river section of the tidal Elbe near St. Margarethen.

Flemming (2000) mentioned, that in deep rivers bed form growth is not limited by water depth and

that bed forms will continue to grow in response to increase in mean flow velocity until a critical suspension threshold for a given grain size is reached. For the study presented here no velocity measurements are available. Zorndt et al. (2011) determined that headwater discharge is strong enough to alter tidal asymmetry and outweighed influence of the tides. Therefore a particular focus of our analysis is the impact of headwater discharge and the impact of water injection procedures (as a human influence factor) on bed form structures in the study area near St. Margarethen.

2. STUDY AREA

The Elbe river with its length of 1.094km is one of the major rivers of central Europe and originates in the Krkonose Mountains in the northern Czech Republic before transverses Germany and enters the North Sea at Cuxhaven (IKSE, 2005). The tidal Elbe river extends from the weir in Geesthacht (Elbe-km 585.9), which is the border between the tidal and the non-tidal part of the river Elbe, to the mouth at Cuxhaven and has a total length of about 140km. The study area is located in the navigation channel in the river bend near St. Margarethen between Elbe-km 685.4 and 689.9 about 60km downstream of the Port of Hamburg (figure 1). The study area has a length of 4300m and a width of 450m. The area is characterized by semi-diurnal tides with a distinct diurnal asymmetry and classified as upper meso- to lower macro-tidal with a maximum tidal range up to 4m at spring tidal conditions (Kappenberg and Fanger, 2007). The river width between the mean high tide level is 2.6 to 2km at the location site. The navigation channel of the tidal Elbe is frequently dredged and the dredged sediments are given back to the river in so-called relocation sites. Major relocation sites are located on both sides next to the navigation channel in the study area (figure 1).

3. DATASETS

5.1. Echo-sounding data

Within the navigational channel the German Federal Waterways and Shipping Administration carries out hydrographical measurements to achieve changes in bathymetry. The survey vessels are equipped with Kongsberg company multi-beam sonar (EM 3002). To determine bed form structures in the study area, we analyzed eleven bed level measurements between 01.03.2010 and 16.08.2010 (table 1). The measurements were conducted during different headwater discharge and tides. The use of a precise differential global positioning system leads to accurate surveying. The point density of the echo-sounding measurements is approximately one point per m^2.

table 1. Overview over evaluated echo-sounding measurements, belonging headwater discharge and determined mean bed from heights and length.

date	headwater discharge [m3.s-1]	bed form height [m]	bed form length [m]
01.03.2010	1004	1,99	70,82
09.03.2010	1874	2,30	91,45
31.03.2010	1614	2,16	87,82
28.04.2010	741	1,81	75,75
10.05.2010	646	1,86	71,10
31.05.2010	920	2,29	89,02
15.06.2010	1370	2,01	76,88
30.06.2010	572	2,44	86,93
12.07.2010	371	2,55	86,14
04.08.2010	519	2,66	84,82
16.08.2010	1296	2,48	83,00

5.2. Headwater discharge

The headwater discharge from the inland river catchment into the tidal Elbe river is measured at the last gauge upstream of the weir Geesthacht at Neu Darchau (Elbe-km 536.4). The headwater discharge is given by means of daily values. The mean headwater discharge amounts 916.8$m^3.s^{-1}$ in 2010. During study period a peak of 1870$m^3.s^{-1}$ occurred on 09.03.2010 and a minimum of 269 $m^3.s^{-1}$ on 22.07.2010. The headwater discharge belonging to each echo-sounding measurement is listed in table 1.

5.3. Bed sediments

The bed sediments in the navigation channel consists mainly of fine and middle sand fractions (BfG, 2012). Based on dataset from 2005, provided by the German Federal Waterways Engineering and Research Institute, in the study area an average grain size distribution was determined with 4% coarse sand, 27% middle

sand, 43% fine sand and 26% silt and clay fractions.

5.4. Dredging and supply

In 2010 the German Federal Water and Shipping Administration has supplied about 2.5 Mio m^3 to the relocation sites near St. Margarethen, a substantial part of 47% of this was relocated within the whole April 2010. Depending on the origin of the dredged material the supplied sediments were covering a wide range of fractions: silt, fine sand and middle sand. When being released from the hopper dredger most of the silty sediments are expected to remain in suspension and drift with the current. For coarser fractions, mainly middle sand, are assumed that they accumulate on the river bed, afterwards they attend in bed-load transport and get in the navigation channel in some places (BfG, 2010). In the study period between March and August 2010 about two to three times a month water injection procedures were carried out in the navigation channel to eliminate individual bed form crests. Due to ice drift no water injection procedures take place during February (Qrefa-Sander, WSA Hamburg, pers. comm.).

4. METHODS

5.1. History

A first version of the dunetracking software DT2D (Dune Tracking in 2 Dimensions) was launched in 1997. A final version of the program, called DT2D 3, was released in 2000 (Wesseling & Wilbers, 2000) and was successfully applied in a large number of studies for the quantification of transport rates in Dutch rivers (e.g. Wilbers, 2004; Frings, 2005a, 2005b; Wilbers and Ten Brinke, 2003; Frings and Kleinhans, 2008). In 2007 the German Federal Institute of Hydrology expressed the wish to convert DT2D into a tool for operational management, which led to a completely new development of the software now being called Rheno Bedfrom Tracking (Rheno BT). Refer to Frings (2011) for further readings about the software.

5.2. Bed form analyses with Rheno BT

Rheno BT software detects bed form structures in echo-sounding data. Data input (I) are three-dimensional echo-sounding data, which represent the height characteristics of the river bed. Using Rheno BT software we could (II) indicate bed forms, (III) calculate bed form properties and finally (IV) determine the bed form migration between two consecutive measurements. First of all, we import the three-dimensional bed-elevation data, after that Rheno BT calculates two-dimensional bed-elevation profiles, called BEPs to the left and to the right of the used tracking axis, in our case in a distance of every 20m. This is executed in two steps and continues as long as the number of points contributing to the BEP did not drop below a certain threshold. Points which contribute in a circuit of 5m to one BEPs are selected. Afterwards the points are projected to BEP separated in sections. In the second part bed forms are identified downstream in two-dimensional longitudinal direction. In order to achieve information about spatial variability Rheno identifies bed forms for several BEPs located next to each other in lateral direction. A periodogram is used to provide us the possibility to determine a window length for the moving average line therefore a power is plotted against distance. The larger the power, the more suitable is the distance as window length. For our analyses we used a window length of 120m and a zero down crossing factor of 0.3m prevents noise to be recognized as bed forms and skip the smaller bed forms. In the third part Rheno BT provides the determination of the bed form properties of the identified bed forms like bed form height, bed form length, bed form area and the shape factor. The shape factor determines the similarity between an identified bed form and a related idealized triangle. In the fourth part we determined the bed form migration based on our three-dimensional bed-elevation data between two consecutive BEPs using a cross correlation procedure with a maximum migration distance of 60 m.

5.3. Post-processing

The post-processing is carried out in the same way for each dataset. Average point density in Rheno BT was determined at one point per m^2. Reflecting the work of Wilbers and Ten Brinke (2003) we supposed that bed form length could determined accurate when the bed form consists at least of ten points. Therefore we deleted bed forms with a length shorter than 10m from our dataset. Also 2% of the largest bed forms were selected and deleted

as outliers. For each dataset and BEP a mean bed form height and length is calculated and all BEPs in the same distance to tracking axis were averaged. Migration rate was calculated using the migration distance which was computed in Rheno BT between seven echo-sounding datasets and dividing it through time interval between the two datasets. Migration rate is plotted against the headwater discharge which is averaged over the corresponding time period. Afterwards we compared our migration rate depending on headwater discharge with results from Nasner (1974) and Zorndt et al. (2011). To describe development of an individual bed forms after water injection, we monitored height of bed form crest in each dataset after the cut back of the crest. We determined a rate of increase by dividing increase of height of the bed form through time interval.

5. RESULTS

5.1. Geometry

The averaged bed form geometry over time and space is about 2.2m in height and 82.2m in length. Figure 2 shows mean bed form heights and lengths averaged for BEPs in the same distance to tracking axis. Bed form length varies between 71m and 95m with the longest bed forms in the middle of the navigation channel close to the tracking axis (0). Minimum bed form lengths were observed in the north eastern part of the navigation channel. Bed form heights vary between 1.7m in the south western part and 2.6m close to the tracking axis. In south western part of the tracking axis the bed forms are not as high as on the north eastern part.

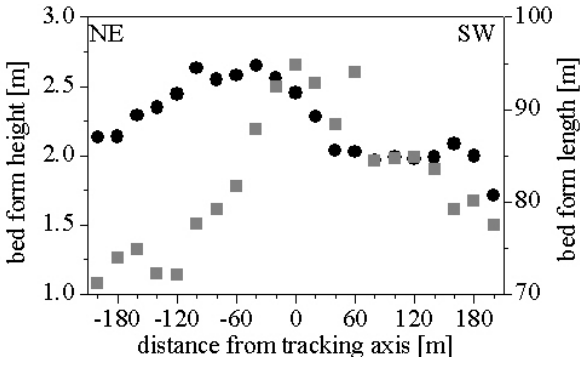

Figure 2. Average bed form height and length in cross section of the navigation channel .

5.2. Geometry and discharge

The mean bed form height and length for each dataset is plotted against headwater discharge in figures 3. There is neither a clear correlation between headwater discharge and bed form height nor between headwater discharge and bed form length.

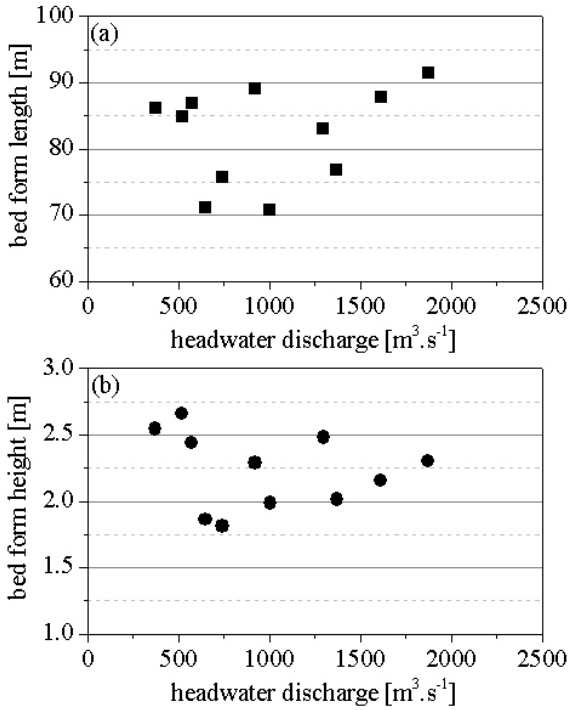

Figure 3. Averaged bed form length (a) and height (b) over time and space against headwater discharge.

5.3. Migration

The migration rate is plotted against headwater discharge in figure 4. A good correlation can be found between these two factors. In the study area near St. Margarethen migration rate was about 0.6 $m.day^{-1}$ in the direction of the North Sea when headwater discharge was higher than $1200 m^{3}.s^{-1}$. During periods of headwater discharge less than 500 $m^{3}.s^{-1}$ the migration rate is close to zero with 0.1 $m.day^{-1}$ in the direction of the North Sea with 0.1 $m.day^{-1}$. Figure 4 also shows our results together with the migration rates determined by Naser (1974) and Zorndt et al.(2011). All studies show a good correlation between migration rate and migration direction with headwater discharge.

To highlight the correlation we used a linear regression. For each location and headwater discharge there might be a point of reversal where bed forms change their migration direction.

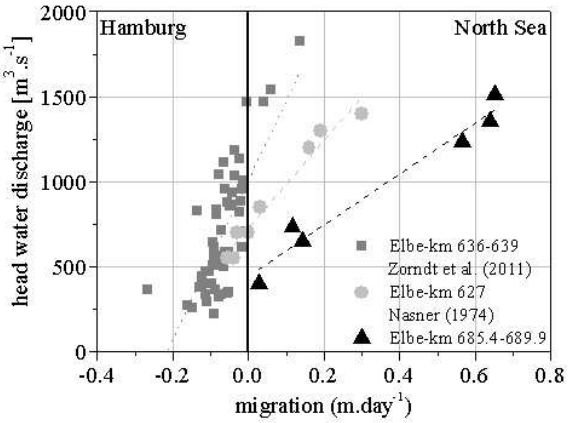

Figure 4. Averaged bed form length (a) and height (b) over time and space against headwater discharge

5.4. Bed form height after water injection

Figure 5 and figure 6 refers to the same individual bed form structure, located 180m northward of the tracking axis within the navigation channel. To maintain the required navigational water depth of -13.9m SKN the crests of these structures were eliminated by water injection procedure on 23.04.2010. The following echo-sounding measurement on 28.04.2010 shows that the crest were cut back from -13.25m SKN to -14.65m SKN. On 12.07.2010 within a few months this individual bed form was observed to reshape and to regain almost its previous height with -13.68m SKN (figure 5).

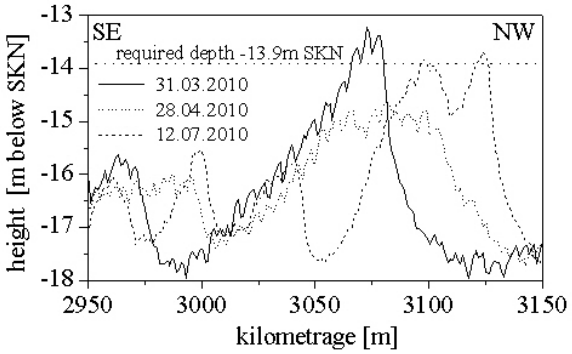

Figure 5. Development of a individual bed form, 180m northward of tracking axis after a water injection.

Figure 6 focuses only the bed form crest. During low headwater discharge the crest increase and during high headwater discharge the crest decrease in height.

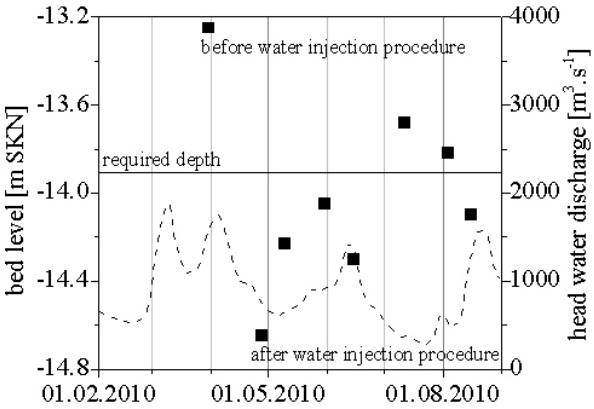

Figure 6. Reshape of bed form crest in relation to headwater discharge after the water injection.

6. DISCUSSION

The applied Rheno BT software and therefore the dune tracking method which are used to analyse bed form structures in the presented study area near St. Margarethen is a reliable tool to determine bed form geometry, migration distance and direction between two consecutive echo-sounding datasets. Rheno BT is a functional and stable software and provides proper and reproducible datasets.

The presented dataset from March to August 2010 covered a period with a range from high headwater discharge in March to low headwater discharge in July. Although the spatial resolution of the dataset is not very high, we were able to determine bed form geometry, migration rate and distance for the period between March and August 2010. We also got an impression of the development of individual bed form structures after water injection procedures.

We found out that geometry of bed form structures varies across the width of the navigation channel in our study area. This seems reliable because our study area is located in a river bend with the inner bend in south western part and outer bend in north eastern part. It is likely that there are different velocities in cross sectional area and therefore bed form height might be higher in north eastern part

than in south western part of the navigation channel. Unfortunately we have no in-situ velocity measurements in the study area to check the assumption.

A correlation between bed form geometry and headwater discharge could not found. Probably bed form structures not yet achieved a equilibrium because of the constantly changing hydrological influences such as current direction and current velocity, headwater discharge or even because of human interventions.

Almost all bed forms in the study area show a asymmetry in shape, which indicates a migration in direction towards the North Sea. In the study area we found out that even during low headwater discharge the residual bed form migration is directed downstream. In river sections located more upstream close to the Port of Hamburg, where the study of Nasner (1974) was conducted, bed form structures migrate upstream during headwater discharge smaller than $700 m^3.s^{-1}$ and downstream during higher discharge (Nasner, 1974). Zorndt et al. (2011) presented a dataset in a flood dominant area downstream of the Port of Hamburg where the bed form migration direction is upstream except during high discharge over $1468\ m^3.s^{-1}$. However, all three studies show the same trends: (I) Bed form migration rate decrease downstream to the North Sea with a decrease in headwater discharge, (II) each study determined a point where bed form migration direction is being turned or becomes almost zero. We suggest that this reversal point is depended on the location in the tidal Elbe river, flood dominance in the river section and headwater discharge.

If we want to correlate bed form geometry to human influences like sediment supply in relocation sites and water injection activities, there is no dataset which is not affected by human influence except that from 01.03.2010, because in February there was ice in the water and therefore no water injection and no artificial supply took place in this area. We know from our experience that individual bed forms especially close to the border of the navigation channel increase in height and impair the safety for navigational purpose. We suggest that the reason for this is the artificial supply on the relocation sites close to the navigation channel during the entire year. The sediments which are coarser than a particular grain size are transported into the channel and participate in the sediment transport and contribute by building bed form structures. We cannot document this with data at the moment, but we know that water injection procedures in the study area were carried out more and more and the frequency increase.

But we were able to document the development of an individual bed form structure after a water injection procedure in April 2010 in the navigation channel which was showed in chapter 5.4. Bed form structures generate to their original height in only a few month. We suggest that this development is a kind of circulation process, because sediments were re-arranged and not removed during water injection procedures and it will not end until water injection procedure stops. But we also mentioned that the observed bed form crest decrease for a while during high headwater discharge, although there was no clear correlation between bed form geometry and headwater discharge in our dataset.

7. CONCLUSION

In this study we applied Rheno BT software as an operational tool for river managers to determine bed form geometry, migration direction and migration rate. The computed results were further investigated to appoint the influence of headwater discharge and water injection procedures on bed form geometry, migration rate and direction in the tidal Elbe river in the study area near St. Margarethen. In total eleven measurements between March and August 2010 were analysed. Moreover daily values of discharge from the gauge Neu Darchau, sediment samples from relocation sites and the navigation channel and information on dredging, artificial supply and water injection procedures were available.

Within the study area 10.000 individual bed form structures with an average bed form height and bed form length of 2.2m and 82.2m were detected. But bed form geometry varies over the navigation channel and over time due to natural fluctuations, to river morphology and to water injection procedures. Therefore neither bed form height nor bed form length in our study area correlate with headwater discharge.

The determined migration rate depends on headwater discharge, we found a migration rate of

$0.6m.day^{-1}$ during discharge $>1200m^3s^{-1}$ and a migration rate smaller than $0.2m.day^{-1}$ during low discharge $<700m^3.s^{-1}$. Studies by Nasner (1974) and Zorndt et al. (2011) show for migration rate results in the same order of magnitude.
We found out that individual bed form structures only need a few month to regain its previous height before their elimination by water injection procedures.
In future research, the development of bed forms after water injection and the development of the crest and troughs will studied in more detail. In addition the results of this study will be used for further calculations of the sediment transport. Modeller are able to use the results to reconstruct the thickness of the active layer and to calculate spatial variations in bed form-related to hydraulic roughness

8. ACKNOWLEDGMENT

The data were collected and provided by the German Federal Water and Shipping Administration in Hamburg, Germany in persons of Dr. Ingo Entelmann and Mamat Qerefa-Sander, which we gratefully acknowledge. The authors are grateful to Kor de Jong from the Utrecht university, the Netherlands, who programmed the software.

9. REFERENCES

BfG 2010. Untersuchungen zur Dynamik von Feststoffen und feststoffgebundenen Schadstoffen für den Verbringbereich bei Elbe-km 688/690. Ergebnisse der Monitoringkampagnen vom Oktober 2008 und März 2009. BfG-1691: 1-92.

BfG 2012. Auswirkungsprognose für die Umlagerung von Baggergut im Verbringstellenbereich zwischen Elbe-km 686 und 690. BfG-1744: 202.

Dammschneider, H.-J. 1983. Morphodynamik, Materialbilanz und Tidewassermenge der Unterelbe. Institut für Geographie der Technischen Universität Berlin 12: 166.

Flemming, B.W., 2000. The role of grain size, water depth and flow velocity as scaling factors controlling the size of subaqueous dunes. Marine sandwaves dynamics. 7

Frings, R.M. & Kleinhans, M.G., 2008. Complex variations in sediment transport at three large river bifurcations during discharge waves in the river Rhine. Sedimentology 55 doi: 10.1111/j.1365-3091.2007.00940.x: 1145-1171.

Frings, R.M., 2005a. Sedimenttransport op de Ijsselkop tijdens hoog- en laagwaterperioden in 2002 en 2004. Utrecht: Centre for Geo-ecological Research ICG 05/2.

Frings, R.M., 2005b. Sedimenttransport op de Merwedekop tijdens de hoogwaterperiode van 2004. Utrecht: Centre for Geo-ecological Research ICG 05/3.

Frings, R.M., 2011. Proposal for the revision of the dunetracking software DT2D. Institute of Hydraulic Engineering and Water Resources Management, RWTH Aachen University.

IKSE 2005. Die Elbe und ihr Einzugsgebiet. Ein geographisch-hydrologischer und wasserwirtschaftlicher Überblick: 16.

Kappenberg, J. & Fanger, H.-U. 2007. Sedimenttransportgeschehen in der tidebeeinflussten Elbe, der Deutschen Bucht und in der Nordsee. Forschungszentrum Geeshacht 20: 123.

Moehl, S. 1996. Sedimenttransport im Bereich der Tideelbe. Formänderungen von Riffeln als Kennwert der Materialumlagerung. Mitteilungen der Geographischen Gesellschaft 86: 109.

Nasner, H. 1974. Über das Verhalten von Transportkörpern im Tidegebiet. Mitteilungen des Franzius-Instituts für Wasserbau und Küsteningenieurswesen der technischen Universität Hannover Heft 40: 149.

Ten Brinke, W. 2005. The river Rhine, a restrained river. Diemen: Van Veen Magazines: 228

Vollmers, H. &Wolf, G. 1969. Untersuchung von Sohlenumbildungenim Bereich der Unterelbe. Die Wasserwirtschaft 140: 269-293.

Wesseling, C. & Wilbers, A.W.E. 2000.Handleiding DT2D versie 2.3 Software voor dune-tracking in twee dimensies. Manual. Utrecht. 24.

Wilbers, A.W.E. & Ten Brinke, W.B.M., 2003. The response of subaqueous dunes to floods in sand and gravel bed reaches of the Dutch Rhine. Sedimentology, 50: 1013-1034.

Wilbers, A.W.E. 2004. The development of hydraulic roughness of subaqueous dunes. Koninklijk Nederlands Aardrijkskundig Genootschap.

Zorndt, A. C., Wurpts, A. & Schlurmann, T. 2011. The influence of hydrodynamic boundary conditions on characteristics, migration, and associated sand transport of sand dunes in a tidal environment. A long-term study of the Elbe Estuary. Ocean Dynamics DOI 10.1007/s10236-011-0452-1: 16.

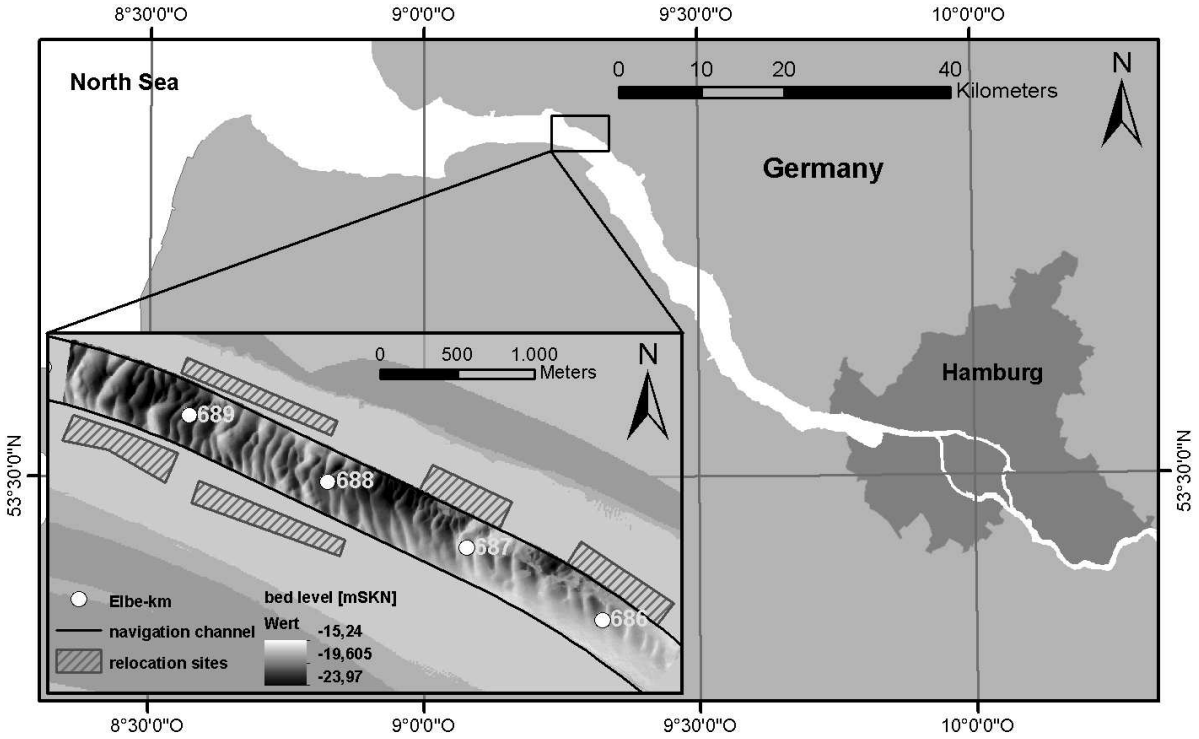

Figure 1. The tidal Elbe river and the study area near St. Margarethen between Elbe-km 685.4 and 689.9.

Numerical Modelling of flumes with moving dunes – TELEMAC3D and Sisyphe

Annalena Goll [1,2] , Rebekka Kopmann [1] and Catherine Villaret [3]

1. Federal Waterways Engineering and Research Institute (BAW), 76187 Karlsruhe, Germany
E-mail: annalena.goll @baw.de
2. Université Paris-Est, Saint-Venant Laboratory for Hydraulics, ENPC, EDF R&D, CETMEF, 78400 Chatou, France
3. EDF R&D Laboratoire National d'Hydraulique et Environnement (LNHE), 78400 Chatou, France

ABSTRACT

The numerical modelling of three dimensional bed form formation remains challenging (quelle?). Indeed, there have been major advances and some successful dune modelling has been shown (i.e. Nabi 2012, Tuijnder 2010). However, it seems that dune modelling is still not applicable in engineering practice, where most projects are 2D-hydrodynamic simulations and bed forms are accounted for by either parametric methods (i.e. Yalin, 1992) or empiric formulations (i.e. v Rijn, 1984).

Dunes are the major bed forms in waterways. If they are only represented indirectly by a dune predictor and an average bed height, they are responsible for high uncertainties concerning water depth and shipping capacity. Not only does the presence of dunes considerably modify the flow structure with vortex creation in the lee of bed forms, also the sediment transport rates are changed.

The prediction of dune characteristic dimensions (height and length) with numerical modules and configurations that are applicable in project work is therefore of high interest.

The objective of this presented work is to validate a full 3D morphodynamics model to represent the bed forms dimensions as well as the characteristic time scales for dunes formation. Here we apply the open source Telemac system (release 6.1).

In the BAW moveable bed experimental flume (in Karlsruhe) three-dimensional dunes have been produced and studied. The flume has a dimension of 30x2m and is filled with uniform sediment with a D50 of 1mm. High resolution measurements provide an excellent data base for the calibration of a numerical model.

The capacity of TELEMAC3D and SISYPHE for modelling dune dynamics and features has been shown in previous studies (Goll and Kopmann, 2012a+b), where the emergence and movement of dunes were successfully reproduced. Nonetheless there were shortcomings: the correct form in terms of skewness of the dune slopes and their curvature (kurtosis) were only partially reproducible. Also a carefully calibrated parameter was necessary and the model results were highly sensible to the choice of turbulence model, bed load formula as well as slope and deviation functions.

To reduce some of the difficulties of reproduction, a second dune study with only two dimensional dunes was calculated with the same calibrated numerical model. The study flume is the one of the Laboratory of Hydraulic Research, Hokkaido University, Japan. The mobile bed region has the dimension of 10x0.1m and the flume is filled with uniform sediment of D50 = 0.28mm. Several studies have been conducted (Giri and Shimizu 2006, Toyama et al 2007) and from this selected runs have been calculated with TELEMAC3D and SISYPHE for this paper. It was possible to explicitly reproduce the 2D dunes of the experimental runs with the same calibrated parameter set as for the BAW flume (see Fig.1). The shape of the dunes has not been considered so far, but the height matches the experimental results already.

Further flumes shall be calculated to find a parameter set that fits a maximum of dune formation scenarios. In the end a configuration for project work will be extracted and the numerical system will be tested on a river stretch comparable to common project work configurations and problems.

REFERENCES

Giri S. and Y. Shimizu 2006. Numerical computation of sand dune migration with free surface flow. Water Resources Research, Vol 42, W10422.

Goll A. and R. Kopmann 2012. Dune simulation with TELEMAC3D and SISYPHE: A parameter study. Proceedings of Telemac Users Club, Oxford (in press).

Goll A. and R. Kopmann 2012. Numerical simulations of groyne influenced dunes. Proceedings of River Flow 2012.

Nabi M. 2012. Computational modelling of small-scale river morphodynamics. PhD thesis, Delft University, Faculty of Civil Engineering and Geosciences, Department of Hydraulic Engineering.

Toyama A. et al 2007. Study of sediment transport rate over dune-covered beds. Proceedings of RCEM 2007.

Tuijnder A.P. and J.S. Ribberink 2010. Development of supply-limited transport due to vertical sorting of a sand-gravel mixture. Proceedings of River Flow 2010.

Van Rijn, L. C. 1984. Sediment transport, part III: Bed forms and alluvial roughness. Journal of Hydraulic Engineering.

Yalin, M. S. 1992. *River Mechanics*. Elsevier, New York.

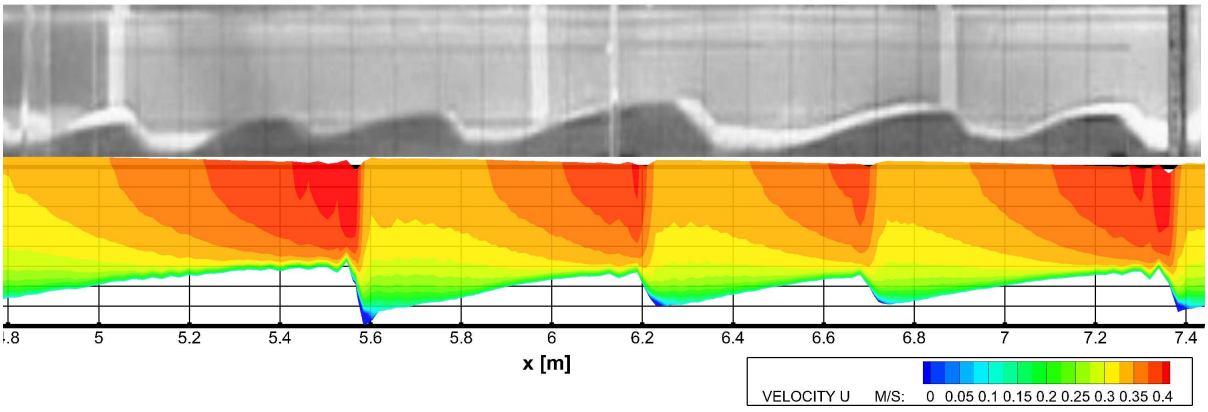

Figure 1: Calculations (preliminary results) with Sisyphe/Telemac3d after 4h simulation time (longitudinal section) in comparison to results from Giri & Shimizu, 2006, run A-1.

Numerical simulation of Dune morphodynamic changes for unsteady flows

Patrick Grover [(1)] and Ana Maria Ferreira da Silva [(1)]

1. Department of Civil Engineering, Queen's University, Kingston, Ontario, Canada K7L 3N6
E-mail: patrick.grover@queensu.ca

ABSTRACT

The morphological evolution of river dunes exposed to unsteady flow conditions presents challenges to engineers trying to predict water levels for navigation, flood and water management. Our long term objective is to develop a coupled hydrodynamic-sediment transport model to predict the evolution of dunes under unsteady flows. This paper presents our preliminary investigation into the hydrodynamics of flows of varying flow depths over rigid dunes. Detailed velocity measurements are collected using LDV over a train of 130cm long and 7.43cm high dunes under various flow depths at our laboratory flume located at the Coastal Lab at Queen's University in Kingston Ontario. A RANS numerical model is developed using the OpenFOAM CFD package and compared to the laboratory measurements. We conduct a detailed investigation into the meshing requirements in the near-wall region order to develop a computationally robust and efficient mesh. We also compare the results of a rigid-lid and a free-surface model using based on the Volume-of-Fluid approach. Finally we present the preliminary results of our sediment transport model.

Evolution of secondary cellular circulation flow above submarine bedforms imaged by remote sensing techniques

I. Hennings [(1)], D. Herbers [(1)]

1. GEOMAR Helmholtz-Zentrum für Ozeanforschung Kiel, Kiel, Germany - ihennings@geomar.de

Abstract

Normalized radar cross section (NRCS) modulation and acoustic Doppler current profiler (ADCP) measurements above submarine sand ribbons and sand waves are presented. The two study areas are located in the Southern Bight of the North Sea at the *Birkenfels* wreck and in the sand wave field of the Lister Tief in the German Bight of the North Sea. These measurements reveal the developments of secondary cellular circulations in tidally induced coastal sea areas. Secondary circulation cells can develop perpendicular as well as parallel to the direction of the dominant tidal current flow. Circulation cells developed perpendicular to the direction of the dominant tidal current flow are associated with marine sand ribbons manifested near an underwater wreck. Secondary circulation cells within the water column observed parallel to the direction of the dominant tidal current flow have been initiated during flood and ebb tidal current phases associated with submarine sand waves. These two types of cellular circulations must obey the Hamiltonian principle of classical mechanics. The current–short surface wave interaction is described by the action balance or radiation balance-equation based on weak hydrodynamic interaction theory. The calculated current gradient or strain rate of the applied imaging theory has the same order of magnitude for both bedforms such as marine sand ribbons and sand waves, respectively.

1. INTRODUCTION

During the last three decades it turned out that the wave-current-bedform interaction mechanism is a rather complex process. Marine remote sensing data gave a certain impulse for the explanation of the different imaging mechanisms in the visible, infrared and microwave parts of the electromagnetic spectrum as well as in the sound waves spectrum. Normalized radar cross section (NRCS) modulation and acoustic Doppler current profiler (ADCP) measurements above submarine sand ribbons and sand waves reveal the development of secondary cellular circulation in tidally induced coastal sea areas. Mathematically and physically such kind of associated hydrodynamics obeys the Hamiltonian principle of classical mechanics (Neumann 1946, Neumann 1949, Alpers & Hasselmann 1978).

Secondary circulation cells can develop perpendicular as well as parallel to the direction of the dominant tidal current flow $\mathbf{U_0}$. In this paper both cases will be presented. Secondary circulation cells developed perpendicular to the direction of $\mathbf{U_0}$ are associated with marine sand ribbons manifested near an underwater wreck in the Southern Bight of the North Sea (Hennings & Herbers 2010). In contrast, secondary circulation cells related parallel to the dominant direction of the tidal flow $\mathbf{U_0}$ are associated with marine sand waves in the tidal inlet of the Lister Tief in the German Bight of the North Sea (Hennings & Herbers 2006).

A similar kind of secondary circulation arising in the water is the vortex pair generated by the ship hull. Lateral current gradients behind the ship have been measured (Marmorino & Trump 1996). Surface strain rates associated with the divergent flow had a value of $\partial u/\partial x = 0.03\ s^{-1}$. This strain rate is of the same order of magnitude as strain rates associated with internal waves, fronts and sea bottom topography in littoral waters (Gasparovic & Apel 1988, Marmorino & Trump 1994, Hennings & Herbers 2010).

The motivation for this study is the mathematical and physical formulation of the imaging mechanism of radar signatures at the sea surface caused by submerged wrecks as well as ADCP measurements above marine sand waves. First, the

formation of wreck marks like sand ribbons at the sea bed and the associated manifestation of radar signatures at the water surface caused by a vortex pair or helical flow cells triggered by unidirectional tidal current flow interacting with a wreck are summarized. Second, the ADCP measurements and the characteristic flow related to marine sand waves in a tidal channel are shown. In section 2, a brief background of the theory is presented. Secondary circulation flow associated with sand ribbons and sand waves are described in section 3. Finally, section 4 contains the discussion and conclusions.

2. THEORY

The equations of Hamiltonian flow in phase space connect position x with momentum p_x through the Hamiltonian H. Volume in phase space is conserved under Hamiltonian flow, a property known today as Liouville's theorem (Nolte 2010). Neumann (1946) already concluded that a cellular current must obey the Hamiltonian principle of classical mechanics. The so called standing cellular wave published by Neumann (1946) is shown in Figure 1. Standing cellular circulation implies that volume or mass is not only be conserved by an acceleration or deceleration of the flow associated with submarine bedforms but that up- and downwelling of the three-dimensional current field is also important (see section 3). According to this fundamental background the current–short surface wave interaction can be described by the action balance or radiation balance equation (Alpers & Hasselmann 1978)

$$\frac{dN}{dt} = \left(\frac{\partial}{\partial t} + \dot{\mathbf{x}} \frac{\partial}{\partial \mathbf{x}} + \dot{\mathbf{k}} \frac{\partial}{\partial \mathbf{k}} \right) N = S(\mathbf{x}, \mathbf{k}, t) \qquad (1)$$

where N is the wave action density spectrum, $\mathbf{x}$ is the space variable, t is the time variable, $\mathbf{k}$ is the wave number and $S(\mathbf{x},\mathbf{k},t)$ is a source function. The waves propagate along trajectories in phase space which are given by the ray equations

$$\dot{\mathbf{x}} = \frac{\partial \omega}{\partial \mathbf{k}} \qquad (2a)$$

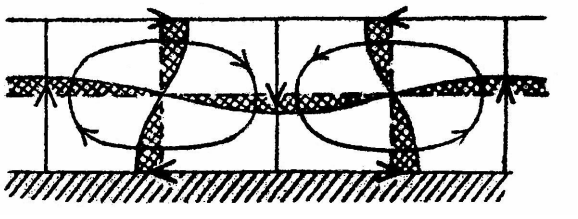

Figure 1. Standing cellular wave dynamics published by Neumann (1946).

$$\dot{\mathbf{k}} = \frac{\partial \omega}{\partial \mathbf{x}} \qquad (2b)$$

where

$$\omega(\mathbf{x}, \mathbf{k}, t) = \omega'(\mathbf{k}) + \mathbf{k} \cdot \mathbf{U}(\mathbf{x}, t) \qquad (3)$$

denotes the angular wave frequency in the moving medium with variable velocity $\mathbf{U}(\mathbf{x},t)$ and $\omega'(\mathbf{k})$ is the intrinsic angular wave frequency.

The relationship between the wave height spectrum $\Psi(\mathbf{k})$, the wave-energy density spectrum $F(\mathbf{k})$ and the wave action density spectrum $N(\mathbf{k}) = F(\mathbf{k})(\omega'(\mathbf{k}))^{-1}$ is defined by (Holliday et al. 1986)

$$F(\mathbf{k}) = \omega'(k) N(\mathbf{k}) = \frac{\omega'(k)^2}{k} \psi(\mathbf{k}) \qquad (4)$$

After transforming the mathematical formulations like described by Alpers & Hennings (1984) have been carried out then the expression for the modulation of the first order perturbed wave energy density spectrum $\delta F/F_0 = (F - F_0)/F_0$, with F_0 as the unperturbed and F as the local wave energy density spectrum, respectively, is derived as a first approximation

$$\frac{\delta F}{F_0} = -(4+\gamma) \frac{\partial u_{perp}}{\partial x_{perp}} \left(\left(\mathbf{c_g} + \mathbf{U_0} \right) \frac{1}{L} + \mu \right)^{-1} \qquad (5)$$

where γ is the relation between the group velocity $\mathbf{c_g}$ and the phase velocity of the short waves, $\partial u_{perp}/\partial x_{perp}$ is the gradient or strain rate of the current velocity component of the secondary circulation perpendicular to the bedform, $\mathbf{U_0}$ is the mean dominant tidal current flow of the undisturbed sea area, L denotes the spatial scale of the flow cell in x_{perp}-direction, and μ is the relaxation rate parameter. Equation (5) describes that the modulation of the first-order perturbed wave energy density spectrum of capillary and short gravity waves is proportional to the current

gradient of the secondary circulation caused by marine bedforms such as sand ribbons (Kenyon 1970) and sand waves (Hennings & Herbers 2010). However, equation (5) is only valid if the one-dimensional model for describing the sea bottom topography-current interaction is applicable. Otherwise, a full three-dimensional approach is required. If it is assumed that the radar is a linear imaging system then the relative radar image intensity modulation $\delta I/I_0$ is equal to the relative normalized radar cross section (NRCS) modulation $\delta\sigma/\sigma_0$ based on quasi-specular scattering. It follows that $\delta\sigma/\sigma_0$ is then proportional to $\delta F/F_0$ defined in equation (5) (Hennings & Herbers 2010).

3. SECONDARY CIRCULATION

Transverse secondary circulation of flow over a rough sea bed is equivalent to Langmuir circulation at the water surface due to wind stress. Circulation patterns associated with Langmuir super cells off the coast of New Jersey of the eastern U.S. coast have been identified by Gargett et al. (2004). The dominant scale of such circulation may be responsible for low-relief sand ribbons in the presence of strong tidal currents. Karl (1980) and Viekman et al. (1992) assumed that helical secondary-flow circulation within a boundary layer is responsible for the lineation development of sand ribbons and sedimentary furrows. Secondary circulations in the sea bottom boundary layer concentrate large, low-density particles in zones where there is flow convergence on the sediment surface. Thereupon, lineations such as sand ribbons can be formed. The schematic representation of the relationship between secondary circulations in the boundary layer, zones of convergence and divergence on the sea bed, sand ribbons, and sedimentary furrows in the model of furrow maintenance is presented in Figure 2 (Viekman et al. 1992). Hulscher (1996) shows that inclusion of vertical flow structures turned out to be necessary to describe the formation, or absence, of all known large-scale regular sea bottom features. The residual component of the vertical velocity is one order of magnitude smaler than the horizontal residual

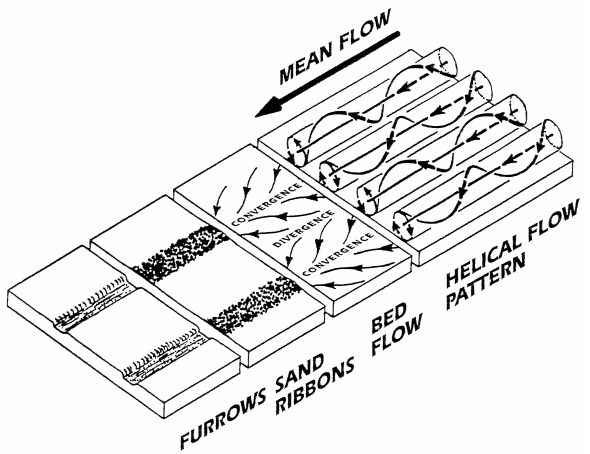

Figure 2. Schematic representation of the relationship between secondary circulations of the boundary layer, zones of convergence and divergence on the sea bed, sand ribbons, and sedimentary furrows in the model of furrow maintenance according to Viekman et al. (1992). Copyright 1992 by the American Society of Limnology and Oceanography, Inc.

velocity. It is directed upward above the crests and downward towards the troughs. These residual flow components cause a residual circulation which favours the growth of the bedform, as outlined in Fig. 2. In situ measurements verify up- and downwelling phenomena of the three-dimensional current velocity field contributing significantly to the interaction between marine sand waves and the tidal flow, which has not been known before in detail (see section 3.2, Alpers & Hennings 2004, Hennings and Herbers 2006). The up- and downwelling regimes cause remarkable depressions at the troughs of sand waves with a maximum depth of 2 m and a width of maximum 50 m (Hennings & Herbers 2006).

An elliptical vortex pair or elliptical helical flow cells are assumed as a first approximation to explain the interactions between the wreck mark, the (tidal) current, the residual flow and the water surface roughness. This assumption was based on the formation of wreck marks such as sand ribbons at the sea bed as shown in Fig. 2 and the manifestation of associated radar signature at the water surface as well as due to spatial considerations presented in section 3.1.

3.1 Sand ribbon associated with secondary circulation flow

The following relation can be derived for $\partial u_{perp}/\partial x_{perp}$ from equation (5) according to Hennings & Herbers (2010):

$$\frac{\partial u_{perp}}{\partial x_{perp}} = \frac{u_{perp} \cdot z}{R}\left(1-2\frac{R^2}{z^2}\right)\times \left(\frac{x_{perp}}{R\cdot z}+\left(z_{\max}-z\right)\cdot 2F_{sp}\cdot\left(x_{perp}-R\right)^2\frac{1}{z^2}\right) \quad (6)$$

where $R = |\mathbf{R}|$ of the space vector of a point on an ellipse in the Cartesian coordinate system, u_{perp} is the tangential current of an elliptical gyre at the sea surface in x_{perp}-direction, z is the water depth, z_{max} is the maximum water depth, and F_{sp} is the so-called shape parameter, which determines the slope of the sand ribbon.

Due to the analysed *Birkenfels* wreck data (Hennings & Herbers 2010) it turned out that only one of the two possible circulation cells downstream of the wreck is responsible for the manifestation of the radar signature (see also Fig. 3). Otherwise the bright and dark signatures as well as the spatial scales of $\delta I/I_0$ are not consistent with the theoretical assumptions. The reason for the manifestation of only one bright as well as one dark radar signature can be due to the following effect: The inactive circulation cell has been not developed to such an extent that the current gradients become too weak to produce a significant NRCS modulation. This can happen due to changing tidal current directions of $\mathbf{U_0}$ relative to the orientation of the wreck and sand ribbon, which has been indeed observed above marine sand waves (Hennings et al. 2000). However, Innes McCartney, a wreck specialist, reported in Divernet, the Diver Magazine Online (2012), that strong tidal currents can be developed at a wreck even in a water depth of 70 m lying in the sea area between the island of Alderny and Cape Le Hague in the English Channel. McCartney discovered the wreck on 4 July 2006 off Cape Le Hague which was the German Navy raider *Komet*. The *Komet* sunk on 14 October 1942. In 2007 it took two days for the divers to work out how to negotiate the treacherous currents in the area. The currents run fiercely over the upturned hull. But the uncertainty over the true nature of the water motion around a wreck underlines just how valuable in situ current measurements would have been in this situation. On the basis of these considerations, Figure 3 presents a schematic view of the radar imaging mechanism of the submerged *Birkenfels* wreck and the associated sand ribbon. More details are described in Fig. 3's caption.

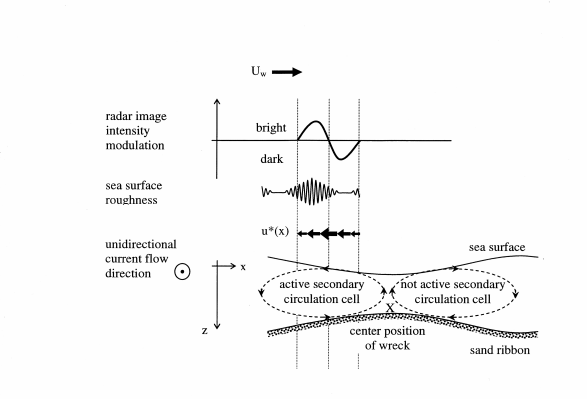

Figure 3. Schematic sketch of the unidirectional ebb tidal current flow (direction coming out of the graphic plane), cross-structure secondary circulation cells above sand waves or sand ribbons, centre position of wreck, marked by the capital letter X, sea surface, horizontal component of the tangential current of the secondary circulation cell $u^* = u_{perp}$ in $x = x_{perp}$-direction at the sea surface, associated sea surface roughness and radar image intensity modulation due to accelerated and decelerated sea surface current velocities of the active secondary circulation cell. The wind direction U_w is indicated by an arrow and the left and right vertical lines indicate schematically the space range of 200 m used for simulations.

The comparison of simulated and measured NRCS modulation as a function of position is shown in Figure 4d. The simulated water depth as a function of position (-100 m $\leq x = x_{perp} \leq$ 100 m) with a total length of x_{perp} = 200 m is presented in Figure 4a and has been used for all simulations. Figure 4b shows the simulated perpendicular current speed $u_{perp} = u^*$ relative to $\mathbf{U_0}$. A maximum current speed of $u_{perp}{}^{max}$ = -0.34 m s^{-1} has been calculated. The strain rate or the gradient of the perpendicular component relative to $\mathbf{U_0}$ of the current velocity $\partial u_{perp}/\partial x_{perp}$ is presented in Figure 4c. Minimum and maximum strain rates varied between -0.0084 s^{-1} and 0.0088 s^{-1}. The comparison of simulated NRCS modulation $(\delta\sigma/\sigma_0)_{sim}$ and measured NRCS modulation $(\delta\sigma/\sigma_0)_{meas}$ as a function of position is shown in Figure 4d. The calculations for $(\delta\sigma/\sigma_0)_{sim}$

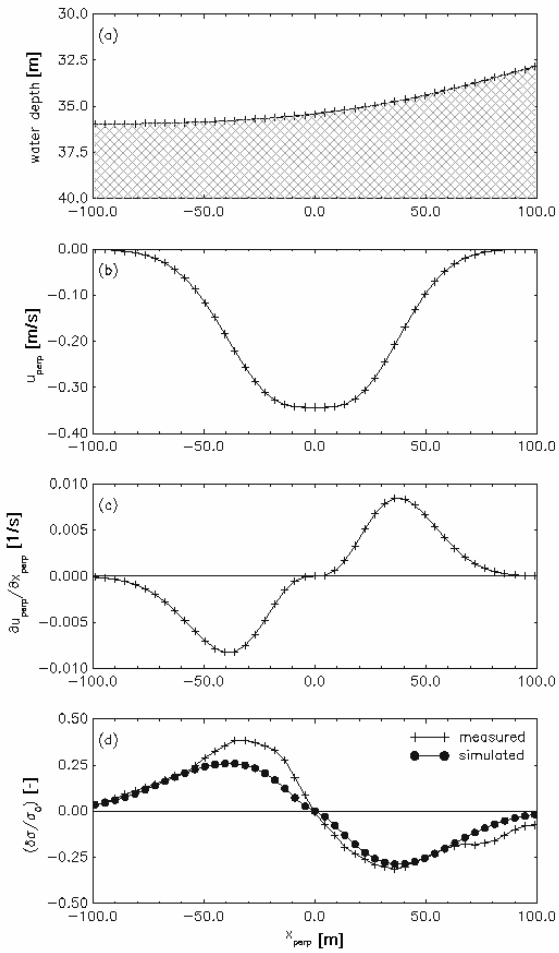

Figure 4. Results of simulations according to Hennings & Herbers (2010): (a) water depth as a function of x_{perp}, (b) perpendicular current speed u_{perp} relative to $\mathbf{U_0}$, (c) strain rate or gradient of the perpendicular component relative to $\mathbf{U_0}$ of the current velocity $\partial u_{perp}/\partial x_{perp}$, (d) comparison of simulated $(\delta\sigma/\sigma_0)_{sim}$ and measured $(\delta\sigma/\sigma_0)_{meas}$ NRCS modulation.

applying equations (1)-(26) from Hennings & Herbers (2010) have been carried out for $\theta_0 = 70^o$, $g = 9.81$ m s^{-2}, $\rho = 1026$ kg m^{-3}, $T = 73 \times 10^{-6}$ m^3 s^{-2}, $B = 4.6 \times 10^{-3}$, $B' = 3.15 \times 10^{-2}$, $k_v = 502.28$ m^{-1}, $U_0 = 0.8$ m s^{-1}, $U_w = 9$ m s^{-1}, $L = 369$ m, $\mu = 1$ s^{-1}, $a = 184.50$ m, $b = 25.04$ m, $h_0 = 5$ m, and $z_{max} = 36$ m. The value for μ is in the range of parameterizations for the K_a band radar as published by Caponi et al. (1988). The direction of $\mathbf{c_g}$ has been assumed equal to the wind direction from 270^o. For all simulations the perpendicular component of $\mathbf{c_g}$ relative to $\mathbf{U_0}$ in the direction of x_{perp} has been used. The simulated NRCS modulation $(\delta\sigma/\sigma_0)_{sim}$ presented in Figure 4d shows a maximum modulation $(\delta\sigma/\sigma_0)_{sim}^{max} = 0.26$ at the minimum strain rate (see Fig. 4c) and the measured maximum NRCS modulation $(\delta\sigma/\sigma_0)_{meas}^{max} = 0.38$ is located also at the minimum strain rate. The measured minimum modulation $(\delta\sigma/\sigma_0)_{meas}^{min} = -0.31$ at the maximum strain rate position agrees fairly well with the simulated modulation $(\delta\sigma/\sigma_0)_{sim}^{min} = -0.29$ with a coinciding phase relation. The results of $(\delta\sigma/\sigma_0)_{sim}$ presented in Figure 4d show the best fit to $(\delta\sigma/\sigma_0)_{meas}$ based on available in situ data and most consistent other parameters like μ.

3.2 Sand wave associated with secondary flow

The vertical flow components u_{vert} of the three-dimensional current field measured by the ADCP over asymmetric marine sand waves on the sea bottom in the study area of the Lister Tief in the German Bight of the North Sea are shown in Figures 5a-b at the end of the paper (Hennings & Herbers 2006). The current field has been measured by the ADCP of the same kind during ebb and flood tidal current phases, respectively. During flood tidal current phase the vertical component of the tidal current is reversed compared to the ebb tidal current phase. Upwelling events during ebb tidal current phase are associated with steep flanks of sand waves and during flood tidal current phase u_{vert} is related to downwelling events at the steep flanks of sand waves. The water depth dependent vertical component u_{vert} of the current velocity as a function of the horizontal space component perpendicular to the sand wave crest x_{perp} is shown in Fig. 5a and varies between -12 cm s^{-1} $\leq u_{vert} \leq$ 16 cm s^{-1} during ebb tidal current phase at 0502-0513 UT on 10 August 2002. Last high water at station List was at 0243 UT on 10 August 2002. The downward orientated vertical component (dark or blue colour) is located at the troughs and gentle slopes of the sand waves. A regular structure of circulation cells of u_{vert} within the water column has been developed during that time of the ebb tidal current phase. The upward orientated vertical component u_{vert} of the current velocity (bright or yellow/red colour) has been developed at the steep flanks of sand waves and is superimposed on the divergent zones of the perpendicular component relative to the sand wave crest of the current velocity gradient $\partial u_{perp}/\partial x_{perp}$.

During flood tidal current phase at 1025-1031 UT on 10 August 2002 u_{vert} varies between -16 cm s^{-1} $\leq u_{vert} \leq$ 12 cm s^{-1} (Fig. 5b). Last low water at station List was at 0829 UT on 10 August 2002. The downward orientated vertical component (dark or blue colour) is located at the troughs and steep slopes of the sand waves and is superimposed on the convergent zones of the perpendicular component relative to the sand wave crest of the current velocity gradient $\partial u_{perp}/\partial x_{perp}$. The upward orientated vertical component (bright or yellow/red colour) is associated with the gentle slopes of the sand waves. These observations confirm the theory of the radar imaging mechanism of sea bottom topography presented by Alpers & Hennings (1984).

4. CONCLUSIONS

The standing cellular wave mechanism published by Neumann (1946) has been visualized by the up- and downward orientated components u_{vert} of the three-dimensional current velocity field measured by the ADCP at stoss faces of asymmetric marine sand waves in the study area of the Lister Tief in the German Bight of the North Sea (Hennings et al. 2004). The so called "waterspouts" have been measured by the ADCP of the same kind during ebb and flood tidal current phases, respectively. During ebb tidal current phase the waterspouts are upwelling events and during flood tidal current phase they are associated with downwelling at the steep flanks of the investigated marine sand waves. It has to be noticed here, that observed vertical velocities over two-dimensional (2-D) dunes in a laboratory channel analyzed by Bennett & Best (1995) are directed downwards above the dune trough and upwards over the stoss during flood tidal phase. The vertical velocities described here have a different phase relationship to the sand waves.

The presented theory is a first-order theory, describing the NRCS modulation in the capillary as well as in the gravity wave ranges of the wave energy density spectrum due to secondary flow circulation or helical eddies caused by the investigated submerged wreck/sand ribbon configuration. The theoretical model proposed in this study is not able to explain all aspects of the NRCS modulation due to submerged wrecks associated with sand ribbons in coastal waters. However, the quasi-specular scattering theory does produce sensible results at this stage in our understanding and can explain certain aspects of the radar signature. This subject has been shown by simulations of the NRCS modulation and by comparison with measured NRCS modulation data caused by the *Birkenfels* wreck of the southern North Sea (Hennings & Herbers 2010). That the quasi-specular theory is capable to explain the radar signature of the wreck/sand ribbon may be due to the fact that the *Birkenfels* wreck is lying more or less sub-parallel to the dominant regional tidal current direction.

From the results derived in this paper the following conclusions can be drawn for the NRCS modulation and ADCP measurements above submarine sand ribbons and sand waves revealing the developments of secondary cellular circulations in tidally induced coastal sea areas:

1. Wreck marks like sand ribbons as well as radar signatures of wrecks are indicators of local (tidal) current directions. Radar image signatures of wrecks associated with sand ribbons are indicators of secondary flow regimes or helical circulation cells triggered by unidirectional (tidal) current flow caused by submerged wrecks.
2. The simulated NRCS modulation $(\delta\sigma/\sigma_0)_{sim}$ and the measured NRCS modulation $(\delta\sigma/\sigma_0)_{meas}$ above the wreck/sand ribbon have the same order of magnitude with a coinciding phase relation. The difference between the maximum simulated and measured NRCS modulation is less than 31.6% and the difference between the minimum simulated and measured NRCS modulation is less than 6.5%. These results are acceptable but need to be improved.
3. The existence of a significant upward orientated vertical component u_{vert} of the three-dimensional current velocity field measured by the ADCP has been recorded. Marked waterspouts of u_{vert} have been measured in a more or less straight line in the vicinity of crests above steep slopes of flood tide oriented marine sand waves. These waterspouts created by u_{vert} produce upwelled water and create turbulence patterns at the water surface. The upward orientated patterns of u_{vert} are simultaneously superimposed on the divergent flow zones of $\partial u_{perp}/\partial x_{perp}$. The downward orientated vertical flow component of u_{vert} is located at the troughs and gentle slopes of the

marine sand waves. A regular structure of circulation cells of u_{vert} within the water column has been initiated during ebb tidal current phase. During flood tidal current phase the vertical component of the tidal current is reversed. This implies that mass is not only be conserved by an acceleration or deceleration of the flow in relation to marine sand waves. Up- and downwelling of the three dimensional current field also contribute significantly to the extensive circulation mechanism above marine sand waves in the study area of the Lister Tief.

5. REFERENCES

Alpers, W. & Hasselmann, K. 1978. The two-frequency microwave technique for measuring ocean wave spectra from an airplane or satellite. Boundary Layer Meteorology 13: 215-230.

Alpers, W. & Hennings, I. 1984. A theory of the imaging mechanism of underwater bottom topography by real and synthetic aperture radar. Journal of Geophysical Research 89(C6): 10529-10546.

Bennett, S.J. & Best, J.L. 1995. Mean flow and turbulence structure over fixed, two-dimensional dunes: implications for sediment transport and bedform stability. Sedimentology 42: 491-513.

Caponi, E.A., Crawford, D.R., Yuen, H.C. & Saffman, P.G. 1988. Modulation of radar backscatter from the ocean by a variable surface current. Journal of Geophysical Research 93(C6): 12249-12263.

Gargett, A., Wells, J. Tejada-Martinez, A.E. & Grosch, C.E. 2004. Langmuir supercells: a mechanism for sediment resuspension and transport in shallow seas. Science 306: 1925-1928.

Gasparovic, R.F. & Apel, J. 1988. An overview of the SAR internal wave signature experiment. Journal of Geophysical Research 93: 12304-12316.

Hennings, I., Lurin, B., Vernemmen, C. & Vanhessche, U. 2000. On the behaviour of tidal current directions due to the presence of submarine sand waves. Marine Geology 169: 57-68.

Hennings, I., Herbers, D., Prinz, K. & Ziemer, F. 2004. First results of the OROMA experiment in the Lister Tief of the German Bight in the North Sea. EARSeL eProceedings 3: 86-104.

Hennings, I. & Herbers, D. 2006: Radar imaging mechanism of marine sand waves at very low grazing angle illumination caused by unique hydrodynamic interactions. Journal of Geophysical Research 111: C10008, doi: 10.1029/2005JC003302.

Hennings, I. & Herbers, D. 2010. A theory of the K_a band radar imaging mechanism of a submerged wreck and associated bed forms in the southern North Sea. Journal of Geophysical Research 115: C10047, doi: 10.1029/2010JC006360.

Holliday, D., St-Cyr, G. & Woods, N.E. 1986. A radar ocean imaging model for small to moderate incidence angles. International Journal of Remote Sensing 7: 1809-1834.

Hulscher, J.M.H. 1996. Tidal-induced large-scale regular bed form patterns in a three-dimensional shallow water model. Journal of Geophysical Research 101(C9): 20727-20744.

Karl, H.A. 1980. Speculations on processes responsible for mesoscale current lineations on the continental shelf, southern California. Marine Geology 34: M9-M18.

Kenyon, N.H. 1970. Sand ribbons of European tidal seas. Marine Geology 9: 25-39.

Marmorino, G.O. & Trump, C.L. 1994. A salinity front and current rip near Cape Hatteras, North Carolina. Journal of Geophysical Research 99: 7627-7637.

Marmorino, G.O. & Trump, C.L. 1996. Preliminary side-scan ADCP measurements across a ship's wake. Journal of Atmospheric and Oceanic Technology 13: 507-513.

Neumann, G. 1946. Stehende zellulare Wellen im Meere. Naturwissenschaften 33: 282-283.

Neumann, G. 1949. Stabilitätsschwingungen und die innere thermische Unruhe im Meer und in der Atmosphäre. Deutsche Hydrographische Zeitschrift 2: 52-67.

Nolte, D.D. 2010. The tangled tale of phase space. Physics Today 63: 33-38.

Viekman, B.E., Flood, R.D., Wimbush, M., Faghri, M., Asako, Y. & Van Leer, J.C. 1992. Sedimentary furrows and organized flow structure: A study in Lake Superior. Limnology and Oceanography 37: 797-812.

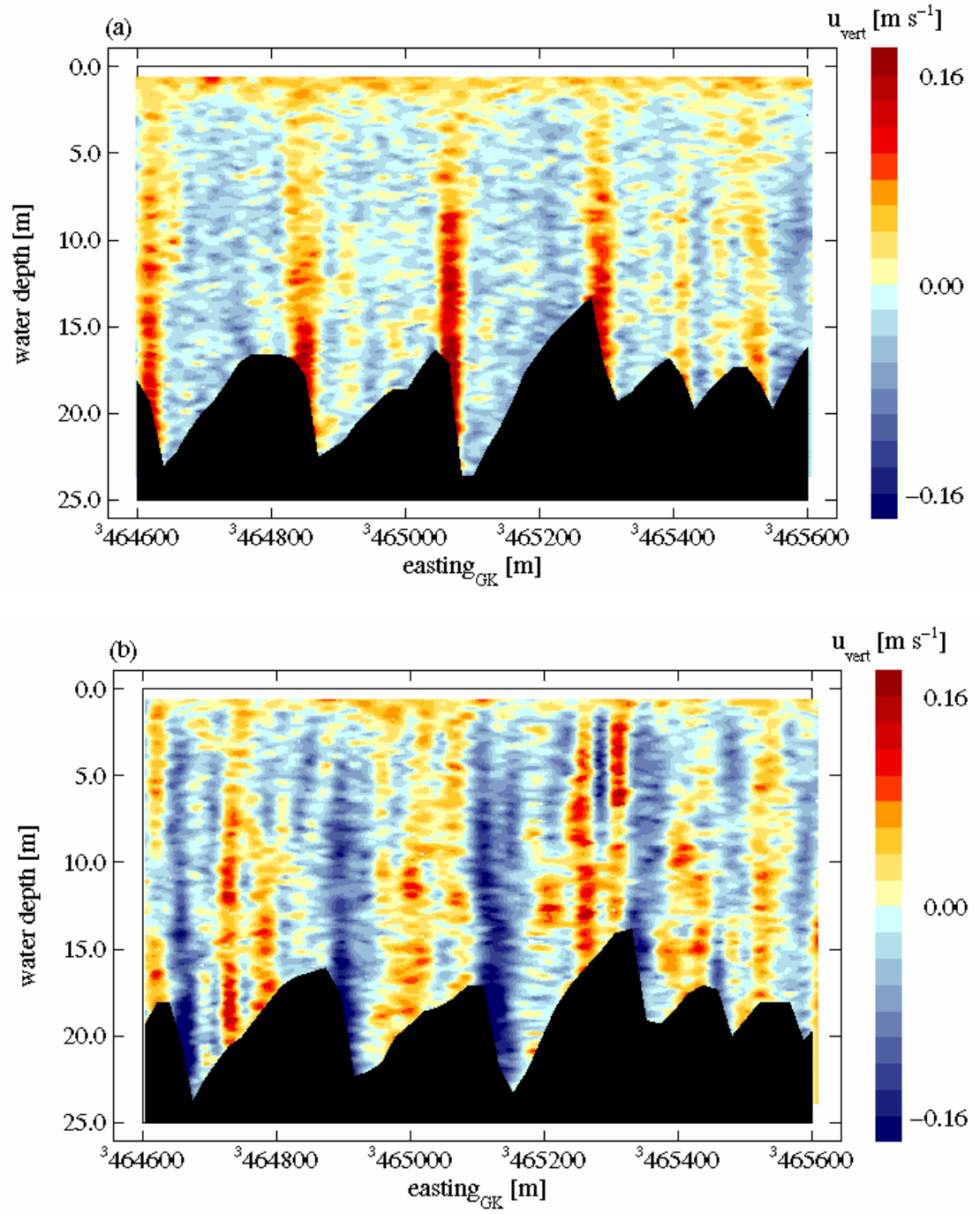

Figure 5. (a) Water depth dependent vertical component u_{vert} of the current velocity as a function of the horizontal space component perpendicular to the sand wave crest x_{perp}. The ADCP data from the near water surface to the sea bed have been obtained on board R.V. *Ludwig Prandtl* during ebb tidal current phase at 0502-0513 UT on 10 August 2002 along the profile *AA'* in the Lister Tief of the German Bight in the North Sea (Hennings & Herbers 2006). Dark or blue colour shows the downward and bright or yellow/red colour the upward orientated vertical component u_{vert}. The direction of the ebb tidal current is from right to left; (b) same as (a) but the data were measured during flood tidal current phase at 1025-1031 UT on 10 August 2002 along the profile *AA'*. The direction of the flood tidal current is from left to right.

Estimation of the friction coefficient induced by marine dune using high resolution bathymetric data

Nicolas Huybrechts [(1)] Hassan Smaoui [(1)], Sophie Le Bot [(2)], Abellatif Ouahsine [(1)], Yann Ferret [(2)] and Robert Lafite [(2)]

1. Roberval Laboratory, LHN (joint research unit UTC-CETMEF), UMR CNRS 7337, Compiègne, France
E-mail: nicolas.huybrechts@developpement-durable.gouv.fr

2. CNRS, UMR 6143 M2C, 76821 Mont-Saint-Aignan Cedex, France.

ABSTRACT

The Somme estuary, located in France in the eastern English Channel, endures a severe sedimentation with an increase of the mean bed level about 1.3 cm/year. The sedimentation is probably induced by the asymmetry of the tidal current and the associated residual sediment flux between the flood and the ebb. This phenomenon is probably increased by different hydraulic structures built during the last centuries to domesticate the tide or river dynamics and to gain farmland. More recently, new hydraulic structures have been planned to limit the sedimentation, such as flush operation from the Somme channel or an experimental realignment project. To predict the bed morphology evolution and the influence of these hydraulic works, it is necessary to estimate the sedimentation rate feeding the bay from offshore. Field surveys (MOSAG07 and MOSAG08 on RV Thalia) conducted offshore, about 30 km away from the mouth in South West direction (Ferret *et al.*, 2010), lighten the presence of marine dunes ranging from 100 m to 1800 m in wavelength. The presence of bedforms, such as dunes, strongly influences the hydrodynamic characteristics and the sediment transport rates. Their influence thus needs to be included into the methodology. The field surveys included high resolution bathymetric data, measurements of tidal currents, wave characteristics and bed material composition. A numerical model of the Somme estuary has been developed using the open source Telemac System (www.opentelemac.org) based on finite element technique. The model comprises a large coastal area (up to 60 km offshore and along shore) in order to predict the sediment feeding from the sea. In numerical model, the dune influence can be reckoned through an equivalent roughness using empirical formulae such as van Rijn 2007 formula. This kind of formula is generally built from datasets collected on river in equilibrium conditions. Their application to estuarine (Huybrechts et al. 2012) or coastal environments is still challenging because of: (1) the unsteady behavior of the flow induced by the tide and the waves, and (2) the lack of *in situ* data to validate the predicted value of the roughness. In the present contribution, it is therefore proposed to analyze how the high resolution bathymetric data can be integrated into the numerical model and can serve to estimate the friction coefficient. In coastal area, the grid resolution is often about 500 to 1000 km. The bedforms are thus not physically represented. Using finer grid may allow to physically represent dunes but it will also require a 3D computation to reckon the 3D flow behaviour induced by dunes. More attention is thus currently paid on the grid resolution regarding the bedform wavelength and the associated roughness treatment.

ACKNOWLEDGMENT

Field measurements have been acquired in the framework of a study supported by the Hydrographic and Oceanographic Office of the French Navy (SHOM) and the Regional Council of 'Haute-Normandie' (France). The SHOM is also thanked for providing complementary bathymetric data. The authors want to thank the crew of the RV 'Côte d'Aquitaine' (INSU/CNRS) and RV 'Thalia' (IFREMER).

REFERENCES

Y. Ferret, S. Le Bot, B. Tessier, T. Garlan, R. Lafite (2010) "Migration and internal architecture of marine dunes in the eastern English Channel over 14 and 56 year intervals: the influence of tides and decennial storms" Earth Surface Processes and Landforms. Vol 35 Issue 12 pp 1480-1493

Huybrechts, N., Villaret, C. and Lyard, F. (2012) “Optimized predictive 2D hydrodynamic model of the Gironde estuary (France)”, Journal of Waterway, Port, Coastal and Ocean Engineering. Vol 138 (4) pp 312-322.

van Rijn, L.C. (2007). “Unified view of sediment transport by currents and waves. 1. Initiation of motion, bed roughness, and bed-load transport”, J. Hydraulic Eng. 133(6), pp 649-667.

Disposal strategy to create ecological valuable habitats in the Western Scheldt estuary

S. Ides [(1)], Y. Plancke [(2)]

1. Antwerp Port Authority, Antwerp, B - Stefaan.Ides@haven.antwerpen.be
2. Flanders Hydraulics Research, Borgerhout, B - Yves.Plancke@mow.vlaanderen.be

Abstract

To guarantee optimal accessibility to the port of Antwerp, a deepening of the navigation channel was proposed within the Long Term Vision for the Scheldt estuary. An environmental impact assessment and an appropriate assessment were carried out for this project. From these studies it was concluded that the most preferred scenario for the enlargement of the navigation channel includes a strategy aiming at disposing dredged material near 3 sandbars in the Western Scheldt, creating opportunities for nature. To determine the optimal disposal strategy on a detailed and more practical level, research was performed by Flanders Hydraulics Research. The main objective of this study was to determine a detailed disposal strategy in order to maximize the ecological benefits, i.e. maximizing the potential creation of low dynamic intertidal and shallow water area. This paper describes the studies undertaken by Flanders Hydraulics Research to determine the most optimal disposal strategy. In a next part the most optimal disposal strategy resulting from the research will also be presented, as well as the strategy being used to evaluate this new disposal strategy.

1. INTRODUCTION

The Scheldt estuary is the maritime access to several ports in Flanders and the Netherlands, the largest being the Port of Antwerp, located at some 100 km from the open sea. The Western Scheldt – the part of the estuary between Vlissingen and the Dutch-Belgian border – is a typical multiple channel system, with the navigation route being mainly located in the ebb channel. Up-estuary the Dutch-Belgian border, the estuary evolves to a meandering single channel system. The main driving force from point of view of hydrodynamics is the tidal penetration from the North sea into the estuary: the tide penetrates up to Ghent (a distance of approximately 160 km from the mouth in the North sea) and is blocked there by a weir. The fresh water discharge is hydrodynamically less important, however it has an important influence on the salinity gradient along the estuary.

In 1999 Flanders and the Netherlands agreed to cooperate closely for managing the Scheldt estuary and set up a "Long Term Vision" (LTV), based on 3 pillars: safety against flooding, port accessibility and nature. Parallel to the LTV, the Antwerp Port Authority asked an international expert team (called Port of Antwerp Expert Team, or "PAET") to investigate the possibilities of a further deepening of the navigation channel. The PAET proposed the idea of morphological management. As a pilot project they proposed to use dredged material to restore the western tip of the Walsoorden sandbar in the Western Scheldt [Meersschaut et al., 2004; PAET, 2003]. This proposal would not only improve the distribution of the flood currents between the ebb and the flood channel, but would also create benefits for ecology. The feasibility of the Walsoorden pilot project was investigated by Flanders Hydraulics Research using in situ measurements, a physical scale model as well as numerical modelling [FHR, 2003]. Final proof of the feasibility of the morphological disposal near the Walsoorden sandbar was brought by 2 in situ disposal tests [FHR, 2006; FHR, 2009a; Plancke et al., 2009].

In the environmental impact assessment of a further deepening of the navigation channel of the Scheldt estuary, different scenarios were investigated for the Western Scheldt. The scenario in which the material from the capital dredging works was disposed near sandbars (i.e.

morphological disposal as introduced by PAET, see Figure 1 for locations) was the most favorable one: this strategy would not induce any negative effects, on the contrary it would create possibilities for the development of nature [Arcadis-Technum, 2007].

Where the environmental impact assessment investigated the overall effects of the channel enlargement (including disposal) on a large estuary wide scale, Flanders Hydraulics Research was asked to conduct research to optimize the disposal strategy near sandbars on a detailed and more practical level.

2. RESEARCH OPTIMIZING THE DISPOSAL STRATEGY

The goal of the proposed disposal strategy along sandbars was to maximize the creation of ecological valuable ecotopes, i.e. subtidal and intertidal areas with low currents, in a sustainable way. Flanders Hydraulics Research used a combination of different tools to investigate the most optimal disposal strategy: analysis of topo-bathymetric maps, field measurements and a high resolution 2D hydrodynamic numerical model [Ides et al., 2010]. Moreover, the experience gained near the Walsoorden sandbar [FHR, 2006; FHR, 2009; Plancke et al., 2009] was used as valuable input during this research.

1.1. Historical topo-bathymetric analysis

Since it is important that the disposal strategy will not work against the natural evolution, a morphological analysis – based on topo-bathymetric maps from 1931 to 2005 – was made for each sandbar location. Besides observation of the morphological evolutions, the causes for these evolutions were investigated trying to understand the morphodynamics of the estuarine system.

1.2. In situ measurements

Insight in the local hydrodynamic conditions was obtained by intensive flow (GPS floats and ADCP) and sediment transport measurements on the 4 potential disposal locations. Besides gaining insight in the local conditions, these measurements would also serve as a T0 situation, in order to evaluate the effect of the disposal.

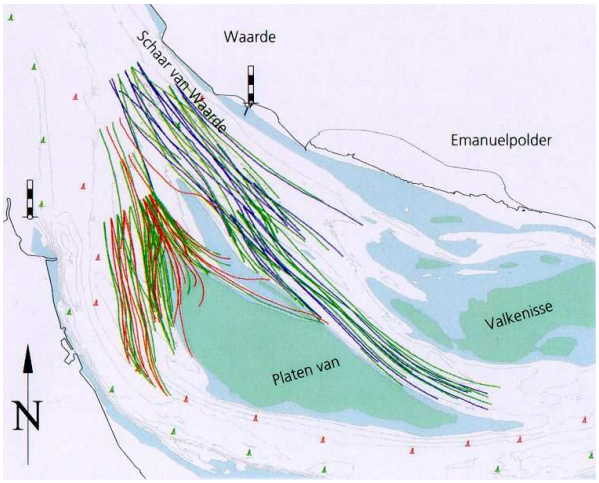

Figure 2. Results of float measurements at the Walsoorden sandbar.

1.3. Numerical hydrodynamic model

As a next step a detailed numerical hydrodynamic model was set up for each sandbar location, which was calibrated using all available measurement data [Ides et al., 2010]. Since local hydrodynamics were to be represented very accurately by the model (cfr. goal to create low dynamic area), special attention was paid to the flow velocities. Where the flow velocities in the deep and shallow water areas were good reproduced by the model, limited data availability in the intertidal area prevented a good calibration of the models in this reach. Therefore an additional validation of the intertidal area was carried out based on the maps of ecotopes, which define several classes in regard to their ecological value. One fundamental aspect in the definition of the ecotopes is the hydrodynamic character, which is related to the flow velocities. Figure 3 shows some results of the calibration of the model based on the maps of ecotopes for the Rug van Baarland.

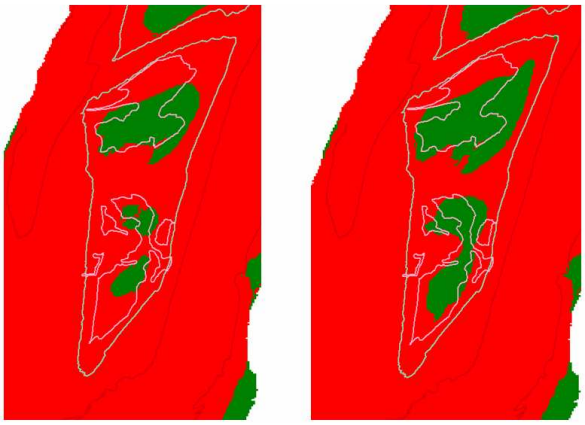

Figure 3. Calibration of the numerical model in the initertidal zone using ecotope classification for Baarland. The green contour indicates the intertidal area, the pink contour indicates the low dynamic intertidal area as indicated on the ecotope classification. The colors indicate respectively high dynamic (red) and low dynamic (green) area as calculated by the numerical model. The 2 figures show different results during the calibration of the model.

3. THE PROPOSED DISPOSAL STRATEGY

The research carried out by Flanders Hydraulics Research revealed that fundamental differences exist between the 4 proposed locations (see Figure 1). On one hand both the locations near the Walsoorden sandbar and the Hooge Platen West are located near the seaward tip of a sandbar, attacked by flood currents. It is expected that sediment disposed at these locations will gradually be transported towards the sandbar. On the other hand the locations near Rug van Baarland and Hooge Platen North are located along a sandbar, guiding the currents. It is expected that sediment disposed at these locations, will be transported along the sandbar.
For the Walsoorden sandbar and the Hooge Platen West (see Figure 4) the disposal strategy aims at creating a subtidal "megadune" which will migrate towards the sandbar under influence of the flood-dominated currents. This can be seen as an application of the "working with nature" principle. This so-called megadune aims for the creation of an underwater barrier which will reduce the currents between the barrier and the sandbar, creating a low dynamic shallow water area.

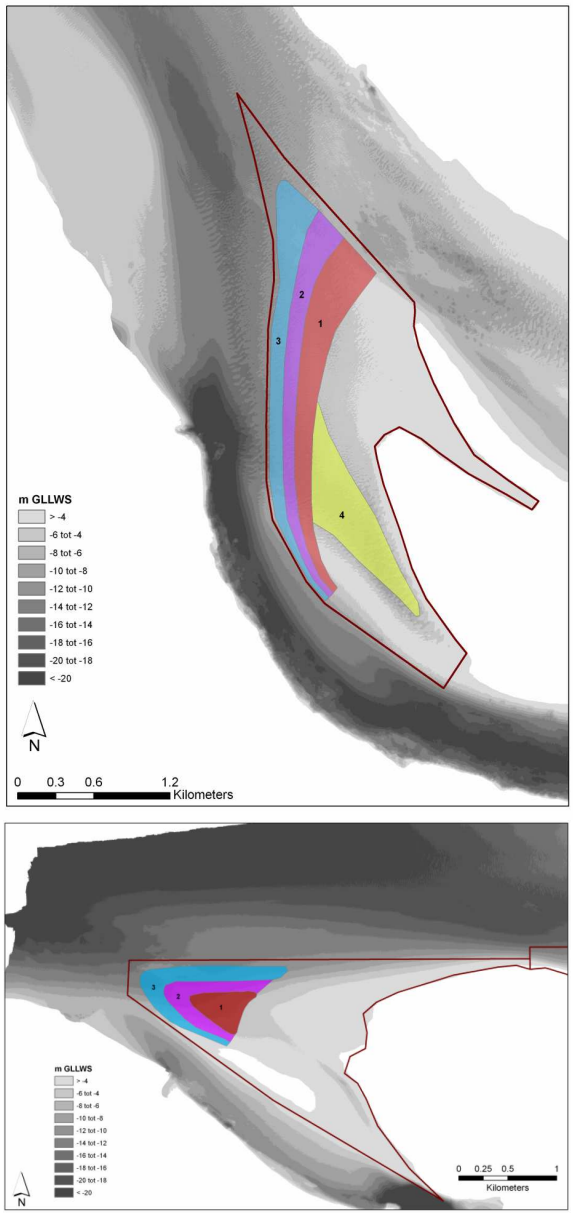

Figure 4. Megadune propsed at Walsoorden sandbar (above) and Hooge Platen West (below).

Near Rug van Baarland and Hooge Platen North (see Figure 5) the disposal strategy aims at constructing a "sand spit" near the tip of the sandbar. This new sand spit, in combination with the existing one, aims for the creation of an underwater barrier reducing the currents

between the barrier and the sandbar, creating a low dynamic shallow water area.

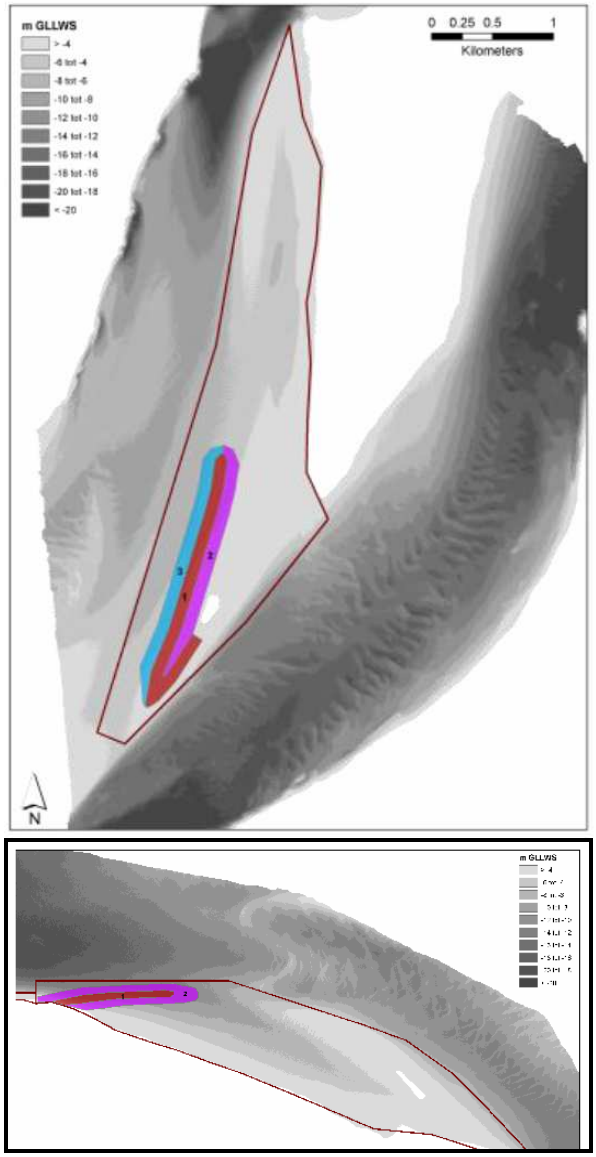

Figure 5. Sand spit proposed at Rug van Baarland (above) and Hooge Platen North (below).

4. EXECUTION & EVALUATION OF NEW DISPOSAL STRATEGY

On February 12th 2010 dredging works for the enlargement of the navigation channel in the Western Scheldt started. During a period of one year all necessary capital dredging works (7,7 Mm³ of sandy material) were executed. The sediments were disposed near the 4 proposed locations along sandbars. In the deeper areas near the sandbars, the disposal was performed using the conventional "clapping" technique with hoppers. In the shallower areas, the trailing suction hopper dredgers connected to a floating line which was connected to a diffuser (see Figure 6). This technique allowed the disposal of sandy material in zones up to 2m below low water. Simultaneously with the capital dredging works, maintenance dredging works had to take place. Part (20%) of the dredged sediments from the maintenance works, are disposed near the sandbars, while the other part is disposed in the main or secondary channels. Over the first 2 years a total of 12.4 Mm³ of sediments have been disposed near all 4 sandbars, which is 63 % of the amount foreseen to be disposed in 5 years (see Table 1).

Figure 6. TSHD connected to floating line (above) and detail of diffuser head (below).

Location	Capacity over 5 yr [Mm³]	Disposal Year 1 [Mm³]	Disposal Year 2 [Mm³]	Disposal Year 1+2 [Mm³]	Stability [%]
Hooge Platen West	8.20	1.95	0.58	2.53	70
Hooge Platen North		3.50	0.51	4.01	105
Rug van Baarland	5.00	0.70	0.58	1.28	268
Walsoorden sandbar	6.50	3.72	0.82	4.54	62

Table 1. Overview of quantities to be disposed near sandbars and initial stability.

To evaluate the possible effects of the deepening of the navigation channel and the new disposal strategy, an extensive monitoring programme was set up [Plancke et al., 2012]. This monitoring programme consists among others of high frequent multi-beam echo soundings, current measurements, RTK height measurement and determination of grain size.

To monitor the stability of the disposed sediment, high frequent multi-beam echo soundings (MBES) of the total disposal area were performed. In the period during the execution and 1 month after the last disposal, one sounding every 2 weeks was made. After this period, the intensity was reduced to one sounding per month and finally to one every 3 months. Additionally to these "disposal zone" soundings, a MBES of a larger area took place twice a year to monitor the morphological changes in case the sediment would be transported out of the disposal zone.

The flow velocities are measured on 10 transects over 2 full spring-neap-tide cycles. Each transect consists of 3 points in the intertidal area (measured with Nortek AquaDopp | 2MHz – figure 7) and 1 undeep subtidal point (RDI ADCP | 1200 kHz). The AquaDopps in the intertidal zone were dug in the sandbar and look upward, allowing maximal vertical resolution when flooded during the tidal cycle. To present measurement data, scatterplots are generated showing the maximum flow velocity (flood or ebb) versus the tidal range (rising or falling) (figure 7). Before the start of the deepening, the reference situation was monitored for all 40 locations, measuring continuously over 2 spring-neap tidal cycles. Since the start of the works, new measuring campaigns at all locations have been executed to evaluate the effect of the disposal activities. During the next 6 years this monitoring will continue, allowing the evaluation of the new disposal strategy on the longer term.

Besides these measurements, a calibrated 2D-numerical model [Ides *et al.*, 2010] is used to evaluate the developments of the flows near the sandbars. Simulations are performed on regular basis (every 3 – 6 months), using the most actual topo-bathymetry near the sandbars. All 40 measurement points are defined in the model and similar analyses is performed. Additionally, spatial maximum flow maps are generated and changes in these maps are evaluated (figure 7).

A special "protocol", containing several morphological (stability of disposed material) and ecological (evolution of ecotopes) criteria is appended to the disposal license to, quasi continuously, evaluate the monitoring data. An independent group of experts ("Commission Monitoring Western Scheldt") will supervise the evaluation of the monitoring and advices at least every 2 years on the disposal strategy.

5. CONCLUSIONS

Within the enlargement project of the navigation channel in the Scheldt-estuary, a new disposal strategy was chosen, aimed at creating new ecological valuable habitats. The combination of the morphological analysis, the in situ measurements, the numerical model as well as the experience with 2 in situ disposal tests at the Walsoorden sandbar resulted in detailed specifications for the disposal strategy. It was found that fundamental differences exists between the 4 proposed locations. On one hand both the locatons near the Walsoorden sandbar and the Hooge Platen West are located near the seaward tip of a sandbar, under attack by flood currents. It is expected that sediment disposed at these locations will be gradually transported towards the sandbar. On the other hand the location near Rug van Baarland and Hooge Platen North are located along a sandbar, guiding the currents. It is expected that sediment disposed at these locations will be rather transported along the sandbar. Therefore a

different disposal strategy was proposed for both type of locations.
An extensive monitoring programme was set up to evaluate the success of this new strategy, focusing on topo-bathymetry (using MBES) and flow characteristics (using Acoustical Doppler techniques). Additionally, hydrodynamic numerical simulations were performed to investigate the changes in flow patterns near the disposal locations. This extensive monitoring and analysis of the measurement data will allow a final evaluation 5 years after the start of enlargement project.

6. ACKNOWLEDGMENT

This research was funded by ProSes2010. A special acknowledgement to the people of the hydrometry department of Flanders Hydraulics Research and the crew of the vessels (Fleet) who assisted during the execution of the field measurements, which allowed us to calibrate and validate the numerical models. Finally we would like to acknowledge the Port of Antwerp Expert Team, and Mr. Jean Jacques Peters and Mr. Jean Cunge specially, for their input during the different steps of the research.

7. REFERENCES

Arcadis-Technum 2007. Environmental impact assessment: main report - Enlargement of the navigation channel in the Lower Sea Scheldt and the Western Scheldt (in Dutch).

Flanders Hydraulics Research 2003. Model 678/1 Alternative dumping strategy Walsoorden. Results physical & numerical modeling.

Flanders Hydraulics Research 2006. Model 754/2C Alternative dumping strategy Western Scheldt. Evaluation of the in situ disposal test 2004 (in Dutch).

Flanders Hydraulics Research 2009. Model 754/3C Alternative dumping strategy Western Scheldt. Evaluation of the in situ disposal test 2006 (in Dutch)

Ides, S., Plancke, Y. & Vos, G. 2010. Validation of a 2D hydrodynamic model within a study to propose the optimal disposal strategy in the Western Scheldt. SIMHYDRO 2010: modèles hydrauliques et incertitudes, Nice, France

Meersschaut, Y., Parker, W., Peters, J.J. & Plancke Y. 2004. A dredging and disposal strategy for managing the Western Scheldt's morphology and ecology. WODCON 2004, Hamburg, Germany.

Port of Antwerp Expert Team 2003. Alternative dumping strategy - The feasibility of morphological dredging as tool for managing the Western Scheldt.

Plancke, Y., Ides, S., Peters, J.J. & Vos, G. 2009. Le projet pilote Walsoorden: la premiere etape dans la gestion morphologique de l'Escaut Occidental, reconciliant la preservation de l'ecologie et l'accessibilité des ports. 31ième Journées de l'hydraulique: «Morphodynamiques et débits solides dans les estuaires, les baies et les deltas» Paris, France.

Plancke, Y., Ides, S., Vos, G., Roose, F. & Peters, J.J. 2010. A new disposal strategy for the Western Scheldt, conciliating port accessibility and nature preservation. 32nd PIANC Congress, Liverpool, UK.

Plancke, Y., Schrijver, M., Vos, G. 2012. High resolution topo-bathymetric and flow measurements and 2D-hydrodynamic numerical modelling to evaluate the effects of the deepening of the navigation channel in the Western Scheldt. HMEM2012, Utah, USA.

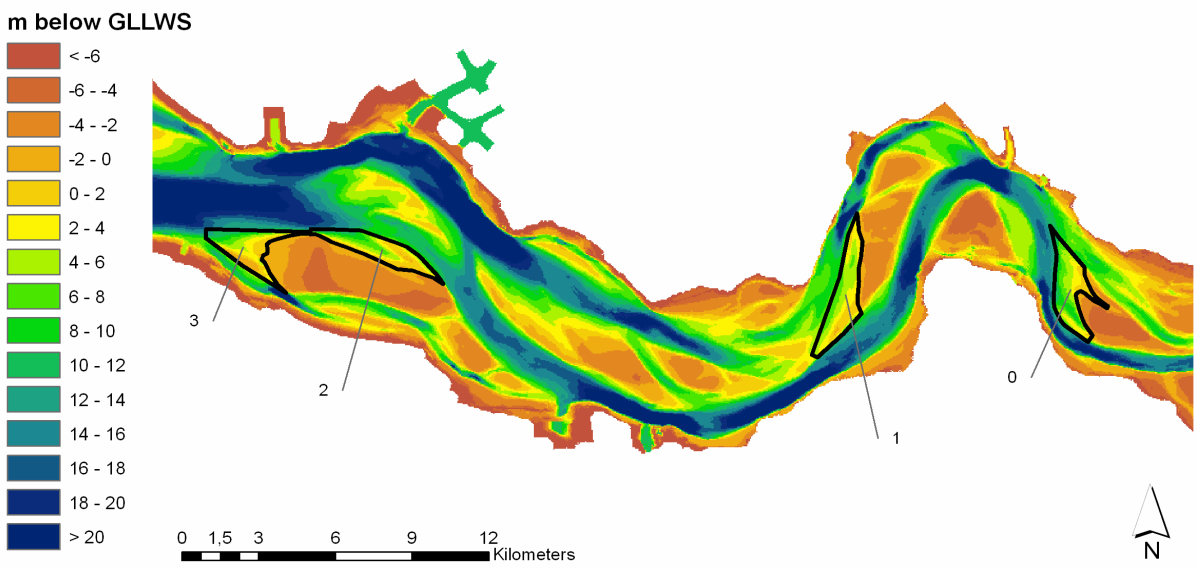

Figure 1. Overview of the present topo-bathymetry of the Western Scheldt (bathymetry expressed in meters below mean low spring water level). The black contours indicate the different disposal areas near sandbars studied in the environmental impact assessment. 0: sandbar of Walsoorden; 1: Rug van Baarland; 2: Hooge Platen North; 3: Hooge Platen West.

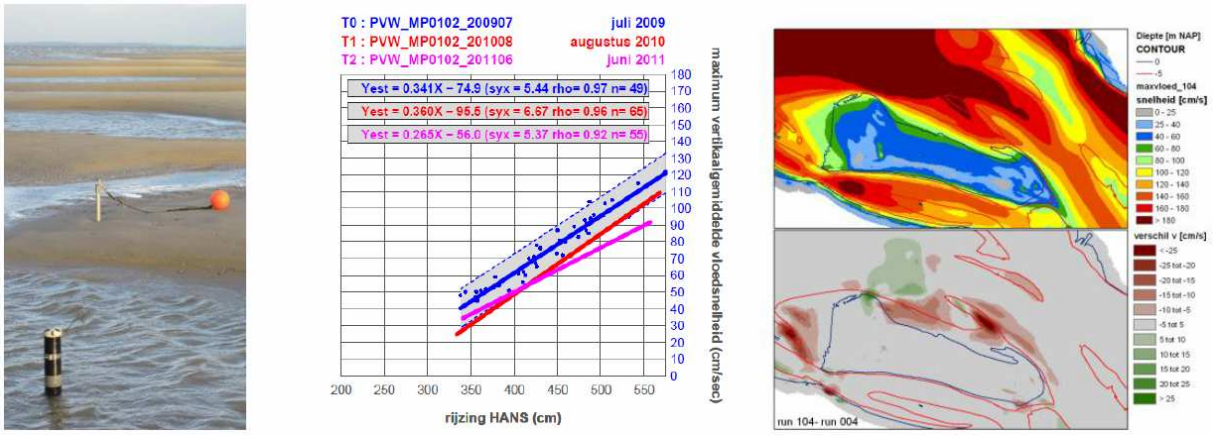

Figure 7. AquaDopp (left), scatterplot from ADP-measurement rising vs. maximum flood velocity (mid) and flood velocities and difference (T0+15months – T0) from numerical model (right).

Flow structure and bedform dynamics around tidally-influenced bars

C.E. Keevil [(1)], D.R. Parsons [(1)], P.J. Ashworth [(2)], J.L. Best [(3,4)], S.D. Sandbach [(5)], G.H. Sambrook Smith [(6)],E.W. Prokocki [(4)], A.P. Nicholas [(5)], C.J. Simpson [(7)]

1. Department of Geography, Environment and Earth Sciences, University of Hull, Hull, HU6 7RX, UK - c.keevil@hull.ac.uk, d.parsons@hull.ac.uk
2. Division of Geography and Geology, School of Environment and Technology, University of Brighton, Brighton, Sussex, BN2 4GJ, UK - p.ashworth@brighton.ac.uk
3. Departments of Geology, Geography and Geographic Information Science, Mechanical Science and Engineering and Ven Te Chow Hydrosystems Laboratory, University of Illinois at Urbana-Champaign, 1301 W. Green St., Urbana, IL, 61801, USA - jimbest@illinois.edu
4. Department of Geology, University of Illinois at Urbana-Champaign, 1301 W. Green St., Urbana, IL, 61801, USA. prokock1@illinois.edu
5. Department of Geography, College of Life and Environmental Sciences, University of Exeter, Exeter, EX4 4RJ, UK - A.P.Nicholas@exeter.ac.uk, S.Sandbach@exeter.ac.uk
6. School of Geography, Earth and Environmental Sciences, University of Birmingham, Edgbaston, Birmingham, B15 2TT, UK - g.smith.4@bham.ac.uk
7. Fulcrum Graphic Communications Inc., TH2-168, Esplanade Avenue East, North Vancouver, BC, V7L 4X8, Canada cjsimpson@fulcrumgraphics.com

Abstract

Tidal bar complexes are common features of fluvio-tidal transition zones. Such features are generated by the complex interplay, across a broad range of spatio-temporal scales, between fluvial, tidal and wave hydrodynamics. This spatio-temporal variability is reflected in the generation and interactions of reach-scale flow structures around and over bar forms, which in turn drive bar-scale sediment transport and bedform scale morphodynamics. However, presently we do not possess adequate data or understanding to enable quantification of these relationships and how they change across the fluvio-tidal transition zone.

This paper reports on the flow structure and morphodynamics around tidal bars through the fluvio-tidal transition in the Columbia River, WA, USA. Detailed flow mapping using an ADCP was conducted from a small launch highlighting the evolution of flow around km-scale tidally-influenced bars during the tidal cycle. These flow data were combined with targeted multibeam echo sounder (MBES) bathymetric surveys conducted from a second launch, thus allowing the link between flow forcing and bar- and bed- form geometries to be examined. Results show how the spatio-temporal variations in the hydraulics around bars are highly dynamic, which controls the likely transitions in bar morphologies as the tidal influence increases distally towards the river mouth and likely governs bar evolution and stability.

1. INTRODUCTION

All river-estuarine systems contain a transitional zone between fully fluvial and fully tidal environments. This region is highly complex with fluvial and tidal currents interacting on daily, seasonal and annual cycles. The interaction of these variable current cycles makes measuring and defining hydrodynamic and sediment transport processes difficult. However, gaining an understanding of these processes is crucial to managing the sensitive environments located within this region, particularly in regard to environmental and sea-level change. As a consequence, the controls on flow and sediment routing and the deposits within the fluvio-tidal transition zone are poorly understood, and specifically the relationships between flow structure, its change through tidal cycles, and the bed-sediment response.

Whilst fluvial and estuarine systems have been investigated in detail (e.g., Dalrymple et al., 1992;

Dalrymple and Choi, 2007; Uncles, 2010; van den Berg et al., 2007), the transition zone has often been largely neglected. To understand the morphodynamic and sedimentary processes occurring within this region, from tidally dominated zones through to tidally-influenced river systems, the flow and the fluid forcing mechanisms must be considered in detail.

2. FIELDSITE

The Columbia River Estuary (WA, USA) has a total drainage area of 660,480 km^2, before entering the Pacific near Astoria, Oregon, USA (Simenstad et al., 2011). The river has an average discharge of 6,700 – 7,300 m^{3}s^{-1} and a maximum tidal range of 3.6 m (Sherwood and Creager, 1990; Fain et al., 2001). It is a large estuarine system with contemporary and historic tidally-influenced bar construction (Figure 1).

Figure 1. The Columbia River Estuary, WA, USA. Well -developed bar complexes can be seen throughout the channel, some of which are vegetated. Data on two bars are presented herein: i. Sandee Bar, where ADCP measurements were carried out (Figs 2 and 3); and ii. Wills Bar where the MBES survey shown in Figure 4 was conducted.

3. METHODOLOGY

The fluid flow, sediment transport and morphodynamics of a 40 km-reach of the river have been studied using acoustic Doppler current profiling (ADCP) and Multibeam Echosounding (MBES). Several bars within the reach were chosen for careful investigation. Herein we present results from two of the bars investigated. At each site, a 1200 kHz RDInstruments ADCP was deployed from a small launch during both 2011 and 2012, covering a number of tidal cycles. This provided measurements of three-dimensional flow velocity and suspended sediment concentration along a set of pre-determined cross-sections around individual bar complexes, to investigate flow forcing and flow structure generated as fluvial-tidal interactions varied during the survey periods. MBES surveys were performed with a RESON SeaBat 7125 and POS-MV system. These surveys were carried out in June 2012 and measured channel bathymetry around the tidal bars. The morphologies obtained have permitted investigation of bedform interactions and bedform steering by tidal bar morphologies.

4. FLUID FLOW

Flow was measured at both high and low tides around a bar head at several cross-sections (Figure 2). Two of these cross-sections lay upstream of the bar head, within a major anabranch of the river, whilst the other two were positioned either side of the bar head itself. The flows measured are shown in Figure 3.

At low tide, flow in all parts of the channel flow field is in a downstream (ebb) direction, with lower velocities seen across topographic highs at the channel and bar edges. Maximum flow velocities in the sections reached over 1 ms^{-1}, concentrated within the deepest parts of the channel. Flow in the shallower channel to the north of the bar head (cross-section D) was considerably lower, with maximum velocities of ~0.3 ms^{-1}.

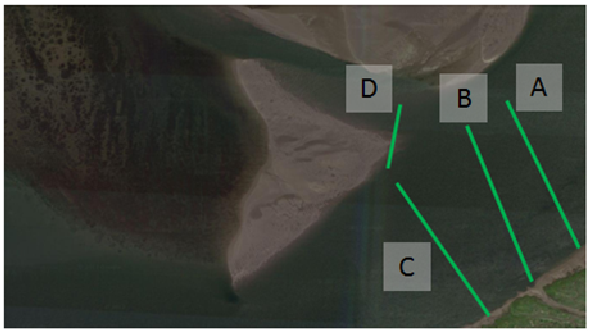

Figure 2. Position of ADCP lines around the bar head at Sandee Bar.

Flows at high (flood) tide had much lower overall velocities, up to a maximum of ~0.4 ms^{-1}, along with a distinct zone of flow reversal seen in two of the sections. Interestingly, flow at cross-section A shows a weak upstream flow in the deepest parts of the main channel, with slightly stronger

downstream flow in the shallower areas of the cross-section to the north. Cross-section D shows an increase in ebb-directed flow during the flood, indicating a significant influence of tidal bar topography in steering the flow driving the incoming flood into the topographic lows, with much higher variability in flow direction across topographic highs in response.

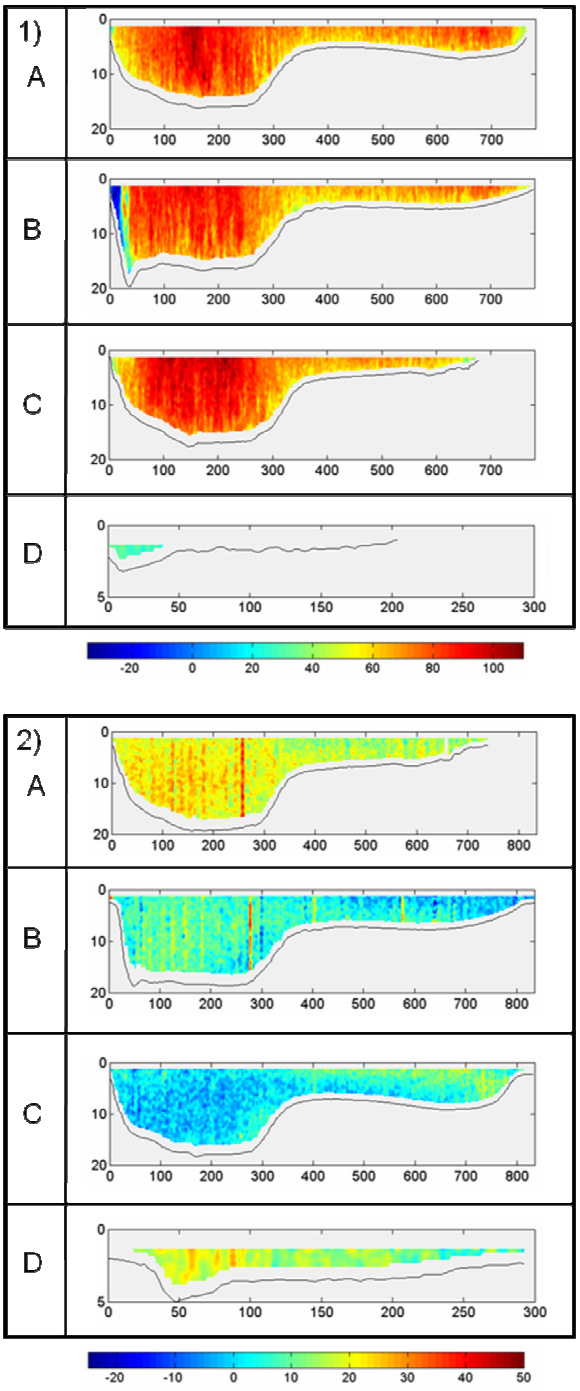

Figure 3. Streamwise flow around a bar head measured at four positions on 1) the outgoing (low/ebb) and, 2) incoming (high/flood) tides. Section positions are shown on Figure 2. All images show flow facing in a downstream direction. Water depth and distance from left bank are shown in metres, while streamwise flow velocity in shown in cms^{-1}. Note scales vary between sub-panels

5. BEDFORMS

Although the region studied shows bi-directional flow through the tidal cycle, the bedforms identified across the bar head at Wills Bar (Figures 1, 4) have dominantly unidirectional, asymmetric, ebb-directed geometries, with long stoss sides with sharp crests. Large dunes are found throughout the estuary system, commonly with flattened crests. Figure 4 shows that dunes upstream of the bar head have crests orientated in a NE-SW direction (normal to the bar head apex). As the channel bifurcates, the orientation of the dunes changes as they are steered around the bar head. In the larger southern channel, flow is deeper and the dunes become longer in wavelength and straighter crested. Here, the dunes crests are N-S in orientation. In the smaller northern channel, the flow is shallower and dune amplitude declines significantly.

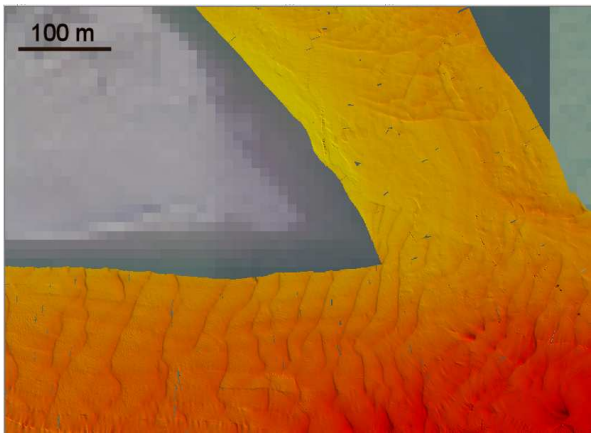

Figure 4. Large dunes showing some steering and pronounced decay around a bar head at Wills Bar (location shown in Figure 1). Flow is diverted from the main river channel at the bottom right of the image and separates around a large bar.

6. CONCLUSIONS

Flow fields around tidal bars have significant variability that is driven by the response and interactions of the tidal flow and topographic forcing. This can result in appreciable steering of flow at tidal bar heads, with notable implications for bar morphodynamics of and their sedimentology. For example, there is little evidence for variation in bedform asymmetry through the reaches examined herein. However, the multibeam surveys presented herein have allowed a first view of this flow steering effect and future repeat surveys will be carried out across a complete tidal cycle to determine sediment transport rates and directions. Full three-dimensional flow data will be examined in the near future to elucidate the secondary flow components and evolution of channel scale helicity and the role it plays in sediment routing round these key features of the fluvial-tidal transition zone.

7. ACKNOWLEDGMENTS

The work in this project was carried out as part of NERC grant NE/H007954/1. Thanks CMOP (Portland), Clatsop College and MERTS in Astoria, OR (Michael Wilkin in particular), Pat and Sandee Killion, and Mike Stecher.

8. REFERENCES

Dalrymple, R.W. & Choi, K. 2007. Morphologic and facies trends through the fluvial-marine transition in tide-dominated depositional systems: A schematic framework for environmental and sequence-stratigraphic interpretation. Earth-Science Reviews 81: 135-174.

Dalrymple, R.W., Zaitlin, B.A. & Boyd, R. 1992. Estuarine facies models: Conceptual basis and stratigraphic implications. Journal of Sedimentary Petrology 62: 1130-1146.

Fain, A.M.V., Jay, D.A., Wilson, D.J., Orton, P.M. & Baptista, A.M. 2001. Seasonal and tidal monthly patterns of particulate matter dynamics in the Columbia River Estuary. Estuaries 24: 770-786.

Sherwood, C.P. & Creager, J.S. 1990. Sedimentary geology of the Columbia River Estuary. Progress in Oceanography 25: 15-79.

Simenstad, C.A., Burke, J.L., O'Connor, J.E., Cannon, C., Heatwole, D.W., Ramirez, M.F., Waite, I.R., Counihan, T.D. & Jones, K.L. 2011. Columbia River Estuary Ecosystem Classification—Concept and Application: U.S. Geological Survey Open-File Report 2011-1228, 54 pp.

Uncles, R.J. 2010. Physical properties and processes in the Bristol Channel and Severn Estuary. Marine Pollution Bulletin 61: 5-20.

van den Berg, J.H., Boersma, J.R. & van Gelder, A. 2007. Diagnostic sedimentary structures of the fluvial-tidal transition zone – Evidence from deposits of the Rhine and Meuse. Geologie en Mijnbouw (Netherlands Journal of Geosciences) 86: 287-306.

Modeling Dune dynamics in situations with bimodal sediment distributions.

M.A.F.Knaapen [(1)], J.Willis [(2)] , J.H. Harris [(3)]

1. HR Wallingford, Wallingford, UK – m.knaapen@hrwallingford.com
2. International Center for Ecohydraulics Research, Southampton, UK. J.Willis@soton.ac.uk
3. HR Wallingford, Wallingford, UK – j.harris@hrwallingford.com

Abstract

Despite the significant progress that has been made in modeling dune dynamics in the marine environment in situations with abundance of movable sand, little progress has taken place in the understanding of dune dynamics in areas of mixed sediment including sand and gravel mixtures. In large parts of the North Sea, sand is transported as migrating dunes over a bed consisting of gravel. This paper presents some initial results from a multi-grain model using a Cellular Automaton type model based on the work of Bishop et al. (2008). The sediment is represented as unit slabs And the movement of these slabs within the model is based on a stochastic set of rules based on the flow and the gradient of the bed sediment. Transport takes place over a given distance that is also dependent on the local bed gradients. As part of this movement the model checks to see if the sediment bed slope exceeds a critical value, and if this value is exceeded avalanching occurs.

1. INTRODUCTION

Cellular automata (CA) have been shown to be capable of capturing the complex patterns of sand wave, ripple and dune formation, which have proven particularly difficult for conventional process-based modeling techniques to reproduce (Nield and Baas, 2008, Bishop et al., 2002, Wilson, 1972, Hammond, 1979).

The original CA models are deceptively simple and were intended to provide an understanding of the fundamental rule system which underlies the patterns and features we observe in nature (Bishop et al., 2002). In order to apply these models for prediction to the real world we need to add complexity and flexibility without losing the essential simplicity that is their major strength. Therefore, the base CA model was adapted to incorporate the ability to represent variable flow fields using process-based hydrodynamic models (in this instance the TELEMAC system), multiple grain sizes, and simplified ecological rule systems.

A series of simplified tests were undertaken to demonstrate the model's ability to reproduce a range of complex bedform patterns that are observed in nature (other than simple dunes and dune fields).

2. CELLULAR AUTOMATA (CA)

CA models are a class of individual based modeling where each particle in the model is restricted to a spatial grid (Fonstad, 2006). The spatial restriction helps reduce computational overhead in calculating millions of iterative steps of movement and these models can, therefore, be used to show how small scale processes can impact large scale patterns. Nevertheless, coding for speed is important, and the size and complexity of these models can be limited by computing power. Any instruction (rule) that is replicated may impact the overall performance severely and so there is always a trade-off between computational efficiency and rule complexity. For instance, the model developed during this project uses a 3-dimensional domain with over 40 million explicit cells, which each need to be classified and tracked through the model runs.

The large scale patterns that develop in the model are called emergent behavior of the model.

Emergent behavior is often difficult to predict from analysis of the simple cellular rules that drive the model. In a 'strict' cellular automaton a cell's state is only determined by its four or eight nearest neighbors (Von Neumann and Moore neighbors, respectively). In the present case, the state of a cell can be determined by cells far distant across the grid, and multiple slabs can be 'stacked' on a single grid position (cell), in an attempt to parameterize the model such that the emergent behavior matches some of the patterns observed in reality.

CA models allow interactions to be defined between cells that are deterministic, probabilistic or rule based (Fonstad, 2006). In comparison to mathematical deterministic models, they are more flexible and often more simple to initialize, understand and operate. CAs have been used to model biological colonization and succession on Aeolian sand dunes (Feagin et al., 2005; Baas and Nield, 2010) and other physical sedimentary dynamics, such as river braiding (Murray and Paola, 1994).

Models specifically aimed at representing complex ephemeral bedforms such as sand dunes are often complicated and reasonably limited to highly theoretical cases (Duran et al., 2010), which is not to say they are inaccurate. On the other hand, theoretical CA models 'look right' and that in itself is an important fact mitigating for their benefit in capturing the essential dynamics (Wolfram, 2002). However, we must exercise extreme caution in suggesting that they are exact representations of reality and in using them for prediction when we have not tested their results rigorously against reality. There is much left to do and the best predictions are always likely to be made by using a combination of all model types (Paola et al., 2006).

3. MODEL DISCRIPTION

The model adopted to describe the underlying sediment processes is the simple one-dimensional model described by Bishop et al. (2002), hereafter called the 'basic model'. This model was then incrementally enhanced to reflect some of the aspects of the real system we wish to model. An outline of the model is given below.

1.1. Basic Model

The model consists of a three-dimensional lattice, which can be considered as a grid of stacked slabs. The model is initialized with a stack of slabs on each cell of the grid. The model operates by picking a cell at random and moving the top slab, the moved slab is shifted forward in the direction of the current (the strength of the current determines a jump length in an integer number of cell widths). The current is parallel to one of the axes of the base grid (a 'one-dimensional' current) and the moved slab is deposited on top of the stack of slabs at the destination cell. A slab reaching a destination cell may 'stick' and remain there or 'bounce' and move again - this process of sticking or bouncing is designed to represent the process of saltation in the real situation where particles sometimes bounce along the ground or surface of the bed (bedload). When a cell is stuck a process of local avalanching is initiated. Avalanching involves a move to a neighboring cell if the slope of the stack of slabs in that direction is higher than the angle of repose (an initialization parameter), and the local avalanching process continues until no more slabs move. (There is a mirror image process at the site which the moving slab left, in which the angle of repose is again maintained by a process we call 'fillback'). Once a slab has moved, and initiated an avalanche and fillback (if either or both are required) then a new cell is randomly selected and moved. A single model step is deemed to have passed once the number of random selections of cells is equal to the total number of cells in the grid - i.e. on average each cell has been selected once.

A key aspect of the basic model is shadowing, without which interesting patterns do not form (Nield and Baas, 2008). Shadows are cast by stacks of slabs downwind of the current direction at the shadow angle (which is an initialization parameter). If a slab is in shadow it does not move if its cell is selected (the selection attempt is still counted against the number for a model step). If a cell moves into a position which is in shadow it always sticks and does not bounce.

Modifications were made to the basic model to improve the application of the model to real world situations.

1.2. Variable direction currents

To vary the flow field during the simulation, a method was developed to advect each slab independently based on a current field that is overlain on the grid. In this case the current grid need not be the same as the cellular grid as long as the current can be interpolated at a center point of each grid cell. The slab is then pushed forward by the current (or in some relationship to the current resolved in 'cell widths') and lands on the cell with the center point closest to the destination. The key difficulty in this scheme is not pushing the cell forward but calculating the shadow, which will be different for each cell relative to its velocity. A critical factor here is speed of processing as any scheme selected for calculation of shadow must be comparable to the basic case where the program merely has to look along the row or column upwind of a cell. A simple straight line calculation was used to look upwind of a cell to determine if it was in shadow and allowed a restriction on the maximum distance that the shadow influence was calculated. This method is restricted to cases of smoothly varying current directions, if the current changes direction significantly within the length of the shadow a method which follows the current (in reverse) to determine shadows would be superior.

1.3. Conical avalanches on a square grid.

The basic model uses an avalanche system that is determined by the 8 nearest neighbors of a cell (Moore neighborhood - In cellular automata, the Moore neighborhood comprises the eight cells surrounding a central cell on a two-dimensional square lattice), therefore, it was assumed that the pyramidal shapes appeared due to the avalanching system not accounting for increased distance of diagonal neighbor cells compared to adjacent neighbor cells (Von Neumann neighbors). This effect was imperceptible for angles of repose relating to lower heights between neighbors as a single slab height was greater than the variation between a direct neighbor and a diagonal neighbor. As such, the random nature of the avalanching system caused approximately conical shapes. An alternative was to move to a system of Von Neumann neighbors for avalanches, however, this produced a square based pyramidal shape at 45° to the one caused by the Moore neighborhood approach.

In an attempt to create a more realistic pyramidal base the height of the diagonal neighbors were divided by the square root of 2 to account for increased distance from the center of the starting cell. This also produced a square pyramidal shape rotated at 45°. However, by taking an equal random choice of the root 2 corners and the normal system (with a similar adjustment to the angle of repose) it produced an almost conical avalanche.

1.4. Multiple grain types

In the real world marine soils are often variable in their makeup and consist of different grain sizes with different characteristics. These different characteristics will affect sediment transport and, therefore, it is considered that by being able to better represent this variability is advantageous when it comes to modeling seabed morphology. One of the principal reasons for trying to use CA type models to simulate sediment transport may well be in trying to understand what may happen when a 'slab' of one soil type of material is overlain by another type. Previous studies have taken a similar approach to explain the patterns found in terrestrial sandstone (Anderson and Bunas, 1993), but there are few studies of fluvial or aquatic dune formation. Anderson and Bunas (1993) describe a typical observed pattern of an aeolian dune, having a thin veneer of coarse particles on the upwind (stoss) slope, a coarser ridge and a finer downwind slope. They attributed this to less saltation for the heavier particles combined with the release of fine particles after impact with a heavy particle (Anderson and Bunas, 1993).

Using sediment slabs representing multiple grain size fractions is straightforward. The pick-up and deposition probabilities are varied depending on the sizes being represented. The heaviest particles might only move through avalanching.

The critical difference between a model that has specific grain types and the basic model which operates with a single sediment type is that each slab in the model needs to be identified and tracked within the computer program. In the basic model a stack of slabs on a cell are all expected to be the same, therefore, the computer needs only to record the height, thus the memory requirement to define the model is restricted to an integer value for each grid cell. However, if there are different

sediment types represented in the model and they occur at different levels within each stack then the memory requirement becomes three dimensional, the model has a 'height' and the absence of a cell is recorded as well as the type when one is present. In the present study 8 bit integer values were chosen for each cell leading to a limit of 255 types including 'no cell' and 'immoveable bedrock' cells. This system was, therefore, logical and simple to use.

4. SCENARIO'S

The results of three scenarios are presented here.

- Mound of mixed sediment in a constant current
- Bimodal sediment bed in a unidirectional variable current
- Bimodal sediment bed in a bidirectional variable current

5. RESULTS

1.5. Scenario 1: Mound of mixed sediment in a constant current

Figure 1 shows how a mixed mound of sediment (10% heavier particles) can be affected by a current travelling in a single direction. The heavier particles are not advected by the current but avalanche as the finer material is moved away, this leads to an armored mound and fine material moving away from the horns of the dune. If there is sufficient fine material it will form a separate smaller Barchan dune moving away with the current.

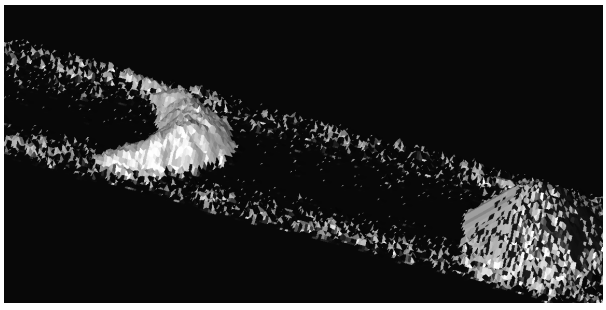

Figure 1. The sediment sorting of a mount of mixed sediments leads to a Barchan dune and ridges of fine material being formed.

1.6. Scenario 2: Bimodal sediment bed in a unidirectional variable current

Figure 2 shows the pattern emerging when the bed composition is bimodal and the forcing flow unidirectional but varying in speed. The first movement was from bottom right to top left aligned with the grid in which all the material moved in a similar way. The second subsequent phase of movement was in the same direction and the various grain sizes behaved differently. The light particles (black) moved whenever selected (and when not in shadow etc.) and the heavier particles (gray) only moved on 10% of occasions when they were picked. The pattern is slightly suppressed than with uniform condition with longer wedge shaped bedforms forming with less mobile particles on the upwind slopes and sorted faces on the downwind slopes. This is similar to the bedforms described in Boyd et al. (2006). Figure 3 shows the presence of coarse material veneers forming in the bed.

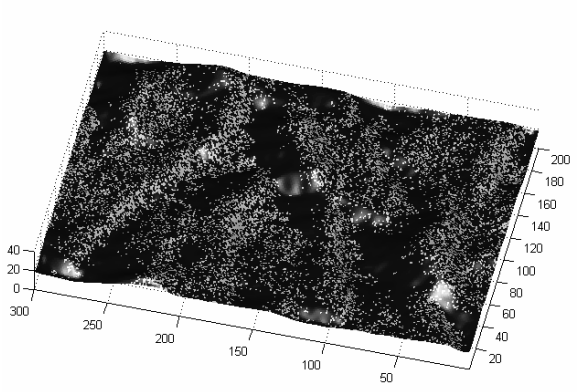

Figure 2. Bed pattern emerging from a bimodal bed under a unidirectional varying flow. Coarse material is gray, the fines are black.

Figure 3. The sorting mechanism leads to veneers of coarse (black) material underneath the mobile fines (gray).

1.7. Scenario 3: Bimodal sediment bed in a bidirectional variable current

Figure 2 shows the pattern emerging when the bed composition is bimodal and the forcing flow unidirectional but varying in speed. The first phase of movement was from bottom right to top left and aligned with the grid in which all the material moved in a similar way. The second subsequent phase of movement was in the normal direction of the grid, bottom left to top right in which the different sizes of grains behaved differently. The light (black) particles moved whenever selected (assuming they were not in shadow etc.) and the heavy (gray) only moved on 10% of occasions when they were selected. The mobile sand sorted into waves of fine material and moving over a veneer of heavy particles.

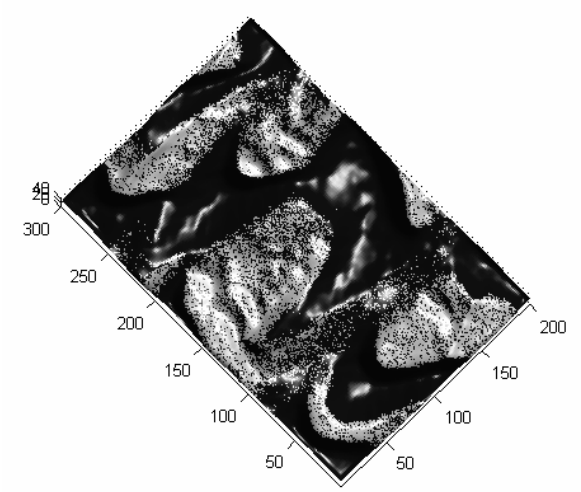

Figure 4. Bed pattern emerging from a bimodal bed under a bidirectional varying flow. Coarse material is green, the fines are blue.

Figure 5. The sorting mechanism leads to veneers of coarse (black) material mostly underneath the mobile fines (gray), but occasionally covering bedforms.

6. DISCUSSION

Two fundamental sediment patterns which occur in the North Sea are sediment sorting in bedforms and the existence of sediment veneers (HR Wallingford, 1995). Sediment sorting leads to progressively finer sediments in the direction of the current and sand wave type bedforms of well sorted finer sand. These patterns of sorting are common, and they have been used to infer the transport characteristics of the North Sea (HR Wallingford et al., 2002, Vanwesenbeeck and Lanckneus, 2000) and nearby UK coastal seas (Flemming and Stride, 1967). In this instance the veneers are defined as thin layers of heavier particles overlaying either fine or mixed sediments. In the southern North Sea the seabed sediments have been described as fine to medium grade sandy sediment overlying the underlying sediment (HR Wallingford et al., 2002). Buried veneers have also been described whereby finer material is drifting over a veneer (Flemming and Stride, 1967). A typical arrangement that is often described in the North Sea is one of sand waves covered with a veneer of heavier particles overlain by well sorted fine sand mega-ripples.

Apart from the armoring process, two processes operate that sort the sediment. First, in weakening flows the sediment to be deposited first consists of the largest grain sizes. Thus the troughs of bedforms are filled with relatively coarse sediment while the bedforms themselves consist of finer sediment. In weakening flows, such as occur over a tidal cycle, more and more sediment is deposited in the bedform troughs, leading to a fining upward sequence in the seabed below the active bedforms. This process is relatively well understood and is predictable using available bedload transport formulae for different size fractions.

The second process is due to the bedload sediment being sorted in the avalanche of grains along the lee side of the bedforms. This process is less well understood. The sediment that is transported over the length of the bedforms is deposited at the lee side of the bedforms. At the top or slightly downstream of the top the sediment avalanches from the dune. Every avalanche forms a new lamina in the set of layers called cross-bedding. During this avalanche the bedload sediment is sorted, with the coarse material being deposited preferentially deeper within the trough. The finer

material is deposited preferentially higher above the trough. The result is a fining-upward sequence in the bedforms.

7. CONCLUSIONS

Bedform formation and development in bimodal beds is simulated using a Cellular automaton. The results show patterns similar to those observed in nature. The model also captures the sorting mechanisms leading to veneers of large material in between and on top of layer of finer material.

8. REFERENCES

Anderson, R.S. & Bunas, K.L. 1993. Grain-size segregation and stratigraphy in aeolian ripples modeled with a cellular-automaton. Nature, 365: 740 - 743.

Baas, A.C.W. & Nield, J.M. 2010. Ecogeomorphic state variables and phase-space construction for quantifying the evolution of vegetated aeolian landscapes. Earth Surface Processes and Landforms, 35: 717 - 731.

Bishop, S.R., Momiji, H., Carretero-Gonzalez, R. & Warren, A. 2002. Modelling desert dune fields based on discrete dynamics. Discrete Dynamics in Nature and Society, 7: 7 - 17.

Duran, O., Parteli, E. J. R. & Herrmann, H. J. 2010. A continuous model for sand dunes: Review, new developments and application to barchan dunes and barchan dune fields. Earth Surface Processes and Landforms, 35: 1591-1600.

Feagin, R.A., Wu, X.B., Smeins, F.E., Whisenant, S.G. & Grant, W.E. 2005. Individual versus community level processes and pattern formation in a model of sand dune plant succession. Ecological Modelling, 183: 435-449.

Flemming, N.C. and Stride, A.H. 1967. Basel sand and gravel patches with separate indications of tidal current and storm-wave paths, near Plymouth. Journal of the Marine Biological Association UK, 47: 433 - 444.

Fonstad, M.A. 2006. Cellular automata as analysis and synthesis engines at the geomorphology-ecology interface. Geomorphology, 77: 217 - 234.

Hammond, F.D.C. 1979) A grain-by-grain computer simulation of sand ripple formation. Marine Geology, 31:53-60.

HR Wallingford 1995. Dredging east of Southwold Area 430. Report No. EX 3039.

HR Wallingford, Cefas/UEA, Posford Haskoning & Dr B. D'Olier 2002. Southern North Sea Sediment Transport Study Phase 2, Sediment Transport Report. Report produced for Great Yarmouth Borough Council, HR Wallingford Report EX4526, August.

Paola, C., Foufoula-Georgiou, E., Dietrich, W.E., Hondzo, M., Mohrig, D., Parker, G., Power, M.E., Rodriguez-Iturbe, I., Voller, V. & Wilcock, P. 2006. Toward a unified science of the Earth's surface: Opportunities for synthesis among hydrology, geomorphology, geochemistry, and ecology. Water Resources Research, 42.

Murray, A.B. & Paola, C. 1994. A cellular-model of braided rivers. Nature, 371: 54 - 57.

Vanwesenbeeck, V. & Lanckneus, J. 2000. Residual sediment transport paths on a tidal sand bank: A comparison between the modified McLaren model and bedform analysis. Journal of Sedimentary Research, 70: 470 - 477.

Wilson, I. G. 1972. Aeolian bedforms - their development and origins. Sedimentology, 19: 173 - 210.

Wolfram, S. 2002. A new kind of science, Wolfram Media.

Morphology of pillow-hollow and quilted-cover bedforms in Lake Geneva, Switzerland

N. Le Dantec [1,2], Y. Akhtman [3], D. Constantin [3], U. Lemmin [2], D.A. Barry [2], O. Pizarro [4]

1. Laboratoire de Génie Côtier et Environnement, Centre d'Etudes Techniques Maritimes et Fluviales, Plouzané, France - nicolas.le-dantec@developpement-durable.gouv.fr
2. Ecological Engineering Laboratory, Swiss Federal Institute of Technology (EPFL), Lausanne, Switzerland - andrew.barry@epfl.ch, ulrich.lemmin@epfl.ch
3. Geodetic Engineering Laboratory, Swiss Federal Institute of Technology (EPFL), Lausanne, Switzerland - yosef.akhtman@epfl.ch, dragos.constantin@epfl.ch
4. Australian Centre for Field Robotics, University of Sydney, Sydney, Australia - o.pizarro@acfr.usyd.edu.au

Abstract

Extensive areas of the bottom of Lake Geneva are covered with bedforms that have been referred to as pillow-hollows and quilted-cover pattern by prior observers, as well as with sediment waves and trenches. These structures are decimeter to meter scale. A large dataset of video recording and stereographic camera imagery of the lake bottom was recently acquired during a campaign with the Russian MIR submersibles. We present a classification of the different types of sediment structures with a focus on distinctive morphological characters. The variations in the observed lake-bottom structures reveal a continuous range of morphologies between the aforementioned bedforms. Although the role of the bottom-dwelling Burbot fish in at least maintaining the bottom landscape has been suggested in previous studies, the origin of the observed bedforms is unclear. On the basis of our preliminary observations, other candidate mechanisms are briefly mentioned, including bottom currents generated by internal waves. Understanding the formation and evolution of lake-bottom morphology is important since the transport pathways of lake sediment condition to a large extent the fluxes and cycle of pollutants.

1. INTRODUCTION

1.1. Sediment structures and benthic processes

Sedimentary structures at the bottom of aquatic environments are of importance to various processes occurring in the bottom boundary layer. The benthic zone provides habitat for a number of species types, from bottom-dwelling fishes to burrowing invertebrates and microbial fauna (Thrush *et al.*, 2001; Hewitt *et al.*, 2005). The nature and properties of surface sediment control the type and rate of chemical reactions taking place near the lake bottom (e.g. Brandl *et al.*, 1990; Mermillod-Blondin and Rosenberg, 2006), which ultimately govern the transformation cycle and fate of the compounds input into the aquatic system (Warren and Haack, 2001). Bedform-scale topography has an ecological function, for example in providing shelter for certain species, in particular during early development stages (Probst, 2008), or foraging grounds for others (Erlandsson *et al.*, 1999). Bedforms are observed at the interface between mobile sediment substrate and overlying fluid. Common in fluvial and shallow marine environments, bedforms also occur in lacustrine and deep marine realms. There, they usually exhibit slower dynamics because fluid forcing is generally weaker and episodic.

1.2. Prior studies in Lake Geneva

First observations of bottom structures in Lake Geneva were reported by Vernet (1966) after several dives with the submersible Piccard. He described a uniform landscape composed of a succession of humps and pits linked together by saddles, which he referred to as a quilted-cover where stitches are randomly distributed. The

hypothesis of interference of ripples generated by distinct current regimes was proposed to explain the formation of the observed morphology, noting that the origin of such currents was not well identified. The role of fish inhabiting the lake bottom in maintaining and enhancing the bedform pattern was already outlined.
Sedimentological studies were carried out on the pillow-hollow structures with radioisotopic, chemical and microbial analyses of short cores (Dominik *et al.*, 1992; Brandl *et al.* 1990). Troughs exhibited a stratigraphic hiatus compared to pillows, where sediment was relatively less consolidated. There were differences in the thickness and age of missing sediment between adjacent troughs. The above results suggested localized erosion and reworking of the surficial sediment with small-scale inhomogeneity in erosive events. Random changes in the intensity and frequency of Burbot fish activity from one structure to the next could explain the variability in the stratigraphy of the troughs.

1.3. Scope of the paper

This paper reports preliminary results on extensive observations of lake-bottom morphology in Lake Geneva using video recording and stereographic imagery. After describing the data acquisition and the analysis and processing methods, we focus on a description of the sediment structures. A classification is derived from the more extensive video record. Examples of 3D models are used to illustrate the added-value of scaled digital terrain models continuously covering long sections of the lake-bottom compared with raw video. The motivation for the study is to understand the mechanisms controlling the development of the observed bedforms. Several potential processes are mentioned, as well as the two main approaches of the analysis, currently in progress, to assess these processes.

2. METHODS

2.1. Data acquisition

Data presented here were acquired with the manned submersibles MIR-1 and MIR-2 operated by the Russian Academy of Sciences during the éLEMO campaign conducted in Lake Geneva in summer 2011 (www.elemo.ch, last accessed 28 February 2013). The éLEMO project is an interdisciplinary research initiative where multiple research groups coming from different Swiss and international institutions have joined their efforts in a comprehensive study of lake processes.
The analysis carried out in the present paper relies on two types of imagery data: raw video and stereographic images. Video was recorded with the submersible's camera attached to the portside robotic arm. The two stereographic cameras were set about 9 cm apart from each other and both fired continuously at a frequency of 2 frames per second. For all dive profiles, the general strategy was to record video and stereographic imagery whenever the submersibles were navigating right over the lake-bottom.

2.2. Lake-bottom classification from video recording

Lake-bottom topography was characterized by visual inspection of the raw video to establish a list of sedimentary structures. The analysis was done using a collaborative, web-based GIS interface (Akhtman *et al.*, 2012) where the video record had been indexed with navigation data. Structures are defined as morphological elements shaping the lake-bottom landscape, consisting of accretions or incisions, with typical size ranging from decimeter to meter. They can be repeated with some degree of regularity in their spatial arrangement (e.g., pillow-hollows or sediment waves), organized in networks (e.g., trenches), or isolated (e.g., single depressions); see section 3.1 for a description of the structures. Structure identification can be affected by certain characteristics of the video record such as perspective, backscatter and image quality. Distinctive characters were used, such as the connectivity of local topographic lows between adjacent bedforms and the extent and uniformity of the lake-bottom coverage by the bedform pattern.

2.3. 3D model reconstruction

Image sequences used to generate 3D models of the lake bottom had to be manually selected to retain only high-quality images. Low-light settings required by underwater photography yield noisy images and the local descriptor-matching approach at the basis of image registration is highly sensitive to noise. Images were preprocessed using edge-detection methods to mask the submersible's

robotic arm which is sometimes present. After applying the resulting mask, images are subjected to histogram equalization before being fed to the commercially available image registration software Agisoft Photoscan Pro. The 3D models are finally scaled using an algorithm calibrated with the known distance between the stereographic cameras. The camera calibration allowed producing reliable 3D models up to 50 meters long, corresponding to sequences of about 1000 images. Depth maps are directly obtained by projection of the 3D models on the plane normal to the orientation of the cameras. The 3D point cloud is then interpolated using a distance-weighted function. Low frequencies are removed from in order to use the entire grayscale of the image to represent sediment structures only. Figure 1 (placed at the end of the paper) shows the products the above processing for one sequence of pillow-depressions used as an example.

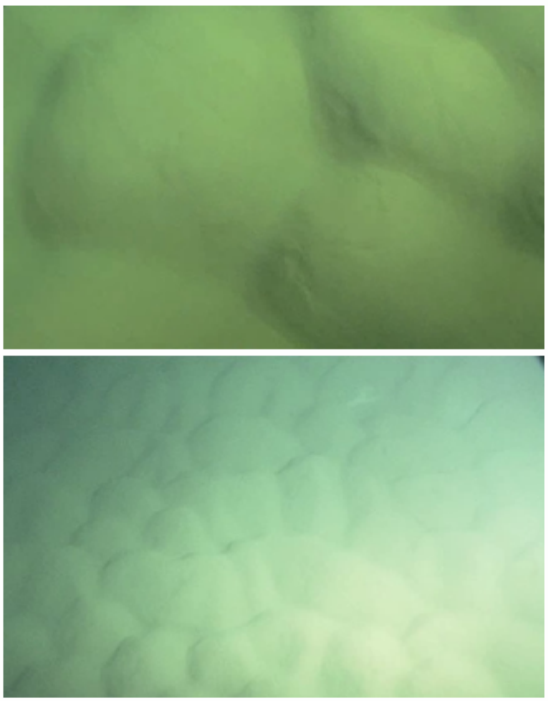

Figure 2. Pillow-hollows (close-up and perspective).

3. RESULTS

3.1. Designation of the sediment structures

A set of observation keys was defined to describe the lake-bottom structures. Representative examples of all structures are shown in Figures 2 to 5, where the image dimension ranges from 1 to a few meters, depending on the distance and angle between the camera on the robotic arm and the bottom. The structures most commonly observed are pillow-hollows, quilted-cover, sediment waves and trenches. Pillow-hollows (Figure 2) are large, well-rounded, cushion-like structures staggered over the lake bottom and usually separated by comparatively narrow troughs. The quilted-cover (Figure 3) consists of local topographic lows (depressions) alternating with local highs (bumps) in a regular and widespread pattern. The depressions are usually circular and smooth, separated by saddles or ridges that prevent the formation of fully connected drainage paths. Sediment waves (Figure 4A) designate sub-parallel ridges extending in one direction, with low-relief crests about 1 m wide and troughs narrower than typical dunes. In general, they are somewhat sinuous and not markedly asymmetric.

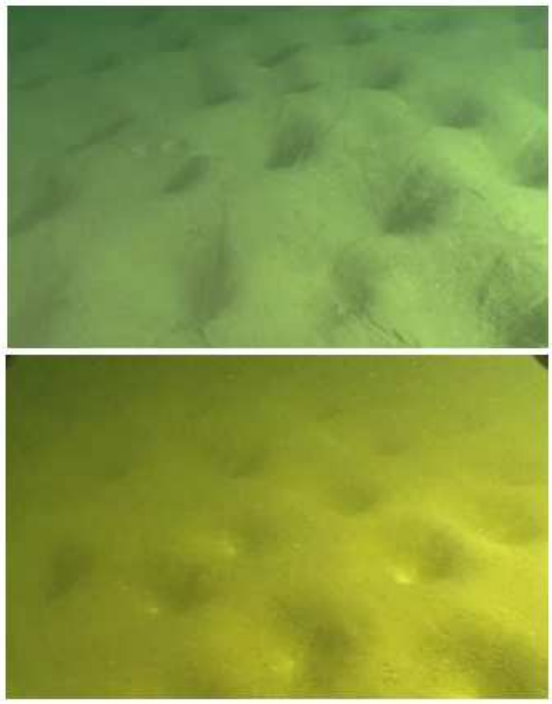

Figure 3. Quilted-cover on two different sediment types.

Trenches (Figure 4B) denote continuous troughs forming branching networks. Areas between trenches may either consist of flat bed or show bedforms, usually pillows and sediment waves.

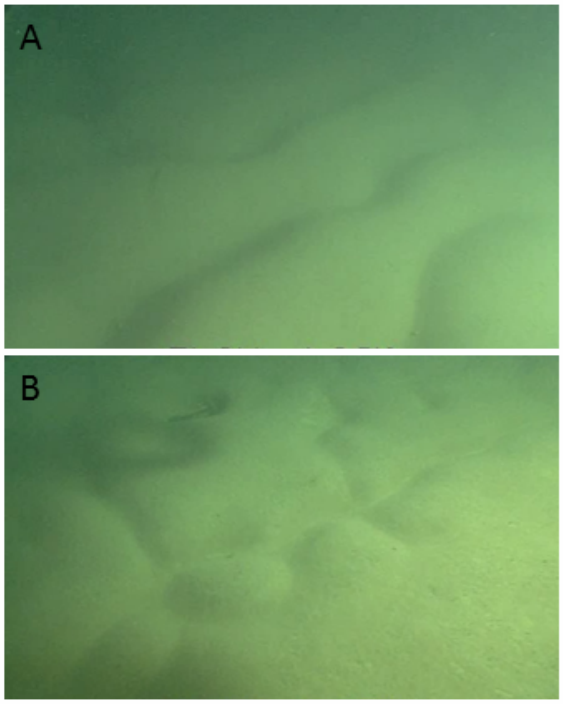

Figure 4. Sediment waves (A) and trenches (B).

Three additional types are defined to describe bedforms corresponding to a transition between structures or a variation on a structure. Pillow-trenches (Figure 5A) naturally refer to the combination of pillows and trenches. Cuspate pillows (Figure 5B) have the same planar geometry as pillow-hollows, but a flatter top and a steep lee side making them more markedly asymmetric than the rounded, cushion-like pillow-hollows. Pillow-depressions (Figure 5C) are similar to the quilted-cover but with lower saddles separating depressions and connecting bumps. Regions of the lake-bottom devoid of topographic structures are labeled as flat bed.

Finally, isolated depressions (Figure 5D) are observed, usually but not exclusively over a flat bed. These local topographic lows are circular with rims either fairly steep or smoothed. Their typical dimension of about 0.1 m is smaller than pockmarks (Wessels *et al.*, 2010) but their shape is similar. They tend to happen in small groups but only cover a small fraction of the lake bottom. In some cases a narrow and shallow channel can connect a few single depressions, but their spatial arrangement is generally random.

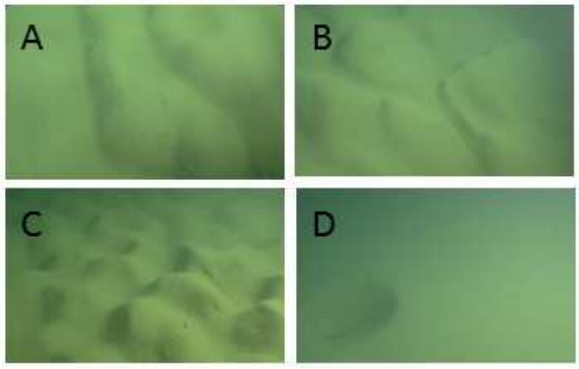

Figure 5. Lake-bottom images representing pillow-trenches (A), cuspate pillows (B), pillow-depressions (C) and an isolated depression (D).

3.2. New insight from selected 3D models

Reconstructed models yield additional information not included in the still images. Figure 6 (placed at the end of the paper) shows examples of 3D models for the four main structures. Continuous extension of the models along the submersible's track provides a spatial context to examine morphological properties and assess the uniformity of the lake-bottom landscape at the level of several consecutive bedforms. For example, models reveal the existence of more or less well-marked networks of channels connecting troughs or depressions in most sequences showing pillows, as can be seen both in the depth maps and in the perspective view (Figures 1 and 6A). Such continuous channel networks are absent in the case of the quilted-cover. For isotropic bedforms like the quilted-cover, the regularity of the pattern is confirmed over extensive sections of the lake bottom (Figure 6B). In the case of 1D-periodic bedforms like sediment waves, lateral continuity and wavelength homogeneity can be examined (Figure 6C).

The combination of multiple adjacent bedforms on a single model also reveals the existence of a low

spatial frequency perturbation on the main slope in most sequences. Removing background lake-bottom undulations enhances the morphology of the sediment structures. Figure 1 shows how the level of connectivity between the depressions more readily stands out after filtering. The height of the saddles separating depressions, which controls connectivity between depressions, can be used as a quantitative parameter to discriminate quilted-cover from pillow-hollows.
Finally, the possibility to manipulate 3D models with texture and shadowing voids biases related to the perspective of still images and ensures more objective assignments of structure types.

4. DISCUSSION

Our overall goal in characterizing the lake-bottom morphology is to infer the nature and origin of the bedforms. Their evolution as well as their interaction with transport and biogeochemical transformation processes may be predicted on the basis of proposed models for their formation.

4.1. Sediment transport driven by hydrodynamic processes

Geotechnical measurements (Stark *et al.*, submitted) as well as sedimentological analyses indicate that bottom sediment mostly consists of fine and poorly consolidated materials with very low shear strength. Small velocity thresholds, on the order of a few mm/sec, are sufficient for sediment resuspension. Most of Lake Geneva is over 200 m deep, so wind-induced surface currents are damped where bedforms are observed. However, some processes locally generate significant near-bottom currents, notably shore-hugging Kelvin waves and density flows acting along the slopes. Caused by a combination of wind stress-induced pycnocline tilting in stratified conditions and Coriolis forcing, Kelvin waves are internal waves rotating counter-clockwise (in the Northern Hemisphere) that are confined to a narrow band along the lake's shore (Lemmin *et al.*, 2005). Rapid cooling of surface waters can occur in shallow areas near the shores of cold-region lakes (alpine or high altitude and high latitude lakes) during winter. The denser water masses near the shores plunge and cascade downslope as density currents (Fer *et al.*, 2002). The orientation of asymmetric bedforms like the cuspate pillows relative the main slope can be used to distinguish these two mechanisms. In addition, episodic currents with velocity on the order of cm/s have been recorded at a long-term monitoring site on the lake bottom (Lemmin, unpublished data). They are assumed to be related to internal wave dynamics of the lake.

4.2. Other processes

Entrainment of sediment from the bottom can arise through mechanisms other than fluid shear. Boyer *et al.* (1990) have observed foraging trenches about 30 cm deep made by Burbot fish in Lake Superior, showing the capacity of Burbot fish to rework large amounts of sediment. Katz *et al.* (2012) report that significant sediment resuspension by bottom-dwelling fish along the oxygenated margins of Saanich Inlet in Bristish Columbia is at the origin of an intermediate nepheloid layer in the inlet. There is no doubt that Burbot fish play a significant role in at least maintaining the depressions in most sediment structures occurring at the bottom of Lake Geneva, as confirmed by repeated observations of turbation activity of Burbot fish at the lake bottom during this and prior campaigns.
Processes occurring within the sediment could also be at the origin of the development of the observed sediment structures. For instance, bioturbation causes local changes in the rheological behavior of the sediment and may induce spatial heterogeneity in the response of the sediment substrate to erosion and deposition processes.
Gas expulsion is known to form craters in immersed granular layers (Varas *et al.*, 2009) and could be responsible for the development of depressions at the lake bottom, in particular the isolated depressions. Significant methane bubbling has been observed in Lake Geneva (Sollberger *et al.*, submitted), although there is no evidence of large pockmarks as in Lake Constance (Wessels *et al.*, 2010).
Finally, in hydrodynamically quiescent environments, slow deformation of lake-bottom sediment under their own weight is possible given their very low strength. Bedform asymmetry could then result from long-term creep.

4.3. Direction of continuing work

Further analysis of the dataset is in progress following two main approaches. First, a distribution map will be generated from systematic classification of the entire video dataset. Correlations with the variations of relevant limnological parameters like depth, topography or near-bottom current velocity will be investigated to assess candidate mechanisms for bedform development. Second, a quantitative analysis of morphological characters will be carried out using the depth maps. Identifying metrics for bedform geometry that yield an objective discrimination will allow validating the visual classification. Contextual analyses of descriptors such as connectivity and anisotropy will be conducted on extensive 3D models.

5. CONCLUSION

With the exception of the isolated depressions, for which the authors are not aware of prior reference in the literature, all structure types described in this paper had been previously reported in Lake Geneva. However, the extent of the video dataset coverage and the 3D model reconstructions enabled a finer assessment of the variations in the observed lake-bottom structures and of their spatial consistency, revealing a rather continuous range of morphologies. Future work on the dynamics of these sediment structures is under consideration. Understanding the formation and evolution of bottom sediment structures is relevant for the benthic processes on which bottom topography has a significant impact.

6. ACKNOWLEDGMENT

Funding for this study was provided via the éLEMO project supported by the “Fondation pour l’Etude des Eaux du Léman”. The authors are grateful to the MIR crew and in particular to the pilots.

7. REFERENCES

Akhtman, Y., Martelletti, L., Grandjean O. & Lemmin U. 2012. Collaborative Web-GIS platform for systematic exploration of Lake Geneva. XXII Congress of the International Society for Photogrammetry and Remote Sensing, Melbourne, Australia, 25 August - 1 September 2012.

Boyer, L.F., McCall, P.L., Soster, F.M. & Whitlatch, R.B. 1990. Deep sediment mixing by burbot (*Lota lota*), Caribou Island Basin, Lake Superior, USA. Ichnos 1: 91-95.

Brandl, H., Hanselmann, K.W. & Bachofen, R. 1990. *In situ* stimulation of bacterial sulfate reduction in sulfate-limited freshwater lake sediments. Federation of European Microbiological Societies, Microbiology Ecology 74: 21-32.

Dominik, J., Loizeau, J.L. & Span, D. 1992. Radioisotopic evidence of perturbations of recent sedimentary record in lakes: a word of caution for climate studies, Climate Dynamics 6: 145-152.

Erlandsson J, Kostylev, V. & Williams, G.A. 1999. A field technique for estimating the influence of surface complexity on movement tortuosity in the tropical limpet *cellana grata gould*. Ophelia 50(3): 215-224.

Fer, I., Lemmin, U. & Thorpe, S.A. 2002. Winter cascading of cold water in Lake Geneva. Journal of Geophysical Research 107(C6): 13.1-13.16.

Hewitt. J.E., Thrush, S.F., Halliday, J. & Duffy, C. 2005. The Importance of Small-Scale Habitat Structure for Maintaining Beta Diversity. Ecology 86(6): 1619-1626.

Katz, T., Yahel, G., Reidenbach, M., Tunnicliffe, V., Herut, B., Crusius, J., Whitney, F., Snelgrove, P.V.R. & Lazar B. 2012. Resuspension by fish facilitates the transport and redistribution of coastal sediments. Limnology and Oceanography 57(4): 945-958.

Lemmin, U., Mortimer C.H. & Bäuerle, E. 2005. Internal seiche dynamics in Lake Geneva. Limnology and Oceanography 50(1): 207-216.

Mermillod-Blondin, F. & Rosenberg, R. 2006. Ecosystem engineering: The impact of bioturbation on biogeochemical processes in marine and freshwater benthic habitats. Aquatic Sciences 68: 434-442.

Probst, W.N. 2008. New insights into the ecology of perch *Perca fluviatilis* L. and burbot *Lota lota* (L.) with special focus on their pelagic life-history. Thesis, University of Constance, 106 pp.

Sollberger, S., Corella, J.P., Girardclos, S., Randlett, M.-E., Schubert, C.J., Senn, D., Wehrli, B. & DelSontro, T. Influence of subaquatic canyons on benthic methane fluxes in the Rhone Delta (Lake Geneva). Submitted to Aquatic Sciences.

Stark, N., Le Dantec, N., Corella, J.P., Barry, D.A., Lemmin, U., Girardclos, S. & Kopf, A. Deployment of a dynamic penetrometer from manned submersibles for fine-scale geomorphology studies.

Submitted to Limnology and Oceanography: Methods.

Thrush, S.F., Hewitt, J.E., Funnell, G.A., Cummings, V.J., Ellis, J., Schultz, D., Talley, D. & Norkko, A. 2001, Fishing disturbance and marine biodiversity: the role of habitat structure in simple soft-sediment systems. Marine Ecology Progress Series 223: 277-286.

Varas, G., Vidal, V. & Géminard, J.C. 2009. Dynamics of crater formations in immersed granular materials. Physical Review E 79(2): 021301.

Vernet, J.P. 1966. Prise de vues sous-lacustres dans le Léman lors de plongées du mésoscaphe Auguste Piccard. Bulletin de la Société Vaudoise des Sciences Naturelles 69: 287-292.

Warren, L.A. & Haack, E.A. 2001. Biogeochemical controls on metal behaviour in freshwater environments. Earth Science Reviews 54: 261-320.

Wessels, M., Bussmann. I., Schloemer, S., Schlüter, M. & Böder, V. 2010. Distribution, morphology, and formation of pockmarks in Lake Constance. Limnology and oceanography 55(6): 2623-2633.

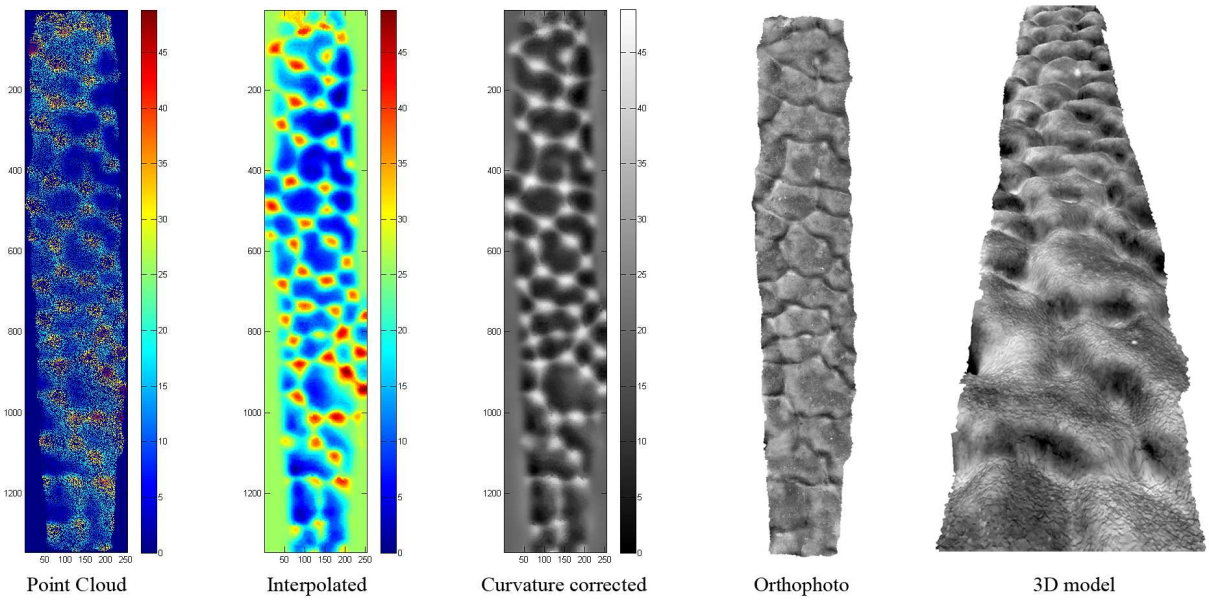

Figure 1. Depth map and model computed at 100 pixels per meter depicting a 14 m × 3 m section of the lake bottom with sediment structures about 0.5 m in height; see section 2.3 for details on the processing steps. Height is positive downward, *i.e.* low-relief is red in color images and white in black-and-white images. All scales are in cm.

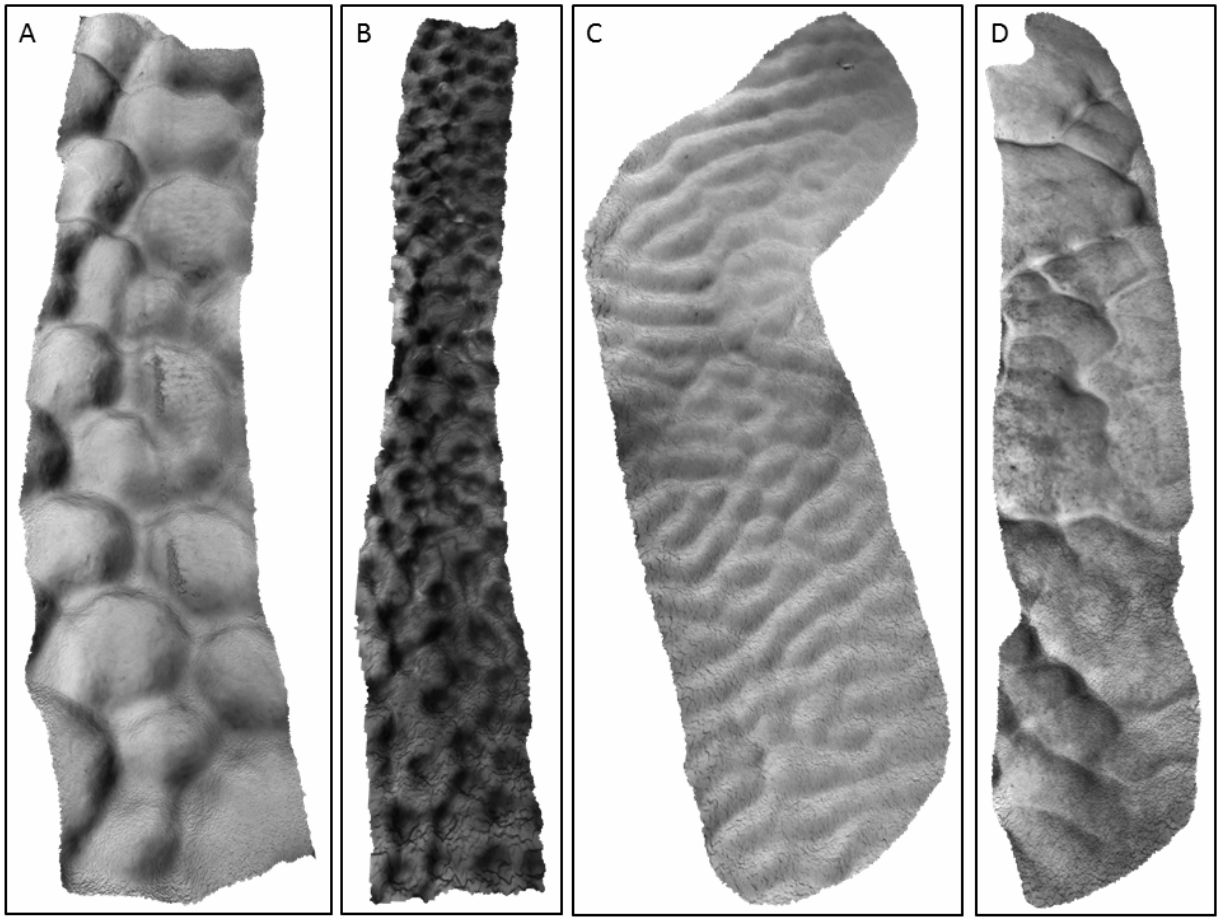

Figure 6. 3D models of pillow-hollows (A), quilted-cover (B), sediment waves (C) and trenches (D).

Selection of bedform morphology in an experimental flume under supply-limited conditions

Nicolas Le Dantec [(1,2)], Julie Dréano [(1)], Dimitri Lague [(3)] and Alexandre Valance [(1)]

1. Institut de Physique de Rennes, CNRS UMR 6251, Université Rennes 1, 35042 Rennes, France
2. Laboratoire de Génie Côtier et Environnement, Centre d'Etudes Techniques Maritimes et Fluviales (CETMEF), 155 rue Pierre Bouguer, Technopôle Brest Iroise - BP 5 - 29280, Plouzané, France, E-mail: nicolas.le-dantec@developpement-durable.gouv.fr
3. Géosciences Rennes, CNRS UMR 6118, Université Rennes 1, 35042 Rennes, France.

ABSTRACT

Our understanding of bedform dynamics is still limited because of the complex coupling between hydrodynamic forcing, sediment transport and bedform evolution, the time dependency of bedform development and the spatial variability of bedform morphology. In the case of exhaustible supply, as for instance in the presence of a thin erodible bed, the influence of sediment availability on bedform development constitutes an additional key control factor on hydrosedimentary processes. Dréano et al. (2010) carried out flume experiments on the development of bedform instabilities at the sediment-water interface in conditions of limited sediment supply. The goal was to identify mechanisms responsible for the selection of bedform morphology, in the context of river dynamics and bedform diversity. Dréano and coworkers studied the properties of equilibrium bedforms by analyzing time series of three-dimensional bed topography obtained in 46 different configurations with varying sediment size, sediment supply rate and water flow rate. Bedform morphology was characterized with parameters evaluated along flow-parallel profiles and averaged in the transverse direction: equilibrium height, length and spacing as well as migration speed. Here, we examine other parameters taking further account of the morphological complexity and heterogeneity of bedforms. The objective is to identify parameters that can be interpreted in terms of relevant near bed hydrodynamics processes, eventually leading to relationships between bedform-scale morphological parameters and mechanisms of sediment entrainment. A threshold applied to the topographic data allows generating binary images on which bedforms are identified. Bedform sinuosity and spatial density, which show little dependence on the threshold value, reveal efficient at discriminating the equilibrium morphologies. Scaling laws are proposed for these two parameters as a function of the sediment flux trapped by the bedform face Qc and the cube of the shear flow velocity u*. Their applicability to bedforms in other environments could be assessed, noting that sinuosity and bedform density may be quantified provided the outline of bedforms can be determined. Additional parameters should be tested, in the idea of better exploiting 3D topographic data of bedforms by extracting local signatures that are relevant to the study of bedforms sensitivity to their formation conditions.

REFERENCES

Dréano J., Valance A., Lague D. and Cassar C. 2010. Experimental study on transient and steady-state dynamics of bedforms in supply limited configuration. Earth Surface Processes and Landforms 35(14):1730-1743.

Variation of flow separation over large bedforms during a tidal cycle

A. Lefebvre[(1)], Y. Ferret[(1)], A.J. Paarlberg[(2)], V.B. Ernstsen[(3)] and C. Winter[(1)]

1. MARUM – Center for Marine Environmental Sciences, Bremen, Germany - alefebvre@marum.de
2. HKV Consultants, Lelystad, The Netherlands.
3. Department of Geosciences and Natural Resource Management, University of Copenhagen, Denmark

Abstract

This study characterizes the shape of the flow separation zone over natural compound bedforms during a tidal cycle and investigates how the flow separation zone depends on changing flow conditions, water levels and bathymetry. Field data collected during a full tidal cycle over large ebb-oriented bedforms provides high-resolution bathymetry and velocity measurements that are used to simulate the hydrodynamics structure during a tidal cycle using the Delft3D numerical model.

During the ebb, a large flow separation zone occurs on the steep lee side (14 to 23°) of each bedform. During the flood, no flow separation developed over the gentle slope of the flood lee side (3 to 5° on average). However, a small flow separation zone is often recognized near the crest, where the slope is locally up to 15°. The shape of the FSZ is not influenced by changes in current velocities or water levels. On the contrary, it is largely influenced by changes in the bed morphology. In particular, variations in the shape of the crest during the tidal cycle results in variations of the length of the FSZ.

1. INTRODUCTION

In tidal inlets and rivers, strong currents and high availability of sandy sediment result in large asymmetric bedforms (having a gentle and a steep side, Figure 1). If the bedform lee slope is steep enough, the pressure gradient at the edge of the bedform crest creates flow separation and the formation of a recirculating eddy is induced within the Flow Separation Zone (FSZ, Figure 1). This FSZ has a strong influence on the resistance that bedforms exerts on the flow due to energy loss through turbulence (Vanoni and Hwang, 1967). Furthermore, it complicates sediment transport above bedforms due to the presence of reverse flow within the FSZ. It is therefore highly relevant for the understanding and modeling of coastal hydro- and sediment dynamics to determine the length and shape of the FSZ for different flow conditions.

The FSZ has been widely studied over bedforms with a lee side close or equal to the angle-of-repose (~30°) which commonly occurs in rivers (see review by Best, 2005). Over such bedforms, a permanent FSZ develops. However, bedforms with a lee side smaller than the angle-of-repose have also been observed to commonly occur in rivers (e.g. Best and Kostaschuk, 2002) and in tidal environments (e.g. Lefebvre et al., accepted) The FSZ over lee sides that are less steep than the angle-of-repose is thought to be non-existent or intermittent. However, the exact slope at which the FSZ becomes permanent has not yet been determined. Paarlberg et al. (2009) considered that flow separation is permanent in time for a slope of 10° or more. Kostaschuk and Villard, (1996) suggested that flow separation may occur intermittently only for lee side slopes up to 19° and Best and Kostaschuk (2002) found that flow separation over bedforms with maximum lower lee side slope of 14° was present for about 4% of the time.

In tidal environments, flow reverses depending on the tidal phase and large bedforms usually keep their asymmetry, typically being oriented with the residual flow direction (e.g. Ernstsen et al., 2006). Therefore, their lee side may be steep or gentle depending on the tidal phase (Figure 1) which

implies that the FSZ varies depending on flow direction. Furthermore, the angle of the steep side of tidal bedforms is often smaller than the angle of repose (typically between 10 and 20°) i.e. in the range of angles over which the presence of a permanent FSZ is still under debate. In addition, the influence on the FSZ of tidally-induced variations of flow velocity, water level and bathymetry is still to be determined; in other words, the effect on the FSZ of tidal flow acceleration and deceleration, tidal range and variations of bathymetry due to sediment movement during a tidal cycle is unknown. This is largely due to the difficulty, if not impossibility, to measure the near-bed flow over bedforms in a natural environment.

This study aims, through numerical modeling, at characterizing the shape of the FSZ over natural asymmetric bedforms during a tidal cycle and investigating how the FSZ varies with changing flow velocities, water levels and bathymetry.

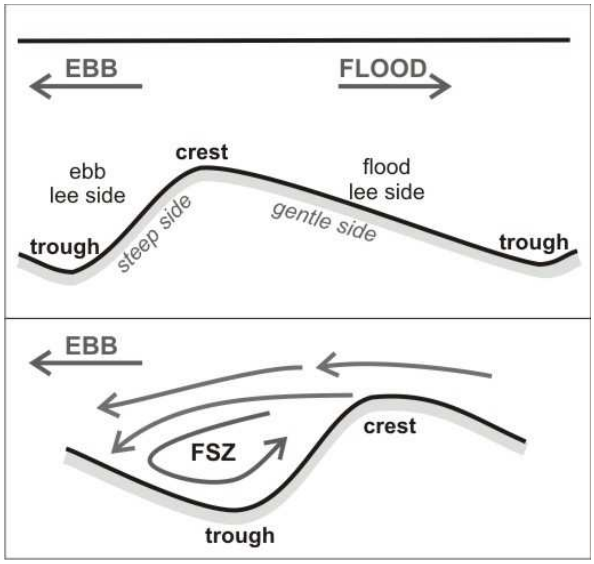

Figure 1. Top: sketch of an asymmetric bedform in a tidal environment; bottom: detail of the Flow Separation Zone (FSZ).

2. METHODS

2.1. Study area

The Knudedyb tidal inlet connects a tidal basin of the Danish Wadden Sea to the adjacent North Sea. The Knudedyb channel is around 8.5 km-long and 1 km-wide with an average water depth of about 15 m (Figure 2). The tides in the area are semi diurnal with a tidal range of 1.6 m on average. The tidal inlet bed is sandy and covered with compound bedforms (Lefebvre et al., 2011): large ebb-oriented bedforms (wavelengths of several hundred meters and heights of several meters) on which smaller bedforms (wavelengths of 3 to 5 m and heights of 0.15 to 0.3 m) are superimposed. These secondary bedforms reverse directions and migrate in the direction of the tidal currents while the primary bedforms stay ebb-oriented throughout the tidal cycle.

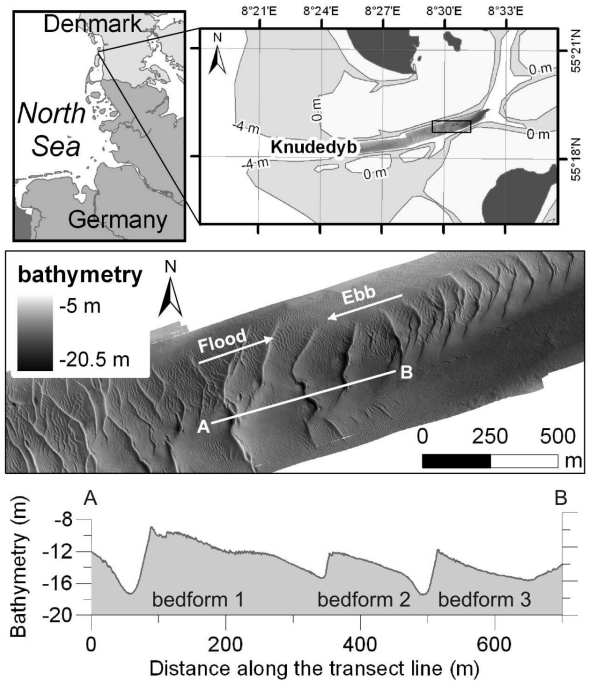

Figure 2. Top: location of the Knudedyb tidal channel and configuration of the inlet. Middle: bathymetry (m under mean sea level) around the measurement site and location of the transect line. Bottom: bed elevation profile along the transect line.

2.2. Field data

Repetitive surveys were conducted over a 700 m-long transect line crossing 3 primary bedforms (Figure 2) with the RV Senckenberg on 17 October 2009 during a full tidal cycle (Lefebvre et al. accepted). Flow velocity magnitudes and directions were measured using an acoustic Doppler current profiler (ADCP) operating at 1200

kHz and the seabed bathymetry was recorded using a high-resolution multibeam echosounder (MBES) operating at 455 kHz. The measurements of seabed bathymetry and flow velocity were performed simultaneously while the vessel was moving against the main tidal current in order to maintain a straight course at a constant and relatively low vessel speed. A total of 16 repetitive runs were carried out.

The ADCP data were used to calculate transect-averaged water levels and depth-averaged velocity magnitude and direction (Figure 3). The tidal range during the survey was 1.8 m. During the flood, the flow direction was 66° N on average (ESE to WNW) and (transect and depth-averaged) maximum velocity was 0.9 m/s. During the ebb, the flow direction was 242° (WNW to ESE) and (transect and depth-averaged) maximum velocity was 1.1 m/s (Lefebvre et al. accepted).

The bathymetric data were gridded with a cell size of 0.5x0.5 m and bed elevation profiles (BEPs) were extracted from the gridded bathymetry along the transect line. The troughs and crests of the large bedforms were determined following Ernstsen et al. (2010) as the lowest and highest elevation along each bedform and used to calculate bedform dimensions.

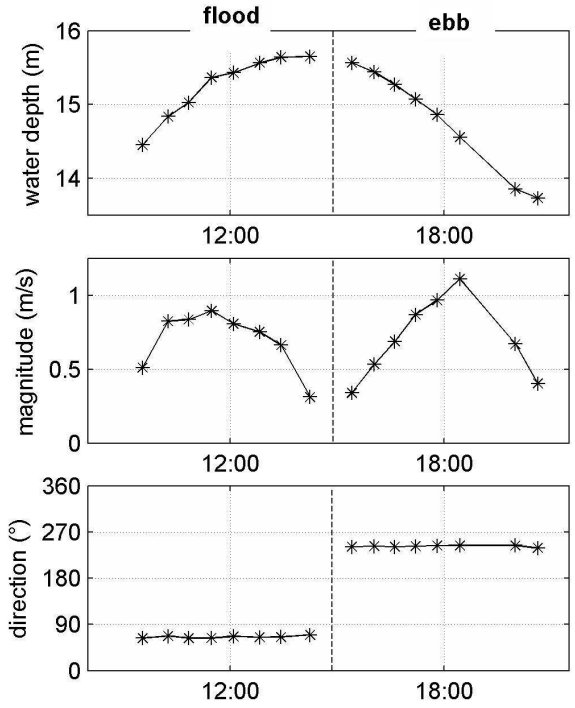

Figure 3. Variations of water depth and transect- and depth-averaged velocity magnitude and direction recorded by the ship mounted ADCP.

2.3. Numerical model

Delft3D (Deltares, 2011) is a process-based open-source integrated flow and transport modeling system. In Delft3D-FLOW the 3D non-linear shallow water equations, derived from the three dimensional Navier-Stokes equations for incompressible free surface flow, are solved. In order to capture the flow circulation above bedforms, the non-hydrostatic version and the k-epsilon turbulence closure are used.

The numerical model has been calibrated and validated against velocity and water level data from the laboratory flume experiments of McLean (1999). It proved to be able to correctly reproduce flow separation over bedforms, in particular the shape and length of the FSZ (Lefebvre et al., 2012).

2.4. Model Experiments

Five experiments were carried out using the numerical model. All simulations were done with the hydrodynamic module (without sediment transport) using velocity as entrance boundary condition and water level as exit boundary conditions. The horizontal grid cell was set to 0.5 m and the vertical grid was composed of 59 non-equidistant layers having a size of 0.2 m between the lowest and highest point of the bed profile (i.e. lowest trough and highest crest), before gradually increasing to a size of 1 m in the water column. The time step was 0.01 second.

The five experiments (Table 1) were designed to investigate the effects of changes in flow velocity, water levels and morphology on the FSZ.

The velocity setting was defined as (a) steady: 16 steady flow simulations were carried out, each simulation using one of the 16 velocity magnitudes calculated from the field data (Figure 3) or (b) tidal: one simulation was carried out with tidally-varying velocity magnitude.

The water level setting was defined as (a) mean: the water level was constant and equal to the mean water level recorded during the field survey, (b) varying: the water level was constant and varied to match the field data or (c) tidal: the water level was tidally-varying.

The morphology setting was defined as (a) mean: the bathymetry used was the mean bathymetry of

the field bathymetry data or (b) varying: each simulation was carried out using one of the 16 field bathymetries.

Table 1. Summary of the simulations carried out with details of the experiment number (exp. number) and the number of simulations for each of these experiments (number of sim.).

Exp. number	Number of sim.	Velocity	Water level	Morphology
1	16	steady	mean	mean
2	1	tidal	mean	mean
3	16	steady	varying	mean
4	1	tidal	tidal	mean
5	16	steady	varying	varying

2.5. Flow separation zone

The precision of the field data being insufficient to accurately determine the position of the FSZ (Lefebvre et al, accepted) the present study concentrates on characterizing the FSZ from the numerical simulation experiments. The method used to determine the presence and shape of the FSZ was adapted from Paarlberg et al. (2007) and Lefebvre et al (2012). The FSZ was sought on the lee of each bedform for each simulation as follow (Figure 4):

- the profiles with negative velocity were found
- the height of zero velocity point was calculated along each velocity profile
- the zero velocity line was determined and parameterized. It was observed to be composed of two segments: (1) upper zero velocity line: over the slip face, i.e. from the first profile with a negative velocity until the profile where the angle of the bed became higher than -12° (MID), the zero velocity line was a straight line and was fitted with a 1st order polynomial and (2) lower zero velocity line: over the trough and stoss side (angle of the bed profile > -12° until last profile with negative velocity) the lower zero velocity line was fitted with a 3rd order polynomial
- the intersection between the upper segment of the zero velocity line and the bed defined the separation point (SEP, beginning of the FSZ)
- the separation points were calculated along each profile by calculating the height at which the integral of the velocity between the bed and that point is zero (see Paarlberg et al. 2007)
- the flow separation line was calculated by fitting a 3rd order polynomial through the flow separation points, assuming that this polynomial went through the separation points
- the reattachment point (RET) was defined as the point where the flow separation line crossed the bed
- the height of the FSZ (H_{FSZ}) was calculated as the height between the separation point and the trough
- the extent of the FSZ (L_{FSZ}) was the horizontal distance between the separation point and the reattachment point
- the normalized extent of the FSZ was calculated, $L'_{FSZ} = L_{FSZ} / H_{FSZ}$

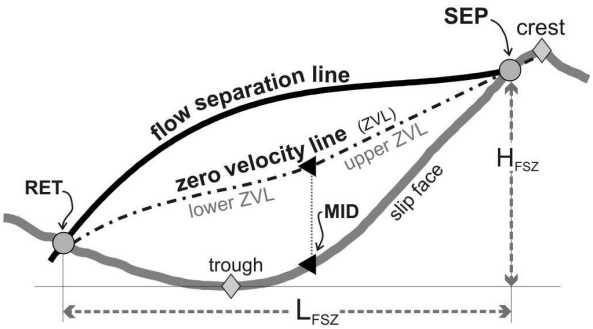

Figure 4. Schematic of the FSZ; SEP = separation point; MID = "middle" of the zero velocity line, i.e. profile where the angle of the bed is higher than -12°; RET = reattachment point; H_{FSZ} = height of the flow separation zone; L_{FSZ} = length of the FSZ.

3. RESULTS

3.1. Overall difference between ebb and flood

Based on the results of all experiments, it is observed that during the ebb a FSZ is present on the steep lee side of all three bedforms (Figure 5). The normalized length of the FSZ was on average 5.7 over bedform 2, and 6.2 over bedforms 1 and 3. Bedform 2 has a complicated morphology near the crest making the flow separates at the edge of the slip face and not close to the crest (highest point along the bedform). Therefore, in this case, the crest is defined as the last point before the trough which has positive bed slope (Figure 5).

In most cases during the flood, no FSZ develops over the gentle lee side, due to the flat bed at the crest (Figure 6). However, a small FSZ is sometimes recognized over the steepest part of the bedform, in general over bedform 1 (Figure 6). This FSZ has a normalized length of 1.3. This

small value shows that this FSZ is not related to the whole bedform but only to the steepest part of the bed near the crest.

3.2. Influence of velocity

Experiments 1 and 2 were designed to test the effect of velocity on the FSZ, specifically whether changes in steady velocity (Exp. 1) or tidally-varying (unsteady) velocity (Exp. 2) influence the length of the FSZ. The results of Experiments 1 and 2 reveals no effects of velocity on the FSZ. The variations in the FSZ during the tidal cycle are due to flow reversal with a small or non existent FSZ during the flood and a permanent well developed FSZ during the ebb (as outlined in Section 3.1.). During the ebb, the FSZs are clearly developed when flow velocity magnitudes becomes larger than 0.2 m s^{-1} (around 20 min after slack water) and stable until flow reversal impacts the velocity directions and hence a clear FSZ can not be distinguished (around 20 min before slack water).

3.3. Influence of water level

Experiments 3 and 4 were performed to test the influence of changing water levels on the FSZ. During the tidal cycle simulated here, the tidal range is 1.8 m (Figure 3) and the relative bedform height (bedform height / mean water depth) varies from 0.52 to 0.59 (bedform 1), 0.22 to 0.25 (bedform 2) and 0.34 to 0.39 (bedform 3). The results show that varying water levels has no influence on the FSZ. Furthermore, bedforms 1 and 3 have a similar normalized length of FSZ despite having different relative height implying that relative height is not a determining factor of the normalized length of the FSZ.

3.4. Influence of morphology

Experiment 5 was designed to test the effect of the changes in morphology on the FSZ. The high-resolution MBES data collected during the field campaign provided bathymetric data that realistically depicted the changes in bathymetry due to sediment transport during a tidal cycle. The troughs of the bedforms did not change significantly during the tidal cycle, whereas the crests were clearly altered by sediment movement. In particular, the crest of bedform 1 developed a flood cap during the flood, i.e. a high and steep crest, which then disappeared during the ebb, as observed over similar large bedforms by Ernstsen et al. (2006).

The results from Experiment 5 show that changing morphology influences the FSZ. Changes of the FSZ observed during the flood are difficult to interpret due to the small size of the FSZ, which provided only a small amount of profiles to characterize the FSZ. During the ebb, the observed variations of the FSZ length are clearly related to changes in morphology. The normalized length of the FSZ varies by 1 to 2% for bedforms 1 and 3. For bedform 2 on the other hand, it varies by up to 10%, with minimal and maximal values of 5.2 and 6.1. More importantly, the position of the separation point clearly changes with changing bathymetry (Figure 7). In particular, it appears that at the beginning of the ebb, the flow separation point is situated relatively down on the lee side due to the gentle slope of the bed towards the crest. At the end of the ebb, sediment movement created a steeper slope at the crest and consequently, the flow separates at the crest.

Considering all experiments, FSZ is present over slip face angles between 12 and 23° and no FSZ is observed for smaller angles.

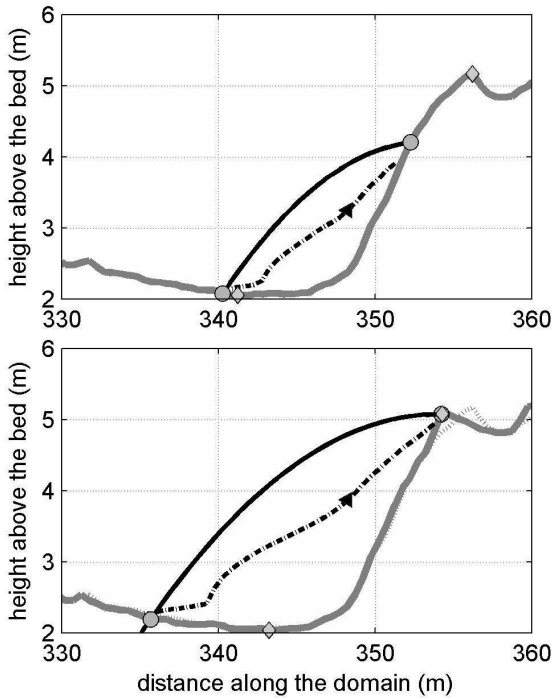

Figure 7. Detail of the FSZ over bedform 2 at the beginning (top) and at the end (bottom) of the ebb.

4. DISCUSSION

The numerical experiments suggest that a permanent flow separation zone develops for lee side angles in excess of 12°. Although this value is smaller than those suggested by Kostaschuk and Villard (1996) and Best and Kostaschuk (2002) (19° and >14° respectively), it agrees well with the assumption of Paarlberg et al. (2009) that flow separation is permanent in time for a slope of 10° or more.

The experiments also show that variations of velocity and water level have no influence on the FSZ within the tested velocity range. This agrees with results from Paarlberg et al. (2007) who, based on results from a large dataset of previous lab experiments, did not find any relationship between length of FSZ and flow velocity or water depth. Importantly, our results suggest that tidal variations of water levels and velocities magnitude do not influence the FSZ.

The only variations of the FSZ are created by changes in the bed morphology, which is in line with the suggestion by Paarlberg et al. (2007) that the slope of the bed at the bedform crest is a critical parameter in determining the shape and length of the FSZ. The flow separation line was always well parameterized by a 3rd order polynomial, as proposed by Paarlberg et al. (2007); however, we found that the normalized length of the FSZ is on average between 5.5 and 6.2 which is much longer than the value of 5.2 that Paarlberg et al. (2007) calculated. The difference can be explained by the fact that the flume experiments all contained very few points in the FSZ which forced them to extrapolate velocity profiles, whereas we had on average 10 times more points available to precisely determine the length and shape of the FSZ. Furthermore, flume experimental settings usually use simple bedform shapes (typically a sinusoidal stoss side and a straight steep lee side) whereas we modeled large compound bedforms derived from field measurements.

5. CONCLUSIONS

A non-hydrostatic numerical model was used to investigate the changes in the flow separation zone (FSZ) over natural compound bedforms in a tidal environment. Several conclusions can be drawn from the model simulations:

- A permanent FSZ is observed on the steep lee sides of the bedforms during the ebb; whereas during the flood, no flow separation zone is generally observed except locally over the steepest part of the bed near the crest.
- Changes in velocity and water levels (steady or tidally-varying) do not affect the size of the FSZ.
- The size of the FSZ is influenced by changes in bed morphology during the tidal cycle, especially by the bed morphology around the crest.

6. ACKNOWLEDGMENT

This study was funded through DFG-Research Center / Cluster of Excellence “The Ocean in the Earth System” and the Danish Council for Independent Research | Natural Sciences under the project “Process-based understanding and prediction of morphodynamics in a natural coastal system in response to climate change” (Steno Grant 10-081102).

7. REFERENCES

Best, J., 2005. The fluid dynamics of river dunes: A review and some future research directions. Journal of Geophysical Research 110 (F04S02): DOI 10.1029/2004JF000218.

Best, J. & Kostaschuk, R., 2002. An experimental study of turbulent flow over a low-angle dune. Journal of Geophysical Research 107 (C9): DOI 10.1029/2000jc000294.

Ernstsen, V., Noormets, R., Hebbeln, D., Bartholomä, A. & Flemming, B.W., 2006. Precision of high-resolution multibeam echo sounding coupled with high-accuracy positioning in a shallow water coastal environment. Geo-Marine Letters 26 (3): 141-149.

Kostaschuk, R. & Villard, P., 1996. Flow and sediment transport over large subaqueous dunes: Fraser River, Canada. Sedimentology 43: 849-863.

Lefebvre, A., Ernstsen, V.B. & Winter, C., 2011. Bedform characterization through 2D spectral analysis. Journal of Coastal Research SI64: 781-785.

Lefebvre, A., Paarlberg, A.J. & Winter, C, 2012. A numerical investigation of flow separation over bedforms. Poster presented at the EGU General Assembly 2012, Vienna (Austria), 22-27 April 2012.

Lefebvre, A., Ernstsen, V.B. & Winter, C., accepted. Estimation of roughness lengths and flow separation over compound bedforms in a natural tidal inlet. Continental Shelf Research.

McLean, S.R., Wolfe, S.R. & Nelson, J.M., 1999. Spatially averaged flow over a wavy boundary revisited. Journal of Geophysical Research 104 (C7): 15743-15753.

Paarlberg, A.J., Dohmen-Janssen, C.M., Hulscher, S.J.M.H. & Termes, P., 2007. A parameterization of flow separation over subaqueous dunes. Water Resources Research 43: DOI 10.1029/2006WR005425.

Paarlberg, A.J., Dohmen-Janssen, C.M., Hulscher, S.J.M.H. and Termes, P., 2009. Modeling river dune evolution using a parameterization of flow separation. Journal of Geophysical Research 114 (F01014): DOI 10.1029/2007JF000910.

Vanoni, V.A. & Hwang, L., 1967. Relation Between Bed Forms and Friction in Streams. Journal of the Hydraulics Division: 121-144

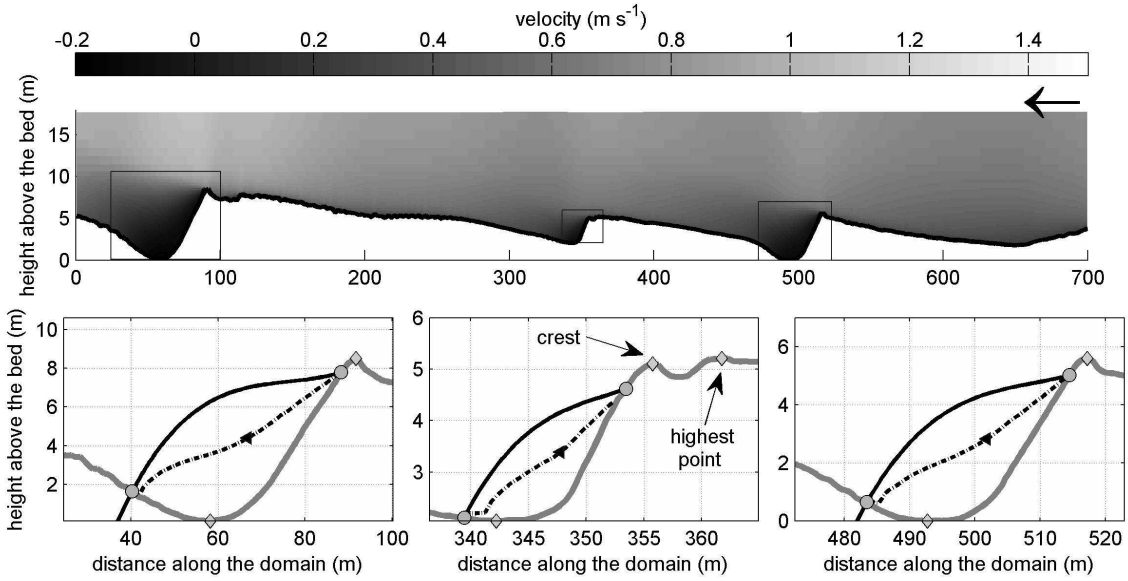

Figure 5. Velocities and FSZ over the 3 bedforms during maximum ebb velocity (see Figure 4 for details of the symbols). The arrow indicates the flow direction.

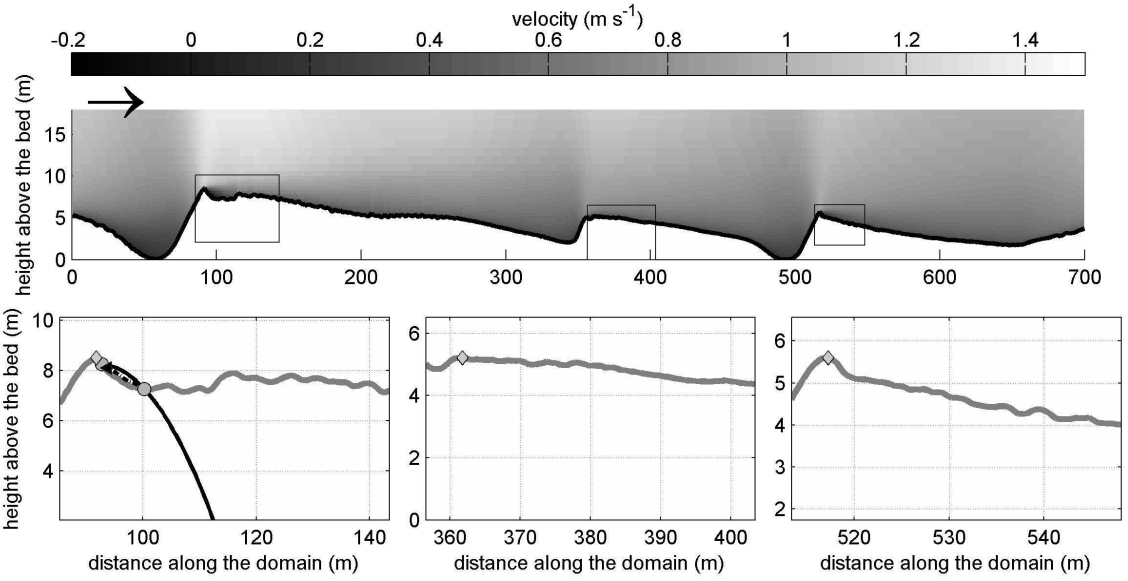

Figure 6. Velocities and FSZ over the 3 bedforms during maximum flood velocity (see Figure 4 for details of the symbols). The arrow indicates the flow direction.

Bedform characterization in river channel through 2D spectral analysis

A. Lisimenka[(1)], S. Rudowski[(1)]

1. Maritime Institute in Gdansk, Gdansk, Poland - sasha@im.gda.pl, starud@im.gda.pl

Abstract

During last decades a multibeam echosounder has become a widely used tool for a high resolution, rapid and, first of all, cost-effective mapping of submerged environments. At the present time, wealthy literature related to the bedform characterization based on the multibeam swath bathymetry systems data collected in different aquatic areas all over the World exist. In this paper, results of the recent bathymetry investigations in the main Vistula river mouth − the Cross-cut artificial channel, which were performed several times during 2009-2012 years are presented. The comprehensive riverbed morphology of the channel is characterized by the set of the different kinds and patterns of sandy bedforms. A detailed analysis of the bottom roughnesses in conjunction with a quantitative parameterization of the primary geometrical characteristics of the bedforms based on two-dimensional spectral analysis (2D FFT) are executed. The obtained results indicates significant changes of the morphology and bedform patterns which are very important in order to estimate and verify the bedload sediment transport phenomena and hydrodynamic processes connected with. Moreover, such information is required for predicting of the flood possibility related to riverine and sea storm surges in the area of interest.

1. INTRODUCTION

Different type of bottom surface roughnesses, such as ripples, megaripples, sandwaves and dunes, are a fundamental seafloor features which reflect and at the same time impact on a variety of physical phenomena including sediment transport and hydrodynamic processes. Characterization of this rhythmic bedforms essential parameters, their spatial distribution, dimension and orientation, as well as its migration and evolution, is with no doubts required for understanding and quantifying the influence of sediment topography on current state of a aquatic system and can be useful for predicting of its natural and anthropogenic changes.

The oceanographers' community manifests growing interest in a quantitative echosounders data analysis in context of the sediment transport estimation since the sonar systems of sea bottom visualization have appeared (among others, Kenyon, 1970, Kenyon *et al.*, 1981). But just in last years, development of the sonar technologies, computer techniques and signal processing methods has led to more fully exploitation of an information obtained by also in case of multibeam echosounder systems (MBES). It has found a reflect in growing numbers of the scientific works encapsulating this topic.

Some classification schemes of the various type of the bedforms were proposed (Ashley, 1990, Mitchell & Hughes Clarke, 1994, Knaapen *et al.*, 2001, Tegowski *et al.*, 2011), models of wind waves and currents interaction with seabottom were created (Davis *et al.*, 2004).

Using of a high-frequency MBES gave a possibility to determine a total volumetric sediment transport in a tidal channel (Bartholomä *et al.*, 2004) and a sand dunes crests migration over a tidal period in a shallow water (Knaapen *et al.*, 2005).

An attempt of finding a relationship between precise morphology, three-dimensional flow structure and sediment transport over a large sand dunes was presented in Parsons *et al.* (2005, 2006). Detailed information about bottom topography changes together with space distribution of the flow speed and grain size analysis of the bed material allowed the direct determination of bed resistance during flood on the Rhine river (Julien *et al.*, 2002).

High variability of the main bedform structures parameters in space and in time requires an appropriate mathematic tool for its determination. In context of scientific problem presented in this paper, results of works of many investigators based on algorithms of two-dimensional Fast Fourier Transform (2D FFT) spectral analysis have indicated a possibility of detailed quantification of the primary bedforms characteristics, determine their space form and dominant surface roughnesses (among others, Percival & Walden, 1993, Lyons *et al.*, 2002, Briggs *et al.*, 2005, Cazenave *et al.*, 2008, Lefebvre *et al.*, 2011, Lefebvre & Lyons, 2011), what is a main term for verification of the bedload sediment transport and hydrodynamic processes connected with.

2. MEASUREMENT AREA

Investigations were carried out in the main Vistula river mouth located in Polish coastal waters (Fig. 1). The Vistula is the longest river in Poland and plays a dominant role as regards both the catchment area size and the amount of discharged water flowing into the Gulf of Gdansk.

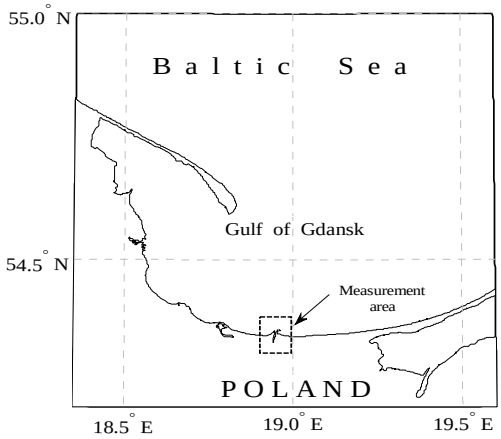

Figure 1. Location of the measurement area.

The main Vistula river mouth is the Cross-cut artificial channel with a *ca* 3000m length, 400m width and up to 10m depth. More than 95% of total Vistula waters outflow into the sea through this channel with the average annual water discharge more than 1000m^3/s (Cyberski, 1997).

Generally, a hydrological conditions in the main Vistula river mouth area, where a river waters mix with sea waters from the Gulf of Gdansk, are formed through interaction of the processes from this two environments. This riverine and marine processes influence superbly on not only current hydrological regime in the area, but seriosly affect on the morphology evolution of this part of the river, coast and neighbouring marine waters in longterm period of time.

Scale of the hydrological conditions related to the magnitude and variation of the water flows during 2009-2012 hydrological years is presented in Fig.2. Average daily water discharge data[1] were obtained from the gauging section located in Tczew, in range of 31.2km upstream the Vistula channel mouth. This gauging section is the last representative place situated in the lower reach of the Vistula river, which covers 99,92% of the catchment area (Augustowski, 1982), and, moreover, is not subjected to the impact of the backwater phenomena connected with the sea storm surge (mainly occurs when strong winds blow from north and west directions during long period of time).

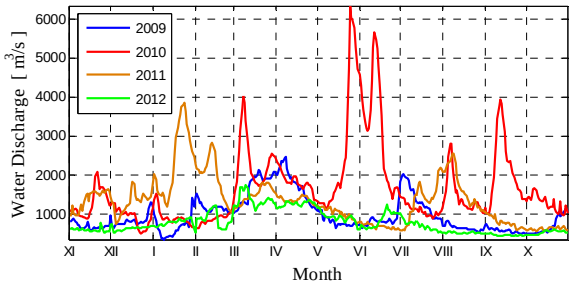

Figure 2. Average daily water discharge during 2009-2012 hydrological years.

In period of time between two measurement campaigns (see Section 3.1), a considerable variations in water discharge were taken place. Several phenomena with extremely high magnitudes connected with a precipitation floods (up to 6360m^3/s in May 2011) and a snow-melt floods (up to 4000m^3/s in January 2011) were observed and with no doubts have significantly

[1] hydrological data source − internet information service of the Institute of Meteorology and Water Management, www.pogodynka.pl

influenced on morphological character of the bottom as well as sediment mass transport in the area of interest.

3. METHODS

3.1. Data acquisition

Bathymetry measurements were carried out several times in 2009-2012 years on the board of the hydrographic boat Imoros 2. In the paper, results of two measurement campaigns which were performed in 20-23 August 2009 and 4-6 June 2012 are presented. An area of the interest was mapped using boat mounted high-resolution Reson Seabat 8101 (before 2012 year) and 7101 multibeam echosounder systems (MBES). The positioning system DGPS RTK Trimble SPS 851 together with Ixsea Hydrins inertial navigation system were integrated with MBES using the QINSy data acquisition software package. During of the each hydroacoustic surveys, the vertical sound speed profiles were measured using the portable model Reson Sound Velocity Probe SVP15.

3.2. Postprocessing

The bathymetric data were gridded with a cell size of 0.25m. The whole dataset was subsequently divided into the sub-domains using by a sliding square windows of 50m side with a 75% overlapping between an adjacent windows. Within a particular window, the mean depth was subtracted from each data sample and then a detrending procedure was applied. In order to minimize the spectral leakage due to the finite length of the data set, the data in each window were pre-multiplying by single orthogonal taper belongs to a family of functions known as discrete prolate spheroidal sequences (DPSS). Next, the spectral analysis based on the 2D Fast Fourier Transform (2D FFT) algorithm was executed:

$$S(f_x, f_y) = \int_{-\infty}^{+\infty}\int_{-\infty}^{+\infty} s(x,y)e^{-2\pi i(f_x x + f_y y)}dxdy \qquad (1)$$

where s(x,y) = spatial signal in the x and y directions, $S(f_x, f_y)$ = two-dimensional amplitude spectrum referred to the appropriate spatial frequencies f_x and f_y.

In order to exclude appearance of false components in spectra associated with the border of the data coverage effect, the 2D FFT was calculated only in sub-domains with a full data coverage (completely wet areas).

Then, the power spectrum density was calculated and direction and spatial frequency of the most energetic peak were determined.

As it was also noted in Lefebvre *et al.* (2011), although the data were detrended before being spectrally transformed, low frequency components were still present and masked the higher frequencies that are of interest. So, frequencies corresponding to wavlengths larger than 25m (half a square window geometrical dimension) were filtered out.

4. RESULTS

The comprehensive morphological character of the bottom is presented (Fig.3). The bottom relief are consist of two biggest forms: sand bar and trough, located along the border of the channel. In August 2009 (Fig. 3a), this main forms occupied almost all of the channel area. But at the end part, the trough is closed by the sandbar and nearly filled the channel mouth, in spite of the left side where an erosional depression is situated. In June 2012 (Fig. 3b), there are significant changes in bottom morphology. The sandbar is become longer, completely covered the erosional depression. By another hand, the trough end is become good formed completely opened the mouth. Moreover, a set of the different bedforms as sandwaves with superimposed megaripples and ripples with various height, wavelength and orientation are observed.

The calculated bedform orientation and wavelength based on the results of the two-dimensional spectral analysis in particular square windows, depicted by black vectors and superimposed on the part of the appropriate bottom relief (depicted by dashed rectangulars in Fig.3) are shown in more detailed scale in Fig.4. The different pattern of the bedform crests and significant changes of the their spatial frequency and orienation as well as distribution are distinctly visible.

5. CONCLUSIONS

The obtained results indicates that the application of the 2D spectral analysis is a good tool for

studies of the bedload sediment transport phenomena, roughnesses character of the bottom and hydrodynamic processes connected with. It should be require for monitoring, modeling and prognosis of the bedload transport and flows, especially related to flood possibility (riverine and/or sea storm surge). The data are also needed to prepare an emergency warning against extreme hydrological conditions for local society by appropriate services.

6. ACKNOWLEDGMENT

The author is grateful to the National Centre for Research and Development for funding this work by grant No PBS1/A2/3/2012.

7. REFERENCES

Ashley, G. M. 1990. Classification of large-scale subaqueous bedforms; a new look at and old problem. J. Sediment. Res. 60(1): 161-172.

Augustowski, B. (ed.). 1982. Dolina dolnej Wisły. Ossolineum, Wrocław (*in polish*).

Bartholomä, A. & Ernstsen, V.B. & Flemming, B.W. & Bartholdy, J. 2004. Bedform dynamics and net sediment transport paths over a flood-ebb tidal cycle in the Grådyb channel (Denmark), determined by high-resolution multibeam echosounding. Danish J. of Geography 104(1): 45-55.

Briggs, K.B. & Lyons, A.P. & Pouliquen, E. & Mayer, L.A. & Richardson, M.D. 2005. Seafloor roughness, sediment grain size and temporal variability. Proc. of Intern. Conf. and Exchib. on UAM, Heraklion, Crete, Greece, pp. 29-37.

Cazenave, P. W. & Lambkin, D.O. & Dix, J.K. 2008. Quantitative bedform analysis using decimetre resolution swath bathymetry. Caris 2008 Conference Proc., 22-26.09.2008, Bath, UK, 12 p.

Cyberski, J. 1997. Riverine outflow into the Gulf of Gdańsk. Oceanol. Stud. 26(4): 65–75.

Davis, J.P. & Walker, D.J. & Townsend, M. & Young, I.R. 2004. Wave-formed sediment ripples: Transient analysis of ripple spectral development. J. Geoph. Res. 109 (C07020): 15 pp. doi:10.1029/2004JC002307

Julien, P. Y. & Asce, M. & Klaassen, G. J. & Ten Brinke, W. B. M. & Wilbers, A. W. E. 2002. Case Study: Bed Resistance of Rhine River during 1998 Flood. J. Hydraul. Eng. 128: 1042-1050.

Kenyon, N.H. 1970. Sand ribbons of European tidal seas. Marine Geology 9: 25-39.

Kenyon, N.H. & Belderson, R.H. & Stride, A.H. & Johnson, M.A. 1981. Offshore tidal sand banks as indicators of net sand transport and as potential deposits. Spec. Public. of the Intern. Assoc. of Sedimentologists. 5: 257-268.

Knaapen, M.A.F. & Hulscher, S.J.M.H. & de Vriend, H.J. 2001. A new type of sea bed waves. Geophysical Research Letters 28(7): 1323-1326.

Knaapen, M.A.F. & van Bergen Henegouw, C.N. & Hu, Y.Y. 2005. Quantifying bedforms migration using multi-beam sonar. Geo-Marine Letters 25: 306-314.

Lefebvre, A. & Ernstsen, V.B. & Winter, C. 2011. Bedform characterization through 2D spectral analysis. J. Coast. Res. Spec. Issue 57: 781-785.

Lefebvre, A. & Lyons, A.P. 2011 Quantification of roughness for seabed characterization. Proc. of 4th Intern. Conf. and Exhib. on UAM, Kos Island, Greece, 20-24 June 2011, 8 p.

Lyons, A.P. & Fox, W.L.J. & Hasiotis, T. & Pouliquen E. 2002. Characterization of the two-dimensional roughness of wave-rippled sea floors using digital photogrammetry. IEEE J. Ocean. Eng. 27(3): 515-524.

Mitchell, N.C. & Hughes Clarke, J.E. 1994. Classification of seafloor geology using multibeam sonar data from the scotian shelf. Marine Geology. 121: 143-160.

Parsons, D. R. & Best, J. L. & Orfeo, O. & Hardy, R. J. & Kostaschuk, R. & Lane, S. N. 2005. Morphology and flow fields of three-dimensional dunes, Rio Paraná, Argentina: Results from simultaneous multibeam echosounding and acoustic Doppler current profiling. J. Geophys. Res. 110 (F04S03): 9 pp.

Parsons, D. R. & Best, J. L. & Lane, S. N. & Hardy, R. J. & Kostaschuk, R. & Shugar, D. & Orfeo, O. 2006. Morphology, flow and sediment transport over a natural 3D dune field: Rio Paraná, Argentina. River Flow 2006 vols 1 and 2: 997-1004.

Percival, D.B. & Walden, A.T. 1993. Spectral analysis for physical application. Cambridge University Press, 616 p.

Tegowski, J. & Nowak, J. & Moskalik, M. & Szefler, K. 2011. Seabed classification from multibeam echosounder backscatter data using wavelet transformation and neural network approach. Proc. of 4th Intern. Conf. and Exhib. on UAM, Kos Island, Greece, 20-24 June 2011, 1257-1264.

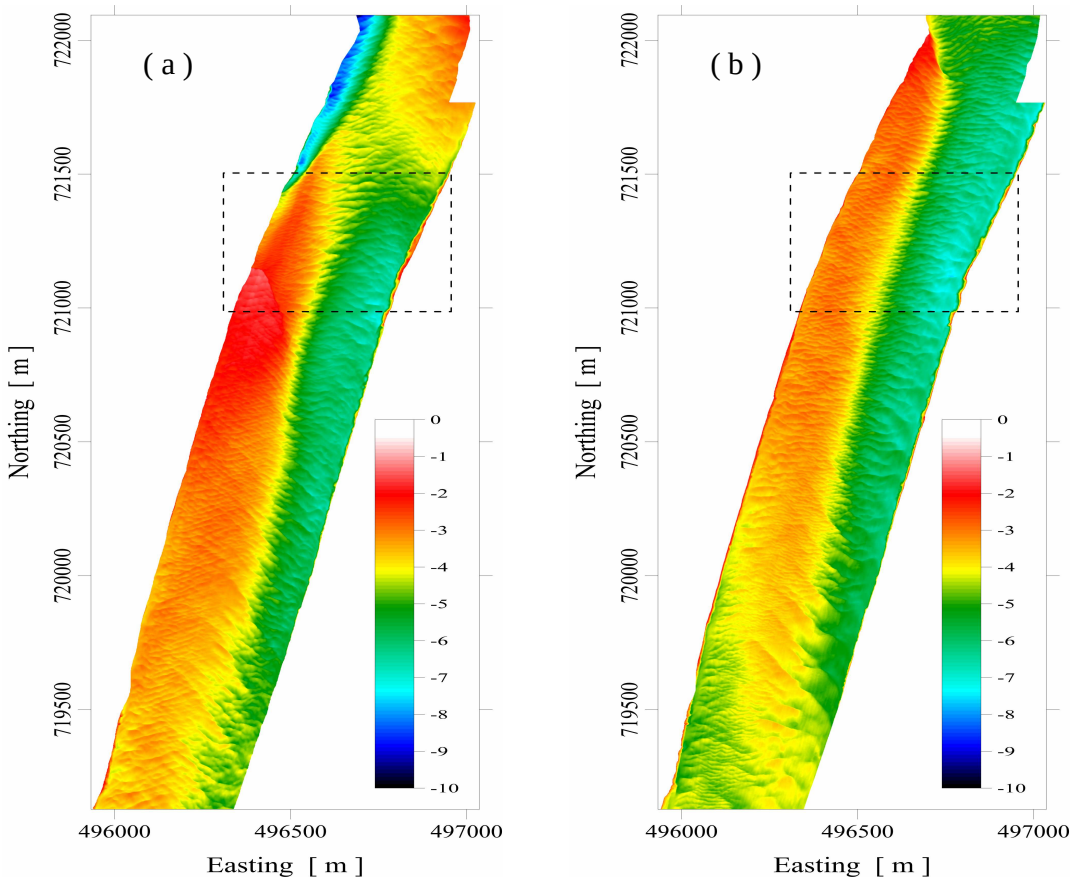

Figure 3. Bathymetry images of the Vistula river channel on the base of measurements performed in August 2009 (a) and June 2012 (b). Coordinates in WGS-84. Colorbar scales in meters.

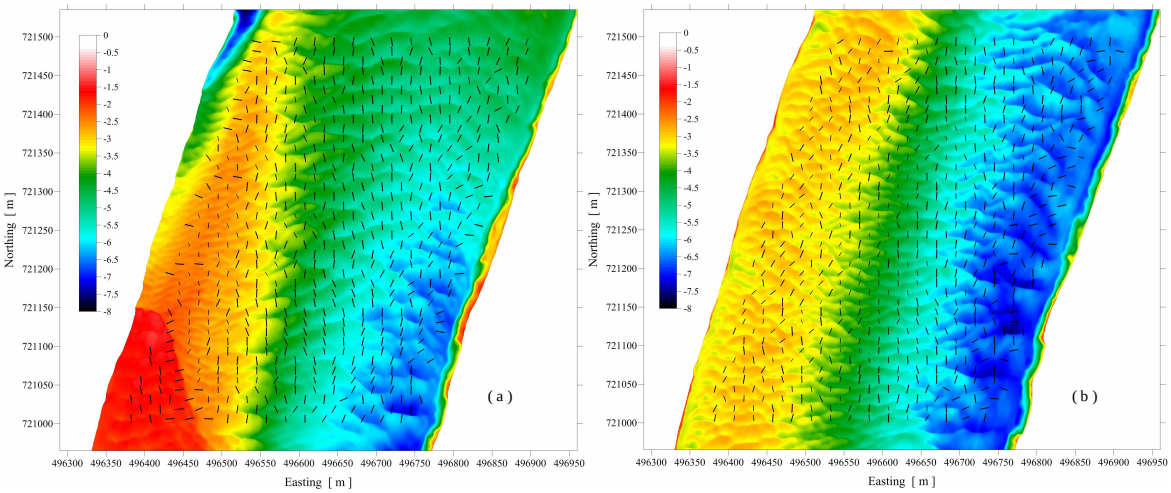

Figure 4. Calculated bedform orientation and wavelength depicted in the black vectors superimposed on the bottom relief of the river channel (part of the Fig.3 in bigger scale) for August 2009 (a) and June 2012 (b) respectively. Length of the black vectors is proportional on bedform wavelength. Coordinates in WGS-84. Colorbar scales in meters.

Sediment transport distribution along equilibrium sand dunes

S. Naqshband [(1)], J. S. Ribberink [(1)], D. Hurther [(2)], S.J.M.H. Hulscher [(1)]

1. University of Twente, Enschede, Netherlands – S.Naqshband@utwente.nl
2. Université de Grenoble, CNRS, Grenoble, France

Abstract

The present study focuses on distribution of sediment transport along mobile dunes in equilibrium. To this end, using ACVP (Acoustic Concentration and Velocity Profiler), we have obtained simultaneous, co-located, high temporal-spatial resolution measurements of the multi-component flow velocity and suspended sediment concentration above dunes. In contrast to previous measurements of flow and sediment dynamics above dunes which are mostly carried out with more than one instrument, we are now able to address sediment fluxes directly for flow scales smaller than the separation distance between different instruments. In this paper, preliminary ACVP results are shown in terms of flow velocities, suspended sediment concentrations and suspended sediment fluxes along dune profiles

.

1. INTRODUCTION

Dunes are the most common bed forms in lowland river channels consisting of sand and gravel, generated by divergences and convergences of sediment over the bed. They act as roughness to the flow leading to increasing water levels. To be able to model dune evolution and dune dimensions adequately, knowledge on flow and sediment transport processes are crucial.

Sediment is transported as bed load and suspended load, of which a part can be wash load. Wash load is fine sediment that is transported in permanent suspension and therefore less important for morphological development of bed forms. Despite the dominance of suspended load in sand bed rivers (Kostaschuk, 2006), it is often assumed that bed load is the dominant transport mechanism in generating and migrating dunes. Suspended load is then neglected in modelling dune morphology and evolution for flood management purposes (Jerolmack et al. 2005; Paarlberg et al. 2009). However, several theoretical as well as field studies have shown significant difference in dune mechanisms under bed load and suspended load dominant transport regimes. Generally, researchers have found that asymmetric dunes with flow separation zones (high-angle dunes) occur when bed load is the dominant transport mechanism while symmetric dunes without flow separation zones (low-angle dunes) develop when most sand is transported in suspension (Smith and McLean, 1977a; Kostaschuk and Villard, 1996; Kostaschuk, 2000; Kostaschuk and Best, 2005). However, it is not yet clear which processes are responsible for this difference between dunes under bed load and suspended load dominant transport regimes.

For a better understanding of flow and sediment dynamics above dunes, to-date velocity and concentration measurements above mobile and immobile dune beds were collected using separate acoustic and or optical measuring systems (Nelson et al. 1993; Venditti and Bennett, 2000; Kostaschuk et al. 2004; McLean et al. 2008; Wren and Kuhnle, 2008), resulting in a limited investigation of sediment fluxes to large scale processes. In particular, turbulence processes e.g. turbulent bursts and turbulence generation in the dune flow separation zones, which are the most important mechanisms of sediment entrainment, could not be directly addressed for flow scales

smaller than the separation distance between the different instruments.

Our aim in this study is to understand and quantify the sediment transport distribution along equilibrium dunes. In particular, we are interested in the contribution of suspended sediment transport to dune migration. To this end, detailed measurements of flow velocity and sediment concentrations have been obtained using the Acoustic Concentration and Velocity Profiler (ACVP), developed by Hurther et al. 2011. ACVP is capable of measuring vertical profiles of the multi-component flow velocity and sediment concentration simultaneously and co-located with high temporal-spatial resolution. In addition, corresponding bed interface position is measured thus providing direct sediment flux measurements along the bed profiles (Hurther and Thorne, 2011). In this paper, preliminary results are shown of the flow velocity, suspended sediment concentration and sediment flux measurements along mobile dunes.

2. LABORATORY EXPERIMENT

2.1. Set up and instrumentation

We have conducted experiments in the Hydraulics Laboratory of the Leichtweiss institute of the Technical University of Braunschweig, Germany. The flume used has a width of 2 m and length of 30 m, where the effective measuring length was approximately 10 m. As we are interested in flow and sediment transport over quasi 2D dunes, the width of the flume was reduced to 0.5 m. This, in addition, reduces the measuring complications that are related to the occurrence of 3D dunes.

The experiments were conducted with uniform, fine sand (see Table 1 for sand properties). Flow discharge to the flume is delivered from a constant head-tank approximately 5 m above the flume level. Using an Inductive Discharge Measurement device (IDM), the desired discharge was set with an accuracy of 1%. The flume slope and the weir at the end of the flume are adjustable, which made it possible to realize equilibrium flow conditions at a predefined discharge and water depth. The sediment at the end of the flume was caught by a funnel and transported back to the upstream end of the flume after the completion of each experiment. At the effective measurement section of the flume (over a length of 10 m), the bed and water levels were measured continuously using echo sensors that were mounted on a semi-automatic measurement carriage. The water level was measured at the centre of the flow, where the bed level measurements were taken at three parallel transects across the flume width. The accuracy of the bed level measurements were determined by repeatedly measuring a fixed bed profile (see Tuijnder et al. 2009). The vertical standard deviation was less than 1 mm, where the horizontal standard deviation was approximately 3 mm. In the horizontal direction the accuracy was limited by the area of the measurement surface of the echo sounders, which was a few centimetres. This makes the echo sounders suitable for studying large-scale features of the dunes, but the grain scale processes cannot be resolved.

In order to determine the sediment fluxes along the dune profiles, flow velocities and sediment concentrations are measured using the ACVP (see also Naqshband et al. 2012). The major advantage of this single system, compared to separate instruments for measuring flow velocity and sediment concentration, is the ability of addressing sediment fluxes to small scale processes. In particular, turbulence processes e.g. turbulent bursts and turbulence generation in the dune flow separation zones, which are the most important mechanisms of sediment entrainment, could not be directly addressed for flow scales smaller than the separation distance between the instruments.

The ACVP was submerged and deployed at approximately 20 cm above the mean bed level. The transmission rate of the ACVP was 1 MHz and the collected data were processed to give horizontal velocity u along the flume, vertical velocity w and sediment concentration profiles at a vertical spatial resolution of 2.5 mm. Furthermore, an Acoustic Doppler Velocimeter and transverse suction sampler (Bosman et al. 1987) were used to measure the flow velocity and sediment concentration at several locations along the dune profile. The data collected with these instruments will be used for the validation of the ACVP.

2.2. Experimental procedure

A sand layer of approximately 25 cm thick was installed over the entire length of the flume and the sand bed was flattened at the beginning of each experiment. For each experiment the water discharge, flume slope and water depth were

predefined (see table 1). The flume was slowly filled with water from both the downstream and upstream end of the flume to make sure the bed was not disturbed. Subsequently, the predefined discharge and weir level were set at the required level and the measurement program was started. Every 2 to 3 minutes, water levels and bed profiles were measured with echo sensors on the carriage, over the entire effective measurement section of the flume. The data were stored and processed after each measurement to monitor the water and bed level development in the flume. The weir level was adjusted if the water levels in the flume significantly differed from the predefined water depth.

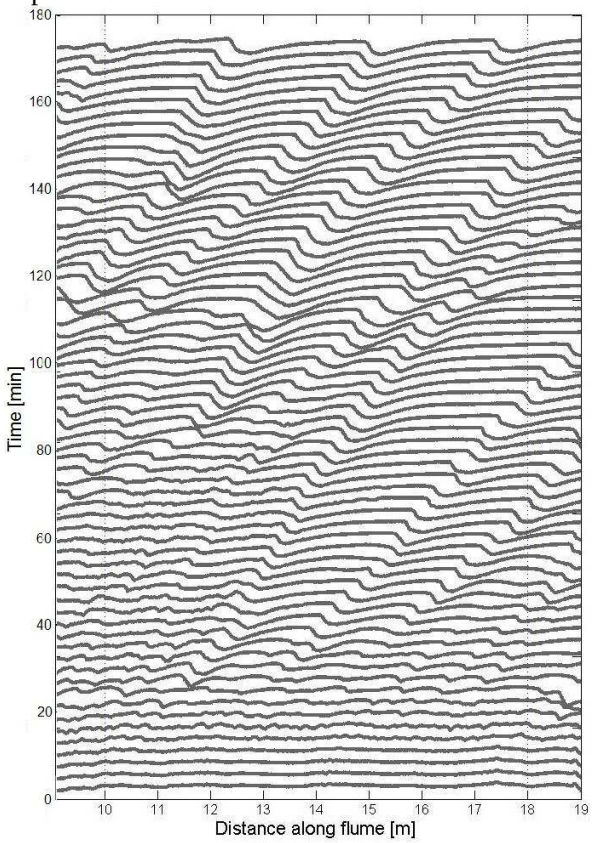

Figure 1. Bed development in time for EXP1 at the effective measurement section of the flume (10-18 m); starting from plane bed towards dunes in equilibrium.

The ACVP measurements were started as soon as equilibrium flow conditions were obtained and the dunes were found to be in a dynamic equilibrium at the effective measurement section of the flume. This dynamic equilibrium is reached when dunes migrate without changing shape as illustrated in Figure 1. Starting from plane bed, ripples develop into dunes and after approximately 150 minutes dunes are migrating with a constant velocity maintaining their shapes.

In addition, average dune heights (Figure 2a) and dune lengths (Figure 2b) together with standard deviations were calculated over the effective measurement section of the flume showing that a dynamic equilibrium is reached after approximately 150 minutes.

During this equilibrium, the carriage with the ACVP was placed at a fixed position along the flume and the dunes migrated underneath the ACVP. After the completion of the measurement program, the discharge through the flume was stopped and the sediment accumulated at the end of the flume was put back to the upstream end of the flume.

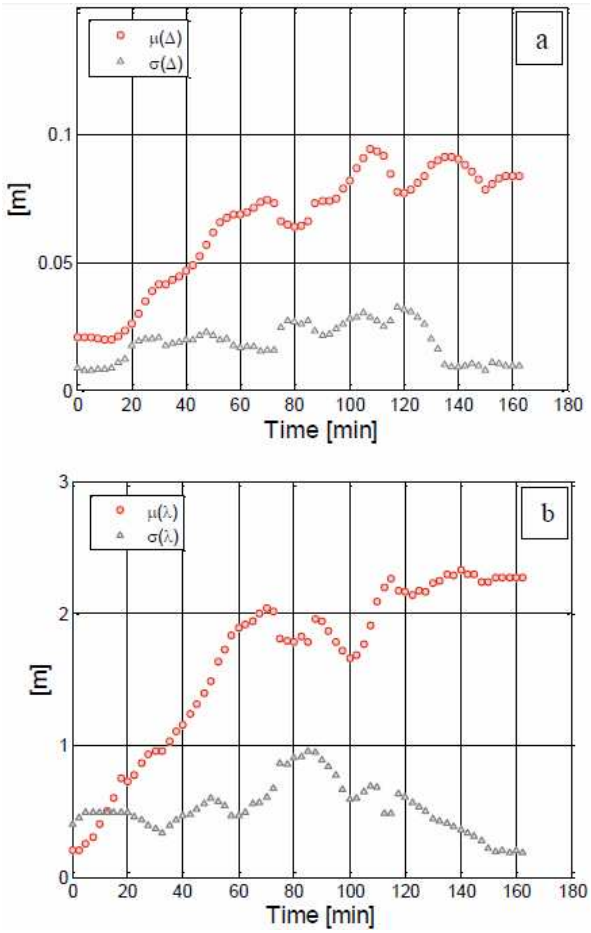

Figure 2. Average bedform heights (a) and lengths (b) in time for EXP1 together with the standard deviations.

2.3. Experimental conditions

Two detailed experiments were carried out, each with a different discharge and flume slope but constant water depth. The results discussed in this paper correspond to experiment 1 (EXP1, Table 1). For this experiment, the equilibrium dune height Δe, dune length Λe and time to equilibrium Te are also shown in the table below.

Parameter	**Value**
Discharge range [L s^{-1}]	80-100
Discharge EXP1 [m3 s^{-1}]	0.08
Flume slope [-]*10-3	1.0
Water depth [m]	0.25
D10 [mm]	0.21
D50 [mm]	0.29
D90 [mm]	0.40
Λe [m]	2.27
Δe [m]	0.084
Te [min]	150

Table 1. Experimental conditions and average equilibrium dune dimensions for EXP1.

3. RESULTS AND DISCUSSION

In this section, preliminary time-averaged ACVP results are shown of the measurements of flow velocity, sediment concentration and corresponding bed interface positions along the dunes. The averaging time for now is chosen to be 60 seconds and needs more attention as the data is sensitive to this averaging time. The sediment flux is calculated directly from the product of flow velocities and sediment concentrations, which is also shown here.

Figure 4 shows the time-averaged horizontal flow velocity corresponding to EXP1. The Flow direction is from right to left and the solid line represents the dune profile as measured by the ACVP. Several characteristics of fluid flow over dunes can be observed in this figure as expected from theory and experimental studies in literature (Raudkivi, 1966; Engelund & Fredsse, 1982; Bennet & Best, 1995; Holmes & Garcia, 2008): (1) a zone of flow separation on the dune crest lee-side with reversing flow velocities; (2) flow acceleration at the dune crest; (3) flow deceleration in the wake region overlying the separation zone and extending downstream; (4) an outer, near-surface region with higher velocities overlying the wake region; and (5) developing of a near-bed boundary layer starting on the stoss-side of the dune towards the dune crest. In addition, good agreement is obtained for the comparison of the time-averaged horizontal flow velocity with data from the ADV as shown in Figure 3.

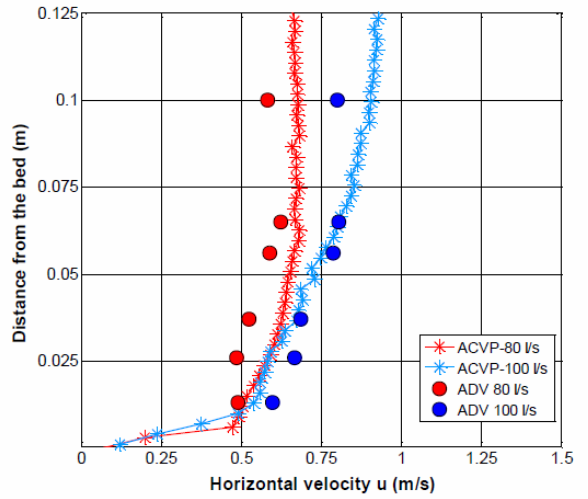

Figure 3. Comparison of time-averaged horizontal velocities between ADV and ACVP for EXP1 (80 L/s) and EXP2 (100 L/s)

The time-averaged sediment concentration corresponding to EXP1 is shown in Figure 5. It can be seen that most of the sediment is concentrated in the lowest 1 to 2 cm from the dune bed. From the dune crest towards the dune trough, the thickness of this high concentrated sediment layer increases. This is due to the flow acceleration at the crest and flow deceleration at the trough, and the corresponding turbulent intensity which is important for sediment entrainment. The turbulent intensity (not shown here) is much higher at the dune trough region due to flow separation.

The product of horizontal velocity and sediment concentration, averaged in time, is shown in Figure 6. It can be seen that most of the sediment is transported near the bed and that sediment flux increases towards the dune crest. A region of relatively small negative flux is observed in the flow separation region which is due to flow reversal. Furthermore, the avalanching of sediment on the lee-side is made visible. These patterns show a good match with previous studies of flow and sediment transport over dunes (e.g. Lapointe, 1992; Kostaschuk et al. 2004; Best, 2005; McLean et al. 2008; Kostaschuk et al. 2009).

4. CONCLUSIONS

The present study discusses preliminary results of mobile dune experiments conducted in the hydraulics laboratory of the Leichtweiss institute (LWI) of the technical University of Braunschweig, Germany. Using the ACVP, simultaneous, co-located, high resolution data was collected of the multi-component flow velocity and suspended sediment concentration over mobile sand dunes. The patterns found in the flow velocity, sediment concentration and sediment transport over dunes show good agreement with previous studies of dune dynamics.

5. FUTURE WORK

In order to quantify the contribution of suspended sediment to dune migration, net suspended sediment fluxes will be derived next. In addition, total sediment transport rates (bed and suspended load) will be calculated from dune migration profiles. Furthermore, the velocity data will be used to derive turbulent bed shear stress formulations.

6. ACKNOWLEDGMENT

This study is carried out as part of the project 'BedFormFlood', supported by the Technology Foundation STW, the applied science division of NWO and the technology programme of the Ministry of Economic Affairs. The authors are grateful to Olav van Duin and Arjan Tuijnder for their contribution to the experiments.

7. REFERENCES

Bennet & Best, 1995. Mean flow and turbulence structure over fixed, two-dimensional dunes; implications for sediment transport and bed form stability. Sedimentology, 42, 491-513.

Best, J. 2005. The fluid dynamics of river dunes: A review and some future research directions. Journal of Geophysical Research, 110 (F04S01), doi:10.1029/2004JF000218.

Bosman, J.J., Velden, E.T.J.M. & van der Hulsbergen, C.H. 1987. Sediment concentration measurements by transverse suction. Coast. Eng., 11, 353-370.

Engelund, F. & Fredsere, J. 1982. Sediment ripples and dunes. Ann. Rev. Fluid Mech., 14, 13-37

Holmes, R.R. & Garcia, M.H. 2008. Flow over bedforms in a large sand-bed river: A field investigation. Journal of Hydraulic Research, 46(3): p. 322-333.

Hurther, D. & Thorne, P.D. 2011. Suspension and near-bed load sediment transport processes above a migrating, sand-rippled bed under shoaling waves. Journal of Geophysical research, Vol. 116, C07001, doi:10.1029/2010JC006774.

Hurther, D., Thorne, P.D., Bricault, M., Lemmin, U., Barnoud, J.M. 2011. A multi-frequency Acoustic Concentration and Velocity Profiler (ACVP) for boundary layer measurements of fine-scale flow and sediment transport processes. Coastal Engineering, 58, 594-605.

Jerolmack, D. J., & D. C. Mohrig 2005. A unified model for subaqueous bed form dynamics. Water Res. Res., 41, W12421, doi:10.1029/ 2005WR004329.

Kostaschuk, R.A. & P.V. Villard 1996. Flow and sediment transport over large subaqueous dunes: Fraser River, Canada. Sedimentology, 43, 849-863.

Kostaschuk, R. A. 2000. A field study of turbulence and sediment dynamics over subaqueous dunes with flow separation. Sedimentology, 47, 519– 531.

Kostaschuk, R.A., P.V. Villard & J.L Best 2004. Measuring velocity and shear stress over dunes with an acoustic Doppler profiler. Journal of Hydraulic Engineering, 130, 932- 936.

Kostaschuk, R., & J. Best 2005. Response of sand dunes to variations in tidal flow: Fraser Estuary, Canada, J. Geophys. Res., 110, F04S04, doi:10.1029/2004JF000176

Kostaschuk, R.A. 2006. Sediment transport mechanics and dune morphology. In: G. Parker and M. Garcia, eds. River, Coastal and Estuarine Morphodynamics: RCEM 2005, Taylor & Francis, London, 795-803

Kostaschuk, R., Shugar, D., Best, J.L., Parsons, D.R., Lane S.N. Hardy, R.J. and Orfeo, O. 2009. Suspended sediment transport and deposition over a dune: Rio Parana, Argentina. Earth Surface Processes and Landforms, 34:1605-1611.

Lapointe, M.F. 1992. Burst-like sediment suspension events in a sand bed river. Earth Surf. Process. Landforms, 17, 253-270.

McLean, S. R., Nelson, J. M., Gary, L. 2008. Suspended sediment in the presence of dunes. In River, Coastal and Estuarine Morphodynamics: RCEM 2007, Dohmen-Janssen CM, Hulscher SJMH (eds). Taylor & Francis Group: London; 611–618.

Naqshband, S., J.S. Ribberink, S.J.M.H. Hulscher & Hurther, D. 2012. Simultaneous, co-located measurements of flow velocity and sediment concentration over mobile dunes. In Murillo Muñoz, R. E. (Ed.). Proceedings of the conference on Fluvial-hydraulics, (River Flow), San José, Costa Rica, pp. 755-760.

Nelson, J.M., McLean, S.R., Wolfe, S.R. 1993. Mean flow & turbulence fields over two-dimensional bed forms. Water Resources Res. 29, 3935–3953.

Paarlberg, A. J., C. M. Dohmen-Janssen, S. J. M. H. Hulscher, & A. P. P. Termes 2009. Modeling river dune evolution using a parameterization of flow separation. Journal of Geophysical Research. Pt. F: Earth surface, 114 (F01014). ISSN 0148-0227.

Raudkivi, A.J. 1961. Bed forms in alluvial channels. J. Fluid Mech., 26, 507-514.

Smith, J.D. & S.R. McLean 1977a. Spatially-averaged flow over a wavy surface. Journal of Geophysical Research, 82, 1735-1746.

Tuijnder, A.P., Ribberink, J.S., & Hulscher, S.J.M.H. 2009. An experimental study into the geometry of supply-limited dunes. Sedimentology, 56(6), 1713-1727.

Venditti, J. G. & Bennett, S. J. 2000. Spectral analysis of turbulent flow and suspended sediment transport over fixed dunes. Journal of Geophysical Research., Vol. 105, No. C9, pp. 22,035–22,047.

Wren, D. G., & Kuhnle, R. A. 2008. Measurements of coupled fluid and sediment motion over mobile sand dunes in a laboratory flume. Int. Journal of Sediment Research. Vol.23, No. 4, pp. 329–337.

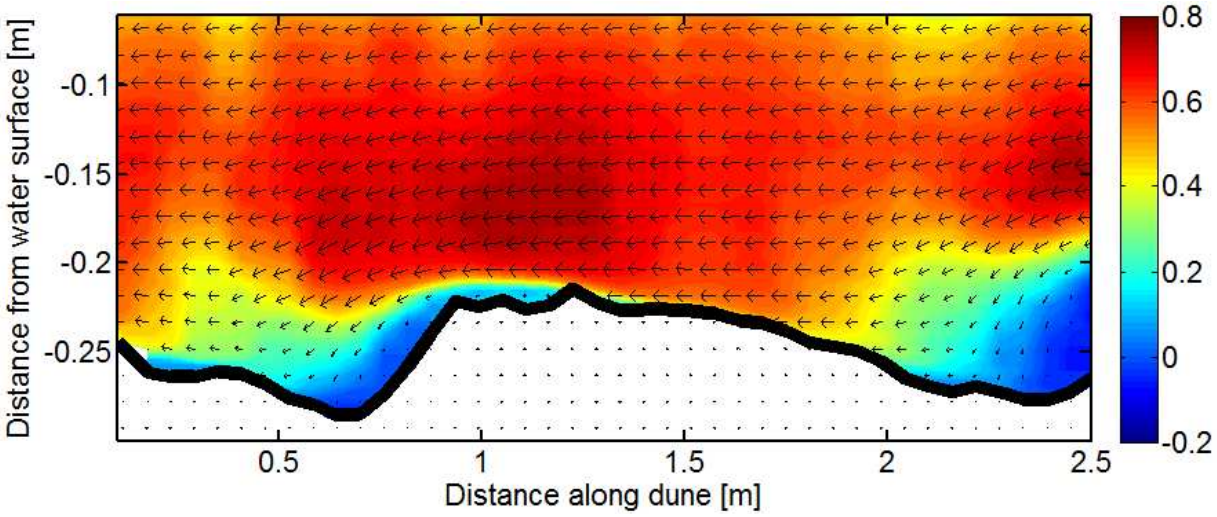

Figure 4. Time-averaged horizontal flow velocity u [m.s-1] over the dune profile, from ACVP measurements of EXP1. The arrows represent the 2D, time-averaged flow direction. Flow is from right to left.

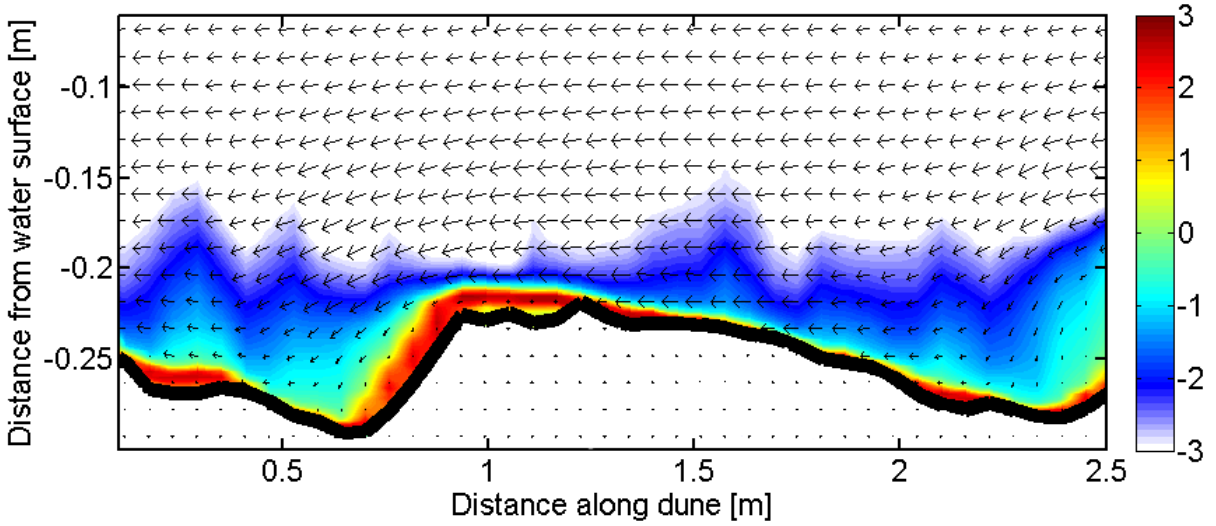

Figure 5. Time-averaged sediment concentration $\log_{10}(c)$ [kg.m^{-3}] over the dune profile, from ACVP measurements of EXP1. The arrows represent the 2D, time-averaged flow direction. Flow is from right to left.

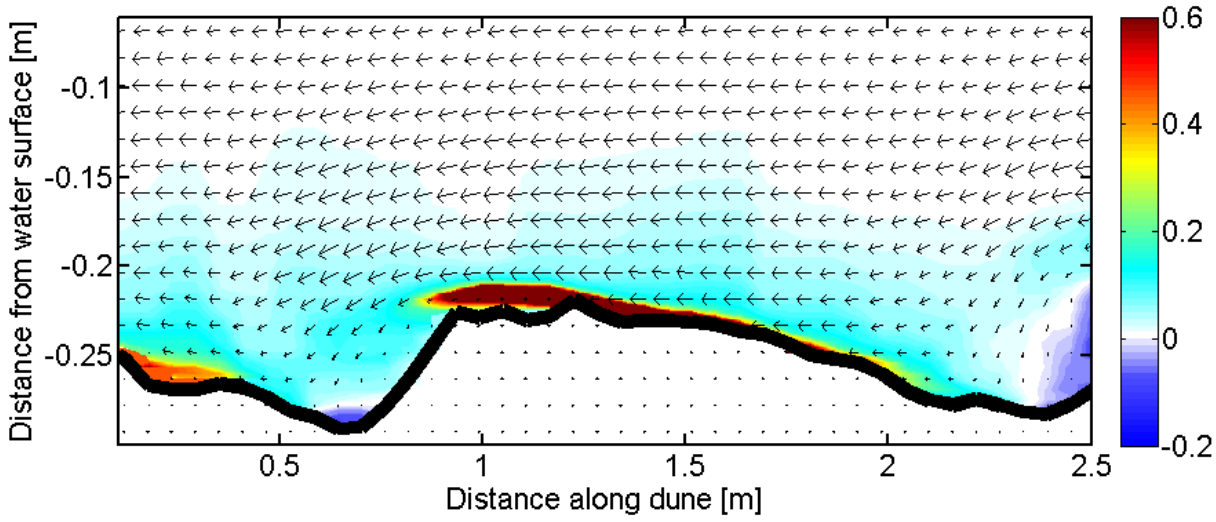

Figure 6. Time-averaged sediment flux uc [kg.m^{-2}.s^{-1}] over the dune profile, from ACVP measurements of EXP1. The arrows represent the 2D, time-averaged flow direction. Flow is from right to left.

Large-eddy simulation of flow over barchan dunes

M. Omidyeganeh [(1)], U. Piomelli [(1)], K. T. Christensen [(2)], and J. L. Best [(2)]

1. Queen's University, Kingston, CA – omidyeganeh@me.queensu.ca, ugo@me.queensu.ca
2. University of Illinois, Urbana-Champaign, USA – ktc@illinois.edu, jimbest@illinois.edu

Abstract

We have performed large-eddy simulations of turbulent flow over barchan dunes in a channel with 5 differing interdune spacings in the downstream direction at moderate Reynolds number, Re_∞=25,160 (based on the free stream velocity and channel height). Simulations are validated against experimental data (at Re_∞=59,000); the largest interdune spacing (2.38λ, where λ is the length of the barchan model) presents similar characteristics as the isolated dune in the experiment, indicating that at this distance the sheltering effect of the upstream dune is very weak. We provide 3D realizations of the mean and instantaneous flow that allows us to explain some features of the flow relevant to sediment transport. Barchan dunes induce two counter-rotating streamwise vortices, along each of the horns, which direct high-momentum fluid toward the centerline symmetry plane and low-momentum fluid near the bed away from the centerline. Distribution of the bed shear stress, characteristics of the separation and reattachment regions, and instantaneous wall turbulence are discussed. The interdune spacing significantly alters the turbulent flow over the stoss side of the dunes. The characteristics of the separated-shear layer are altered quantitatively; the separation bubble is smaller, the separated-shear layer is stronger, and the bed shear stress is larger at smaller interdune spacings.

1. INTRODUCTION

The interaction of turbulent flow fields with a mobile sand bed, when the flow is unidirectional and sand supply is limited, results in the formation of barchan dunes in aeolian and fluvial environments. Barchans have a crescentic topography with horns elongated in the downstream direction (Kroy *et al.* 2005), and are extensively observed in deserts on Earth (Bagnold 1941; Lancaster 1995) and on Mars (Breed *et al.* 1979), but only rarely in rivers and oceans (McCullogh *et al.* 1964; Allen 1968). The linear relationship between the width of the dune, its height and length and its three-dimensional shape are well understood (Bagnold 1941; Hesp *et al.* 1998). Barchans rarely exist as isolated forms and may occur in large fields (Hersen *et al.* 2004) of a few hundred square kilometers in area (Lettau *et al.* 1969). Their significant effects on the flow field and sediment transport have attracted researchers to study fluid and morphological dynamics in environments with barchans.

Most of the measurements and calculations of flow and sediment transport have been performed on the streamwise-wall-normal symmetry plane of barchans, over the windward stoss side (Lancaster 1985; Lancaster *et al.* 1996; Wiggs *et al.* 1996; McKenna *et al.* 2000; and Palmer *et al.* 2011). Theoretical efforts have also usually considered transverse dunes (Lancaster 1985; Frank *et al.* 1996; Lancaster *et al.* 1996; Wiggs *et al.* 1996; McKenna *et al.* 2000) and assumed the law-of-the-wall to be valid, although velocity profiles often do not obey the logarithmic law of the wall over barchan dunes (Frank *et al.* 1996; Wiggs *et al.* 1996; McKenna *et al.* 2000). Although transverse dunes share some mean-flow features with barchan dunes, such as the separation of the flow at the crest, the separated-shear layer over the lee side and the developing internal boundary layer, the three-dimensional mean flow around barchans introduces additional complexities that affect the turbulence.

A few numerical studies have been conducted of flow over three-dimensional barchan dunes (Wippermann *et al.* 1985; Takahashi *et al.* 1998); they generally suffer from a low grid resolution and inaccurate models. Reynolds-averaged Navier-Stokes solvers in 2D (Parsons *et al.* 2004) and 3D (Hermann *et al.* 2005) provide mean-flow characteristics (flow acceleration/deceleration, separation, reattachment, and reversal) with qualitative agreement with the literature, but do not provide

information on the instantaneous flow structures observed in experiments (McKenna *et al.* 2000; Franklin *et al.* 2011) and their importance; for instance, elongated sand streaks observed on the stoss side of dunes represent significant contribution of wall turbulence to sediment transport (Franklin *et al.* 2011; Charru *et al.* 2012).

The effects of interdune-spacing on dune dynamics have been largely ignored, despite the fact that the spacing affects the flow on the lee side of the upstream dune and the stoss side of the downstream dune (Fernandez et al., 2006), and may change the mechanisms of sediment transport (Walker *et al.* 2003; Baddock *et al.* 2007; Palmer *et al.* 2011). The importance of secondary flows in the lee side on intermittent sediment transport over the stoss side of the downstream dune was studied by Walker *et al.* (2003); high shear-stress variability at the reattachment zone inhibits sediment deposition and can cause deformation of the stoss side of the downstream dune. At interdune spacings close to the separation-bubble size, regular deformation models (McLean *et al.* 1986) cannot explain the flow physics, even for transverse dunes (Baddock *et al.* 2007). Palmer *et al.* (2011) conducted a series of novel experiments on the effects of interdune spacing on the features of the separated shear-layer, separation bubble size and approaching turbulence structures on the downstream dune stoss side over the centerline symmetry plane. The sheltering effect of the upstream dune on the flow over the downstream dune was identified, in which the separated vortices are advected downstream and transported energy to smaller scales.

However, all efforts so far lack an accurate representation of the bed shear-stress, which provides insight on the sediment transport mechanisms in a three-dimensional view. Turbulent flow over the lee side of the dune, where the flow separates at the crest and broad ranges of length- and time-scales are introduced into the turbulence spectrum, is poorly understood. The three-dimensional mean flow and turbulence characteristics have yet to be studied with reasonable resolution. The significant contribution of the interdune spacing on the mean-flow and instantaneous flow features has also to be examined in detail. Herein, we aim to perform a series of resolved large-eddy simulations of flow over a model barchan dune (Palmer *et al.* 2011) at various interdune spacings, in order to obtain a more comprehensive 3D understanding of mean flow characteristics and turbulence coherent structures.

2. PROBLEM FORMULATION

In large-eddy simulations, the velocity field is separated into a resolved (large-scale) and a subgrid (small-scale) field, by a spatial filtering operation (Leonard 1974). The non-dimensionalized continuity and Navier-Stokes equations for the resolved velocity field are

$$\frac{\partial \overline{u_i}}{\partial x_i} = 0, \tag{1}$$

$$\frac{\partial \overline{u_i}}{\partial t} + \frac{\partial \overline{u_i}\,\overline{u_j}}{\partial x_j} = -\frac{\partial \overline{p}}{\partial x_i} - \frac{\partial \tau_{ij}}{\partial x_j} + \frac{1}{\mathrm{Re}_\infty}\frac{\partial^2 \overline{u_i}}{\partial x_j \partial x_j}, \tag{2}$$

where $Re_\infty = U_\infty h/\nu$, h is the channel height, and U_∞ is the free-stream velocity of an equivalent open channel flow simulation without surface roughness (dune). x_1, x_2, and x_3 are the streamwise, vertical and spanwise directions, also referred to as x, y and z. The velocity components in these directions are, respectively, u_1, u_2 and u_3 (or u, v and w). An overline denotes a filtered quantity, and $\tau_{ij} = \overline{u_i u_j} - \overline{u_i}\,\overline{u_j}$ are the subgrid stresses, which were modeled using an eddy-viscosity assumption

$$\tau_{ij} - \delta_{ij}\tau_{kk}/3 = -2\nu_T \overline{S_{ij}} = -2C\overline{\Delta}^2 \left|\overline{S}\right| \overline{S_{ij}}. \tag{3}$$

Here, $\overline{\Delta} = 2\left(\Delta x \Delta y \Delta z\right)^{1/3}$ is the filter size, $\overline{S_{ij}} = \left(\partial \overline{u_i}/\partial x_j + \partial \overline{u_j}/\partial x_i\right)/2$ is the resolved strain-rate tensor and $\left|\overline{S}\right| = \left(2\overline{S_{ij}}\,\overline{S_{ij}}\right)^{1/2}$ is its magnitude. The coefficient C is determined using the dynamic model (Germano *et al.* 1991) with the Lagrangian averaging technique proposed by Meneveau *et al.* (1996), and extended to non-Cartesian geometries by Jordan (1999) and Armenio *et al.* (2000).

The governing differential equations (1) and (2) are discretized on a non-staggered grid using a curvilinear finite-volume code. The method of Rhie *et al.* (1983) is used to avoid pressure oscillations. Both convective and diffusive fluxes are approximated by second-order central differences. A second-order-accurate semi-implicit fractional-step procedure (Kim & Moin 1985) is used for the temporal discretization. The Crank-Nicolson scheme is used for the wall-normal diffusive terms, and the Adams-Bashforth scheme for all the other terms.

Fourier transforms are used to reduce the three-dimensional Poisson equation into a series of two-dimensional Helmholtz equations in wave-number space, which are solved iteratively using the Bi-Conjugate Gradient Stabilized method. The code is parallelized using the Message-Passing Interface and the domain-decomposition technique, and has been extensively tested for turbulent flows (Silva Lopes *et al.* 2006; Omidyeganeh *et al.* 2011).

The barchan model (Figure 1) was generated from the model used in the experiments of Palmer *et al.* (2011), which reflects a typical curvature of barchans in nature (Hersen *et al.* 2004). The aspect ratio of the current model falls in the range of laboratory and field measurements (Palmer *et al.* 2011). The barchan model has a length of $\lambda=3.62h$, width of $W=3.62h$, and height of $H=0.135h$. The ratio of the dune height to the channel height is equal to the ratio of the dune height to the boundary layer thickness in the experiment (Palmer *et al.* 2011). The simulation adopts an immersed boundary method based on the volume of fluid (VOF) technique (Scotti 2006) to model the barchan. On the bed, the no slip boundary condition is used. Periodic boundary conditions are used in the streamwise (x) and spanwise (z) directions. The flow is driven by a pressure gradient that maintains a constant streamwise flow-rate in time. The top surface is assumed to be rigid and free of shear stress: the vertical velocity is set to zero, as are the vertical derivatives of the streamwise and spanwise velocity components. The Reynolds number is Re_∞=25,160 and is less than half of the experiments of Palmer *et al.* (2011; Re_∞=59,000).

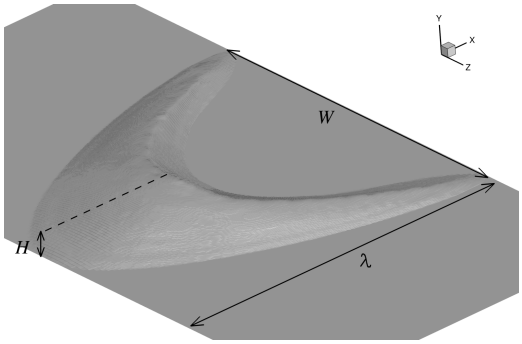

Figure 1. Geometry of the barchan dune model.

A series of simulations is conducted to study the effects of interdune spacing on the physics of flow (Table 1). A Cartesian mesh is generated; the grid distribution in the wall-normal direction is uniform up to the highest point of the dune, and then stretched by a hyperbolic tangent function. The grid in the spanwise direction is uniform, while in the streamwise direction a higher resolution is used over the lee side of the dunes, since the bed slope is significant in this zone and flow separates. For all cases mentioned in Table 1, the grid distribution is the same. We performed a grid refinement study for Case 1 with a focus on the resolution of the VOF model over the lee side of the dune as well as the convergence of statistics. Three simulations with 64 158 128, 128 158 256, and 160 281 512 grid points are examined and the finest simulation produces grid-converged results with resolution $\Delta x^+<28.86$, $\Delta y^+<0.83$, and $\Delta z^+<10.55$, where the plus sign in the superscript represents normalization with respect to the local bed-shear velocity u_τ and kinematic viscosity ν. First- and second-order statistics were within *5%* of each other for all resolutions. Only the results obtained with the finest grid resolution are shown in the following results. Note that the grid spacings above are comparable to those used in many Direct Numerical Simulations of the Navier-Stokes equations.

Table 1. Properties of the test cases. The interdune spacing is defined as the distance between the streamwise location of the horns of upstream dune and the upstream stoss side of the downstream dune.

Case No.	Spacing	$N_x \times N_y \times N_z$
1	0.00λ	160 281 512
2	0.34λ	192 281 512
3	0.68λ	224 281 512
4	1.02λ	256 281 512
5	2.38λ	384 281 512

The equations were integrated for $900H/U_\infty$ time units to remove transient effects. Then, statistics were accumulated over $1200H/U_\infty$ time units. To increase the sample size, averaging was also performed over the symmetric points in the spanwise direction. To verify the adequacy of the sample, we compared statistics obtained using only half of the sample with those obtained using the complete sample, and found that the mean velocities differed by less than *3%*, and the root-mean-square (rms) intensities by less than *7%*.

3. RESULTS

Mean streamwise velocity contours and streamlines on the centerline symmetry plane are shown for Case 5 in Figure 2. The flow separates at the crest and reattaches on the bed at $x_r/H \approx 5.6$. The reattachment length in the experiments is slightly smaller, which is explained by the faster flow over the crest in the simulations caused by the induced secondary flow (Figure 4). Decreasing the interdune spacing decreases the reattachment length not because of the speed of the approaching flow, but due to the bedward motion upstream of the dunes caused by the sheltering effect of the upstream dune.

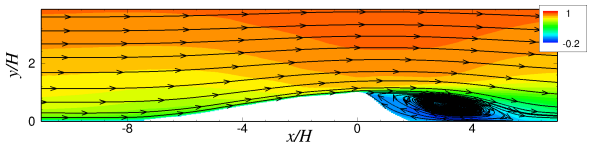

Figure 2. Contours of streamwise velocity normalized by the free stream velocity and streamlines on the centerline plane of Case 5.

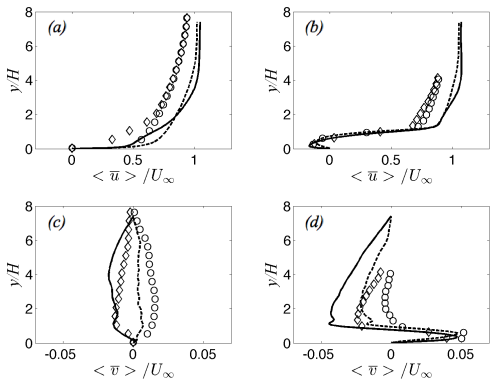

Figure 3. Normalized streamwise *(a,b)* and wall-normal *(c,d)* velocity profiles at *(a,c) x/H=-9.0*, and *(b,d) x/H=2.0*; — Case 5, - - - Case 1, **O** isolated dune, and ◊ zero interdune spacing in the experiment (Palmer *et al*. 2011).

Validation of our simulations is shown in Figure 3 for velocity profiles at two vertical lines upstream of the dune, *x/H=-9.0* and over the lee side of dune, *x/H=2.0*. The developed secondary flow across the channel in our simulations (Figure 4) drives high-momentum fluid into the centerline plane and causes the difference in the normalized bulk velocity profiles. Fluid moves faster on the centerline plane of the simulations, but the behavior of the velocity profiles is similar to the equivalent experiments (Palmer *et al.* 2011). The streamwise velocity profiles upstream of the dunes, in the zero-spacing cases, show a two-layer structure in which the wake with higher momentum overlies the internal boundary layer at the wall, and the two layers still interact. On the other hand, the isolated case shows a single layer similar to a boundary layer profile, and also similar to the largest interdune-spacing (Case 5), which indicates that there is a negligible wake effect at this distance (*60H* from the upstream crest). The two layer profiles have disappeared over the lee side (Figure 3*(b)*). The separation bubble is represented by negative streamwise velocities (Figure 2 and Figure 3*(b)*) and positive vertical velocity (Figure 3*(d)*) near the bed, *y/H<0.7*; here our simulations agree quantitatively with the experiments (Palmer *et al.* 2011).

Upstream of the dunes (Figure 3*(c)*), vertical velocity is positive for Case 5 and for the isolated dune in the experiments (Palmer *et al.* 2011) as the flow reacts to the windward slope. However, the upstream dune changes this feature; the approaching flow moves toward the bed (negative vertical velocities in Figure 3*(c)* for Case 1 and for the experiment with a zero spacing). This phenomenon influences the flow in the lee side of the downstream dune; the separation bubble shrinks due to the bedward bulk flow, and the reattachment length decreases.

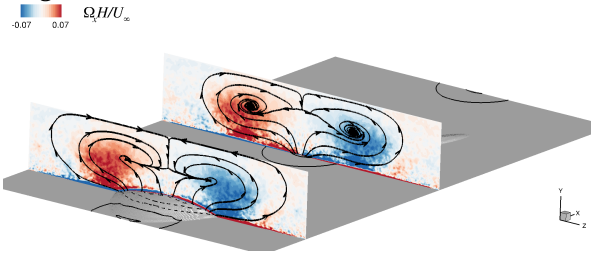

Figure 4. Contours of mean streamwise vorticity on two vertical planes across the channel at the crest and at the barchans toe for Case 3. Streamlines tangential to these planes show the secondary flow. Contour lines of the mean pressure are shown on the bed surface.

The profiles of the turbulence statistics show quantitative agreement with our simulations and with the experiments (Figure 5). Two peaks in the vertical profile of the turbulent kinetic energy (Figure 5*(b)*) for Case 1 represent two shear layers, with the overlying one being weaker. At the dune toe,

there is a near-bed peak representing the developing boundary layer on the stoss side for both simulations, while the second peak represents the wake region of the upstream dune for the zero-spacing case. Over the lee side, the outer-layer peak is still effective (at $y/H \approx 2.5$) while all cases show significant turbulent kinetic energy in the separated-shear layer. Reynolds shear stress is significant in the separated-shear layer as compared to the developing boundary layer.

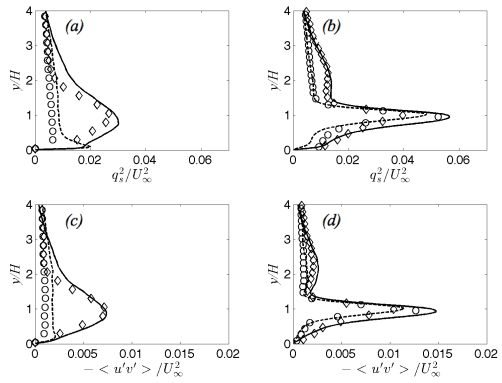

Figure 5. *(a,b)* Planar turbulent kinetic energy, $q_s^2 = \left(\langle u'u' \rangle + \langle v'v' \rangle\right)/2.0$, and *(c,d)* Reynolds shear stress at *(a,c) x/H=-9.0*, and *(b,d) x/H=2.0*; — Case 5, - - - Case 1, **O** isolated dune, and ◊ zero interdune spacing in the experiment (Palmer *et al.* 2011).

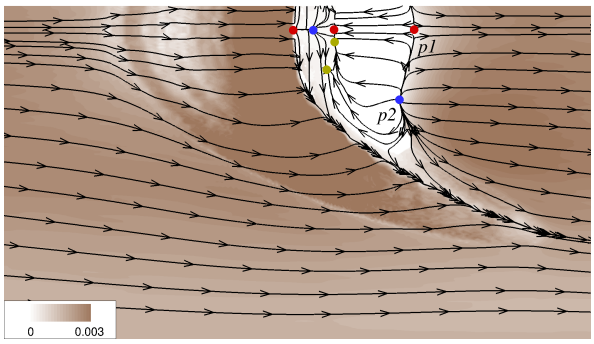

Figure 6. Contours of bed shear stress for Case 5. Streamlines represent the flow direction at the first grid point above the bed surface.

The bed shear-stress is strong over the stoss side of dunes close to the crest (Figure 6). At the toe, the flow diverges from the centerline plane, and the bed stress is decreased, but away from the centerline and along the horns the stress is large, as the flow rises up the stoss side. Figure 6 shows the size of the separation bubble that is not extended towards the horn. The separated flow at the crest reattaches to the bed and due to the three-dimensionality of the separation line, a nodal point of attachment is located away from the symmetry plane (point *p2* in Figure 6). The bed shear stress is larger downstream of this point where high-momentum fluid that separated at the crest reattaches, increases the pressure and the stress. Compared to the streamlines around the nodal point of reattachment, a saddle point of separation appears downstream of the dune on the symmetry plane (point *p1* in Figure 6) where the shear stress is small and the near-bed flow converges to the centerline plane from the sides. The separation bubble contains a large secondary flow, and a few small secondary flow regions over the lee side of the dune, which cause weak points of separation and attachment. These features close to the bed are often observed in the separation bubble of three-dimensional objects (Chapman *et al.* 1991). All other cases in our simulations present a similar trend; even the bed shear stress does not change significantly with the spacing. From a series of streamlines from the stoss side of the dune, we note that the separation bubble and the reattached flow converge to a single streamline along the horn and leave the dune from that side, consistent with 3D realizations of near-bed streamlines shown in Figure 7. The observation that barchan dunes loose sediment from the horns (Hersen *et al.* 2004 and Franklin *et al.* 2011), is explained by our results.

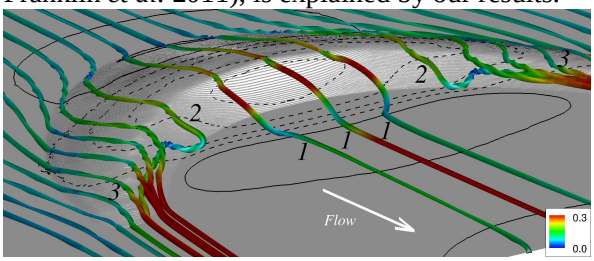

Figure 7. Streamlines close to the bed for the barchan dune of Case 3. Streamlines are colored with the magnitude of the velocity vector. Contour lines of mean pressure are shown on the bed surface; — $\langle \bar{p} \rangle = 0$, - - - $\langle \bar{p} \rangle = -0.005 \rho U_\infty^2$.

We show streamlines near the bed in Figure 7. Streamlines close to the centerline plane diverge and rise on the stoss side, then separate at the crest and move toward the bed while they are advected downstream (labeled by number 1). Away from the centerline plane, the streamlines diverge significantly toward the horns and separate at the crest,

but enter the separation bubble and meander in the recirculation region toward the horns while remaining near the bed (labeled by number 2). Streamlines far away from the centerline plane diverge toward the horns and never separate (labeled by number 3). Contours of the velocity magnitude show that streamlines moving toward the horns are accelerated.

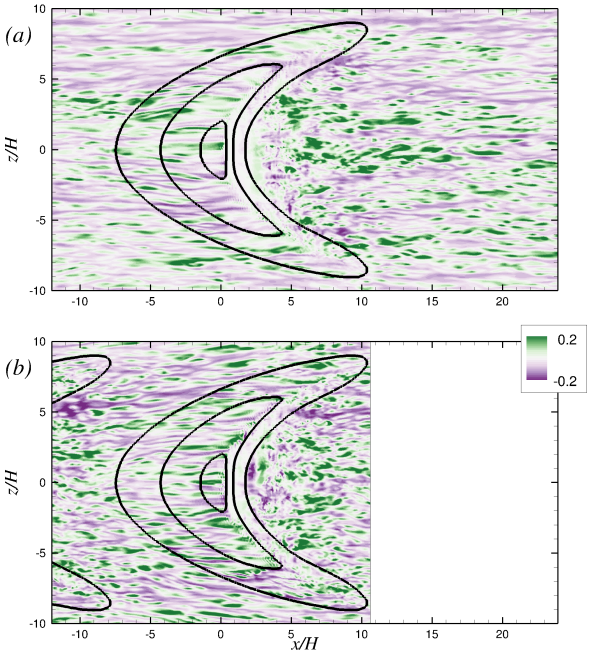

Figure 8. Contours of the streamwise fluctuating velocity on a plane parallel to the bed surface with a distance 0.025*H* for *(a)* Case 5, and *(b)* Case 1. The lines correspond to the bed levels at *y/H=0.03, 0.5 0.9*.

A realization of *u'* on a plane parallel and close to the bed is provided in Figure 8 for Case 5, with the largest interdune spacing, and Case 1, with the smallest interdune spacing. The flow approaching the dune in Case 5 has characteristics of a smooth open channel flow with alternating stripes of low- and high- momentum fluid. It seems that acceleration of flow over the stoss side of the dune elongates the streaks (Figure 8*(a)*). Franklin *et al.* (2011) observed streamwise stripes with regular spacing on the stoss side of their barchan dune. In the lee side of the dune, spanwise oriented structures are observed in between the horns. Around the reattachment region, the contours show a chaotic distribution of structures and after that, as the flow is advected downstream, the structures are reorganized and within a distance of an order of the dune length, the low- and high- speed streaks are reformed (Figure 8*(a)*). Case 1 (Figure 8*(b)*) presents different characteristics; the streaks are shorter and represent footprints of overlying turbulent events. The magnitude of fluctuations at the same distance from the bed is larger for Case 1 with smaller interdune spacing; hence this closely spaced arrangement of dunes enhances the wall turbulence and thus sediment transport in mobile bed barchans.

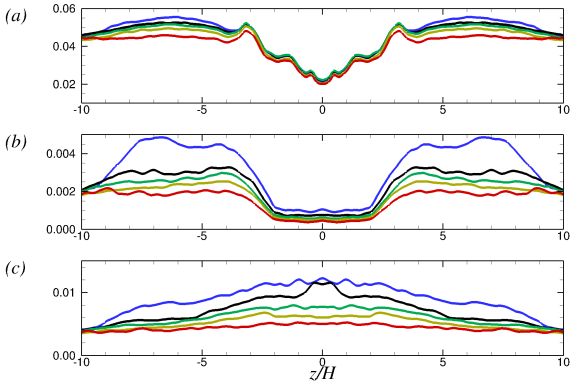

Figure 9. *(a)* Bed shear velocity, *(b)* wall-normal Reynolds normal stress, and **(c)** spanwise normal Reynolds stress at the centre of the stoss side *x/H*=-5.0 across the channel at a uniform distance from the bed. — Case 1, — Case 2, — Case 3, — Case 4, — Case 5.

At *x/H*=-5.0, in the middle of the stoss side, the mean bed-shear stress is not affected significantly by the interdune spacing (Figure 9*(a)* from -3.5<*z/H*<3.5), but the turbulent activities are significantly altered; *e.g.*, the spanwise normal Reynolds stress (Figure 9*(c)*) has a peak on the centerline of the dune and is larger for a smaller interdune spacing. Around the edges of the dune surface, at *z/H*≈±3.5, the wall-normal stress (Figure 9*(b)*) is boosted and is larger for closely spaced dunes.

Instantaneous flow structures are shown by the *Q* criterion, where

$$Q = -\frac{1}{2}\frac{\partial \bar{u}_j}{\partial x_i}\frac{\partial \bar{u}_i}{\partial x_j} \qquad (4)$$

for Cases 1 (Figure 10) and 5 (Figure 11). A population of coherent structures over the stoss side is evident in Case 1. Away from the dunes, typical wall turbulence structures are observed, but coherent eddies generated in the separated-shear layer due to Kelvin-Helmholtz instability are dominant. Separated vortices in Case 5 are advected away

from the centerline plane by the secondary flow (Figure 4) and dissipate before reaching the downstream dune. In Case 1, the production of these structures is more frequent, and they do not diverge from the centerline plane since the spacing between the dunes is small. Hence, we observe more structures in Case 1 between the horns.

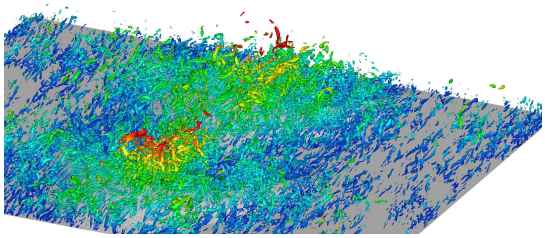

Figure 10. Isosurfaces of the second invariant of the velocity gradient tensor, $QH^2/U_\infty^2=0.7$, colored by distance from the bed for Case 1 (refer to Figure 11 for the scales).

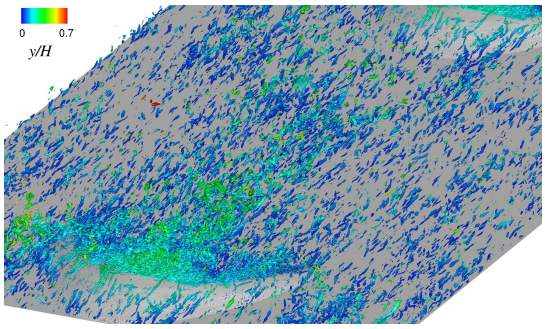

Figure 11. Isosurfaces of the second invariant of the velocity gradient tensor, $QH^2/U_\infty^2=0.7$, colored by distance from the bed for Case 5.

4. CONCLUSIONS

Flow over barchan dunes has some characteristics in common with that over transverse dunes (deceleration and acceleration of flow over the stoss side, separated flow and formation of a shear layer at the crest, reattachment of flow on the bed and development of internal boundary layer), but the complex three-dimensional shape of barchans introduces mean secondary flow across the channel and alters turbulence over the stoss side. The current simulations are validated against experiments (Palmer *et al.* 2011) and provide a comprehensive three-dimensional realization of mean flow characteristics and instantaneous flow structures.

Barchan dunes induce two counter-rotating streamwise vortices, each along one of the horns. These vortices direct high-momentum fluid toward the centerline symmetry plane and low-momentum fluid near the bed away from the centerline. In our configuration with barchans aligned in the spanwise direction, and with the periodic boundary condition we use, the streamwise vortices become stable.

The three-dimensional flow visualization explains some features of sediment transport near the bed reported in the literature; the flow decelerates at the toe of the dune and moves toward the closest horn, hence bed shear stress increases on the sides of the barchan while it decreases on the centerline plane. Separation of the flow at the horns is intermittent; 3D streamlines show that the flow at the crest may enter the separation bubble and meander toward the horns and leave the dune while accelerating. We note that flow in the separation bubble is likely capable of transporting high concentrations of sediment and exiting the dune from the horns, which explains many observations in nature and laboratory measurements that barchans loose sediment downstream via their horns.

The interdune spacing quantitatively alters the mean flow; the secondary flow is stronger at smaller spacings, and the sheltering effect of the upstream dune is observed in the turbulence characteristics; coherent high- and low-speed streaks are shorter and the spanwise Reynolds normal stress is significantly higher where the interaction between the wake region and the internal boundary layer is strong.

5. ACKNOWLEDGMENTS

The authors are grateful to the High Performance Computing Virtual Laboratory (HPCVL), Queen's University site, for computational support. MO acknowledges the partial support of NSERC under the Alexander Graham Bell Canada NSERC Scholarship Program. UP also acknowledges the support of the Canada Research Chairs Program and of the Natural Sciences and Engineering Research Council (NSERC) under the Discovery Grant program.

6. REFERENCES

Allen, J. 1968. Current ripples: their relation to patterns of water and sediment motion. North-Holland Pub. Co.

Armenio, V. & Piomelli, U. 2000. A Lagrangian Mixed Subgrid-Scale Model in Generalized Coordinates. Flow. Turb. Combust., 65, 51–81.

Baddock, M. C., Livingstone, I. & Wiggs, G. F. S. 2007. The geomorphological significance of airflow patterns in transverse dune interdunes. Geomorphology, 87, 322–336.

Bagnold, R. A. 1941. The Physics of Blown Sand and Desert Dunes. Methuen, London.

Breed, C. S., Grolier, M. J. & McCauley, J. F. 1979. Morphology and distribution of common 'sand' dunes on mars: Comparison with the earth. J. Geophys. Res., 84, 8183–8204.

Chapman, G. T. & Yates, L. A. 1991. Topology of flow separation on three-dimensional bodies, Appl. Mech. Rev., 44(7), 329–345.

Charru, F. & Franklin, E. M. 2012. Subaqueous barchan dunes in turbulent shear flow. part 2. fluid flow. J. Fluid Mech., 694, 131–154.

Fernandez, R., Best, J. and Lopez, F., 2006 Mean flow, turbulence structure and bedform superimposition across the ripple-dune transition, Wat. Resources Res., 42, W05406, doi:10.1029/2005WR004330.

Frank, A. & Kocurek, G. 1996. Toward a model for airflow on the lee side of aeolian dunes. Sedimentology, 43, 451–458.

Franklin, E. M. & Charru, F. 2011. Subaqueous barchan dunes in turbulent shear flow. part 1. dune motion. J. Fluid Mech., 675, 199–222.

Germano, M., Piomelli, U., Moin, P. & Cabot, W. H. 1991. A dynamic subgrid-scale eddy viscosity model, Phys. Fluids A, 3, 1760–1765.

Hermann, H. J., Andrade Jr., J. S., Schatz, V., Sauermann, G. & Parteli, E. J. R. 2005. Calculation of the separation streamlines of barchans and transverse dunes. Physica A, 357, 44–49, doi:10.1016/j.physa.2005.05.057.

Hersen, P., Andersen, K. H., Elbelrhiti, H., Andreotti, B., Claudin, P. & Douady, S. 2004. Corridors of barchan dunes: Stability and size selection. Phys. Rev. E, 69 (011304), 1–12.

Hesp, P. A. & Hastings, K. 1998. Width, height and slope relationships and aerodynamic maintenance of barchans. Geomorphology, 22, 193–204.

Jordan, S. A. 1999. A large-eddy simulation methodology in generalized curvilinear coordinates, J. Comput. Phys., 148(2), 322–340.

Kim, J. & Moin, P. 1985. Application of a fractional step method to incompressible Navier-Stokes equations. J. Comput. Phys., 59, 308–323.

Kroy, K., Fischer, S. & Obermayer, B. 2005. The shape of barchan dunes. J. Phys. Condens. Matter, 17, S1229–S1235.

Lancaster, N. 1985. Variations in wind velocity and sand transport rates on the wind-ward flanks of desert sand dunes. Sedimentology, 32, 581–593.

Lancaster, N. 1995. Geomorphology of desert dunes, Routledge, New York.

Lancaster, N., Nickling, W. G., McKenna Neuman, C. & Wyatt, V. E. 1996. Sediment flux and airflow on the stoss slope of a barchan dune. Geomorphology, 17, 55–62.

Lettau, K. & Lettau, H. H. 1969. Bulk transport of sand by the barchans of la pampa la hoja in southern Peru. Zeitschrift fūr Geomorphologie, 13, 182–195.

McCullogh, D. S. & Janda, R. J. 1964. Subaqueous river channel barchan dunes. J. Sed. Petrol., 34, 694.

McKenna Neuman, C., Lancaster, N. & Nickling, W. G. 2000. The effect of unsteady winds on sediment transport on the stoss slope of a transverse dune, silver peak, NY, USA. Sedimentology, 47, 211–226.

Meneveau, C., Lund, T. S. & Cabot, W. H. 1996. A Lagrangian dynamic subgrid-scale model of turbulence. J. Fluid Mech., 319, 353–385.

Omidyeganeh, M. & Piomelli, U. 2011. Large-eddy simulation of two-dimensional dunes in a steady, unidirectional flow. J. Turbul., 12 (42), 1–31.

Palmer, J. A., , Mejia-Alvarez, R., Best, J. L. & Christensen, K. T. 2011. Particle-image velocimetry measurements of flow over interacting barchan dunes. Exp. Fluids, pp. 1–21.

Parsons, D. R., Wiggs, G. F. S., Walker, I. J., Ferguson, R. I. & Garvey, B. G. 2004. Numerical modelling of airflow over an idealised transverse dune. Env. Mod. Soft., 19, 153–162, doi:10.1016/S1364-8152(03)00117-8.

Rhie, C. M. & Chow, W. L. 1983. Numerical study of the turbulent flow past an airfoil with trailing edge separation. AIAA J., 21, 1525–1532.

Scotti, A. 2006. Direct numerical simulation of turbulent channel flows with boundary roughened with virtual sandpaper. Phys. Fluids, 18, 031,701.

Silva Lopes, A., Piomelli, U. & Palma, J. M. L. M. 2006. Large-eddy simulation of the flow in an S-duct. J. Turbul., 7 (11), 1–24.

Takahashi, S., Du, M., Wu, P., Maki, T. & Kawashima, S. 1998. Three dimensional numerical simulation of the flow over complex terrain with windbreak hedge. Env. Mod. Soft., 13, 257–265.

Walker, I. J. & Nickling, W. G. 2003. Simulation and measurement of surface shear stress over isolated and closely spaced transverse dunes in a wind tunnel. Earth Surf. Proc. Landf., 28, 1111–1124.

Wiggs, G. F. S., Livingstone, I. & Warren, A. 1996. The role of streamline curvature in sand dune dynamics: evidence from field and wind tunnel measurements. Geomorphology, 17, 29–46.

Wippermann, F. K. & Gross, G. 1986. The wind-induced shaping and migration of an isolated dune: a numerical experiment. Bound.-Lay. Meteorol., 36, 319–334.

Burial Recording Mines: a valid technique to study bedform migration and storm impact above the sea-floor

Sonia Papili [1,2], Thomas Wever [3] and Yves Dupont [4]

1. Belgian Navy, Zeebrugge, BE, - sonia.papili@mil.be,
2. Ghent University, Ghent, BE - sonia.papili@ugent.be
3. WTD 71 / FWG, Kiel, D - thomaswever@bundeswehr.org
4. Belgian Navy, Zeebrugge, BE, - yves.dupont@mil.be

Abstract

Initially, Burial Recording Mines (BRMs) were used to understand the sea mine burial. It was a technique predominantly related to military purpose. The first experiment was made 1974. Now a day, it is used as a valid tool for marine science. This methodology gives the rare opportunity to observe and analyze the processes acting on the seafloor directly, making the estimation closer to the reality.

During MARIDIV, we present the results of 3 months experiment using burial recording mines. The experiment was performed between September 2008 and January 2009. The Wandelaar region on the Belgian Continental Shelf was chosen as suitable test area. 10,000 measurements of the sediment height around the cylindrical object were recorded, each one of those every 15 minutes. The dataset collected, together with sediment characterization and hydrological and meteorological information, allowed the understanding of the bedform migration.

During the experiment, 2 storms passed the test area, in October and November 2008. Using Burial Recording Mines gave the rare opportunity to observe and analyze the storm impact directly on the sea-floor.

Processes during and after the second storm will be revealed.

1. INTRODUCTION

Burial recording mines are instruments collecting data directly on the sea-floor. They perform a recording of the sand mobility in four dimensions. Due to their massive but smooth body they are not affected by heavy storms. Those objects were initially used for military purpose (Wever et al, 2004) for the understanding of the sea mine burial. The knowledge coming out from this methodology results valuable to figure local small scale scenario during bedforms migration (Wever et al., 2008). Moreover, it reveals mechanisms regarding the storm influences on man-made structures. Storms are uncontrollable and can be destructive. It is not always possible to get on-scene data measurements due to large involved forces. This technology gives possibilities in the understandings the storm impact on sediments surrounding objects laying on the sea-floor with a confidence level of centimeters in space and minutes in time.

2. STUDY AREA

2.1. Area of investigation

The Wandelaar region is located at 12 km distance from the port of Zeebrugge (fig.1) in the vicinity of the main navigation channels on the Belgian part of the North Sea. In these channels, every year about 1.4 10^6 T dry matters (TDM) of sand and mud are dredged to maintain the accessibility of the port (Lanckneus et al., 2001). Given the strategic position of the area, permanent stations for hydro-meteorological measurements are localized nearby. The tidal regime amplitude is between 3.5m and 5m producing strong rectilinear current ellipses prevail with the main axis oriented in a SW-NE direction (Lanckneus et al, 2001).

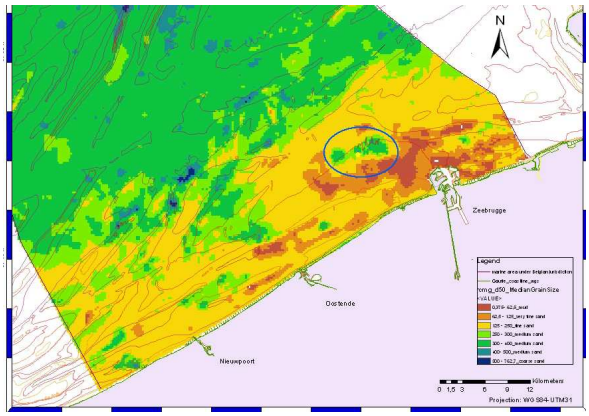

Figure 1. Extract from a grain size map of the Belgian continental shelf (Verfaillie et al., 2006). UTM coordinates. Sandy sediments are represented in green; the Wandelaar area is contoured in Blue.

The Wandelaar consists of a sandy bottom and is characterized by the presence of small to large dunes (sensu Ashley, 1990), of up to 2 meters in height.

Substrate characteristics and morphology, together with hydrological and meteorological conditions contribute to the dynamics and the evolution of the Wandelaar zone. Studies on the morphology of the large dunes revealed that in the near coastal zone the crests are dominantly oriented in a northeastern direction (Lanckneus et al., 2001). This is in agreement with the rectilinear current ellipses described above.

All bedforms are affected by hydro-meteorological factors (currents, waves), including occasional strong events and storms (Lanckneus et al., 2001). The superficial sand dune layers directly respond to these stresses (Van Lancker, 1999), but the residual effect on these bedforms can be evaluated only over a time scale of years (Wever, 2003). Different is the situation for smaller bedforms such as megaripples: they can be seriously affected by current, waves and current-wave interaction, on a time scale of hours. They can even be destroyed (Langhorne, 1976) to form again under normal conditions. Episodic strong storm effects dominate over processes related to current-induced bedform movement.

3. METHODS

3.1. Description of burial registration mine (BRM)

Four burial registration mines (BRMs) of FWG (Forschungsanstalt der Bundeswehr für Wasserschall und Geophysik, now Forschungsbereich für Wasserschall und Geophysik of WTD 71) were deployed to study sediment dynamics in the Wandelaar area.

The BRM (fig.2) has a cylindrical shape, is 1.70 m long and has a diameter of 0.47 m. The weight in air is 500 kg. BRMs were built to determine the sediment height surrounding the object as function of time. For this purpose BRMs are equipped with three rings of 24 led bridges ("sensors") equally spaced around the object at 15°. All electronics and energy supply is installed within the BRM. Up to 10,000 measurements of all 72 sensors can be recorded. The sensors emit light at pre-set intervals. The light bridges (light emitter and receiver) are in small housings at a distance of 4 cm. The light sensors detect the presence of sediment by recording the value "1" if sediment occludes the space between emitter and receiver (the led bridges are blocked) otherwise they record "0". The led bridges of each ring are numbered from 1 to 24. The rings are located on both ends and the centre of the BRM at a distance of 60 cm (fig.2). The rings are named "Stern", "Centre" and "Bow". The bow ring is at the truncated side.

Figure 2. BRM, length: 1.70m, diameter: 47cm, weight: 5.0 kg. Bow ring at the right side (Wever et al. 2004).

In addition to the burial status, accelerometers inside monitor the movement of the object and allow to calculate the Pitch and the Roll of the object and its variation in time. Figure 3 shows the used convention defining the positive and the negative side for both Pitch and Roll. The magnetic steel casing does not permit to monitor of the BRMs heading with a compass.

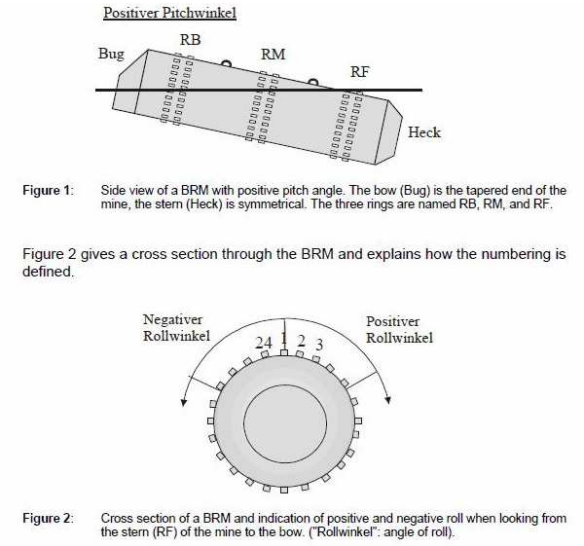

Figure 3. Used convention defining the positive and negative position for pitch and roll measurement.

The Pitch has positive values when the Bow side is up with respect to the horizontal position. Watching from Stern towards Bow the roll has positive values when the object rotates to the right side.

It is important to underline that the geometry of the object produces, at a small scale, different modalities of sedimentation of the sand. Both end rings are around 25 cm from the ends. The Bow and Stern rings are exposed to stronger water acceleration and consequently stronger erosion than the Centre ring. On the contrary, the sediment deposits behind the Centre ring are in a "current shadow".

3.2. Experiment

Four BRMs were deployed on 25th September 2008 in the Wandelaar region (fig.1).

Always two instruments are deployed together, one having 15 minutes and one having 60 minutes recording intervals. Figure 4 gives a sonar image of one pair of BRMs after deployment. The BRM called "Seestern" was recovered from the seafloor on 15th January 2009. It recorded the sediment height every 15 minutes. With this setting the Seestern had a maximum recording time of 104 days until 6th January 2009. The other instruments were buried and could not be recovered yet.

Initially, a quality control for the elimination of obviously wrong recordings was performed; subsequently, data were analyzed and interpreted. Only very few records had the necessity to be corrected showing that the measurements were achieved in optimal conditions.

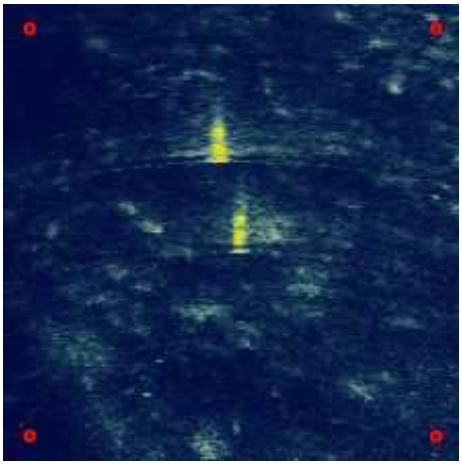

Figure 4. Hull-mounted sonar image of two BRMs directly after deployment. The three rings with the sensors are perfect sonar reflectors and allow identifying the systems.

3.3. Hydrometeorological datasets

Hydrological and meteorological data were recorded at different monitoring stations in the vicinity of the Wandelaar. They included wind measurements, velocity and direction, recorded by the *Wandelaar* waverider (Fig.5), ca. 3 km southwest of the Seesterns's position.

Wave height and period were recorded by the *A2* buoy (Fig.5), ca. 6 km southeast of Seestern. The direction of high and low frequency waves was observed at the *Bol van Heist* waverider (Fig.5), ca. 11 km to the southeast. All of these data originated from the Flemish Hydrography, Flemish Authorities.

Current data are recorded at the measuring pile MOW0 (Fig.5) located ca. 2 km north of the BRM. The data give information about speed and direction of the current at different water depths. Starting at the surface there is a measure of current velocity and direction every 2 meters of depth.

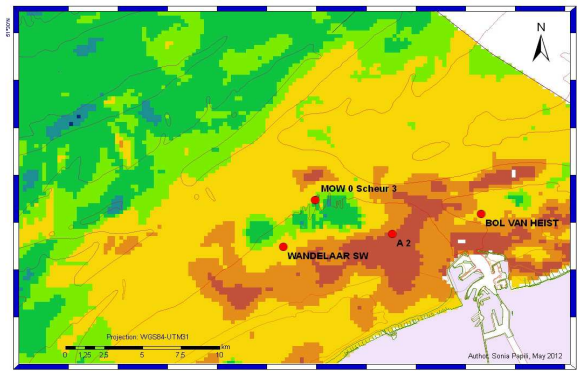

Figure 5. Hydrological and meteorological monitoring stations in the vicinity of the Wandelaar area.

3.4. Time references

The time references (local time and UTC) were a parameter that asked some recalculation. The current and the hydro-meteorological data were recorded in UTC time, the tide data were recorded in local time: UTC time+1h during winter and UTC time+2 during summer period; the "Seestern" recording were in Central European Time (CET): UTC time+2. To facilitate the interpretation all data were reconverted in UTC time. In addition, data were recorded at different time intervals, for instance, current data every 10 minutes, mine burial and wave height every 15 minute, wave direction every 30 minutes. Only simultaneous measurements were correlated and compared.

4. RESULTS

4.1. Interaction sediments-object.

The recordings made by the BRM are visualized on figure 9 at the end of the present document. They show the sediment displacement around a cylindrical object in a shallow dynamic environment. Remembering that the instrument was programmed measuring every 15 minutes, the picture we got is close by to an on-scene scenario.
Figure 9 is a composite figure where 3 different diagrams are displayed.
The first one indicates the variation during the 3 months experiment for pitch and roll values. The second one shows the BRM burial volume in percentage and the third one is the combination of both.
Watching the burial curve (b) we can identify 3 significant stages in the recording.
The first one, with values less than 20% burial; the second one with a medium burial oscillating between values of 60-70% and the third one with a medium value oscillating around the value 80-90%.
Two crucial moments delimiting the three stages are visible in the recordings, they correspond to storm events. Storm events represent the only circumstances where the object reaches minimum value of burial and has the possibility to roll. We will go deeper into this matter in the next paragraph.
During the 3 months experiments, 7 cycles of neap-spring tide are counted. This alternation is reflected in the measured data. Under stronger tidal neap and spring currents the megaripples show an enhanced mobility (back-and-forth movement) which is easily recognized in the recordings by 6-hour peaks in response to a changing current direction. This has been shown for wider areas by Wever et al. (2008). During neap tide, the environment is less subject to turbulences; as a consequence the sediment mobilization around the object is minimal not exceeding 5% of burial variation.
On the contrary, during spring tide the sediments are affected by increased local turbulence producing short moments of complete burial (peaks). Both periods are recognizable in the burial volume curve (b).

4.2. Storms

Storms along the Belgian coast are caused by a low pressure system over Scandinavia associated with reinforced Azores high pressure systems. The atmospheric pattern leads to a strong Southwest-Northeast pressure gradient associated with onshore winds blowing from the western sector in the southern part of the North Sea (Ullmann et al., 2009).
Two storms passed the experiment site off the Belgian coast in October and in November 2008. The effects of both storm passages are well documented in recordings. The second storm is discussed in the following.

4.2.1. Storm 21st -24th November 2008

On Thursday 20th November 2008 a high pressure system developed on the Atlantic Ocean together

with a low pressure above the Baltic Sea. As a consequence a cold front passed along the Northern coasts around the midday of the 20th November 2008; from Friday the 21st, winds blew from northerly direction and affected the Belgian coast and inland. The combination of cold arctic airs with relatively warm water from the sea started an instable situation with the beginning of a storm. (Storm archive, Royal Meteorological Institute, 2008).
Meteorological measurements show a wind blowing from WNW-NWN during the 20th, 21st and 22nd November with 10 to 22 m/s (5 to 8 Bft), with gusts of 28 m/s (10Bft) at 22:10 h on the 21st November and 33 m/s (12 Bft) at 04:50h on 22nd November (fig.6).

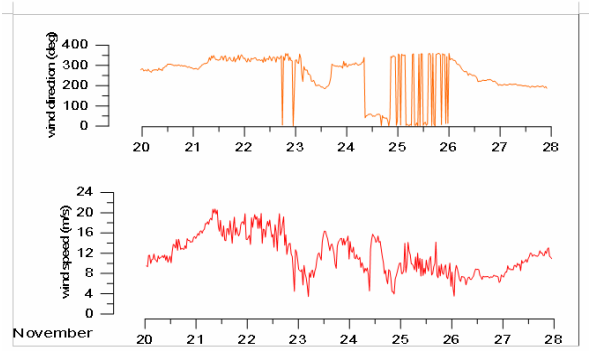

Figure 6. Wind direction (a) and wind speed (b) between the 20th and the 28th November 2008. The graph illustrates only measurements recorded every 30 minute. Therefore, the maximum values discussed on the results section are not visible.

The significant wave height increases during this period reaching almost 3.50 m. Peaks of maximum wave height of 6 m were measured during the 21st and the 22nd (fig.7).

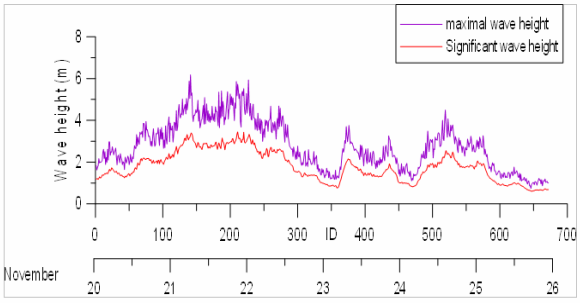

Figure 7. Maximum (blue curve) and significant (red curve) wave heights measured between 20th and 26th November 2008.

The tidal cycle was during 21st and 22nd November in neap tide regime with a maximum water depth variation of 3.47 meters.
Before the storm, the BRM lay almost horizontally on the sea floor with the Bow side (pitch value -2) oriented slightly downwards. At that time it was partially buried for 60% of its volume. A flattening of megaripples already during the rise of the storm is clearly visible as reported by Langhorne (1976).
Between the 20th November at 10:45h and the 23rd November at 09:15h the significant wave height recorded at sea (red on fig.8a) was much higher than the calculated critical wave heights for sediment mobilization (gray on fig.8a). The storm caused forces at the seafloor that were able to move easily the sediments in the main phase of the storm. On 21st November at 11:00h the storm has a peak water height of 6.17 m of producing energy of 48,000 J/m² in an estimated water depth of 9.5 m. The wind blew with 18.5 m/s from NNW (337.4°) whereas the tidal current at a depth of 10 m had a direction of 275°. The combined action at the seafloor is scouring around the mine leaving only 4.8 % of the total mines volume buried (fig.8b). During this phase the sediment cone underneath the BRM collapsed and the mine rolled 97° towards NW and 26° back in the following 30 minutes (Table 1). The burial increased to more than 80% in the following hours.

Date	Time (UTC)	Significant wave height(cm)	Relative buried volume (%)	Roll
20/11/08	11:01	330,570007	**4**	**+39**
21/11/08	11:16	339,890015	15	**-58**
21/11/08	11:31	335,670013	31	**-47**
21/11/08	11:46	325,26001	45	**-32**

Table 1: comparison between significant wave height, relative mine buried volume and roll on 21st November 2008

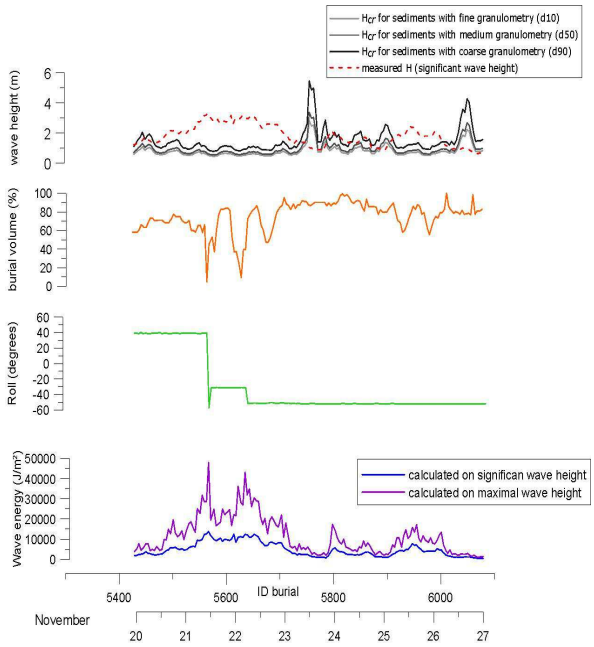

Fig. 8. Storm in November 2008. (a): comparison between measured curve of real wave height (red-dashed) and calculated curves of critical wave height (different tone of grey); (b): curve of burial volume; (c): curve of roll measurements; (d): curve of wave energy.

On 22nd at 04:00h a second minimum burial of 9.5% was recorded (Table 2). The estimated water depth was 8.7 m. During this minimum of water depth a wave height peak of 5.8 m is measured producing wave energy of 43.200 J/m². The tidal current had a direction of around 250°. The combined action of wave and current caused scouring around the mine. This allowed an additional roll of 20° towards W.

Date	Time (UTC)	Significant wave height(cm)	Relative buried volume (%)	Roll
22/11/08	3:31	297,329987	26	-31
22/11/08	3:46	302,73999	**9**	-30
22/11/08	4:01	313,01001	**10**	**-32**
22/11/08	4:16	335,140015	24	**-52**
22/11/08	4:30	344,779999	27	-52

Table 2: comparison between significant wave height, relative mine buried volume, and roll on 22nd November 2008.

The sediment deposition phase started in the evening of the 22nd November. It is characterized by a fast drop in wave energy (fig.8d). The sediment settling around the object covered it to about 90% of its total volume during the next day. On 23rd November at 17:45h the minimum value of wave energy (2,024 J/m²) is recorded.

5. CONCLUSIONS

Through the use of the burial recording mines (BRM) seabed processes could be studied; also during storms. Especially the flattening of megaripples under high-energetic conditions could be proven.

In shallow water, both current and waves affect the sea-floor and are able to mobilize fine to medium sands. The tidal variation during neap and spring period produces different scenarios, respectively steady or turbulent. During storms, a rapid erosion of sand around the object is observed. It starts with scouring at both BRM ends. The scour holes eventually merge leaving the BRM almost uncovered. At this stage it rolls to a deeper level within the merged scour pits. The subsequent sedimentation phase favours reaching a higher percentage of burial volume. More in detail, the BRM data showed during the experimental period, a burial of 60% after the first storm (October 2008) and 80% after the second storm (November 2008). It remained in this condition until the end of the 3 months experiment.

The burial recordings display a rapid (within two days) generation of megaripples after the decay of the storm thus proving a quick adjustment to normal hydrodynamic conditions.

Burial recording mines are reliable tools to investigate local phenomena in 4 dimensions. They can be a supporting method for analyzing small scale scenarios and they are perfect for in situ measurements during storm events.

6. ACKNOWLEDGMENT

The author is grateful to the Belgian Navy founder of this project and to Ghent University, particularly to RCMG (Renard Centre of Marine Geology) for the facilities and the precious intellectual support; to Forschungsanstalt der Bundeswehr für

Wasserschall und Geophysik, now Forschungsbereich für Wasserschall und Geophysik of WTD 71, owner of the BRMs kindly supporting this experiment. The author is also grateful to the crew of the MH vessel Lobelia especially the diving team that deployed and recovered the BRM Seestern.

7. REFERENCES

Ashley, G.M. (1990). Classification of large-scale subacqueous bedforms: a new look at an old problem. J. Sedim.Petrol., 60, 1: 160-172

Lanckneus, J., Van Lancker, V., Moerkerke, G., Van den Eynde, D., Fettweis, M., De Batist, M., Jacobs, P. (2001). Investigation of the natural sand transport on the Belgian continental shelf (BUDGET). Final Report. Federal Office for Scientific, Technical and Cultural Affairs (OSTC), 104p. = 87p. Annex.

Langhorne, D.N. (1976). Consideration of meteorological conditions when determining the navigational water depth over a sand wave field, 15th Annual Canadian Hydrographic Conference, Ottawa. (illustrated Figure: Plate 4.2 in A.H. Stride (1982) (ed.): Offshore Tidal Sands, Chapman and Hall, London).

Ullmann A., Sterl A., Van den Eynde D., Monbaliu J. (2009). Storm surges and atmospheric circulation: an analysis since 1950 for the Belgian coast and forecast for the 21th century. Internal Report Hydraulics Laboratory.

VanLancker, V. (1999). Sediment and morphodynamics of a siliciclastic near coastal area, in relation to hydrodynamical and meteorological conditions: Belgian continental shelf. Unpublished Ph.D. Thesis, Universiteit Gent, Gent, 194 pp.

Verfaillie E., Van Lancker V;, Van Meirvenne M. (2006). Multivariate geostatistics for the predictive modelling of the surficial sand distribution in shelf seas. Continental Shelf Research 26. p. 2454-2468

Wever, Th. (2003). Speed of Migrating Bedforms on the Sea Floor – A Review, FWG Report 50, 20 p. plus appendices.

Wever, Th.F., Lühder, R., Stender, I.H. (2004). Burial Registration Mines – 30 Years of Seafloor-Mine-Interaction Research, Sea Technology 45/11, 15-19.

Wever, Th., Voß, H., Lühder, R**.** (2008). High-resolution observation of small-scale variability in a bedform field, Marine Sandwaves and River Dynamics III (MARID 2008), International Workshop, 1.-3. April 2008, Leeds University, Proceedings, D. Parsons, T. Garlan, JBest (eds), 331-335.

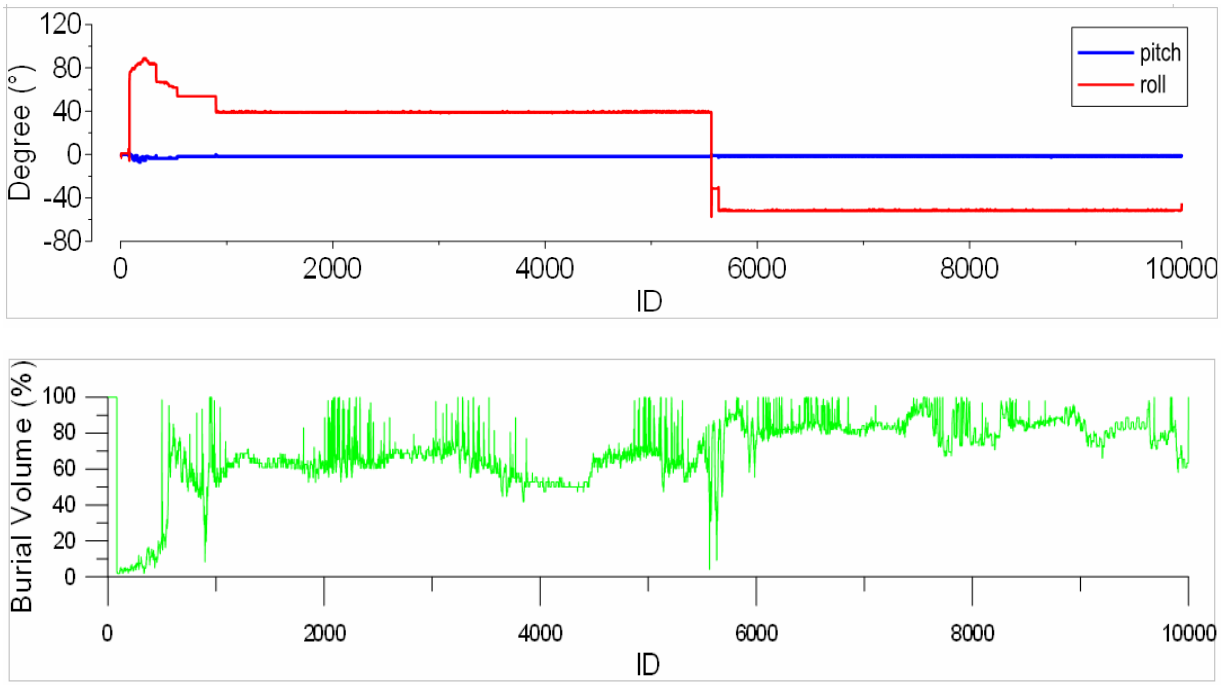

Figure 9. Pitch and roll measurements during the all experiment, (a). Mine burial volume during the all experiment. 2 storm events are recognizable: lowest values at around 1000 and 5500 recording number, (b). combination pitch-roll and burial volume. Roll events are encountered during storm events,

.

Decifering Mega-Ripple variability in an anthropogenically-steered environment: implications for mine burial studies.

Sonia Papili[1,2], Matthias Baeye[3], Vera Van Lancker[3]

1. Belgian Navy, Marinebasis Zeebrugge, Graaf Jansdijk 1, 8380 Zeebrugge, Belgium Email: sonia.papili@mil.be,
2. RCMG (Renard Centre of Marine Geology), Department Geology and Soil Science, Ghent University, Krijgslaan 281-S8, 9000 Gent. Belgium. Email: sonia.papili@ugent.be
3. Royal Belgian Institute of Natural Sciences. Management Unit of the North Sea Mathematical Models. Gulledelle 100, 1200 Brussels, Belgium. Email: Vera.vanlancker@mumm.ac.be, Matthias.Baeye@mumm.ac.be

ABSTRACT

In 2007 the Ministery of Defence, in collaboration with Ghent University, developed a project on the understanding of mega-ripple variability in view of improving mine burial prediction models in sandbank areas. Results will assist in the monitoring of sea-mines, heritage of two World Wars, nowadays partially or totally buried by sandy bedforms.

In this paper we will present results from 'The Vlakte Van De Raan – Akkaert Bank' region, a sandbank area on the Belgian Continental Shelf where intensive disposal of dredged material takes place. Five years time series of multibeam echosoundings (Kongsberg Simrad EM1002-EM3002) were built-up.

Migration of dunes (2-3m in height) has been observed of up to 20m in a South West direction opposite to the dominant North East current direction. Magnitudes of migration are largest near to the disposal ground (Van Lancker et al., 2012). Megaripples has been observed too, but their variability was not quantified. During this study a series of parallel profiles, aligned transversally to the dunes, were investigated in time. Profiles with ebb-dominance were analyzed separately from those with a flood-dominance. Differences are highlighted between those closely settled to the disposal ground and those further located.

From the bedform migration, a volume quantification was performed following the results of Duffy (2012). Results are being analysed against hydro-meteorological influences and volumes of dumped material.

REFERENCES

V. Van Lancker, M. Baeye, I. Du Four, R. Janssens, S. Degraer, M. Fettweis, F. Francken, J.S. Houziaux, P. Luytan, D. Van den Eynde, M. Devolder, K. De Cauwer, J. Monbaliu, E. Toorman, J. Portilla, A. Ullman, M. Liste Munõz, L. Fernandez, H. Komijani, T. Verwaest, R. Delgado, J. De Schutter, J. Janssens, Y. Levy, J. Vanlede, M. Vincx, M. Rabaut, N. Vandenberghe, E. Zeelmaekers, A. Goffin. (2012). *Quantification of Erosion/Sedimentation patterns to trace the natural versus anthropogenic sediment dynamics 'QUEST4D'*. Final report Brussels : Belgian Science Policy Office.103 p. (Research Program Science for a Sustainable Development).

Garret P; Duffy, John E. Hughes Clarke. (2012). Measurement of bedload transport in a coastal sea using repeat swath bathymetry surveys: assessing bedload formulae using sand dune migration. International Association of Sedimentologists and published for them by Blackwell Publishing Ltd. 44, pag 249-272

Three-dimensional spatial variations of suspended sediment concentration over vortex ripples

A. M. Penko[(1)] and J. Calantoni[(1)]

1. Naval Research Laboratory, Stennis Space Center, MS, USA – Code7434@nrlssc.navy.mil

Abstract

A three-dimensional mixture theory model (SedMix3D) was used to simulate the flow and sediment transport over vortex ripples for scaled laboratory conditions. SedMix3D treats the fluid-sediment mixture as a continuum of varying density and viscosity with the concentration of sediment and velocity of the mixture calculated using a sediment flux equation coupled to the Navier-Stokes equations for the mixture. Mixture theory allows the model to simulate the three-dimensional flow and sediment concentration within and above an evolving sediment bed. Grid spacing was on the order of a sediment grain diameter and time steps were $O(10^{-5}$ s). The simulation was forced with a time series of free-stream velocity measured in a free-surface laboratory flume. Spatial variations in the simulated suspended sediment concentration were primarily associated with the non-uniform generation of vortex structures over the ripple flanks. The suspended sediment was initially picked up in regions of high vorticity, and then caused a damping of the vorticity while being advected through the water column.

1. INTRODUCTION

Bedforms on the seafloor in the neashore coastal and continental shelf regions impact erosion and deposition, waves and currents, and coastal infrastructure. Ripples are ubiquitous in sandy coastal regions, generally covering the seafloor in depths up to 20 m during temperate weather (i.e, during non-extreme wave events). Ripples drastically affect the total sediment transport and wave energy dissipation; however, it is difficult to quantify their total effect due to the complexity that ripples bring to the hydrodynamics of bottom boundary layer flow.

The hydrodynamics above sand ripples are dominated by the coherent vortices formed on the ripple flanks and ejected into the water column at flow reversal. This process erodes sediment off the surface of the ripple and suspends it into the water column where it is then advected with the flow (Thorne et al., 2003, van der Werf et al., 2006).

Recent advances in high performance computing hardware and software have allowed us to implement three-dimensional, high-resolution simulations to study small-scale bedform dynamics. Experimental (laboratory and field) and complex numerical models are all necessary to better understand and quantify the effect of ripples on sediment transport and the turbulent dynamics of the wave boundary layer. However, most research examining sediment transport over three-dimensional dynamic beds has been limited to laboratory and field studies. Recent advances have allowed for the measurement of vortex dynamics and sediment transport in the laboratory (van der Werf, 2006) and field (Traykovski, 1999; Hurther and Thorne, 2011). Few three-dimensional, high-resolution models exist to study small-scale sediment dynamics in detail. Here we use a mixture theory model to study the dynamic coupling of vorticity and suspended sediment and their spatial variability over dynamic sandy rippled beds.

2. METHODOLOGY

2.1. Numerical model

Using the three-dimensional Navier-Stokes solver, SedMix3D, we performed a high spatial and temporal resolution simulation of oscillatory flow over a sandy rippled bed for 18 wave periods.

The model equations are based on the mixture velocity (the velocity of the sediment and fluid as a continuum) as defined by mixture theory. SedMix3D is a one-phase continuum model, with a scalar quantity of sediment concentration that determines the mixture's bulk properties (density, viscosity, settling velocity) at every grid point (Penko et al., 2011). The mixture is treated as a continuum of varying density and viscosity with the concentration of sediment and velocity of the mixture calculated with a sediment flux equation coupled with the Navier-Stokes equations for the mixture. The mixture continuity equation was derived by combining the fluid and sediment phase continuity equations,

$$\frac{\partial \rho}{\partial t} + \nabla \cdot (\rho \mathbf{u}) = 0 \quad (1)$$

where **u** is the mixture velocity and ρ is the mixture density,

$$\rho = \phi \rho_s + (1-\phi)\rho_f \quad (2)$$

where □ is the sediment volumetric concentration, and ρ_s and ρ_f are the sediment and fluid densities, respectively.

The mixture momentum equation was derived from the sum of the fluid and sediment phase momentum equations,

$$\frac{\partial \rho \mathbf{u}}{\partial t} + \rho \mathbf{u} \cdot \nabla \mathbf{u} = -\nabla P + \nabla \cdot (\mu \nabla \mathbf{u}) + \mathbf{F} - \rho \mathbf{g} - S_b \mathbf{u} \quad (3)$$

where P is the mixture pressure, μ is the effective viscosity, **F** is the external driving force vector per unit volume, **g** is gravitational acceleration (981 cm/s^2), and S_b is the particle pressure parameterization.

SedMix3D employs a modified Eilers equation (Eilers, 1941) to represent effective viscosity, μ, here scaled by the pure water viscosity, μ_f,

$$\frac{\mu}{\mu_f} = \left[1 + \frac{0.5[\mu]\phi}{1-\phi/\phi_m}\right]^2 \quad (4)$$

where [μ] is the intrinsic viscosity, a dimensionless parameter representing the sediment grain shape, and 0.0 < □ < 0.63, with the lower bound representing pure water and upper bound roughly corresponding to the maximum concentration of a packed sediment bed.

The concentration of sediment is modeled with a sediment flux equation (Nir and Acrivos, 1990) that balances the temporal gradients in sediment concentration with advection, gravity, and shear-induced diffusion,

$$\frac{\partial \phi}{\partial t} + \mathbf{u} \cdot \nabla \phi = D \nabla^2 \phi - \frac{\partial \phi W_t}{\partial z} \quad (5)$$

where W_t is the concentration dependent settling velocity (Richardson and Zaki, 1954) and Re_p is the particle Reynolds number. The shear-induced diffusion of sediment, D, is a function of grain size, volumetric concentration, and mixture stresses (Leighton and Acrivos, 1986),

$$D = \frac{1}{4} d^2 \beta(\phi) |\nabla \mathbf{u}| = 0 \quad (6)$$

and where d is the grain size diameter, α is an empirical constant, and β is an empirical function of concentration. Previously, SedMix3D demonstrated good agreement with detailed laboratory observations using particle image velocimetry to measure vortex dynamics over rippled beds with uniform grain size (Penko et al., 2013). Here, we initialized the numerical simulation with the measured bed profile and imposed hydrodynamic conditions.

2.2. Simulation set-up

The simulation had a domain size of 19.0 cm x 2.4 cm x 14.2 cm with approximately 1.5 million grid points and ran on 96 processers on a Department of Defense high performance computer. The 36 s real-time simulation took approximately 170 wall-clock hours to complete. The laboratory data used to initialize and force the model simulation were collected using Particle Image Velocimetry (PIV) in a free-surface wave flume with a wave generator that produced regular sinusoidal waves 5 cm in height with 2 s periods over an artificial sediment bed.

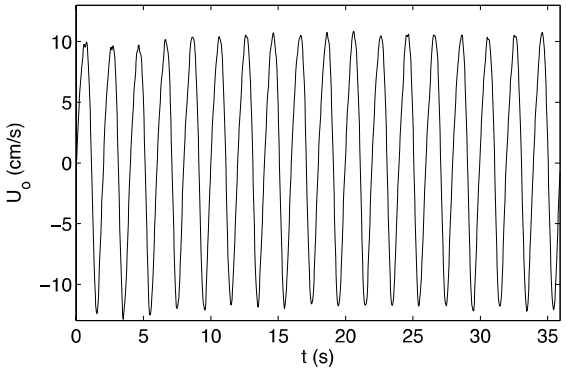

Figure 1. Free stream velocity time series recorded by an ADV in a free surface flume that was used as forcing in the simulations.

Two–dimensional ripples persisted during the experiment with wavelengths of ~5 cm and heights of ~2 cm. The simulation was forced with a time series of free stream velocity recorded with an ADV (Figure 1) for a total of 18 wave periods (36 s). The first 9 wave periods of the simulation were discarded for model spin-up and not included in the data analysis.

The initial bed consisted of four ripples (height~2 cm, length~5 cm) extracted from profiles measured in the laboratory (Figure 2). The initial bed profile was determined from the measured laboratory bed profile at the beginning of the experiment and then evolved with the oscillatory flow.

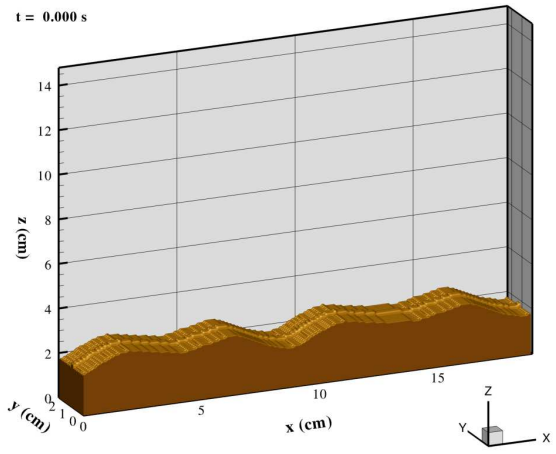

Figure 2. The initial simulation bed profile in the simulation coordinate system.

The bed profile reached equilibrium in the simulation by the seventh wave period and the ripples remained in equilibrium for the remainder of the simulation. Due to a lengthy model spin-up time, only the last 9 wave periods were used in the analysis. The model output of velocity and concentration was ensemble-averaged over the 9 wave periods and the results are presented in the following section.

3. RESULTS

SedMix3D outputs the three-component velocity vector and volumetric concentration of sediment (0 < □ < 0.63) at every grid point within the domain. The mixture theory approach is advantageous for examining sand ripple dynamics because the model simulates the velocity and concentration everywhere, from the top of the boundary layer to the packed sand bed, including the highly concentrated bedload layer that is very difficult to measure in situ and arbitrary in thickness. One can also directly examine the dynamically coupled effect of the suspended sediment on the vorticity and conversely, the vorticity on the transport of sediment.

A plan view (x-y) of the vorticity magnitude and the suspended sediment concentration contour levels for □ = 0.01 (blue solid line) and □ = 0.1 (magenta dashed line) at an elevation of z = 2.86 cm is plotted in Figure 3. The insets in the upper left corners denote the phase of the wave for each subfigure. Note the significant variability of the vorticity and bursts of suspended sediment in the cross-flow (y) direction (Figure 3a). Immediately before flow reversal, sediment was picked up in the regions of strong vorticity (Figure 3a). Once suspended in the water column, the sediment began to damp the vorticity, causing pockets of decreased vorticity and consequently causing a spatial variability in the vortex dissipation (Figure 3b). As the flow began to accelerate, the model produced strong and spatially uniform vortex structures over ripple crests (Figure 3c). However, over the troughs, where the flow decelerated, vortices broke-up and dissipated at random, producing more three-dimensional variability than in the accelerated flow over the crests (Figure

3a,b). Also just after flow reversal, the suspended sediment concentrated in the leading (left) edge of the ejected vortex, damping out most of the vorticity before maximum flow (Figure 3b,c).

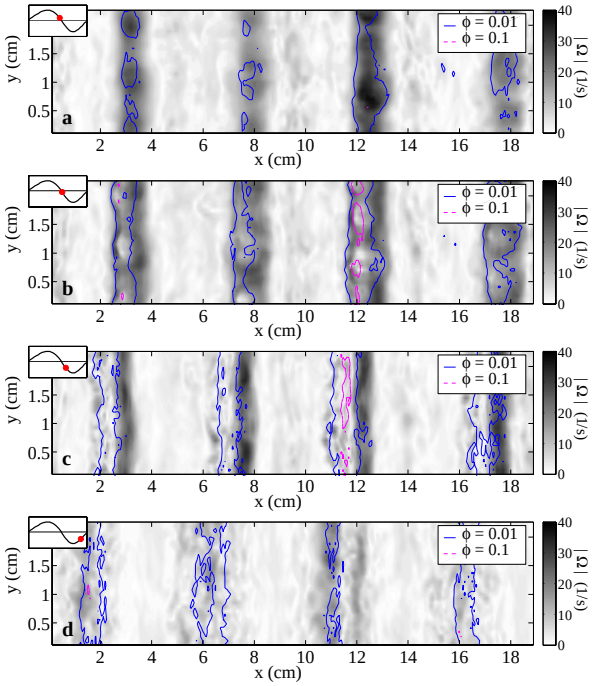

Figure 3. Plan view of the ensemble-averaged vorticity magnitude (filled black and white contours) and suspended sediment concentration (blue solid and magenta dashed contour lines) at z = 2.86 cm. Insets show the ensemble-averaged free stream velocity (black line) and the position of the wave for each figure (red dot).

The simulation also showed a suspended sediment burst on the flank of the ripples after maximum flow, despite relatively low vorticity, which is a behavior we have observed in laboratory experiments of oscillatory flow over sand ripples (Figure 3d).

The cross-flow variability is also evident in a plot of the three-dimensional swirling strength (Figure 4). Swirling strength is a scalar quantity of the vorticity that identifies the closed rotational vortex structures in turbulent flow (Zhou et al., 1999). The method is effective in determining the location of vortex cores by excluding the voriticity due to boundary-generated shear, but does not identify the rotational direction. At flow reversal (Figure 4a), the vortices over the troughs were very three-dimensional with high spatial variability, especially in the cross-flow direction. However, where the flow accelerated over the ripple crests, the vortices were more uniform, with very little variability in the cross-flow direction. After maximum flow (Figure 4b), the vorticies are stretched and dissipated by the strong flow. The vorticies dissipate randomly, especially over the ripple troughs.

4. CONCLUSIONS

To the authors' knowledge, no one previously has been able to simulate the three-dimensionality of small-scale boundary layer processes in this amount of detail. SedMix3D allows for detailed examinations of the three-dimensional boundary layer processes occurring due to oscillatory flow over sand ripples. Here, we present three-dimensional model results of vorticity and suspended sediment concentrations throughout the phase of a wave. Over ripple crests and during the accelerated portion of the flow the model produced strong uniform vortex structures. However, over the troughs, where the flow decelerated, vortices broke-up and dissipated at random, producing more three-dimensional variability than in the accelerated flow over the crests. Spatial variations in the simulated suspended sediment concentration were primarily associated with the non-uniform generation of vortex structures over the ripple flanks and non-uniform vortex dissipation as flow accelerated. The suspended sediment was initially picked up in regions of high vorticity, and then damped the vorticity while being advected through the water column. The simulation also showed bursts of suspended sediment concentration when vorticity was low, similar to observations of laboratory experiments.

5. ACKNOWLEDGMENT

AMP was supported by the Jerome and Isabella Karle Distinguished Scholar Fellowship Program at the Naval Research Laboratory. JC was supported under base funding to the Naval Research Laboratory from the Office of Naval

Research. This work was supported in part by a grant of computer time from the DoD High Performance Computing Modernization Program at the NAVY, AFRL, and the ERDC DSRC.

6. REFERENCES

Eilers, H. 1941. The viscosity of the emulsion of highly viscous substances as function of concentration. Kolloid-Zeitschrift 97(3): 313–321.

Hurther, D. & Peter, D.T. 2011. Suspension and near-bed load sediment transport processes above a migrating, sand-rippled bed under shoaling waves. J. Geophys. Res. Oceans 116: C07001.

Leighton, D. & Acrivos, A. 1986. Viscous resuspension. Chem. Eng. Sci. 41(6): 1377–1384.

Nir, A. & Acrivos A. 1990. Sedimentation and sediment flow on inclined surfaces. J. Fluid Mech. 212: 139–153.

Penko, A.M., Slinn, D.N., & Calantoni, J. 2011. Model for mixture theory simulation of vortex sand ripple dynamics. J. Waterw. Port. Coast. Eng. ASCE 137(5): 225–233.

Penko, A.M., Calantoni, J., Rodriguez-Abudo, S., Foster, D.L., & Slinn, D.N. 2013. Three-dimensional mixture simulations of flow over dynamic rippled beds. J. Geophys. Res. Oceans 118: doi:10.1002/jgrc.20120.

Richardson, J.F., & Zaki, W.N. 1954. Sedimentation and fluidisation: Part 1. T. I. Chem. Eng. 32: 35–53.

Thorne, P.D., Davies, A.G., & Williams, J.J. 2003. Measurements of near-bed intra-wave sand entrainment above vortex ripples. Geophys. Res. Letters 30(20): 2028.

Traykovski, P., Hay, A.E., Irish, J.D., & Lynch, J.F. 1999. Geometry, migration, and evolution of wave orbital ripples at LEO-15. J. Geophys. Res. Oceans 104(C1): 1505–1524.

Van der Werf, J.J., Ribberink, J.S., O'Donoghue, T., & Doucette, J.S. 2006. Modelling and measurement of sand transport processes over full-scale ripples in oscillatory flows. Coastal Engineering 53: 657–673.

Zhou, J., Adrian, R.J., Balachandar, S., & Kendall, T.M. 1999. Mechanisms for generating coherent packets of hairpin vortices in channel flow. J. Fluid Mech. 387: 353–396.

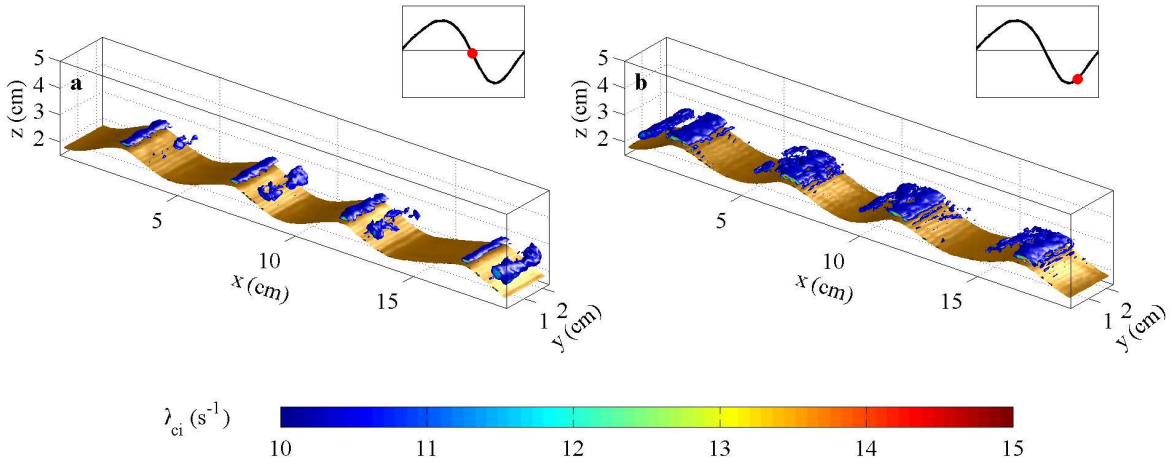

Figure 4. The plot shows the ensemble-averaged isosurface of the three-dimensional swirling strength at two phases of the wave. The blue surface indicates a swirling strength of 10 s^{-1} and the color contours represent the swirling strength inside a vortex that intersects the edge of the domain. The brown isosurface represents the instantaneous bed at 57% concentration by volume.

The response and hysteresis of alluvial dunes under transient flow conditions

Arjan Reesink[(1)], Dan Parsons[(1)], Phil Ashworth[(2)], Richard Hardy[(3)], Jim Best[(4)], Christopher Unsworth[(1)], Stuart McLelland[(1)] and Brendan Murphy[(1)]

1. Department of Geography, Environment and Earth Sciences, University of Hull, Hull, HU6 7RX, UK - a.reesink@hull.ac.uk
2. Division of Geography and Geology, School of Environment and Technology, University of Brighton, Brighton, Sussex, BN2 4GJ, UK.
3. Department of Geography, Durham University, Durham, DH1 3LE, UK.
4. Departments of Geology, Geography and Geographic Information Science, Mechanical Science and Engineering and Ven Te Chow Hydrosystems Laboratory, University of Illinois at Urbana-Champaign, 1301 W. Green St., Urbana, IL, 61801, USA.

Abstract

Bedforms perpetually adjust to spatially non-uniform and temporally unsteady flow conditions, with marked changes in flow causing hysteresis-effects in bed response. The rates and styles of adjustment are likely to differ depending on the relative magnitudes of changes in water surface slope, and thus bed shear stress, and flow depth. Slope and depth are likely to be temporally disconnected during the passage of flood waves, but also vary in spatially in their magnitude, for instance between the thalweg and shallower parts of the channel. This paper describes the first of a series of experiments set up to identify the relative roles of slope and flow depth for the morphodynamic adjustments of dunes under a range of transient flow conditions. Initial results suggest that the morphodynamics of dune growth and decay are controlled by four key factors: i) the bedform stability range, ii) spatial variability in bedform stability, iii) bedform kinematics, iv) the relative magnitudes of water surface slope and depth. Bed morphology was most sensitive to changes in water depth. In particular, the development of trains of superimposed bedforms on the stoss of larger dunes was observed following an increase in water depth and not in decreasing water depths. This association suggests that an abundance of superimposed bedforms is not unique to dune decay by cannibalisation, but related to a disequilibrium between dune geometry and the flow over the stoss slope. Fuller understanding of the causes for, and constraints on, dune adaptation to changing flows requires robust quantification of the flow field over out-of-equilibrium dunes.

1. INTRODUCTION

Bedforms in river channels perpetually adjust to non-uniform and unsteady flow conditions, with marked changes in flow causing hysteresis-effects in bed roughness, sediment transport rates and morphodynamic adjustments. Recent work indicates that the reduction in dune size through cannibalization (e.g. Kleinhans, 2002) by smaller superimposed dunes differs fundamentally from bedform amalgamation during dune growth (Coleman and Melville 1994; Raudkivi and Witte, 1990). Such differences are consistent with changes in water-surface slope and absolute flow depth being out-of-phase with one another during the passage of a flood wave (Figure 1). Water-surface slope commonly increases during the arrival of a flood wave, such that the maximum bed shear stress precedes the maximum water level for a given flood (Van Rijn, 1994). In contrast, water surface slope and bed shear stress decline prior to absolute flow depth during falling stage (Figure 1). The separation of water surface slope and depth supports a separation of '*true hysteresis*' of different bedform growth and decay processes (Martin and Jerolmack, 2013), '*rate-dependent hysteresis*' related to the time needed for bedform adaptation to reach an equilibrium form (Paarlberg *et al*., 2010; McElroy and Mohrig, 2007), and *'naturally variability'* in dune geometries (Parsons

et al., 2005; Rubin and McCulloch, 1980). The shape of flood waves and the phase-relation between water surface slope and water depth varies between floods from highly asymmetrical flash-floods to monthly changes in base-flow. In addition to such temporal variability related to flood waves, the magnitudes of changes in flow depth and water surface slope differ i) within a river channel between the deeper areas, such as the thalweg, and shallower areas such as bar tops where depth increases are much larger, and ii) along a the course of a river from steep and shallow tributaries to a comparatively deep and low-gradient river mouth. In order to understand the morphodynamic response of river beds to transient flows, it is necessary to identify the mechanisms of erosion and deposition associated with adaptions to changing water depths and water surface slopes.

This paper presents preliminary results from a series of laboratory experiments in which bedform response was measured for different magnitudes of changes in water depth and discharge (flow velocity).

2. METHODS

A recirculating flume 16m long, 2m wide and 0.5m deep was constructed in the Total Environment Simulator in The Deep at the University of Hull, UK. The flume contained a sand bed with a D_{50} of 239µm. The experimental runs covered a range of transient conditions, where the magnitudes and rates of change in discharge (and hence flow velocity) and depth were carefully controlled and systematically increased and decreased. In this paper, we present data from: 1) an increase water depth for a fixed discharge; 2) a decrease in water depth for a fixed discharge, 3) an increase in discharge for a fixed water depth, and 4) a decrease in discharge for a fixed water depth. Water-depth and water surface slope were measured along the flume at 2Hz using 7 wave height probes. Flow velocity was measured at 25 Hz with 4 ADV's set at 40% of the water depth at 4 locations in the test section to provide an approximation of the depth average flow velocity. Froude numbers were calculated using the depth-averaged flow velocity measured with the 4 ADVs. Bed elevation was measured over a 5 m test section at repeat intervals of 7.5 and 300 s throughout the 120 hrs of experiments using a multi-frequency (1, 2 and 4 MHz) acoustic backscatter profiler that measured bed elevation together with suspended sediment concentration. Vertical resolution of the bed elevation measurements was 2.5 mm and horizontal resolution was 5 mm.

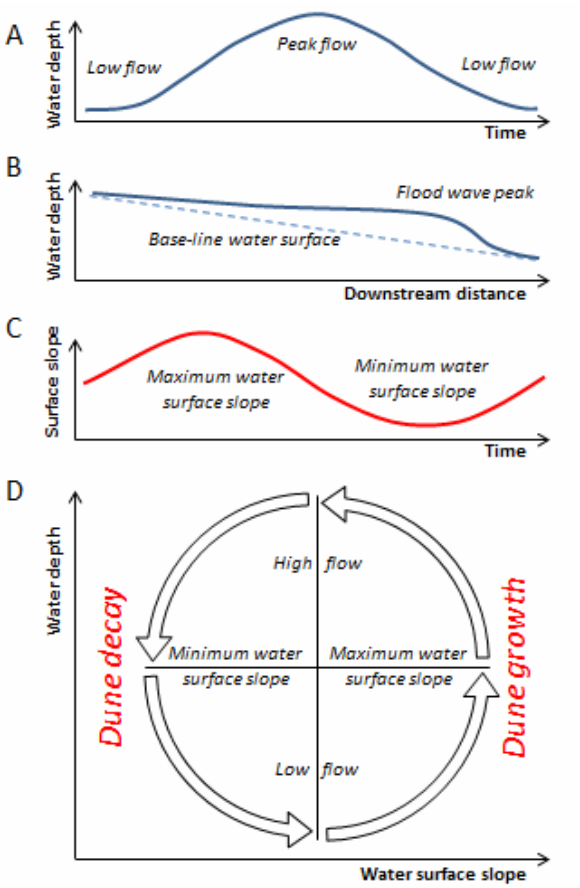

Figure 1. The passage of a flood wave at a location over time (A) and at a time over a downstream distance (B): both result in a water surface slope (C) that is out-of-phase with water depth at a location (A). This depth-slope association affects the nature of alluvial dune growth and decay in unsteady flows (D).

3. RESULTS

Four step-wise changes in flow conditions (Figure 2) are described herein to illustrate differences in bedform adaptation that were observed during the experiments for:

1) an increase in flow depth
2) a decrease in flow depth

3) a decrease in discharge (flow velocity)
4) an increase in discharge (flow velocity)

The flow was kept within the limits of the stability range of dunes. The effects on the morphology of these changes in flow are then compared below.

3.1. Increase in flow depth

An increase in water depth was followed by a decrease in dune migration rate, a decrease in trough scour, and the development of trains of superimposed bedforms on the stoss slopes of two dunes (Figure 2A, Label 2). The presence of these two new clusters of smaller superimposed bedforms was also linked to preceding merger of bedforms upstream (Figure 2A, Label 1). The superimposed bedforms gradually decreased in number and increased in height and length until the dune-bed had re-established itself at a new condition. Dune trough scour decreased following the increase in flow depth (Figure 2A, Label 3). The depth increase presented here was a 30% increase in flow depth, from 0.175 to 0.225m. This increase in flow depth caused a decrease in water surface slope from $-1.9 \pm 0.6 * 10^{-3}$ to $-1.2 \pm 0.4 * 10^{-3}$ and a decrease in the Froude number from 0.59 to 0.50.

3.2. Decrease in flow depth

A decrease in water depth was followed by an increase in trough scour (Figure 2B, Label 4) and a lengthening of the dunes (Figure 2B, Label 5). Trains of superimposed bedforms remained absent during the decrease, and merger of bedforms was not followed by the development of superimposed bedforms on the downstream bedforms. The decrease in flow depth presented here was a reversal in flow depth from 0.175 back to 0.225m. This decrease in water depth caused an increase in water surface slope from $-1.6 \pm 0.5 *10^{-3}$ to $-2.3 \pm 0.8 *10^{-3}$, and an increase in the Froude number from 0.46 to 0.58.

3.3. Increase in discharge (flow velocity)

An increase in flow velocity was followed by an increase in dune migration rate, an increase in scour depth (Figure 2C, Label 4) and crest height of the dunes (Figure 2C, Label 6), and a reduction in the number and size of superimposed bedforms. The increase in discharge (velocity) presented here, from 1.8 to 0.2 m s^{-1} at a fixed water depth of 0.175 m caused an increase in water surface slope from $-1.4 \pm 0.5 *10^{-3}$ to $-2.1 \pm 0.8 *10^{-3}$ and an increase in the Froude number from 0.49 to 0.53.

3.4. Decrease in discharge (flow velocity)

A decrease in flow velocity was followed by a decrease in dune migration rate and an increase in the number superimposed bedforms (Figure 2D, Labels 1-2). The development of a train of superimposed bedforms occurred in an area where the crest-to-crest distance had increased following the merger of bedforms upstream. The decrease in discharge presented here, from 2.2 to 2.0 m s^{-1} at a fixed water depth of 0.175 m caused a decrease in water surface slope from $-1.6 \pm 0.8 *10^{-3}$ to $-1.4 \pm 0.7 *10^{-3}$ and a change in the Froude number from 0.56 to 0.52.

4. DISCUSSION

4.1. Bedform adaptation and bedform stability in spatially variable flow

The causal association of bedform response to changes in flow is complicated by naturally occurring variability in bed morphology at different locations in the stability range of dunes (Van den Berg and Van Gelder, 1993) and dune kinematics (Gabel, 1993; Leclair and Bridge; 2002). For example, the distinct increase in superimposed bedforms (Figure 2, Label 2) occurred following decreases in dimensionless bed shear stress and hence the bed becoming nearer to the stability range of ripple-covered beds. Under these conditions, closer to the stability range of ripple-covered beds, flow can be hydraulically smooth locally on dune stoss slopes even though time- and space-averaged flow remains hydraulically rough (Bridge, 2003; Reesink and Bridge, 2009). Such localised hydraulically smooth flow allows ripples to develop, and potentially even persist, outside their stability field if the separated flow in their lee is sufficiently erosive. Thus, dune adaptation is likely to vary depending on bedform stability, which varies spatially over bedforms that are sufficiently large in size.

4.2. Bedform adaptation, local flow conditions and dune kinematics

In addition to differences in bedform stability, the development of trains of superimposed bedforms was associated with preceding merger of dunes upstream from the newly developed bedforms (Figure 2, Label 1). The merger of two bedforms generates a gap in the crest-to-crest spacing of the primary bedforms. Trains of superimposed bedforms form preferentially in such enlarged areas of flow deceleration. Thus, the results indicate that antecedent bed morphology and kinematics affect the location and frequency of processes such as cannibalisation of large dunes by smaller bedforms.

4.3. Superimposition as an adaptation mechanism

Superimposition of bedforms, like other changes in bedform geometry, is non-unique and occurs naturally in any dune population. However, increased superimposition of smaller bedforms on dunes has been described as a mechanism for growth by amalgamation (Raudkivi and Witte, 1990), as a mechanism for decay by cannibalisation (Kleinhans, 2002; Martin and Jerolmack, 2013), and as a characteristic of the re-establishing boundary layer on the stoss slope (Rubin and McCulloch, 1980). Superimposed bedforms can significantly increase bed roughness through modification and interactions of coherent flow fields over bedforms of various scales (Fernandez *et al.*, 2006). Despite their importance, the hydrodynamic controls that allow superimposed bedforms to develop and persist on dune stoss slopes are poorly constrained. In these experiments, the development of superimposed bedforms occurred primarily following a decrease in flow competence, forming on stoss slopes in areas where the crest-to-crest distance was relatively high. Overall dune dimensions ultimately increased as a consequence of the increase in flow depth (Figure 2A). Conversely, initial increase in dune length observed in decreased flow depths were not associated with increased bedform superimposition. Thus, the results of the experiments suggest that an abundance of superimposed bedforms is not unique to dune decay by cannibalisation, but related to a disequilibrium between primary dune geometry and flow over the stoss slope.

4.4. Separate effects of water depth and water surface slope?

The magnitudes of adaptation effects (increased superimposition, trough scour, increase in crest height, bedform lengthening) were more pronounced for the changes in water depth compared to the changes in discharge/velocity (Figure 2), even though all the investigated changes represented significant steps within the stability range of dunes. Flow velocity and water depth have different effects on the geometry and strength of the separated flow and re-establishing boundary layer (Balachandar *et al*., 2007), and such differences may explain the differences in bed response to changing flow. Further research is needed to improve our understanding of out-of-equilibrium flow over dunes, in particular the nature of the separated flow and re-establishing boundary layer on the stoss of downstream bedforms (Unsworth et al., this volume) and its role in initiating and sustaining, or supressing, superimposed bedforms.

5. CONCLUSIONS

The absolute and relative magnitudes of water surface slope and water depth differ spatially along river channels and temporally between different flood waves. These temporal changes are known to exhibit significant out-of-phase behaviour in which maximum water surface slope precedes maximum water depth. In the experiments presented herein, the morphodynamics of dune growth and decay are attributed to four factors: i) the bedform stability range, ii) spatial variability in bedform stability, iii) bedform kinematics, and iv) the relative magnitudes of water surface slope and depth. Morphology was more sensitive to changes in water depth than flow velocity. In particular, the development of trains of superimposed bedforms on the stoss of larger dunes was observed following an increase in water depth as opposed to a decrease in discharge, and was associated with areas of flow deceleration that were enlarged by preceding merger of dunes. This association suggests that an abundance of superimposed bedforms is not unique to dune decay by cannibalisation, but related to a disequilibrium between primary dune geometry and flow over the stoss slope. Fuller understanding of the causes for, and constraints on, dune adaptation to changing

flows awaits quantification of the flow field over out-of-equilibrium dunes.

6. ACKNOWLEDGMENT

This research was supported by grant NE/I014101/1 from the UK Natural Environment Research Council (NERC).

7. REFERENCES

Balachandar, R., Hyun, B.-S., & Patel, V.C., 2007, Effect of depth on flow over a fixed dune, Canadian Journal of Civil Engineering 34, 1587–1599

Bridge J.S., 2003, Rivers and Floodplains, Forms, processes and sedimentary record. Blackwell Publishing 491 p.

Coleman , S.E. and Melville B.W., 1994, Bed form development. Journal of Hydraulic Engineering, 120, 544-560

Fernandez, R., Best, J., & Lopez, F., 2006 Mean flow, turbulence structure, and bed form superimposition across the ripple–dune transition: Water Resources Research, 42(5), p. 948–963

Gabel, S., 1993, Geometry and kinematics of dunes during steady and unsteady flows in the Calamus River, Nebraska, USA, Sedimentology, 40(2), 237-269

Kleinhans, M.G., 2002 Sorting out sand and gravel: sediment deposition in sand-gravel bed rivers. PhD Thesis Universiteit Utrecht, NGS 293, 227 p.

Leclair, S. and Bridge, J.S., 2002, Preservation of cross-strata due to the migration of subaqueous dunes: an experimental investigation, Sedimentology, 49(6), 1157–1180

Martin R.L. & Jerolmack D.J., 2013, Origin of hysteresis in bed form response to unsteady flows. Water Resources Research, accepted article

McElroy, B. & Mohrig, D., 2007, Correlation decay and dynamic equilibria in sandy transport systems. River, Coastal and Estuarine Morphodynamics; RCEM 2007, 891-896.

Paarlberg, A.J., Dohmen-Janssen, C.M., Hulscher, S.J.M.H., Thermes, P., & Schielen, R., 2010, Modelling the effect of time-dependent river dune evolution on bed roughness and stage. Earth Surface Processes and Landforms, 35, 1854-1866

Parsons, D.R., Best, J.L., Orfeo, O., Hardy, R.J., Kostaschuk, R. & Lane, S.N., 2005, Morphology and flow fields of three-dimensional dunes, Rio Parana, Argentina: Results from simultaneous multibeam echo sounding and acoustic Doppler current profiling. Journal of Geophysical Research-Earth Surface, 110.

Raudkivi, A.J. & Witte, H-H., 1990, Development of bed features. Journal of Hydraulic Engineering, 116, 1063-1079

Reesink, A.J.H. & Bridge, J.S., 2009, Influence of bedform superimposition and flow unsteadiness on the formation of cross strata in dunes and unit bars - Part 2, further experiments. Sedimentary Geology, 222, 274-300

Rubin, D.M. & McCulloch, D.S., 1980, Single and Superimposed bedforms – A synthesis of San Francisco Bay and flume observations. Sedimentary Geology, 26, 207-231.

Unsworth, C.A., Parsons, D.., Reesink, A., Best, J., Ashworth, P. and R. Hardy, R., 2013, Flow Structures over Fixed 2D Bedforms in Transient States. This volume.

Van den Berg, J.H. & Van Gelder, A., 1993, A new bedform stability diagram, with emphasis on the transition of ripples to plane bed in flows over fine sand and silt. In Alluvial Sedimentation (Eds. Marzo, M and Puidefabregas, C.) IAS Special Publication 17, 11-21

Van Rijn, L.C., 1994, Principles of fluid flow and surface waves in rivers, estuaries, seas and oceans. Aqua Publications, Amsterdam.

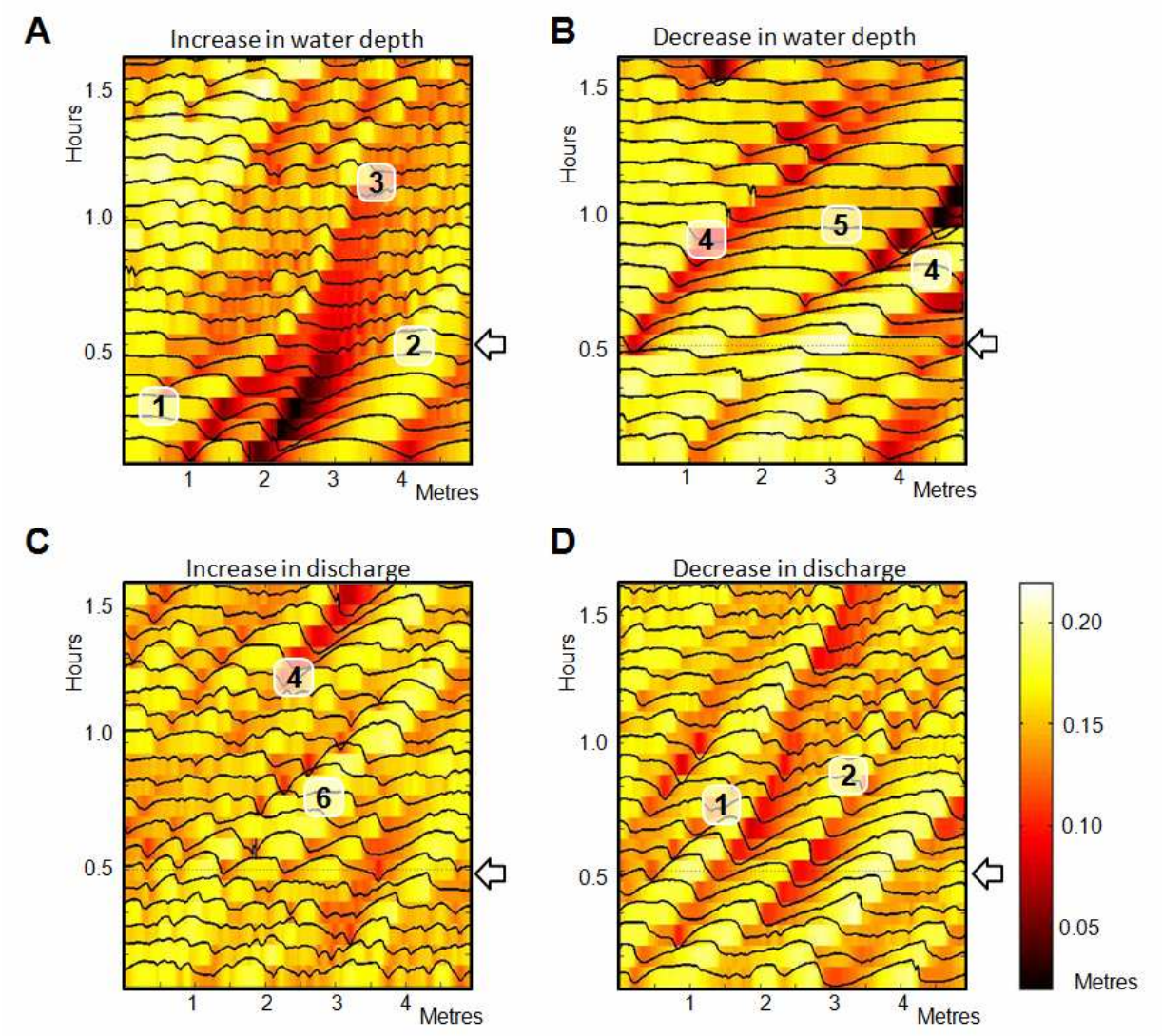

Figure 2. Plots of consecutive bed elevation profiles over time: A) an increase in water depth, B) a decrease in water depth, C) an increase in discharge, and D) a decrease in discharge. The background-colour represents bed elevation. Arrows indicate the point of change, and labels indicate the effects of this change on the morphology: 1) dune merger, 2) increased superimposition of bedforms, 3) decreased trough scour, 4) increased trough scour, 5) lengthening of dunes, and 6) increased dune height.

Morphobathymetric and sediment dynamics analysis on the Gulf of Valencia continental slope (NW Mediterranean)

Marta Ribó[(1)], Pere Puig[(1)], Juan Acosta[(2)], Araceli Muñoz[(3)], Hans van Haren[(4)], Claudio Lo Iacono[(1)], María Gómez Ballesteros[(2)]

1. Institut de Ciències del Mar, ICM-CSIC, Pg. Marítim de la Barceloneta, 37-49, PO Box 08003, Barcelona, Spain, E-mail: mribo@icm.csic.es
2. Instituto Español de Oceanografía, IEO, Pg. Corazón de María,8, PO Box 28002, Madrid, Spain
3. TRAGSATEC - Secretaria General de Pesca, C. José Ortega y Gasset,57, PO Box 28006, Madrid, Spain
4. Royal Netherlands Institute for Sea Research, NIOZ Landsdiep 4, PO Box 1797 SZ, 't Horntje, Texel, The Netherlands

ABSTRACT

The Gulf of Valencia (GoV) continental margin is located in the north-western Mediterranean Sea between the Ebro margin and the promontory Cap La Nao. The morphology of this margin is mainly controlled by the deposition of post-Miocene prograding sequences (Díaz del Río *et al*., 1986). Early studies described the morphological features and sedimentary processes observed on the inner and outer shelf of the GoV (Maldonado *et al*., 1983; Rey and Díaz del Río, 1983; Díaz del Río *et al*., 1986; Rey *et al*., 1999). In the central part of the outer shelf and extending onto the continental slope, a series of sediment undulations aligning sub-parallel to the isobaths were observed (Rey and Díaz del Río, 1983). These features were described in the literature as a result of sliding (Díaz del Río *et al*., 1986) and/or creep (Díaz del Río and Fernández Salas, 2005). These interpretations came from the seismic profiles where the sediment undulations appeared to be affected by the neotectonic fracture systems, which produced mass movements of material towards the continental slope along gliding planes subparallel to the seafloor (Díaz del Río *et al*., 1986).
Recently, new multibeam data sets and several seismic profiles were acquired on board of R/V García del Cid and R/V Vizconde de Eza, respectively. These data sets were analyzed to describe the seafloor morphology and the relevant morphologic features of the study area. In addition, a mooring line, including a string of high frequency temperature sensors, and an ADCP and ten OBS, was deployed on the GoV continental slope. These time series showed the presence of internal waves and their role with the sediment transport. Results of this study provide a new point of view on the sediment dynamics on the GoV continental slope and the origin of the sediment undulations observed, suggesting a relation between the sediment dynamics and the observed morphological features.

REFERENCES

Díaz del Río, V., Rey, J., Vegas, R., 1986. The Gulf of Valencia continental shelf: extensional tectonics in neogene and quaternary sediments. Marine Geology, 73: 169-179

Díaz del Río, V., Fernández Salas, L., 2005. El margen continental del levante español y las islas baleares. Mapa Geomorfológico de España y del margen continental. Instituto geológico y minero de España pp. 177-187

Maldonado, A., Swift, D., Young, R., Han, G., Nittrouer, C., DeMaster, D., Rey, J., Palomo, C., Acosta, J., Ballester, A., Castellvi, J. 1983. Sedimentation on the Valencia Continental Shelf: preliminary results. Continental Shelf Research, 2: 195-211

Rey, J., Díaz del Río, V., 1983. Aspectos geológicos, sobre la estructura poco profunda de la plataforma continental del levante español. Estudio Oceanográfico de la Plataforma Continental

E.O.P.C. Cádiz 15-18 Marzo 1983. Gráficas Buper S.A., pp.53-74

Rey, J., Fernández Salas, L., Blázquez, A., 1999. Identificación de las unidades morfosedimentarias cuaternarias en la plataforma interna del litoral del País Valenciano: el rol de los factores morfoestructurales y eustáticos. Geoarquología i Quaternari litoral. Memorial M.P. Fumanal: 403-418.

Essential facts of the monitoring of the sand extraction and its impact on the Flemish banks on the Belgian continental shelf from 2003 to 2012.

M. Roche[(1)], K. Degrendele[(1)], L. De Mol[(1)], R. Milano[(2)], R. Van den Branden[(3)] and G. De Schepper [(3)]

1. FPS Economy, Continental Shelf Service, B - Marc.Roche@economie.fgov.be, Koen.Degrendele@economie.fgov.be, Lies.DeMol@economie.fgov.be
2. FPS Economy, Statistics - Methodology, B - Robert.Milano@economie.fgov.be
3. Management Unit of the North Sea Mathematical model, B - R.Vandenbranden@mumm.ac.be, G.DeSchepper@mumm.ac.be

Abstract

The monitoring of sand extraction on the Flemish sandbanks of the Belgian continental shelf is based on multiple types of data: statistics derived from the extraction registers, data from the Electronic Monitoring System (EMS = “black-boxes”) on board the dredging vessels (complete records are available since 2003), and regular bathymetric surveys with the multibeam echosounders (MBES) EM1002 and EM3002D (installed on the R/V Belgica) across the sandbanks along parallel lines and on specific areas. The analysis of the various types of data provides a 4D (space and time) view of the evolution of the extraction and admits robust and pragmatic conclusions about the real impact of the sand extraction on the marine environment. From 2003 to 2012, the global bathymetric evolution, based on MBES EM1002 and EM3002D measurements along lines across the control zones, confirms the straightforward relation between the extraction and the bathymetrical evolution. On a larger scale, virtually all of the bathymetric variation can be explained by the extraction itself. In areas without any extraction, no significant trend of the bathymetry is observed.

1. INTRODUCTION

According to the Belgian law of 13 January 1969 (Article 3, § 2, 3) which states that "the exploration and exploitation are subject to an ongoing review of the influence of the activities concerned on the movement of sediments and the marine environment ", the Continental Shelf Service conducts a regular monitoring of the sand extraction on the Belgian Continental Shelf since November 1999.

This monitoring is based on different types of data: statistics derived from the extraction registers, data from the Electronic Monitoring System (EMS = “black-boxes”) onboard the dredging vessels, and regular bathymetric surveys with the multibeam echosounders (MBES) EM1002 and EM3002D (installed on the R/V Belgica) on monitoring areas and across the sandbanks along the old DECCA lines. The analysis and combination of these different types of data provide a 4D (space and time) view of the evolution of the extraction and allow the assessment of its environmental impact.

The impact of the extraction on the seafloor is studied on two different levels. First, a number of reference areas are surveyed several times each year. The delimitation of these monitoring areas is based on the constant monitoring of the extraction activities with the EMS: they coincide with the most extracted areas. These monitoring zones are studied in detail, with resulting grids of 1x1 m, and provide a good idea of the local impact of the most intense extraction on the seafloor.

Based on this local approach on the most dredged areas, a first internal report summarizes the data acquired from 1999 to 2001 on the impact of

extraction on the Kwintebank (Degrendele et al., 2002). Later, many issues relating to the impact of dredging on the marine environment have been widely discussed in the context of multidisciplinary scientific projects: the international project EUMARSAND (01/11/2002-31/01/2006) funded by the EU and the national projects MAREBASSE (01/02/2002-30/04/2006), SPEEK (15/12/2003-30/04/2006) and QUEST4D (01/01/2007-31/01/2011) funded by the Belgian Science Policy (BELSPO).

From the perspective of sustainable management of the sandbanks, lessons from the European project EUMARSAND and the resulting recommendations (Van Lancker et al., 2010) are of prime importance. Sedimentological and morphological analysis based on data acquired from 1999 to 2005 (before and after extraction) shows the stability of the depression of the Kwintebank after cessation of dredging on February 15, 2003. MBES data demonstrates that regarding the bathymetry and the geomorphology, the extraction has a local non-cumulative impact and that potential recovery is nonexistent (Bellec et al., 2010, Degrendele et al., 2010). The project EUMARSAND also demonstrates that at decadal scale, the sand of the Kwintebank should be considered as a non-renewable resource and that extraction has a local non-cumulative impact.

In addition to this local approach by monitoring restricted areas, the regular surveying of a large number of straight parallel lines along the "DECCA" (old positioning radio system lines) across the sandbanks and the channels in the extraction areas provides us with valuable information on the global evolution of the bathymetry of the sandbanks and the channels and allows a comparison between extracted and non-extracted areas.

This contribution aims to provide a summary of this large scale approach with data acquired between 2003 and 2012. Since 2003, EMS is operational on all vessels operating on the Belgian waters and the resulting database allows an accurate evaluation and mapping of the extracted volumes for any area and time period. From 2008 to 2012, 5 sets of "DECCA" lines across the Flemish banks and their adjacent channels have been recorded with the high resolution EM1002 and EM3002D MBES.

To quantitatively evaluate the impact of the extraction on the bathymetry on a large spatial and temporal scale, these five annual MBES surveys along DECCA lines are correlated with the extracted volumes based on EMS - black boxes data. This approach allows an extension of our spatial and temporal point of view and leads to more robust and pragmatic conclusions on the impact of the sand extraction on the marine environment.

2. EMS DATA

The EMS is a fundamental tool for the control of the extraction because it assesses the extracted volume for any area and for any time interval.

The operating principle of the EMS is summarized in the following paragraphs and in figure 1. The EMS automatically records the following parameters: identification of vessel, code of concessionary, date, time, geographical position, speed, status of dredging pump(s) and dredging activity. All necessary sensors are installed to enable the recordings of the parameters above-mentioned. The acquisition rate depends on the ships' activity with additional records during anomalies of the EMS. The EMS is designed to record the sand and gravel extraction activities on the Belgian part of the North Sea: (1) to verify if the trailing suction hopper dredgers are extracting in the designated areas and (2) to verify the average speed of the ships while dredging. Part of the data processing also involves retrieving metadata fields of the dredging operation, such as date, start time, stop time, concession code, average speed, geographical position recognition and distance calculations of tracks inside or outside the designated areas.

As the EMS is not equipped with sensors to record the load of dredged materials in real-time, a method is developed to estimate the extracted volume of a trailing suction hopper dredger within a certain timeframe. This method is based on the following assumptions:

- The extracted volume (m^3) per second is constant, and is based on the known fixed loading capacity of a ship and the duration (in seconds) of the dredging operations.

- The ship is completely empty when the dredging activity starts.
- The ship is completely loaded when the dredging activity ends.

Based on these assumptions and on the calculated time difference between consecutive data points, the extracted volume (m^3) is computed for each EMS record. The EMS database can then be used to evaluate the extracted volumes within any timeframe and within any area.

The reliability of the estimation of the extracted volumes from EMS data can be evaluated by comparing the total annual volume calculated from EMS data with the total annual volume independently calculated from the extraction registers. These registers are the extraction quantities that are declared by the extraction vessels. A mean deviation of 3% is observed between the two data sets. This low deviation confirms the validity of the assumptions used as basis for calculating the extracted volumes from EMS data.

3. MBES DATA

Since 2008, one MBES survey has been performed in spring each year along DECCA lines across the Flemish banks in zone 2 (Kwintebank, Buiten Ratel and Oostdyck). Table 1 provides the codes, dates and MBES types of the surveys used in this contribution:

Survey	Date	MBES
C0810	21-25 April 2008	EM1002
C0911	15-17 April 2009	EM3002D
C1011	26-30 April 2010	EM3002D
C1115	16-20 May 2011	EM3002D
C1213	07-11 May 2011	EM3002D

Table 1: table of surveys, dates and MBES types

These measurements are repeated each year around the same period in order to evaluate the global evolution of the sandbanks. More specifically, the impact of the extraction (e.g. Buiten Ratel) or even the possible recovery (e.g. Kwintebank) can be studied on a larger scale using these data.

All data were acquired onboard the R/V Belgica with the EM1002 (2008) and EM3002D (2009-2012) MBES. The quality of the measurements has been evaluated in relation to the reigning hydrographical norm (IHO standards for hydrographic surveys, 5th Edition, 2008, Special Publication N°44). Both vertically and horizontally the EM1002 and EM3002D measurements are within the scope of the confidence interval of the Special Order standard from IHO.

After the processing of the data (position, tide and draught correction, data cleaning) the soundings are modeled. The resulting grids are subtracted from the reference model based on MBES surveys from 2003, showing the bathymetrical evolution since 2003 (Figure 2). A positive difference corresponds with an increase in amount of sediment while a negative difference indicates a decrease.

Compared to the singlebeam echosounder that provides a simple set of bathymetric values along the navigation line, the great advantage of the MBES is the acquisition of a corridor of variable width (function of the depth) with a high density of soundings. Under normal survey conditions the EM3002D, with its 508 beams distributed over an opening angle of 140° and with its ping rate up to 15 Hz, has an average density of 3-4 soundings/m^2. The high sampling rate combined with a precise real-time correction for heave, roll and pitch gives the data from the EM3002D an unbeatable advantage in statistical credibility and accuracy. For this reason, the bathymetric models of the corridors recorded along the DECCA lines with the EM3002D allow us to assess with a high reliability and precision the bathymetric variation with a reference model.

4. EMS -MBES CORRELATION

The full dataset will enable a joint assessment of the bathymetric variations and volumes of sand extracted during a period of ten years across the the Flemish sandbanks. To quantitatively evaluate the impact of the extraction on the bathymetry on this large spatial and temporal scale, MBES datasets surveyed along DECCA lines results are correlated with the extracted volumes computed from the EMSdata.

This assessment is based on the two following independent datasets (Figure 3 A, B and C):

- For each survey the data are merged to produce a single grid of 5x5 m resolution covering zone 2 of the Flemish banks; each grid represents the bathymetric variation along the DECCA lines between the date of the survey and 2003, date of the reference grid.
- For each survey a grid (100x100 m resolution) of the extracted volumes in zone 2 is estimated from EMS data (black boxes). For each grid cell, the total extracted volume is computed for the same time interval as the bathymetric data.

Using the extracted volume grid, masks are created for successive extracted volume intervals. For each mask, the statistics of all the grid cells included inside the mask are computed for both the extracted volume grid and the DECCA difference grid. Using the extracted volume statistics computed for each mask, an estimation of the mean bathymetric difference due to the extraction is obtained by dividing the mean extracted volume (in m^3) with the surface of the mask (in m^2). This value represents the theoretical bathymetric (ΔZ component) difference caused by the extraction.

For each survey, the predicted bathymetric differences caused by the extraction activities are compared with the bathymetric differences measured with the EM3002D along the DECCA lines. Tables 2 and 3 and figure 4 summarize the results.

A very high linear correlation is observed between the bathymetric differences measured with the MBES and the bathymetric differences caused by the extraction. It must be underlined that for the whole area where the mean extracted volume is null (no extraction), the bathymetric difference is practically equal to zero (mean value of the 5 surveys = -0.03 m). A slight error on the draft measurement of the ship is sufficient to explain variation as low. Finally, a simple linear regression (weighted by the number of observations and without constant) Y=X allows to summarize the relationship between the extraction and the bathymetric variation observed on the Flemish sandbanks and their adjacent swales with a high statistical level of significance (see table 3 and figure 4 for the detailed statistics).

5. CONCLUSIONS

On the Flemish sandbanks and within a period of 10 years, on a mean point of view, a simple linear relationship is observed between the bathymetric differences measured with the MBES and the bathymetric differences caused by the extraction. At the time scale considered, our results show that the extraction can explain most of the measured bathymetric variations and demonstrate also the natural stability of the Flemish sandbanks.

6. ACKNOWLEDGMENT

The Management Unit of the Mathematical Model of the North Sea and the Scheldt Estuary (MUMM) provided ship time on board the R/V Belgica. The crew of R/V Belgica is thanked, for its flexibility and assistance during the campaigns.

3. REFERENCES

Bellec, V., Van Lancker, V., Degrendele, K., Roche, M. & Le Bot, S., 2010. Geo-environmental characterization of the Kwinte Bank. Journal of Coastal Research, SI, 51: 63-76.

Degrendele, K., Roche, M. and Schotte, P., 2002, Synthèse des données acquises de novembre 1999 à avril 2001 quant à l'incidence des extractions sur le Kwintebank, Rapport Fonds pour l'extraction de sable, Ministère des affaires économiques de Belgique.

Degrendele, K., Roche, M., Schotte, P., Van Lancker, V.R.M. & Bellec, V., 2010. Morphological evolution of the Kwinte Bank central depression before and after the cessation of aggregate extraction. Journal of coastal research, SI, 51: 77-86.

Van Lancker, V.R.M., Bonne, W., Garel, E., Degrendele, K., Roche, M., Van den Eynde, D., Bellec, V., Brière, C., Collins, M.B. & Velegrakis, A.F., 2010. Recommendations for the sustainable exploitation of tidal sandbanks. SI, 51: 151-164.

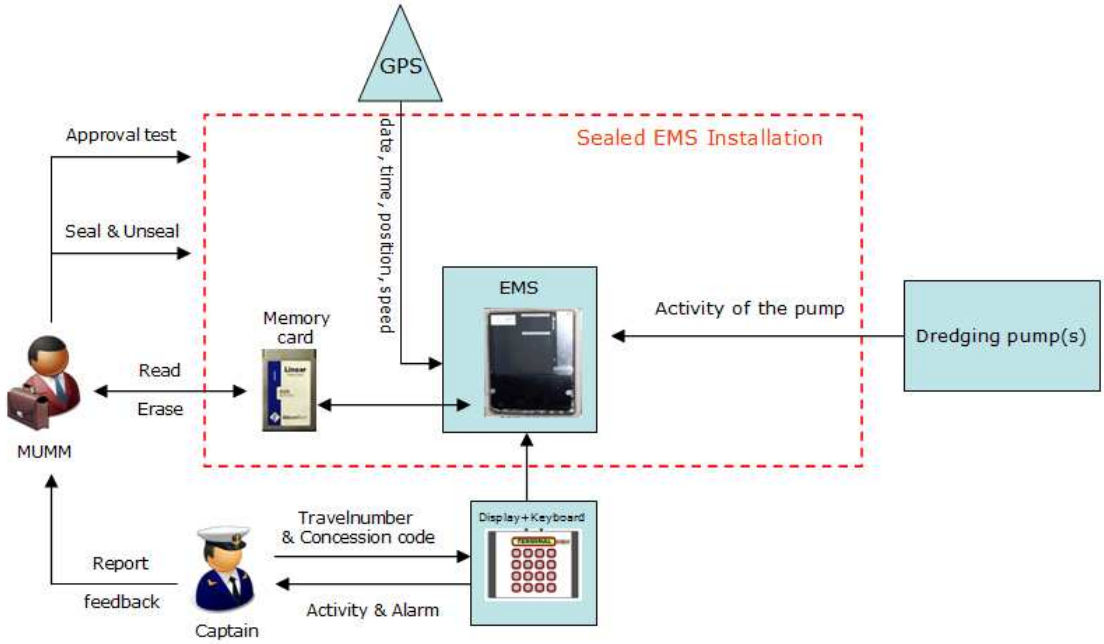

Figure 1: Electronic Monitoring Systems (EMS = "black-boxes").

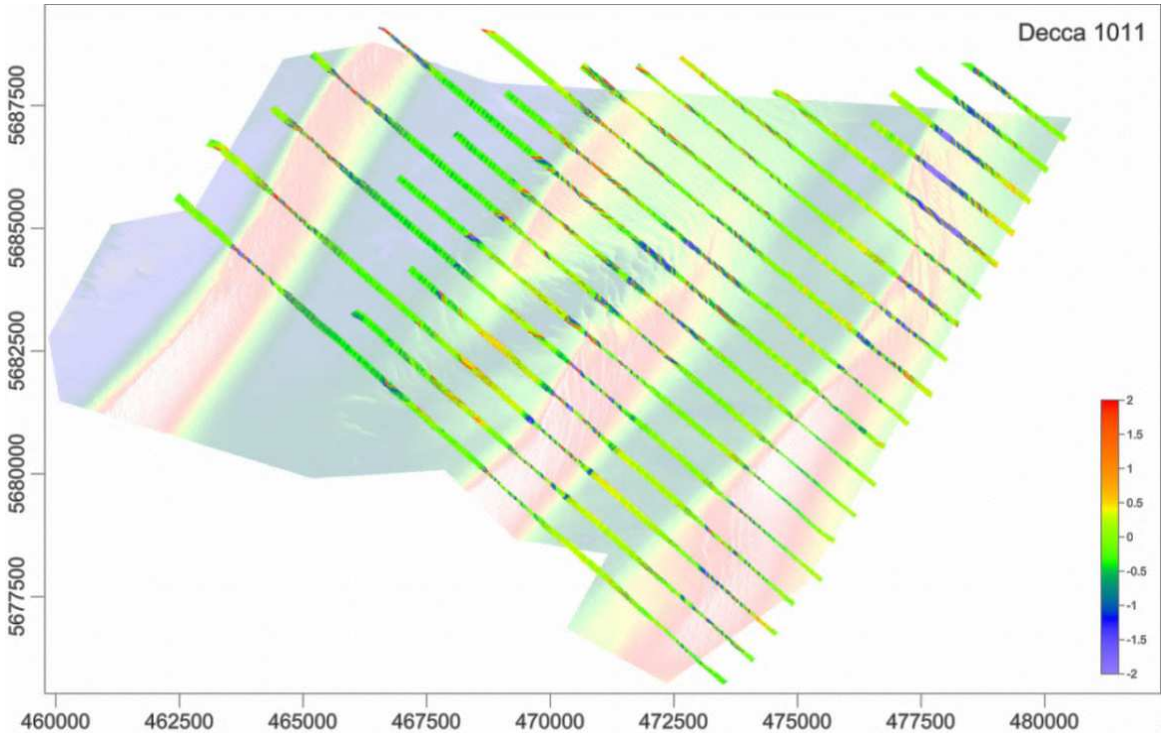

Figure 2. Overview of the MBES survey along the DECCA lines in zone 2, obtained during the Belgica 2010/11 campaign, showing the difference (scale bar in meters) with the reference model obtained in 2003 (background image). Orange to red colors indicate an increase in sediment while blue to purple colors indicate a decrease in amount of sediment. Green represents stable areas. Map coordinates are UTM zone 31N and in meter.

A

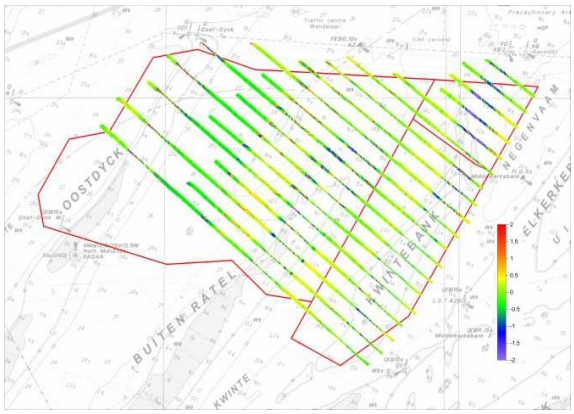

B

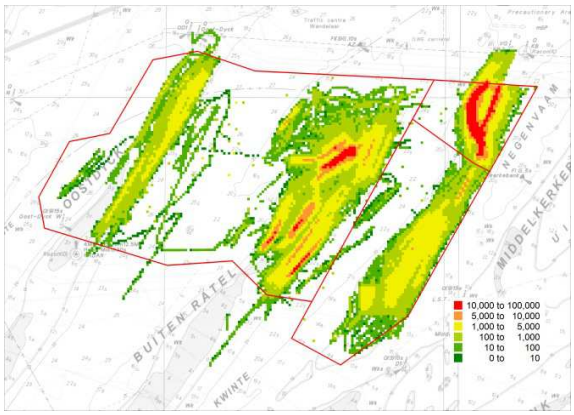

C

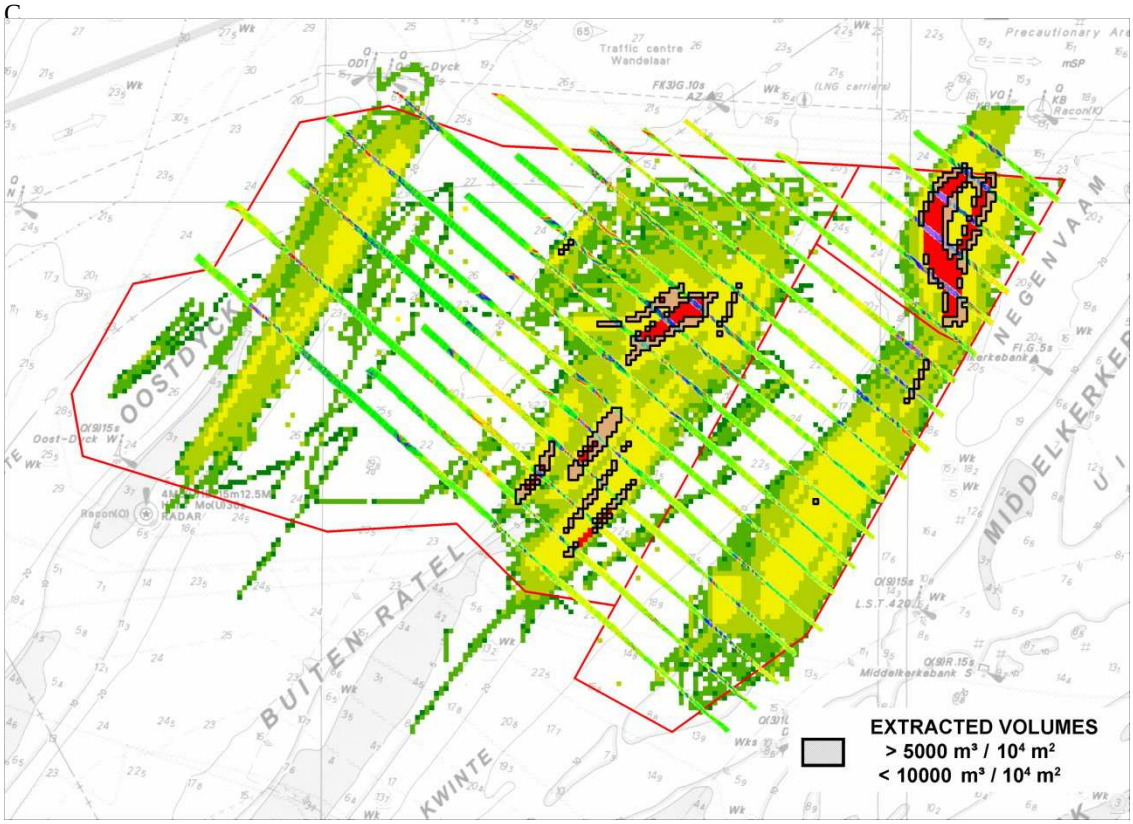

Figure 3 A, B and C: Analysis of the correlation between extracted volumes computed from the EMS data and bathymetric differences measured along the DECCA lines with the MBES; both datasets = same time interval.

A: Bathymetric difference measured with MBES along DECCA lines minus reference model 2003 (in m);

B: Extracted volume (m^3/ha or $m^3/10^4m^2$) from the EMS from 2003 to the MBES survey date;

C: Creation of a mask for a volumetric intervals (e.g. 5 10^3 m^3 < v < $10^4 m^3$); statistics of all grid cells inside the mask are computed for both layers A and B.

CAMPAIGN	VOLUME INTERVALS (10^3 m³/ha)	BATHYMETRIC DIFFERENCE DEDUCED FROM EMS			BATHYMETRIC DIFFERENCE BASED ON MBES MEASUREMENTS		
		mean	std	nb grid cells	mean	std	nb grid cells
C0810	0	0.00	0.00	16740	-0.13	0.41	613784
	>0 and ≤1	-0.02	0.02	6905	-0.13	0.65	415863
	>1 and ≤2	-0.14	0.03	748	-0.24	0.59	43122
	>2 and ≤3	-0.24	0.03	333	-0.31	0.53	21318
	>3 and ≤4	-0.35	0.03	187	-0.39	0.60	9888
	>4 and ≤5	-0.45	0.03	109	-0.61	0.69	8218
	>5 and ≤10	-0.68	0.14	186	-0.88	0.79	13323
	>10 and ≤15	-1.23	0.15	65	-1.31	0.86	3917
	>15 and ≤20	-1.72	0.14	44	-1.97	1.11	3440
	>20 and ≤25	-2.18	0.15	38	-2.66	1.22	3950
C0911	0	0.00	0.00	15768	0.04	0.39	730065
	>0 and ≤1	-0.02	0.02	7335	0.03	0.62	562207
	>1 and ≤2	-0.15	0.03	912	-0.10	0.62	74905
	>2 and ≤3	-0.24	0.03	534	-0.20	0.60	43640
	>3 and ≤4	-0.35	0.03	241	-0.24	0.68	21189
	>4 and ≤5	-0.44	0.03	133	-0.44	0.72	12528
	>5 and ≤10	-0.71	0.15	256	-0.67	0.83	25690
	>10 and ≤15	-1.22	0.15	70	-1.15	0.86	5832
	>15 and ≤20	-1.71	0.14	44	-1.97	1.21	4341
	>20 and ≤25	-2.18	0.15	38	-2.59	1.27	4898
C1011	0	0.00	0.00	15606	0.01	0.42	478146
	>0 and ≤1	-0.02	0.02	7225	0.00	0.64	398929
	>1 and ≤2	-0.14	0.03	978	-0.14	0.62	57576
	>2 and ≤3	-0.24	0.03	555	-0.22	0.56	32063
	>3 and ≤4	-0.34	0.03	284	-0.32	0.70	19013
	>4 and ≤5	-0.45	0.03	168	-0.40	0.80	14480
	>5 and ≤10	-0.70	0.14	318	-0.69	0.77	24003
	>10 and ≤15	-1.22	0.15	94	-1.06	0.87	6425
	>15 and ≤20	-1.72	0.15	59	-1.66	1.10	5186
	>20 and ≤25	-2.18	0.14	42	-2.59	1.30	4032
C1115	0	0.00	0.00	15547	-0.04	0.44	339484
	>0 and ≤1	-0.02	0.02	6734	-0.05	0.66	253207
	>1 and ≤2	-0.15	0.03	992	-0.18	0.65	37725
	>2 and ≤3	-0.25	0.03	606	-0.27	0.63	20526
	>3 and ≤4	-0.35	0.03	294	-0.34	0.68	11408
	>4 and ≤5	-0.45	0.03	186	-0.54	0.83	8810
	>5 and ≤10	-0.70	0.15	363	-0.76	0.83	17383
	>10 and ≤15	-1.21	0.14	142	-1.21	0.90	7621
	>15 and ≤20	-1.71	0.14	71	-2.09	1.27	3073
	>20 and ≤25	-2.21	0.15	57	-2.72	1.28	3880
	>25 and ≤30	-2.67	0.13	17	-1.62	1.23	460
C1213	0	0.00	0.00	15271	-0.03	0.45	308798
	>0 and ≤1	-0.02	0.02	6807	-0.04	0.66	255822
	>1 and ≤2	-0.15	0.03	918	-0.13	0.70	34954
	>2 and ≤3	-0.25	0.03	652	-0.29	0.66	24377
	>3 and ≤4	-0.35	0.03	390	-0.30	0.66	16603
	>4 and ≤5	-0.45	0.03	192	-0.46	0.83	8718
	>5 and ≤10	-0.70	0.14	394	-0.72	0.84	17948
	>10 and ≤15	-1.24	0.15	167	-1.04	0.84	8148
	>15 and ≤20	-1.70	0.13	99	-1.45	1.10	5212
	>20 and ≤25	-2.22	0.15	57	-2.23	1.29	3974
	>25 and ≤30	-2.68	0.12	28	-2.67	0.99	431
	>30	-3.64	0.47	38	-2.91	1.44	2042

Table 2: Correlation EMS - MBES measurements. Table of results per survey

	REGRESSION PARAMETERS			CORRELATION	
	Coefficient Y= a X	Standard Error	p-Value	Adjusted Squared Multiple R	Standard Error of Estimate
C0810	1.225	0.198	0.000	0.809	0.188
C0911	1.043	0.079	0.000	0.951	0.090
C1011	1.012	0.045	0.000	0.983	0.050
C1115	1.119	0.062	0.000	0.970	0.065
C1225	0.900	0.037	0.000	0.982	0.049
ALL DATA	1.035	0.041	0.000	0.925	0.103

Table 3: Results and statistics of weighted linear regressions without constant Y (MBES) = a X (EMS) Table of results per survey and for all the data together.

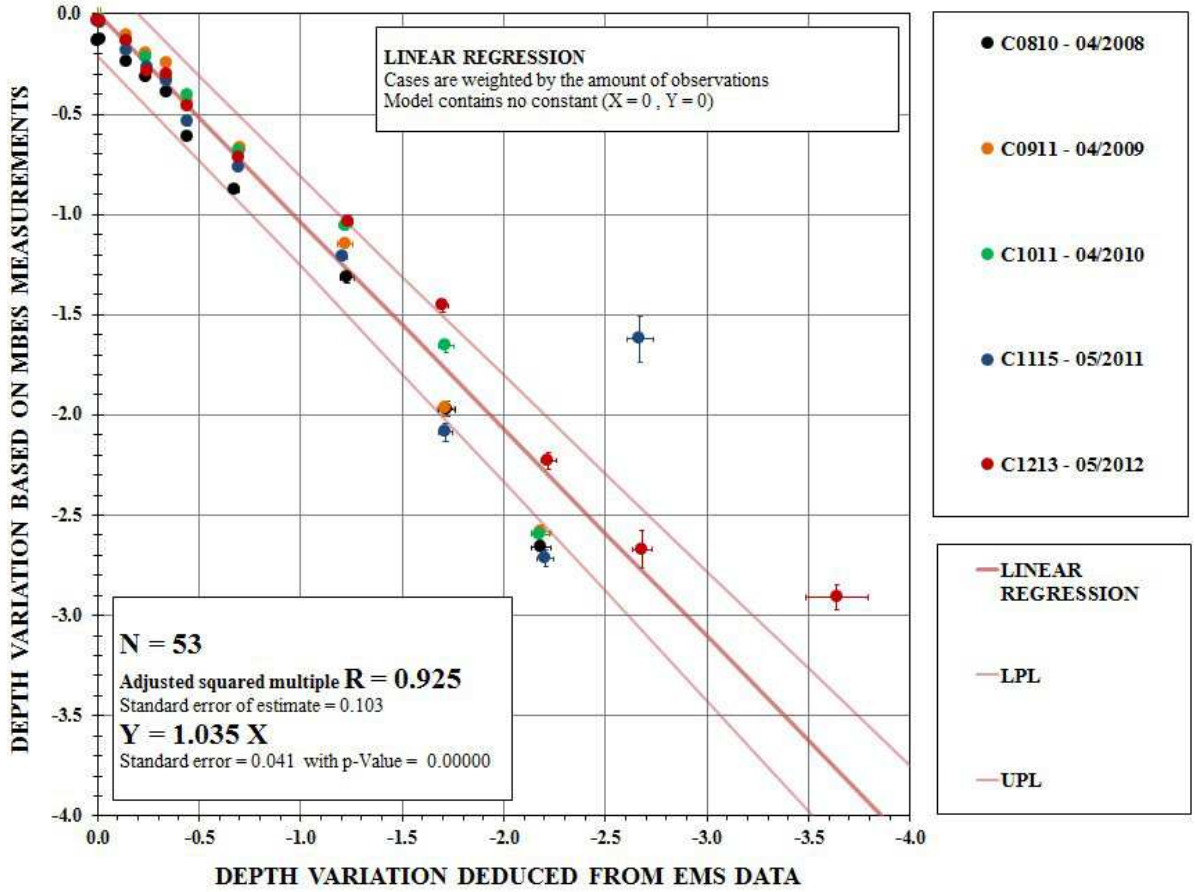

Figure 4: Plot of the bathymetric difference measured with the MBES *versus* the bathymetric difference deduced from EMS data; standard error of each measurement; weighted linear regression line without constant based on all the data together and related statistics.

Analysis of the behavior of sand waves at Boqueirão channel

Adriana Capelo Rodrigues [(1)], Lucas Martins Pion [(1)], Moysés Gonsalez Tessler [(2)] and José Carlos de Melo Bernardino[(1)]

1. FCTH, Fundação Centro Tecnológico de Hidráulica, Escola Politécnica da Universidade de São Paulo, Av. Pedroso de Morais, 1619 - cj 507/508, 05419-001. São Paulo, São Paulo, Brasil. E-mail: adriana.rodrigues@fcth.br

2. Instituto Oceanográfico da Universidade de São Paulo, Departamento de Oceanografia Física, Química e Geológica, Praça do Oceanográfico, 191, Cidade Universitária. 05508-900. São Paulo, São Paulo, Brasil

ABSTRACT

At Boqueirão channel, located at São Luís, state of Maranhão, Brazil, it is possible to observe bedforms denominated sandwaves, composed of non-cohesive sediments. These sediments are transported by strong ocean currents, which confer wave form to the ground. These bedforms are more than 10m long, reaching until hundred meters, and are higher than 0.75m (FENSTER et al., 1990). The tide is semidiurnal, with average amplitude about 4.6m. The amplitude can reach up to 7m on equinoctial syzygy. Current's main direction is N-S.

This study has been done with the objective of identifying patterns of sedimentary movements on the ground, to make viable the construction of a new pier in this area, with two berths. The study area was delimited to comprehend near the pier. Monthly bathymetries made on the study area from April/2011 to February/2012 were analyzed. The analysis was based on level surfaces and transversal and longitudinal profiles, apart from comparison surfaces and volumes variation between sequent months.

Analyzing the level surfaces, it is possible to visualize the characteristic form of sandwaves, elongate and which axis is perpendicular to the flow. The chosen area for the new pier coincides with the area of sandwave migration, complicating ship mooring.

On comparison surfaces between sequent months, it is possible to observe that, on most of months, the new pier area is where most sedimentary movement occurs, compared to the rest of study area. It is possible to notice sedimentary loss areas on the side of sedimentary gain areas, with the gain areas always on the north. These forms characterize the sandwave migration to north. On the rest of study area, it is possible to observe depth variations up to 2m.

The order of magnitude of volumetric variation observed trough sequent months on the study area is compatible with low average depth variation, about 20cm. However, the greatest variations are observed on the sandwave migration areas, where they can reach up to 10m, depending on the period. Besides, it is possible to notice that the monthly ground variation resultant tends to natural balance.

The longitudinal profiles indicate that there are two stability zones on the study area. The first is about 300m long and is located about 200m south to the new pier installation area. The second one is about 600m long and is located about 350m north to the new pier. This last one refers to the nearby of Cabeço do Mearim, a rock formation. Observing the transversal profiles, it is possible to notice the slope inclination on the proximities of the new pier area, which is about 1V:30H. The profiles also show the natural depths on the future berths area.

To reach and maintain the appropriate depth on the berths region (25m), implantation and maintenance dredging will be necessary. On the north berth, the situation is more critical, because depths are up to 7m over the appropriate.

REFERENCES

Fenster, M.S., Fitzgerald, D.M., Bohlen, W.F., Lewis, R.S. and Baldwin, T.: “Stability of giant sand waves in eastern Long Island Sound”, páginas 207-225, vol 91, Marine Geology, U.S.A., 1990.

Influence of dunes on alternate bar migration in a sandy gravel river: the Loire (France)

Stéphane Rodrigues[(1)], Nicolas Claude[(2)], Benjamin Gandubert[(1)], Coraline Wintenberger [(1)], Philippe Jugé[(3)] and Jean-Gabriel Bréhéret[(1)]

1. GéoHydrosystèmes COntinentaux, EA 6293 GéHCO, Université François Rabelais de Tours, Faculté Sci. et Tech. Parc de Grandmont, F-37200 Tours, France - srodrigues@univ-tours.fr
2. EDF – LNHE / laboratoire St Venant, 6 quai Watier, F-78401 Chatou, France
3. Cetu Elmis Ingénieries, Université François Rabelais de Tours, 11 quai Danton, F-37500 Chinon.

ABSTRACT

The control exerted by dunes on the formation and migration of alluvial bars has been identified on several large rivers. With only a few exceptions, none of the many field investigations carried out on dunes examined the influence of their migration on bar dynamics. The exceptions are studies by Ashworth et al. (2000) and Villard and Church (2005) who provided a comprehensive analysis of dune-bar. However, the interactions between dunes and alternate bars are seldom investigated. These macroforms consist in consecutive diagonal fronts with low slope riffles located upstream. Their spatial pattern varies from simple- to multiple-row configurations depending on the width-to-depth ratio of the channel.

In the downstream reaches of the River Loire (France), near the city of Nantes, several secondary channels allow the study of interactions between alternate bars and superimposed dunes since they are disconnected during low flows. In one of these channels, hydraulics, high frequency bathymetrical surveys and sedimentary sequences were analyzed to detail the influence of dune migration on the dynamics of five alternate bars during a 4-year flood event.

Bathymetrical surveys performed demonstrate that height and length of dunes varied according to a counterclockwise hysteresis. Although the height and length of dunes were higher during the falling limb of the hydrograph than during the rising limb, the evolution of these parameters was more important during the rising limb, specifically just before the flood peak. For these flow conditions, the increase in dunes length was significant while the increase in height was moderate. During the peak discharge, the height and length of dunes strongly increased on most of the bars while the morphological response of dunes to discharge variation differed according to the bar considered after the flood peak. Consequently, the average dune steepness was characterized by a clockwise hysteresis during the same flood event. The results show that the average steepness of the dunes is equal to 0.023. This value is low in comparison to the minimum value of steepness 0.06 commonly admitted for equilibrium dunes and can be attributed to a depth limitation. In terms of hydraulics, values of the roughness parameter (ks) proposed by Van Rijn (1984) increased on bars in the downstream direction during the flood peak. The lateral evolution of the height of dunes on each alternate bar was also analyzed. Bars located near a geometrical discontinuity of the channel banks show a strong correlation between the height of dunes and distance from the bank. In other words, the increase in dunes' height is more important for high flow depths located near the bank opposite to the bar. This can be attributed to the lateral variation of flow depth associated with the transverse slope of these bars. On the other bars (located in a straighter part of the channel) this trend was not observed. Due to high values of Shields mobility parameter, the sediments of the bars were easily reworked and a lateral spreading governed by a re-direction of dunes towards the inner part of the channel was observed after the

flood peak. This process also influences the sedimentary products associated with the bars (Rodrigues et al. 2012).
Results given are the basis of a conceptual model of alternate bars/dunes interactions for unsteady flow conditions in large sandy gravel rivers.

REFERENCES

Van Rijn L.C. 1984. Sediment transport, part I: bed load transport. Journal of Hydraulic Engineering 110 (10), 1431–1456.

Rodrigues S, Claude N, Jugé P, Bréheret J.G. 2012. An opportunity to connect the morphodynamics of alternate bars with their sedimentary products. Earth Surface Processes and Landforms 37, 240–248

Influence of time- and depth-dependent eddy viscosity on the formation of tidal sandwaves

P. C. Roos[(1)], H. M. Schuttelaars[(2)]

1. Water Engineering and Management, University of Twente, Enschede, Netherlands – p.c.roos@utwente.nl
2. Delft Institute of Applied Mathematics, Delft University of Technology, Delft, Netherlands – h.m.schuttelaars@tudelft.nl

Abstract

Existing model studies on sandwave dynamics point to the importance of turbulence, and particularly its temporal and spatial structure. We present an idealized model of sandwave formation, in which turbulence is accounted for by adopting a time- and depth-dependent eddy viscosity. Following linear stability analysis, the basic and perturbed flow solutions are obtained using a spectral method involving eigenfunctions that simplify the vertical stress term. First model results show favourable convergence properties of the basic state, expressing the generation of higher harmonics due to the time-dependent eddy viscosity. The perturbed state, which requires further investigation in detail, reveals large flow gradients close to the bed.

1. INTRODUCTION

1.1. Tidal sandwaves

Tidal sandwaves are dynamic bed forms observed in tide-dominated shallow seas, characterized by wavelengths of hundreds of meters, heights of several meters and migration rates up to tens of meters per year. Sandwaves may pose a hazard to navigation and the safety of pipelines and wind farms. Understanding sandwave dynamics thus helps improving/optimizing the design and maintenance of pipelines and wind farms, the dredging operations in approach channels and the survey strategies for nautical charting.

1.2. Sandwave modelling

Tidal sandwaves have been explained as an inherent instability of a flat seabed subject to tidal motion (Hulscher 1996). Wave-like bottom undulations perturb the water motion such that vertical residual circulation cells are formed with a near-bed flow directed from trough to crest. If sufficiently strong to overcome gravity, this flow transports sediment from trough to crest, thus causing the undulation to grow. This formation process was described by a linear stability analysis, which produces growth rates as a function of the topographic wave number k and orientation with respect to the tidal current. Instability is expressed by the occurrence of positive growth rates, the maximum of the growth curve defines the so-called fastest growing mode. Hulscher (1996) considered symmetric tidal forcing, a schematized turbulence model (constant and uniform vertical eddy viscosity with partial slip at the bed) and bed load transport. Later on, this model was extended to explain sandwave migration due to residual currents and overtides in the forcing (Németh et al. 2002, Besio et al. 2004), role of higher harmonics in the perturbed flow (Gerkema 2000, Besio et al. 2003a) and the representation of turbulence and suspended load transport (Blondeaux & Vittori 2005ab). Although the characteristics of the fastest growing mode generally agree with observations from e.g. the North Sea, these linear models suffer from two shortcomings: (*i*) their validity is restricted to small amplitudes and (*ii*) they fail to

suppress the growth of 'ultra-long' sandwaves (near $k = 0$).
The first shortcoming, actually a restriction of linear stability analyses in general, has inspired the development of nonlinear models. (e.g., Németh et al. 2007, Sterlini et al. 2009). These models describe sandwave evolution towards equilibrium, but the modelled equilibrium heights exceed those observed in the field. Furthermore, simulations of patterns with multiple sandwaves (on a spatially periodic domain) ultimately develop into a single feature with a wavelength equal to the length of the computational domain. This is physically unrealistic and probably related to the second shortcoming, i.e. the failure of suppressing ultra-long sandwaves.

1.3. Turbulence representation

Resolving this problem requires a closer investigation of the representation of turbulence and sediment transport. Komarova & Hulscher (2000) showed that adopting a time-dependent eddy viscosity of a particular form helps to suppress the growth of very long sandwaves. They considered bed load transport and continued to use the schematized turbulence model with a uniform eddy viscosity and partial slip at the bed. Although computationally appealing (basic flow analytically available), it involves a slip parameter that is hard to quantify and an unknown thickness of the constant-stress layer tacitly excluded from the water column. Blondeaux & Vittori (2005ab) avoided these drawbacks by adopting Dean's (1974) eddy viscosity profile combined with a no-slip condition at the bed. They assumed a time-independent eddy viscosity as their focus was on the inclusion of suspended load rather than the behaviour near $k = 0$ (which still showed positive growth rates). Recent numerical simulations of sand wave formation carried out with a k-epsilon model by Borsje et al. (2011) reveal both the depth- and time-dependency in the vertical eddy viscosity A_v. The profiles are nearly parabolic, whereas the M4 component of A_v is about half the residual component, with an almost identical parabolic vertical shape and a phase that is nearly constant over the water column. Borsje et al. (2011) found negative growth rates near $k = 0$, which was attributed to suspended load transport. Because of the different approaches, it is hard to interpret the conclusions from Komarova & Hulscher (2000), Blondeaux & Vittori (2005ab) and Borsje et al. (2011) in a unified manner.

1.4. Goal

The main goal of this study is to develop a new modelling framework that allows us to systematically investigate the implications of the (combined and separate) depth- and time-dependencies of the eddy viscosity on sand wave formation. Since numerical simulations are not suitable for such a task (time-consuming and difficult to analyse), we adopt an idealized modelling approach following a linear stability analysis. Since incorporating a k-epsilon model is unfeasible, we seek a parameterization of the key features of the eddy viscosity as found in the numerical simulations above (Borsje et al. 2011). This structure, parabolic in the vertical and with a significant M4-component, is further supported by the literature on estuarine hydrodynamics (McGregor 1972, Ianniello 1977). Our parameterization of the eddy viscosity allows for a spectral solution method, expressing the flow solution as a superposition of analytically obtained vertical profiles. This provides a computationally attractive alternative to the finite difference schemes used in other studies mentioned above. The innovation of our study is therefore twofold: (*i*) the inclusion of time-dependency in a depth-dependent vertical eddy viscosity representation in an idealized sandwave model, (*ii*) the use of a spectral solution method regarding the vertical structure of the flow.

2. MODEL FORMULATION

2.1. Hydrodynamic conservation laws

Consider tidal flow of angular frequency ω and typical depth-averaged flow velocity amplitude U in an offshore region of a shallow shelf sea, far away from coastal boundaries. The mean water depth H is of the order of tens of meters. Let $\mathbf{u} = (u,w)$ denote the flow velocity vector with components u and w in the (horizontal) x-direction and in the (vertical) z-direction, respectively. Ignoring rotation, we assume uniformity and zero flow in the y-direction. The free surface elevation is located at $z = \zeta$ around the still water level $z = 0$. The seabed is located at $z = -H + \eta$, where $\eta(x)$ represents the topographic undulations. These undulations are characterized by a bed amplitude h

that is small with respect to the water depth and a topographic length scale $L = 2\pi/k$ of about 10^2-10^3 m, i.e. well below the tidal wavelength.
Next, we assume hydrostatic pressure ($H \ll L$) and adopt the eddy viscosity concept as turbulence closure. Conservation of momentum and mass is then expressed by the 2DV (two-dimensional vertical) shallow water equations:

$$u_t + u\,u_x + w\,u_z = -g\,\zeta_x + A_h u_{xx} + [A_v N(\check{z}) b(\omega t) u_z]_z, \qquad (1)$$

$$u_x + w_z = 0. \qquad (2)$$

Here, subscripted coordinates denote derivatives, g is the gravitational acceleration. The horizontal kinematic eddy viscosity, with typical magnitude A_h (in $m^2\ s^{-1}$), is assumed constant in time and space. Alternatively, the vertical kinematic eddy viscosity is written as the product of a dimensional reference value A_v (in $m^2\ s^{-1}$) and two dimensionless order one functions $N(\check{z})$ and $b(\omega t)$, which separately account for the vertical and temporal variations. This representation allows us to impose the eddy viscosity as obtained with the recent numerical model results of sandwave formation (Borsje et al. 2011).

2.2. Vertical eddy viscosity representation

Following McGregor (1972) and Ianniello (1977), we propose a parabolic profile of the vertical eddy viscosity (Figure 1), given by

$$N(\check{z}) = 1 - [\beta(\check{z}+\delta)]^2, \qquad (3)$$

with $\beta = (1 - R)^{1/2}/(1 - \delta)$. Equation (3) is a function of a re-scaled vertical coordinate $\check{z} = z/(H - \eta)$, ranging from -1 at the bed to 0 at the free surface. As shown in figure 1, N attains a small value R ($0 < R < 1$) at the bed (at $\check{z} = -1$) and reaches a maximum of unity near mid-depth (at $\check{z} = -\delta$ with $0 < \delta < 1$). Positive N-values everywhere in the water column are warranted by requiring $N(0) = 1 - \beta^2\delta^2 > 0$, which is equivalent to the constraint $\delta^{-1} > 1+(1-R)^{1/2}$. Default values used throughout this study are $R = 0.01$ and $\delta = 0.5$. Importantly, the dependency of $\check{z}$ on $\eta(x)$ implies that, in the case of a non-horizontal bed, the viscosity also depends on the horizontal coordinate x.

The temporal structure of the eddy viscosity is represented as a truncated Fourier series according to

$$b(\omega t) = \Sigma_p B_p \exp(ip\omega t), \qquad (4)$$

with the summation ranging from $p = -P$ to P (with truncation number P) and complex coefficients B_p, contained in a column vector $\mathbf{B} = (B_{-P},\ldots,B_P)^T$ and satisfying $B_{-p} = B_p^*$ because $b(\omega t)$ is real (an asterisk denoting complex conjugation).

2.3. Boundary conditions and forcing

Regarding boundary conditions, we require zero perpendicular flow and no stress at the free surface as well as no slip at the bed. This implies $u_z = w = 0$ at $z = 0$ and $u = w = 0$ at $z = -H + \eta$, where we have adopted a rigid-lid approach, by which the upper boundary of the computational domain is set at $z = 0$ (rather than $z = \zeta$).
Recalling that k is the topographic wave number, we consider a spatial domain of length $L = 2\pi/k$ with spatially periodic boundary conditions. Finally, the problem is forced by a prescribed time-periodic pressure gradient. More precisely, the spatial average of the pressure gradient $g\zeta_x$ in equation (1) is prescribed. We adopt parameter values that are typical for sand wave regions in the North Sea. The dimensional vertical eddy viscosity magnitude is calculated from $A_v = c_d HU$ (Bowden et al. 1959), with drag coefficient $c_d = 2.5\times10^{-3}$.

2.4. Sediment transport and bed evolution

Finally, the bed evolves as a result of the divergence of the bed load sediment flux, which is modelled as a simple power law of the bed shear stress, supplemented with a bed slope correction. Defining the volumetric bed shear stress according to

$$\tau_b = A_v\,R\,b(\omega t)\,u_z \qquad \text{at } z = -H + \eta, \qquad (5)$$

we thus write

$$(1-\varepsilon_{por})\,\eta_t + [\,\alpha|\tau_b|^\gamma(\tau_b/|\tau_b| - \mu\,\eta_x)\,]_x = 0. \qquad (6)$$

Here, ε_{por} is the bed porosity (dimensionless). The term in square brackets is the bed load sediment flux, which contains three constants: a proportionality coefficient α (dimension $m^{2-2\gamma}\ s^{2\gamma-1}$), a dimensionless transport power $\gamma \sim 3/2$ and a

dimensionless (yet non-scaled) bed slope correction coefficient μ.

2.5. Scaling and linear stability analysis

Without reporting the details, we proceed by performing a scaling procedure. We thus reformulate our model in terms of dimensionless unknowns, and identify a set of dimensionless key parameters. Furthermore, it provides a justification of the so-called *quasi-stationary approach*, which allows us to consider the seabed fixed while solving the hydrodynamic problem. The seabed thus effectively evolves as a result of the tidally averaged divergence of the sediment flux. We therefore distinguish a 'fast' hydrodynamic time coordinate t (within tidal cycle) and a 'slow' morphodynamic time coordinate τ for the bed evolution (in the order of years).

Following the principles of a linear stability analysis, we then consider the bed profile as a small perturbation of a horizontal bed, i.e.

$$\eta = a(\tau) \cos kx \,, \qquad (7)$$

with a time-dependent bed amplitude $a(\tau)$ that is small with respect to the water depth. Defining $\varepsilon = a_{init}/H \ll 1$, we now expand the solution in powers of ε. This is symbolically represented as

$$\Psi = \Psi_0 + \varepsilon \Psi_1 + \text{h.o.t.}, \qquad (8)$$

where the vector Ψ contains (the dimensionless counterparts of) the flow velocity components, the free surface (gradient) and the sediment flux (higher order terms denoted by h.o.t.). Importantly, we must also expand the vertical structure of the eddy viscosity in powers of ε according to $N = N_0 + \varepsilon N_1 +$ h.o.t..

We subsequently solve for the basic state Ψ_0 and the perturbed state Ψ_1. In doing so, analogous to equation (4), we expand the temporal structure of the unknowns as a truncated Fourier series in time, where – for the flow components u and w – the associated complex coefficients are functions of the vertical coordinate z. The next step is to resolve the vertical structure of these quantities.

2.6. Superposition of vertical profiles

Essential and novel in our solution method is the fact that we express the horizontal flow velocity components as a superposition of vertical profiles for which the vertical stress term (the one in square brackets in equation (1)) simplifies considerably. These are:

- A finite number of *eigenfunctions* $\phi_m(\check{z})$, with corresponding eigenvalue λ_m, which satisfy $[N_0 \phi_{m,z}]_z + \lambda_m \phi_m = 0$, as well as $\phi_{m,z}(0) = \phi_m(-1) = 0$. These eigenfunctions, which form a complete set, can be expressed in terms of Legendre functions (e.g., Abramowitz & Stegun 1964; see Figure 2a).
- A so-called *residual flow's shape function* $\phi_{res}(\check{z})$, which satisfies $[N_0 \phi_{res,z}]_z = 1$ and $\phi_{res,z}(0) = \phi_{res}(-1) = 0$.
- A *constant function* $\phi_{bed}(\check{z}) = 1$, which (trivially) satisfies $[N_0 \phi_{bed,z}]_z = 0$ and $\phi_{bed,z}(0) = \phi_{bed}(-1) = 0$.

The inclusion of f_{res} and f_{bed} helps to improve the convergence properties of our method. With the aid of equation (2), the vertical flow velocity components are expressed as a superposition of the vertical integrals of the above profiles, denoted by Φ_m, Φ_{res} and Φ_{bed} (see Figure 2b). This implies that our flow solution exactly satisfies continuity in the entire water column. For sake of brevity, further details of the solution method to find Ψ_0 and Ψ_1 are omitted.

3. RESULTS

Simulations with our model indicate spectral convergence of our solution regarding the basic state, i.e. the flow over the flat bed. They also show the generation of higher harmonics due to the time-dependency in the vertical eddy viscosity. For example, if forced by an M2 pressure gradient, the time-varying eddy viscosity generates higher harmonics in the flow solution of the basic state. In classical stability models, this only occurs in the perturbed state as the result of the advective interaction (i.e., the terms $u_0\, u_{1,x}$ and $w_1\, u_{0,z}$ in the first order momentum equations) between the basic and the perturbed flow.

First results from the perturbed state, and hence the growth rates, which have not yet been investigated in detail for small R-values, display large flow gradients near the bed.

4. CONCLUSIONS

We have presented a new modelling framework that allows us to systematically investigate the implications of the (combined and separate) depth- and time-dependencies of the eddy viscosity on sand wave formation. Key features are the spectral method, that allows us to express the flow solution as a superposition of eigenfunctions and other vertical profiles.
First simulations with our model indicate favourable convergence properties (regarding basic state). The results from the perturbed state, and hence the growth rates, have not yet been investigated in detail.
Our simulations further show that in the near-bed region (where the eddy viscosity becomes small), the vertical flow gradients of the perturbed flow become very large. This is as expected, yet should be kept in mind when interpreting results from finite-difference numerical models with usually only a limited number of vertical grid points ('sigma-layers'). Finally, future extensions of our model may include the incorporation of suspended load, which is likely to require a different set of eigenfunctions.

5. REFERENCES

Abramowitz, M. & Stegun, I. A. 1964 Handbook of Mathematical Functions with Formulas, Graphs, and Mathematical Tables, 9th edn. New York: Dover.

Besio, G., Blondeaux, P., Brocchini, M. & Vittori, G. 2004 On the modeling of sand wave migration. J. Geophys. Res. 109, C04018.

Besio, G., Blondeaux, P. & Frisina, P. 2003 A note on tidally generated sand waves. J. Fluid Mech. 485, 171–190.

Blondeaux, P. & Vittori, G. 2005a Flow and sediment transport induced by tide propagation: 1. The flat bottom case. J. Geophys. Res. 110, C07020.

Blondeaux, P. & Vittori, G. 2005b Flow and sediment transport induced by tide propagation: 2. The wavy bottom case. J. Geophys. Res. 110, C08003.

Borsje, B. W., Roos, P. C., Kranenburg, W. M. & Hulscher, S. J. M. H. 2011 Modeling sand- wave formation in a numerical shallow water model. In RCEM 2011, 7th IAHR symposium on River, Coastal and Estuarine Morphodynamics, Beijing, China. (eds X Shao, Z Wang & G Wang). IAHR.

Bowden, K. F., Fairbairn, L. A. & Hughes, P. 1959 The distribution of shearing stresses in a tidal current. Geophys. J. R. Astr. Soc. 2, 288–305.

Dean, R. D. 1974 Aero report. Tech. Rep. 74-11. Imperial College, London.

Dodd, N., Blondeaux, P., Calvete, D., de Swart, H. E., Falqués, A., Hulscher, S. J. M. H., Rozynski, G. & Vittori, G. 2003 Understanding coastal morphodynamics using stability methods. J. Coast. Res. 19 (4), 839–865.

Gerkema, T. 2000 A linear stability analysis of tidally generated sand waves. J. Fluid Mech. 417, 303–322.

Hulscher, S. J. M. H. 1996 Tidal induced large-scale regular bed form patterns in a three-dimensional shallow water model. J. Geophys. Res. 101 (C9), 20,727–20,744.

Ianniello, J. P. 1977 Tidally induced residual currents in estuaries of constant breadth and depth. J. Mar. Res. 35, 755–786.

Komarova, N. L. & Hulscher, S. J. M. H. 2000 Linear instability mechanism for sand wave formation. J. Fluid Mech. 413, 219–246.

McGregor, R. C. 1972 The influence of eddy viscosity on the vertical distribution of velocity in the tidal estuary. Geophys. J. R. Astr. Soc. 29, 103–108.

Németh, A. A., Hulscher, S. J. M. H. & van Damme, R. M. J. 2007 Modelling offshore sandwave evolution. Cont. Shelf Res. 27 (5), 713–728.

Németh, A. A., Hulscher, S. J. M. H. & de Vriend, H. J. 2002 Modelling sand wave migration in shallow shelf seas. Cont. Shelf Res. 22 (18–19), 2795–2806.

Sterlini, F. M., Hulscher, S. J. M. H. & Hanes, D. M. 2009 Simulating and understanding sand wave variation: A case study of the Golden Gate sand waves. J. Geophys. Res. 114, F02007.

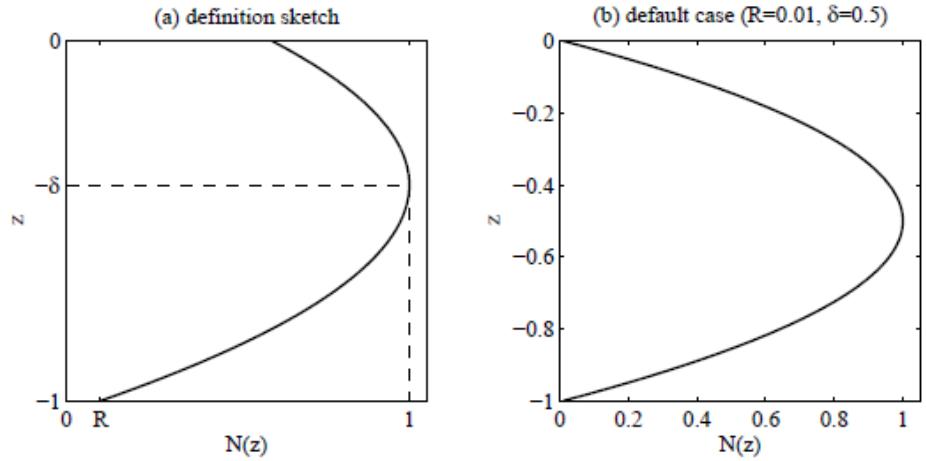

Figure 1. Parabolic viscosity profile *N(ž)* according to equation (3): (a) general definition sketch showing the bottom value *R* and a maximum of unity at $\check{z} = -\delta$, (b) default case with $R = 0.01$ and $\delta = 0.5$.

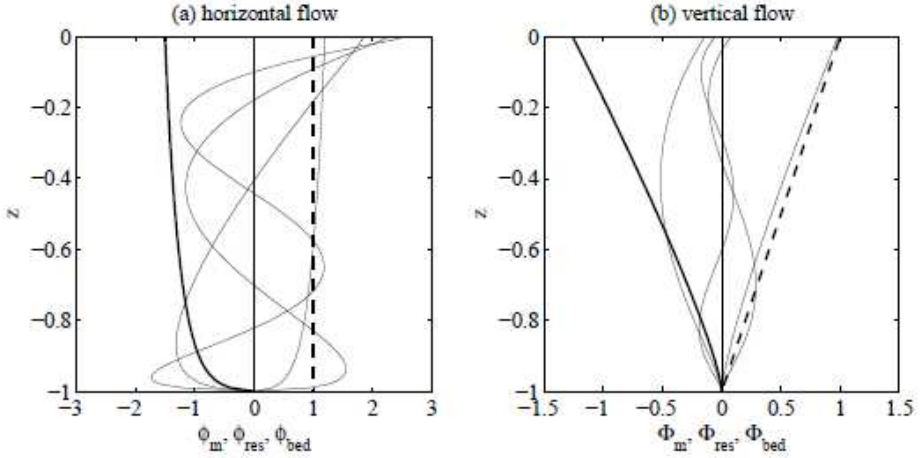

Figure 2. Overview of the functions used in the horizontal and vertical flow solution, respectively: (a) eigenfunctions Φ_m (thin lines, $m = 1,2,3,4$), residual flow's shape function Φ_{res} (thick line) and constant function Φ_{bed}; (b) integrated eigenfunctions Φ_m (thin lines, $m = 1,2,3,4$) and integrated shape functions , Φ_{res} (thick solid line) and Φ_{bed} (thick dashed line). Parameter values $R = 0.01$, $\delta = 0.5$.

Hydrodynamic modeling over a sand wave field at São Marcos Bay, Brazil

L. Samaritano[(1)], F.M. Chagas[(1)], J.C.M. Bernardino[(1)], E. Siegle[(2)], M. G. Tessler[(2)], S. Uemura[(1)]

1. FCTH, Fundação Centro Tecnológico de Hidráulica da Escola Politécnica da Universidade de São Paulo, Avenida Pedroso de Morais, 1619 - cj 507/508, 05419-001, São Paulo, Brasil. - leonardo.samaritano@fcth.br
2. IOUSP, Instituto Oceanográfico da Universidade de São Paulo, Departamento de Oceanografia Física, Praça do Oceanográfico, 191, Cidade Universitária, 05508-900, São Paulo, Brasil.

.

Abstract

Sand wave studies indicate that flow patterns and local hydrodynamic regime are essential elements to determinate orientation, asymmetry, height and migration of subaqueous features. The goal of this work is to characterize the small scale hydrodynamics that control sediment transport at São Marcos Bay, along Ponta da Madeira Port Complex, at São Luís (Maranhão state, NE Brazil). Numerical modeling was based on bathymetric campaigns, topographic data, sediment samples and 4 velocity ADCP monitoring stations along east margin of the bay. Tidal levels reach 7.0 m high, 3.5 m being the mean value and 6.0 m the mean high water level, producing overall ebb dominated strong currents that reach up to 3 m/s on ebb spring tides. Neap currents are weaker and reach 1.9 m/s and 2.0 m/s on flood and ebb tides, respectively. Local morphology determinates the occurrence of intense gyres, which allied to absolute sediment availability, dominate by fine sand, allows 0.5 m to 6.0 m sand waves height development.

1. INTRODUCTION

Hydrodynamic structures, sediment transport patterns and bottom features migration are the subjects of innumerous studies to better understand the evolution of rhythmic features at coastal areas around the world (e.g. Allen, 1968; Allen & Collinson, 1974). Bartholomä et al. (2008) indicates various studies with two-three dimension morphodynamic models as tools to assess bed evolution at tide dominated regions (e.g. Hulscher, 1996; Nemeth et al., 2007; Soulsby & Damgaard, 2005).

Bottom features generated by currents are frequently denominated as subaqueous dunes or sand waves (Bartholdy et al. 2002), while some authors restrict the former to features generated by tide-forced flows. Linear stability analysis (Gerkema, 2000) enforced this denomination, indicating that relevant differences are observed between features formed under tide conditions to the ones from stationary flows.

Shape, asymmetry, height and migration of sand waves provide important information about sediment dynamics and orientation of bottom transport in estuaries and coastal channels. Barnard (2012) indicates that flow structure, regional sediment transport regimes, boundary conditions and the residual hydrodynamic patterns can be described through the cited variables (e.g. Langhorne, 1982; Belderson et al., 1982; Kubo et al., 2004).

To characterize the morphodynamic behavior of sand waves, Flemming (2000) indicates that water column thickness, critical shear velocity and thus sediment granulometry are limiting factors to bottom features growth in shallow waters. Considering this, maximum potential heights tend

to occur at the presence of relative coarser sediments and intense flows, showing the importance of hydrodynamic mapping at sand waves regions. Recent study of Barnard et al. (2011) characterized the dynamics end evolution of subaqueous features at San Francisco Bay (USA) through wave parameters calculation and numerical modeling. Computational simulations described small scale bed dynamics, reinforcing the idea that modern echo sound systems allied to numerical models raise the potential to predict migration on coastal sand wave fields.

Model results generated the hypothesis that sediment transport gradients control migration patterns. Changes on tidal phases and bathymetric features also define the direction of subaqueous dunes migration.

Activities that can potentially influence the hydrodynamics of these systems, such as mineral resources exploitation, beach nourishment, aggregate mining, dredging, navigation and port operations depend on the knowledge about sedimentary budget and transport directions, making sand waves to exercise a fundamental role in this relation.

The main goal of this study is to assess the small scale hydrodynamics that control sediment transport at São Marcos Bay, along Ponta da Madeira Port Complex (São Luís, Maranhão state, Brazil), through numerical experiments of the estuarine channel hydrodynamics.

2. STUDY AREA

Ponta da Madeira Port Complex (PDM) represents one of the greatest exportation sectors of the world in terms of cargo shipping (Amaral, 2010). It is located at the coast of São Luís city, capital of the northern Brazilian state of Maranhão, representing a natural exportation corridor of the geoeconomic important region of the Oriental Amazon (Amazônia Oriental).

At the eastern margin of São Marcos Bay, where PDM helds its port operations, shallow sandbanks are formed next to the navigation route. The sand waves assessed in this study are located in this important socioeconomic area (Fig. 1).

Despite of its great environmental relevance, there are few scientific studies available about sediment processes in São Marcos Bay. Local tide regime is characterized by semidiurnal frequency and macrotidal heights, reaching 7 m in equinox periods. Spring tide amplitudes observed may generate strong currents (Pereira & Harari, 1995), reaching up to 3 m/s in the main channels of the bay.

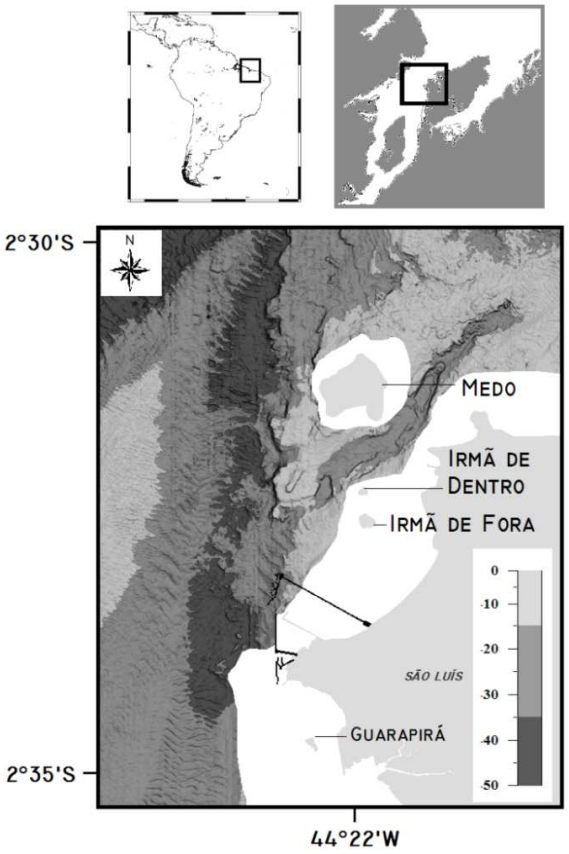

Figure 1. Hill-shaded bathymety map of the study area, indicating the locations of Medo, Irmãs and Guarapirá Islands at São Luís city, adjacent to the east margin of São Marcos Bay.

Climatology of Maranhão state indicates two distinct stations and the important influence of the trade wind system. Rainy season in the region is from January to June, while dryer periods occur from August to December, according to the Brazilian National Institute of Meteorology (INMET).

Superficial sediments are composed by sand, covering the entire subaqueous dunes area. The dominant fraction is composed by fine to very fine sand (> 90%).

3. NUMERICAL MODELING

The applied numerical model is the hydrodynamic (HD) module of the MIKE 3 software (DHI Water & Environment). It simulates unsteady three-dimensional flows, taking into account density variations, bathymetry, tidal elevations, currents and river fluxes.

3.1 Field data

Field data set used in this study was collected from March 2011 to June 2012. Temporal series are composed by flow intensity and direction, water level, conventional and multi-beam bathymetry. Additional information of local depths and sediments at non-measured areas was taken from nautical charts of the Brazilian Navy (DHN).

Velocity data was registered each 15 minutes through the water column, divided by cells of 0.5 meters, with an Acoustic Doppler Current Profiler (ADCP) which has 600 KHz of frequency. Large mooring structures have been used to avoid burial or damage to the instruments.

Five observation points were monitored with ADCPs, distributed in two regions adjacent to PDM. Points identified as P16, P17, P18, P19 and 15H (Fig. 2) have been considered in this study.

Bathymetric surveys have been carried out from November 2011 to June 2012. The tide gauge is recording since October 2011, at a five minutes frequency. 55 superficial sediment samples have been collected with a Van Veen sampler.

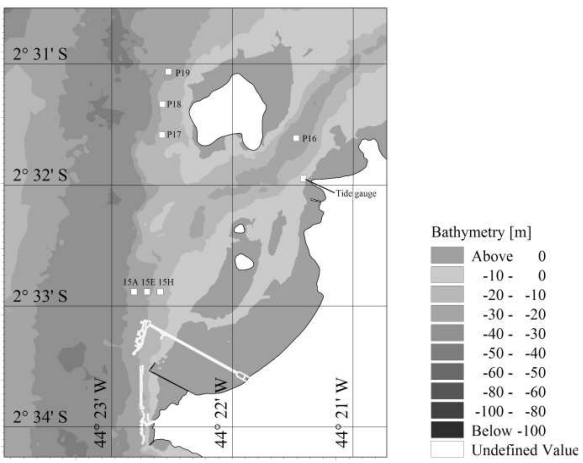

Figure 2. Location of the current monitoring points investigated with acoustic doppler current profiler.

3.1 Model calibration

Comparison between modeled results and field data has been done at four velocity observation points (P16 to P19) and tide levels were compared at the tide gauge location.

Statistical parameters have been applied to evaluate the model adjustment to in situ data. Relative Mean Absolute Error (RMAE) and Adjusted Relative Mean Absolute Error (ARMAE) parameters (Table 1 - van Rijn et al, 2003) provided a quantitative assessment of the modeled outputs.

Table 1. Qualification of agreement between field and modeled data through RMAE (Relative Mean Absolute Error) and ARMAE (Adjusted Relative Mean Absolute Error).

Classification	RMAE	ARMAE
Excelent	< 0.1	< 0.2
Good	0.1 – 0.3	0.2 – 0.4
Reasonable/fair	0.3 – 0.5	0.4 – 0.7
Poor	0.5 – 0.7	0.7 – 1.0
Bad	> 0.7	> 0.2

3.3 Numerical parameters

The present study consists of an application of the hydrodynamic module of MIKE 3 software. It simulates flow conditions descretizing momentum equations at a flexible mesh, using finite volume method.

Variables are determinated in the central points of each element of the numerical mesh through semi-implicite time differencing. As bidimensional flows occur, typical of macrotidal areas, density stratification influence has been neglected, thus only barotropic effect have been taken into account in the modeling process.

Mesh elements have variable resolution, ranging from 900 m far from the area of interest to 30 m next to PDM. Figure 3 presents the numerical mesh for the entire model domain. Bed resistance varied at the model domain proportionally to depth values.

Open ocean boundary condition consisted of amplitude and phase information obtained from a gauge station located near PDM, maintained by the Brazilian Navy. Two southwestern river

boundaries were set up with constant discharges and lateral boundaries were closed considering null normal velocity. Wetting and drying were applied on the intertidal zone to adequately represent water inflow to the bay, simulating periodic changes at surface water level and its effects in the area of interest.

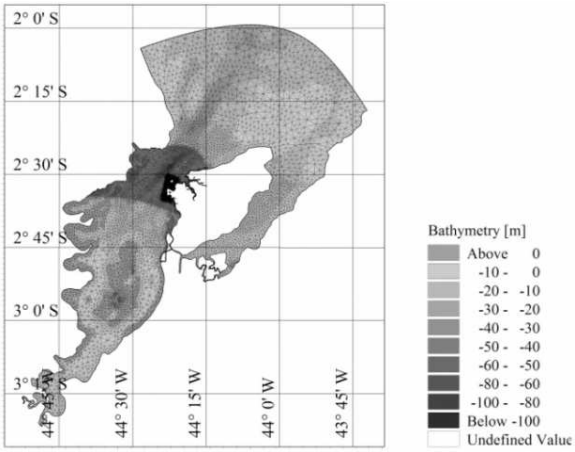

Figure 3. Computational mesh and bathymetry of the hydrodynamic model domain.

Open ocean boundary condition consisted of amplitude and phase information obtained from a gauge station located near PDM, maintained by the Brazilian Navy. Two southwestern river boundaries were set up with constant discharges and lateral boundaries were closed considering null normal velocity. Wetting and drying was considered on the intertidal zone to adequately represent water inflow to the bay, simulating periodic changes at surface water level and its effects in the area of interest.

Horizontal viscosity was considered constant (0.28) and its effect calculated following Smagorinski formula. Vertical viscosity was variable (0.4 m^2/s to $1.8x10^{-6}$ m^2/s) following the logarithmic law.

Final output results were obtained after a series of simulations, varying input data to assess the model sensitivity and output quality.

4. RESULTS AND DISCUSSION

Field data and model output analysis have been used to properly assess the hydrodynamics of São Marcos Bay.

4.1 Measured velocities

Intensity and direction of ADCP data have been processed to obtain temporal series of velocity at the observation points. Tide level reached 6.3 m at the period considered in this study (Fig. 4), where diurnal inequalities and high amplitudes, even at neap tides, can be observed.

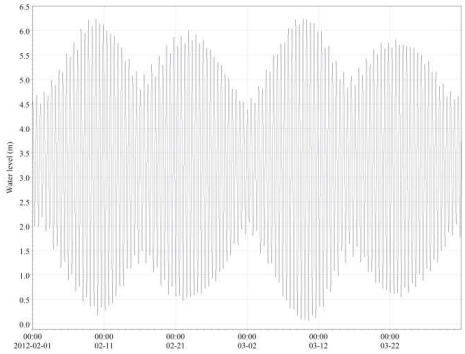

Figure 4. Water level time series registered in the coastal tide gauge.

Figure 5 presents real field data, measured at the points used to calibrate the model in terms of depth-averaged velocity.

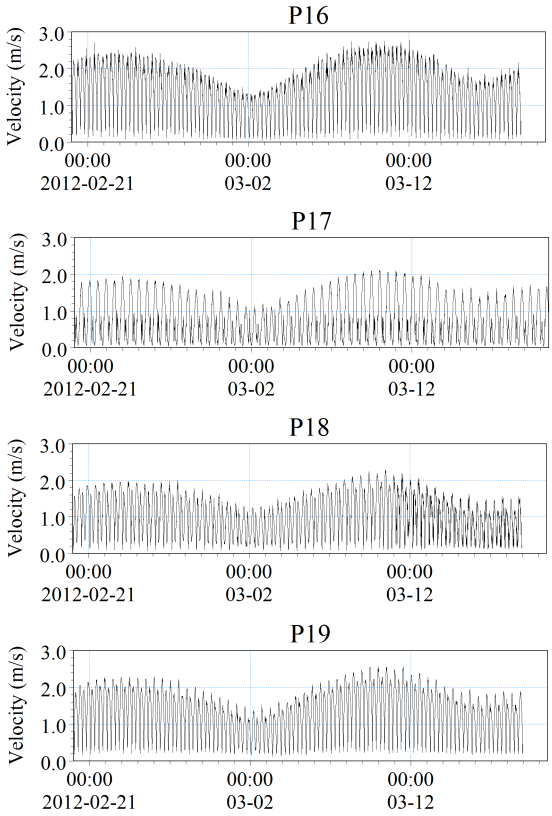

Figure 5. Depth-averaged velocity measured at the observation points P16, P17, P18 and P19.

Maximum flow intensity values are of up to 2.75 m/s at the observed sites, while to southeastern direction these values decrease. In terms of comparison, maximum intensities at point 15H are of 1,86 m/s, showing that the center channel of São Marcos Bay presents higher velocities. Jetties along the east coast of the bay are certainly influencing this hydrodynamic pattern and, consequently, sand waves migration in this area.

Different intensities are observed between ebb and flood tides, where the latter is dominant near the margin. In some areas, such as point P17, ebb currents are much stronger and may double the flood currents. River discharge system and the presence of Medo Island probably act decreasing flood currents that are only forced by periodic changes of water level.

4.2 Model calibration

Sensitivity analysis of the model has been done through changes in key parameters such as bed resistance, time step, mesh element size, horizontal and vertical viscosity.

Comparison of the model and field data through RMAE and ARMAE shows the statistic calculation, assessed at the points P16, P17, P18 and P19 (Tab. 2).

Table 2. Statistical classification of model calibration. U indicates the east-west velocity component and V indicates the north-south velocity component. Mod is the resulting vector.

	P16	**P17**			
	U	V	Mod	U	V
RMAE	0.6	0.6	0.4	1	0.6
ARMAE	0.6	0.6	0.4	0.2	0.6

	P18	**P19**			
	U	V	Mod	U	V
RMAE	0.8	0.5	0.4	0.5	0.5
ARMAE	0.6	0.5	0.3	0.4	0.4

Statistical parameters RMAE and ARMAE show good to fair agreement between model results and field data. The numerical model can be considered well calibrated, mainly near Medo Island, thus able to help in the better understanding of the flood and ebb currents that flow above sand waves next to the eastern margin of the bay.

A comparison between modeled and measured flow velocity time series at four observation points are shown in Figure 6, showing the overall good agreement in the compared series.

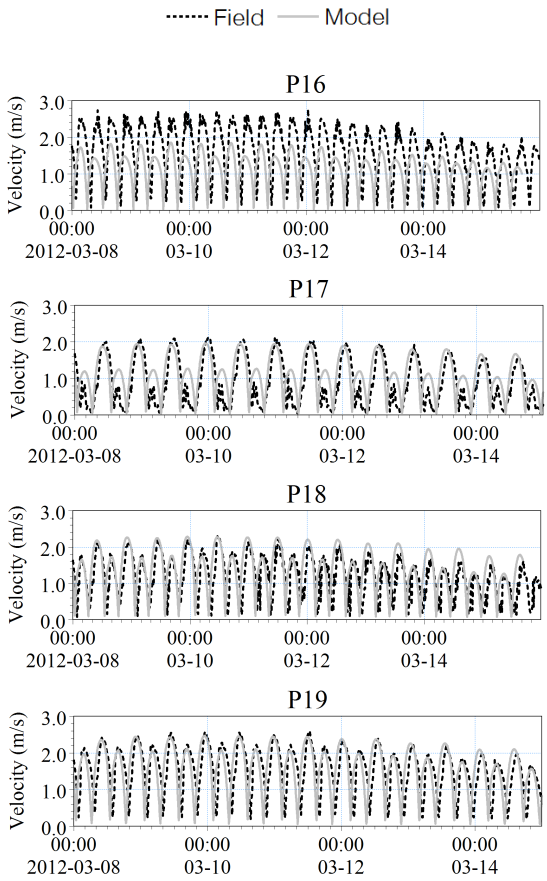

Figure 6. Comparison between modeled results (continuous line) and field data (dashed line).

4.3 Currents vector field

Numerical simulations are an important tool to better understand the overall hydrodynamic process that control sand wave fields, mainly in macrotidal areas. In this study, 6.0 m height tides were simulated generating strong currents that reach up to 3.0 m/s in spring tides. Neap velocities are weaker, although reaching up to 1.9 m/s and 2.0 m/s at flood and ebb tides, respectively.

Regions adjacent to the jetties present intermittent gyres and recirculation forms between the small embayment formed by Irmãs Islands and the harbor structures (Fig. 7).

These specific gyres migrate, weakening and strengthening along the year due to changes in tidal currents. As important hydrodynamic features these fluxes play an essential role on the migration of sand waves, mainly to the north at areas where ebb flux dominate (center channel of Sao Marcos Bay) and to the south where flood currents are stronger, as in the Boqueirão Channel between Medo Island and Irmã de Fora Island.

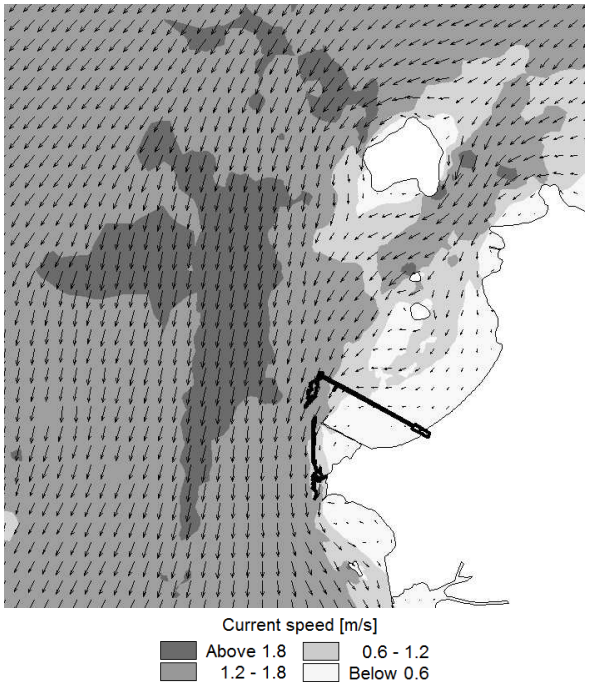

Figure 7. Typical maximum flood currents at São Marcos Bay.

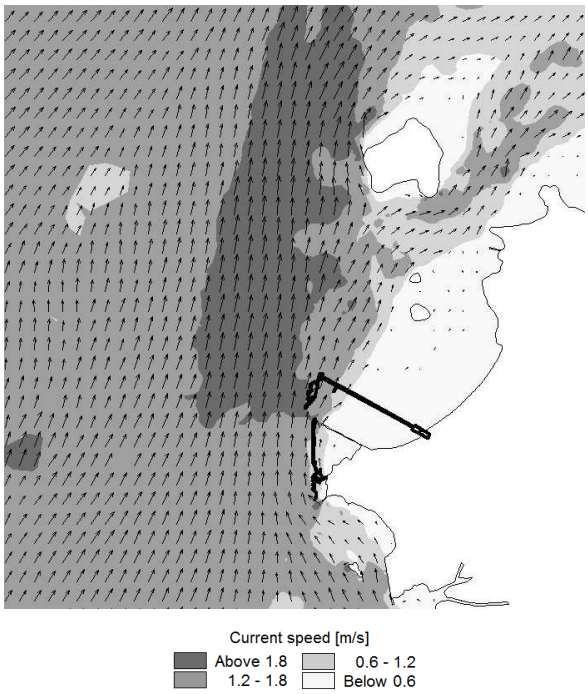

Figure 8 . Typical maximum ebb currents at São Marcos Bay.

5. CONCLUSIONS

Field data analysis and hydrodynamic modeling experiments provide essential information to build up the knowledge about sand waves migration at São Marcos Bay. As indicated in previous studies, tidal forcings are the main hydrodynamic controls in the estuary, where intense currents observed at the numerical model reached 3.0 m/s during spring tides.

Simulations show interesting features near the coast, which are characterized by gyres and recirculation patterns between Irmãs Islands and the port structures. East margin geomorphology and jetties control the development of circular flows.

These important dynamic features play an essential role to the systems residual bottom movement, as indicated by the vector fields. The transport is mainly to the north at ebb dominated flows, for instance at the center channel of Sao Marcos Bay, and to the south where flood currents are stronger, as at the Boqueirão Channel between Medo Island and Irmã de Fora Island.

The gyres move along the year due to tidal variations, thus the understanding of long time sand waves migration is extremely dependent on the residual flows present in the bay. Currents are also sufficient to transport the local sediment as bed and suspended load, influencing greatly the formation, amalgamation and dissipation of sand waves.

6. ACKNOWLEDGMENTS

The authors thank VALE S.A company for the partnership on our studies at São Marcos Bay and for providing part of the data set used in this study.

7. REFERENCES

Allen, J. R. L. 1968. Current Ripples. North Holland Publishers Company Amsterdam: 433 pp.

Allen, J. R. L.; Collinson, J.D. 1974. The superimposition and classification of dunes formed by unidirectional aqueous flows. Sed. Geol. 12: 169-178.

Amaral, R.F.; Alfredini, P. 2010. Modelação hidrossedimentológica no Canal de Acesso do Complexo Portuário do Maranhão. Revista Brasileira de Recursos Hídricos, v. 15, p. 5-14.

Barnard, P.L.; Erikson, L.H.; Kvitek, R.G. 2011. Small-scale sediment transport patterns and bedform morphodynamics: new insights from high-resolution multibeam bathymetry. Geo-Mar Lett. 31 (4),227-236.

Barnard, P.L.; Hanes, D.M.; Erikson, L.H.; Rubin, D.M.; Dartnell, P.; Kvitek, R.G. 2012. Analyzing bedforms mapped using multibeam sonar to determine regional bedload sediment transport patterns in the San Francisco Bay coastal system. In: Li, M., Sherwood, C., and Hill, P. (Eds.), International Association of Sedimentologists Sp. Pub., 33 pp.

Bartholdy J, Bartholomae A. and B.W. Flemming 2002. Grainsize control of large compound flow-transverse bedforms in a tidal inlet of the Danish Wadden Sea. Mar. Geol. 188: 391–413

Bartholomä A, Schrottke K, Winter C, 2008. Sand wave dynamics: Surfing between assumptions and facts. In: Parsons, D., T. Garlan and J. Best (eds) Marine and River Dune Dynamics, p. 17-24

Belderson, R.H.; Johnson, M.A.; Kenyon, N.H. 1982. Bedforms. In: Stride AH (ed) Offshore tidal sands, processes and deposits. Chapman and Hall, London, pp 27–57

Flemming, B.W. 2000. The role of grain size, water depth and flow velocity as scaling factors controlling the size of subaqueous dunes. In: Trentesaux, A. and Garlan, T. (Eds) Marine sandwave dynamics. International Workshop, March 23-24 2000), University of Lille I, France. Proceedings, 55-60.

Gerkema, T., 2000. A linear stability analysis of tidally generated sand waves. J. Fluid Mech. 417, 303-322.

Hulscher, S. J. M. H. 1996. Tidal-induced large-scale regular bed form patterns in a three dimensional shallow water model. J. Geophys. Res. 101(9):20,727-744.

Kubo, Y.; Soh., W.; Machiyama, H.; Tokuyama, H. 2004. Bedforms produced by the Kuroshio Current passing over the northern Izu Ridge. Geo-Mar Lett. 24(1):1–7.

Langhorne, D.N. 1982. A study of the dynamics of a marine sandwave. Sedimentology. 29:571–594.

Nemeth, A. A.; Hulscher, S. J. M. H.; Van Damme, R. M. J. 2007. Modelling offshore sand wave evolution. Cont. Shelf Res. 27(5), 713-728.

Pereira, J.E.R. & Harari, J. 1995. Modelo numérico tri-dimensional linear da plataforma continental do Estado do Maranhão. Bol. Inst. Oceanogr., 43(1):11-26.

Soulsby, R.L. and Damgaard, J.S. 2005. Bedload sediment transport in coastal waters. Coast. Eng. 52 (8): 673-689.

van Rijn, L.C., Walstra, D.J.R., Grasmeijer, B., Sutherland, J., Pand, S., & Sierra, J.P., 2003. The predictability of cross-shore bed evolution of sandy beaches at the time scale of storms and seasons using process-based Profile models. Coast. Eng. 47, 295-337

Analysis of coherent flow structures over alluvial dunes revealed by multi-beam echo-sounder acoustic backscatter

S.M. Simmons[(1)], D.R. Parsons[(1)], J.L. Best[(2)], O. Orfeo[(3)], J.A. Czuba[(4)], J.A. Boldt[(5)], K.A. Oberg[(5)]

1. Department of Geography, Environment and Earth Sciences, University of Hull, Hull, HU6 7RX, UK. s.simmons@hull.ac.uk; d.parsons@hull.ac.uk.
2. Departments of Geology, Geography and Geographic Information Science, Mechanical Science and Engineering and Ven Te Chow Hydrosystems Laboratory, University of Illinois at Urbana-Champaign, 1301 W. Green St., Urbana, IL, 61801, USA. jimbest@illinois.edu
3. CECOAL-CONICET, Corrientes, Argentina. oscar_orfeo@hotmail.com
4. U.S. Geological Survey, Tacoma, Washington, USA. jon.czuba@gmail.com
5. U.S. Geological Survey, Urbana, Illinois, USA. jboldt@usgs.gov; kaoberg@usgs.gov

Abstract

Large-scale coherent flow structures, or macroturbulence, produced by alluvial sand dunes are reasoned to dominate the flow field and result in significant transport of suspended bed sediment. Macroturbulence, and its interaction with the free flow surface, is also thought to influence the creation and maintenance of the dune bed morphology. Recent physical and numerical modelling has demonstrated the structure and origin of such turbulence, and field data obtained along vertical profiles using acoustic Doppler current profilers have also recently enabled a quantification of such turbulence from within natural channels. We have recently developed a novel method, based upon acoustic backscatter from multibeam echo sounding systems, which allows for the simultaneous quantification of suspended sediment dynamics and estimates of flow velocity (see Simmons et al., 2010; Best et al., 2010). This paper presents a full application of this new technique to data collected over dune bedforms in two large rivers: the Rio Paraná and the Mississippi River. An analysis of the mean velocity components and turbulence intensity across the flow field and the quadrant analysis of the flow structures, together with a description of the temporal length scales revealed by wavelet analysis, are presented. These field results are compared with recent numerical modelling of coherent macroturbulence over dune-covered beds, allowing verification of our conceptual models of these key features of many river flows.

1. INTRODUCTION

Simultaneously quantifying, at sufficiently high resolutions, the interactions between turbulent flow, sediment transport and bed morphology has long been known to be key to improved understanding of the morphodynamics of bedforms. Recent advances in Multibeam Sonar (MBES) technology, which allow recording of the full water column acoustic backscatter data, have opened up this possibility (Simmons et al., 2010; Best et al., 2010). The theory relating the acoustic backscatter to sediment concentrations and flow velocities has been well developed and employed over the course of the last two decades (see Thorne and Hanes, 2002). Combining these theoretical and technological advances, Simmons et al. (2010) and Best et al. (2010) were able to advance a methodology based upon MBES that permitted quantification of the suspended sediment concentration and velocity vectors across the two-dimensional MBES swath fan, enabling the simultaneous measurement of these related sediment transport parameters across the flow field above a dune field in a large alluvial river.

2. FIELD SITES AND METHODS

The results presented herein were derived from data collected at two field locations: the Mississippi River near the confluence with the Missouri River, USA (38°48'N, 90°7'W) and the Rio Paraná near the confluence with the Rio Paraguay, Argentina (27°18'S, 58°35'E). Data were collected at both locations using a RESON 7125 SeaBat 396 kHz MBES deployed on a survey

vessel that was moored at a single stationary location over the lee-side of a low-angled sand dune in the Mississippi and at three separate stationary locations along the streamwise axis of a sand dune in the Rio Paraná.

The MBES was mounted with the acoustic interrogation swath aligned parallel to the streamwise flow, enabling the two-dimensional imaging of the development of turbulence-related suspensions of sediment in the streamwise direction. Data were collected over 256 acoustic beams at the Mississippi site and 512 beams at the Paraná site, both over a swath of 128° with an acoustic frequency of 398 kHz and with a sample-spacing of ~2.1 cm. The MBES ping collection rate was set to 10Hz for the Mississippi and 30Hz for the Paraná. The distance to the river bed at the field sites locations varied between ~6.8 to ~9.0 m.

Figure 1 shows the raw acoustic magnitude data for a single ping at Paraná Position 3 (furthest downstream). The strong acoustic reflection from the bed can be seen bisecting the swath approximately horizontally at *c.* 8 m depth below the transducers. The areas of the water-column near to the bed on both sides of the swath are dominated by an acoustic artifact known as sidelobe interference. The region of study herein is therefore the sector bounded by the arc of the nearest distance to the bed that is free from such interference. Suspended sediment bursts are discernible within this volume, advecting with streamwise flow from left to right. It should be noted that suspended sediment backscatter is a relatively weak signal and the data in the image has been clipped to a maximum of 2500 MBES counts to enhance the contrast with the strong bed echoes.

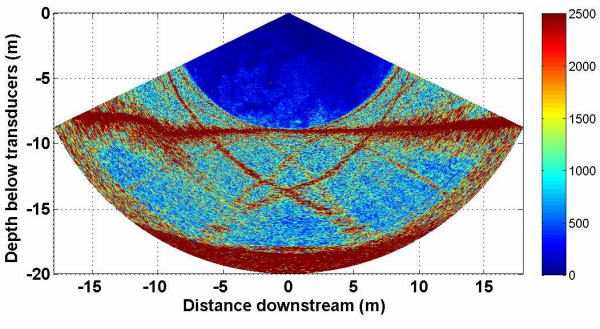

Figure 1. Raw data from a single ping obtained over the lee of a sand dune in the Paraná (Position 3).

The results presented herein were derived from flow field vectors obtained by using a method of comparing the mean quadratic difference (MQD) between two-dimensional areas of consecutive pings. The magnitude data were first adjusted for acoustic propagation losses and averaged over a local area to account for the random nature of acoustic backscatter from small particles. Details of the flow field velocity method are fully described by Best et al. (2010) and the spatial averaging and conversion to suspended sediment concentration by Simmons et al. (2010). In short, data were corrected for acoustic propagation losses, averaged with a circular spatial filter of radius 6.5cm and interpolated to Cartesian co-ordinates on a rectangular grid (cell size 2.5 x 2.5 cm) to allow the MQD between area windows in consecutive pings to be calculated. The flow field vectors were allocated to the position at the centre of the window in the first ping, with the streamwise and vertical velocity vector determined by considering the distance to the centre of the window with the lowest MQD in the next ping and the delay between the two pings. The MBES system at the Mississippi site recorded at a ping rate consistent with the set parameter of 10Hz; however the system used at the Paraná site recorded at a variable ping rate with delays between 0.03 - 0.5 s (typical mean of ~ 0.12 s) as the system lacked sufficient processing power to write the large quantities of data to the hard disk at the set ping rate parameter of 30Hz.

3. RESULTS AND DISCUSSION

3.1. Flow field time series analysis

The Mississippi data consists of a single recording over a period of 600 s. The mean flow field streamwise (u) and vertical (w) components of velocity for the entire period are displayed in Figure 2. u increases with height above the bed, rising to ~1.7 ms^{-1} high in the water column, and w decreases from ~0 - 0.01 ms^{-1}. The area shown is not as extensive as the full sector to the bed (transducer-to-bed range is 6.85 m) as the method is less accurate near the area boundaries where the window size decreases. Data were screened above a MQD quality threshold, although some artifacts can be seen near the boundaries, e.g. the far right-hand side of the w component. Figure 3 shows u

and *w* along the vertical profile directly below the transducers.

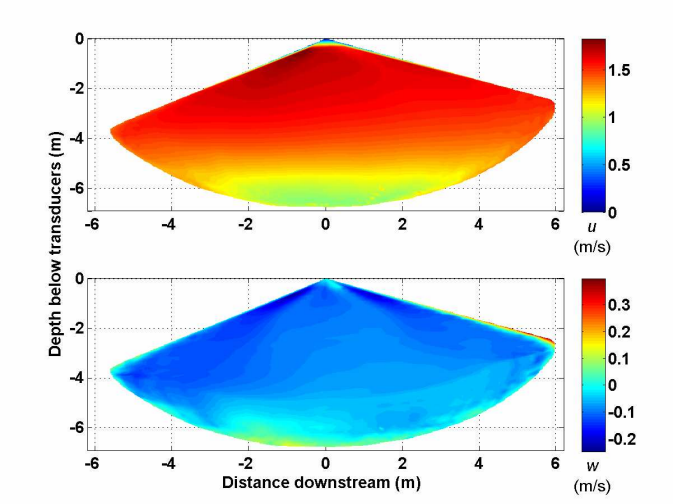

Figure 2. Mean *u* (top) and *w* (bottom) velocities across the analysis area of the multibeam swath at the Mississippi site.

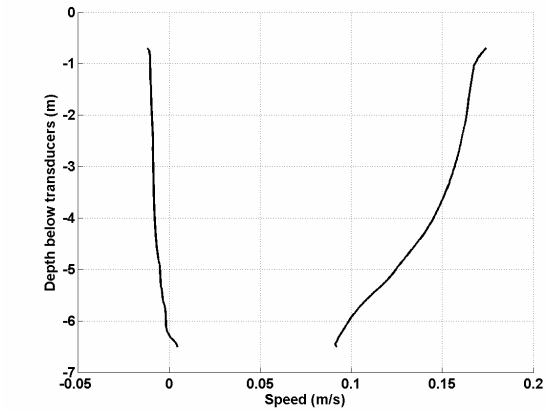

Figure 3. Mean vertical profile of *u* (right) and *w* (left) derived from the time series for the vertical profile beneath the MBES transducers at the Mississippi site.

Figures 4 & 5 display the time series for *u* & *w* respectively for three single points in the vertical profile below the transducers at heights above the bed, *z*, of 0.75, 0.5 and 0.25 of the flow depth, *h*. The RMS of the deviatoric components of velocity increase, with turbulence intensity, towards the bed: 1.37 cms^{-1} (*u*, 0.75 *z*/*h*), 1.59 cms^{-1} (*u*, 0.5 *z*/*h*), 2.21 cms^{-1} (*u*, 0.25 *z*/*h*) , 0.56 cms^{-1} (*w*, 0.75 *z*/*h*), 0.65 cms^{-1} (*w*, 0.5 *z*/*h*), 1.24 cms^{-1} (*w*, 0.25 *z*/*h*). Quadrant analysis has been previously utilized to discriminate turbulent events in the boundary layer (e.g. Lu and Willmarth, 1973; Bennett and Best, 1995). Four quadrants are defined for deviations from the mean: Quadrant 1 (positive *u* & *w*), Quadrant 2 (negative *u*, positive *w*), Quadrant 3 (negative *u* & *w*) and Quadrant 4 (positive *u*, negative *w*).

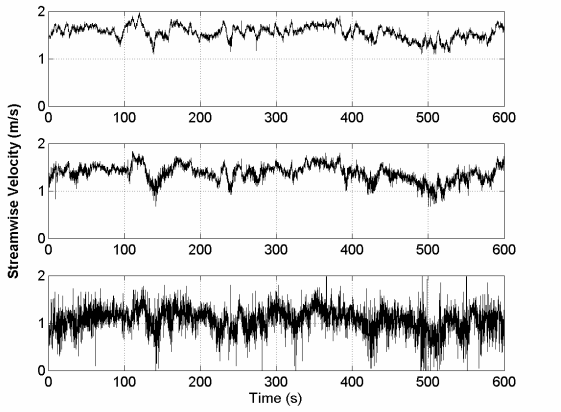

Figure 4. Time series of U at 0.25 *z*/*h* (bottom), 0.5 *z*/*h* (middle), 0.75 *z*/*h* (top) at the Mississippi site.

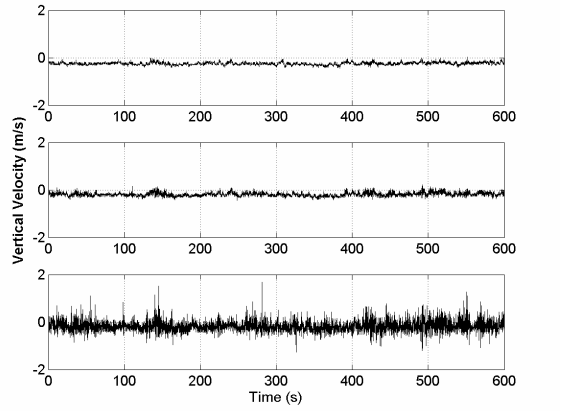

Figure 5. Time series of *w* at 0.25 *z*/*h* (bottom), 0.5 *z*/*h* (middle), 0.75 *z*/*h* (top) at the Mississippi site.

Figure 6 shows the result of quadrant analysis applied to the vertical profile below the MBES, showing the frequency of occurrence beyond a 'hole' size of one standard deviation. The results show how Q1 and Q3 events dominate lower in the water column, but that Q2 and Q4 events dominate away from the bed. Wavelet analysis was also applied to the time series shown in Figures 4 & 5 to examine how the scales of variability evolved temporally and spatially as a function of time. Wavelet analysis produces power values for a range of frequencies and a set of locations in time, and has been previously applied for the analysis of turbulence (e.g., Farge, 1992). The Morlet wavelet

was applied to derive the results shown in Figures 7 & 8 for the *u* and *w* components respectively at the three heights above the bed. Distinct frequencies are apparent in both of the wavelet power spectra, with coherence between the streamwise and vertical components. Both spectra also show a trend of the filtering of higher frequencies with distance from the bed. Distinct clustering of events is also apparent in the time series, which is likely produced by shear layer flapping and vortex shedding.

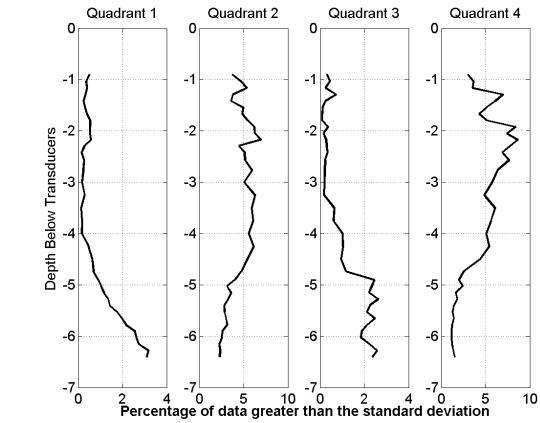

Figure 6. Quadrant analysis of the time series for the vertical profile beneath the MBES transducers at the Mississippi site.

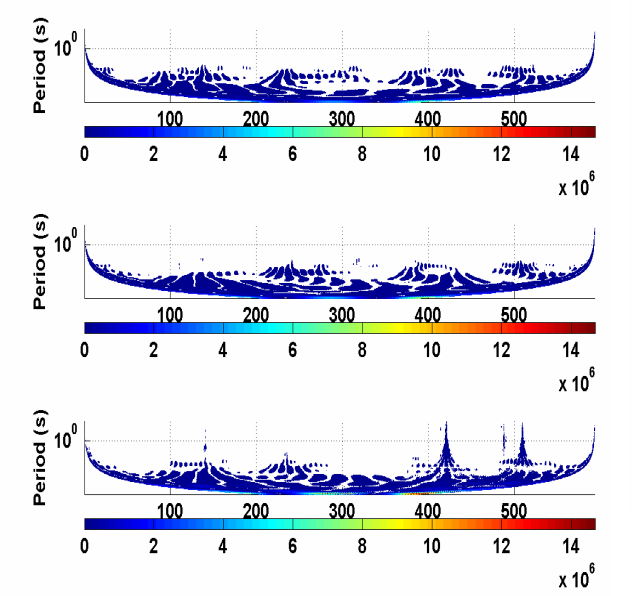

Figure 7. Wavelet analysis of the *u* time series for 0.75 *z*/*h* (top), 0.5 *z*/*h* (middle), 0.25 *z*/*h* (bottom).

3.2. Spatial Variability and Evolution

The data recorded at the Paraná site was obtained over a single sand dune at three stationary locations separated by increasing distance in the downstream direction from Position 1 to Position 3. The data from the Paraná site was found to be poorer in quality as the result of two factors related to the ping rate. Firstly, the processor was incapable of recording at 30Hz, which led to a variable delay between successive pings. Secondly, when the delay was small (usually less than 0.1 s) large and varying magnitudes of surface reverberation were observed across the swath. Heavily contaminated pings at less than 0.07 s delay were therefore rejected from the analysis, thus increasing the average delay between the remaining pings. A time series analysis of the data would require interpolation to a uniform temporal sampling rate. Reverberation was a particular problem at the edge of the swath, as was the presence of the mooring cable that can be seen on the left-hand side of Figure 1 Herein, we show the results for the mean *u* and *w* components of flow velocity across the central section of the swath sector from beams 165 to 348 that span 45.5°.

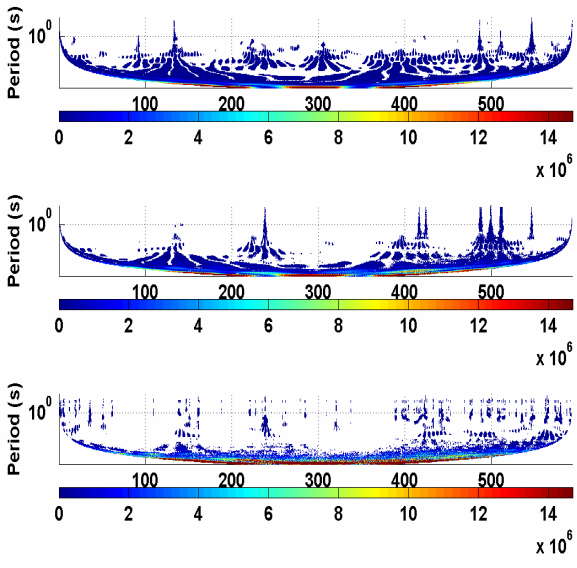

Figure 8. Wavelet analysis of the *u* time series for 0.75 *z*/*h* (top), 0.5 *z*/*h* (middle), 0.25 *z*/*h* (bottom)

Figure 9 shows the mean vertical *u* and *w* profiles for the three positions. The usable data were recorded over shorter time periods than for the

Mississippi site: Position 1 (181 s), Position 2 (52 s) and Position 3 (33 s). The three *w* profiles show a very similar variation with depth above the bed. The *u* profile shows a sharp gradient above the bed for the furthest upstream (near crest) and shallowest position, Position 1.

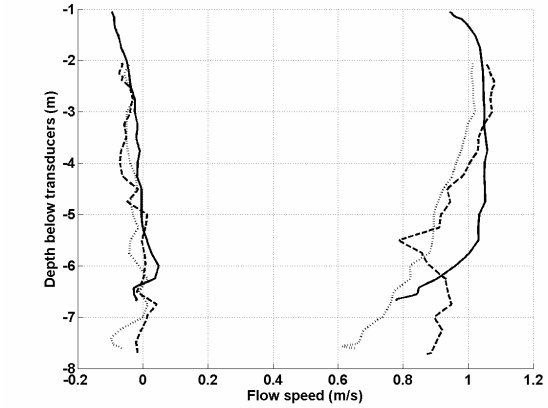

Figure 9. Mean vertical profile of *u* (right) and *w* (left) derived from the time series for the vertical profile

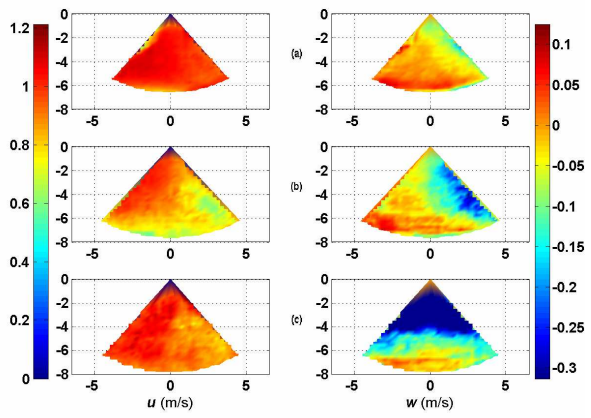

Figure 10. *u* (left) and *w* (right) flow fields obtained from the analysis of data collected at three locations in the lee of a sand dune in the Rio Paraná. Position 1 (a), Position 2 (b) and Position 3 (c)

The Position 2 profile shows a more gradual increase in flow speed with depth above the bed, while the Position 3 profile shows a similar gradient between ~ 2 - 5.5 m but with a notable increase in flow velocity in the lower two metres of the profile, perhaps related to a re-attachment point and/or intense turbulence that results in the incorporation of some temporal variation, particularly given the short length of the time series. Figure 10 shows the variation of mean *u* and *w* across the central region of the swath.

4. CONCLUSIONS

Methods for deriving the suspended sediment concentration and flow field velocity vectors across a two-dimensional flow field at a stationary position over a sand dune have previously been demonstrated by Best et al., (2010). The results in the present paper demonstrate how an analysis of the spatial and temporal variation of the flow field velocities obtained with this method can reveal insights into the turbulent behavior of flow over a dune. Work is ongoing to further characterize the variations in turbulent behavior, use the spatial richness of the MBES data to link the periodicities identified in the wavelet analysis to the structures responsible for the signals. Additionally, effort is been focused into further quantifying the uncertainties associated with this new and promising method, particularly with some of the technical issues encountered at the Rio Paraná site.

5. REFERENCES

Bennett, S.J., & Best, J.L. 1995. Mean flow and turbulence structure over fixed, two-dimensional dunes: Implications for sediment transport and dune stability, Sedimentology, 42: 491– 513, doi:10.1111/j.1365-3091.1995.tb00386.x.

Best, J., Simmons, S., Parsons, D., Oberg, K., Czuba, J. & Malzone, C. 2010. A new methodology for the quantitative visualization of coherent flow structures in alluvial channels using multibeam echo-sounding (MBES), Geophys. Res. Lett., 37. doi: 10.1029/2009GL041852.

Farge, M. 1992. Wavelet transforms and their application to turbulence. Ann. Rev. Fluid Mech., 24: 395– 457, doi:10.1146/ annurev.fl.24.010192.002143.

Lu, S.S. & Willmarth, W.W. 1973. Measurements of structure of Reynolds stress in a turbulent boundary layer, J. Fluid Mech., 60: 481–511, doi:10.1017/S0022112073000315.

Simmons, S.M., Parsons D.R., Best J.L., Orfeo, O., Lane, S.N., Kostaschuk, R., Hardy, R.J., West G., Malzone, C., Marcus, J. & Pocwiardowski, P. 2010. Monitoring Suspended Sediment Dynamics Using MBES, Journal of Hydraulic Engineering. Volume 136, Issue 1: 45-49.

Thorne, P.D., & Hanes, D.M., 2002. A review of acoustic measurement of small-scale sediment processes, Cont. Shelf Res. 22: 603–632.

Sand ripple volume generator for underwater acoustic models, a cellular automaton Monte-Carlo approach.

P. Staelens[(1)], Y. Dupont[(2)], J.-P. Henriet[(3)]

1. dotOcean N.V., Brugge, B – peter@dotocean.eu
2. Belgian Navy, Brussels, B – yves.dupont@mil.be
3. Renard Centre of Marine Geology Ghent University, Gent, B – jeanpierre.henriet@ugent.be

Abstract

Cellular automata have been successfully used to model the sand dynamics of aeolian dunes and ripples. The cellular automata Monte-Carlo model proposed in this paper expands the capabilities of cellular automata models to under water ripple formation introducing not a two dimensional matrix but two three dimensional volumes, being a sand volume and a water volume. The proposed model has the capability to generate optimal environmental data to input in other mathematical models in need of environmental data. The following enhancements were implemented: optional abstraction levels of the hydrodynamic behavior, morphological formation of underwater ripples under unilateral currents in any direction as well as morphological formation of underwater ripples under wave current interaction, grain size distribution of the sand in every time step in the entire volume and compaction distribution in every time step in the entire sediment volume. The proposed cellular automata model is a closed toroidal system. The toroidal approach of the model enables to build up infinite rippled surfaces by using the generated sediment volumes as tiles; this solves boundary problems in for example acoustic models. Using the fractal properties of the sand ripples, infinite surfaces containing rippled dunes can be generated.

1. INTRODUCTION

A sandy seafloor is covered with bedforms, the bedform dynamics themselves sorting and compacting the sediment (Soulsby 1997). Understanding the complex non-random sediment dynamics in general and the interaction with sea mines is essential to understand the resulting acoustic response of sediment and semi buried or buried mines. Bedforms can be observed in any sandy environment where the shear stress caused by a current over a sand bed exceeds a certain threshold (Soulsby 1997). Once the threshold is exceeded, the granular medium reorganizes itself from a rough, relatively flat morphology into a ripple pattern. Sand ripples and dunes can be seen as self organizing patterns with a fractal character (Tian-De, Qing-Song et al. 2001). The fractal property will prove to be useful in the acoustic models. Ripples and dunes may be generated by a sub aqueous current or by the wind (aeolian ripples). Aeolian generated patterns have been described and modeled by Nishimori and Ouchi (Nishimori and Ouchi 1993), Anderson and Bunas (Anderson and Bunas 1993), Landry and Werner (Landry and Werner 1994), Yizhaq et al. (Yizhaq, Balmforth et al. 2004) gives a brief overview of some existing aeolian models and model approaches. Many expansions on these models have been made in the recent decade. Soulsby (Soulsby 1997) explains the sub aqueous transport mechanisms, but does not propose any model. The aeolian sediment transport processes and formulae as described (Anderson and Bunas 1993; Nishimori and Ouchi 1993; Landry and Werner 1994; Tian-De, Qing-Song et al. 2001; Zhang and Miao 2003; Yizhaq, Balmforth et al. 2004) do not apply in sub aqueous environments, but the resulting shapes and some patterns are similar. Therefore first existing aeolian models were evaluated and found to be inapplicable in underwater acoustic models. The models proved to be inapplicable in underwater acoustics because they were not designed to generate the parameters such as grain size distribution and compactions. Upgrading the models to an applicable level for underwater acoustics appeared to be impossible. Nevertheless a lot can be learned from the methodological approach some of the authors

have. In this paper the toroidal cellular automaton approach will be used. On the application level, to prevent algorithmic implementation effects in the data, a Monte-Carlo method has been used to trigger the automata. The goal is not to regenerate the sediment volume using exact rules corresponding fully with nature; the goal of this model is to generate artificial sediment with a correct distribution of required properties and to avoid synthetically looking surfaces generating synthetic results in mathematical models where the generated volumes are used as input. The distribution at a micro level often is random; on higher levels the distribution often appears to have unique but recognizable patterns. The properties covered in this paper will be: topography, grain size distribution, compaction and acoustic impedances.

2. METHOD

The cellular automata technique used in this paper is based upon the behavioural description of one single sand grain, called a cellular automaton, in a cellular automata system. The 3D cellular automata matrix used in the presented simulations typically includes a layered set of 5.000.000 automata, all having the same rules, but with different attributes such as weight and dimensions. As previously stated, the automata are triggered using a Monte-Carlo method and only sand grains exposed to fluid flow can be triggered. This generally reduces the amount of activated automata per time step, in the presented simulations, to about 0.1% or 5.000. The model as such does not contain every sand grain available in a real life system, but reduces the behaviour of a predefined zone or bin of sand to one single sand grain called the cellular automaton. The bin dimensions are defined by the user.

Four transport mechanisms are active in a sub aqueous sand dynamic system. The transport mechanisms are implemented on the cellular automata, they are; avalanche, roll, saltation and creep. In this model a combination of roll and saltation is the driving mechanism of sub aqueous sediment transport; a grain rolls or hops up the ripple following the least energy-consuming path to the crest where it may avalanche until it settles down in the current shadow. If a pile of grains exceeds a certain stability angle, the pile will fail and grains will avalanche until a specific stability angle has been restored. The stability angle of sand in a non-energetic environment is about 32°-37° (Soulsby 1997). Saltation is the most energy consuming way of transport. Saltation means that grains are ejected from the sand bed, float in the water column and splash down downstream. Saltation is thought to be the driving mechanism for aeolian ripple formation (Anderson and Bunas 1993; Nishimori and Ouchi 1993; Landry and Werner 1994; Tian-De, Qing-Song et al. 2001; Yizhaq, Balmforth et al. 2004). When fixed time step increments are introduced, a grey region between roll and saltation emerges. A single grain may have contact several times with the seabed in a single time step. In order to reduce the complexity of the model and allow the usage of fixed time step intervals, saltation and roll are approached as being one mechanism. All grain movements influenced by more than one small scale feature of the sand bed during one discrete time increment (hopping) follow the roll equations. Since most of the bedload transport happens near to the seabed, most of the saltation movements can be described as 'hopping' in the proposed model. Other forms of saltation can be implemented, but will be ignored in this implementation. The fourth mechanism is the creep mechanism; some grains have minimal exposure to the current and destabilize, they however do not receive enough energy to roll up the ripple. These grains will modify their position on the ripple slope, they might move to an adjacent bin. This mechanism can be seen as the settling of the sand grain in a nearby optimal position and makes the surface smoother and more realistic looking.

2.1. Two dimensional implementation

Starting with a simplified 2D approach of ripple formation, the model adopts the following sedimentological rules. Figure 9 shows a ripple and a coordinate system. The current flows in the positive X direction. The transport mechanisms can be subdivided in two groups: energy consuming mechanisms such as saltation, roll and creep and energy producing mechanisms as avalanching and sometimes creep. The system will receive energy from the avalanching when a slope gradient in the system exceeds the stability angle,

that angle is called α. The energy consuming mechanisms also have some stability angles. The angle β defines the maximum slope of the stoss side of the ripple. The current shadow is defined as h_x-h_{x-1}< 0. Where h is the topographic height of the considered bin, x and x-1, and the direction of the main current is along the positive X axis.

Consider now one single grain, with a diameter gd. An increasing force is imposed on it, forcing it to move or roll. The grain will have the potential to move once the implied force is higher than the friction force keeping the grain on its position. The model will translate the exerted force to energy. Per bin, per discrete unit of time a grain can spend a maximum accumulated amount of energy: Ex. Exposed grains and grains positioned on a slope exceeding the stability angle β will be transported over a distance s, following equation 1

$$s = \sum \Delta s \qquad (1)$$

With every discrete space step Δs defined as:

$$\Delta s = \sqrt{\Delta x^2 + (\Delta h + gd)^2} \quad (1)$$

The stoss side stability angle or β-function is not yet determined, β is set to an acceptable constant 7°, but is supposed to be related to the horizontal component of the water velocity vector on the sea floor, grain mass and smallest current impact surface of a grain. A similar approach can be made for the β_2-function related to vortices (Figure 1).

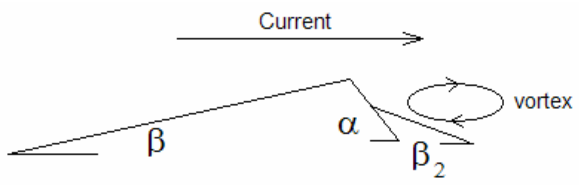

Figure 1. Stability angle schematics

A moving grain will spend an amount of energy per discrete space step.

$$E = \sum \Delta e \qquad (2)$$

Where Δe is defined as the energy used in a movement between two adjacent bins. The grain will stop rolling as soon as the grain enters a bin where E ≥ E_x.

The last rule of the roll movement defines that all grains in a current shadow, h_x-h_{x-1} < 0, will not move at all, the hydrodynamics matrix can provide that information. The α-function, or avalanche function, is set to a constant: 32°. The summary of formulae for the energy consumption in roll, with a current in the positive X direction, is given in the equation set 3.

$$\begin{cases} E = \sum \Delta e \\ E \le E_x \\ E_x = 0 \Leftrightarrow h_x - h_{x-1} < 0 \\ E_x = 0 \Leftrightarrow \begin{cases} h_x - h_{x-1} < h_{x+1} - h_x \\ \dfrac{h_x - h_{x+1}}{\Delta x} < \beta \end{cases} \end{cases} \qquad (3)$$

The discrete energy consumption Δe is defined as the sum of the energy used to overcome the friction (Efriction) and the energy used to lift up the grain (Egravity). Efriction is a function of mass and travelling distance, while Egravity is a function of mass and the difference in height between two adjacent bins x and x+1:

$$\Delta e = E_{friction}(m, \Delta s) + E_{gravity}(m, \Delta h) \qquad (4)$$

The grain movement rules for roll and bed load saltation are:

$$\begin{cases} h_x = h_x - gd \\ h_{x+1} = h_{x+1} + gd \end{cases} \Leftrightarrow \quad \Delta e > 0 \qquad (5)$$

And the grain movement rules for the avalanche:

$$\begin{cases} h_x = h_x - gd \\ h_{x+/-1} = h_{x+/-1} + gd \end{cases} \Leftrightarrow \quad \frac{h_x - h_{x+/-1}}{\Delta x} > \alpha \qquad (6)$$

Implementing this simple set of rules will generate a 2D section of a ripple taken parallel to the current. The avalanche mechanism is simplified, but demonstrates well the idea.

2.2. Three dimensional implementation

Imagine a number of 2D systems are set parallel to the flow current in a three dimensional matrix. Using the above rules, ripple shapes will appear in the matrix but no ripple pattern, all grains will move along the X axis. A ripple pattern is formed when a communication between each 2D ripple shape is possible. Here Δs, equation 2, as distance will be expanded to equation 7:

$$\Delta s = \sqrt{\Delta x^2 + \Delta y^2 + (\Delta h + gd)^2} \qquad (7)$$

As described in the sedimentation rules, a grain will follow the least energy consuming path, as a result in the roll movement there will be three options to roll to instead of one. The 3D expansion of the 2D rules for roll is given in equation 8 (assuming that roll is possible):

$$\Delta e_{optimal} = \min \begin{bmatrix} \Delta e_{x,y \to x+1,y-1} \\ \Delta e_{x,y \to x+1,y} \\ \Delta e_{x,y \to x+1,y+1} \end{bmatrix} \quad (8)$$

Avalanching will be similarly expanded, instead of two avalanche directions there will now be eight directions of avalanche (diagonals are included; most of the implementation applies calculations in an 8-cell Moore neighbourhood). The result of these expansions will be a 3D ripple like pattern (Figure 4, Figure 6, Figure 9). Avoiding undesired effects related to the discretisation can be done using the creep method or the implementation of a low pass filter along the Y axis. The stability angle γ for destabilized creeping grains will be related to the energy lost in friction and will be along the Y axis. This mechanism is of high importance to expand the 2D model to a 3D model since it will act as a low-pass filter along the Y axis. Filters along the Y axis are often implemented in the code implementation of the described aeolian ripple models. Implementing filters gives optimal topographic results but reduces the model to a topographic model. Since we aim to derive some basic parameters such as compaction and grain size distribution, filters cannot be implemented in this application. The creep method allows a grain to move to one adjacent bin in the Von Neumann neighbourhood if the grain is exposed to the current. Creep movement will not take energy out of the system. In order to have creep, a grain must have sufficient exposure to the flow current, hcreep is a Boolean derived from the formula below and defines whether a grain can move or not (reduced Moore neighbourhood).

$$h_{creep} = \min \begin{bmatrix} h_{x-1,y-1} \\ h_{x-1,y} \\ h_{x-1,y+1} \end{bmatrix} \leq h_{x,y} - gd - \gamma \Delta s \quad (9)$$

The creeping grain can be exposed but must also be able to settle, this time, in a reduced Von Neumann neighbourhood. The Boolean hoptimalset defines whether the grain can settle.

$$h_{optimalset} = \min \begin{bmatrix} h_{x,y-1} \\ h_{x,y+1} \\ h_{x+1,y} \end{bmatrix} \leq h_{x,y} - gd - \gamma \Delta s \quad (10)$$

If both hcreep and hoptimalset are true, a creep motion will be invoked and the grain will move to an adjacent cell with minimum height.

2.3 The hydrodynamic volume

The hydrodynamic volume generator is separated from the sedimentological model and is activated after each run or time step of the sedimentological model. In the presented data, the hydrodynamic volume generator applies a simple set of rules. Infinite complexity of the hydrodynamic volume generator is not possible without adapting some of the rules applied in the sedimentological model. The decision of the cellular automaton or sand grain to follow the lowest energy consuming path is equal to what the water particles would do. Implementing similar rules in the hydrodynamic module would accelerate the particles. One has to make the choice on where to apply what set of rules. The hydrodynamic model used in the presented simulations is one that generates a current shadow behind the ripple crest (Figure 2).

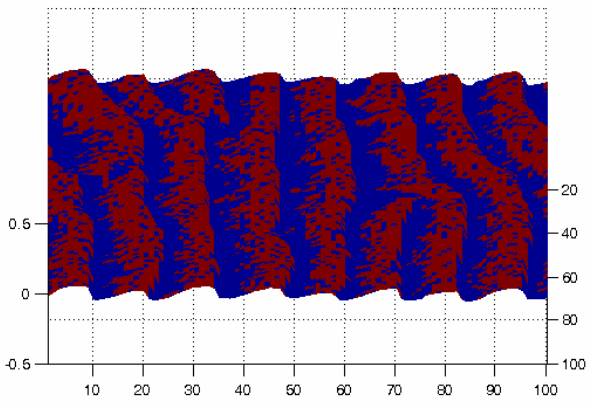

Figure 2. In red are the grains in motion, blue shows the grains in the current shadow.

The hydrodynamic model starts with horizontally slicing the water volume and implements a speed vector to all slices that encounter no obstruction. When passing an obstruction or ripple crest the

bins behind the obstruction are set to zero over a predefined distance. Every hydrodynamic slice drags the underlying slice with a predefined delay in the space domain. Depending on the height of the crest, the topography behind the crest, the number of horizontal hydrodynamic slices and the viscosity rules set, the water flow will pick up speed again closer or further behind the crest.

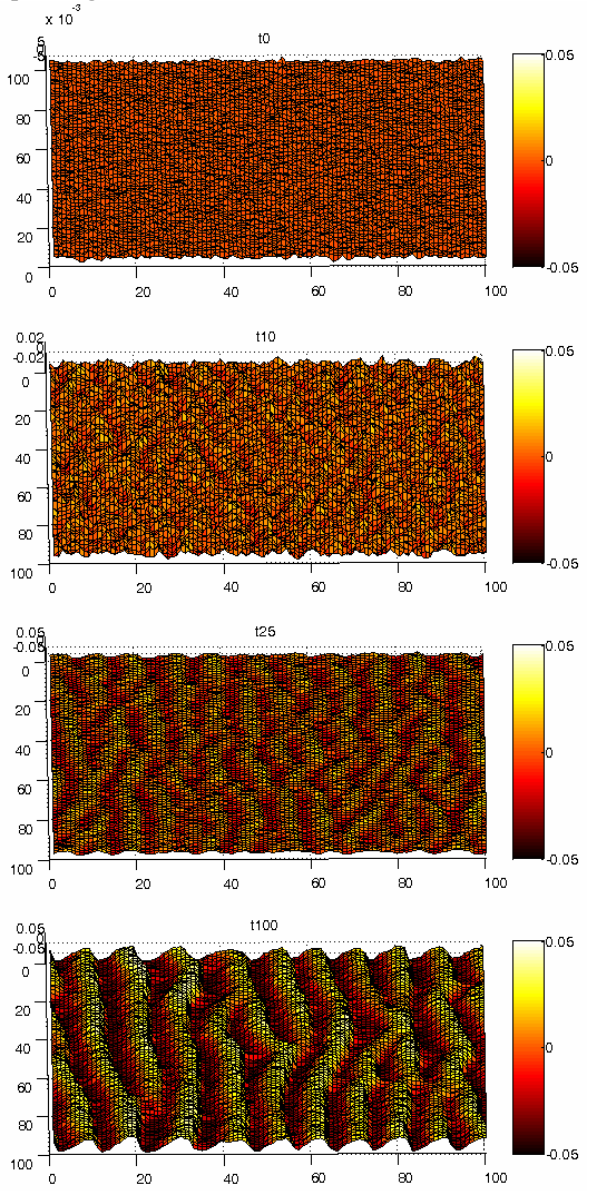

Figure 3. Topographic evolution from a rough surface to a rippled surface is demonstrated. Initial condition t0 is the top figure followed by time steps t10, t25 and t100.

3. RESULTS AND APPLICATIONS

The cellular automaton rules set and explained are the basic rules for a simple model and are subject to modification. Extra restrictions or open up restrictions is possible. The proposed rules compensate largely for small scale hydrodynamic variations but not for vortices.

3.1 Evolution of a ripple field

Figure 3 displays the evolution in 4 time steps of a rough flat sand surface to a ripple field. This example has been generated using a unilateral current. Simulating wave interaction using the proposed cellular automata rules is possible.

3.2 Acoustic impedance distribution

The generated results appear to be sufficient for acoustic modelling (Staelens (2009)). Next to topography, acousticians are also interested in acoustic impedances. The acoustic impedance of a sediment is a function of the sound speed trough the sediment and the density of the sediment. Densely packed sand has higher acoustic impedance than loosely packed sand. A complex mechanism as sand ripple evolution and migration generates a sorted sediment with a potential of very strong impedance changes. A simulation containing a compaction module generates Figure 4, the surface distribution of acoustic impedances in a ripple field.

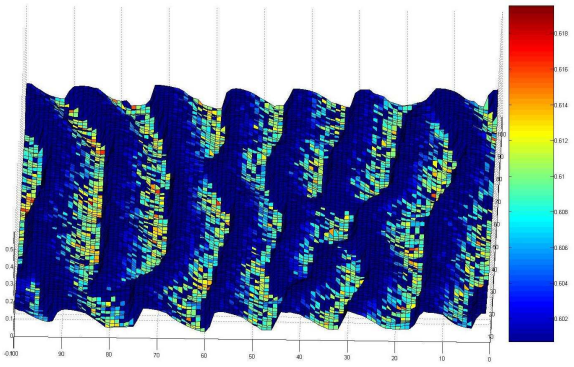

Figure 4. Generated acoustic impedance distribution on the surface of a ripple field, generated from a compaction module implemented on the sand ripple generator (dark blue is lower impedant)

3.3 Acoustic ray tracing

Another acoustic modelling application is ray tracing and formation of shadows. Acoustic ray bending in the simplest form is function of the sound velocity variations in the water column and the opening angle of the sonar. The formation of shadows depends upon the vertical sound velocity profile, the sonar opening angle and the seafloor (Figure 5).

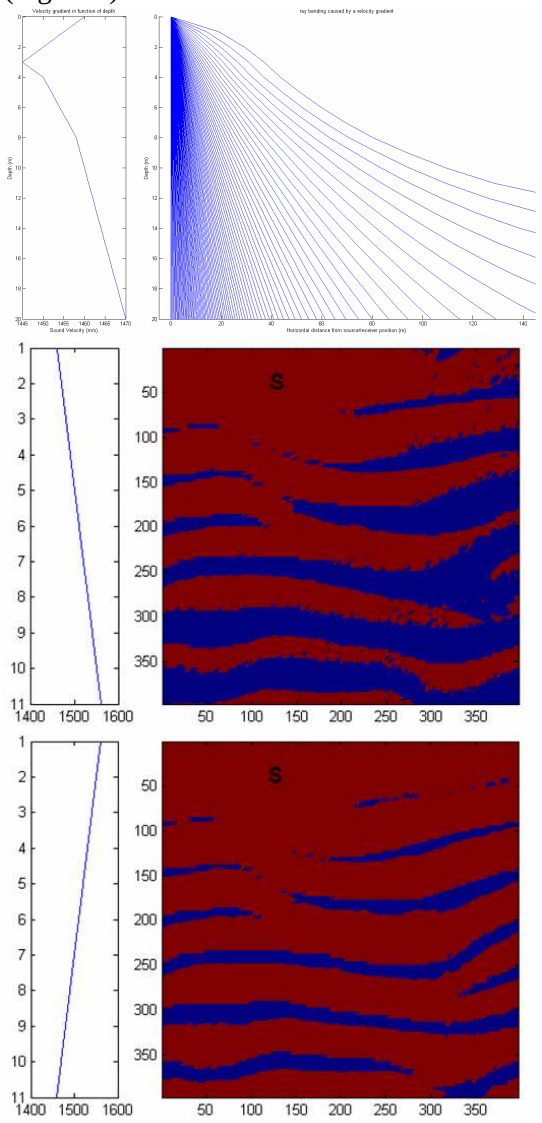

Figure 5. All figures have on the left the sound velocity variation in function of depth. The top figure shows the principle of ray tracing in function of the opening angle of the sonar. The centre and bottom figure display the effect on shadowing based on a sound velocity profile, S is the position of the acoustic transducer.

3.4 Generating an infinite surface

Tiling up the artificial environment is possible (Figure 6) and allows the generation of continuous infinite surfaces without holes or gaps. The neighboring tiles can be tiles from the same time step or, since changes in between time steps are relatively small, can be from different but close time steps. The last feature described allows the generation of ripple patches. Fractal properties of dunes can be used to generate rippled dunes (Figure 9)

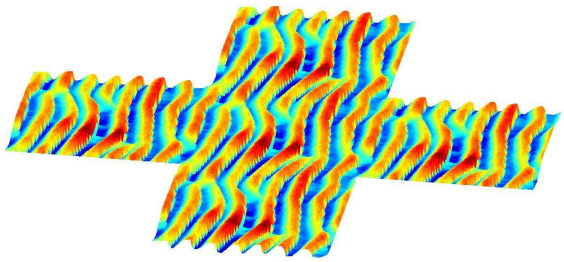

Figure 6. Ripple tiles are being used to generate an infinite surface without boundary gaps

3.5 Grain size distribution

A vertical section through the sediment volume displays a sorting of the sediment (Figure 7). Finer grains appear to concentrate in the ripples features. Figure 8 shows the grain size distribution on the surface of the ripple. This observation is to be verified.

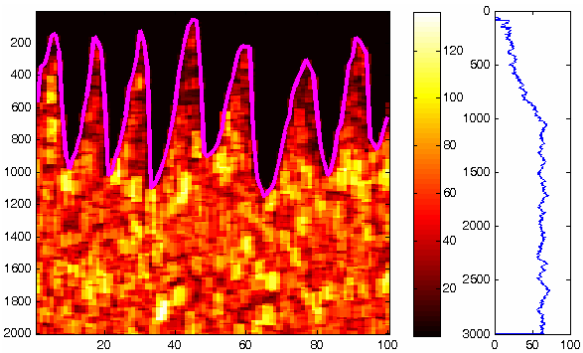

Figure 7. grain size distribution after an 8-cell Moore neighborhood average filter in a vertical section of the generated sediment volume (left) and the average grain size evolution in function of depth over the profile (right)

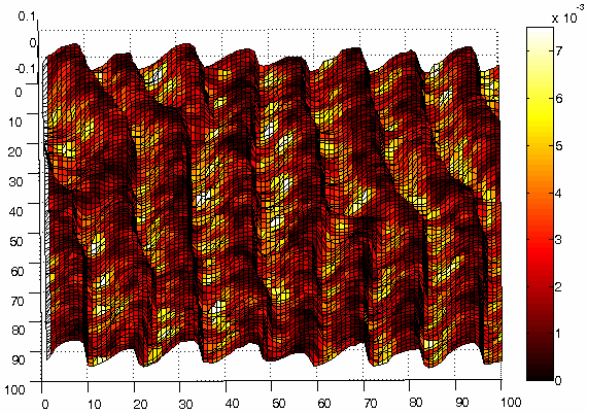

Figure 8. Grain size distribution on the surface after an 8-cell Moore neighborhood average filter. In the ripple through the larger or heavier particles appear to concentrate.

4. CONCLUSIONS

Modeling sand dynamics using cellular automata in combination with a Monte Carlo method implementation appears to deliver high quality data for mathematical models in need of unbiased sediment input data. Correct implementation of the methodology allows the generation of additional parameters needed in for example underwater acoustic models. The major advantage of using digital generated sediment volumes instead of, for example multibeam echosounder generated maps, in underwater acoustic models is that the digital sediment volume is free of interpretation and allows as such validation of for example backscatter interpretations and fundamental research on sonar imaging technology. Applying additional modules on the cellular automata model allows the generation of new parameters. The demonstrated grain size distribution effects need to be validated on the field or in lab conditions. This validation will probably add additional rules to the cellular automata but will increase reliability of the model.

5. ACKNOWLEDGMENT

This research was funded by the Belgian Navy and supported by Ghent University.

6. REFERENCES

Anderson, R. S. and K. L. Bunas 1993. Grain-Size Segregation and Stratigraphy in Aeolian Ripples Modeled with a Cellular-Automaton. Nature 365(6448): 740-743.

Nishimori, H. and N. Ouchi 1993. Formation of Ripple Patterns and Dunes by Wind-Blown Sand. Physical Review Letters 71(17): 2841-2841.

Landry, W. and B. T. Werner 1994. Computer-Simulations of Self-Organized Wind Ripple Patterns. Physica D 77(1-3): 238-260.

Soulsby, D.H. (1997). Dynamics of marine sands. A manual for practical applications, Thomas Telford Publications, London, England, 249 p.

Staelens, P.J.M. 2009. Defining and modeling the limits of high-resolution underwater acoustic imaging. Ph.D. thesis, UGent. 178 pp.

Tian-De, M., M. Qing-Song, et al. 2001. Computer simulation of aeolian sand ripples and dunes. Physics Letters A 288(1): 16-22.

Yizhaq H., Balmforth N.J., Provenzale A. (2004). Blown by wind: nonlinear dynamics of aeolian sand ripples. Physica D 195: 207-228.

Zhang, Q. H. and T. D. Miao 2003. Aeolian sand ripples around plants. Physical Review E 67(5).

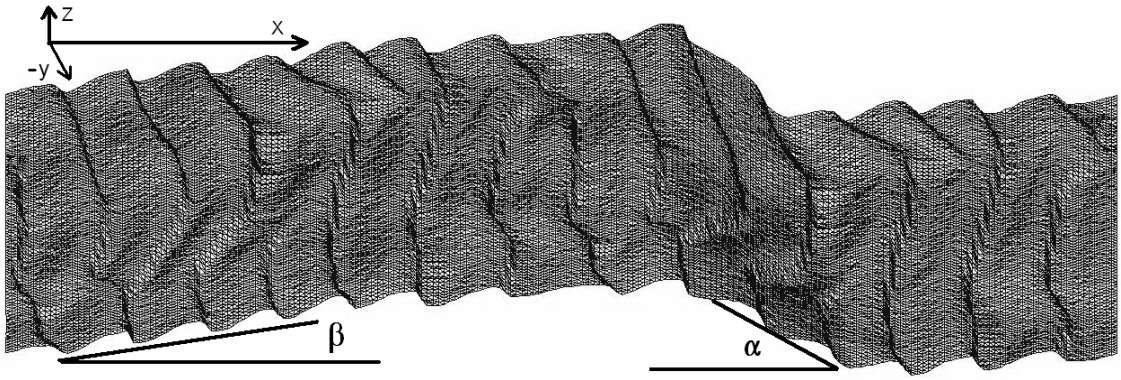

Figure 9. The coordinate system used during the simulations displayed on a fractal implementation of the generated ripple topography.

Equilibrium beach-evolution model

Imen Turki[(1)], Raul Medina[(2)], Mauricio Gonzalez[(2)], Giovanni Coco[(2)]

1. UMR CNRS 6143 Continental and Coastal Morphodynamics 'M2C' University of Rouen, 76821 Mont-Saint-Aignan Cedex, France. imen.turki@univ-rouen.fr
2. Environmental Hydraulics Institute IH 'Cantabria', University of Cantabria, c/Isabel Torres 15, 39011 Santander, Spain.

ABSTRACT

Changes in the shoreline location of sandy beaches are the result of a large number of processes and mechanisms which interact on a variety of spatial and temporal scales (*e.g., DeVriend 1993*). Beaches are in fact complex dynamic systems and respond to waves and currents through a series of changes that can occur at different time scales. In the last decade, several approaches have been developed for predicting beach changes induced by wave action. The approaches can be broadly divided into two categories: data-driven, process-based. The term data-driven refers to models that entirely rely on the presence of a pre-existing data-set to develop what is usually a site-specific predictor. An example of a simple data-driven model is a regression analysis relating changes in shoreline position to the some averaged measure of the previous offshore wave climate. Analyses of this type have been presented by several authors also for the study of beach rotation on embayed or pocket beaches (*e.g., Ojeda et al., 2008; Turki et al., under review*).

The focus of the present work is the development of a robust model based on kinetic equations and capable of forecasting shoreline changes over long timescales and with a quantifiable degree of accuracy. Sediment transport theories were used for the development of an analytical model which assumes that the instantaneous changes to the planview shape of the shoreline depend on the long-term equilibrium planview shape (*Kriebel and Dean, 1985*). Based on this assumption, a 1-D approach was developed to compute the instantaneous shoreline response as a function of the initial shoreline response and terms depending on the wave energy and the physical characteristics of the beach.

The novel simple beach-evolution model was applied to estimate the shoreline rotation at sandy pocket beaches. Two years of hourly wave time series, calculated at the coast of Barcelona, on the north-eastern coast of Spain (NW Mediterranean), were used as an input for the analytical model to compute the shoreline response of three artificially embayed beaches. Modelled results were validated by weekly observed shoreline positions, extracted from video images (ARGUS) of Barcelona, and have shown an excellent agreement with an RMSE less than 1.5 m.

The finding presented an new beach-evolution model which successfully reproduced the shoreline response over a range of scales (months and years). For its simplicity and its computational efficiency, the model provides a powerful tool to understand the dynamics regulating the evolution of pocket beaches and predict temporal patterns in beach rotation.

REFERENCES

De Vriend, H. J. D., M. Capobianco., T. Chesher, and T. Swart (1993), Approaches to long-term modelling of coastal morphology, Coastal Engineering, 21, 225-269

Kriebel, L. D., and R. G. Dean (1985), Numerical simulation of time-dependent beach and dune erosion, Journal of Waterway, Port, Coastal and Ocean Engineering, 9, 221-245.

Ojeda, E., and J. Guillén (2008), Shoreline dynamics of embayed beaches, Marine Geology, 253, 51-62. doi: 10.2112/07-0886.1

Turki, I., R. Medina., M. Gonzalez, and G. Coco, Natural variability of shoreline position: observations at three pocket beaches, Marine Geology, under review.

Flow Structures over Fixed 2D Bedforms in Transient States

C.A. Unsworth[(1)], D.R. Parsons[(1)], A.J.H. Reesink[(1)], J.L. Best[(2)], P.J. Ashworth[(3)] and R.J. Hardy[(4)]

1. Department of Geography, Environment and Earth Sciences, University of Hull, Hull, HU67RX, UK *E-mail: C.A.Unsworth@2011.hull.ac.uk
2. Departments of Geology, Geography and Geographic Information Science, Mechanical Science and Engineering and Ven Te Chow Hydrosystems Laboratory, University of Illinois at Urbana-Champaign, 1301 W. Green St., Urbana, IL, 61801, USA
3. Division of Geography and Geology, School of Environment and Technology, University of Brighton, Brighton, Sussex, BN24GJ, UK
4. Department of Geography, University of Durham, Durham, DH13LE, UK

Abstract

Flow processes measured in the laboratory over fixed, 2D or 3D bedforms have mostly been conducted at one flow depth and with bedform dimensions set by scaling laws based upon "equilibrium" flow conditions. These results thus have limited applicability to many natural situations where bedforms and flow fields are co-evolving at different rates in response to transient conditions, such as changes in flow depth and flow discharge associated with a flood. The research presented herein investigates flow processes over 2D fixed bedforms under a range of non-equilibrium, transient, states in order to quantify the spatio-temporal changes in turbulence associated with steady conditions that are set at non-equilibrium depths and velocities. Flow field information was obtained at steady states for a range of flow depths and mean flow velocities, mimicking conditions during the transient evolution of flow and bedforms during a flood wave. This allowed quantification of flow fields over bedforms under transient boundary conditions, including shear stress profiles and the spatial variation in the dynamics of the separation zone. These findings provide data for a preliminary assessment of the link between sediment transport lag and transient flow dynamics, and facilitate an analysis of the implications of variable dune height: flow depth for flood wave propagation and bedform response.

1. INTRODUCTION

The flow structure over dunes has been extensively measured in laboratory conditions and there is general agreement on the nature of the flow field over idealised dune forms (e.g. Nelson et al., 1993; Nezu and Nakagawa, 1993; McLean et al., 1994; Bennett and Best, 1995; Nelson et al., 1995; Kadota and Nezu, 1999; Fedele and Garcia, 2001; Best, 2005a,b; Garcia, 2008). However, these laboratory experiments have only quantified the flow fields over dunes in steady flows that are scaled to a flow-morphology equilibrium condition. Detailed understanding of flow-bedform interactions during unsteady or transient conditions, which commonly results in a flow-morphology hysteresis, is currently lacking. Yet the quantification of such flow-form interactions is vital to understand these unsteady dynamics and mutual adjustments that occur in natural flows.

It is well known that stoss side flow acceleration and lee side flow separation associated with dunes produces shear layer turbulence and fluid ejections (e.g. Bennett and Best, 1995) and that the point of flow reattachment may be important in suspending large quantities of bed sediment. However, there is currently a lack of understanding on how these processes change when the flow and bedforms are not under scaled equilibrium conditions. This research aims to investigate how the flow structure over fixed, idealised, 2D dunes changes with variations in flow depth and flow velocity.

2. METHODS

A large recirculating flume that had dimensions 1 m wide, 1 m deep, and 10 m long was used herein. Three 2D idealised dune forms were fixed to the flume bed. They were 0.08 m high and with an angle-of-repose lee face (~30 degrees), and a crest to crest wavelength of 0.80 m. Detailed two-dimensional (streamwise (u) and vertical (w)) flow velocities were quantified using a Dantec 100 Hz Particle Imaging Velocimetry (PIV) system. The PIV was positioned along the centreline of the flume and centred on the mid-stoss of the third dune form. Velocities were measured for ~130 seconds per run, yielding an array of ~9000 images at 1280x800 pixels. Vectors were calculated using an adaptive correlation on a 32x32 grid, with sub-pixel

refinement. Outliers were identified and replaced by a combined automated penalised least squares approach with a discrete cosine transform and cross-validation (Garcia, 2011).

A suite of experimental conditions were investigated using this set-up, where the depth and/or flow velocity were systematically changed over the same fixed bedforms. Herein, we present results on the first 5 experiments conducted, at 0.28m flow depth (Table 1).

Table : List of experimental conditions. No.= run number, D = average flow depth (m), $\bar{U}$ = depth-averaged flow velocity over crest (ms^{-1}) , Fr = Froude number, Re = Reynolds Number, Q = discharge ($m^3\ s^{-1}$)

No.	D	$\bar{U}$	Fr	Re	Q
1	0.28	0.14	0.08	38535	0.039
2	0.28	0.30	0.18	83218	0.083
3	0.28	0.70	0.42	194491	0.195
4	0.28	0.76	0.46	213297	0.214
5	0.28	0.92	0.56	258427	0.259

3. RESULTS

3.1. Mean velocities

Figure 1 (see end of article) shows the time-averaged normalised flow velocity profiles for the streamwise and vertical components of flow for several locations across the dune. For the streamwise velocity, *u*, the largest variation in the shape of the velocity profile between all the runs occurs over the crestal locations (Fig. 1 A), although there is no obvious trend with increasing flow velocity.

The mean velocity over the trough and near the reattachment point along the dune (Fig. 1 C, E) shows similar shaped profiles of streamwise velocity, notably at and beneath the shear layer (Fig. 1 C), but with a slight variation above the distinct kink in the profiles. The spatial variation in mean *u* on the stoss slope shows the impact of the lee side wake layer on the recovery of the time-averaged flow field, with the highest *u* velocities systematically shifted into the upper portions of the profile along the stoss side.

The vertical (*w*) component of velocity shows significant spatial variation along the dune and between each of run conditions (Figure 1, B,D,F,H,J). Although the shape of the normalised vertical velocity profiles converges towards the bed between the various conditions, there are significant divergences above this zone, which show a systematic trend with changing flow conditions. The normalised vertical velocity profiles in the dune trough (Figure 1D) are largely consistent until the shear layer (around crest height, at x=200), showing how strongly coupled the flow field is to the bedform morphology. However, the shape of the vertical flow profile for the different incoming velocities changes dramatically around the reattachment point. This is a key indication of where, and how much, flow is directed towards the bed on the stoss side of the dune within the region of flow recovery.

This result indicates that there is a substantial variation in normalised flow directed towards the bed with increasing flow velocity, and thus the spatial location of the maximum bed shear stress will also vary with mean flow velocity.

3.2. Flow reattachment point

The most significant change in flow over dunes in these experiments concerns the point of flow reattachment. Herein, the reattachment point was calculated for each condition by finding the streamwise location of the highest time-average magnitude in flow vorticity at the bed. The length of the shear layer, and thus reattachment point, for Runs 2-5 shows some systematic variation (plotted as distance from the crest to the near-bed vorticity maximum, Figure 2). The slowest condition (Run 1, 0.14 ms^{-1}, Re=38535) does not fit this trend and given the very low velocities in this run may display different interacting processes (see discussion).

3.3 Quadrant Analysis

Quadrant analysis was performed using the same methodology applied in Bennett and Best (1995) with a threshold value (hole size) of one standard deviation. Figure 3 (see end of article) displays contour plots of the quadrants (% contributions) for two runs; Run 1 (0.14 ms^{-1}, Re=38535) and Run 3 (0.70 ms^{-1}, Re = 194491), displayed in the left and right series of panels of Figure 3 respectively, and shows the spatial change in the turbulent flow structure over the dune.

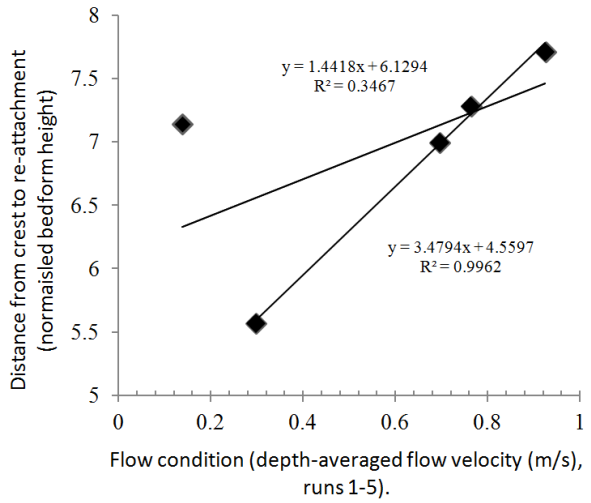

Figure 2: Reattachment length for Runs 1-5.

Quadrants 2 and 4 neatly highlight the position of the shear layer and wake, with Q2 events (ejections) being concentrated into the separation zone and Q4 (inrushes) dominating along the shear layer interface for both conditions (Figure 3). There are, however, some distinct changes between the two runs, with Q4 in Run 1 being significantly more dominant across a larger area than in Run 3 where Q4 events are mostly confined to the shear layer and a zone just above the stoss side. The wake from the upstream bedform can be seen in the Q2 contours for both flow velocities shown here (above the crest). However, there is a significant change in the dominance and position of the wake between these two conditions. In Run 3, the Q2 region extends well beyond the downstream crest and stacks above the developing shear layer and boundary layer of the downstream dune stoss side, whilst this stacking is almost non-existent for the slower velocity Run 1. The wake stacking above a shear layer seen here is similar to that shown by Fernandez et al. (2006), where superimposed bedforms created two stacked shear layers that interacted to enhance the turbulence produced around the flow separation zone. Therefore, this phenomenon should lead to larger and more energetic eddies being produced along the shear layer and at flow reattachment and thus a likely increased bed shear stress through this zone, particularly given that the position of Q2 ejections along the whole stoss region of the downstream dune are closer to the bed for the higher velocity Run 3 (Figure 3D).

4. DISCUSSION

The overlapping nature of the normalised downstream (u) velocities (Figure 1) masks a significant amount of variability in the flow field data presented herein. The differences in the normalised vertical (w) velocities provide an indication of the scale of relative change in the flow structure with increasing mean flow velocity and flow Reynolds Number. These results also demonstrate how strongly the bedform shape controls the velocity profiles in, and near, the shear layer. Nevertheless, the systematic increase in reattachment length with increasing flow velocity for Runs 2-5 shows that this phenomenon does change with flow velocity and is not just controlled by bedform geometry as described by Kadota and Nezu (1999). The variation between Runs 2-5 and run 1 is possibly explained by the lack of a wake overlapping the shear layer (as shown by quadrant analysis). Nelson et al. (1993, 1995) discuss the importance of the wake region on the stoss of dunes in controlling the initiation, growth and stability of dunes. This region is subject to a developing boundary layer due to the flow reattachment zone of the preceding separation zone, and the turbulent events that emanate from this zone. These pulses of turbulent flow produce localised high bed shear stress events that are responsible for the majority of sediment motion on the stoss of dunes (Nelson et al., 1993, 1995).

The spatial variation in quadrant contributions to the flow between Runs 1 and 3 (Figure 3 A,C,E,F for Run 1, B,D,F,H for Run 3) displays the dramatic changes that occur due to increasing flow velocity and Reynolds number. There is a major shift in the stacking of wake structures (notably Q2 events) with the increase in mean flow velocity. This stacking will result in enhanced turbulence as the wake zones from neighbouring dunes interact, which in turn will likely result in enhanced bed shear stresses in the flow recovery zone on the dune stoss side. A similar phenomenon is described by Fernandez et al. (2006) for superimposed bedforms. These results therefore begin to explore the relationships between flow structure zonation, bed shear stress and bedform morphology, and how these relations alter away from a flow-morphology equilibrium conditions.

5. CONCLUSIONS

Quantification of out-of-equilibrium flow over fixed, idealised, 2D dunes indicates that:

1. An increase in mean flow velocity causes substantial migrations in the locations of maximum turbulence generation and dissipation.
2. This change in turbulence zonation does not extend to, and does not appear to have a significant impact on, the height of flow separation. There is a possible relationship between increasing mean flow velocity and the length flow separation zone.
3. The flow field downstream of reattachment changes with flow velocity and Reynolds number. The zone of Q2 events extends downstream of the crest over the lee side separation region and also moves closer towards the bed over the subsequent dune stoss, which has significant implications for bed shear stress distributions and thus sediment dynamics.
4: The presence of wake stacking, from upstream dunes, over the flow separation region in the lee of the dune can occur without a change in bedform geometry and will likely contribute to morphological adjustment on the dune stoss side in response to flow variability.

6. ACKNOWLEDGMENTS

The authors would like to thank Dr. Gareth Keevil for his work in collection of the data in the Sorby Laboratory, University of Leeds. Unsworth would like to thank the University of Hull for his PhD. Scholarship. This research was partly supported by grant NE/I014101/1 from the UK Natural Environment Research Council (NERC).

7. REFERENCES

Bennett, S. J. and Best, J. L. 1995. Mean flow and turbulence structure over fixed, two-dimentional dunes: implcations for sediment transport and bedform stability. *Sedimentology,* 42**,** 491-513.

Best, J. 2005a. The fluid dynamics of river dunes: A review and some future research directions. *Journal of Geophysical Research,* 110.

Best, J. 2005b. The kinematics, topology and significance of dune-related macroturbulence: Some observations from the laboratory and field. *In:* Blum, M. D., Marriott, S. B. and Leclair, S. (eds.) *Fluvial Sedimentology VII* Special Publication of the International Association of Sedimentologists.

Fedele, J. J. and Garcia, M., H. 2001. Alluvial roughness in steams with dunes: A boundary-layer approach. *In:* Seminara, G. and Blondeaux, P. (eds.) *River, Coastal and Estuarine Morphodynamics.* New York. Springer.

Fernandez, R., Best, J. and López, F. 2006. Mean flow, turbulence structure, and bed form superimposition across the ripple-dune transition. *Water Resources Research,* 42.

Garcia, M., H. (ed.) 2008. *Sedimentation Engineering,* Reston, Virginia, USA: American Society of Civil Engineers.

Garcia, D. (2011). A fast all-in-one method for automated post- processing of PIV data. *Experiments in Fluids.* 50,1247–1259.

Kadota, A. and Nezu, I. 1999. Three-dimensional structure of space-time correlation on coherent vortices generated behind dune crest. *Journal of Hydraulic Research,* 37**,** 59-80.

Mclean, S. R., Nelson, J. and Wolfe, S. R. 1994. Turbulence structure over two-dimensional bed forms: Implications for sediment transport. *Journal of Geophysical Research,* 99, 12,729-12,747.

Nelson, J.M, Shreve, R.L; Mclean, S.R, Drake, T.G. 1995. Role of Near-Bed Turbulence Structure in Bed Load Transport and Bed Form Mechanics. *Water Resources research,* 31, 8, 2071-2086.

Nelson, J., Mclean, S. R., Wolfe, S. R. 1993. Mean Flow and Turbulence Fields Over Two Dimensional Bed Forms. *Water Resources Research,* 29**,** 3935-3953.

Nezu, I., Nakagawa, H. 1993. *Turbulence in Open Channel Flows.*, Rotterdam, A.A. Balkema.

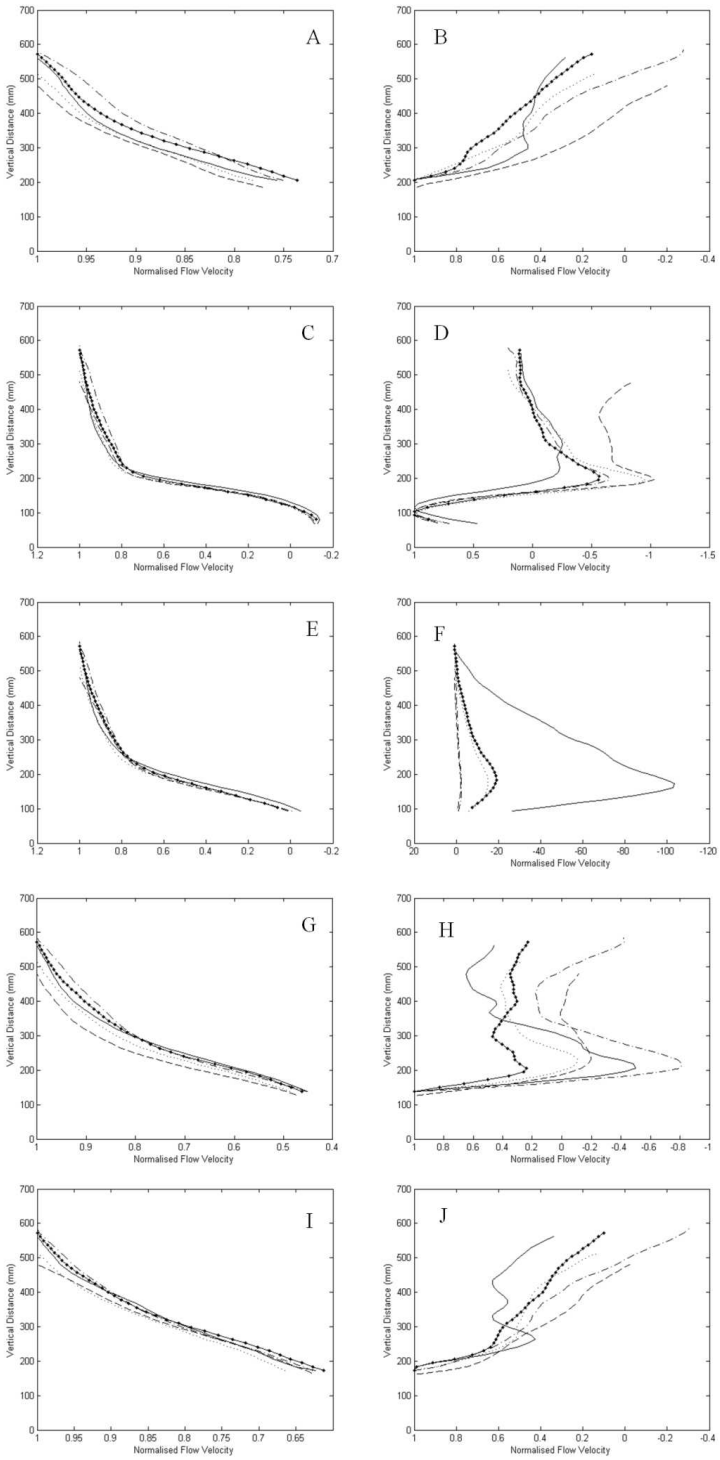

Figure 1: Normalised time-averaged velocity profiles with streamwise velocity component *u* (left) and vertical component *w* (right). Sequence A-E shows different locations across the dune (A-B y= 180 (at crest); C-D y= 400, (at trough); E-F y= 650 (near reattachment), G-H y=1200 (at mid-stoss of downstream dune), I-J y=1500 (upper stoss)). Solid black = 0.14ms^{-1}, line-diamonds = 0.30ms^{-1}, small-dash = 0.70 ms^{-1}, dot-dash = 0.76ms^{-1}, large-dash = 0.92ms^{-1}. Y axis is the vertical height in mm, X axis is normalised by the maximum flow velocity for each run.

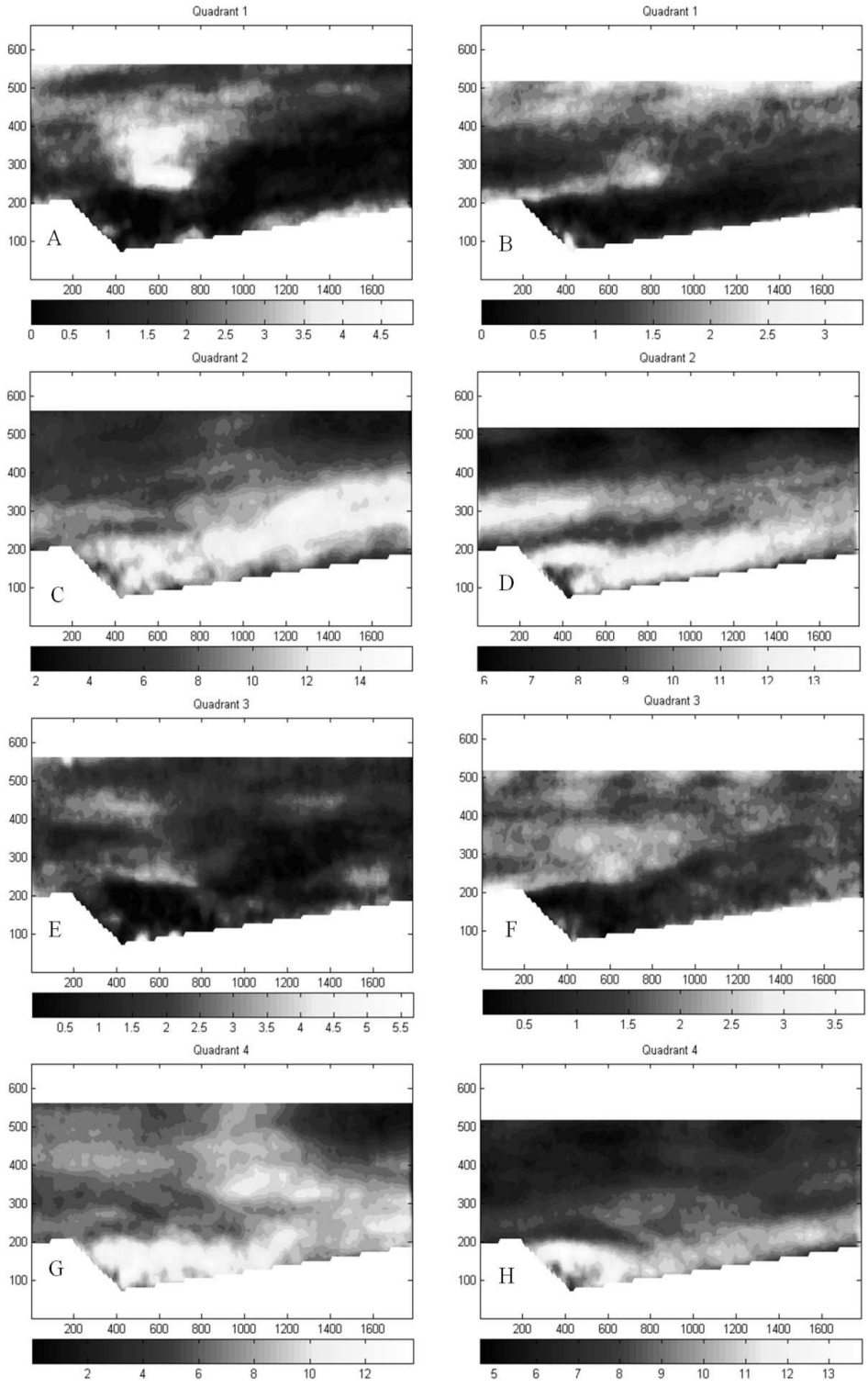

Figure 3: Quadrant analysis for Run 1 (left) and Run 3 (right) - A-B = Q1, C-D=Q2, E-F=Q3, G-H=Q4. Panels A,C,E and G are for Run 1 (at 0.14ms^{-1}) and Panels B,D,F,H are for Run 3 (at 0.7ms^{-1}). Note the changing contour values between panels. X and Y axis labels refer to distances in mm.

Impact evaluation of marine aggregate extraction through adaptive monitoring of bottom shear stress in bedform areas

V. Van Lancker[(1)], M. Baeye[(1)], F. Francken[(1)], S. Legrand[(1)], D. Van den Eynde[(1)], K. Degrendele[(2)], L. De Mol[(2)], & M. Roche[(2)]

1. Royal Belgian Institute of Natural Sciences.
Management Unit of the North Sea Mathematical Models (MUMM). Gulledelle 100, B-1200 Brussels, Belgium - vera.vanlancker@mumm.ac.be
2. Continental Shelf Service, FPS Economy, SMEs, Self-Employed and Energy. Bd Albert II 16, 1000 Brussels, Belgium

Abstract
Dedicated monitoring programmes are needed for the evaluation of the effects of the exploitation of non-living resources on the territorial sea and the continental shelf. Related to physical impacts, hydrodynamics and sediment transport, together with sedimentological and morphological evolution, need investigation. Overall aim is to increase process and system knowledge of both natural and exploited areas, with a particular focus on the compliancy of extraction activities with respect to European Directives (e.g., European Marine Strategy Framework Directive and Habitat Directive). More specifically assessments are needed of changes in seafloor integrity and hydrographic conditions, two descriptors to define Good Environmental Status within Europe's Marine Strategy Framework Directive.

An important parameter is the bottom shear stress, with knowledge needed on both natural and anthropogenically-induced variability. Bottom shear stress measurements are used for the validation of numerical models, necessary for impact quantification in the far field. Extensive data-model integration is critical for adequate assessments of the status of the marine environment, a prerequisite for sustainable use of living, and non-living resources.

1. INTRODUCTION

Mineral and geological resources can be considered to be non-renewable on time-scales relevant for decision-makers. During the last decade, socio-economic demands for marine aggregate resources in the North-East Atlantic or OSPAR region have increased at an unprecedented pace. During the past few years, hundreds of millions m^3 of offshore sand and gravel have been extracted for coastal maintenance, harbour extensions and onshore industrial use. Future aggregate demands will be even higher. Increasing volumes of nourishment sand are needed as accelerating sea-level rise will leave our coastlines ever more vulnerable. In addition, vast quantities of sand and gravel will have to be extracted to realize the large infrastructural works that are the key components of many visions on coastal zone and offshore development.

Sustainable use of marine resources is required and is inevitably linked to good environmental status (GES) of the marine environment. This is the 2020 goal of the Marine Strategy Framework Directive (MSFD, 2008/56/EC). Furthermore, following the Habitat Directive (92/42/EEC), Natura 2000 sites have been implemented in the marine environment. Appropriate assessments are needed of any plan or project that may affect such sites.

To allow monitoring of the evolution towards GES, a series of descriptors have been defined. Related to physico-chemical seabed attributes, descriptor 6 on seafloor integrity and descriptor 7 on hydrographic conditions are relevant in the context of aggregate extraction. GES for seafloor integrity refers to the structure and functions of the ecosystems that need safeguarding, without

adversely affecting benthic ecosystems, whilst GES for hydrographic conditions means that permanent alteration of hydrographical conditions does not adversely affect marine ecosystems. 'Not adversely affected' can be interpreted as meaning that impacts may be occurring, but all impacts are sustainable such that natural levels of diversity, productivity, and ecosystem processes are not degraded (Rice et al. 2012). Hence, there is a clear need for methodologies and tools that allow quantification of natural and man-made changes that, in combination with geological knowledge bases, define sustainable exploitation thresholds. Only then assessments can be made whether or not recovery from perturbations will be rapid and secure, and whether changes will remain within the range of natural variation.

For the first cycle of MSFD (2012-2018), Belgium put forward some physical indicators that should allow monitoring progress towards good environmental status (Belgische Staat 2012).
(1) For seafloor integrity, they are related to particular sediment classes (cf. predominant habitat types), of which the spatial extent and distribution should remain equal, or at least within its margins of uncertainty (Van Lancker & van Heteren 2013, for a discussion). Furthermore, the ecological value of gravel beds is recognized and an indicator is proposed that stipulates that the ratio of the surface of hard substrate (i.e., surface colonized by hard substrata epifauna) against the ratio of soft sediment (i.e., surface on top of the hard substrate that prevents the development of hard substrata fauna), does not show a negative trend. This relates directly to exploitation-induced increases in turbidity that may lead to siltation in areas where those gravel beds occur.
(2) Bottom shear stress is chosen as an indicator to assess changes in hydrographic conditions. Using validated mathematical models, it is calculated over a 14-days spring-neap tidal cycle. An impact should be evaluated when one of the following conditions is met: (i) There is an increase of more than 10% of the mean bottom shear stress; (ii) The variation of the ratio between the duration of sedimentation and the duration of erosion is beyond the "-5%, +5%" range; (iii) The impact under consideration should remain within a distance equal to the square root of the area occupied by this activity and calculated from the inherent outermost border.
All developments need compliance with existing regulations (e.g., EIA, SEA, and Habitat Directive Guidelines) and legislative evaluations are necessary in such a way that an eventual potential impact of permanent changes in hydrographic conditions is accounted for, including cumulative effects. This should be evaluated with relevance to the most suitable spatial scale (ref. OSPAR common language).

This paper outlines the monitoring programme that should allow quantifying the effects of marine aggregrate extraction and evaluating the compliancy with respect to European Directives. The natural dynamics of the seabed, and of its bedforms in particular, complicate the debate. The monitoring programme has started in 2013 with pre-investigations in 2012.

2. STUDY AREA

Over a 10-yrs period intensive extraction of marine aggregates (up to 2.9 million m³ over 3 months) is allowed on the Hinder Banks, a sandbank complex located 40 km offshore in the Belgian part of the North Sea (BPNS). Depths are from 5 m to 30 m (Fig. 1). The sandbanks are superimposed with a hierarchy of dune forms, often more than 6 m in height. The channels in-between the sandbanks reach 40 m of water depth. Such intensive extraction activities are new practice in the BPNS, for which the environmental impact is yet to be determined. Furthermore, a Habitat Directive Area is present at a minimum of 2.5 km from the southernmost exploitation sectors. In this area, highest biodiversity is found in the troughs of barchans dunes (Houziaux et al. 2008).

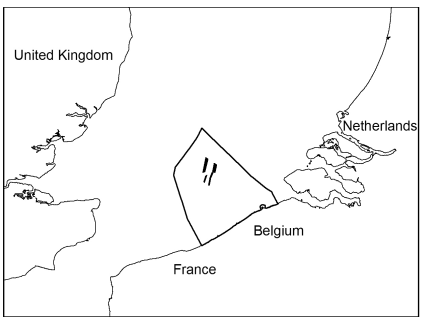

a

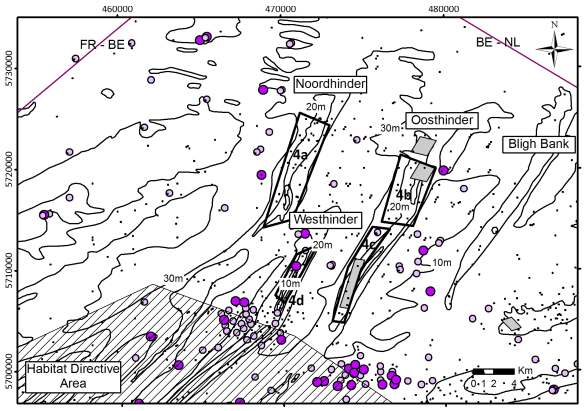

b

Figure 1. The Belgian part of the North Sea (a) and the area of the Hinder Banks (b), where intensive marine aggregate extraction is allowed in 4 sectors (black polygons). A Habitat Directive Area is present at a minimum of 2.5 km from the southernmost sectors. The size of the dots represents relative amounts of gravel with a minimum of 20 %. Borders with France (FR-BE) and the Netherlands (BE-NL) are indicated. In the grey shaded areas repetitive multibeam recordings.

3. MONITORING PROGRAMME

The monitoring programme is steered towards the testing of impact hypotheses, that are based on 30-yrs of extraction practices and its related research on the effects (Van Lancker et al. 2010, for an overview):
(1) Seabed recovery processes are very slow; (2) Large-scale extraction leads to seafloor depressions; these do not impact on the spatial connectedness of habitats (MSFD descriptor 6); (3) Impacts are local, no far field effects are expected; (4) Resuspension, and/or turbidity from overflow during the extraction process, will not lead to an important fining of sediments (e.g., siltation); (5) Marine aggregate extraction has no significant impact on seafloor integrity, nor it will significantly lead to permanent alterations of the hydrographical conditions (MSFD descriptor 7) (i.e., no change of sediment transport pathways); (6) Cumulative impacts with other sectors (e.g., fisheries) are minimal; and (7) Large-scale extraction does not lead to changes in wave energy dissipation that impact on more coastwards occurring habitats.

A tiered approach is proposed consisting of in-situ measurements and modelling. Critical is to assess potential changes in hydrographic conditions, as a consequence of multiple seabed perturbations (e.g., depressions) and their interactions. In short, current measurements along transects are needed to depict spatial variability over the sandbank areas, in combination with quantification of turbidity to assess changes due to the release of fines throughout the extraction process. Consequently, insight is needed in the dispersion of the fines and the probability of siltation in the nearby Habitat Directive area.

3.1 In-situ measurements

Three campaigns a year are aimed at and include: (1) Transect-based measurements (Fig. 2) of the full three-dimensional current velocity and direction, together with turbidity based on the acoustic backscatter over 13-hrs cycles (hull-mounted acoustic Doppler current profiler). (2) Very-high resolution acoustic measurements (Kongsberg-Simrad EM3002 multibeam, MBES) to obtain depth, backscatter, and water column data. Repetitive MBES measurements allow identifying erosion and/or deposition areas, estimating bedload transport pathways and magnitude from the asymmetry and rate from the migration of sand dunes, and assessing seabed sediment changes. (3) Water column measurements at fixed stations, over 13 hrs windows, to study temporal variations in salinity, temperature and depth (CTD), turbidity (optical backscatter sensor, OBS), and particle size distributions (Sequoia type C 100 X Laser In-Situ Scattering and Transmissometry, LISST). Water samples are taken for calibration of the OBS measurements.

To investigate near-bottom processes, it is envisaged to use a benthic tripod, instrumented with sensors dedicated to the measurement of currents, using ADP (Acoustic Doppler Profiler) and ADV (Acoustic Doppler Velocimeter) instruments, and turbidity (OBS). Bottom shear stress will be calculated (Francken & Van den Eynde 2010). At least, recordings of 14 days spring/neap tidal cycles are aimed at.

Seabed sediment samples are taken in function of increasing the reliability of sediment maps that serve as input to sediment transport models (e.g.,

bottom roughness). Changes in seabed sediment samples (e.g., siltation) are evaluated.

Optimal positions of the in-situ measurements are based on the results of the acoustic measurements (ADCP and MBES), and model results.

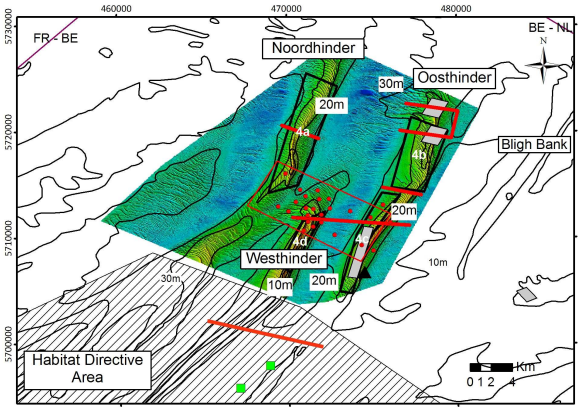

Figure 2. Sandbanks and troughs in the area of the Hinder Banks. Cross-sectional lines show the locations of ADCP profiling. Along the transects, water sampling and vertical profiling is performed. Repetitive MBES measurements are performed in the grey zones and within the rectangle covering the central zone of the Hinder Banks, together with sediment samples. The triangle indicates the position of longer-term measurements of sediment processes. Small rectangles in the Habitat Directive area are the locations of ecologically valuable gravel beds. Background bathymetry: FPS Economy, Self-Employed and Energy.

3.2 Quantitative model validation

Measurements will feed into numerical models (250 m x 250 m grid resolution) for conducting impact assessments under various scenarios of extraction activities.

Hydrodynamic models (OPTOS-BCZ, Luyten 2010), driving sediment transport and advection-diffusion models, need validation to allow quantification of their accuracy, critical to detect changes in time. Statistical analyses of the differences between model results and observations will be executed.

Sediment transport models (MU-SEDIM, Van den Eynde et al. 2010) need refinement: e.g., bottom shear stress calculated with the numerical model, will be compared with the bottom shear stress, derived from the ADV and ADP measurements (see above). An adjustment of the modelled shear stress to the observed shear stresses will be executed, by fitting the bottom roughness. Using all available data, an analysis of the variability of the resulting bottom roughness, as a function, amongst others, of grain-size distribution, will be executed. Furthermore the predicted sediment transport magnitude and directions will be compared to the sediment transport estimates, derived from sand dune migrations and asymmetries.

Advection-diffusion sediment transport models (MU-STM, Fettweis & Van den Eynde 2003; Van den Eynde 2004) will be refined allowing quantifying erosion and deposition of fine-grained material and (fine) sand in the water column. Results will be compared with the measurements and observations along areas where the probability of settling of finer sediments is highest. The significance of increases in turbidity will be determined from statistical analyses of the longer time series of turbidity (from benthic lander).

4. DISCUSSION

As stated in the introduction, the monitoring programme should allow quantifying the impacts of marine aggregate extraction and evaluating its compliancy with European Directives. The latter is relatively new and the monitoring requires extensive testing of the effectiveness and sensitivity of the indicators that should allow assessing progress towards good environmental status. For assessing changes in hydrographic conditions, the ranges in calculated bottom shear stress will identify whether or not an impact should be further evaluated. If this is the case, it is still acceptable as long as the impacted area remains within a certain buffer. For the exploitation in the Hinder Banks region this buffer is indicated in Fig. 3. Clearly, the area of impact can have significant dimensions. Following this concept, no impact is allowed in the Habitat Directive area, just south of the exploitation zone. Whether or not this indicator would be an early warning, preventing adverse effects on the ecosystem, remains to be investigated.

Furthermore, the influence of varying bedform properties and dynamics is not clear yet.

Calculation of bottom shear stresses is far more complicated in bedform areas, and can potentially not be modelled with conventional techniques. The dynamics of large bedforms and the relation with ecological functions they can provide is poorly studied. According to their setting, dimensions and morphology, some of them are more effective in trapping fine sediments (Van Lancker et al. this volume). In many cases such areas host a richer biodiversity. Whether or not exploitation-induced siltation will adversely affect the ecosystem requires further investigation and debate.

Hence, monitoring programmes should be adaptive, with approaches that are adjustable following external input and new insights. It is a learning process with the aim of reducing uncertainties and allowing calculation of risks when certain environmental goals are not reached (Laane et al. 2012). Extensive data-model integration is needed, that should allow showing the societal relevance of the measures that are proposed to monitor progress towards good environmental status of the marine environment.

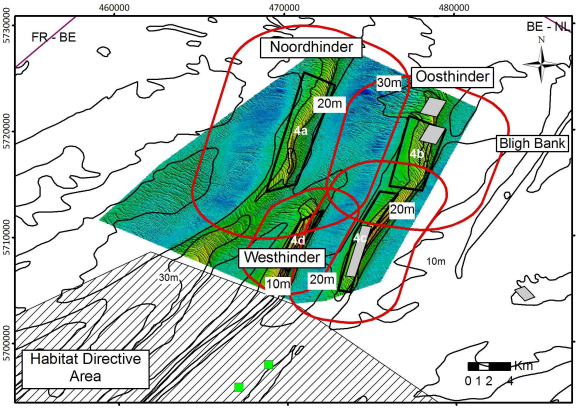

Figure 3. Buffer of acceptable change in bottom shear stress in the Hinder Bank region where marine aggregate extraction is allowed in 4 sectors. Calculations according to Belgische Staat (2012).

5. CONCLUSIONS

A monitoring programme is proposed that should allow quantifying the impacts of marine aggregate extraction and evaluating its compliancy with European Directives. Most importantly, monitoring should allow assessing progress towards good environmental status. This is relatively new and requires extensive testing of effectiveness and sensitivity of indicators. One of the indicators is bottom shear stress and should allow evaluating changes in hydrographic conditions due to human impact. It is stipulated that extensive data-model integration is needed for adequate assessments of the status of the marine environment, a prerequisite for sustainable use of living and non-living resources.

6. ACKNOWLEDGMENT

The evaluation of the effects of marine aggregate extraction forms part of a continuous monitoring programme, paid from the revenues of extraction activities (ZAGRI). The Flemish Authorities, Agency for Maritime Services and Coast fund the dedicated research in the area of the Hinder Banks.

7. REFERENCES

Belgische Staat 2012. Determination of Good Environmental Status and establishment of environmental Targets for the Belgian marine waters. Art. 9 & 10: 33 pp. Brussels: Federal Public Service Health Food Chain Safety and Environment.

Fettweis, M. & Van den Eynde, D. 2003. The mud deposits and the high turbidity in the Belgian Dutch coastal zone, Southern bight of the North Sea. Continental Shelf Research 23: 669-691.

Francken F. & Van den Eynde D. 2010. Calculation of current and wave induced turbulence from high frequency ADV measurements: 14 pp. Brussels: MUMM report.

Houziaux, J.-S., Kerckhof, F., Degrendele, K., Roche, M.F. & Norro, A. 2008. The Hinder banks: yet an important area for the Belgian marine biodiversity?: 248 pp. Brussels: Belgian Science Policy.

Laane, R.W.P.M., Slijkerman, D., Vethaak, A.D., & Schobben, J.H.M. 2012. Assessment of the environmental status of the coastal and marine aquatic environment in Europe: A plea for adaptive management. Estuarine. Coastal and Shelf Science 96: 31–38.

Luyten P. 2010. COHERENS - A coupled hydro-dynamical-ecological model for regional and shelf seas: User Documentation. Version 2. Brussels: Management Unit of the North Sea Mathematical Models.

Rice, J., Arvanitidis, C., Borja, A., Frid, C., Hiddink, J. G., Krause, J., Lorance, P., Ragnarsson, S. A., Skold, M., Trabucco, B., et al. 2012. Indicators for Sea-floor Integrity under the European Marine Strategy Framework Directive. Ecol. Indicators 12: 174–184.

Van den Eynde, D. 2004. Interpretation of tracer experiments with fine-grained dredging material at the Belgian Continental Shelf by the use of numerical models. Journal of Marine Systems 48: 171-189.

Van den Eynde, D., Giardino, A., Portilla, J., Fettweis, M., Francken, F. & Monbaliu, J. 2010. Modelling The Effects Of Sand Extraction On The Sediment Transport Due To Tides On The Kwinte Bank. Journal of Coastal Research, SI 51: 106-116.

Van Lancker, V.R.M., Bonne, W., Bellec, V., Degrendele, K., Garel, E., Brière, C., Van den Eynde, D., Collins, M.B. & Velegrakis, A.F. 2010. Recommendations for the sustainable exploitation of tidal sandbanks. Journal of Coastal Research SI51: 151-161.

Van Lancker, V. & van Heteren, S. 2013b. Case Study 4: Revisiting the spatial distribution of EUNIS Level 3 North Sea habitats in view of Europe's Marine Strategy Framework Directive, pp. 86-93. In: V. Van Lancker & S. van Heteren (eds.). Standardisation and harmonisation in seabed habitat mapping: role and added value of geological data and information. EU-FP7 Geo-Seas Deliverable 10.5.

Van Lancker, V., Houziaux, J.S., Baeye, M., Van den Eynde, D., Rabaut, M., Troost, K., Vermaas, T. & van Dijk, T.A.G.P. this volume. Biogeomorphology in the field: bedforms and species, a mystic relationship: 1-7.

Biogeomorphology in the field: bedforms and species, a mystic relationship

V. Van Lancker[(1)], J.S Houziaux[(1)], M. Baeye[(1)], D. Van den Eynde[(1)], M. Rabaut[(2)], K. Troost[(3)], T. Vermaas[(4)] and T.A.G.P. van Dijk[(4,5)]

1. Royal Belgian Institute of Natural Sciences. Management Unit of the North Sea Mathematical Models (MUMM). Gulledelle 100, B-1200 Brussels, Belgium
   E-mail: vera.vanlancker@mumm.ac.be
2. Ghent University. Marine Biology Section, Belgium. *Present address: Cabinet Johan Van de Lanotte, Deputy Prime Minister and Minister of Economy, Consumer Affairs and North Sea
3. IMARES, The Netherlands
4. Deltares. Dept. of Applied Geology and Geophysics, The Netherlands
5. University of Twente, Dept of Water Engineering & Management, The Netherlands

Abstract

Fine-scale seabed mapping (<5 m resolution) (e.g. surficial sediments, morphology and benthos) was conducted along the ebb-tidal delta of the Westerschelde estuary, Belgian and Dutch part of the North Sea. To understand variations in habitat and species distributions, mapping was combined with measurements of currents and turbidity throughout 13-hrs cycles and with sediment transport modelling results.

Results showed that highest abundances of some ecosystem engineering species (e.g. the tubeworm *Owenia fusiformis*, and the razor clam *Ensis directus*) occur near bedload convergence zones resulting from a mutually evasive flood- and ebb-dominant channel system. Such zones are at the end of the channels, hence also fine-grained sediments, food and larvae are trapped. The combination of the coarser-grained bedload with the deposition of fines is indeed the optimum for a lot of suspension and detritus feeders. Still, highest abundances occur at the fringes of such a system where stress levels are intermediate. Hypotheses were successfully tested along the Dutch coastal zone. Those insights are important to assess changes in seafloor integrity and hydrographic conditions, two descriptors to define Good Environmental Status within Europe's Marine Strategy Framework Directive.

1. INTRODUCTION

Biogeomorphology is a field in which the understanding of benthic species in relation to their surrounding landscape is critical. In the marine environment, observations of both components remain relatively scarce, but increase steadily as multibeam technology allows capturing, visualizing and quantifying benthic and terrain variables on both small- and large-scales (e.g. Van Lancker et al. 2012). However, feedback mechanisms between geomorphology and benthos are not always clear. Complexity increases where also humans affect the benthos-landscape relationship. This is the case along the ebb-tidal delta of the Westerschelde estuary ('Vlakte van de Raan'), where disposal of dredged material is regular practice for already 30 yrs. This paper discusses the relative occurrences of macrobenthic species in this area in relation to its driving forces.

2. STUDY AREA

Measurements and observations have been made along the Belgian and Dutch part of the North Sea, a siliciclastic macro-tidal environment (tidal range of 4.5 m), comprising several groups of sandbanks (Fig. 1). Sediment transport is mainly driven by tidal currents (max. 1.2 m/s), though wind-induced currents may have a direct effect on sediment resuspension and bedform morphology. Along the Vlakte van de Raan sediment dynamics become more complex. Increased sediment fluxes arise from the disposal activities, but along its delta front, and more offshore, bedform patterns are very complex with varying rates and directions of migrating sand dunes (Fig. 1). Also on the disposal

ground itself a series of large sand dunes is present (Du Four & Van Lancker 2008) (Fig. 1). On this location, biodiversity is low, but regional observations of macrobenthos (species larger than 1 mm) did show higher abundances in this area (Fig. 2).

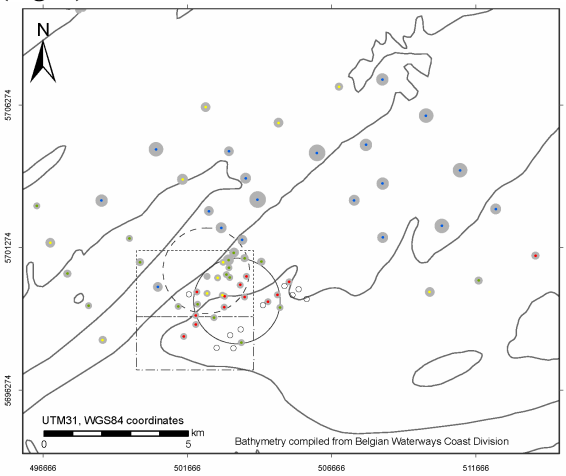

Figure 2. Macrobenthos densities and communities along the western part and delta front of the Vlakte van de Raan (Belgian part). Low species densities to no fauna (open circles) characterize the disposal ground; densities (sized circles) amount up to more than 25.000 ind. m^{-2} with up to 43 species per 0.1 m^2 (Macrodat@UGent, Degraer et al. 2006). Along the delta front the *Abra alba* community thrives, being the most rich and diverse macrobenthic community on the Belgian part of the North Sea. Location see Fig. 1.

Also, the razor clam *Ensis directus*, being the most important invasive species on the Belgian part of the North Sea thrives in this area (Houziaux et al. 2011). This species is commercially exploited in the Dutch part of the North Sea. Yearly stock assessments take place, though the monitoring would benefit from a revised survey design based on the habitat preferences of the species (Troost et al. 2012).

3. METHODOLOGY

High resolution multibeam acoustic data were acquired (Kongsberg Simrad EM1002/99 kHz and EM3002/300 kHz) for seabed mapping and habitat characterization (yearly surveys in the period 2006-2011). Depth and backscatter data were processed and data grids were produced at a resolution lower than 5 m. This allowed quantifying fine-scale sediment and terrain variation, as also bioturbation. Some species indeed alter the acoustic response of the seafloor (e.g. Degraer et al. 2008; Van Lancker et al. 2012), with dense colonies of tubeworms forming mounds of up to 40-50 cm. For the area, these were observed through fine-scale terrain analyses. For the time series analyses, vertical dynamics are quantified from the calculation of a linear trend in time over the available bed levels on a cell-by-cell basis (Van Dijk et al. 2011). Additionally, current and backscatter profiling (Acoustic Doppler Current Profiling, ADCP) was carried out along a transect perpendicular to the delta front, covering periods of 13 hrs tidal cycles. Sediment and macrobenthos samples (> 1 mm) were taken, both in the Belgian and Dutch sector. In this paper, multibeam results will be discussed in more detail.

4. RESULTS

In the area of highest macrobenthos abundances (Fig. 2), a complex of large to very large dunes was revealed (Fig. 3). Bathymetry data showed that the highest dunes occurred where the channel, separating the Vlakte van de Raan from the Akkaert Bank, gradually shallows. The ending of the channel and its higher relief is caused by the interaction of flood and ebb tidal currents, on a residual basis. This is typical in an area where the interaction between the tidal flow and the local or regional bottom topography leads to unequal strengths and duration of the flood and ebb tidal currents. Both currents evade from each other leading to bedload deposition in their interaction zone. This is called a mutually evasive sediment transport system, *sensu* Harris (1988).

In the present case the flood is most dominant and has created a so-called flood channel. ADCP profiling showed strong and rectilinear currents along its axis (Fig. 6). Bedforms are clearly flood-dominated, but become more symmetrical near the end of the channel. Analysis of the morphology, asymmetries and migration rates through time, showed that the northwestern side of the flood channel was merely characterized by ebb-dominated dunes (Fig. 3). A similar evasive system occurs higher up the delta front, though the ebb-dominancy, as also the transport pathway is more difficult to evidence. In any case, currents are weaker here and the tidal ellipse is more rotary (Fig. 6). Generally, the dune area along this side of

the flood channel is more depositional. Figure 4 shows the differences in vertical dynamics along the NW, Central and SE side of the axis of the flood-channel. Note that the dynamics are only high at the end of the flood-channel.

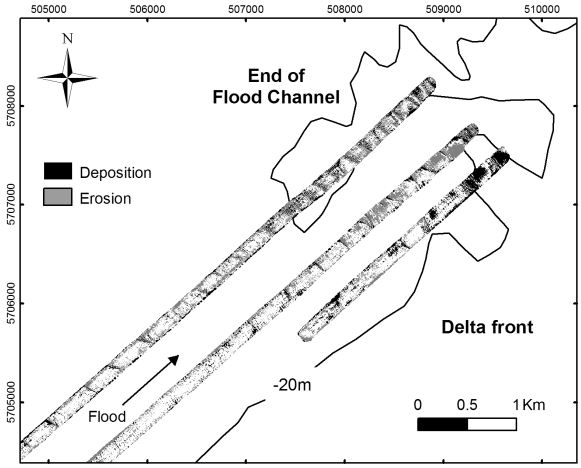

Figure 4. Trends of vertical dynamics based on multibeam time series, here in 2008 and 2009. Along the northern profile erosion and deposition alternate, because of alternating flood and ebb dominancy of the dunes; centrally the dunes are mostly erosive; to the southeast, up the delta front, mostly deposition occurs.

Regarding the occurrence of macrobenthos, high resolution multibeam recordings showed extensive small-scale mounds in-between large to very large dunes in water depths around -20 m (Fig. 5). These were related to colonies (up to 6000 ind. m^{-2}) of the tube-building polychaet *O. fusiformis* (Fig. 5). They occupy areas of up to 12 km^2.

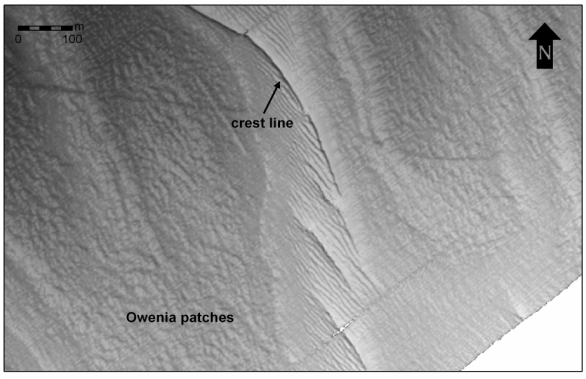

Figure 5. Detailed shaded relief map of an area with very large dunes; in the troughs extensive fields of *O. fusiformis* are present (rectangle on Fig. 3). The Owenia mounds are up to 40-50 cm high.

However, higher up the delta front densities increased with a maximum of macrobenthos abundance along the upper slope, from -16 m onwards (Fig. 6). This is the fringe area, where flood and ebb residual currents mutually evade. Up to 11881 ind. m^{-2} were found of *O. fusiformis* and more than 500 ind. m^{-2} of *E. directus*. ADCP-derived backscatter profiling showed that this zone is regularly affected by transient turbidity plumes descending the delta front during the ebbing phase of the tide. Dispersion modelling showed that the fine-grained material could originate from the disposal activities, though any fines, whether naturally-, or anthropogenically-induced, would be transported downwards.

Hypotheses were tested along the Dutch Voordelta where it was aimed at predicting highest abundances of *E. directus* from multibeam bathymetry. From the observations described above, an area with a similar setting was chosen for time- and cost-efficient monitoring: from large-scale bathymetry the end of a flood channel was selected (Fig. 1) and surveyed using high resolution multibeam technology. Again a complex of large to very large dunes was revealed with macrobenthos sampling results showing highest abundances (a so-called Ensis bed) at the southeast fringe of the dune system (Fig. 7).

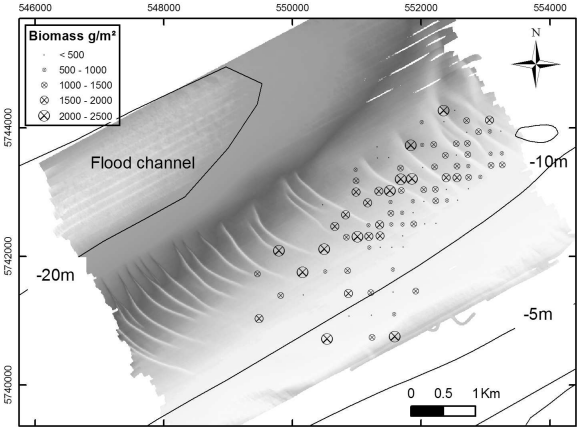

Figure 7. Distribution of biomasses of large Ensis (width > 16 mm), sampled by boxcores (IMARES monitoring Autumn 2012), projected on a multibeam-derived digital terrain model. Note the ebb-shape of the dunes, regardless the overall flood-dominancy of the area. Location see Fig. 1.

Results are important in the framework of Europe's Marine Strategy Framework Directive requiring Good Environmental Status (GES) of its marine waters by 2020. Related to physico-chemical seabed attributes, descriptor 6 on seafloor integrity and descriptor 7 on hydrographic conditions are relevant here. GES for seafloor integrity refers to the structure and functions of the ecosystems that need safeguarding, without adversely affecting benthic ecosystems, whilst GES for hydrographic conditions means that permanent alteration of hydrographical conditions does not adversely affect marine ecosystems. Given the benthos-landscape relationship major changes to flood- and ebb tidal channel systems will undoubtedly affect the benthic ecosystem. Results also indicate that the deposition of fine-grained material, e.g. as resulting from increased human activities, is not necessarily adverse to the structure and function of the ecosystem. Definition of allowable ranges is a challenge for all disciplines.

5. CONCLUSIONS

Extensive fine-scale seabed mapping (e.g. surficial sediments, morphology and benthos), in combination with current and turbidity profiling, was carried out along the delta front of the ebb tidal delta of the Westerschelde, Belgian and Dutch part of the North Sea. It was shown that highest abundances of macrobenthos occurred in areas where fine-grained material naturally deposits on top of relatively coarser substrates. This combination is most favourable for suspension feeders (e.g. ecosystem-engineering tube worms and clams) that profit from the stable substrate, of which its coarseness is favourable for detritus trapping and for better oxygenation. In addition, the passing to deposition of fines provides ample opportunities for filtering food resources. Such zones are found: (1) Near bedload convergence zones, at the end of mutually evasive flood- and ebb-dominant channels. Higher dynamics results in the combination of relatively coarser sediments that are enriched with fine-grained material that is, together with food and larvae, transported through the channel systems. Species that can withstand the overall higher dynamics will be sheltered in the troughs of the large to very large dunes. Though, highest abundances are found at intermediate stresses at the edge of such systems. (2) Up-slope delta fronts, abundances are higher since the edge zones are also enriched with fines that are deposited from turbidity plumes. Whether naturally or anthropogenically-driven (e.g. from disposal activities) these are transported downwards the slope during the ebbing phase of the tide. High abundances of macrobenthos were found in similar settings along the Dutch Voordelta area.

6. ACKNOWLEDGMENT

Data were acquired in the framework of the Belgian Science Policy projects QUEST4D (SD/NS/06B) and EnSIS (SD/NS/09A). Ghent University, Renard Centre of Marine Geology is thanked for the use of multibeam processing software Sonarscope (Ifremer). Ifremer granted the use of the CARAIBES software in the framework of the EU-FP7 Geo-Seas project. Officers and crew of RV Belgica are particularly acknowledged.

7. REFERENCES

Degraer, S., Moerkerke, G., Rabaut, M., Van Hoey, G., Du Four, I., Vincx, M., Henriet, J.P. & Van Lancker, V. 2008. Very high resolution side-scan sonar mapping of biogenic reefs of the tube-worm Lanice conchilega. Remote Sensing of Environment 112 : 3323-3328.

Degraer, S., Wittoeck, J., Appeltans, W., Cooreman, K., Deprez, T., Hillewaert, H., Hostens, K., Mees, J., Vanden Berghe, W. & Vincx, M. 2006. Macrobenthos Atlas of the Belgian part of the North Sea: 163 pp. Brussels: Belgian Science Policy. ISBN 90-810081-5-3.

Du Four, I. & Van Lancker, V. 2008. Changes of sedimentological patterns and morphological features due to the disposal of dredge spoil and the regeneration after cessation of the disposal activities. Marine Geology 255(1-2): 15-29.

Harris, P.T., 1988. Large scale bedforms as indicators of mutually evasive sand transport and the sequential infilling of wide-mouthed estuaries. Sedimentary Geology 57: 273–298.

Houziaux, J.-S., Craeymeersch, J., Merckx, B., Kerckhof, F., Van Lancker, V., Courtens, W., Stienen, E., Rabaut, M., Perdon, J., Goudswaard, P.C., Van Hoey, G., Vigin, L., Hostens, K., Vincx, M. & Degraer, S. 2011. 'EnSIS' - Ecosystem Sensitivity to Invasive Species. Final Report: 100 pp. Brussels: Belgian Science Policy, Research Programme Science for a Sustainable Development.

Troost, K., Van Asch, M., Baeye, M., Brummelhuis, E., Davasuuren, N., Van den Ende, D., & Van Lancker, V. 2012. KBWOT 2012: the use of an acoustic technique in mapping beds of razor clams (Ensis sp.): 23 pp. Den Haag: Stichting DLO Centre for Fisheries Research (CVO). Commissioned by EL&I Directie Kennis).

Van Dijk, T.A.G.P., van der Tak, C., de Boer, W.P. Kleuskens, M.H.P., Doornenbal, P.J., Noorlandt R.P. & Marges, V.C. 2011. The scientific validation of the hydrographic survey policy of the Netherlands Hydrographic Office, Royal Netherlands Navy. Delft: Deltares, report 1201907-000.

Van Lancker, V., Moerkerke, G., Du Four, I., Verfaillie, E., Rabaut, M. & Degraer, S. 2012. Fine-scale geomorphological mapping for the prediction of macrobenthic occurrences in shallow marine environments, Belgian part of the North Sea, ***in***: Harris, P. and E. Baker (Eds.) 2012. Seafloor Geomorphology as Benthic Habitat: GeoHab Atlas of seafloor geomorphic features and benthic habitats: 251-260. Elsevier Insights.

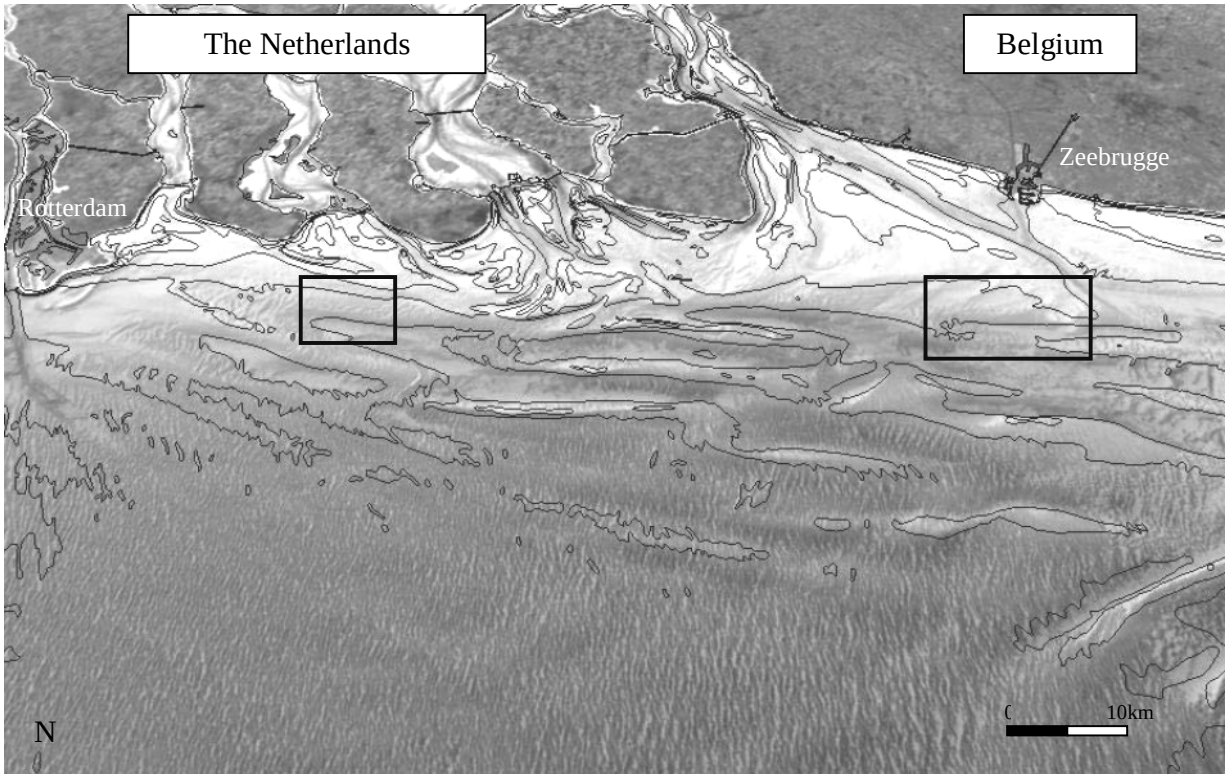

Figure 1. Deltas from the rivers Rhine, Meuse and Scheldt impacting on the Belgian-Dutch coastal zone. Note the complex offshore bathymetry with sandbanks and gullies. Bathymetric data compiled from Flemish Hydrography and Deltares 2011 (Nederlandse Hydrografische Dienst & Rijkswaterstaat Dienst Noordzee). Rectangles indicate the study areas of the Vlakte van de Raan (Belgium) and along the Dutch Voordelta (The Netherlands).

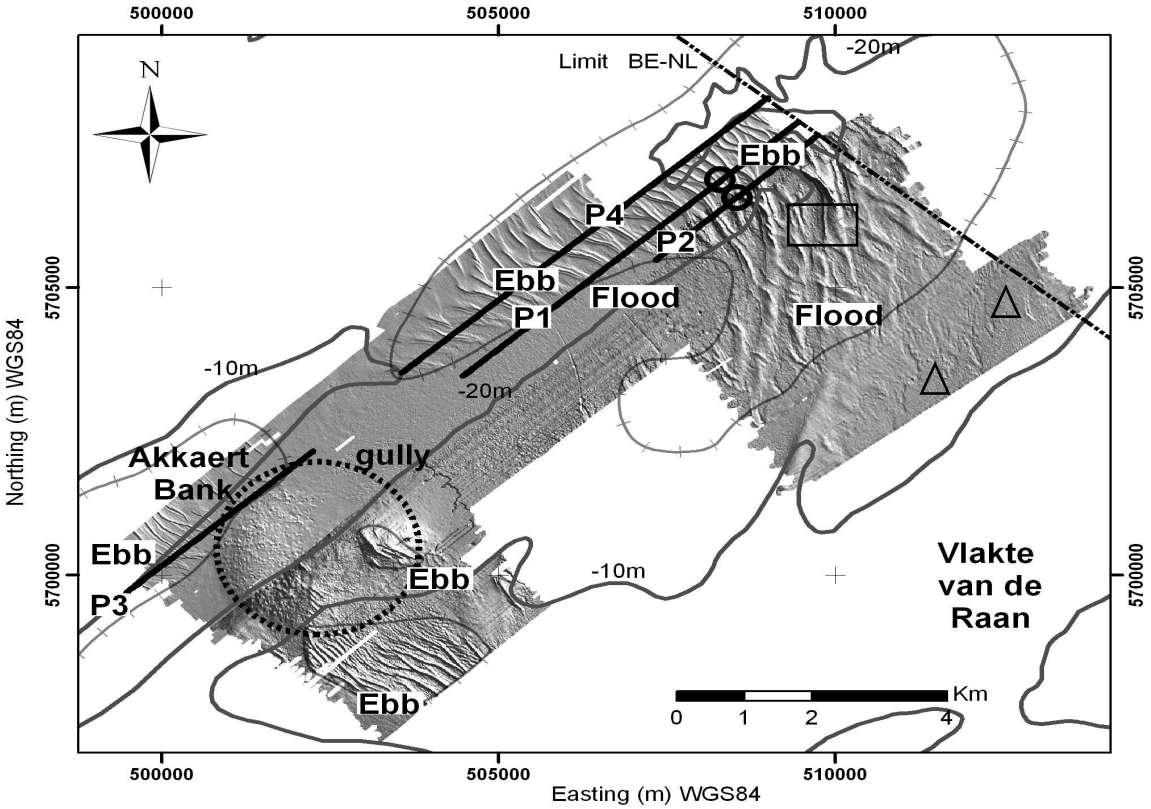

Figure 3. Detailed seabed morphology, as derived from multibeam seabed mapping. Areas with large dunes are observed south and north of the present disposal ground of dredged material (dashed circle). At the northeast extremity of the gully, a series of large complex dunes (up to 4 m) are present. In the axis of the gully and towards the slope their asymmetry is clearly flood-dominated; this gully is a flood-dominated channel. However, in the prolongation of the Akkaert Bank, dunes show an ebb-dominancy. The broad end of the flood channel is a bedload convergence zone, resulting from mutually evasive flood- and ebb-dominated transport zones. Here, colonies of the tube worm *O. fusiformis* occur in the troughs of the dunes (rectangle, see Fig. 6 for a detailed view), as also large quantities of *E. directus* juveniles, American razor blade and most important invasive species along the Belgian part of the North Sea. Higher up the delta front higher densities of *O. fusiformis* and *E. directus* adults occur (triangles). Four profiles (P1 to P4) are indicated along which bedform evolution was followed (see Fig. 5). The circles on profile P1 and P2 indicate where flood- and ebb-dominated dunes converge. The intersected line represents the maximum extent of the bedform area, as derived from broad-scale DTM's.

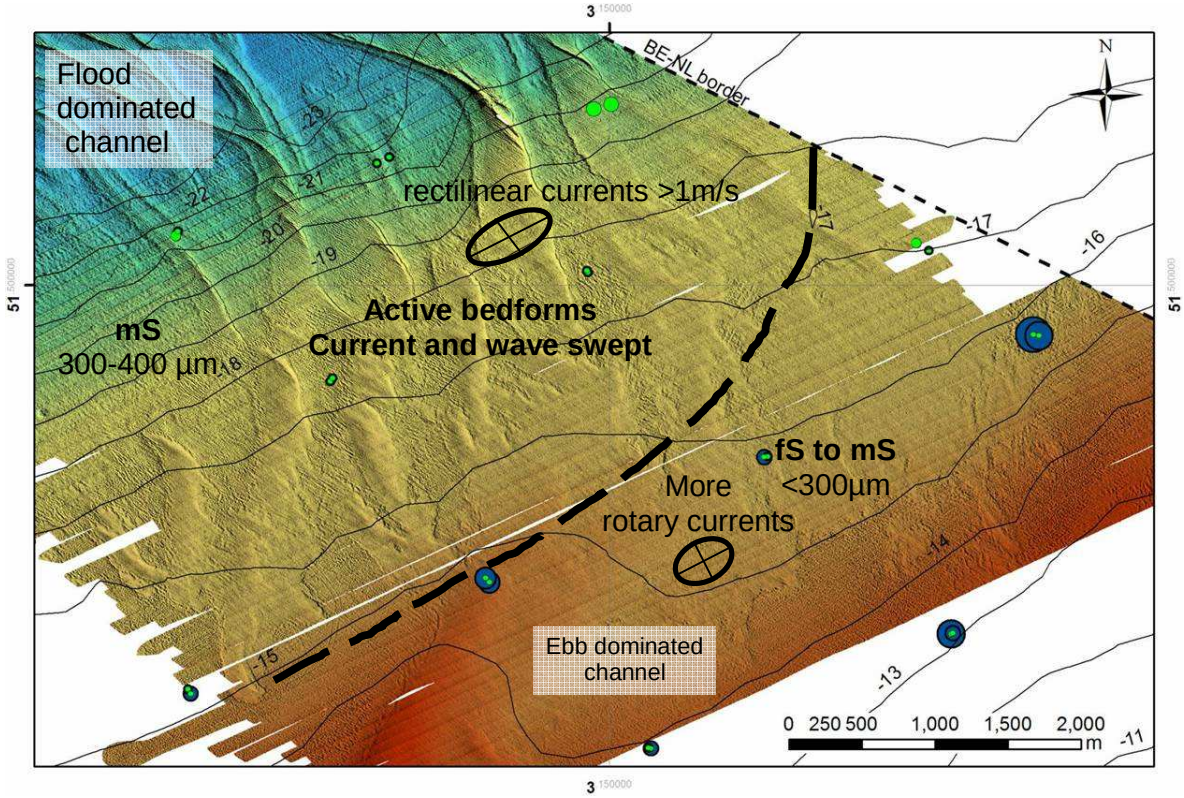

Figure 6. Synthesis figure of sediment dynamics, as derived from acoustic measurements (multibeam and ADCP). Recently reworked sand dunes were observed (without major trawling traces, in contrast to earlier observations that mostly witnessed ripped-up seafloors). In this zone of active transport medium sands (mS) prevail. The dashed line delimits the zone of highest dynamics. Higher up the delta front sediments become finer (fS) and currents became more rotary and less in strength. The ebb current is here important. Highest densities and species richness occur in this upper slope area (e.g. *O. fusiformis* ~ 11.000 ind. m^{-2} *E. directus* (dark grey circles) > 500 ind. m^{-2}). Light grey circles correspond with the occurrence of *E. directus* juveniles; they are most abundant near the end of the flood-dominant channel. The upper slope area is most frequently subdued to transient turbidity plumes, naturally and anthropogenically-induced. Only, stress-resistant species can survive.

Amplified Sediment waves in the Irish Sea (AmSedIS)

Katrien Van Landeghem[(1)], Giovanni Besio[(2)], Helge Niemann[(3)], Claire Mellett[(4)], Dei Huws[(1)], Lea Steinle[(3)], Shane O'Reilly[(5)], Peter Croker[(6)], Dave Hodgson[(4)] and David Williams[(7)]

1. School of Ocean Sciences, Bangor University, Menai Bridge, Wales, UK - katrien.vanlandeghem@gmail.com
2. Department of Civil, Chemical and Environmental Engineering, Università degli Studi di Genova, Genova, Italy
3. Department of Environmental Sciences, Universität Basel, Basel, Switzerland
4. School of Environmental Sciences, University of Liverpool, Liverpool, UK
5. School of Chemical Sciences, Dublin City University, Glasnevin, Dublin 9, Ireland
6. Previously at Petroleum Affairs Division, Dublin 2, Ireland
7. Agri-Food and Biosciences Institute (AFBI), Newforge Lane, Belfast, UK

Abstract

Exceptionally high, straight-crested and trochoidal sediment waves have recently been observed on shelf seas world-wide, and reach heights of up to 36 m in the Irish Sea. It is uncertain how the interplay between geological, biogeochemical and hydrodynamic processes influences the migration and extreme growth of these sediment waves. The AmSedIS project thus sets out to (1) investigate the role of sediment granulometry and sediment availability on both “extreme” and “normal” sediment wave development and (2) investigate the potential association of methane derived carbonate formation with extreme sediment wave growth. The preliminary findings are: (1) The crests of unusually high and trochoidal sediment waves still migrate over several meters per year and they consist of coarser, more poorly sorted sediments in comparison to the "normal" sediments waves; (2) Methane seepage is not considered a factor in extreme sediment wave development; (3) The excess of mobile sediment supply seems to allow for "extreme" sediment wave growth, and is linked to palaeo-tunnel valleys and the finer sediments that fill them or with converging sediment transport pathways; (4) The variation in sediment from sediment wave trough to crest to trough will form the basis for more advanced numerical modelling.

1. INTRODUCTION

Large sediment waves are striking yet poorly understood seabed features in many shelf seas. Very large sediment waves (3–18 m in height) are documented to migrate up to 70 m per year (over time scales >> the tidal period) in the Irish Sea (Van Landeghem et al., 2012). Such transport of enormous sediment volumes can endanger the stability of pylons, cables and pipes on and beneath the seabed and causes a highly mobile benthic habitat. In addition, straight-crested, trochoidal, symmetrical and unusually high sediment waves (>18 m) have recently been observed adjacent to “normal-sized” sediment waves on shelf seas world-wide (Barrie et al., 2009; Valentine et al., 2002; Van Landeghem et al., 2009) reaching heights up to 36 m in the Irish Sea and comprise over 1/3 of the water column. These immense sediment waves contrast in their cross sectional form with normally shaped sediment waves that have a gentle stoss slope and a steep lee slope. Figure 1 illustrates this contrast.

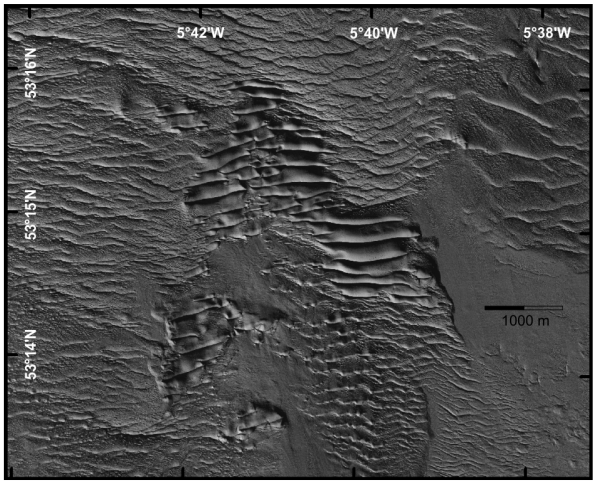

Figure 1. Pockets of straight-crested, trochoidal sediment waves amidst "normal" sediment waves. This data was collected by the INFOMAR project.

As part of the project AmSedIS (Amplified Sediment waves in the Irish Sea), a team of marine geoscientists, geochemists and numerical modellers from the UK, Italy, Switzerland and Ireland embarked on an 11-day survey on the RV Celtic Voyager in April 2012 to survey various sites in the Irish Sea (Fig. 2). The dataset collected includes swath bathymetry data, boomer and sparker seismic profiles, CTD transects, water sampling and Shipek grab sampling. Some bad luck stood in the way of collecting vibrocores.

Figure 2. Scientists and crew members on the RV Celtic Voyager about to collect data for the AmSedIS project.

1.1. Characteristics of sediment waves

From the relatively few studies on unusually high sediment waves, the suggestions thus far have been that they
(i) scale with water depth (Barrie et al., 2012),
(ii) are immobile and moribund (Van Landeghem et al., 2009),
(iii) are formed in response to the bi-directionality of tidal currents (Allen, 1980; Valentine et al., 2002; Van Landeghem et al., 2009),
(iv) are amplified as a result of gas seepage (Hovland, 1993; Judd et al., 2007),
(v) form due to standing internal waves from stratified water flowing across a step in the sea floor (Cartwright, 1959) and/or
(vi) represent differences in sediment grain sizes (Bartholdy et al., 2002; Valentine et al., 2002).

Unusually high sediment waves do not scale with water depth, they are not always associated with a step in the seafloor and they are still mobile with migration rates of up to 2 meters per year (Van Landeghem et al., 2009; 2012). The biogeochemical aspects of methane oxidation are complex and the causal link with sediment wave growth remains un-tested. To improve our understanding on the dynamics of these sediment waves, we thus investigate the effect of sediment grain size variability, mobile sediment supply and gas seepage.

1.2. Influence of sediment size and sorting on sediment wave dynamics

The sediment wave sizes are reported to increase with grain size until about 0.5 mm, after which they decrease (Dalrymple and Rhodes, 1995). This relationship has been further quantified (Bartholdy et al., 2002), but the correlations are likely site-specific and the question remains what the variation of grain size is within sediment waves. In unusually high sediment waves, the variation in grain size in the series of deposits within the bedform will influence its stability.
In sediments with mixed grain-sizes, coarser grains become more exposed to the near-bed currents, while the finer grains become hidden behind or in between large grains. This hiding-exposure effect alters the threshold of entrainment of differently sized sediment in a layer and will define which proportion is actively mobile (Van Oyen and Blondeaux, 2009), thus allowing sediment waves to grow larger. As mixed sediments are progressively sorted during sediment wave formation, this hiding-exposure effect is expected to change over time. Well-sorted sediment would accommodate faster growth rates. Poorly sorted sediment would dampen growth in weak tidal currents and strengthen it in strong currents (Van Oyen and Blondeaux, 2009). This time-dependent effect thus likely plays a more significant role in sediment wave dynamics than previously thought and is represented by the dimensions of sediment waves and the nature of the sediments inside them.

1.3. Influence of sediment availability on sediment wave dynamics

The infill of flooded landscapes scoured by glacial processes in the Irish Sea is expected to increase the amount of mobile sediment available for sediment wave formation. The spatial relationship of tunnel valleys and unusually high sediment waves has been documented tentatively (Van Landeghem et al., 2009), but is investigated further in this work.

In the Juan Fuca Strait (British Colombia), the occurrence of unusually high sediment waves is related to the entrapment of coarse sand in seafloor depressions (Barrie et al., 2009). These seafloor depressions occur in the Irish Sea as well, and so it is investigated whether these seafloor depressions host amplified sediment wave formation or if they are created subsequently from intensive scour around the huge sediment waves.

1.4. Influence of gas seepage on sediment wave dynamics

When methane migrates upwards through the sediment column (cold seeps), it may be oxidised with sulphate, leading to the precipitation of methane-derived authigenic carbonates (MDAC). These carbonate minerals cement the seabed sediments to a hard, rock-like structure. Cold seeps and the mechanism of methane oxidation has tentatively been linked to extreme sediment wave growth in the North Sea (Hovland, 1993). The cemented layers would make the sediment more difficult to displace, accommodating aggradation rather than migration and therefore amplifying sediment wave growth. The presence of shallow gas seeps and MDAC coincide with the presence of sediment waves in the Codling Fault Zone and in the Western Trench (Judd et al., 2007). Recent work by the Joint Nature Conservation Committee identified a large area with MDAC in the central Irish Sea. Between these "Croker Carbonate Slabs", abnormally high sediment waves also occur. We thus investigate, for the first time, evidence for past and present methane seeps in the sediments of sediment waves and, if methane by-passes the benthic microbial filter, in the water column above the bedforms.

2. SURVEY RESULTS

2.1. Overview of survey areas

Figure 3 illustrates the several areas in the Irish Sea and Liverpool Bay where swath bathymetry data, seismic profiles, CTD transects and Shipek grab samples were collected.

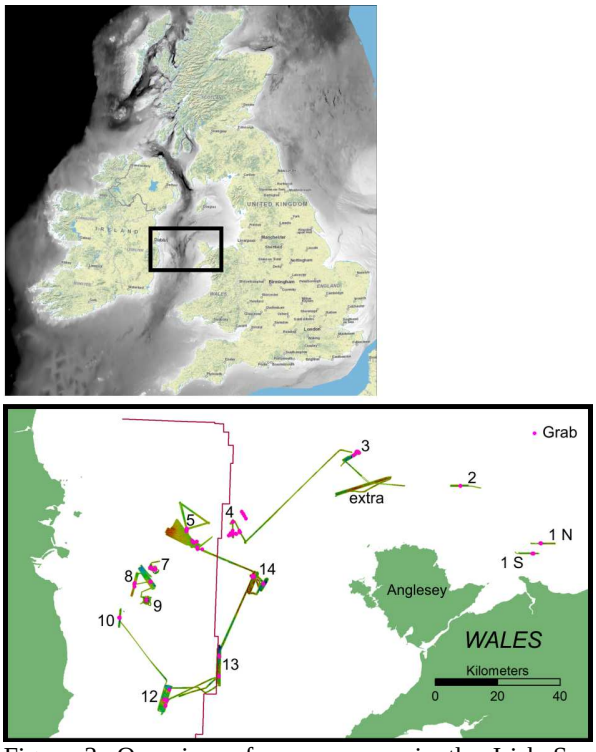

Figure 3. Overview of survey areas in the Irish Sea during the AmSedIS survey in April 2012.

2.2. Variation in sediment wave sizes and migration speeds

Repeated swath bathymetry data permits sediment wave sizes and migration rates to be documented. The data from April 2012 largely confirmed the distribution of sediment wave sizes and migration rates previously published (Van Landeghem et al., 2012), with sediment waves of all sizes typically migrating a few meters per year, locally amplified where currents are deflected around regional bathymetric changes. In the deep central Irish Sea (areas 12 and 13), the largest of Irish Sea sediment waves (25–35 m high) are still mobile (Fig. 4). The migration of the lateral edges is usually significantly higher than the migration of the highest part - the middle part- of the sediment wave. These lateral edges thus seem important in the overall sediment transport mechanism from one bedform to another.

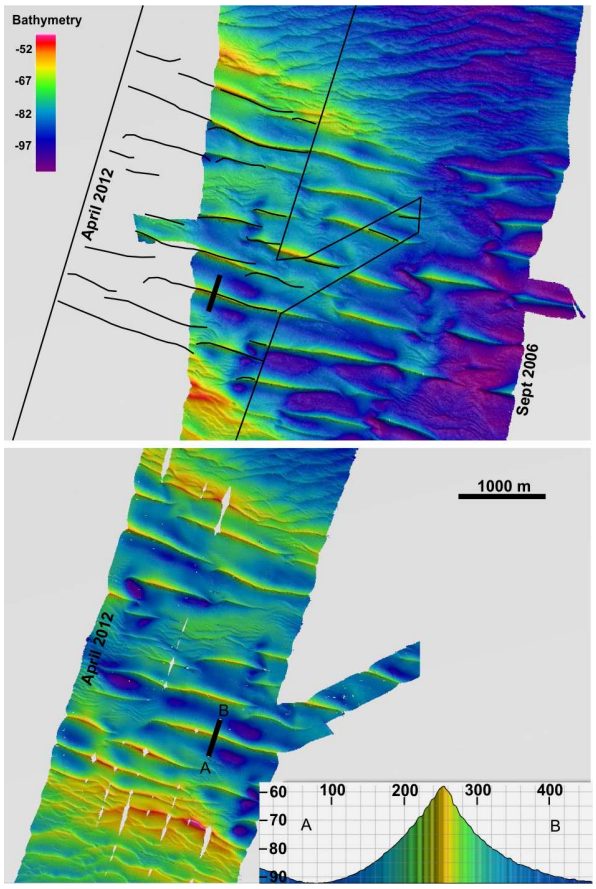

Figure 4. Repeated swath bathymetry data in the central Irish Sea (area 12). The unusually high sediment waves with their trochoidal shape (see profile) have moved and re-arranged a little in the 5.5 years' time difference between both surveys.

2.3. Variation in grain size distribution over differently sized and actively migrating sediment waves.

Granulometric variations across sediment waves can be indicative of differences in effective sediment transport, which defines the potential of the sediment waves to migrate over time. Sand-sized sediment is usually better sorted than gravel and mud as it is easier transported in the energetic shelf sea environments. Gravel is often too "heavy" to be transported, while silts are often aggregated in clusters. As a consequence, from silt to sand we see a coarsening of the sediment with better sorting, whilst from sand to gravel we see a coarsening of the sediment with poorer sorting.

From 22 sediment waves in various places of the Irish Sea, sediment grabs were collected in transect and analysed for granulometric variations. The coarsest sediments -coarse sands to fine gravels- are found in the central Irish Sea (Area 12), where also the largest bedforms occur. Both the mean sediment grain size and the sorting are more variable in the fields of trochoidal sediment waves. With likely stronger currents in the past, perhaps the initially poorly sorted sediments would have strengthened sediment wave growth due to the hiding-exposure effect.

Many of those grab samples were taken in transect over sediment waves of various shapes and sizes. Compared to the sediments over normal sediment waves, the average sediment over trochoidal sediment waves is coarser, and the sediment sorting is highly variable from one sediment wave to the next. Particle size distributions over the trochoidal sediment waves are multi-modal, while the neighbouring "normal" sediment waves are mostly composed of uni-modal sediments.

2.4. Sediment availability underneath unusually high sediment waves.

The field with the largest Irish Sea sediment waves, the middle of area 12, is flanked both in the south and the north by normal sediment waves that migrate towards that field. Mobile sediment is thus steadily supplied towards this field with the world's largest sediment waves. In area 13 and in area 9, the same sediment convergence occurs where the sediment waves are straight-crested, trochoidal and unusually high (Van Landeghem et al., 2012). This systematic abundance in mobile sediments must thus be a critical factor in extreme sediment wave growth.

In area 9 (see Figure 1), seismic profiles were collected to investigate the depositional architecture of the sediment wave field. Was there a pre-existing depression in the seafloor to "trap" the sediment in this convergence zone, or has subsequent erosional scour created somewhat of a depression around the unusually high sediment waves? It seems now that in fact that both factors play an important role. The scour around the coarse grained sediment waves has cut in the originally horizontal sediment layers around the field, and will have over time remobilized a considerable amount of sediment. This is an additional source of the mobile sediment fraction needed to build such large sediment waves.

In area 5, the seismic profiles indicate the presence of a steeply dipping layer (roughly coinciding with

the glacial incision delineated by the British Geological Survey). The incision in the subsurface is expressed by a change in sediment wave orientation and an increase in sediment wave height. The sediment waves in this area are completely immobile. The medium sands can either no longer be mobilised by the relatively weak currents in area 5, or the shallow gasses in this area (Croker, 1994) have dampened the mobility of the bedforms via methane-derived authigenic carbonate (MDAC) cements in between the sand grains. The sediments from the sediment waves have, however, shown no evidence of MDAC and there is no increase of methane concentrations relative to the background values, see section 2.5.

2.5. Methane concentrations in sediment wave fields.

The sediments from the unusually high sediment waves in the Irish Sea do not show any increase in methane concentrations compared to background values. Only in area 4 (fig. 5), shallow gas was clearly observed underneath sediment waves.

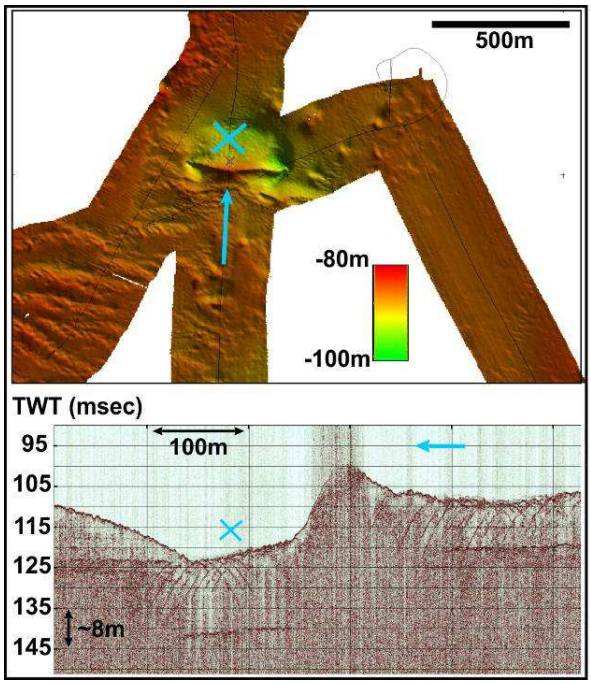

Figure 5. Boomer seismic profiles under the seabed in area 4. The acoustic signal (a strong, consistent top reflection and acoustic turbulence below) is indicative of shallow gas.

High concentrations of methane in sediments near sediment waves were found in this area 4 (the Croker MDAC slabs), but no increase in methane values were found in the sediments that make up the unusually high sediment waves.

3. CONCLUSIONS

Unusually high, straight-crested and trochoidal sediment waves reach unique heights of up to 36 m in the Irish Sea. The preliminary findings on these bedforms that differentiate them from normal sediment waves is that (1) they consist of considerably coarser, more poorly sorted sediments, (2) a continuous and abundant supply of mobile sediment is crucial. This abundant mobile sediment is likely supplied to the sediment wave fields from glacially scoured channel-fills, due to convergence in sediment transport pathways and/or due to scour around coarse-grained sediment waves additionally dislodging the mobile fraction from the coarse lag deposits. Methane seepage is not considered a defining factor in the development of these enigmatic features. Instead, AmSedIS' efforts to better understand these bedforms will focus on the underlying geology, sediment transport pathways and the mixture of sediments found from sediment wave crest to trough. This dataset is envisaged to allow for more advanced numerical modelling of sediment wave development in these particular circumstances.

4. ACKNOWLEDGMENT

The research leading to these results has received funding from the European Union Seventh Framework Programme (FP7/2007-2013) under grant agreement n° [228344], [EUROFLEETS]. Extra ship time on the RV Celtic Voyager was funded by the Petroleum Affairs Division, which is part of the Department of Communications, Energy and Natural Resources that regulates, protects and develops the Natural Resources of Ireland. The project partners at Bangor University, the University of Liverpool, Universität Basel and Università degli Studi di Genova funded a supplementary day offshore and are funding all the data analyses.

5. REFERENCES

Allen, J.R.L. 1980. Sand waves: a model of origin and internal structure. Sedimentary Geology 26: 281–328.

Barrie, J.V. et al. 2009. Large-scale sedimentary bedforms and sediment dynamics on a glaciated tectonic continental shelf: Examples from the Pacific margin of Canada. Continental Shelf Research 29: 796–806.

Bartholdy, J. et al. 2002. Grain-size control of large compound flow-transverse bedforms in a tidal inlet of the Danish Wadden Sea. Marine Geology 188: 391–413.

Cartwright, D.E. 1959. On submarine sand-waves and tidal lee-waves. Proceedings of the Royal Society of London, Series A 253: 218–241.

Croker, P.F. 1994. Shallow gas in the Irish Sea and associated seafloor morphology. Paper presented as poster at the 3rd International Conference on Gas in Marine Sediments, Texel, The Netherlands: 25–28.

Dalrymple, R.W. & Rhodes, R.N. 1995) Estuarine dunes and bars, in: G.M.E. Perillo ed.) Geomorphology and Sedimentology of Estuaries, Developments in Sedimentology 53: 359–422.

Folk, R.L.. & Ward, W.C. 1957) Brazos River bar: a study in the significance of grain size parameters. Journal of Sedimentary Petrology 27: 3–26.

Hovland, M. 1993. Submarine gas seepage in the North Sea and adjacent areas. Petroleum Geology of Northwest Europe: Proceedings of the 4th Conference: 1333–1338.

Judd, A. et al. 2007. Extensive methane-derived authigenic carbonates in the Irish Sea. Geo-Marine Letters 27, 259–267

Valentine, P.C. et al. 2002. Backscatter intensity and sun-illuminated sea floor topography of Quadrangles 1 and 2, map E, in: Valentine, P.C. (Ed.), Maps showing sea floor topography, sun-illuminated sea floor topography, and backscatter intensity of Quadrangles 1 and 2 in the Great South Channel region, western Georges Bank: U.S.G.S. Geologic Investigations Series Map I-2698.

Van Landeghem, K.J.J. et al. 2009. Post-glacial sediment dynamics in the Irish Sea and sediment wave morphology: Data–model comparisons. Continental Shelf Research 29: 1723–1736

Van Landeghem, K.J.J. et al. 2012. Sediment wave migration in the Irish Sea, NW Europe: a reappraisal of the validity of geometry-based predictive modelling and assumptions. Marine Geology 295–298: 95–112

Van Oyen, T. & Blondeaux, P. 2009. Grain sorting effects on the formation of tidal sand waves. Journal of Fluid Mechanics 629: 311–342

Comparing field observations of sorting patterns along tidal sand waves with theoretical predictions

T. Van Oyen[(1)], P. Blondeaux[(2)] and D. Van den Eynde[(3)]

1. Department of Civil Engineering, Ghent University, Technologiepark 904, B-9052, Ghent, Belgium
2. Department of Civil, Environmental and Architectural Engineering, University of Genoa, Via Montallegro 1, 16145 Genova, Italy
3. Royal Belgian Institute of Natural Sciences, Management Unit of the North Sea Mathematical Models, Gulledelle 100, B-1200 Brussels, Belgium

Abstract

We present a site-by-site comparison between field observations and model predictions of grains size variations over tidal sand waves at six sites in the North Sea. To drive the model, at each location, local sediment characteristics are derived from the described field data, while hydrodynamic conditions are determined from a numerical model for tidal wave propagation in the North Sea. It is found that the theoretical model provides reasonable estimates of the occurring tidally generated bed forms. Moreover, at five of the six locations, the model describes a sorting pattern which concurs with the observed sediment grain size variation, indicating that the model provides a fair description of the processes governing the phenomenon.

1. INTRODUCTION

Tidal sand waves are prominent bed features observed in many coastal seas where an abundance of sand is present and tidal currents are dominant (macro-tidal conditions), e.g. the North Sea, San Francisco Bay, (Terwindt, 1971; Barnard *et al.* 2006). The bed features are characterized by a regularly undulating bottom profile, with crest-to-crest distances between 100 and 1000 m and with crest lines organized approximately orthogonal with the dominant direction of the tidal current. The amplitude of tidal sand waves can grow up to a few meters, and the bed forms are found to be able to migrate, with speeds up to tens of meters a year (van Dijk and Kleinhans, 2005). Consequently, the bed forms are hazardous for pipe lines and navigation channels such that a clear understanding of their dynamics is required to derive a long-term management strategy of the coastal zone.

The mechanism leading to the generation of tidal sand waves was first described by Hulscher (1996); and lateron by Gerkema (2000), and Besio *et al.* (2006). These studies reveal that the formation of the bed forms is controlled by the interaction between the periodic tidal flow field and the wavy bottom topography which leads to a steady component of the flow directed from the troughs to the crests of the bed forms; dragging thus sediment from the bottom towards the top. Sediment, on the other hand, is transported down slope due to gravitational effects. The occurrence of the phenomenon is thus a balance between both mechanisms.

Field observations reveal striking sediment sorting patterns over tidal sand waves (Van Lancker and Jacobs, 2000; Roos *et al.*, 2007).

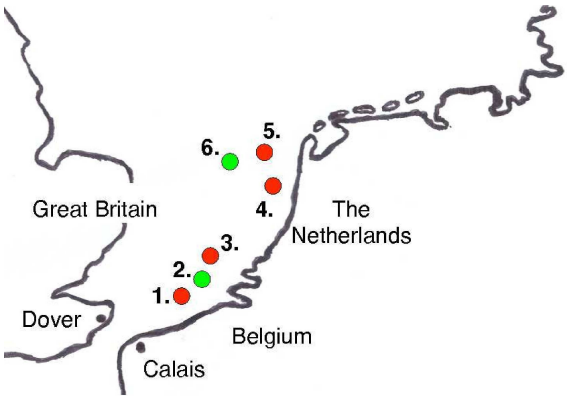

Figure 1. Illustration of the locations of the sites described by Van Lancker & Jacobs (2000) and Roos *et al.*, (2007), respectively number 1 and numbers 2 to 6. The green (red) dots indicate a site where a fining (coarsening) of the sediment towards the crest is observed.

Intriguing, however, these patterns are not persistent; i.e. at some locations, coarser grains are found at the crest while at others, measurements reveal a reverse pattern, see figure 1.

A first study on this phenomenon was conducted by Roos *et al.*, (2007), on the basis of a numerical model for sand wave evolution (van den Berg & van Damme, 2005), resulting in a coarsening of the crest of the bed form. Van Oyen & Blondeaux (2009a,b) also analyzed the process leading to the sorting of grain sizes, using the approach introduced by Besio *et al.* (2006). These studies suggest that the apparently conflicting observations could be the result of two mechanisms which, combined, govern the grain size distribution. The first mechanism follows from a balance between reduced mobility, favoring the transport of finer grains and prevailing for moderate tidal currents; and hiding/exposure effects which enhances the transport of coarse grains for strong tidal currents. The second mechanism occurs only for strong tidal currents and results from the different tidal excursion lengths for distinct grain sizes and can reverse the sorting process, see Van Oyen and Blondeaux (2009b).

To validate the theoretical model, Van Oyen and Blondeaux (2009b) compared model results with three locations in the North Sea. Here, we extend this comparison with three additional sites such that a more clear picture can be derived on the performance of the model.

In the next section, the model of Van Oyen and Blondeaux (2009b) is summarized for the self-consistency of the present work after which the data (Section 3) and the results (Section 4) are described. Conclusions are formulated in Section 5.

2. MODEL

A three-dimensional model (Blondeaux and Vittori, 2005a,b) is adopted to describe the tidally induced flow field related to the M2 component. The model is governed by continuity and momentum conservation, taking into account the Coriolis force. Reynold stresses are described by introducing a scalar eddy viscosity which is time-independent, though varies in the vertical as suggested by Dean (1974). The following boundary conditions are considered:

(i) No-slip condition at the bottom boundary.
(ii) Vanishing of shear stresses and kinematic boundary condition at the free surface.

Using the model introduced by Blondeaux and Vittori (2005a,b), the flow field is determined once the magnitude of the maximum depth averaged flow velocity during the tidal cycle u, the local depth h, the geometric mean grain size d and the eccentricity (i.e. the ratio between the minor and major axis of the tidal ellipse) is specified.

The heterogeneity of the bottom composition is described by considering a number of grain size classes, each with a certain probability of occurrence. Sediment fluxes, of each grain size class n, during the tidal cycle are evaluated by considering both sediment transport in suspension ($\boldsymbol{q}_{s,n}$) and bedload transport ($\boldsymbol{q}_{b,n}$). The latter is calculated following the empirical relation provided by van Rijn (1984a,b), modified to account for slope effects. Suspended sediment transport is evaluated by evaluating the flux of sediment concentration in suspension, which, in turn is governed by an advection –diffusion equation, see Van Oyen & Blondeaux (2009b) for details. Both the bedload and suspended load transport are adjusted to capture the influence of hiding effects, following Ashida and Michiue (1972), and reduced mobility effects.

To describe the evolution of the bed profile, we adopt the active layer approach, as proposed by Hirano (1971), which considers a top layer of the bed (with thickness L_a) in which the sediment is

well mixed and instantaneously available for transport. Hence, for each grain size class *n* it follows that

$$(1-s)\left\{-p_n\frac{\partial}{\partial t}(h+L_a)+\frac{\partial}{\partial t}(p_nL_a)\right\}= -\nabla\cdot\boldsymbol{q_n}. \quad (1)$$

Here, *s* denotes the sediment porosity and p_n the probability of occurrence of the grain size class *n* in the active layer. Summation of (1) over all the grain size classes then provides a relation which describes the evolution of the bed.

To evaluate the formation of sand waves and the related sorting pattern, the model considers a stability analyses; i.e. small wavy perturbations are imposed to a flat bed and their influence on the flow field, sediment transport and bottom evolution is evaluated. Considering observations and the results of Besio *et al.* (2006), the wavy perturbations are aligned orthogonal to the direction of the major axis of the tidal ellipse and are characterized by a wavenumber α_x. Only small perturbations are considered which has as advantage that the perturbed equations can be linearized. The drawback, however, is that, formally, the analysis is only valid for the initial formation of the bed forms.

It turns out that (see Van Oyen and Blondeaux, 2009b), the amplitude *A(t)* of each wavy perturbation with wavenumber α_x develops exponentially in time as

$$A(t)=A_0\exp\{\Gamma t\}. \quad (2)$$

Hence, when Γ is positive (negative), the perturbation is amplified (suppressed) in time. Moreover, we consider that the wavenumber with the largest value of Γ will dominate the other wavelengths and corresponds to the bed forms observed in the field.

Concurrently, the sediment sorting pattern along the sand wave is evaluated. Considering two grain size classes to describe the mixture, it is found that the time development of the probability density (of class 1) is linear in time and controlled by the value of Π, i.e.

$$p_1(t)=\Pi t. \quad (3)$$

Taking class 1 to be related to the coarse grain size fraction, it follows from (3) that a positive (negative) value of Π indicates that the coarse (fine) grains are found at the crests of the sand wave.

3. OBSERVATIONS

To evaluate the performance of the model, we compare field observations of sediment sorting patterns along tidal sand waves which are reported by Van Lancker & Jacobs (2000) and Roos *et al.* (2007).

Van Lancker & Jacobs (2000) describe echo-sounding and side-scan sonar measurements of the bottom profile at a sand wave field near the Baland Bank on the Belgian continental shelf (site number 1, figure 1, Blb). Sand waves with wavelengths of about 150 m and heights of approximately 1 m are observed in water depths between 3 and 15 m. Bottom samples reveal a sediment composition with mean grain sizes between 0.3 and 0.4 mm, and illustrate a coarsening of the sand wave crests.

Sorting patterns over tidally generated bed forms at five locations in the North Sea are described by Roos *et al.* (2007). The first site is located on the Thornton Bank (location 2, Tnt). Based on measurements using a cylindrical box corer to analyse the bottom composition, Roos *et al.* (2007) describe that the mean grain size is finer at the crest (0.397 – 0.421 mm) of the bed forms than in the troughs (0.436 – 0.530 mm). In contrary, as reported by Roos *et al.* (2007), a coarsening of the grain size diameter at the crest is observed at three other sites in the southern North Sea:

(i) west-southwest of Hoek van Holland (Hvh, location 3)
(ii) a coastal site near Zandvoort (Znv, location 4)
(iii) a site 50 km off shore of Egmond aan Zee (Egm, location 5).

The final site discussed by Roos *et al.* (2007) is located along the Brown bank (Bnb, site number 6 in figure 1). At this location, the grain size distribution over the tidal sand waves is only based on two measurements of the bottom composition and is not pronounced, i.e. the median grain size at the trough is only slightly higher (0.316 mm) than that at the crest (0.314 mm). A fining is thus observed, even though the measurements appear to be non-conclusive.

In order to describe the observed bottom composition with the model, the reported mean

grain size diameters (and sorting coefficients) are used to construct a cumulative probability curve of the grain sizes (in the □-scale), for each site respectively. Based on this distribution, we evaluate the values of $□_{33}$ and $□_{66}$ to fix the diameters of the coarse and fine grain size, respectively.

The hydrodynamic and bathymetric conditions used as input to compute the tidal flow field are obtained from numerical results computed by the Management Unit of the North Sea Mathematical Models (MUMM) as this information is not provided in the literature. Here, it is worth to note that the numerical grid for the sites Blb, Tnt and Hvh is much finer (750 m x 750 m) than for the other sites (4 km x 4 km).

4. RESULTS

Adopting the derived data and information provided by MUMM, we use the theoretical model to compute at each site the wavelength which is characterized by the largest value of Γ and thus is assumed to be dominant since it is the "*fastest growing mode (fgm)*". For this wavelength, we then evaluate the value of Π in order to recognize the sorting process occurring concurrently with the formation of the bed forms.

For example, figure 2 illustrates the computed value of Γ for perturbations characterized by different wavenumbers α_x,

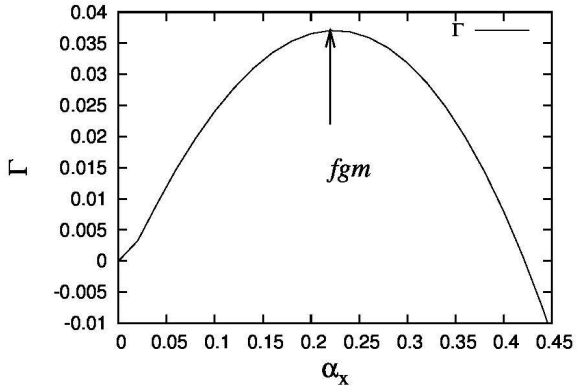

Figure 2. The value of Γ for bed forms with different wavelengths (wavenumbers α_x). Hydrodynamic, bathymetric and bottom characteristics representative for the conditions at Egmond aan de Zee are considered.

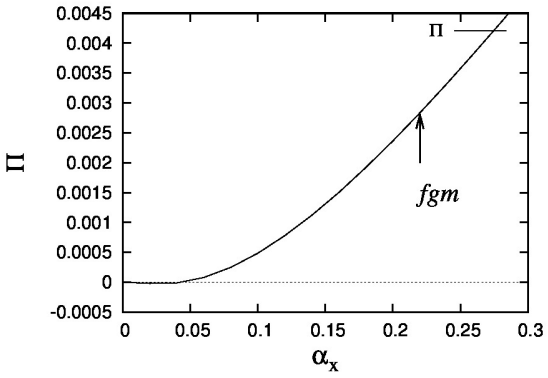

Figure 3. Plot of the value of Π as function of the wavenumber α_x. Hydrodynamic, bathymetric and bottom characteristics representative for the conditions at Egmond aan de Zee are considered.

Table 1. Summary of the observed and predicted wavelength at each site.

Location	Obs. λ [m]	Pred. λ [m]
1. Blb	150	329
2. Tnt	145	173
3. Hvh	350	435
4. Znv	760	327
5. Egm	203	685
6. Bnb	206	556

which allows to evaluate the fastest growing mode (here, $\alpha_{x,max}$ is equal to 0.22). The corresponding wavelength is then computed as $\lambda = 2\pi h/\alpha_{x,max}$. The model, in addition, can compute the value of Π for different wavenumbers, as shown in figure 3. Considering the value of Π for the fastest growing mode, it follows that a coarsening of the crest is predicted since Π_{max} *is positive*.

For each site, the fastest growing wavelength and the concurrently occurring sorting process is evaluated. Table 1 summarizes the observed (obs. λ) and predicted (pred. λ) wavelength for the six locations. It appears that the model provides reliable wavelengths for the locations Tnt and Hvh, while leading to a fair estimate at the other locations.

In addition, by evaluating the value of Π for the fastest growing mode, the predicted sorting patterns are found; i.e. a positive (negative) value of Π for the fastest growing mode corresponds to a coarsening (fining) of the crest. In Table 2 the observed trends are compared with the obtained results.

Table 2. Comparison of the observed sorting trends with the predicted grain size distribution.

Location	Observed	Value of Π	
1. Blb	Coarsening	pos.	✓
2. Tnt	Fining	neg.	✓
3. Hvh	Coarsening	pos.	✓
4. Znv	Coarsening	pos.	✓
5. Egm	Coarsening	pos.	✓
6. Bnb	Fining	pos.	✗

It is found that for five out of the six locations the theoretical model correctly reproduces the qualitative sorting pattern.

The results thus indicate that the model provides (at least) a fair estimate of the occurring wavelength. Moreover, the comparison between the observed and predicted sorting pattern suggests that the model describes adequately the governing processes controlling the grain size distribution along the tidally generated bed forms; especially taking into account the non-conclusive field data obtained at Bnb.

Nevertheless, caution should be taken upon considering this model as a conclusive prediction model since (i) the approach is not able to describe correctly the hydrodynamics and related sediment transport for tidal sand waves of finite amplitude (due to the linear stability approach) and (ii) the model omits hydrodynamic processes which, surely, also effect the wavelength and sorting trend such as wind waves, other components of the tidal wave and wind-induced currents. Moreover, further comparison with more sites based on better quality input data seems required.

5. CONCLUSIONS

A comparison between field observations of grain size segregation along tidal sand waves and a theoretical model is performed for six locations in the southern North Sea. The predicted wavelength compares reasonably with the observed crest-to-crest distances for all the sites. For five out the six sites, the model is found to correctly predict the qualitative sediment distribution along the sand waves (i.e. coarsening or fining of the crests). The results thus indicate that the model provides a fair description of the dynamics leading to the formation of the bed forms. However, care should be taken to adopt the model as a predictive model for coastal management due to the inherent limitation of the model (being based on a linear stability analysis) and since the model, presently, omits important processes such wind wave induced sediment transport, interactions between several tidal components, etc.

6. ACKNOWLEDGMENT

The first author is grateful to the Ghent University (Special Research Fund) for his post-doctoral grant. T.A.G.P. van Dijk is gratefully acknowledged for accommodating the coordinates of the sites described by Roos *et al.* (2007).

7. REFERENCES

Ashida, K. & Michiue, M. 1972 Study on hydraulic resistance and bedload transport rate in alluvial streams. Trans. Japan Soc. Civil Eng. 206

Barnard, P.L., Hanes, D.M., Rubin, D.M.& Kvitek, R.G. 2006 Giant sand waves at the Mouth of the San Fransisco Bay. Eos. Trans. AGU 87 (29)

Besio, G., Blondeaux, P. & Vittori, G. 2006 On the formation of sand waves and sand banks. J. Fluid Mech. 557

Blondeaux, P. & Vittori, G. 2005a Flow and sediment transport induced by tide propagation. Part1: The flat bottom case. J. Geophys. Res. 110

Blondeaux, P. & Vittori, G. 2005b Flow and sediment transport induced by tide propagation. Part2: The wavy bottom case. J. Geophys. Res. 110

Dean R. D. 1974 Aero report 74 – 11. Tech. rep., Imperial College, Londen.

Gerkema, T. 2000. A linear stability analysis of tidally generated sand waves. J. Fluid Mech. 417

Hirano, M. 1971 On river bed degradation with armouring. Trans. Japan. Soc. Of Civil Eng. 3

Hulscher, S.J.M.H. 1996. Tidal-induced large-scale regular bed form patterns in a three-dimensional shallow water model. J. Geophys. Res. 101

Roos, P, Hulscher, S., van der Meer, F., van Dijk, T.A.G.P., Wientjes, I. G.M., van den Berg, J. 2000. Grain size sorting over offshore sand waves: Observations and modelling. In: Dohmen-Janssens, C., Hulscher, S.

Terwindt, J.H.J. 1971. Sand waves in the southern bight of the North Sea. Mar. Geol. 10, 51 - 67.

van Dijk, T.A.G.P & Kleinhans, M.G. 2005 Processes controlling the dynamics of compound sand waves

in the North Sea, The Netherlands, J. of Geophys. Res. 110

Van Lancker,V., & Jacobs, P., 2000 The dynamical behaviour of shallow marine dunes. In: Trentesaux, A., Garlan, T. (Eds.), Int. Workshop on Marine Sandwave Dynamics. University of Lille 1, France.

Van Oyen T., & Blondeaux, P., 2009a Grain sorting effects on the formation of tidal sand waves. J. Fluid Mech. 629

Van Oyen T., & Blondeaux, P. 2009b Tidal sand wave formation: Influence of graded suspended sediment transport. J. Geophys. Res. 114

van Rijn, L.C. 1984a Sediment transport, part 1: bed load transport. J. Hydraul. Engineering 110

van Rijn, L.C. 1984a Sediment transport, part 2: suspended load transport. J. Hydraul. Engineering 110

Deep-water bottom current dynamics: processes, products & challenges

D. Van Rooij[(1)]

1. Ghent University, Dept. Geology & Soil Science, Ghent, Belgium - david.vanrooij@ugent.be

Abstract

Contourites are deep-water sedimentary deposits created under the influence of predominantly along-slope bottom currents. They are considered to be excellent deep-water recorders of global climatic change. Over the last decade, the improvement of deep-water survey technology enabled better visualising and understanding their driving processes, recognizing these deposits in more complex areas and in shallower depositional environments (such as shallow seas and lakes). Unfortunately, there still is no uniform and unequivocal classification, since the coupling between geological and hydrographic processes is rather vaguely defined due to the lack of good "in-situ" observations, in contrast to shallow marine and river systems. This paper aims to introduce the challenges and potential benefits that are ahead of us in contourite research, and aspires to open a dialogue between the deep and shallow water sediment dynamic communities.

.

1. INTRODUCTION

The ocean basins floor, from their shallow shelf down to the abyssal plains, is swept by a large variety of bottom currents, originating from different processes. Whereas shallow marine and riverine bedforms are (also) influenced on (semi-)diurnal basis, they are however rather poor recorders of the geological or climatic log-book. Conversely, in deeper water, some of the large-scale bedforms or depositional elements driven by along-slope bottom currents are regarded as some of the best sedimentary recorders (Rebesco & Camerlenghi, 2008). Although these deposits, called contourites or sediment drifts, have been known since the 1960's (Heezen et al., 1966), and their fundamental role in the construction and evolution of continental margins has already been clearly documented (Stow et al., 2002, Rebesco & Camerlenghi, 2008), it is only recently that their importance and relevance is coming back into the spotlights (Hernández-Molina et al., 2011). There is a vast need to improve our understanding of the involved processes, products and controls.

This present paper aims to introduce the challenges and potential benefits that are ahead of us in contourite research, and will show that a lot of knowledge can be gained from their shallow water counterparts and vice versa.

2. PROCESSES & PRODUCTS

Whereas initially the erosive and depositional features associated to contourites where only attributed to the deep thermo-haline circulation, it is now clear that they are formed under the complex interplay oceanographic processes, pre-existing seabed morphology, sediment supply and climate change (Hernández-Molina et al., 2011). Based upon this, the most recent classification of large-scale contourite drifts has been proposed by Rebesco and Camerlenghi (2008), following upon the seismic work of Faugères et al. (1999). Some of these have an elongation of over hundreds km (giant elongated drifts, abyssal sheet drifts), some may be restricted by obstacles or gateways (confined drifts, mounded drifts), or just locally attached to the margin (plastered drifts). All types may occur separately, or combined over space and

time in contourite depositional systems (Hernández-Molina et al., 2011). A very wide variety of oceanographic processes, among which the internal tides are gaining importance, will leave characteristic bedforms behind, allowing to reconstruct the along-slope bottom current pattern that is responsible for the shaping of these giant drift bodies. A compilation has been made by Stow et al. (2009), based upon seabed imagery and bottom current measurements (Fig. 1).

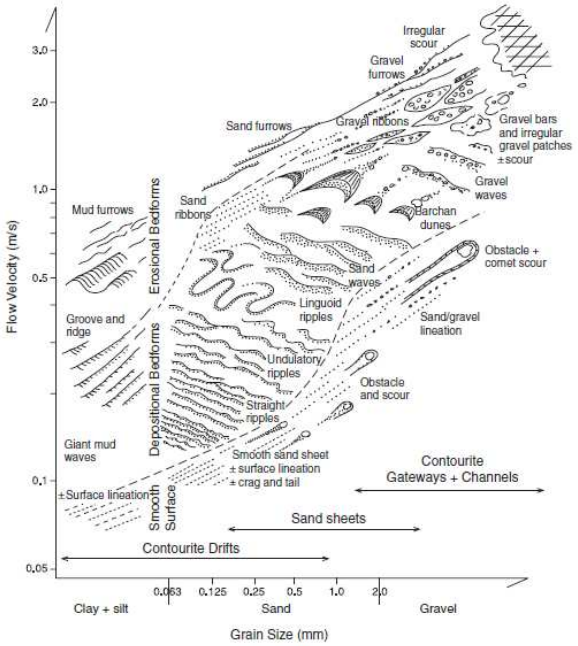

Figure 1. Bedform-velocity matrix for deep-water bottom current systems, showing mean grain size of sediment versus flow velocity at or near seafloor, with schematic representation of bedforms present under specific velocity-grain-size conditions (Stow et al., 2008).

However, they only indicate the present day current direction and strength, whereas during the depositional history of the entire sediment body, both direction as intensity may have changed significantly. On a larger scale, 3D seismic geomorphology may assist in better visualizing palaeotopographic features, whereas only through coring and drilling the fine-scale bottom current intensity changes may be deciphered. Unfortunately, the contourite sedimentary record only sporadically leaves behind traces of the wealth of present-day bedforms.

Although their study has been one of the most active lines in marine geoscience research over the last decades, necessitating an interdisciplinary approach that encompasses sedimentology, physical oceanography, stratigraphy, bio-geochemistry, geophysics, palaeoceanography and paleoclimatology, the visualising and under-standing of their driving processes is largely dependent of (and restricted to) the improvement of deep-water geophysics, coring and drilling facilities and oceanographic monitoring tools (Faugères et al., 1999; Rebesco, 2005; Hernández-Molina et al., 2011).

3. RELEVANCE & CHALLENGES

Contourite processes cover a specific part of all bottom currents, actively distinguished from the better studied downslope processes, forming turbidite deposits, organised in deep-sea fans. It is largely the economic interest of the latter that pushed research to bottom-parallel currents into the shade. Ironically, it is a renewed economic interest (Viana et al., 2007) that has put the spotlight on these deposits. Besides this, the relevance of contourite studies to science and society is manifold, despite their presence is little known and even less understood.

3.1 Palaeoceanography & global change

In the first place, both deep and shallow water circulation is driven by climate. Hence, continuous contouritic deposits, accumulated under enhanced sedimentation rates, are excellent recorders of past climate change (either local or global) and assist in better understanding the modulating role of the deep ocean in our climate's system (Rebesco, 2005). However, deconvolving the different signatures (bottom current intensity, bottom water temperatures & salinities, source fingerprinting,…) from these records is not straightforward. A multidisciplinary approach is required for better relating ocean circulation and bottom currents to their deposits and therefore for determining how best to read the palaeoceanographic or palaeoclimate signatures from contourite deposits.

3.2 Geohazards

Contourite deposits are observed all over the Earth's continental margin, predominantly as vast

sheets of fine-grained material (Rebesco & Camerlenghi, 2008). The combination of these deposits, together with oversteepened slopes, (isostatic) seismicity, oversedimentation, free gas and overpressure may lead to geo-hazards, especially in polar continental margins. They lie at the origin of major slope instabilities, leading to catastrophic slope collapse and consequent damage to subsea installations and cables. Slope collapse can lead directly to major tsunami events and likely devastation to coastal regions (cfr. Storegga Slide (Bryn et al., 2005)), whereas high velocity bottom currents can erode subsea structures, undercut seafloor pipes and chafe submarine cables (Rebesco, 2005).

3.3 Earth resources

Similar to turbidite systems, also contourites may generate well-sorted deep-water sands (Stow et al, 2009). They occur in nearly any complex environment where sandy contourites are a new reservoir play for subsurface oil and gas; muddy contourites may act as potential source rocks, reservoir seals or unconventional reservoirs. Moreover, the role of deep-water circulation on the growth and distribution of ferromanganese nodules is still under debate.

3.4 Ecosystems & environmental change

Over the past decade it has become clear that most of the deep-water ecosystems (cold-water corals) are highly influenced by the presence of deep-water circulation (Hernández-Molina et al., 2011). These deep-water bottom currents are essential for the construction and maintenance of entire deep-water habitats, some of which are still little known to science and some of which provide ideal nurseries for several fish species. A better understanding of the role of bottom currents in the continued "health status" of such ecosystems will help our appreciation of the impact of climate change (long term) or oil spills (short term).

3.5 Oceanographic processes

Although the contourite paradigm has existed for over 40 years, there still seems to be a missing dialogue between physical oceanography and sedimentary observations. Nevertheless, contourite studies may greatly contribute to reconstruct past oceanographic regimes in great detail. However, in order to perform this, we first need to better understand the true interface between the "sediment processes" and "water processes".

3.6 Challenges

Despite the increasing relevance of contourite studies, many challenges lie ahead (Hernández-Molina et al, 2012). There still is no uniform and unequivocal classification, since the coupling between geological and hydrographic processes is rather vaguely defined due to the lack of good "in-situ" observations. However, there is further good potential for achieving a fundamental break-through in our understanding of ocean circulation and how the associated physical processes relate directly to sedimentary processes and their products (e.g. contourites). This area at the boundary between the often disparate disciplines of physical oceanography and sedimentology has been relatively neglected. Associated to this, more unambiguous diagnostic criteria, based upon a better integration of geophysical, sedimentological and geochemical observations may assist in better recognizing land sections, which are poorly documented and fully underrepresented.

Contourites have previously passed beneath the radar when it comes to the assessment of potential economic resources along continental margins and in deeper basin settings. However, as a principal constituent of deep-water sedimentary systems, they must constitute an essential element in the exploration of progressively deeper waters by the hydrocarbon industry. During IODP Expedition 339, for the first time, several 100 m of sandy contourites with reservoir quality were drilled (IODP Expedition Scientists, 2012).

Furthermore, palaeoceanographers are developing more advanced geochemical proxies to better reconstruct the physical and (biogeo)chemical properties of the water-masses. The most challenging task, however, is to identify, document and understand shallow-water contourites, observed in shallow seas and lakes. In terms of geometry, a lot of similarities are observed with respect to their deep-sea counterparts, but since they are predominantly dependant of (near-) surface wind-driven currents, the responsible processes and the palaeoceanographic potential are

poorly known. Ultimately, no real definition has been defined where the "upper" boundary of the contourite occurrence is located, and where this (almost literally) flows over to sandbank and dune dynamics.

4. CONCLUSIONS

It is not by chance that this paper is presented during the "Marine and River Dune Dynamics" conference. The previously stated challenges have recently lead to the initiation of both the IGCP project n° 619, entitled "Contourites: geological record of ocean-driven paleoclimate, accomplice of submarine landslides and reservoir of marine geo-resources" and INQUA project n° 1204 "The Quaternary Contourite Log-book: a deep-water record(er) of variability in palaeoclimate, palaeoceanography and deep-water ecosystems". Both projects, which basically represent research networks, are grouped under the website http://www.contourites.org, aspire to bring together scientists from over the entire marine (geo)science community in order to try to bridge the knowledge gaps. The association of bedforms and their responsible oceanographic processes is key to both the contourite as shallow water community. In contrast to shallow marine and river systems, good and frequent "in-situ" observations are scarce, due to the demanding logistic challenges of deep-water research. Nevertheless, both communities can significantly contribute to each other. Therefore, the major aim of this paper is to aspire and promote an open dialogue between the deep and shallow water sediment dynamic communities.

5. ACKNOWLEDGMENT

The author is grateful to UNESCO for sponsoring the IGCP n°619 project (Contourites: processes and products) and to INQUA for sponsoring the n°1204 project (The Quaternary Contourite Log-book). The co-proponents of both projects are F.J. Hernández-Molina (UVigo, Spain), D.A.V. Stow (Heriot-Watt University, UK), M. Rebesco (OGS, Italy), A. Viana (Petrobras, Brazil), P. Puig (ICM-CSIC, Spain), A. Voelker (LNEG, Portugal) and R. Brackenridge (Heriot-Watt University, UK).

6. REFERENCES

Bryn, P., Berg, K., Forsberg, C.F., Solheim, A. & Kvalstad, T.J., 2005. Explaining the Storegga Slide. Marine and Petroleum Geology 22: 11-19.

Expedition Scientists, 2012. Mediterranean Outflow: environmental significance of the Mediterranean Outflow Water and its global implications. IODP Preliminary Report 339: doi:10.2204/iodp.pr.339.2012.

Faugères, J.-C., Stow, D.A.V., Imbert, P. & Viana, A.R., 1999. Seismic features diagnostic of contourite drifts. Marine Geology 162: 1-38.

Heezen, B.C., Hollister, C.D. & Ruddiman, W.F., 1966. Shaping of the Continental Rise by Deep Geostrophic Contour Currents. Science 152: 502-508.

Hernández-Molina, F.J., Serra, N., Stow, D.A.V., Llave, E., Ercilla, G. & Van Rooij, D., 2011. Along-slope oceanographic processes and sedimentary products around the Iberian margin. Geo-Marine Letters, 31 (5/6): 315-341.

Rebesco, M., 2005. Sedimentary environments: Contourites. In R.C. Selley, L.R.M. Cocks & I. Plimer (eds), Encyclopedia of Geology: 513-528. Oxford: Elsevier.

Rebesco, M. & Camerlenghi, A., 2008. Contourites. Developments in Sedimentology 60. Amsterdam: Elsevier.

Stow, D.A.V., Hernandez-Molina, F.J., Llave, E., Sayago-Gil, M., del Rio, V.D. & Branson, A., 2009. Bedform-velocity matrix: The estimation of bottom current velocity from bedform observations. Geology 37: 327-330.

Stow, D.A.V., Pudsey, C.J., Howe, J.A., Faugères, J.-C., Viana, A.R., 2002. Deep-Water Contourite Systems: Modern Drifts and Ancient Series, Seismic and Sedimentary characteristics. London: Geological Society Memoir 22.

Viana, A.R., Almeida, W., Nunes, M.C.V. & Bulhões, E.M., 2007. The economic importance of contourites. In: A.R. Viana & M. Rebesco (eds), Economic and Palaeoceanographic Significance of Contourite Deposits: 1-24 London: Geological Society Special Publication 276

An equivalent bottom for navigation above irregular bottoms

M. Vantorre[(1)], E. Lataire[(1)], M. Candries[(1)], J. van Doorn[(2)], and D. van Heel[(2)]

1. Ghent University, Division of Maritime Technology, Ghent, B – marc.vantorre@ugent.be
2. MARIN, Wageningen, NL

Abstract

An algorithm is suggested for converting the raw sounding data of a sea bottom with local depth variations into manageable dredging maps and electronic chart systems (ECS). The resulting "equivalent bottom" can be considered to offer a comparable safety as a horizontal bottom with the same depth, and therefore does not jeopardize safe sailing behaviour of a vessel, even if the bottom is locally more shallow than the equivalent depth. On the other hand, accounting for the most shallow spots of a navigation area would result into a lower allowable draft for the vessels or a significant increase of dredging costs. The proposed algorithm has been developed for the access channels for maritime shipping traffic connecting the Western Scheldt estuary with open sea, which is partly characterized by ripples in the bottom. The more theoretical outlines of the principles behind the concept of the equivalent bottom are explained, followed by a more pragmatic approach offering the advantage of a more straightforward implementation.

1. INTRODUCTION

In 2012, a research project was carried out on behalf of the common Dutch-Flemish Nautical Authority to determine a scientifically based algorithm to create ECS-charts in the access channel to the mouth of the Western Scheldt. This research was carried out by Ghent University (Maritime Technology Division) and MARIN.

The presented research suggests an algorithm that converts the raw sounding data of a bottom with local depth variations into manageable dredging and ECS-charts. In general, the conversion of millions of data points resulting from multi-beam soundings to a readable chart is a challenging task. A conservative algorithm, based on the shallowest measured points of the navigation area, will result into safe charts, but will lead to a lower allowable draft for the vessels or a significant increase of dredging costs. A too progressive algorithm, on the other hand, may jeopardise shipping traffic safety.

The present research looks for a compromise by defining the "equivalent bottom", which can be considered to offer a comparable safety as a horizontal bottom with the same depth, and therefore does not jeopardize the safe sailing behaviour of a vessel, even if the bottom is locally more shallow than the equivalent depth.

The proposed algorithm must take account of relevant parameters that determine a ship's safety during navigation in restricted channels. The under keel clearance should be sufficient to keep the probability of bottom touch due to squat, response to waves and other causes of vertical ship motions acceptably low and to guarantee the controllability and manoeuvrability of the ship. On the other hand, the conversion of raw sounding data to charts must be possible with reasonable resources, which implies that the algorithm should be robust and simple. This suggests an algorithm that converts the original raw sounding data into one equivalent value for each grid cell. The vessels that use this equivalent water depth have enough information to transit the seaway in a safe manner. Also for maintenance dredging purposes, the resulting charts are sufficiently detailed to localize critical zones but neglect local spots without relevance.

The equivalent water depth concept is even more relevant in some very specific regions in the Belgian territory of the North Sea characterised by rippled bottoms and/or marine dunes. It is in this type of bathymetry that different algorithms can result in different water depths plotted on the charts and, hence different levels of safety.

2. BOTTOM SURVEY IN *SCHEUR OOST* ACCESS CHANNEL

The dredged channels Scheur West/Oost and Wielingen are of great importance for the shipping traffic to the Western Scheldt giving access to the ports of Flushing (NL), Terneuzen (NL), Ghent (B) and Antwerp (B). These channels are partly located on Belgian and Dutch territory, so that bottom survey is performed under the responsibility of both Rijkswaterstaat and the Coastal Department of the Flemish Government. Although both services make use of the same survey techniques, i.e. multi-beam sonar combined with a Real Time Kinematic positioning system (RTK), several post-processing algorithms can be applied to reduce the huge amount of measurements (5 to 10 data points per square meter) to a limited but relevant number that can be displayed on nautical charts and dredging maps. After filtering the data and removing irrelevant spikes, basic statistical characteristics of the measurements within grid cells of 1 m² are determined, such as average (avg1), minimum (min1), standard deviation (std1).

Further data reduction can be performed by many different algorithms. Over squares of *n***n* 1m² grid cells, either the average or the minimum value can be taken of the n^2 individual average or minimum values; the results are denoted min*n*_min1, avg*n*_min1, min*n*_avg1, avg*n*_avg1.

In areas with a relatively flat bottom, the results are less sensitive with respect to the reduction algorithm. However, some areas are characterized by the formation of ripples with crests perpendicular to the main current direction , a "dune length" of 0.6 to 30 m and a top-to-crest height between 0.4 to 1.5 m. In such areas, different algorithms may lead to significantly different values.

An area of 419 * 464 m² in the access channel *Scheur Oost* was selected as a test case. The results of multi-beam soundings was performed by Flemish Hydrography; the 2.3 10^6 measurements, reduced with the avg1 algorithm, are displayed in Figure 1. The area contains some rather flat, uniform zones at the edges (north and south) of the channel, and a central zone with clear ripples. Bottom samples taken in this area by Rijkswaterstaat revealed that the bottom is composed of mostly clay or sand; in the troughs between the ripples mud is sometimes found. The bottom can therefore be considered as solid, non-penetrable for navigation.

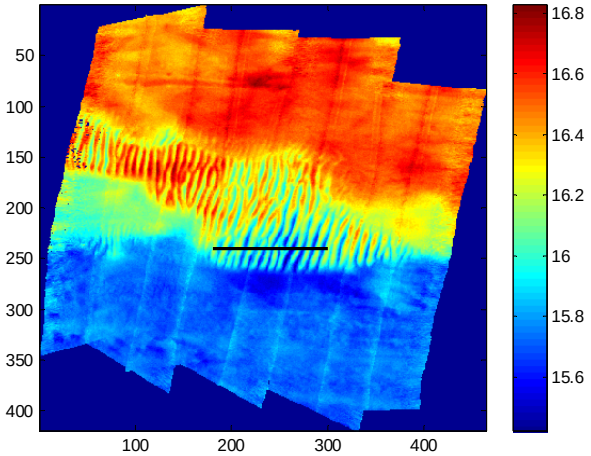

Figure 1. Test section in channel *Scheur Oost*: average values of the multi-beam soundings per grid cell of 1*1 m² (avg1). Horizontal and vertical scale: distance in m (north up); color scale: depth in m with respect to LAT.

A cross section along the east-west line shown in Figure 1 provides a typical view of the ripples, with a height of up to 0.6 m and a wave length of 7 to 10 m, see Figure 14. The difference between avg1 and min1 fluctuates between 0.04 m and 0.20 m, the lower values occurring for grid cells in the troughs and on the crests, the higher values on the slopes. Also the standard deviation over the grid cells (std1) varies correspondingly.

The values for avg1 – min1 and for std1 appear to be very small in uniform zones and on the ripple crests and troughs, so that the average value over 1 m² square grid cells, avg1, was agreed to be a suitable starting point for further analysis. The question remains how these avg1 values can be reduced to suitable values for larger areas.

3. EQUIVALENT BOTTOM FOR DETERMINISTIC CHANNEL ACCESS POLICY

3.1 Analysis of available UKC

Deep-drafted vessels are allowed to navigate in the channels giving access to the Western Scheldt mouth and the Flemish coastal harbours (see Figure 2) based on their gross under keel clearance (UKC), i.e. the difference between the water depth (as a function of place and time) and the static draft of the ship at rest in still water. For Scheur and Wielingen, a gross UKC of 15% of the ship's draft is required, for Pas van het Zand and Western Scheldt 12.5% is needed. These percentages are considered to be sufficient as an allowance for the vertical motions of the ship and as a margin for the uncertainty on the level of the bottom, the free water surface and the ship's draft. The depth of the *Scheur* channel varies between 15.4 m and 16.2 m below LAT, which implies that at zero water level ships can pass with a draft of 13.4m to 14.1m, leaving a gross UKC of 2.0 – 2.1 m.

Taking account of the type of vessels, their speed range and the local wave climate, a rough sub-division of this gross UKC can be made.The following fractions of the gross UKC are assumed to be required for the different types of allowance:

- Squat: abt. 6.0% abt. 0.8 m
- Waves: abt. 7.5% abt. 1.0 m
- Other: abt. 1.5% abt. 0.2 m

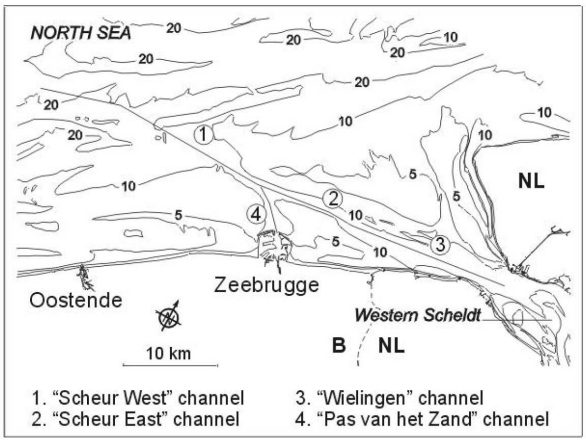

Figure 2. Access channels to the Western Scheldt Estuary and the Belgian coastal harbours (Vantorre et al, 2008).

Assuming that a gross UKC of 15% of the ship's draft offers a sufficient safety margin with respect to a horizontal, flat bottom, the effect has to be estimated of a bottom with variable depth on the required UKC.

3.2 Effect of depth variations on squat

The sinkage and dynamic trim of a ship due to her own forward motion depends on a large number of parameters: ship's speed, ship geometry, water depth, channel bathymetry, … (Briggs et al, 2010). Many empirical methods an formulae have been developed for estimating squat. The water depth is an important parameter in this respect: a decrease of water depth results into a stronger return flow, which increases the sinkage of the water level around the ship and, hence, the ship's squat. The effect of bottom variations has been investigated only sporadically; relevant studies have been carried out at BAW (Hamburg) on the effect of bottom ripples on the squat of container vessels (Uliczka and Kondziella, 2003, 2006). It could be concluded that the squat of a ship navigating above a ripple bottom is approximately equal to the squat above a horizontal bottom at the average level.

A ship navigating above an arbitrary variable bottom will therefore experience less squat compared to a situation of a horizontal bottom at a level corresponding with the most shallow point of the bottom. This squat reduction allows a somewhat smaller UKC with respect to this shallowest point, or allows to define an equivalent bottom level resulting in the same margin with respect to this shallowest point. This is illustrated in Figure 3:

- The sinkage of a ship due to squat above a real, variable bottom can be approximated by the sinkage the ship would experience above a horizontal bottom with a depth equal to the average bottom profile.
- The squat the ship would experience if navigating above a horizontal bottom above the shallowest point of the channel is greater than the squat above the real bottom.
- As a result, the margin between the keel and the bottom is larger in the case of the real bottom compared to the case of the horizontal bottom through the shallowest point.

- The equivalent bottom (with respect to squat) can therefore be defined in such a way that the real margin is kept. The equivalent bottom is located below the minimum bottom level; the level difference equals the difference in squat between the real and the minimal bottom.

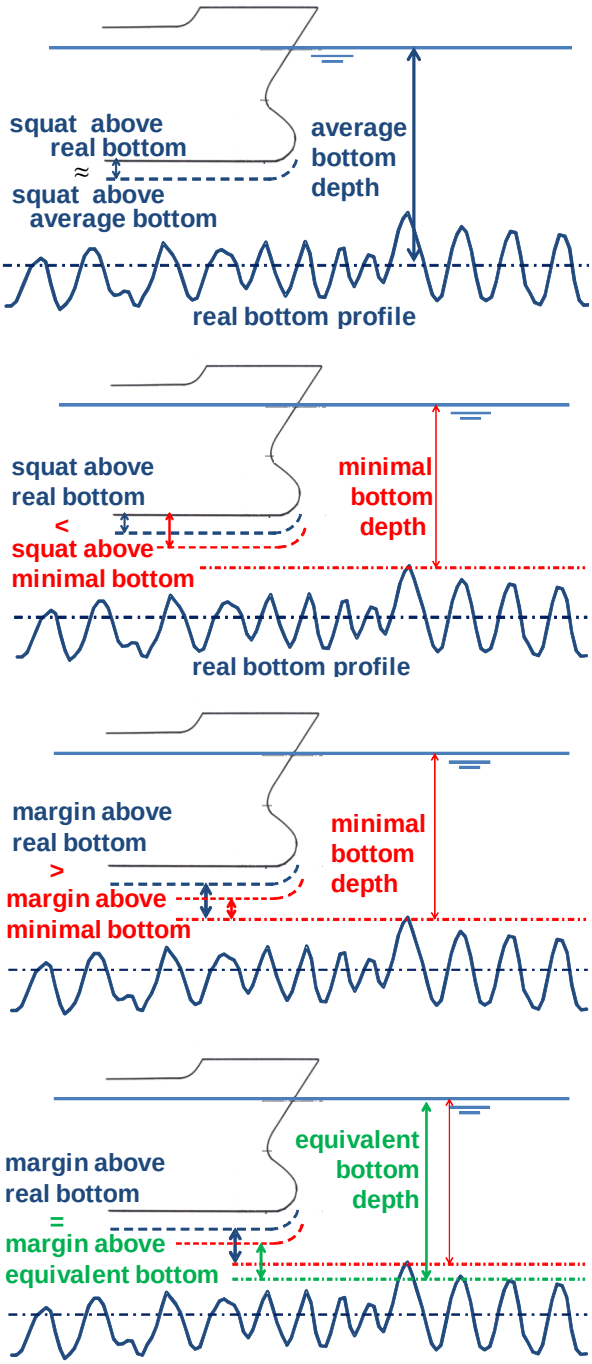

Figure 3. Equivalent bottom with respect to squat.

The effect of an average increase of the water depth on the squat of a ship within the mentioned draft range with a gross UKC of 15% resulting in a squat of 0.8 m was investigated for a number of realistic cases. It was concluded that, in the considered cases, the difference between the squat above a horizontal bottom at a level h_{min} and the squat above a real bottom with average level h_{avg} is about 10% of the difference between both levels.

This leads to the following expression for the equivalent bottom with respect to squat:

$$h_{eq}^{(squat)} = h_{\min} + 0.10\left(h_{gem} - h_{\min}\right) = 0.90h_{\min} + 0.10h_{gem} \quad (1)$$

For a zone with ripples with a trough to crest height of 1 m, the reduction equals 0.05 m, which is only marginal. It is important to mention that the average depth should be considered over an area with dimensions comparable to the horizontal dimensions of deep-drafted vessels.

3.3 Vertical ship motions due to waves

Principally, the fraction of the UKC needed for allowing vertical wave induced ship motions can only be determined in a probabilistic way, as the maximum wave height that will be encountered during the passage of a vessel cannot be predicted with certainty. One can only make predictions about the probability of exceeding a certain level; for such predictions the significant wave height Hs has to be known. This principle can be extended to all (linearly dependent) consequences of wave action, such as vertical ship motions. The vertical position of a point of the ship's keel oscillates about an average level; the time series of the instantaneous level of this point is characterized by a significant amplitude, which is 2.0 times the standard deviation σ_{VM} of the vertical position. The knowledge of this significant amplitude and the fraction Z_{VM} of the UKC available for wave induced motions allows to calculate the probability of bottom contact, see Figure 4. As this study aims at defining the equivalent bottom within the frame of the present deterministic access policy, the quantitative value of this probability is not considered, but realistic values for Z_{VM} and σ_{VM} will be taken as a starting point.

Figure 4. Vertical ship motion above horizontal bottom

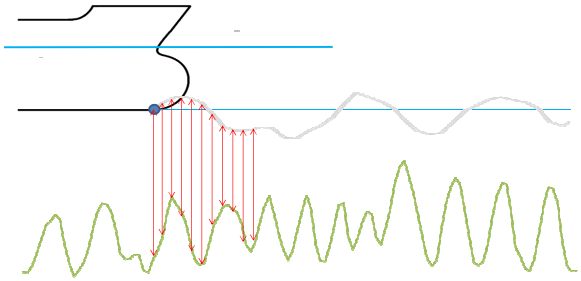

Figure 5. Relative vertical motion of a point of the ship's keel with respect to a variable bottom.

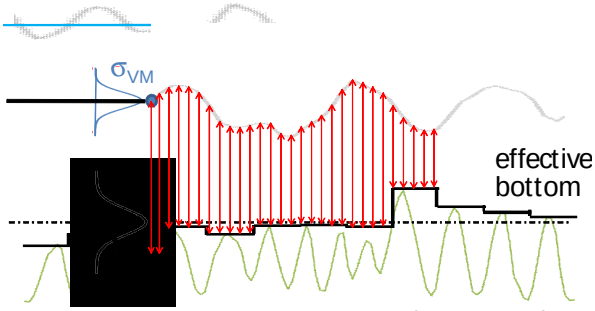

Figure 6. Relative vertical motion of a point of the ship's keel with respect to the effective bottom.

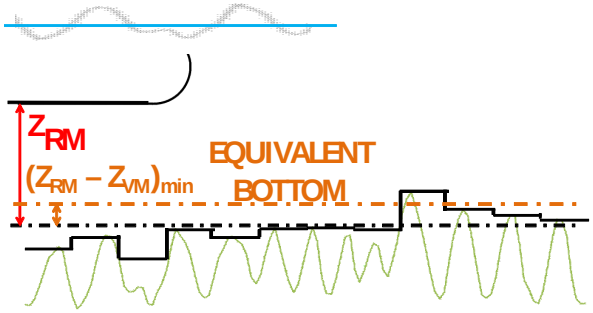

Figure 7. Equivalent bottom with respect to wave induced motions.

Instead of the absolute vertical motion of (a point of) the ship, the relative motion of such a point with respect to the bottom with variable depth can be considered, based on superposition of the the vertical oscillations of the ship and the vertical oscillations of the bottom (see Figure 5). However, this superposition does not make sense in a zone characterized by short ripples, as an arbitrary point of the ship's keel cannot fully make use of the vertical space between the ripple crests.

For this reason, the real bottom is replaced by a so-called *effective bottom*. The area is subdivided in grid cells of 10*10m²; the effective bottom in each grid cell is a horizontal plane through the min10avg1 value. This means that the real bottom is replaced by the shallowest point based on the average depth of all 100 1*1 m² grid cells of which every 100 m² cell is composed, see Figure 6.

Over a larger area, with dimensions which are relevant to the ship's main horizontal dimensions, an average effective depth h_{avg}^{eff} and a standard deviation σ_B^{eff} can be defined. For this study, rectangles of 100*50 m² were considered, containing 50 cells of 10*10m².
The relative vertical motion of the ship with respect to the effective bottom oscillates around a mean value with a standard deviation σ_{RM}^{eff} (RM denoting "relative motion"), defined as:

$$\sigma_{RM}^{eff} = \sqrt{\sigma_{VM}^{\ 2} + \sigma_B^{eff\ 2}} \qquad (2)$$

Above a horizontal bottom, it assumed that the UKC fraction Z_{VM} results in a sufficient degree of safety for allowing a significant absolute vertical ship motion with standard deviation σ_B^{eff}. An equal degree of safety would be provided by a margin Z_{RM} between the average levels of the ship's keel and of the effective bottom equal to:

$$Z_{RM} = Z_{VM}\left(\sqrt{1+\left(\frac{\sigma_B^{eff}}{\sigma_{VM}}\right)^2}\right) \qquad (3)$$

Tdhe required clearance between the average level of the ship's keel and the average effective bottom, Z_{RMmin}, is apparently larger than the required clearance with respect to a horizontal bottom, Z_{VMmin}. A ship navigating above a horizontal bottom located at a vertical distance $Z_{RMmin} - Z_{VMmin}$ above the average effective bottom would therefore experience the same degree of safety as she would have above a realistic, variable bottom. Thus, this level can be considered to be the *equivalent bottom* (Figure 7)

$$h_{eq} = h_{avg}^{eff} - Z_{VMmin}\left(\sqrt{1+\left(\frac{\sigma_B^{eff}}{\sigma_{VM}}\right)^2}\right) \quad (4)$$

For the considered channel, Z_{VMmin} = 1.0 m and σ_{VM} = 0.25 m appear to be suitable estimations.

3.4 Provisional proposal for equivalent bottom

Combining the effect of a bottom with variable depth on squat and on the required clearance for wave induced motions, the following proposal can be formulated for the level of the equivalent bottom, to be determined in 50*100m² rectangles.

$$h_{eq} = h_{avg}^{eff} - 1.0\,\mathrm{m}\left(\sqrt{1+\left(\frac{\sigma_B^{eff}}{0.25\,\mathrm{m}}\right)^2}\right) + 0.10\left(h_{avg} - h_{\min}\right) \quad (5)$$

with

h_{avg}^{eff} = avg50_100min10avg1:
average value of the 50 minimum values of the depth in each of the 10*10m² grid cells composing the 50*100m² rectangle;

σ_B^{eff} = std50_100min10avg1:
standard deviation of these 50 minimum values;

$h_{\min}$ = min50_100min10avg1:
minimum of these 50 minimum values;

h_{avg} = avg50_100min10avg1:
average of these 50 minimum values;

the minimum values of the 10*10m² grid cells being based on the average values determined within each 1*1m² grid cell.

For the selected test section, Figure 8 to Figure 11 show the values for h_{avg}^{eff}, $h_{\min}$, σ_B^{eff} and h_{eq}.

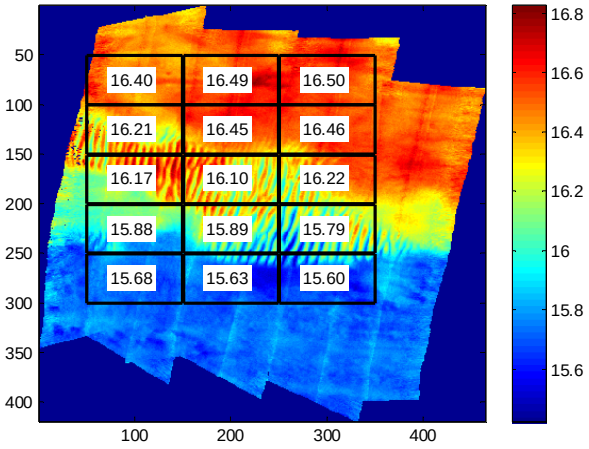

Figure 8. Test section: average effective bottom depth avg50_100min10avg1, with avg1 in the background.

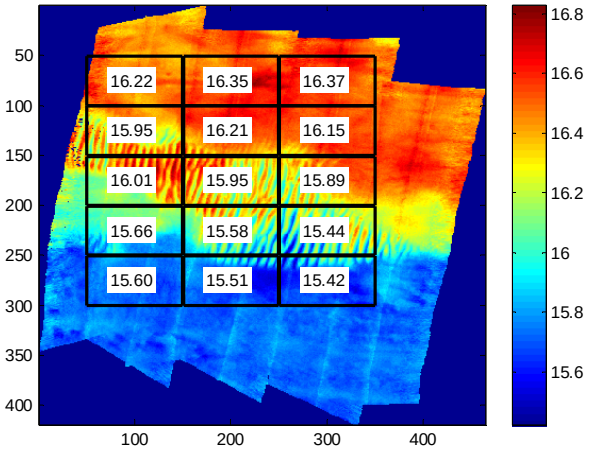

Figure 9. Test section: minimum effective bottom depth min50_100min10avg1, with avg1 in the background.

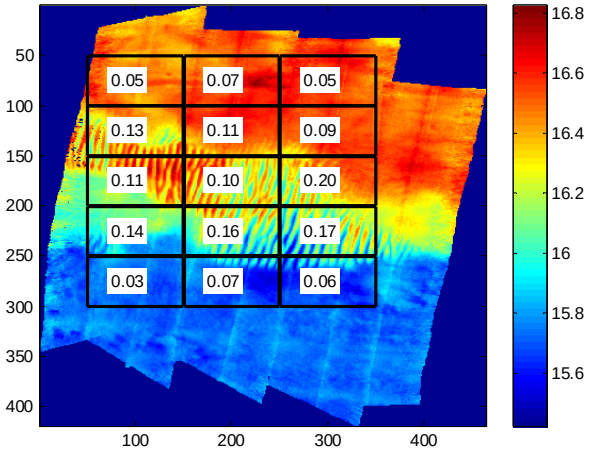

Figure 10. Test section: std50_100min10avg1 values, with avg1 in the background.

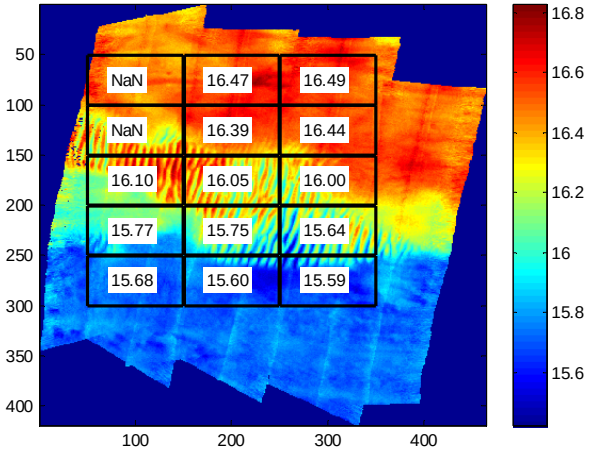

Figure 11. Test section: eq50_100 (equivalent bottom), with avg1 in the background.

4. PRACTICAL IMPLEMENTATION

Although the calculation of the equivalent bottom as described in section 3 only requires average values, minimum values and standard deviations over grid cells, the proposed algorithm deviates considerably from the present methodology for analyzing multi-beam surveys. For this reason, an alternative way of representing the bottom was sought.

The easiest way to reduce the large number of measurements is to consider average values over square grids of $n*n$ m² (avg$n$). The test section was analyzed in such a way, with n = 1,2,3,4,10. For each 50*100 m² rectangle, the minimum value of avg$n$, denoted min50_100avg$n$, was calculated and compared to the equivalent bottom depth eq50_100.

For the considered test sections, n = 3 appeared to result in slightly conservative values for the equivalent bottom depth, see Figure 12, so that avg3 was selected as an alternative practical way for calculating the equivalent bottom. Figure 13 illustrates that averaging the depth over 3*3m² squares leaves sufficient detail to recognize local variations.

The proposed avg3avg1 was implemented by the Flemish Hydrographic Services for issuing charts of the access channels in the Belgian North Sea for nautical purposes and managing dredging activities.

5. CONCLUSIONS

The implementation of the average over 3*3m² grid cells gives satisfactory results for the present practice. The implementation of the equivalent bottom as described in section 3.4 in the short run, on the other hand, is less straightforward. Firstly, the present analysis software does not directly allow such an implementation. Secondly, the implementation would imply a loss of too many details that are of interest for other shipping traffic and for dredging purposes.

In a long-term perspective, the principles of the effective bottom can be integrated in the implementation of a probabilistic access policy for deep-drafted ships, based on an acceptable probability of bottom touch (Vantorre et al, 2008). As the uncertainty of the bottom position, both spatial and temporal, contributes to the stochastic character of the relative motion of the ship's keel with respect to the channel bottom.

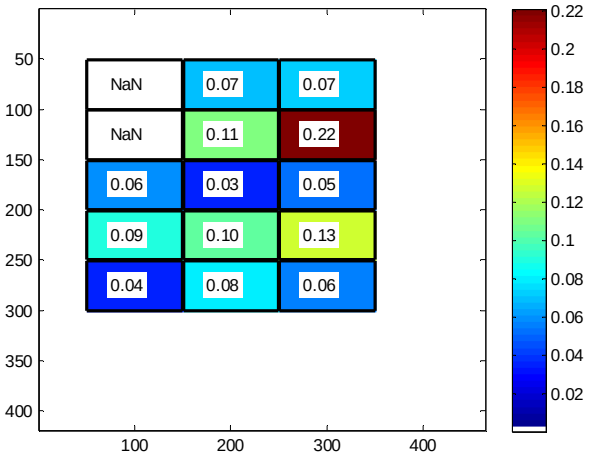

Figure 12. Test section: eq50_100 – min50_100avg3. Positive values suggest a conservative approximation of avg3 for the equivalent bottom depth.

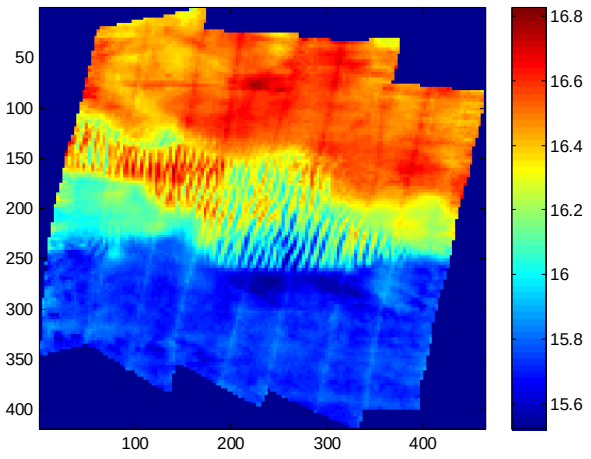

Figure 13. Test section in channel *Scheur Oost*: average values of the multi-beam soundings per grid cell of 3*3 m² (avg3avg1). Horizontal and vertical scale: distance (m, north up); colour scale: depth (m) referred to LAT.

6. ACKNOWLEDGEMENTS

The authors would like to express their gratitude to the State of the Netherlands and the Flemish Government who commissioned the study.

7. REFERENCES

Uliczka, K. & B. Kondziella. 2003. Dynamisches Fahrverhalten extrem großer Containerschiffe unter Flachwasserbedingungen. Mitteilungsblatt der Bundesanstalt für Wasserbau 86: pp. 83-88.

Uliczka, K. & B. Kondziella. 2006. Dynamic Response of very large Container Ships in extremely Shallow Water. 31st PIANC Congress, Estoril, Portugal: pp. 11

Briggs, M.; Vantorre, M.; Uliczka, K. & Debaillon, P. 2010. Prediction of squat for underkeel clearance. Handbook of coastal and ocean engineering. World Scientific: pp. 723-774.

Vantorre, M.; Laforce, E.; Eloot, K.; Richter, J.; Verwilligen, J.; Lataire, E. 2008. Ship motions in shallow water as the base for a probabilistic approach policy. Proceedings of the 27th International Conference on Offshore Mechanics and Arctic Engineering (OMAE 2008), Estoril, Portugal.

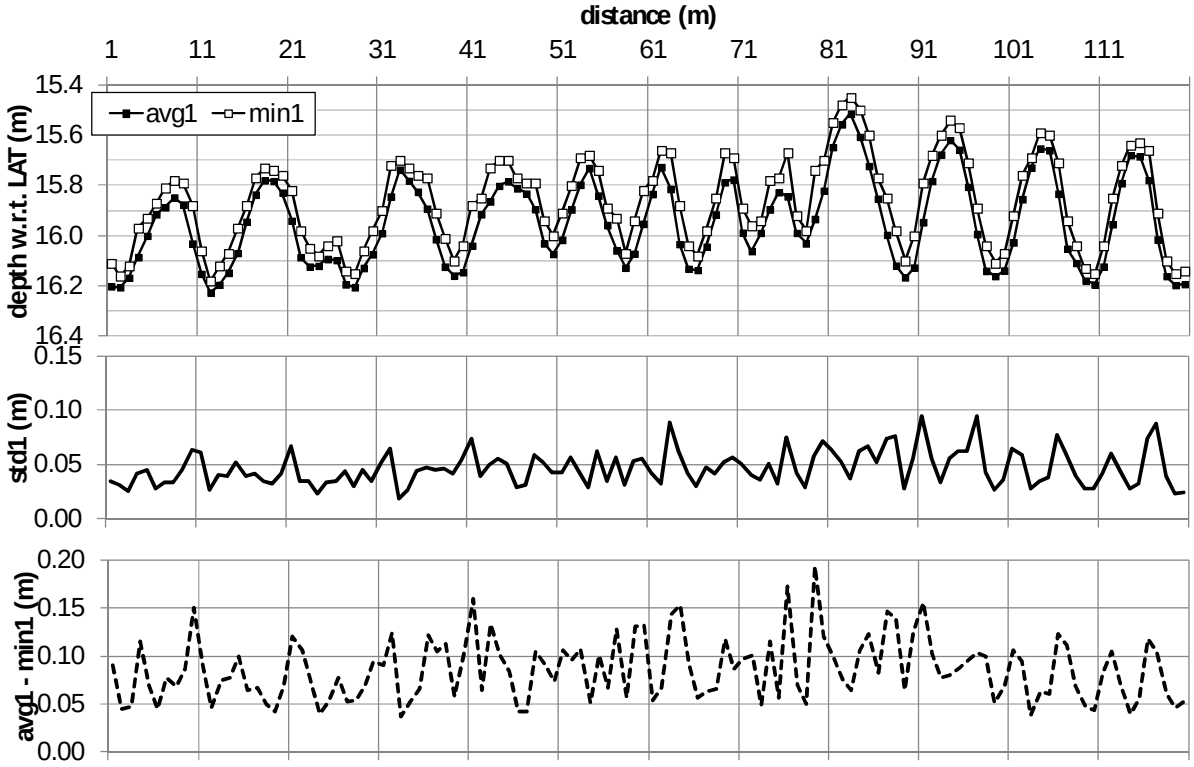

Figure 14. Variation of bottom depth parameter along line [240,180]-[240,300] (see Figure 1).

Gravel dunes generated during ice-jam floods, Tom River, Western Siberia

A. Vershinin[(1)], V. Zemtsov[(1)], N. Inishev[(1)], Y. Korotkova[(1)] and R. Kostaschuk[(2)]

1. Department of Hydrology, Tomsk State University, Tomsk, Western Siberia, Russia.
daversh@rambler.ru
2. Department of Geography, Simon Fraser University, Burnaby, BC, Canada
rkostasc@sfu.ca

Abstract
Dunes are ubiquitous features in sand-bedded lowland rivers but gravel dunes are relatively uncommon. Here we describe gravel dunes exposed on the beds of secondary channels of the Tom River, Western Siberia, Russia. The secondary channels are almost dry most of the time and flow only during floods that are often caused by ice-jams. Flow distribution depends on the location of the ice-jam and in some cases secondary channels can transfer most of the discharge. Dune heights and lengths and bed particle size were measured at three locations in secondary channels in 2009. Dune height ranged from 0.07-0.73 m, length from 5-22 m, and median bed particle size from 11-12 mm. Dune and sediment properties were used to estimate characteristics of the ice-jam flows in the secondary channels using a model for equilibrium dunes. Estimates of flows in 2009 based on the model are much smaller than measurements from an acoustic Doppler current meter, probably because dunes were generated by shallower and faster flows during the falling stage of the flood. In recent years, ice jam floods in this reach of the Tom have become more frequent, causing damage to local villages and engineering structures. Studies such as this provide critical information on flood characteristics and as such are an important component of planning.

1. INTRODUCTION

Dunes are extremely common in sand-bedded rivers but are rarely reported in gravel-bed channels. Carling (1999) conducted an extensive review of the literature and attributed the paucity of information on gravel dunes to their relatively rare occurrence and generic confusion with other gravel features such as antidunes and gravel bars. Carling (1999) examined flume and field data and found that gravel dunes ranged in height from 0.1 to 16 m and in length from 0.6 to greater than 100 m. Flume experiments on gravel dune initiation by Carling et al. (2005) showed that bed defects and incipient dunes developed from lower-stage plane gravel beds during near-threshold conditions of sediment motion and long periods of bed load transport. Equilibrium two-dimensional dunes developed from the defects after several days of gravel transport. Carling et al (2005) suggested that small-scale turbulent sweeps initiated bed defects, but larger-scale, coherent turbulent structures in the outer flow were related to dune development.

In this study we examine gravel dunes exposed in secondary channels in a gravel reach of the Tom River in Western Siberia, Russia (Fig. 1). The secondary channels only flow during floods, many of which are due to ice-jams in the Main Channel.

2. METHODS

Discharge in the Main and secondary channels in the study reach has been measured from a research launch since 1984. A 1000 kHz Sontek acoustic Doppler current profiler (aDcp) has been used since 2008. Dune and sediment properties were used to estimate paleohydraulic and paleohydrologic properties of the flows using the model of van Rijn (1984). Flow depth, h, was determined from dune length, λ:

$$\lambda = 7.3h \quad [1]$$

and dune height, Δ, was used to determine bed shear stress due to skin friction:

$$\Delta = 0.11h\left(\frac{D_{50}}{h}\right)^{0.3}\left(1-e^{-0.5T}\right)\left(25-T\right) \quad [2]$$

where D_{50} is median bed particle size and T is the transport stage parameter for skin friction:

$$T = \left(\frac{\tau_0 - \tau_{cr}}{\tau_{cr}}\right) \quad [3]$$

where τ_0 is the bed shear stress due to skin friction and τ_{cr} is the threshold bed shear stress for sediment motion. Threshold bed shear stress was determined from the threshold Shield's parameter, θ_{cr}, using the equation of Soulsby (1997):

$$\theta_{cr} = \frac{0.3}{1+1.2D_{\square}} + 0.055\left(1-e^{-0.02D_{\square}}\right) \quad [4]$$

where θ_{cr} is:

$$\theta_{cr} = \frac{\tau_{cr}}{g\left(\rho_s - \rho\right)D_{50}} \quad [5]$$

where g is the acceleration of gravity, ρ_s is sediment density, and ρ is water density. Dimensionless grain size, $D_{\square}$ is:

$$D_{\square} = \left[\frac{g\left(s-1\right)}{v^2}\right]^{1/3} D_{50} \quad [6]$$

Dune length and height were measured at three Sites (Fig. 1) with a total station after an ice-jam flood in 2009. Sediment samples were collected at each Site and analyzed using sieves.

where $s = \rho_s / \rho$ and v is the kinematic viscosity of water.

Mean flow velocity, U, is determined from the bed shear stress due to skin friction using the quadratic stress equation:

$$\tau_0 = \rho C_D U^2 \quad [7]$$

where C_D is the drag coefficient:

$$C_D = \frac{g}{C^2} \quad [8]$$

and C is the Chezy coefficient for skin friction:

$$C = 18\log\left(\frac{12h}{k_s}\right) \quad [9]$$

where k_s is the grain roughness:

$$k_s = 3D_{90} \quad [10]$$

and D_{90} is the 90th percentile of the bed particle size distribution.

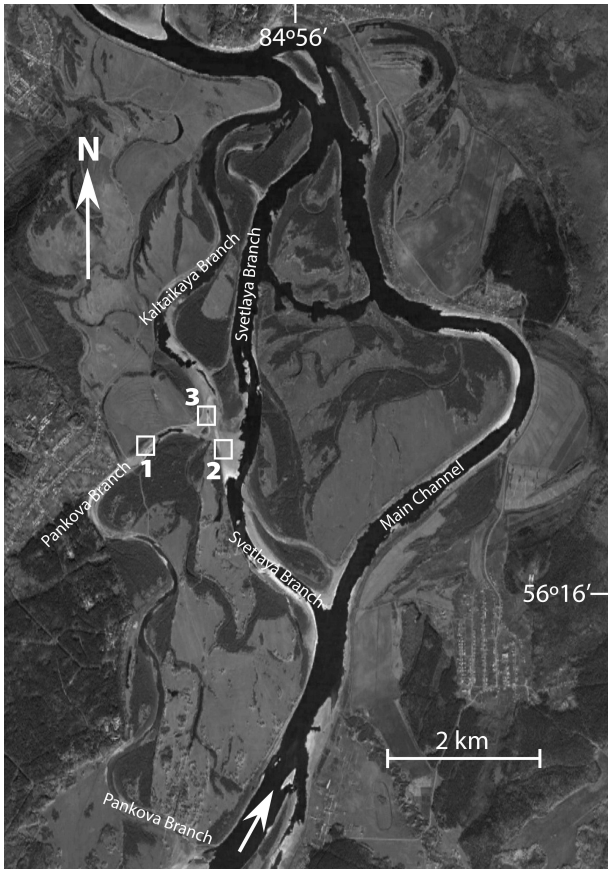

Figure 1. Study reach of the Tom River. The numbers 1-3 refer to Sites of gravel dunes. The image was taken during low flow on October 9 2003. Image from Google Earth.

3. RESULTS AND DISCUSSION

Ice-jam floods in the spring have occurred annually about 40% of the time over the period 1998-2011. Ice-jams in the reach follow three typical patterns (Fig. 2), Firstly, the obstruction occurs in the meander bend of the Main Channel (Fig. 2a). The ice accumulates in the Main Channel and extends upstream to the entrance to the Svetlaya Branch (Fig. 1, 2a). Flow in the Main Channel is diverted primarily into the Svetlaya Branch, which rejoins the Main Channel downstream of the bend. Secondly, ice accumulates at the downstream end of the Svetlaya Branch, diverting flow into the Kaltaikaya Branch (Fig. 1, 2b). Thirdly, ice accumulates in the Main Channel and blocks the entrance to the Svetlaya (Fig. 1, 2c), diverting flow into the Pankova Branch and then the Kaltaikaya Branch (Fig. 1, 2c). The ice is eventually flushed through the reach and all of the channels are actively flowing (Fig. 2d).

Flows in the secondary channels generated gravel dunes at three locations in 2009 (Fig. 1, 3). Dunes have a long, gently-sloping stoss side and a short, steep (>30°) lee side (Fig. 4). Most of the dunes have slightly sinuous crests (Fig. 4) and can be classified as two-dimensional. The crestal areas of dunes often display scours caused by ice blocks.


Figure 3. Field of gravel dunes in May 2012 at Site 2 on the Svetlaya Branch (Fig. 1). Flow was from top left to bottom right.


Figure 4. Gravel dune in May 2012 at Site 2 on the Svetlaya Branch (Fig. 1). Flow was from the left.

Table 1 summarizes mean values of measurements of dune geometry and bed particle size for Sites 1-3 in 2009. Table 2 presents flow characteristics estimated from dune and sediment properties using the van Rijn (1984) models, and Table 3 provides results from aDcp measurements on May 7 2009 just after the ice-jam.

Site	λ (m)	Δ (m)	D_{50} (m)	D_{90} (m)
1	17.5	0.61	0.012	0.023
2	6.4	0.14	0.011	0.017
3	11	0.18	0.012	0.015

Table 1. Mean dune length (λ) and height (Δ), and median (D_{50}) and coarse fraction (D_{90}) bed particle size for 2009.

Site	h (m)	U (m/s)	W (m)	Q (m^3/s)
1	2.4	2.37	118	670
2	0.88	1.67	463	678
3	1.5	1.85	255	711

Table 2. Mean flow depth (h), velocity (U), channel width (W) and discharge (Q). W was measured from the 2010 satellite image taken just after the ice-jam (Fig. 2). h and U were estimated from the van Rijn (1984) models using the 2009 dune and particle size measurements (Table 1).

Site	h (m)	U (m/s)	W (m)	Q (m^3/s)
1	5.0	1.07	117	670
2	5.6	1.61	330	2966
3	7.3	0.71	267	1381

Table 3. Mean flow depth (h), velocity (U), channel width (W) and discharge (Q) measured using an aDcp on May 7 2009.

Dunes were largest in the Pankova Branch (Site 1), followed by the Kaltaikaya (Site 3) and the Svetlaya (Site 2). Bed particle size was similar at all Sites (Table 1). Flow depth is smaller and mean velocity is larger when estimated from the van Rijn models (Table 2) compared to the aDcp measurements (Table 3). Width measured from the 2010 satellite image (Table 2) is greater than the aDcp measurement in 2009 (Table 3) because aDcp measurements are limited to deeper sections of the channel, or because the satellite image was taken during a higher flood stage in 2010 compared to 2009.

Discharge estimated from the van Rijn models (Table 2) is consistent for all three Sites but is much less than the aDcp measurements (Table 3). The aDcp measurements were taken when all of the channels were actively flowing in 2009 and the ice had been removed from the reach. Discharge measured from the aDcp is highest in the largest channel, Svetlaya, followed by the Kaltaikaya and the Pankova.

The results summarized on Tables 1-3 indicate that the dunes measured in 2009 were generated by much shallower and faster flows than those measured with the aDcp. It may be that the flows that created the dunes occurred during the falling stages of the flood when the depth was lower and the velocity higher. It is also possible that the dunes are non-equilibrium features. A compilation of a large amount of data for sand dunes and ripples by Ashley (1990) showed that dune length (λ) and height (Δ) were related as a power function of the form:

$$\Delta = 0.0677\,\lambda^{0.8098} \qquad [11]$$

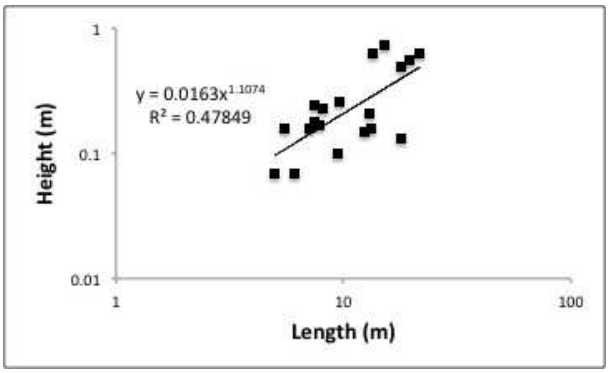

Figure 5. Dune length, λ , and height, Δ , for Sites 1-3 in 2009.

Carling (1999) found that dune length and height for three-dimensional gravel dunes had an exponent similar to that of Ashley (1990) and he concluded that they were probably in equilibrium with the flow. Carling (1999) also suggested that the two-dimensional gravel dunes that he examined were not in equilibrium. The flume experiments of Carling et al. (2005) however showed that, given sufficient time, near-equilibrium two-dimensional dunes can develop. The exponent for the two-dimensional Tom gravel dunes (Fig. 5) is larger than of the Ashley (1990) relation, suggesting that the dunes may not be in equilibrium. It must be noted however that scour by ice blocks may affect the relation on Fig. 5. It is also possible that the Ashley (1990) function for sand dunes does not apply to equilibrium gravel dunes.

4. CONCLUSIONS

Ice-jam floods are common in the Tom River of Western Siberia. Flow distribution between the Main and secondary channels depends on the location of the ice-jam and in some cases secondary channels can transfer most of the flow. Gravel dunes are exposed on the beds of secondary channels during low flows. Dune and sediment properties measured in 2009 were used to estimate characteristics of the ice-jam flows in the secondary channels using a sediment transport model. Estimates of flows in 2009 based on dunes are much smaller than acoustic Doppler current meter measurements during ice-jam flood flows, probably because the dunes were generated by of shallower and

faster flows during the falling stage the flood. Ice jam floods in the Tom have become more frequent in the past decade, causing damage to local villages and engineering structures. An improved understanding of ice-jam flood characteristics is critical for planning.

5. ACKNOWLEDGMENT

We would like to thanks students and staff in the Department of Hydrology, Tomsk State University, for their able assistance. Funding was provided by the Russian Foundation for Basic Research (Grant 10-05-00625a) and the Natural Sciences and Engineering Research Council of Canada.

6. REFERENCES

Ashley, G.M. 1990. Classification of large-scale subaqueous bedforms - a new look at an old problem. Journal of Sedimentary Petrology: 60, 160–172.

Carling, P.A. 1999. Subaqueous gravel dunes. Journal of Sedimentary Research: 69, 534-545.

Carling, P.A., Richardson, K & Ikeda, H. 2005. A flume experiment on the development of subaqueous fine-gravel dunes from a lower stage plane bed. Journal of Geophysical Research: 110, F04S05, doi:10.1029/2004JF000205.

Soulsby, R. 1997. Dynamics of Marine Sands: A Manual for Practical Applications. Thomas Telford, London, 249 p.

van Rijn, L.C. 1984. Sediment transport: Parts I-III. Journal of Hydraulic Engineering: 110, 1431-1454.

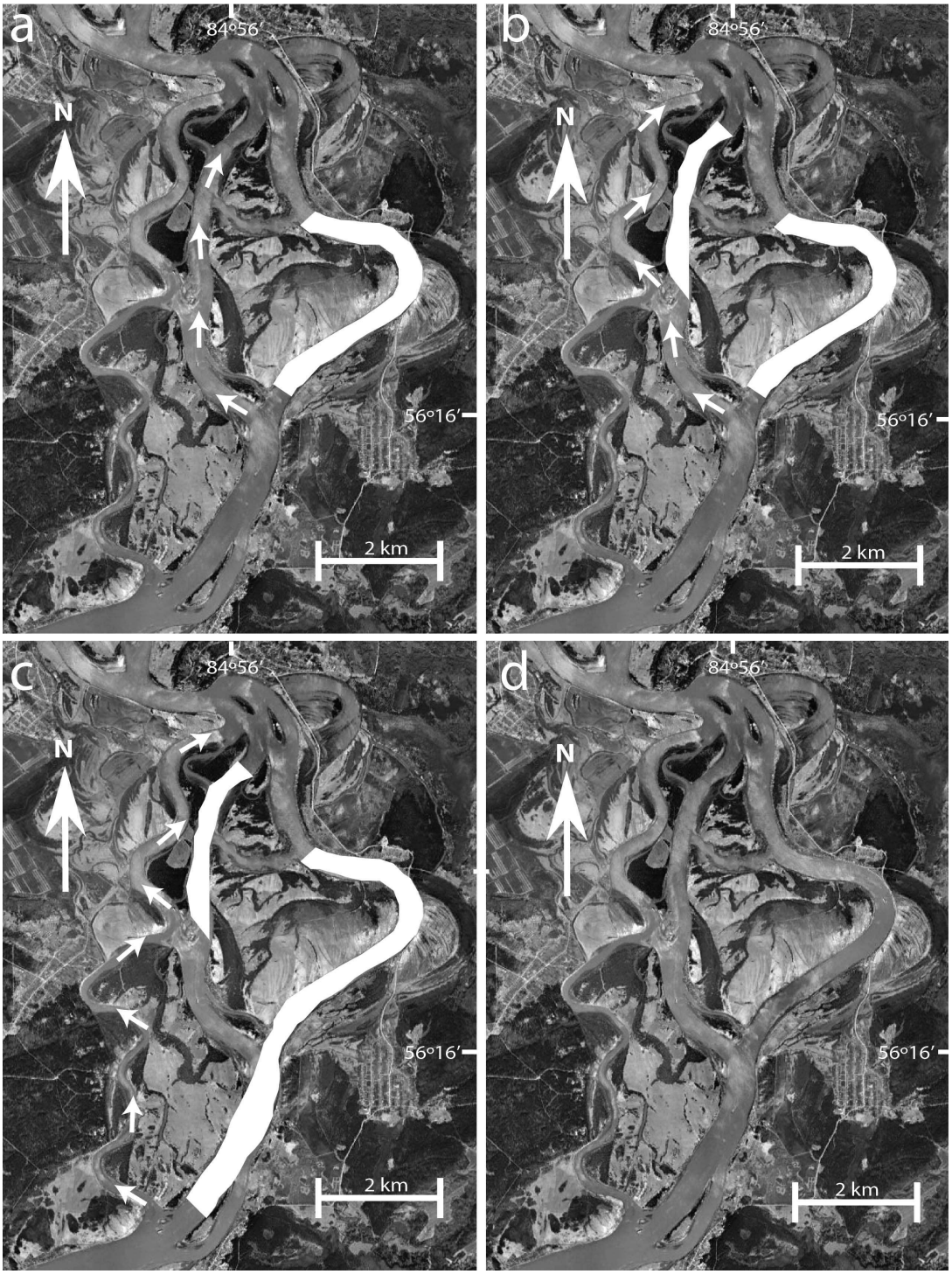

Figure 2. Typical patterns of ice-jam flooding in the study reach of the Tom River. Ice is indicated in white. See text for explanation.

A first phase in the habitat classification for the Zeeschelde: Bed form classification.

G.R. Vos[1,2], T. Maximova[1], Y.M.G. Plancke[1], A. Van Braeckel[3], R. De Sutter[2]

1. Flanders Hydraulics Research, Antwerpen, Belgium - yves.plancke@mow.vlaanderen.be
2. Antea Group, Antwerpen, Belgium – gwendy.vos@anteagroup.com
3. Instituut voor Natuur- en Bosonderzoek, Brussel, Belgium – alexander.vanbraekel@inbo.be

Abstract

Within the scope of the long term vision of the Schelde Estuary and the Development Outline 2010 low dynamic intertidal and shallow water areas are considered to be of high ecological value. Little is known about the occurrence of such valuable areas in the Schelde Estuary, nor are the physical and morphological processes which determine the occurrence of these areas fully understood. Based on the results and recommendations of a 2008-2009 research project in the Westerschelde, a new research project was defined to determine relationships between abiotic (bedforms, hydrodynamics, sediment) and biotic (benthos) characteristics in the Zeeschelde (Belgium) and to set up a classification of deep and undeep subtidal areas. A first phase in the habitat classification comprises of the analysis of bed form occurrence and the setup of a bed form classification based on multibeam echo sounding data. Results show within the different sub areas a variation in bed forms going from hard bed layers to no bed forms to ripples (H ~ 0,1 to 0,3 m | L ~ 10 m) and smaller dunes (H ~ 0,5 to 1 m | L ~ 15 to 25 m). On-going research investigates relationships between the bed form characteristics and flow and sediment characteristics. Preliminary results show weak relationships between flow velocity and bed form size, and between depth and bed form size.

1 INTRODUCTION

Within the scope of the long term vision of the Schelde Estuary and the Development Outline 2010, low dynamic intertidal and shallow water areas are considered to be of high ecological value. These areas are in fact linked to eutrophic foraging zones for birds and young fish and to refugees for tidal migrators as shrimps. However, this assumption is based on experiences in other areas and there is no evidence that all parts of the shallow water area are equally valuable. Little is known about the occurrence of such valuable areas in the Schelde estuary, nor are the physical and morphological processes which determine the occurrence of these areas fully understood. Therefore, a research project was defined in 2008-2009 to investigate the relation between on one hand the bed forms, hydrodynamics and sediment properties and on the other hand the ecological value of the shallow water areas (Plancke, Y. 2009). This 'Walsoorden' research project was conducted by NIOZ-CEME in collaboration with Flanders Hydraulics and IMARES, focused on the area near the Walsoorden Sandbar in the Westerschelde (the Netherlands). This study resulted in a criterion based on abiotic parameters (depth and duration during a full tidal cycle in which flow velocity exceeds 65 cm/s) that was able to predict habitats with a high ecological value. Where this criterion was found for only one specific area of the Schelde Estuary, a validation is necessary. Therefore 2 new studies were started: one to validate the criterium in the Westerschelde, a second one to validate it in the Zeeschelde. This paper describes the results of the abiotic analysis in the Zeeschelde, the Belgian upstream part of the Schelde Estuary. In a first phase a bed form classification was made for 4 specific subareas (spread over the full salinity gradient), based on multibeam echo sounding data. In a second phase the hydrodynamics were analyzed, while in the third phase it was investigated whether relations existed between bed form and hydrodynamic characteristics.

2 BED FORM ANALYSIS

2.1 Study area and used data

Within the Zeeschelde detailed research has been conducted in 4 subareas. These subareas were

selected based on the salinity zones in the Zeeschelde and the occurrence of a vast undeep water area. The selected subareas are:

- Mesohaline: Schaar van Ouden Doel and Galgenschoor area
- Oligohaline: Notelaer and Ballooi area
- Freshwater with long residence time: Branst area
- Freshwater with short residence time : Appels area

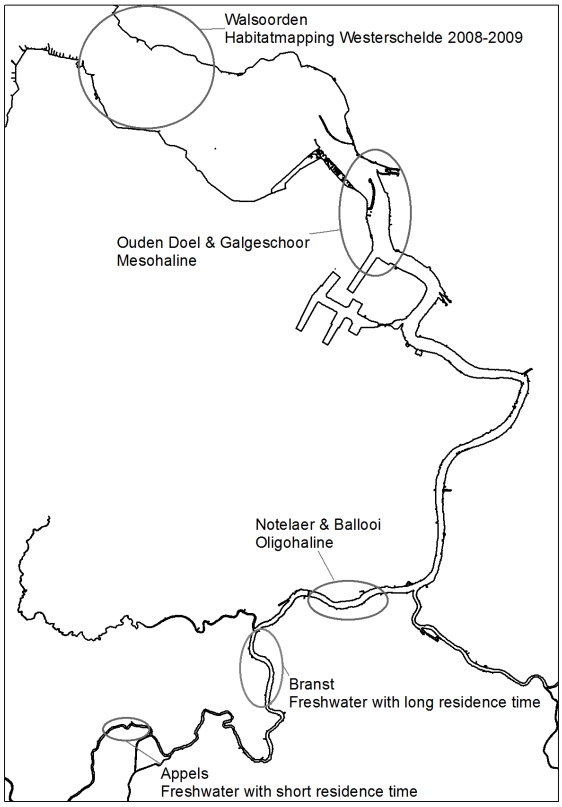

Figure 1. Location of analyzed subareas in the Schelde estuary

The bathymetry of the mesohaline area in the Beneden-Zeeschelde is based on multibeam echo sounding measurements from 2011, the bathymety for the more upstream areas in the Boven-Zeeschelde is composed of data from 2009, 2010 and 2011. For the intertidal area LIDAR data from 2011 is used.

2.2 Methodology

The analysis was executed using the following steps:

1 Visual classification in zones, starting from the shaded view image of the area
2 Selection of zones without bed forms
3 Definition of several longitudinal transects (along the direction of the flow) within each zone with bed forms
4 Analysis of average bed form characteristics in each transect such as length, height, asymmetry and steepness of the bed forms
5 Classification of the sub area in a limited amount of bed form classes

2.2.1 Visual classification in sub areas

A so-called 'shaded view' map was used as a base for the visual classification in sub areas. This computer-generated map shows a simulated cast shadow of sun upon a raised bathymetry. The angle of the sun on the bathymetry has been chosen to discern the bed forms optimally. The optimal angle was found to be parallel to the direction of the flow, because the direction of bed forms is expected to be perpendicular to the direction of the flow.

Based upon this 'shaded view' images, different sub areas were delimited (see zoom detail in Figure 3). Boundaries were defined visually in those places where differences in bed forms appeared to occur.

2.2.2 Selection of zones without bed forms

While determining the zones without bed forms, a distinction was made between flat zones and zones with irregular bed forms (caused by geological hard layers or human interference such as sediment disposal or extraction). This distinction is not always clear on the basis of topo-bathymetric maps. Especially the recognition of hard layers, which can have both irregular and a flat appearance, is often difficult. The in situ sediment sampling campaign that has been conducted in the scope of this research, will make this distinction more clear.

2.2.3 Definition of longitudinal transects

Within every subarea some longitudinal transects were defined, assuming that these sections are representative for the whole subarea. If possible, the length of the transects was chosen long enough to ensure a sufficient number of bed forms within one transect, in order to be able to conduct a representative analysis. The depth values of these

sections were exported from a 1m*1m raster covering the study area using GIS-software.

2.2.4 Analysis of the transects to obtain bed form characteristics

For every longitudinal transect following characteristics were deduced:

- Length of the individual bed forms
- Height of the individual bed forms
- Asymmetry of the individual bed forms
- Average steepness of the bed forms per transect

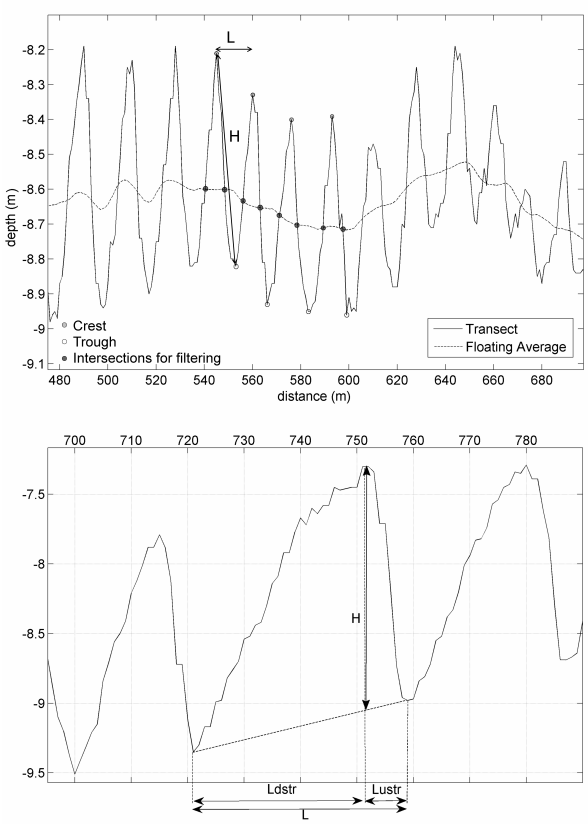

Figure 2. Methodology for determining characteristic parameters, above: step 1 – 4, below: step 5 – 7

This analysis was executed using a self-developed Matlab routine, based on the methodology used in the Bed form Tracking Tool (van der Mark et al. 2007). This routine consists out of the following steps to define the characteristic parameters of the bed forms in a certain transect (Figure 1) :

1 Choosing a period for a floating average to remove trends (large scale depth variation) from the section without losing the individual bed forms.
2 Detrending of the section by subtracting the floating average from the original data.
3 Determining the intersections of the detrended signal and the zero-line.
4 Determining the crests and troughs, based upon the assumption that between two intersections with the zero-line, a crest or a trough can be found.
5 Determining the length of every individual bed form, defined as the distance between 2 successive crests.
6 Determining the height of every individual bed form, defined as the difference between the height of a crest and the following trough.
7 Determining the asymmetry of every individual bed form, defined as the ratio between the inclination length (Ldstr) and the declination length (Lustr) of the bed form (from trough to trough).
8 Determining the average steepness per transect, defined as the ratio between the average height and the average length of the bed forms (from trough to trough) in that section.

Next, the characteristics of the individual bed forms were averaged per transect. The resulting average values for length, height and asymmetry were filtered to minimize outlier-effects: all values outside the interval [0,25*average: 1,75*average] were discarded and a new average was calculated using the remaining values.

The transects were always defined from down-estuary to up-estuary side. Thus, an asymmetry value greater than 1 implies a bed form where the seaward side is longer than the landward side. This indicates flood dominance. A value smaller than 1 indicates ebb dominance.

2.2.5 Classification of the study area in a limited amount of bed form classes

In order to group the different sub areas in a feasible amount of classes, the averaged characteristics were compared and classified according to the classification used in the 2008-2009 Walsoorden research project, which makes it easier to compare results of the Zeeschelde research project with those of the Westerschelde research project.

Class	Length	Height
1	< 10 m	< 5 cm
2	~ 10 m	15 – 30 cm
3	10 – 15 m	30 – 50 cm
4	15 – 25 m	50 – 100 cm
5	15 – 30 m	100 – 150 cm
6	> 30 m	> 150 cm
7	> 30 m	< 100 cm

Table 1 :Overview of length/height classes

Class	Asymmetry
1	< 0,90 (ebb dominance)
2	0,90 – 1,10 (no dominance)
3	1,10 – 1,50 (flood dominance)
4	> 1,50 (strong flood dominance)

Table 2 :Overview of asymmetry classes

Table 1 shows the classification based on length and height of the bed forms, table 2 shows an overview of the asymmetry classes.

2.3 Results

Based on the mean length, height and asymmetry of the bed forms per transect, each of the zones is attributed to one of the bed form and asymmetry classes. A class 0 is also defined, holding the zones with irregular bed-surface. Where small bed forms are superposed on larger ones (e.g. dunes of class 5 with superposition of ripples of class 2), a combined class number is attributed (e.g. class 5,2). In figure 3 an example of the length/height classification for the subarea Notelaer/Ballooi can be found, figure 4 shows the length/height classification for the upstream subarea Appels.

The most downstream subareas Ouden Doel and Galgeschoor in the Beneden-Zeeschelde are strongly influenced by human interference (disposal/sand extraction). This means only few zones contain bed forms, which makes it difficult to draw general conclusions on the occurrence of bed forms. Most of the bed forms in this area are small ripples (class 2).
In the other sub areas, in the upstream Boven-Zeeschelde, bed form characteristics are more diverse. Next to zones with small ripples, sub areas Notelaer/Ballooi and Branst also contain dunes and dunes with superimposed ripples. In most upstream sub area Appels no dunes can be found, but ripples from class 3 are present, next to the small class 2 ripples.

It was noticed that most of the classes with bed forms are located in the deeper, central parts of the river.

The classification in asymmetry classes is executed using the classes in table 2. Class 0 is again used for zones with irregular bed surface, while a class 5 was defined for zones where different transects are characterised by different asymmetry.

Most areas are flood dominant, but within each sub area ebb dominant zones (or zones with no dominance) are found. No relationship can be found though between location of the zones and dominance class.

3 HYDRODYNAMIC ANALYSIS

In a next phase of the study the relation between the occurrence of bed forms and hydrodynamic parameters has been analysed.

3.1 Used data

A 2D validated numerical model is used as a base for the hydrodynamic analysis (Maximova, T. 2013). This model is a refined version of the NEVLA-model (Maximova, T. 2009; Verheyen, B. 2012), which was too coarse to be able to predict the velocities in sufficient detail for this study in the upper part of the estuary.
The downstream boundary of the model is located at Walsoorden in the Westerschelde; the upstream boundary is located at the tidal border. Measured water levels at Walsoorden (HMCZ database) are used as a downstream boundary condition. Measured discharges are used as an upstream boundary condition. The time step used for the model simulations is 3s. For the bathymetry, the multibeam and LIDAR data from the bed form analysis is used in the model.
Every 10 minutes a 'map file' with flow fields was exported for the period from 26/06/2009 to 27/06/2009 (spring tide conditions).

3.2 Methodology

Based upon the flow fields, following characteristic hydrodynamic parameters were deduced:

- Average flood velocity
- Average ebb velocity

- Ratio average flood velocity to average ebb velocity
- Maximum flood velocity
- Maximum ebb velocity
- Duration that flow velocities exceed 65 cm/s during one spring tidal cycle (figure 5 shows the duration map for Appels).

Similar to the bed form analysis, the hydrodynamic analysis was performed using 2 types of classification: first a classification based on the magnitude of average velocities, second a classification based on the ratio between average velocities.

For the first classification, the used boundary values are related to characteristic velocity boundaries for e.g. initiation of sediment transport (Flanders Hydraulics Research, 2007) and low versus high dynamic conditions (Bouma et al., 2005). For every point in the flow field, ebb as well as flood velocity has been classified using these boundary values. Based on the combination of ebb and flood velocity the eventual classification is made (see Table 5).

[cm/s]	*< 50*	*[50, 60]*	*[60, 80]*	*[80, 100]*	*> 100*
< 50	1	2	3	4	5
[50, 60]	6	7	8	9	10
[60, 80]	11	12	13	14	15
[80, 100]	16	17	18	19	20
> 100	21	22	23	24	25

Table 5: Classification based on hydrodynamic characteristics.

3.3 Results

The hydrodynamic analysis shows as can be expected an increase of velocities with increasing depth. The duration during which flow velocities are higher than 65 cm/s exceeds 240 minutes almost everywhere, except along the river banks and on the leeward side of the guiding wall. Flood/ebb ratio shows a similar pattern in all sub areas, namely an alternating pattern of ebb and flood dominated zones along each river bank.

4 ON-GOING RESEARCH

Based on the bed form classification the Research Institute for Nature and Forest has taken ca. 200 samples, stratified random over the different classes and subareas. At this moment the samples are being analysed on both grain size and the density and number of benthic species. These results will be used to investigate potential relations between abiotic characteristics presented in this paper, and biotic characteristics.

5 CONCLUSIONS

Based on the bed form classification and hydrodynamic classification a relationship between both aspects has been investigated. Therefore the hydrodynamic characteristics were attributed to the bed form classes by calculating the average value per bed form zone for each of the hydrodynamic parameters. Figure 6 shows an example of the classification, based on the ratio between average flood and ebb velocity.

Additionally the relationship between the occurrence of certain types of bed forms and each of the hydrodynamic characteristics was examined Figure 7 shows a weak positive trend between average ebb velocity and length/height classes.

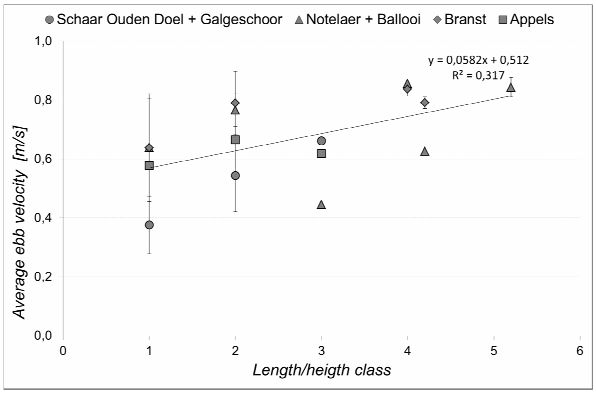

Figure 7: Relationship between length/height class and average ebb velocity

A clear relationship between hydrodynamic and bed form characteristics could not be found. A general increase of the size of the bed forms with increasing velocities can be determined, but the scatter is fairly high. However, the linear relationship between depth and bed form size explained 56% of the variation ($R^2 = 0,568$).

6 ACKNOWLEDGMENT

This study was performed within the scope of the long term vision of the Schelde estuary

commissioned by the Flemish Maritime Division and the Dutch Rijkswaterstaat.

7 REFERENCES

Bouma H., de Jong D.J., Twisk F., Wolfstein K. 2005. Zoute wateren Ecotopenstelsel (ZES.1) – Voor het in kaart brengen van het potentiële voorkomen van levensgemeenschappen in zoute en brakke rijkswateren, juli 2005.

Maximova, T., Ides, S., De Mulder, T., Mostaert, F. 2009. Verbetering 2D randvoorwaardenmodel. Deelrapport 4: Extra aanpassingen Zeeschelde. WL Rapporten, 753_09. Flanders Hydraulics Research, Antwerp, Belgium

Maximova, T., Vanlede, J., Plancke, Y., Verwaest, T., Mostaert, F. 2013. Habitatmapping ondiep water Zeeschelde: Deelrapport 2 - Numeriek 2D model. Version 1.2. WL Rapporten, 00_028. Flanders Hydraulics Research. Antwerp, Belgium

Plancke Y., Vos G., De Mulder, T., Mostaert, F. 2009 Habitatmapping Westerschelde – Deelrapport 1: classificatie op basis van bodemvormen en hydrodynamica. WL Rapporten, 754-06. Waterbouwkundig Laboratorium, Antwerpen, Belgie.

van der Mark C.F., Blom, A. 2007. A new and widely applicable tool for determining the geometric properties of bedforms. april 2007.

Verheyen, B., Leyssen, G., Vanlede, J., Schramkowski, G., Mostaert, F. 2012. Verbetering randvoorwaardenmodel: Deelrapport 7: Afregeling van het 3D Scheldemodel. WL Rapporten, 753_09. Flanders Hydraulics Research & IMDC: Antwerp, Belgium

Vos, G., Plancke, Y., Verwaest, T., Mostaert, F. (2013). Habitatmapping Zeeschelde: Deelrapport 3 – Relaties abiotiek. Versie 1_3. WL Rapporten, 00_028. Waterbouwkundig Laboratorium: Antwerpen, België.

Waterbouwkundig Laboratorium Borgerhout (WLB), 2007. M754/2B Alternatieve stortstrategie Westerschelde – Verslag 13u meetcampagnes Walsoorden, mei 2007.

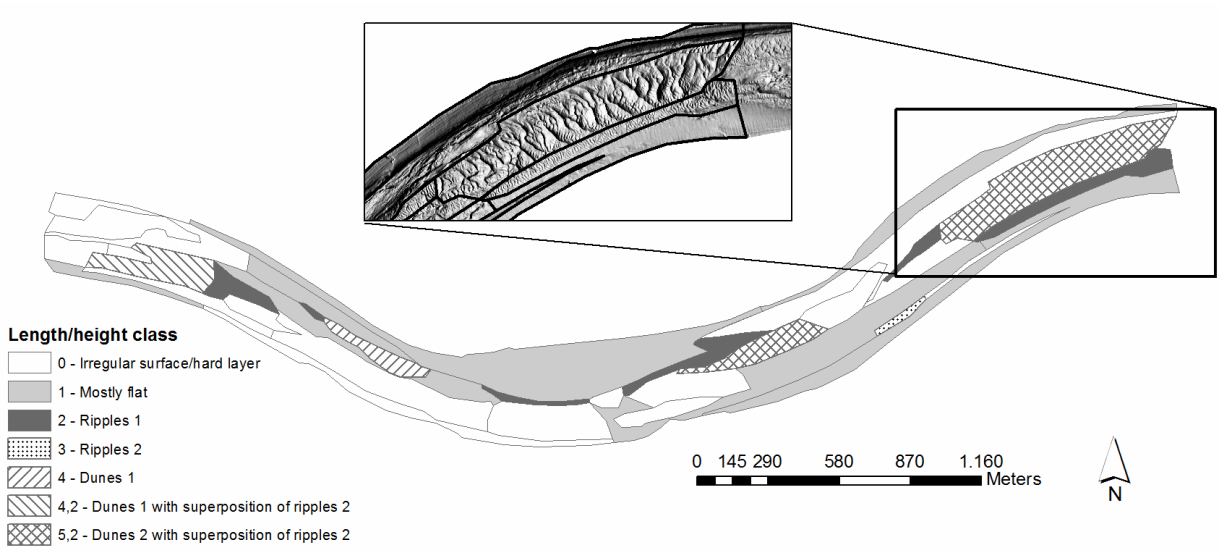

Figure 3. Notelaer and Ballooi: classification in length/height classes, based on shaded view map

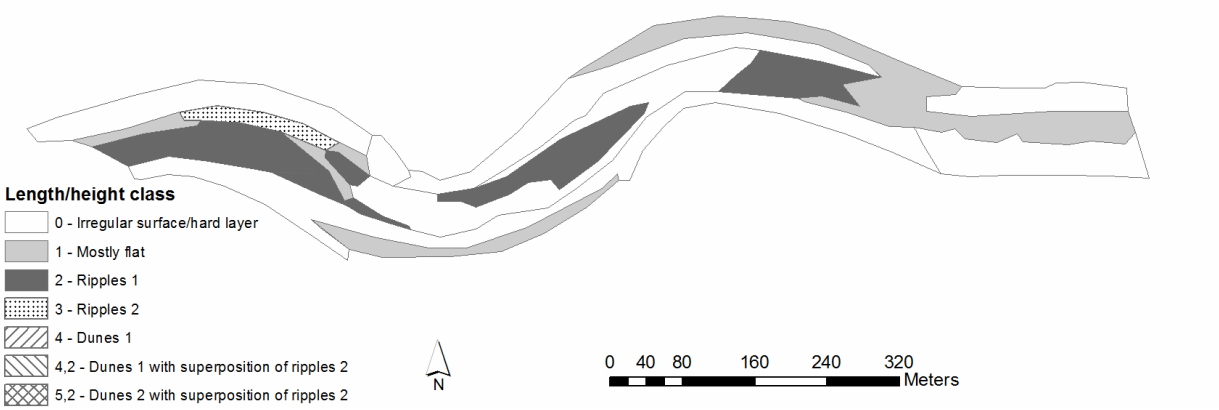

Figure 4. Appels : classification in length/height classes

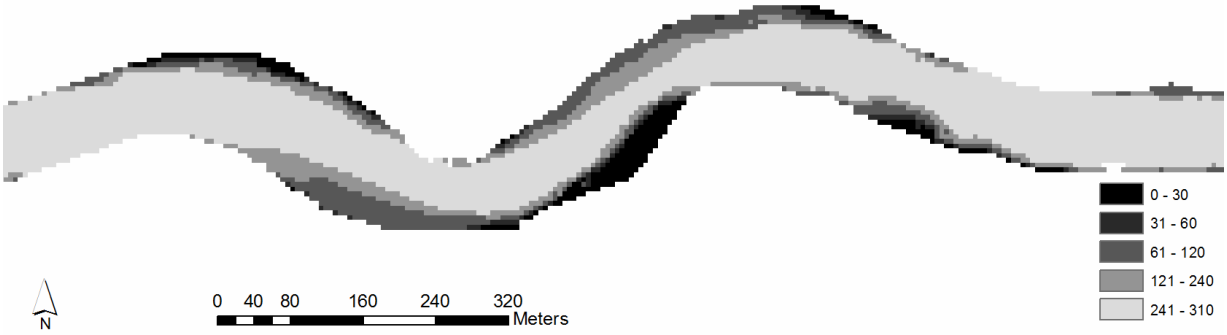

Figure 5: Appels: duration that flow velocities exceed 65 cm/s during one spring tidal cycle

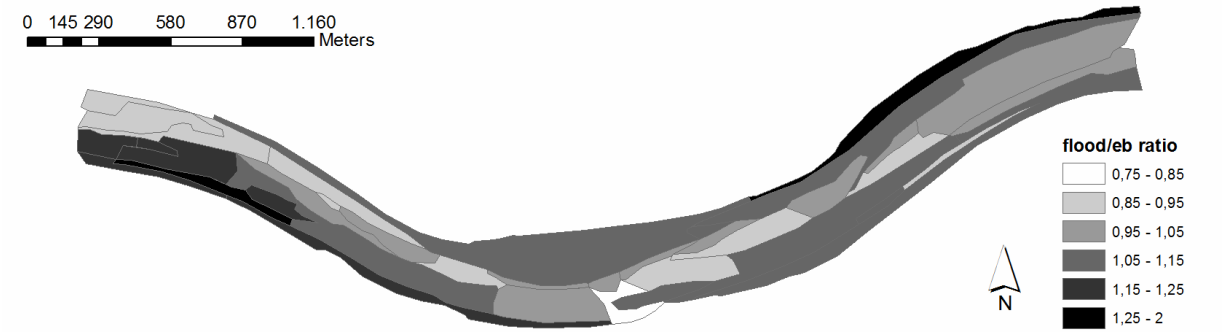

Figure 6. Notelaer and Ballooi: classification in hydrodynamic classes based on flood/eb ratio

Evolution of bed form height and length during a discharge wave

J.J. Warmink[(1)], R.M.J. Schielen[(2)], C.M. Dohmen-Janssen[(1)]

1. Department of Water Engineering and Management, University of Twente, Enschede, The Netherlands – j.j.warmink@utwente.nl
2. Centre for Water Management, Rijkswaterstaat, Lelystad, The Netherlands

Abstract

This research focusses on modeling the evolution of bed form during a discharge wave for application in operational flood forecasting. The objective of this research was to analyze and predict the bed form evolution during a discharge wave in a flume experiment. We analyzed the data of a flume experiment and show that dune length is determined by development of secondary bed forms during the receding limb of the discharge wave. Secondly, three models were compared to predict the bed form evolution: an equilibrium model, a time-lag model and the physically-based, numerical model of Paarlberg et al. (2010). We show some preliminary results and show that the numerical model seems promising for modeling bed form evolution for operational flood forecasting.

1. INTRODUCTION

Accurate forecasts of flood levels are essential for flood management. While a lot of improvements have been made in the field of hydraulic modeling, the roughness values of the main channel and floodplains are still largely uncertain (Warmink et al., 2007, 2012a). This research focusses on the roughness of the main channel, which is mainly determined by the bed forms that develop on the river bed.

Rivers dunes are the dominant bed forms in many rivers. The height is in the order of 10 - 30% of the water depth and their length in the order of 10 times their heights. Under flood conditions the bed is highly dynamic; dunes grow and decay as a result of the changing flow conditions.

River bed forms act as roughness to the flow, thereby significantly influencing the water levels. Accurate and fast computer models are required to predict daily water level forecasts for operational flood management and forecasting. It is essential to predict the time evolution of bed forms and assess their influence on the hydraulic roughness.

Observations in flumes and in the field have shown that dunes of different lengths and amplitude co-exist (Carling et al., 2000; Warmink et al. 2012b). Carling et al. (2000) described the morpho-dynamics of bed forms in the river Rhine under supply limited conditions. They distinguished three scales of bed forms, ripples, small dunes (length < 5 m) and large dunes (length > 10 m) and show that the latter two strongly interact.

Recently, several successful attempts were made to model bed form evolution and associated roughness using detailed numerical modeling (e.g. Giri and Shimizu, 2006, Nabi, 2010). However, these models require long computational times and are therefore not applicable for operational flood management.

Paarlberg et al. (2009, 2010) developed a process-based model for bed form evolution that requires limited computational effort. This model accounts for flow separation and is able to predict bed form development towards equilibrium conditions.

The objective of this research was to analyze and predict the bed form evolution during a discharge wave. Firstly, the data of a flume experiment were

analyzed to determine the most important processes in dune evolution during a discharge wave. Secondly, three models were compared to predict the bed form evolution: an equilibrium model, a time-lag model and the physically-based, numerical model of Paarlberg et al. (2010).

2. OBSERVATIONS FROM DATA

Many flume experiments are available that show the height of bed forms under different discharge conditions (e.g. Guy et al. 1966, Wijbenga and Van Nes 1986, Venditti 2005). However, most of these measurements were carried out for a constant flow discharge. These data do not show the hysteresis effect. We used the flume data from Wijbenga and Van Nes (1986) who imposed a discharge wave in the flume (scaled to observed discharge waves in the Dutch river Rhine) and measured the bed form evolution and associated flow characteristics. The discharge ranged between 0.03 and 0.15 m^3/s resulting in water depths, h ranging between 0.15 and 0.47 m. The width of the flume was 0.5 m and the measuring section was 30 m long. Bed material consisted of uniform sand with D50 = 0.78 mm.

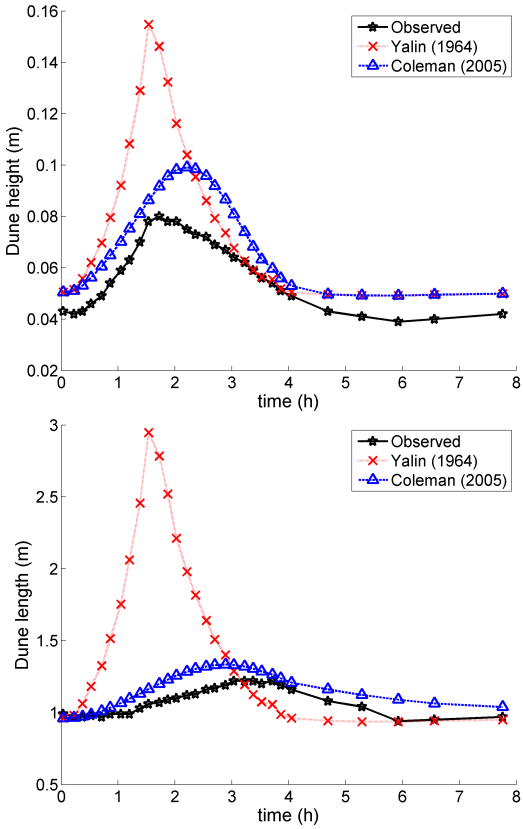

Figure 1. Observed and predicted dune height (top) and length (bottom) from Wijbenga and Van Nes

Figure 1 shows the observed and predicted dune heights, Δ (m) and lengths, Λ (m). The predicted dune dimensions are computed using Coleman et al. (2005) see section 3 and the equilibrium predictors of Yalin (1964) where *h* is water depth (m):

$$\Delta = 0.33\ h \quad (1)$$

$$\Lambda = 6\ h \quad (2)$$

The dune dimensions predicted by Yalin indicate the variation in water depth. The observed dune height shows a small time-lag and is clearly lower than the equilibrium dune height (predicted using eq (1)). This time-lag and attenuation of the dune height is commonly observed under a discharge wave in the field.
The observed dune length shows a similar trend, with a time-lag and attenuation compared to predicted equilibrium dune length. However, the time-lag and attenuation are larger for dune length than for dune height. This shows that dune length has a much longer adaptation time than dune height.

Figure 2 shows the detailed bed profiles measured by Wijbenga and Van Nes (1986) during the discharge wave. The vertical axis shows the normalized time for Twave=3.5h. The right panel shows the normalized discharge, Q, dune height, Δ and dune length, Λ. The left panel shows the corresponding bed profiles at different times during the discharge wave. Initially, at t/Twave=0, a flat bed with small bed forms is visible. As discharge increases dunes grow both in height and length. At t/Twave≈0.5, the bed pattern consists of regular large dunes. Few, small secondary dunes are visible in the bed profiles on top of the primary dunes. In due time, these regular bed forms become longer and lower. After t/Twave=1.24, the regular dunes becomes more irregular and individual dunes are difficult to distinguish. At t/Twave=2, the bed profile is similar to the initial bed profile.
Figures 2 and 3 show that initially, dune length is relatively small and as discharge increases, both the dune height and length grow. However, dune height grows faster than dune length. Just after the peak of the discharge wave, dune height is at its

maximum, while dune length is still growing. At a certain point during the receding limb of the discharge wave, secondary dunes start to develop on top of the primary dunes. At this point, the primary dunes decrease in height, while the secondary dunes grow in height. At the same time, both the primary and secondary dunes grow in length. However, because the secondary dunes grow, they erode the underlying primary dune, leading to reduction of the average dune length as shown in the right panel of figure 2. Figure 3 also shows that at T/t=0.06 many short dunes exist. The small ones grow in length (t/T=0.5) and at t/T>=1.25 both long and short dunes co-exist. This implies that the secondary dunes become dominant and 'took over' the primary dunes. This process is reflected in the observed dune length and essential for describing dune evolution during a discharge wave.

3. TIME-LAG APPROACH

As a first attempt to predict dune evolution under a discharge wave, we used the time-lag method following Coleman et al. (2005). Coleman et al. (2005) adopted the commons scaling relationship for sand-wave development from an initially flat bed from Nikora & Hicks (1997):

$$\frac{P}{P_e} = \left(\frac{t}{t_e}\right)^{\gamma} \quad (\text{for } 0.01 < \frac{t}{t_e} < 1) \qquad (3)$$

where P is the average value of dune length or height, P_e is the equilibrium value (using Yalin, 1964; eq. (2)), t is time, t_e is the time to achive P_e, and γ is a growth rate parameter. Coleman et al. (2005) derived a relation for γ, based on many flume experiment with a discharge step. They showed that growth rate was different for dune height and dune length and only depended on sediment size, D:

$$\gamma_H = 0.22 D_*^{0.22} \approx 0.37 \qquad (4)$$

$$\gamma_L = 0.14 D_*^{0.33} \approx 0.32 \qquad (5)$$

with

$$D_* = D_{50} / \left(g(s-1)/\upsilon^2\right)^{1/3} \qquad (6)$$

Using this approach for the data from Wijbenga & Van Nes (1986) yielded γ_H=0.42 and γ_L = 0.37.

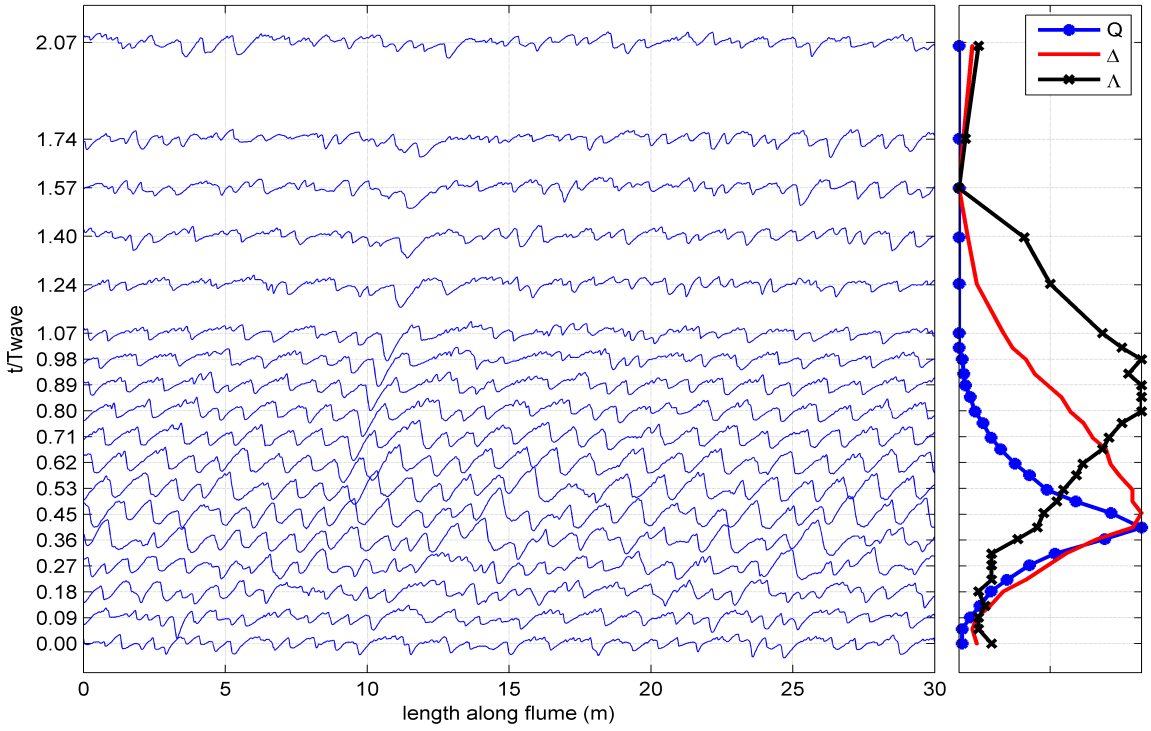

Figure 2. Left: measured bed profiles from test 5 of Wijbenga and Van Nes (1986). Right: corresponding discharge (Q), dune height (Δ) and dune length (Λ) at the same time during the discharge wave (t/Twave). The black solid lines connect individual dune troughs

Coleman et al. (2005) used their data to derive for dunes (7):

$$t_e\left[\frac{u_*}{D_{50}}\right] = 2.05\cdot 10^{-2}\left[\left(\frac{D_{50}}{h}\right)^{-3.5}\right]\left[\left(\frac{\theta}{\theta_{cr}}\right)^{-1.12}\right]$$

Coleman et al. (2005) assumed that the times to equilibrium are equal for dune height and dune length, based on flume experiments with a sudden step in discharge that show that after a certain period of time (after a perturbation in the flow) dunes reach their equilibrium. However, observed dune heights during a flood wave from Wijbenga and Van Nes (1986) show that the maximum dune height is reached long before the maximum dune length is reached (Warmink et al. 2012b; Figure 2). Calibration showed that for dune height, the t_e values need to adapted with a factor 0.01 to yield realistic dune heights for the Wijbenga and Van Nes (1986) data. Figure 1 shows the predicted dune height (a) and length (b) using this time-lag approach. The times to equilibrium from equation (7) ranged between 250,000 to 27,000,000 seconds, which is 3 to 320 days. These values seem unrealistic, but resulted in a reasonably good fit to the observed dune dimensions.

Calibration of t_e for dune height was required, which is not feasible and limits the practical applicability for flood forecasting. Furthermore, the process of overtaking of the primary dunes by the secondary dunes is not taken into account.

4. NUMERICAL MODELING

We used the model developed by Paarlberg et al. (2009, 2010) to reproduce the observed dune evolution of Wijbenga & Van Nes (1986). The Paarlberg et al. (2009) model consists of a flow module, a sediment transport module and a bed evolution module. Flow and bed morphology are solved in a decoupled manner. The flow is described by the two-dimensional shallow water equations in a vertical plane (2-DV), assuming hydrostatic pressure conditions. The model applies a parameterization of the flow separation zone. In the region of flow separation, the separation streamline forms an artificial bed (Paarlberg et al. 2009), which enables the computation of the hydrostatic flow over the dunes. Paarlberg et al. (2009) used the model with a domain length equal to the wave length of the fastest growing mode as determined by a stability analysis (see Paarlberg et al. 2009). This wave length and thereby the domain length changes during the model run, as the flow depth adjusts to the evolving dune. Effectively, the Paarlberg et al. (2009) model computes the lag-time and associated attenuation of the dune height, based on an imposed discharge and equilibrium dune length. We used the dune length predicted by Yalin (eq. 2) as input for the

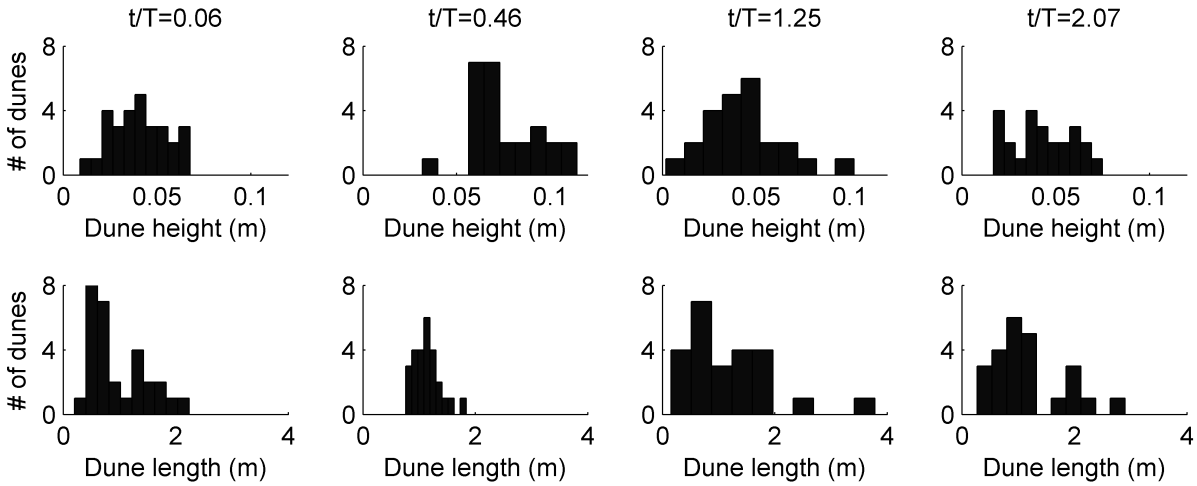

Figure 3. Histograms of dune height and length of profiles in Figure 2, for four times during the discharge wave. The total number of dunes in the flume was 29, 26, 24, 24, respectively. At the peak of the discharge wave (t/T=0.46), dune height is at its maximum, while dune length keeps growing after the peak. The variation in dune length, indicating the amount of secondary bed forms is smallest during the peak.

model instead of the stability analysis, which yielded similar results, but reduces computational time.

For the computation of the discharge wave, the Paarlberg et al. (2009) model was coupled with a 1D hydrodynamic model, Sobek, based on a schematization of the flume. This coupled model is referred to as SobekDune (Paarlberg et al. 2012). Dune dimensions were calculated with the dune evolution model of Paarlberg et al. (2009), using the reach-averaged channel slope, the average water depth in the main channel (as computed by Sobek) and the bed material as inputs (Paarlberg and Schielen, 2012). The model was calibrated by adapting the partial slip model to match the observed discharge. The calibration parameters β1 and β2 were adapted using flow A as reported by Venditti et al. (2005) following Paarlberg et al. (2009).

The dune roughness coefficient of the main channel is specified as a Nikuradse roughness height. This roughness height is translated into a Chézy coefficient for use in Sobek using White-Colebrook. Following Van Rijn (1984), the roughness height of the bed can be found from a summation of a contribution due to grains (k_grains) and due to dunes (k_dunes). Following Paarlberg and Schielen (2012), we adopted the roughness predictor of Van Rijn (1984) for the relation between computed dune dimensions and bed roughness:

$$k_{dunes} = 1.1\Delta\left(1-\exp\left(\frac{-25\Delta}{\Lambda}\right)\right) \qquad (8)$$

where Δ is dune height (m) and Λ is dune length (m). The dune length for computing the roughness was derived using Coleman et al. (2005).

Figure 4 shows the results of the SobekDune model compared to the dune dimensions that were observed and predicted by the Yalin (eq. 1-2) and Coleman (eq 3-7) models. The left frame of Figure 4, shows that the model is capable of reproducing the time-lag in the dune height. Also, the dune height is attenuated compared to the equilibrium dune height predicted by the Yalin model, However, SobekDune overestimates the dune height. This might be caused by erroneous values of the partial slip model coefficients, which were not recalibrated for the Wijbenga and Van Nes (1986) data. In further research, the model will be recalibrated. Adaptation of these parameters will result in a decrease of the flow velocity and therefore a decrease in the sediment transport and dune height.

The dune height predicted using the Coleman et al. (2005) model shows a better fit to the observed dune height. However, it should be noted that this model it is not physically based and therefore has less predictive capacity.

5. ROUGHNESS IMPLICATIONS

The right frame of Figure 4 shows the roughness evolution during the discharge wave in the flume, based on the dune dimensions of the three models of Yalin, Coleman and SobekDune. The observed roughness is based on measured water level slope during the flume experiment. The roughness due to the three models is computed using eq. (8) with the predicted dune dimensions as input.

The roughness based on the dune dimensions from the equilibrium model of Yalin does not show a time-lag. Furthermore, the roughness is slightly underpredicted due to an overprediction of the dune length. The roughness based on the dune

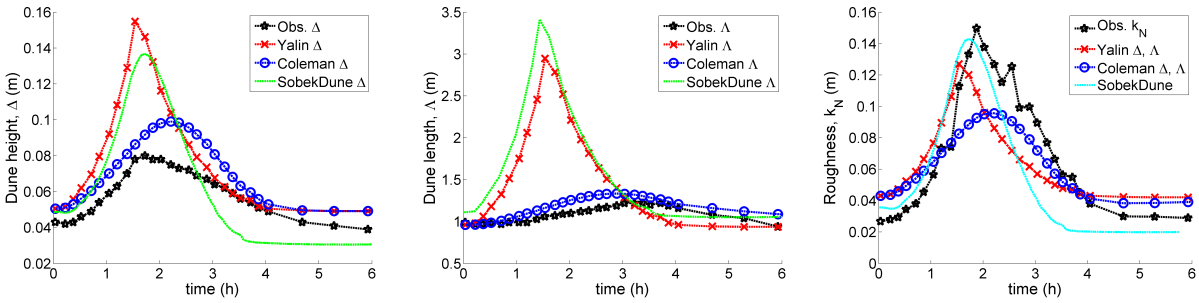

Figure 4. Observed and predicted dune height (left), dune length (middle) and Nikuradse roughness (right) for the three models of Yalin (1964), Coleman et al. (2005) and SobekDune.

dimensions from the Coleman model are slightly lower than the observed roughness values, although the dune dimensions are well represented. This might indicate that the Van Rijn (1984) model underpredicts the roughness for this case.
The roughness based on dune dimensions from SobekDune are similar to the observed roughness values. However, it should be noted that these are only preliminary results and the dune height is overestimated by the SobekDune model.

6. DISCUSSION

The benefit of the SobekDune model is that it is physically-based and can be applied to other conditions as well, while the Coleman model required calibration for the dune height. However, a thorough analysis of validity of the calibration coefficients for the SobekDune model is still required.
Based on these preliminary results, the SobekDune model seems promising for computation of the evolution of bed forms under varying discharge. It represents both the time-lag and attenuation in the dune height, which are essential for prediction of the hydraulic roughness and resulting water levels. The computational time is small compared to existing physically based models for bed form evolution (e.g. Giri and Shimizu, 2006, Nabi, 2010), which makes it feasible for use in operational flood forecasting.
The flattening of the primary dunes and overtaking by the secondary dunes as observed in the data from Wijbenga and Van Nes (1986) is not represented in the three models. In further research, we will include the flattening of the primary dunes and generation of secondary dunes during the receding limb of the discharge wave in the SobekDune model to better simulate the physical processes in bed form evolution in rivers. This potentially increases the predictive capacity of the model and might increase the accuracy of roughness and water level predictions for operational water level predictions.

7. CONCLUSIONS

The objective of this research was to predict and model bed form evolution during a discharge wave. We compared three models: an equilibrium model, a time-lag model and a numerical model for a discharge wave in a flume experiment. We conclude that:

1) The adaptation time for dune length is much larger than for dune height for lower-regime conditions during a discharge wave.
2) Primary dunes are eroded by superimposed secondary dunes that develop during the receding limb of the discharge wave.
3) The time-lag approach of Coleman et al. (2005) yielded realistic result for dune dimension prediction during a discharge wave, however, calibration of the time-to-equilibrium was required for dune height.
4) The SobekDune model seems promising for modeling bed form evolution during a discharge wave, although the modeling results are preliminary.

In further research, we will include the physical processes observed in the flume experiment to increase the accuracy of roughness and water level predictions for operational flood forecasting.

8. ACKNOWLEDGMENT

This study is carried out as part of the project ‘BedFormFlood’, supported by the Technology Foundation STW, the applied science division of NWO and the technology programme of the Ministry of Economic Affairs. The authors are grateful to Andries Paarlberg from HKV Consultants for his assistance.

9. REFERENCES

Carling, P.A., Gölz, E., Orr, H.G. & Radecki-Pawlik, A. 2000. The morphodynamics of fluvial sand dunes in the River Rhine near Mainz, Germany. I. Sedimentology and morphology. Sedimentology 47, 227-252.

Coleman, S.E., Zhang, M.H., Clunie, T.M. 2005. Sediment-wave development in subcritical water flow Journal of Hydraul. Eng. 131, 106-111. Doi: 10.1061/(ASCE)0733-9429(2005)131:2(106)

Giri, S. & Shimizu, Y. 2006. Numerical computation of sand dune migration with free surface flow Water Resources Research 42, W10422

Guy, H.P.; Simons, D.B., Richardson, E.V. 1966. Summary of alluvial channel data from flume experiments. Geological survey professional paper, Sediment transport in alluvial channels 462-I, 95

Nabi, M. 2010. Computational modelling of three-dimensional bedform evolution In: Dittrich et al. (Eds.) Proceedings of River Flow 2010, Braunschweig, Germany, pp. 905-911

Nikora, V.I., and Hicks, D.M. 1997. Scaling relationships for sand wave development in unidirectional flow. J. Hydraul. Eng., 123(12), 1152–1156.

Paarlberg, A.J., Dohmen-Janssen, C.M., Hulscher, S.J.M.H., Termes, P. 2009. Modeling river dune evolution using a parameterization of flow separation. Journal of Geophysical Research 114, F01014

Paarlberg, A.J., Dohmen-Janssen, C.M., Hulscher, S.J.M.H., Termes, P., Schielen, R.M.J. 2010. Modelling the effect of time-dependent river dune evolution on bed roughness and stage. Earth Surface Processes and Landforms 35, 1854-1866

Paarlberg A.J., Schielen, R.M.J. 2012. Integration of a dune roughness model with a large-scale flow model. In: Murillo (Ed.) Proc. of River Flow 2012, Costa Rica, pp. 155-161

Van Rijn, L.C. 1984. Sediment transport, part III: bed forms and alluvial roughness. Journal of Hydraulic Engineering 110, 1733-1754

Venditti, J.G., Church, M.A., Bennett, S.J. 2005. Bedform initiation from a flat sand bed. Journal of Geophysical Research, 110 (F01009), doi: 10.1029/2004JF000149.

Warmink, J.J., Straatsma, M.W., Huthoff, F., Booij, M.J., Hulscher, S.J.M.H. 2012a. Uncertainty of design water levels due to combined bed form and vegetation roughness in the Dutch river Waal. Journal of Flood Risk Management, doi: 10.1111/jfr3.12014.

Warmink, J.J., Schielen, R.M.J., Dohmen-Janssen, C.M. 2012b. Bed form evolution under varying discharges, flume versus field. In: Murillo (Ed.) Proc. of River Flow 2012, Costa Rica, pp. 183-190.

Wijbenga, A. and Van Nes, X. 1986. Flow resistance and bedform dimensions for varying flow conditions; results of flume experiments with flood waves. WL|Delft Hydraulics research report. R657, M1314 Part XIII.

Yalin, M.S. 1964. Geometrical properties of sand waves. Journal of the Hydraulics Division, 1964, HY5, 105-119

Object Burial by Bedforms: Results from instrumented modules, new data analysis concepts

Th. Wever[(1)], and C. Jenkins[(2)]

1. WTD 71 / FWG, Kiel, D - thomaswever@bundeswehr.org
2. INSTAAR, Boulder, CO, USA - chris.jenkins@colorado.edu

Abstract

Results from deployments of burial-recording instrumented modules in the Jade area of the German Bight (North Sea) are reported. The time series show significantly changing patterns of burial activity under megaripples from quiescent periods to stages of repeated burial/unburial. The bedforms reached heights of 0.5 m and migrated past the modules on twice daily time scales. As an adjunct, a scanning sonar installation showed stages of quiescence and also stages of rapid (hourly) migration, splitting and merging activity for megaripple-scale bedforms.

The experiments are designed to help predict frequencies of seabed man-made object burial and unburial. They raise issues on the connection between data and models in this practical application. We review the nature of datasets dealing with the migration behavior of larger (megaripple, sandwave) bedforms and propose that some new approaches are needed. They include: (i) adoption of meta-analysis formalisms, (ii) invention of metrics for a bedform's stage of development; (iii) more use of larger experiment scales, manipulative experiments and instrumented modules; (iv) the gathering of a corpus of data on bedform migration. With these tools improved prediction of object burial by bedforms is feasible.

1. INTRODUCTION

The prediction of the presence and the properties of megaripples and higher sand dunes is of importance for many shipping routes, some of which require regular removal of the bedform tops. Similarly, for safety of navigation, objects at the seafloor under shipping routes need to be detected and perhaps removed despite patterns of burial and unburial. A high prediction accuracy for presence and evolution of active bedforms is a relevant cost factor in such situations.

2. BEDFORM ENVIRONMENTS

We focus on current-generated bedforms which are generated either by oscillating tidal currents, unidirectional flows, or a combination of those. These contrasting current regimes cause typical expressions of bedform features: under tidal influence a more regular back and forth movement ("swinging") of bedform crests is observed (Langhorne 1982), perhaps with some migration (Besio & others 2003). Under constant current influence a unidirectional migration is typical. Subject to the combined action of tidal and unidirectional currents, bedforms show a characteristic unidirectional downstream progress and "swinging crests" (Wever & others 2008).

Tidally active bedforms composed of sand and capable of burying significantly sized objects are important seaward of many river mouths where unidirectional current impacts fade and marine influences such as tides become important.

One example of this situation is in the Jade area of the southern German Bight (North Sea) where our experiments were performed. Water depths there are 10-15 m. The area is protected against swell influence by the coast and a barrier system. The tidal flood and ebb currents have almost exactly opposite directions and peak tidal flows are up to 3 knots (1.5 m/s) at the surface. Occasionally tidal currents of 1 m/s have been observed 1 m above bottom at the site. There is no significant riverine outflow at the site. The megaripples of the area vary greatly in individual lengths and heights, even locally. Sediment character is medium-coarse sand with scattered shell remains.

3. VARIABILITY OF BEDFORM MOBILITY

A central difficulty in bedform research has been the position accuracy of repeated measurements. This inaccuracy can be overcome by using permanent burial recording modules on the seafloor. These modules mimic objects on the seafloor and have the approximate shape, size and weight distribution of the casings of naval mines. In the field experiments of Wever & Stender (2000) much was learnt from these modules about megaripple migration.

3.1 Burial recording module records

A many weeks long time series of bedform migration verified the high temporal variability of megaripple movement. Figure 1 displays a typical example that shows the irregularity of bedform migration.

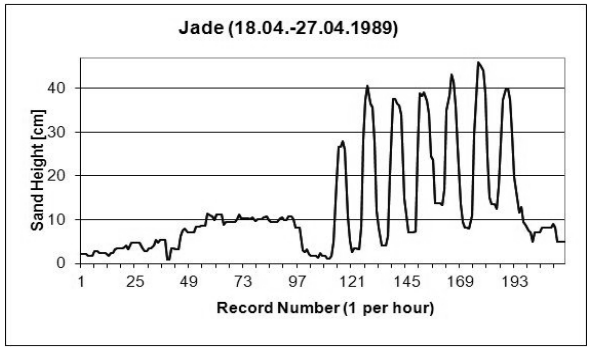

Figure 1. Recorded sand height around a burial recording module during nine days at the Jade site. Recording interval: 1 hour. Only moderate sand height changes around the burial recording module are observed for 4.5 days followed by 4 days of extreme sand height changes which are thought to be the passage of a megaripple.

After a period of little change a set of strong (0.4 m; Figure 1: rec. no. 110-200) changes takes place. That set is interpreted as back and forth movement of a megaripple in response to the tidal current. The period of prominent changes is followed by another "quiet" phase. Weather conditions cannot explain this difference.

In a second phase of experiments arrays of burial recording modules were laid out to study the small-scale changes of bedform migration. Figure 2 displays the result of a typical experiment with an array of six systems with separations of 48-53 m.

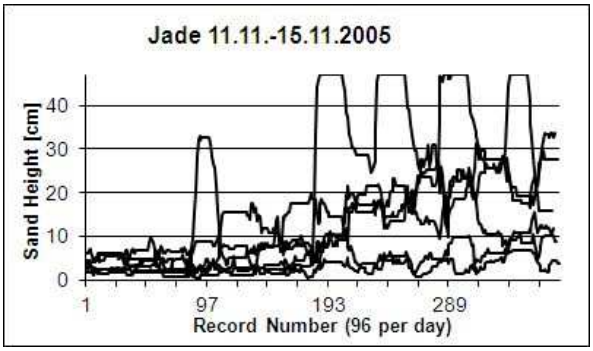

Figure 2. Six curves of recorded sand height around six burial recording modules (48-53 m distance) during a 4 day period at the Jade site. Recording interval: 15 min. The individual maximum sand heights observed by the six burial recording modules were 7, 11, 25, 25, 31, and 47 cm.

Such experiments with many systems were helpful to estimate small-scale variations among migrating bedforms. The repeated deployments of systems at close distance regularly showed similar time-series of burial due to bedforms at the recording modules. However, the observations pointed to new open questions which could not be answered solely by the point data at the recording modules.

3.2 Differential bedform movement

Accordingly, in a third series of experiments at the Jade site an area-covering rotating scanning-sonar was deployed. The 380 kHz frequency sonar was mounted at 4.8 m height on a tower which was positioned on the seafloor. Having a range of 50 m, the system covers a circular area of 7.850 m^2 (Wever & others 2008). Complete areal scans were obtained by the system each 3 minutes over a period of 25 hours, and at 10 minutes over periods of 7 and 9 days respectively. The recorded data showed for example: splittings of megaripples into segments; a sudden stopping of movement for such segments or whole bedforms; mergings with following bedforms. The 3 minute scans showed that these processes happen quickly - on scales of <60 minutes.

Another important aspect revealed by the rotating sonar is the three-dimensionality of bedform shapes and water flow. One short-interval, long-term scanning of an area with bedforms revealed

small sand ripples at the lee side foot of a steep sand dune. They indicated the action of crest-parallel currents. The water appeared to be moving in these cases at least partly on corkscrew-like paths first across and then parallel to sand dunes. Hence, even under purely reversed current situations without a tidal ellipse in the Jade area the bedforms had 3D characteristics as large-scale side scan sonar mappings ahead of sonar tower or burial recording module deployments showed.

4. SUBTIDAL DUNE MIGRATION

These experimental programs have raised important questions for those who are interested in the practical importance of subtidal dune migration. There is a need to understand the probabilities for burial (disappearance) of objects of ~1m size under megaripples and sandwaves, in different environments. Unburial is also of interest. Modeling of large-bedform migration offers one avenue for progress. Besio & others (2003) analysed the relation of sandwave migration to tidal constituents and bottom configurations and proposed morphodynamic scalings for sandwave migration. Now, most likely, further progress on the issue will be through closer data-model combination, especially if the model results (above) are to be applied to a wide set of areas and to the megaripples superimposed on the sandwaves.

4.1 Limiting Environmental conditions

A traditional approach to data on bedforms is the narrative form of analysis in which limiting conditions for presence of active bedforms are set out. This at least gives a highly useful 'epidemiological' view of the problem by defining the areas where burial of objects can be discounted.

For example, in sedimentology: (a) Fenster & others (1990) find no bedforms when the sediment's gravel content exceeds 12%, though (b) gravel bedforms are observed in the English Channel. Bokuniewicz & others (1977) (c) do not observe sand waves when >12% of the grains exceed 1 mm though (d) Harris (1989) reports sand waves composed of sediments with a d_{50} of 0.8 mm.

For the fine constituents of the sediments there is some agreement: (e) Fenster & others (1990), report no sand wave development where silt exceeds 10%; (f) Terwindt (1971), finds no sand waves where mud content exceeds 15%; (g) Salsmann & others (1966), report megaripples with 6% of particles <0.062 mm; (h) Bokuniewicz & others (1977), absent sand waves where silt >10%, (i) Dalrymple & Rhodes (1995) put the limits for dune development at 0.13 mm, and for megaripple development at 10-15% silt/mud content.

A further set of limitations can be imposed based on near-bottom current speeds. Salsman & others (1966) (a) observed megaripple height reduction with increasing current speed; (b) Terwindt & Brouwer (1986) reported that sand wave height increases around the times of spring tide, and decreases around neap tide. Langhorne & Malcolm (1979) (c) found highest bedforms during lowest current velocities and a flattening during higher currents of spring tide. Support comes (d) from observations of Nasner (1975) in Elbe river where he found an inverse correlation of ebb current speed and sand dune height. Idier & others (2002) (e) reported height increases during quiet weather conditions. The rotating sonar records (f) show a flattening of megaripples when current speed at 1 m above seafloor exceeds 0.6 m/s (Wever & others 2008), height determinations are not possible.

Controversially, Soulsby (1997) (g) sees bed shear stress as well as water depth determining the dimensions ("*rough guide … wavelength is 6 times water depth*"). Bartholdy & others (2004) (h) argue against this and refer to reports where flow depth did not control dune dimensions (see, for example Flemming 1978) (i).

Extraneous factors such as irregularly occurring major storms also affect bedform heights: (j) Langhorne (1976) and Houthuys & others (1994) observed the storm-induced disappearance of megaripples, Houthuys & others (1997) (k) reported a flattening of sand dunes by 1.2 m during storms.

Conflicting reports in the literature of both crestwards sediment fining on large bedforms (Harvey 1966; Anthony & Leth 2002) and a coarsening (Terwindt 1970; Stolk 1996; Wells & Ludwick 1974; Fenster & others 1990; Chakhotin 1977) may be due to the action of waves (Perillo & Ludwick 1984). The same may apply for conflicting observations on the heights of megaripples on large sand dunes. Some authors

(Terwindt 1971; Stender 1996) report higher megaripples near the crests of sand dunes. Others (Langhorne, 1977) report the opposite.

4.2 Synthesizing the data

It goes without saying that a better understanding of the entire matrix of environmental controls on bedforms is needed. First, narrative forms of synthesis should be replaced with more formalized methods. We envision a systematic meta-analysis of that corpus as is done in medical sciences and ecology (Stewart 2010). This would enlarge the available pool of data and overcome the heterogeneities between individual, small and local studies. Plus, importantly for practical burial problems, a large-as-possible corpus of data on bedform mobilities and dimensions versus key environmental controls is needed.

In terms of modeling, successful models should be able to explain the collated data on environmental controls, not just implement them *ab initio* in code.

4.3 Dune development

Allowance will have to be made in data syntheses on whether the subject dunes are fully developed, of composite structure, and in equilibrium with surrounding environment. Much existing data is likely to refer to non-ideal states of dune development. It would help to have metrics for stages of bedform completeness of development so that their attending data can be assessed. To an extent this is a matter of the scales of dune dimensions and longevities versus stability of their environment.

The sensitivity of subtidal dune development to sediment supply is well known (Dalrymple & Rhodes 1995). Laboratory work such as by Tuijnder & others (2009) quantitatively addresses ripple scale phenomena, but the excursion paths for the building and migration of megaripples and sandwaves appear to scale over distances and durations well beyond flume scales. To examine the issues of sediment supply controls at appropriate scales, large-scale long-term experiments are needed – including manipulative experiments like trenching into dunes or changing sediment loads (see Nasner 1983; Wienberg & Hebbeln 2005). There may be a role for the instrumented burial recording modules in such experiments.

The simplicity of bedforms is also an issue for rating the reliability of existing data in formal data synthesis. Many large subtidal bedforms have sub-structure that involves layering from alterations in the prevailing flow patterns (e.g., Berne & others 1993), storm induced layering, and varied patterns for their smaller surficial (superimposed) bedforms and sediment textures.

5. CONCLUSIONS

For practical applications such as safe navigation and object burial a knowledge of bedform occurrence and movement is of highest relevance. The immense costs of dredging puts pressure on responsible agencies and bureaux to reduce such operations to a safe minimum. To attain that goal reliable prediction models are desirable which can cope with varying environmental conditions.

Those models could be of the numerical-process type, morphodynamic, expert system, or geographic information system (GIS). In all these cases a good connection between models and data must be a high priority and we advocate a new approach with that in several ways: (i) more systematic meta-analysis of existing data, especially in terms of bedform dynamics; (ii) construction of a corpus of reliable data; (iii) rating that data in terms of bedform development stage; (iv) renewed effort with larger-scale, perhaps manipulative, experiments that use instrumented modules.

From our perspective existing combinations of data and model do not yet provide sufficient predictive capability for practical problems of object burial under bedforms.

6. REFERENCES

Anthony, D., & Leth, J. 2002. Large-scale bedforms, sediment distribution and sand mobility in the eastern North Sea off the Danish west coast. Marine Geology 182: 247-263.

Bartholdy, J., Flemming, B., Bartholomä, A, Ernstsen V. 2004. On the dimensions of depth-independent, simple subaqueous dunes. In S. Hulscher, T. Garlan, & D. Idier (eds), Marine Sandwaves and River Dynamics II: 9-16, International Workshop, Enschede, 1.-2. April 2004.

Berné S, Castaing P, LeDrezen E, Lericolais G. 1993. Morphology, internal structure and reversal of asymmetry of large subtidal dunes in the entrance to Gironde estuary (France). Jl Sedimentary Petrology 63: 780–793.

Besio, G., Blondeaux, P., Brocchini, M. & Vittori, G. 2003. Migrating sand waves. Ocean Dynamics 53: 232–238.

Bokuniewicz, H., Gordon, R. & Kastens, K. 1977. Form and migration of sand waves in a large estuary, Long Island Sound. Marine Geology 24: 185-199.

Chakhotin, P. 1977. Some results of a study of the tidal sand waves in the White Sea. Oceanology 17: 182-188.

Dalrymple, R., & Rhodes, R. 1995. Estuarine Dunes and Bars. In: G.M.E. Perillo (ed.), Geomorphology and Sedimentology of Estuaries: 359-422, Amsterdam: Elsevier.

Fenster, M., Fitzgerald, D., Bohlen, W., Lewis, R., Baldwin, C. 1990. Stability of giant sand waves in the eastern Long Island Sound, USA. Marine Geology 91: 207-225.

Flemming, B. 1978. Underwater sand dunes along the southeast African continental margin – observations and implications. Marine Geology 26: 177-198.

Harris, P. 1989. Sand wave movement under tidal and wind-driven currents in a shallow marine environment: Adolphus Channel, Northeastern Australia. Continental Shelf Research 9: 981-1002.

Harvey, J. 1966. Large sand waves in the Irish Sea. Marine Geology 4: 49-55.

Houthuys, R., Traintesaux, A., De Wolf, P. 1994. Storm influence on a tidal sandbank's surface (Middelkerke Bank, southern North Sea). Marine Geology 121: 23-41.

Idier, D., Ehrhold, A., & Garlan, T. 2002. Morphodynamique d'une dune sous-marine du d'etroit du pas de Calais. C.R. Geoscience 223: 1079-1085.

Langhorne, N. 1976. Consideration of meteorological conditions when determining the navigational water depth over a sand wave field, 15th Annual Canadian Hydrographic Conference, Ottawa.

Langhorne N. 1977. Consideration of meteorological conditions when determining the navigational water depth over a sand wave field, International Hydrographic Review 54: 19-30.

Langhorne, D. 1982. The stability of the top metre of the sea bed. Its importance to engineering and navigational projects. International Hydrographic Review 59: 79-94.

Langhorne, D. & Malcolm, J. 1979. A study of mine burial in monitored hydrodynamic and sedimentological conditions, Start Bay, Devon. Institute of Oceanographic Sciences Internal Document 55.

Nasner, H. (1975). Zur Frage der Baggerung von Riffeln in Tideflüssen, Nassbaggerberichte: 4/75.

Nasner, H. (1983). Dredging of tidal dunes, Int. Harbour Conference, Antwerp, Belgium.

Perillo, G. & Ludwick, J. 1984. Geomorphology of a sand wave in Lower Chesapeake Bay, Virginia, U.S.A.. Geo-Marine Letters 4: 105-112.

Salsman, G., Tolbert, W. & Villars, R. 1966. Sand-ridge migration in St. Andrew Bay, Florida. Marine Geology 4: 11-19.

Soulsby, R. 1997. Dynamics of Marine Sands. London: Thomas Telford.

Stender, I. 1996. Burial of ground mines by migrating bedforms, FWG Forschungsbericht FB 1996-1.

Stewart, G. 2010. Meta-analysis in applied ecology. Biological Letters 6: 78-81.

Stolk, A. 1996. Analysis and control of internal structures by coring; Middelkerke Bank area: sedimentological investigations. In Heyse, I. & G. de Moor (eds.), Sediment Transport and Bedform Mobility in a sandy Shelf Environment, Final Report of the STARFISH Project to the Commission of the European Community, Directorate General VII, Brussels, 16.1-16.33.

Terwindt, J. 1970. Observation on submerged sand ripples with heights ranging from 30 cm to 200 cm occurring in tidal channels of S.W. Netherlands, Geologie en Mijnbouw 49: 489-501.

Terwindt, J. 1971. Sand waves in the southern bight of the North Sea. Marine Geology 10: 51-67.

Terwindt, J., Brouwer, M. 1986. The behaviour of intertidal sandwaves during neap-spring tide cycles and the relevance for paleoflow reconstructions, Sedimentology 33: 1-31.

Tuijnder, A., Ribberink, J. & Hulscher, S. 2009. An experimental study into the geometry of supply-limited dunes. Sedimentology 56: 1713-1727.

Wells, J. & Ludwick, J. 1974. Application of multiple comparisons to grain size on sand waves, Journal Sedimentary Petrology 44: 1029-1036.

Wever, Th. 2004. Bedforms and bedform migration – a data review. In S. Hulscher, T. Garlan, & D. Idier (eds), Marine Sandwaves and River Dynamics II: 330-337, International Workshop, Enschede, 1.-2. April 2004.

Wever, Th. & Stender, I. 2000. Strategies for and results from the investigation of migrating bedforms in the German Bight. In A. Trentesaux, & T.E. Garlan (eds.), Marine Sandwave Dynamics: 221-226, Lille, 23.-24. March 2000.

Wever, Th., Voß, H. & Lühder, R. 2008. High-resolution observation of small-scale variability in a bedform field. In D. Parsons, T. Garlan, & J. Best (eds.), Marine Sandwaves and River Dynamics III: 331-335, Leeds, 1.-3.April 2008.

Wienberg, C. & Hebbeln, D. 2005. Impact of dumped sediments on subaqueous dunes, outer Weser Estuary, German Bight, southeastern North Sea. Geo-Marine Letters 25: 43–53.

Geometric properties of hydraulically-relevant tidal bedforms

C. Winter[(1)], Y. Ferret[(1)], A. Lefebvre[(1)] and V. B. Ernstsen[(2)]

1. MARUM - Center for Marine Environmental Sciences, University of Bremen, Leobener Str, D 28359 - Bremen, Germany, E-mail: cwinter@marum.de
2. Department of Geography & Geology, University of Copenhagen, Øster Voldgade 10, DK-1350 Copenhagen, Denmark

ABSTRACT

Large compound tidal bedforms (also termed dunes, sandwaves, megaripples by different authors) constitute prominent roughness elements in tidal channels and estuaries. Quantitative knowledge on their geometry, dynamics and hydraulic effect is crucial for coastal system understanding and process based numerical modelling. The ubiquitous large bed elements (lengths 10-1000m, heights 1-10m, celerity 10-100m/year) are often asymmetric (with steep slopes facing in the dominant tidal direction) and display super-imposed highly mobile secondary smaller bedforms. As a deterministic prediction of bedform genesis and dynamics is not yet available, various empirical descriptors have been formulated based on extensive data compilations (e.g. Allen, 1968; Flemming, 1988; Francken, 2004). Mean bedform heights H and lengths L were found to scale, e.g H = a * L b in which a=0.03-0.07 and b=0.7-0.9. Due to technical constraints and data reduction the (historic) data bases mostly are restricted to information on mean geometrical states, whereas individual bedform properties are often not reported. Recently Lefebvre et al. (2011) showed that the hydraulic effect of asymmetric compound tidal bedforms depends on the tidal stage: Whereas the secondary bedforms act as roughness elements throughout the tidal cycle, the large primary bedforms dominate the hydraulics when the tidal flow is in the (dominant) direction of the bedform orientation (e.g. ebb-directed primary bedforms act during ebb currents) when the bedforms are expected to induce flow recirculation behind the steep lee side.

Based on the analysis of a large high-resolution bathymetric dataset (multi beam echo sounder mapping of the tidal channel Jade, and Weser and Elbe estuaries, German North Sea coast in 2008), approximately 40,000 individual datasets on bedform geometry (heights, lengths, slopes, etc.) have been identified and analysed. These bedforms range in heights from 0.05 to 8.9m and lengths from 4 to 490m; less than 40% of which scale with the known relations. Bedforms here are defined as "hydraulically-relevant" if they feature a lee slope of 10° or more; which is considered as a threshold condition for the development of flow separation and recirculation eddies in the bedform lee. Only 4.2% of all identified bedforms meet this criterion (n=1,250). These scale with $H=0.1923L^{0.6311}$ ($R^2=0.92$) when taking into account weighted bedform heights (generalized extreme value method).

It is stressed out that the majority of the latter subset scales well above the mentioned mean relationships: 91% of these are steeper than predicted by Allen, 89% steeper than predicted by Flemming, 96% are steeper than predicted by Francken.

It is concluded that common relationships describe independent datasets to some extent (approximately 40% of all bedforms in our case). If the hydraulic effect of bedforms needs to be considered in the analysis or the development, set-up and application of numerical models, the mentioned formulations underestimate the height of bedforms. For these cases a new relationship is proposed. The common formulations form a lower limit of bedform steepness (H/L), as more than 89% of the identified hydraulically relevant subset exceeded their dimensions.

REFERENCES

Allen, J.R.L., 1968. The nature and origin of bed-form hierarchies. Sedimentology, 10(3), 161-182.

Flemming, B.W., 1988. Zur Klassifikation subaquatischer, strömungstransversaler Transportkörper.

Bochumer geologische und geotechnische Arbeiten, 29, 44-47.

Francken, F., Wartel, S., Parker, R., Taverniers, E., 2004. Factors influencing subaqueous dunes in the Scheldt Estuary. Geo-Marine Letters, 24(1), 14-21.

Lefebvre A, Ernstsen VB, Winter C, 2011. Influence of compound bedforms on hydraulic roughness in a tidal environment. Ocean Dynamics.

MARINE AND RIVER DUNE DYNAMICS - MARIDIV

Provincial Court, Bruges, 15-17 April 2013

DRAFT PROGRAMME (8/3/2013)

PROGRAMME DAY 1 – 15 April

08:30 – 10:00 **Registration & Poster set-up**

10:00 – 10:10 **Welcome by the organizers**
Vera Van Lancker
Royal Belgian Institute of Natural Sciences, Belgium
Guest professor at Ghent University, Belgium

10:10 – 10:40 **OPENING KEYNOTE: Gaps in understanding of sedimentary bedforms in the ancient, the present, the extraterrestrial and the kitchen**
Maarten Kleinhans
Professor at Utrecht University, The Netherlands

10:40 – 10:50 **1-minute poster presentations**

1 *Ephemeral bed forms caused by fluid mud dynamics*
M. Baeye et al.
2 *Bedform morphology across the fluvio-tidal transition, Columbia River, USA*
J. Best et al.
3 *A GIS-based hydrographic resurvey strategy of the Belgian Continental Shelf*
N. Bos et al.
4 *Developments in the North Sea wide resurveying and charting of dynamic sand wave areas*
L. Dorst, T. Dehling & C. Howlett
5 *Sand waves morphology and small-scale migration at a macrotidal tropical estuary (São Marcos bay, Brazil)*
F. Chagas et al.
6 *Complex morphology and organisation of dunes in a giant dunes field*
T. Garlan et al.
7 *Decifering mega-ripple variability in an anthropogenically-steered environment: implications for mine burial studies*
S. Papili, M. Baeye & V. Van Lancker
8 *Influence of dunes on alternate bar migration in a sandy gravel river: the Loire (France)*
S. Rodrigues et al.
9 *Impact evaluation of marine aggregate extraction through adaptive monitoring of bottom shear stress in bedform areas*
V. Van Lancker et al.

10:50 – 11:10 **Coffee break**

11:10 – 12:30 **SESSION 1: BEDFORM EVOLUTION AND PROPERTIES**
Chair: Alain Trentesaux
Professor at Lille University, France

11:10 – 11:30 *Short and long term evolution of deep giant submarine dunes in continental shelf environment: the example of the "Banc du Four" (Western Brittany, France)*
P. Franzetti et al.

11:30 – 11:50 *Amplified sediment waves in the Irish Sea (AmSedIS)*
K. Van Landeghem et al.

11:50 – 11:57 *Geometric properties of hydraulically-relevant tidal bedforms*
C. Winter et al.

11:58 – 12:05 *Bedform characterization in river channel through 2D spectral analysis*
A. Lisimenka & S. Rudowski

12:06 – 12:13 *Burial Recording Mines: a valid technique to study bedform migration and storm impact above the sea-floor*
S. Papili, T. Wever & Y. Dupont

12:14 – 12:21 *Morphobathymetric and sediment dynamics analysis on the Gulf of Valencia Continental Slope (NW Mediterranean)*
M. Ribó et al.

12:21 – 12:30 Questions

12:30 – 14:00 Lunch and poster session

14:00 - 14:30 KEYNOTE: Modelling Offshore Sandwaves: Approaches, Biological Interaction and Applications
Suzanne J.M.H. Hulscher
Professor at Twente University, The Netherlands

14:30 – 15:45 SESSION 2: HYDRODYNAMIC AND MORPHODYNAMIC MODELLING
Chair: Daniel Parsons
Professor at Hull University, United Kingdom

14:30 – 14:50 *The dynamics of bedform amalgamation: new insights from a very thin flume*
J. Best et al.

14:50 – 15:10 *The response and hysteresis of alluvial dunes under transient flow conditions*
A. Reesink et al.

15:10 – 15:17 *Modelling sediment pick-up and deposition in a dune model*
O. van Duin et al.

15:18 – 15:25 *Large-eddy simulation of flow over barchan dunes*
M. Omidyeganeh et al.

15:26 – 15:33 *Numerical simulation of dune morphodynamic changes for unsteady flows*
P. Grover & A. Ferreira da Silva

15:33 – 15:43 Questions

15:45 – 16:00 1-minute poster presentations

1 *An experimental investigation of 3D subaqueous interacting barchan dunes and their morphodynamic processes*
G. Blois et al.
2 *Numerical Modelling of flumes with moving dunes – TELEMAC3D and Sisyphe*
A. Goll, R. Kopmann & C. Villaret
3 *Sand transport over a barchan dune*
F. Charru & V. Laval
4 *Estimation of the friction coefficient induced by marine dune using high resolution bathymetric data*
N. Huybrechts et al.
5 *Flow structures and bedform dynamics around tidally-induced bars*
C. Keevil et al.
6 *Selection of bedform morphology in an experimental flume under supply-limited conditions*
N. Le Dantec et al.
7 *Using video imaging techniques for field data collection at coastal areas*
I. Turki et al.
8 *Effects of disposed sediments on local sediment transport and meso-scale morphology*
W. Vandenbruwaene, G. Vos & Y. Plancke
9 *Biogeomorphology in the field: bedforms and species, a mystic relationship*
V. Van Lancker et al.
10 *An equivalent bottom for navigation above irregular bottoms*
M. Vantorre, M. Candries & E. Lataire

16:00 – 16:30 Coffee break

16:30 – 17:45	**SESSION 3: BIOGEOMORPHOLOGY** **Chair: Katrien Van Landeghem** Lecturer at Bangor University, United Kingdom
16:30 – 16:50	*Biogeomorphological self-organization in sandy shelf seas* B.W. Borsje et al.
16:50 – 17:10	*Physical and biological cohesion within mixed sand-mud beds: implications for erosion and bedform development* J.H. Baas & J. Malarkey
17:10 – 17:17	*A first phase in the habitat classification for the Zeeschelde: Bed form classification* G.R. Vos et al.
17:18 – 17:25	*Disposal strategy to create ecological valuable habitats in the Western Scheldt estuary* S. Ides & Y. Plancke
17:25 – 17:32	*Morphology of pillow-hollow and quilted-cover bedforms in Lake Geneva, Switzerland* N. Le Dantec et al.
17:32 – 17:45	**Questions**
18:30	**Reception at the City Hall of Bruges** **Welcome address by Marc Mosar, City of Brugge**

PROGRAMME DAY 2 – 16 April

08:30 – 09:00	**KEYNOTE: Acoustic developments for the measurement of sediment processes over bedforms** **Peter D. Thorne** Professor at National Oceanography Centre, United Kingdom
09:00 – 10:25	**SESSION 4: HYDRODYNAMIC AND MORPHODYNAMIC MODELLING** **Chair: Jim Best** Professor at University of Illinois at Urbana-Champaign, United States
09:00 – 09:20	*Modeling Dune dynamics in situations with bimodal sediment distributions* M.A.F. Knaapen, J.Willis & J.H. Harris
09:20 – 09:40	*Sediment transport distribution along equilibrium sand dunes* S. Naqshband et al.
09:40 – 10:00	*Influence of time- and depth-dependent eddy viscosity on the formation of tidal sandwaves* P.C. Roos & H.M. Schuttelaars
10:00 – 10:07	*Numerical simulation of turbulent sediment transport* O. Durán, B. Andreotti & P. Claudin (Presentation by P. Claudin)
10:08 – 10:15	*Sand ripple volume generator for underwater acoustic models, a cellular automaton Monte-Carlo approach* P. Staelens, Y. Dupont & J.-P. Henriet
10:15 – 10:25	**Questions**
10:25 – 10:55	**Coffee break**

10:55 – 12:10	**SESSION 5: BEDFORM EVOLUTION AND PROPERTIES** **Chair: Sophie Le Bot** Maître de Conférences at Rouen University, France
10:55 – 11 :15	*Object Burial by Bedforms: Results from instrumented modules, new data analysis concepts* T. Wever & C. Jenkins
11:15 – 11:35	*Analysis of coherent flow structures over alluvial dunes revealed by multi-beam echo-sounder acoustic backscatter* S.M. Simmons et al.
11:35 – 11:42	*Evolution of secondary cellular circulation flow above submarine bedforms imaged by remote sensing techniques* I. Hennings & D. Herbers
11:43 – 11:50	*Sorting patterns over tidal sand waves: comparing field observations with theoretical predictions* T. Van Oyen, P. Blondeaux & D. Van den Eynde
11:51 – 11:58	*Deep-water bottom current dynamics: processes, products & challenges* D. Van Rooij
12:00 – 12:10	**Questions**
12:10 – 13:30	**Lunch and poster session**
13:30 - 14:00	**KEYNOTE: Large-eddy simulations in dune-dynamics research** **Ugo Piomelli** Professor at Queen's University, Canada
14:00 – 15:05	**SESSION 6: HYDRODYNAMIC AND MORPHODYNAMIC MODELLING** **Chair: Tomas Van Oyen** Postdoc researcher at Ghent University, Belgium
14:00 – 14:20	*On the influence of bed permeability on flow in the leeside of coarse-grained bedforms* G. Blois et al.
14:20 – 14:27	*Flow structures over fixed 2D bedforms in transient states* C.A. Unsworth et al.
14:28 – 14:35	*Three-dimensional spatial variations of suspended sediment concentration over vortex ripples* A.M. Penko & J Calantoni
14:36 – 14:45	*Variation of flow separation over large bedforms during a tidal cycle* A. Lefebvre et al.
14:46 – 14:55	*Hydrodynamic modeling over a sand wave field at São Marcos Bay, Brazil* L. Samaritano et al. (Presentation by F.M. Chagas)
14:55 – 15:05	**Questions**
15:05 – 15:35	**Coffee break**
15:35 – 17:10	**SESSION 7: PRACTICAL APPLICATIONS AND HUMAN INFLUENCES** **Chair: Yves Plancke** Senior Research Engineer at Flanders Hydraulics Research, Belgium
15:35 – 15:55	*Bed form dynamics in relation to headwater discharge and human influences in the tidal Elbe river, Germany* N. Gehres et al.
15:55 – 16:15	*How the Belgian wind farm business made us discover the challenging environment of marine sand dunes*

	A. Bolle, M. Mathys & P. Haerens
16:15 – 16:35	*Gravel dunes generated during ice-jam floods, Tom River, Western Siberia* A. Vershinin et al. (Presentation by R. Kostaschuk)
16:35 – 16:42	*On the role of fine-sand dune dynamics in controlling water depth changes in Rio Parapeti, Serrania Borebigua (Southern sub-Andean zone of Bolivia)* N. Deville, D. Petrovic & M.A Verbanck
16:43 – 16:50	*Evolution of bed form height and length during a discharge wave* J.J. Warmink, R.M.J. Schielen & C.M. Dohmen-Janssen
16:51 – 16:58	*Essential facts of the monitoring of the sand extraction and its impact on the Flemish banks on the Belgian continental shelf from 2003 to 2012* M. Roche et al.
17:00 – 17:10	**Questions**
17:10 – 17:30	**Future of MARID** **Thierry Garlan** Senior scientist (Dr) at the French Naval Hydrographic and Oceanographic Service
17:30 – 17:45	**AWARDS**
19:00	**Conference dinner at Brewery Halve Maan, Bruges**

PROGRAMME DAY 3 – 17 April

FIELD TRIP

Organizers: Yves Plancke & Tomas Van Oyen
Senior Research Engineer at Flanders Hydraulics Research, Belgium
Postdoc researcher at Ghent University, Belgium

Schedule

8h00	Departure from Bruges towards Breskens, Western Scheldt
09h00 – 13h	Boat trip
13h45 – 17h	Guided Tour Zwin Nature Reserve
17h30	Arrival Bruges

FLANDERS HYDROGRAPHY

Ensuring safe and smooth shipping traffic at sea from and to the coastal ports and the River Scheldt is a core task of the Agency for Maritime and Coastal Services. The MCS-Coastal Division supports the safety of shipping through its team **FLANDERS HYDROGRAPHY.**

Anyone involved in shipping, either professional shipping or pleasure cruising, makes use of products that result from the hydrographic and hydro-meteorological activities of **FLANDERS HYDROGRAPHY**.

A number of data is vital and hence indispensable for a trip to the sea or at sea. Everyone wants to know in advance when it will be low or high tide, how deep the water is, where the channels are located, where the wrecks and banks in the River Scheldt and off the Flanders Coast are situated exactly. Weather conditions are also important to ensure safe sailing.

FLANDERS HYDROGRAPHY provides all this supporting information.

A mission of **FLANDERS HYDROGRAPHY** is to measure and describe the Belgian Continental Shelf, the River Scheldt and all maritime means of access in view of enhancing the safety of navigation and all other marine objectives and activities, including offshore activities, scientific research, protection of the marine environment and shipping forecast services.

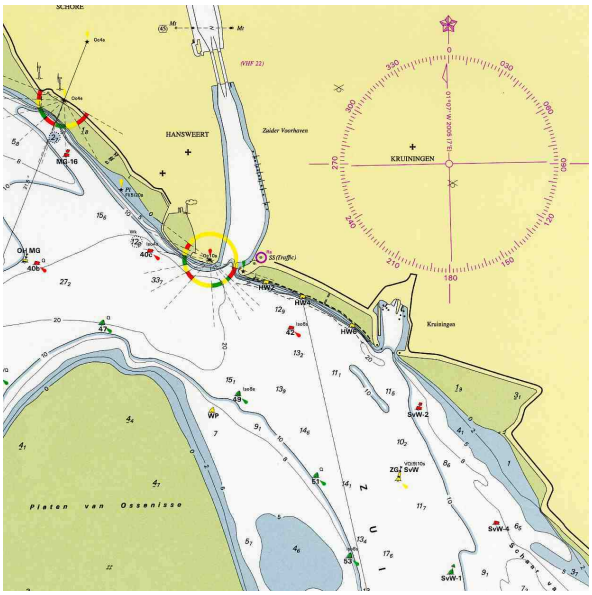

FLANDERS HYDROGRAPHY produces nautical sea charts of the VLAAMSE BANKEN, the Belgian-Dutch and the French-Belgian coast and navigational charts of the River Scheldt. Apart from the traditional paper charts there is also a production of electronic nautical charts (ENCs).

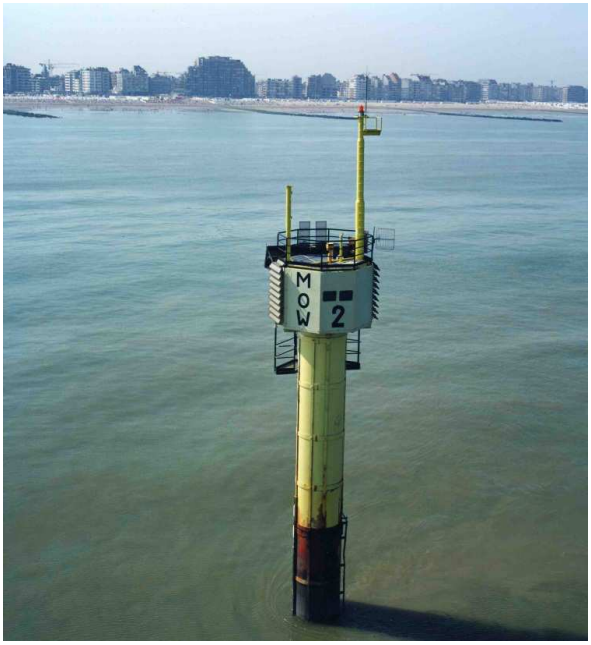

On the Belgian Continental Shelf, in the channels to Zeebrugge and the Western Scheldt, and on platforms on the Westhinder and Oostdyck Bank, a network of measuring poles, buoys and beacons is installed.

This important VLAAMSE BANKEN Monitoring Network is fully managed and maintained by **FLANDERS HYDROGRAPHY.**

agentschap
Maritieme Dienstverlening
en Kust

VLAAMSE HYDROGRAFIE

MARID 2013 PARTNERS

MARID 2013 SPONSORSHIPS

Golden

Silver

ISBN 978-2-11-128352-7